Determining the drivers of harmful algal blooms and their impact on public water supply resilience during droughts

Helen Cantwell

School of Earth and Environmental Sciences

Cardiff University

Submitted in partial fulfilment of the requirements for the degree of

Doctor of Philosophy

March 2021

Abstract.

Climate change poses a significant risk to water supply resilience. Reduced summer rainfall combined with elevated temperatures are likely to threaten both water quantity and water quality. With respect to water quality, shallow warmer reservoirs can increase risk of biological causes of poor quality, for example due to harmful algal blooms, cyanobacteria toxins and taste and odour metabolites. This was investigated at Llandegfedd, the largest potable water reservoir and a critical water supply system in Wales. The overarching aim addressed in this thesis was to determine if the reservoir would be vulnerable to poor water quality events in the future. To this end, the project comprised four main areas of research: 1. Historical data; 2. Water nutrient dynamics; 3. Sediment nutrient dynamics; 4. Effects of extreme weather events upon water quality.

Analysis of water samples indicated phosphorus limitation and the reservoir overall was classified as oligotrophic; unusual for a lowland reservoir. Mass balance analysis demonstrated low internal loading potential even in summer months, which was supported by sediment phosphorus measurements. Allochthonous sources of phosphorus were responsible for the low levels of bioavailable P in the water column. In contrast, the shallowest site at the northern end of the reservoir, adjacent to the main pumped inflow, was eutrophic and at highest risk of water quality deterioration, cyanobacterial growth and geosmin production. Analysis of extreme weather events indicated this risk to be compounded by pulse rainfall events. The reservoir relied upon an allochthonous source of phosphorous, with the refilling process also changing nutrient dynamics through increasing phosphorous concentrations.

An additional finding of this study was that analysis of nutrients pre and post water abstraction tower failure around 1999/2000 indicated that the current water abstraction method is inappropriate for monitoring water quality risk at this site, demonstrating the need for enhanced monitoring.

This study has shown that Llandegfedd Reservoir remains oligotrophic despite potential for internal P loading, suggesting possible future issues with water quality at the site. This is compounded by extreme weather events and patterns of drawdown and refilling. This is an important warning to the wider Water Industry that oligotrophic water supply reservoirs still require significant monitoring to assess water supply resilience in the face of climate change.

Acknowledgements and gratitude. This is for them.

I would not have had the strength or confidence to complete this thesis without the ever-present love and support of my Mam and Dad. Through the turmoil endured throughout the course of my PhD, my parents have been a constant in my life, reassuring me and encouraging me to follow my love for science and not give up in the face of adversity. I am, because of them.

My husband has been my rock throughout and also my protector, insulating me from negativity, reassuring me during times of doubt and drinking with me to celebrate the good times. He has carried me through the toughest of times and always put me before himself.

My children are so well behaved, polite and a pleasure to be with. They've made me laugh through difficult times and taught me to hold my head high when confidence and strength had left me. They gave me cwtches when I was down, and when I wasn't. They are my Love.

My supervisor gave me his time and patience. There were occasions when more patience was required than others. No other teacher has been as supportive and honest.

And Smotyn, without whom, I would never have taken on such a challenge as this in the first place.

Chapter 1: An introduction to water quality and Llandegfedd reservoir

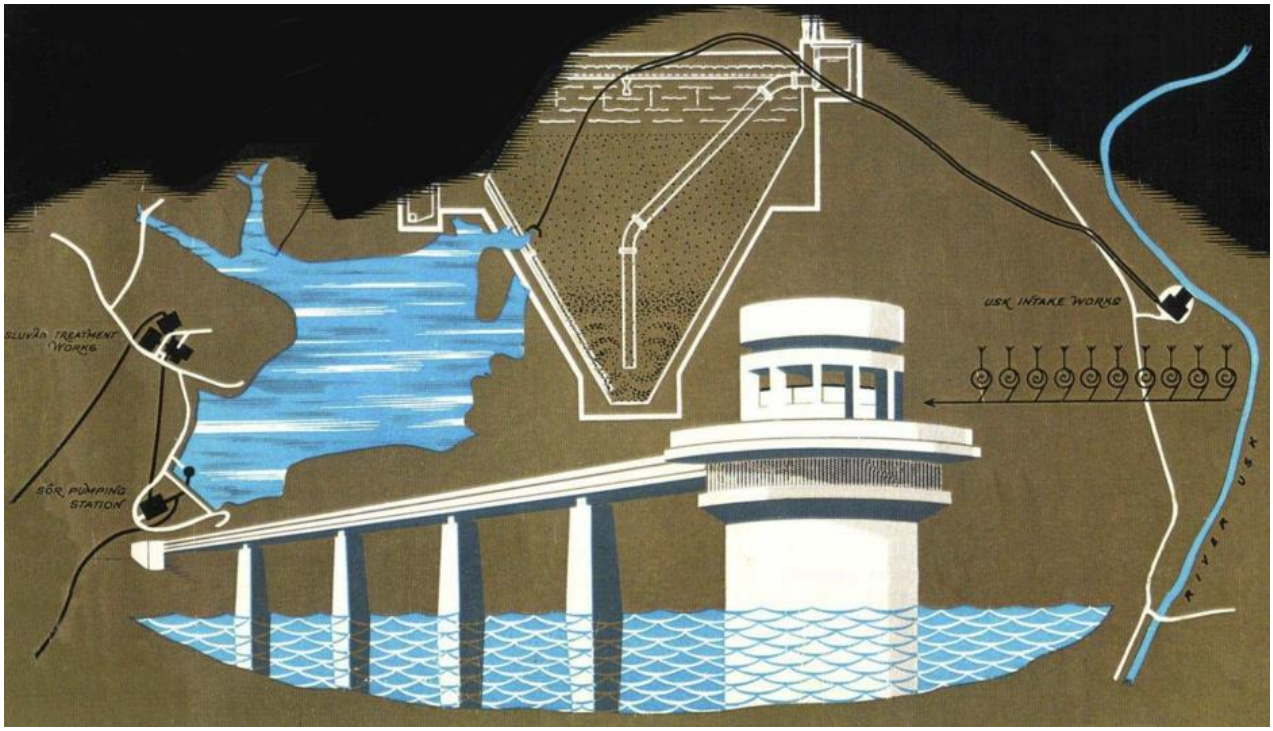

1.1 The importance of nutrient supply in reservoirs

Freshwater represents 0.8% of the worlds' surface and only 0.01% of the water over the world (Crossetti *et al.,* 2008). The freshwater demand imposed by the increasing global population density coupled with the consequences of climate change and restrictions to water treatment rates may further limit the amount of freshwater suitable for treatment to meet the high-water quality standards required for human consumption (Ammar *et al*., 2017).

Maintaining the balance of nutrients within a reservoir such as nitrogen and phosphorous is critical to ensure the survival of native species while avoiding nutritional conditions (shortage or excess) that may lead to a change in ecological community composition. Species native to a reservoir help preserve the nutritional balance required in order to maintain a healthy environment. Undesired nutritional changes may lead to detrimental water quality. Such changes may result in loss of native species through competition with invasive species (Bonito *et al*., 2019), and the inability of an organism native to the reservoir to survive in the changing conditions.

Excessive nutrient supplied to a reservoir may lead to cyanobacterial dominance (Wang *et al.,* 2019), due to the ability of some strains of cyanobacteria (e.g., *Microcystis*) to store excessive phosphorous which may be used during periods of nutrient deficiency. Nitrogen and phosphorous may be introduced to the reservoir in excess, however, very low concentrations of nitrogen and phosphorous favour diazotrophic cyanobacterial dominance. Therefore, the balance of nutrients supplied to a reservoir directly or indirectly, intentionally or otherwise, may lead to the disruption of an established healthy environment *(Poikane et al*., 2019).

Global warming will affect temperature and rainfall; therefore, river flows and water resources are likely to change (Arnell, 2006), with air temperature increasing by 2°C to 3°C and winter rainfall increasing by 10-30% but summer rainfall decreasing by up to 40% around the UK by 2080 (UKCIP). Lakes and reservoirs are sentinels for climate change due to their sensitivity to the environment and can rapidly change in response to changes in the catchment (Adrian *et al.,* 2009). However, changes to nutrient dynamics of a reservoir is site-specific and is dependent upon their characteristics and geographical location (Williamson *et al.,* 1999; Freeman *et al*., 2004; Frey and Smith 2005).

Anthropogenic disturbances within or near aquatic ecosystems contribute to eutrophication events (Dalu *et al.*, 2018). Eutrophication is a consequence of the over-enrichment of a reservoir/lake with nutrients such as phosphorous (P) and nitrogen (N) (Chen *et al.,* 2018), and has been linked to an increase in the establishment and success of cyanobacteria in lakes and reservoirs (Carey *et al*., 2012), leading to water quality deterioration. An indication of deteriorating water quality is the detection of geosmin (4,8a-dimethyl-decahydroaphthalen-4a-ol) or 2-Methylisoborneol (2-MIB) which are metabolic by-products of cyanobacteria (by species of *Dolichospermum, Oscillatoria, Aphanizomenon)* and *Streptomyces* (terrestrial bacteria) (Wu *et al.,* 1988), organisms which are believed to be principal producers within and around reservoirs (Olsen *et al.*, 2016). Geosmin and 2-MIB within drinking water can result in an undesirable earthy taste which remains following treatment (Olsen *et al.*, 2016).
Previous and continuing anthropogenic activities both directly and indirectly affecting freshwater ecology through reshaping our physical environment and disrupting nutrient flow and availability to reservoirs require monitoring and managing to limit the deleterious consequences upon water quality.

1.2. Harmful Algal Blooms (HABs) and other problems in reservoir management

Cyanobacterial blooms releasing toxic by-products are referred to as Harmful Algal Blooms (HABs). 25% to 75% of global cyanobacterial blooms are toxic (Chorus, 2001; Bláhová *et al*., 2007; 2008). These toxins are classified according to the target of their toxicity, as hepatotoxins (liver), neurotoxins (nervous system) and dermatoxins (skin).

A high abundance of cyanobacteria within a reservoir used in the supply of raw water for treatment is a significant concern to water companies, specifically reservoirs hosting water sports activities concerning the cyanobacterial production of hepatotoxins and neurotoxins. Cyanobacterial toxins are one of the highest risk factors of waterborne toxic biological substances (Carvalho *et al.*, 2011).
Microcystins are a family of monocyclic heptapeptides (more than 70 variants have been identified) with the characteristic feature, unusual β-amino acid, Adda (3-amino-9-methoxy-2,6,8-trimethyl-10-phenyldeca-4E, 6E-dienoic acid) (Bláha, 2009). The Adda side chain is consistent between microcystins (Harris *et al.*, 2016), and is used in their identification.

The most frequently found hepatotoxins in freshwater are the cyclic hepta-and pentapeptide microcystins and nodularins (Sivonen, 2019). Humans may be exposed to the toxins while taking part in water sport activities and drinking contaminated water. Heptapeptide is the most common form of microcystin produced by cyanobacteria and is a potent liver toxin (Bullerjahn *et al*., 2016) known to be hazardous to many organisms (Baptista *et al.*, 2006). Heptapeptides may cause severe hepatic damage by inhibiting protein phosphatases (Miller *et al.,* 2017, Camargo *et al.,* 2006). Microcystins are produced by *Microcystis, Planktothrix* and *Dolichospermum* species (Dolman *et al.,* 2012), and may be released into the surrounding water during a period of cyanobacterial senescence.

The presence and concentration of each cyanotoxin within the water is dependent on the composition of cyanobacterial communities present, as different species produce different toxins. The most likely cause leading to changes in toxin production is climate change (Burford *et al.*, 2014) with the growth of various cyanobacterial species and their toxin production is greatly influenced by temperature, pH and available nutrients (Neilan *et al*., 2013; Häder *et al.,* 2014; Rastogi *et al*., 2014), where a positive correlation exists between an increase in water temperature, growth rate and nutrients concentrations.

Phosphate concentrations have no direct impact upon microcystin production by cyanobacteria, but act indirectly by affecting growth rate (Briand *et al.,* 2005), and has a direct correlation with toxin production quantities (Briand *et al.,* 2005). Existing water treatment methods are incapable of removing 100% of cyanobacterial growth by-products such as geosmin, potentially resulting in their distribution throughout the water (Otten *et al.,* 2016). Research carried out by Kull (2004) concluded that chlorine does not efficiently oxidise microcystin in drinking water due to the slow rate of degradation to non-toxic products (Kull *et al.,* 2004).

1.3. Taste and odour metabolites in reservoirs

Cyanobacteria are the most common source of the taste-and-odour (T&O) compounds geosmin and 2-MIB (2-methylisoborneol) (Jung, 2010). 2-MIB is dominant during the live growth phase of cyanobacterial blooms (Ma *et al*., 2013), whereas geosmin is released from cyanobacterial cells during lysis following senescence (Jung, 2010), and is not biomass-related (Perkins *et al*. 2019), therefore, cyanobacterial cell counts would be decreasing, while geosmin concentrations will be increasing. Geosmin production is difficult to anticipate

(Komatsu *et al*., 2008), due to its production and release being dependent on many variables (Zuo *et al*., 2009).

Geosmin can be located both extra- and intracellularly and is species-dependent (Jung *et al.,* 2010). Stress, senescence, cell damage and a period of rapid cyanobacterial growth may result in the release of cell-bound geosmin to the surrounding environment (Asquith *et al.,* 2018).

High levels of inflow from the peripheral sediment into the reservoir during periods of high rainfall volume can carry geosmin and 2-MIB produced by akinetes, terrestrial bacteria and fungi (Klausen *et al.,* 2005; Zaitlin *et al.,* 2006; Jüttner *et al.* 2007).

Harris *et al.,* (2016) concluded that geosmin occurred more frequently during periods of low Total Nitrogen: Total Phosphorous ratio (TN:TP) (<30:1 by mass) compared with higher TN:TP ratios. This is likely due to the increased cyanobacterial productivity at lower TN:TP ratios. Additionally, geosmin production increases during periods of a low NO_3^-: NH_4^+ ratio (Harris *et al.,* 2016).

1.4 Phosphorous in reservoirs.

Phosphorous (termed 'P' and 'TP' (Total Phosphorous) hereafter) is an essential element for all organisms and is often a limiting nutrient in reservoirs and lakes, with an excess potentially leading to eutrophication (Wang *et al*. 2008; Schindler, 1977, 2012). Inorganic phosphorous (phosphate) has been found to instigate and fuel cyanobacterial blooms (Ame *et al.,* 2003). However, both nitrogen and phosphorus are essential in the establishment of cyanobacteria within a reservoir (Conley *et al.,* 2009; Paerl *et al*., 2011; Moss *et al*., 2013). P can be available in various forms, the form of which is dependent upon its source, environmental conditions and its location within the water column. P may be sourced from an internal supply where a pool of P may be accumulated in the sediment surface following senescence of an organism, be bound to redox-sensitive iron compounds or fixed in labile organic forms (Søndergaard *et al.*, 2003). Therefore, many processes may result in the release of P into the water column from the sediment including the mineralisation of organic matter, the desorption and dissolution of P bound in precipitates and inorganic materials and the diffusion of dissolved P from sediment pore waters (Petterson, 1998; Moore, 1994). Internal P release may result in continued eutrophication (Hou *et al.*, 2013). Alternatively, phosphorous may be transported to the lake or reservoir by inflow from a river or by entrainment following precipitation.

1.5 The nature of phosphorus in water

Phosphorous exists in either organic or inorganic form. The individual components of organic phosphorus (OP) are difficult to identify and isolate due to the complexity and variety of bound forms (Wang *et al.,* 2019). Inorganic phosphorous within the sediment is bound to aluminium (Al-P), iron (Fe-P) or calcium (Ca-P). Fe-P can dissociate into the water and is dependent upon redox conditions (Watts, 2000), suggesting a high potential for P release from anoxic sediment (Tu *et al.,* 2019). Fe-P is biologically labile and is available for uptake by phytoplankton (Tu *et al.,* 2019). Al-P and Ca-P are generally unavailable and subject to burying within the sediment. Labile/acid hydrolysable phosphate is biologically labile. It is recycled via bacterial mineralisation of organic P.

Total phosphorous (TP) describes the total concentration of inorganic and organic-P within a sample. Bioavailable P is the sum of immediately available P and the P that can be transformed into available P by naturally occurring processes (Boström *et al.,* 1988). Acid Hydrolysable Phosphorous (AHP) is a refractory form of phosphate and can be used to determine the concentration of condensed-P (Dong *et al*., 1990). AHP is unavailable for biological assimilation until changes to the water environment, such as changes to the pH lead to the hydrolysis of orthophosphate (Hupfer *et al.*, 2004).

Condensed-P comprises meta-, pyro- and polyphosphates (Dong *et al*., 1990). Orthophosphate (PO_4^{3-}) is the most readily available form of P to algal and cyanobacterial cells. Polyphosphate (Poly-P) is a polymer of orthophosphate molecules. The acidity of the water catalyses the hydrolysis of AHP, where a decreasing pH results in an increase in the rate of hydrolysis, with an increasing rate of hydrolysis of condensed-P to OP as the pH decreases below 6.0 (Hupfer *et al.*, 2004, Mistry *et al.,* 2013). The potential for reversion increases as the pH rises above 7.5. Condensed-P has increased solubility and a reduced potential for precipitation relative to that of OP and therefore, may be retained longer in the reservoir (Hupfer *et al.*, 2004). Some fractions of condensed-P are resistant to spontaneous hydrolysis under normal physiological conditions (Mistry *et al*., 2013). Therefore, condensed phosphates are biologically available under certain natural conditions. Condensed-P can be stored in cells as part of 'luxury uptake' by some species of cyanobacteria (e.g., *Microcystis*). However, if P-stressed cells experience a spike in P availability, they over-

produce polyphosphates in excess of luxury uptake levels, leading to the "overplus" response (Martin *et al.,* 2014).

The ferric ion (Fe_3^+) exists in aerobic conditions and easily combines with phosphorous to create phosphate precipitate (Jensen *et al*., 1992). However, ferric hydroxide becomes soluble in anaerobic conditions, increasing the potential for eutrophication following an increase in the release of P (Martin *et al.,* 2014). Wu *et al.* (2014) determined that more P may be released under alkaline conditions and concluded two of the most significant variables determining P release from sediments were temperature and pH (Wu *et al.*, 2014). An increase in water temperature positively correlates with P release from the sediment (Jensen *et al*., 1992), as a consequence of increased microbial metabolic activity during the summer period. Increased metabolic rates lead to anoxic conditions and a decrease in redox potential, which fuels sediment-bound P release (Wu *et al*., 2014). Anoxic conditions lead to P release when Fe^{3+} is reduced to Fe^{2+}.

Jensen (1992) concluded that P release is significantly associated with pH, temperature and NO_3^-, but by pH when these three parameters are found to vary within the normal seasonal range (Jensen, 1992). Nitrate increases sediment P release through increasing metabolic activity of bottom-dwelling bacteria by providing a source of N.

1.6 Internal Phosphorus loading

The sediment represents both the largest source and sink of P (Boström *et al*., 1982; Hou *et al*., 2013), and is therefore a critical factor in the overall nutrient dynamics of reservoirs (Søndergaard *et al.,* 2003). The P equilibrium in oxic conditions also contributes towards the dissolved P-regulation within a reservoir (Kim *et al.,* 2003; Hupfner *et al.*, 2004, Caraco *et al.,* 1993).

Non-calcareous sediment is an efficient sorbent of P as a consequence of the high concentration of oxyhydroxides, Fe^{3+} and aluminium (Reddy, 1995). Iron hydroxides are sensitive to both the redox conditions and pH of the water, whereas aluminium hydroxides are sensitive to the water pH (Reddy, 1995). The phosphate ion competition for iron-binding sites leads to an increase in the P-binding capacity as the pH increases.

Photosynthesis influences the pH of the water, whereby the removal of CO_2 from the water raises the pH. Periods of raised pH may lead to the release of increasing quantities of P

through desorption of P from ferric hydroxide through replacing the P with hydroxide (Jensen *et al*. 1992). However, the majority of P is released in the form of biologically available orthophosphate (Cooke *et al*. 2005). Therefore, increasing photosynthetic rates as a consequence of raised orthophosphate concentrations fuel the rise in pH, leading to the release of more P from the sediment.

Through maintaining a lowered redox potential, sulphides and irons are reduced. Sulphur removes the iron from the water as an iron sulphide precipitate (FeS), decreasing available binding sites of P with iron within the sediment, resulting in a higher concentration of P released into the water (Caraco *et al.,* 1993).

The adsorption of P from the water column to bottom sediments is a transient process (Haggard *et al*., 2005). P equilibrium between Fe-bound and Al-bound P in sediments regulates the P net mobilisation under anaerobic conditions to the interstitial water (Koski-Vahala *et al.,* 2001).An increase in the Fe:P ratio decreases the concentration of P released to the water due to a higher availability of Fe^{3+} adsorption sites within the sediment. The rate of oxic-P release increases when Fe:P ratios are <15 (Jensen *et al.* 1992), due to a decrease in the number of binding sites of P with Fe^{3+}.

The pH and DO levels within a reservoir vary diurnally and seasonally as a consequence of photosynthesis, leading to a dynamic internal P release from the sediment (Ahlgren, 2006). However, the rate of P release is steady over short periods, but drastic or sudden environmental changes may induce a change to the rate of internal P loading (Ahlgren, 2006). There is a seasonal cycle in P concentrations (Chen *et al*., 2014). Bottom-dwelling bacteria deplete nitrate for use as an electron acceptor. The increased summer temperatures lead to thermal stratification, trapping nutrients both above and below the thermocline, preventing mixing along the water column. The depletion of nitrate during denitrification leads to anoxic conditions and a decrease in the redox potential, releasing sediment-bound P into the interstitial water.

1.7 Redox-mediated P-release

The phosphate binding capacity mediated by Fe^{3+} minerals decreases with an increasing pH in a pH range between 5 and 8 as a consequence of competition of hydroxyl ions for binding sites (Ahlgren, 2006; Lijklema, 1980; Reddy *et al*., 2008). Ferric hydroxides are reduced to

ferrous iron by bacteria when redox potentials are below 300 mV or oxygen concentrations below 0.1 mg L^{-1}, releasing phosphate occluded in hydrated coatings of the ferric hydroxide (Golterman, 2004; Reddy *et al.,* 2008). Redox potentials of less than −100 mV are indicative of anaerobic environments, and values >100 mV are indicative of aerobic environments (Suthersan, 2001). The term 'anoxic' is the term given to conditions where oxygen is absent from the environment, whereas the term 'anaerobic' refers to environments that are devoid of any universal electron acceptor such as oxygen, nitrate or sulphate (Christophoridis *et al.*, 2006).

An oxidised surface microlayer created under oxic conditions acts as a protective film, restricting P release from the sediment (Christophoridis *et al.,* 2006). Oxic conditions within sediment or at the sediment/water boundary create a high redox potential status (James *et al*. 2001), leading to the decrease of free electrons within solution, increasing the rate of P binding to the metals. Conversely, a decrease in oxygen concentrations which lead to anoxic conditions increases free electrons, increasing the release rate of P through metal reductions (Moore *et al.,* 1998). The Eh value can reach as low as -240mV, whereas a high redox potential may reach 500 to 920mV (Miao, 2006). Due to the relationship between phosphorous and Fe/Mn, the redox conditions are strongly positively associated with the amount of P released into solution (Miao, 2006).

Cyanobacterial blooms increase pH and decrease the redox potential of the water as a direct consequence of respiration (Cao *et al.,* 2016) which potentially leads to sediment P release leading to an increase in bioavailable P at sediment surfaces and in the water column during blooms (Brunberg *et al*., 1992). An indirect means of microbial contribution of P from the sediment is through the metabolism of bioavailable carbon. The metabolism of organic carbon is oxygen-consuming, leading to an anoxic region at the sediment-water interface (James *et al*. 2001) and the reduction of Fe^{3+} from insoluble Fe(III)-P to soluble Fe(II)- and P. TP concentrations decline after drawdown possibly due to its assimilation by biota (James *et al*. 2001).

1.8 Phosphorus uptake by phytoplankton and bottom algae and cyanobacteria

Cyanobacterial cell growth and phosphorus metabolism is highly dynamic and varies with varying phosphorus concentrations (Ghaffar *et al.,* 2017). A non-linear relationship exists

between P availability and cyanobacterial growth rates which changes with time between external phosphorus concentrations, intracellular phosphorus storage and cellular growth rates (Ghaffar *et al.,* 2017). Cyanobacteria use light energy to build new cell material from carbon, nitrogen, and phosphorus, the supply rate of which determines the cyanobacterial growth rate (Riegman, 1986).

The ability of cyanobacteria to access P in a water column is dependent upon certain ecophysiological traits. Traits advantageous to cyanobacterial establishment include a high affinity P uptake system, which is activated during periods of low P concentrations, the production of extracellular polyphosphatase enzymes to access P which may be organically bound or sediment-bound P, the ability to store P during periods of P availability (luxury uptake) (Healey, 1982; Jacobson, 1982), and an ability to regulate buoyancy through the generation of gas vesicles (Chu, 2007), allowing access to P in various localities within a reservoir (Guedes *et al*., 2019).

Vertical migration is common to cyanobacteria with strong buoyancy controls such as *Dolichospermum, Aphanizomenon* and *Microcystis* (Xiao *et al*., 2016). During periods of low nutrient concentrations in the epilimnion, buoyancy control allows cyanobacteria to descend through the water column to the colder, darker hypolimnion where the storage of P may be higher, especially during anoxic conditions. Cyanobacteria may also return to the warmer epilimnion where conditions are lighter during more favourable conditions.

P-limiting conditions inhibit biomass growth (Chl a) and photosynthesis but the phosphatase activity and P assimilation rate increases (Li *et al.*, 2016)

Alkaline phosphatase increases the uptake of inorganic-P during periods of low internal and external P concentrations through catalysing the degradation of complex organic phosphate substrate into a biologically available inorganic phosphorous (Bar-Yosef *et al.* 2010). Inorganic phosphatase increases the availability of inorganic-P to the cell generating the alkaline phosphatase and to neighbouring cells not simultaneously secreting the extracellular phosphatase (Raven, 2010). Some strains of cyanobacteria (*A. ovalisporum*) capable of extracellular phosphatase production can induce the secretion of alkaline phosphatase in neighbouring strains of cyanobacteria through generating a cyanotoxin to increase the available inorganic-P in the water (Bar-Yousef *et al.*, 2010).

1.9 External Phosphorus loading

A strong correlation exists between external P loading and phytoplankton biomass (Knoll *et al.,* 2003), where excessive P from a terrestrial source significantly increases reservoir productivity (Schindler, 2012). Climate change triggers cyanobacterial and algal blooms through increasing the allochthonous nutrient inflow to a reservoir during periods of heavy rainfall (Lapota, 2019). The surrounding agricultural land if often applied with fertiliser which has the potential to be carried into the reservoir during periods of heavy rainfall. Therefore, periods of heavy rainfall as a consequence of climate change is correlated with an increased soluble phosphorus fraction from agriculturally dominated catchments (Kane *et al.,* 2014). The concentrations of labile phosphorus and algal biomass have increased globally since 1995 (Baker *et al.,* 2014; Conroy *et al.,* 2005a). As a direct consequence of higher winter rainfall, phosphorus loading from land to streams is expected to increase in the UK (Jeppesen *et al.*, 2009). Symptoms of eutrophication may decrease during periods of decreased external nutrient loading through dilution as a consequence of inflow, however, this result is often delayed as a consequence of internal loading from sediments rich in organic matter accrued over many years (Phillips *et al.,* 2005; Turner *et al.,* 2008).

Anthropologically derived P has several routes into a reservoir, each dependent upon the source of phosphorous. Zebra mussels (*Dreissena polymorpha*) invade and occupy the peripheral sediment of many reservoirs (Conroy *et al.* 2005), following the unintended transport of the organism from its source. The mussels may stimulate phytoplankton productivity through nutrient remineralisation (Arnott *et al.,* 1996, Conroy *et al.* 2005). Phosphorous released during the decaying process of mussel colonies may be carried into the reservoir during periods of heavy inflow or during periods of raised reservoir levels, where it may be assimilated by algal and cyanobacterial cells (Hupfner *et al.,* 2004).

1.10 The nature of Nitrogen in water

Nitrate is stable in aerobic water. Nitrite (NO_2^-) is typically an intermediate product during ammonium oxidation to nitrate. Therefore, nitrite does not remain in solution for long periods. The maximum solubility of N_2 in water can be reached at times of lower temperatures (Wetzel, 2001). The warmer temperatures reduce the solubility of N_2, leaving the epilimnion depleted of N_2 (Vincent, 2018). However, despite a warming of the water

column, the metalimnion and hypolimnion may become supersaturated with N_2 due to hydrostatic pressure retaining the molecule within the water column (Su *et al*., 2019). Denitrifying bacteria inhabiting the sedimentary surface may decrease the concentration of N_2, decreasing the N_2 concentrations within the hypolimnion (Adam *et al*., 2016).

1.11 Nitrogen in reservoirs.

Reservoir sediments act as a sink for nitrogen. Nutrient concentrations are higher in the interstitial water than those in surface water creating a concentration gradient which in part controls the release of nutrients from sediments (Wang *et al.,* 2018). The high organic material content of the sediment can absorb large amounts of nitrogen and causes nitrogen deposits to build within sediments (Wang *et al.,* 2018).

Nitrogen-containing compounds serve as a source of nutrition for algae and cyanobacteria as it is an essential component of proteins, enzymes, ATP and genetic material. Reduced (NH_4^+) and oxidised (NO_3^-) forms of N are readily available for assimilation by algae within the reservoir (Zhang *et al*., 2020). Despite nitrogen being abundant within our atmosphere (78%), very little is available for uptake by phytoplankton without nitrogen fixation (Allen *et al.*, 2019). Atmospheric nitrogen exists as a dinitrogen molecule (N_2). The triple bond of the dinitrogen molecule renders the gas inert (Vincent, 2018), and as such, eukaryotic organisms are incapable of breaking the bond to create the required reduced form.

Diazotrophic N_2-fixation of atmospheric N is essential in the supply of atmospheric N to non-diazotrophic organisms within a reservoir (Adam *et al*., 2016), and is a significant source of new nitrogen. Cyanobacteria such as *Aphanizomenon* and *Nostoc* spp. carry out N-fixation (Schoffelen *et al.,* 2019), and become essential to the food-chain through supplying eukaryotic organisms with otherwise unavailable nitrogen (Adam *et al*., 2016). Once dinitrogen has been fixed by bacteria (Figure 1.11.1), the resultant ammonium/nitrate enters the reservoir following senescence of the diazotrophic organism. N_2-fixation by *Aphanizomenon* and *Nodularia* is sufficient to provide their N-requirements while also releasing ~ 35% of their newly fixed nitrogen to the surrounding water (Ploug *et al*., 2011). N-NH_4^+ is nitrified to N-NO_2^- and N-NO_3^- by bacterio-plankton, with nitrate being the most dominant form of N (Debrowski *et al*., 2017). Biological oxidation of the NH_4^+ released by cyanobacteria increases the NO_3^- concentration (Harke *et al.* 2012).

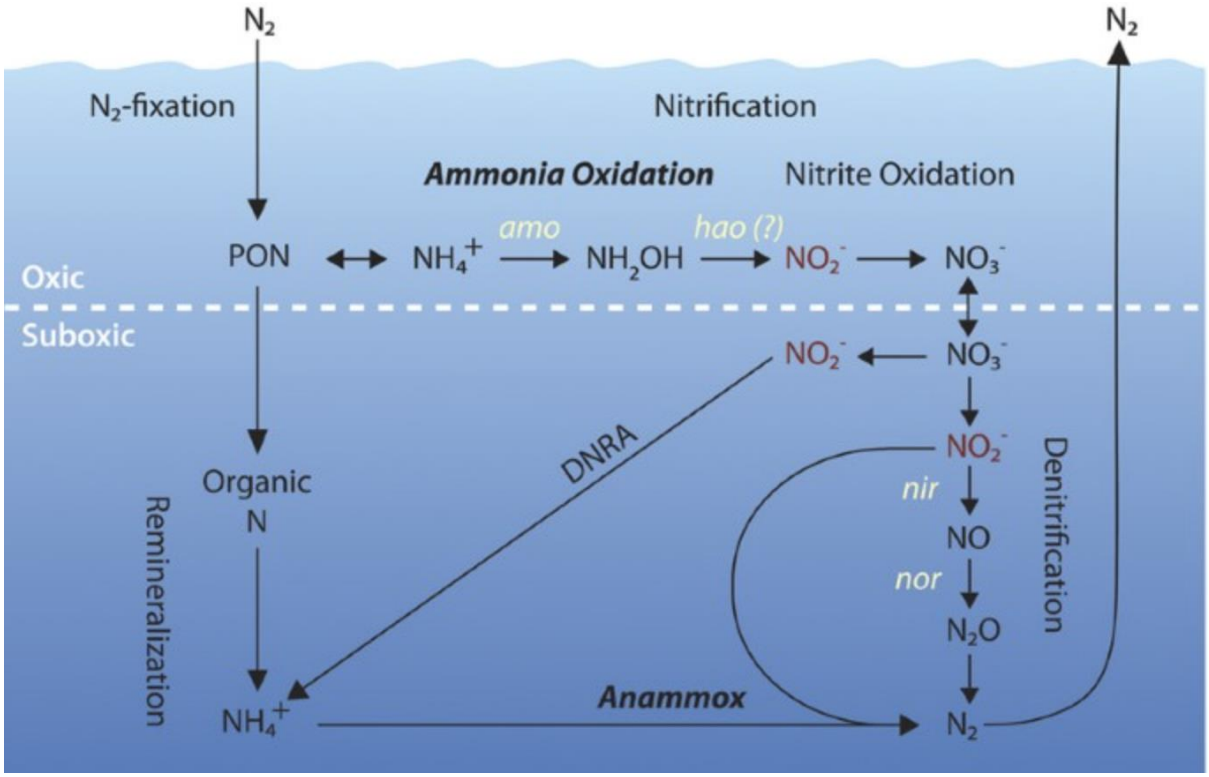

Figure 1.11.1. Nitrogen transformation cycle within a reservoir (Francis et al., 2007).

The release of newly fixed N by a new cyanobacterial bloom during the spring season may stimulate and fuel pelagic production and microbial food-webs. However, some nitrogen fractions are not bioavailable, and some nitrogen is retained within sediments (Wang *et al*., 2018).

Sediments can release nitrogen into the water column under certain conditions (e.g., low pH, anaerobic conditions and disturbance) (Barber *et al.,* 2014), up to 88% greater in aerobic environments compared with that under anaerobic environments (Austin, 1973).

Organic-N from decaying material at the sediment surface is mineralised predominantly to NH_4^+ (Wang *et al.,* 2018). During the degradation of organic matter, the organic compounds are broken down to NH_4^+ and NH_3^+ and CO_2 through the mineralisation process (Isidorova *et al.*, 2019). The mineralisation and immobilisation of organic-N in the sediment layer can provide a source of inorganic-N for a water body (Percuoco *et al.,* 2015). The NH_4^+ may also be nitrified by autotrophic bacteria for use as an electron donor. Denitrification carried out by facultative anaerobic bacteria reduce the nitrate to nitrite, which is then denitrified from nitrite to dinitrogen (Zhou *et al.,* 2016).

The process of denitrification requires <10% oxygen and uses organic matter as an electron acceptor. N_2 escapes to the atmosphere (Adam *et al.*, 2016), leading to a decrease in TN concentrations within the water (Yang *et al*., 2013).

1.12 Sources of nitrogen

Anthropogenic sources of N contribute towards the N load within a reservoir. Nitrogen is frequently applied to the land as fertiliser in the form of NH_4^+. However, excess fertiliser is prone to run-off during periods of heavy rainfall, making agricultural processes among the worst N polluters within the UK (Galloway *et al.,* 2008). In non-polluted areas, much of the combined atmospheric nitrogen is in the form of NH_3^+, a significant amount of which originated from the decomposition of terrestrial organic matter (Hutchinson, 1944).

The main source of entry for N into reservoirs is through organic waste (fish, bird, mammal) and via run-off from fertilised land during a period of heavy rainfall (Grey *et al.*, 2002). Dinitrogen enters a reservoir through diffusion from the atmosphere but is not an available source of N to organisms incapable of nitrogen fixation (Adam *et al.,* 2016). Seasonal reservoir characteristics directly influence nitrogen dynamics within the sediment and water of the reservoir (De Groot *et al.,* 1993). When a reservoir is drawn down (lower water levels) during the summer season, nitrogen is released from the peripheral sediment into the reservoir during episodes of heavy rainfall (Xiao *et al.*, 2017).

Plant uptake within exposed sediment during the summer period can significantly reduce sediment N during periods of growth through removal and assimilation of N-fractions during the growing phase (Caffrey *et al*., 1992; James *et al.,* 2001; Clarke, 2002) but is returned to the reservoir following plant senescence and decay, resulting in a net gain of N (Weisner *et al*., 1994; Nowicki *et al*., 1999; Kleeberg *et al*., 2004). Rooted plants can contribute significantly to N cycling (Caffrey *et al.*, 1992; Fischer *et al.*, 1995; Eriksson *et al.*, 1999) by oxygenating sediments (Kleeberg *et al.*, 2004), promoting coupled nitrification and denitrification. The process decreases the concentration of reduced nitrogen, while an increase in nitrification promotes the oxidative production of TON (Cavanaugh *et al.*, 2006).

1.13 Nitrogen utilisation by phytoplankton and bottom algae and cyanobacteria

Nutrients and climate change are indicators of future cyanobacterial blooms (Persaud *et al.,* 2015). Cyanobacteria release ammonium following N_2-fixation and P from the sediment into

the surrounding water through cellular leakage, parasitism by bacteria or fungi, decomposition of dead cells and dead cyanobacterial colonies (Cottingham, 2015).

Nitrogen fixation requires specialised structures that provide the required intracellular environment in order to carry out N-fixation, such as the absence or very low concentration of O_2. Heterocyst formation is critical to the nitrogen fixation process (Qiu *et al.,* 2019). It is the site of the nitrogenase complex and is formed through filamentous cell differentiation in conditions of low dissolved inorganic nitrogen concentrations (Schoffelen *et al*., 2019). The heterocyst evolved a thick cell wall to prevent the diffusion of O_2, and the removal of photosystem II, thereby preventing O_2 production which would otherwise inhibit nitrogenase formation (Miller *et al*., 2020). Consequently, only photosystem I is located within a heterocyst for ATP production. The heterocyst is highly sensitive to the presence of oxygen; high levels of O_2 can negatively affect the cyanobacteria through suppressing the formation of nitrogenase complexes (Miller *et al*., 2020). Cyanobacteria have evolved to reduce nitrogen-fixing activities during turbulent conditions where oxygen is actively mixed into the water (Gallon, 1992). Residing within oxygen-depleted zones of a reservoir protects the heterocyst from oxygen-induced damage (Wetzel, 2001).

The oxygenic photosynthetic and nitrogenase processes have been spatially separated in filamentous diazotrophic cyanobacteria to limit the negative effect of O_2 upon N-fixation. Additionally, N-fixation is carried out during the night and photosynthesis during the day (Stewart *et al.*, 1986) to further reduce the risk of N-fixation damage by oxygen. Nitrogen-fixing photosynthetic bacteria are capable of fixing nitrogen in the absence of light, but at a reduced rate (<10%) relative to that carried out in the light (Wetzel, 2001).

Although the presence of sunlight is essential to the fixation process (Miller, 1991), nitrogen-fixation is inhibited in full sunlight such as when at the water surface, but reaches maximum productivity below the surface, before an exponential decrease in productivity is seen with greater depth and associated light attenuation (Miller, 1991). NH_4^+ rapidly switches off nitrogenase activity in photosynthetic bacteria (Reich, 1985). Therefore, ammonium released as a consequence of microbial activity may negatively impact nitrogen fixation. The high affinity for NO_3^- of cyanobacteria allow some species to use NO_3^- at a low ambient concentration and the ability to fix N_2 may permit exploitation of the large pool of nitrogen (Binhe, 1992).

The assimilation of N-NO_3^- requires more energy than that of N-NH_4^+ (Riegman *et al.* 1992, Hallegraeff 1993, Riegman 1995, McCarthy *et al*., 2009, Glibert *et al.* 2016, Ruan *et al.*, 2017, Watzer, 2019), therefore, at times of low energy and in the presence of both nitrate and ammonium, N-NH_4^+ is the molecule of choice. The assimilation rate of ammonium correlates positively with temperature as a consequence of increased microbial metabolism (Williamson *et al.,* 2016). Therefore, a higher availability of ammonium than other N-source is beneficial to cyanobacteria and could potentially lead to a cyanobacterial bloom.

Phytoplankton use alternative forms of nitrogen when NH_4^+ concentrations are insufficient to meet the nitrogen requirement. Urea becomes the next choice, and if its concentration is inadequate to satisfy the needs, the third option of using NO_3^- is selected (Takamura *et al*. 1987). Low concentrations of NH_4^+ may not completely suppress NO_3^- uptake and N_2 fixation (Binhe, 1992). An inadequate supply combined with weak affinity for certain forms of nitrogen (e.g., NH_4^+) may allow simultaneous uptake of several forms of nitrogen by cyanobacteria (Binhe, 1992). The rise in the abundance of NH_4^+ may lead to rapid growth in the cyanobacterial population, forcing selection of the alternative metabolic pathway leading to toxin production. A study by Adam (2016), found that *Aphanizomenon* released 50% of its newly fixed N_2 as NH_4^+. However, the NH_4^+ was transferred to microorganisms within approximately 5 hours of its release and did not accumulate in the water (Adam *et al.*, 2016). Ammonium concentrations are generally low in natural habitats (Rees *et al.*, 2006). Therefore, cyanobacteria can maximise ammonium uptake during periods of low ammonium concentrations by utilising high-affinity ammonium permeases.

Ammonium uptake by cyanobacteria taken up either from the outer medium or produced intracellularly, is incorporated into carbon skeletons mainly through the glutamine synthetase-glutamate synthase cycle (GS/GOGAT) (Herrero, 2001), where the carbon skeletons required for ammonium assimilation are supplied in the form of 2-oxoglutarate (2-OG) (Florencio, 2002). Cyanobacteria coordinate the flow rates of carbon and nitrogen assimilation by using signal transduction systems to maintain their metabolic homeostasis. The signal transduction systems integrate signals from the existing status of the carbon and nitrogen metabolic activity and regulate the level of glutamine synthetase (GS) and glutamate synthase (GOGAT) activity (Muro-Pastor *et al.,* 2001). Nitrogen control by cyanobacteria relies upon the repression of pathways of assimilation of some nitrogen sources, allowing expression of reductase genes in the presence of a more easily assimilated sources of nitrogen

such as ammonium (Herrero, 2001) (Figure 1.13.1). The nitrogen-controlling ability is not universal for all species (Drath *et al.*, 2008; J. Li *et al.*, 2016).

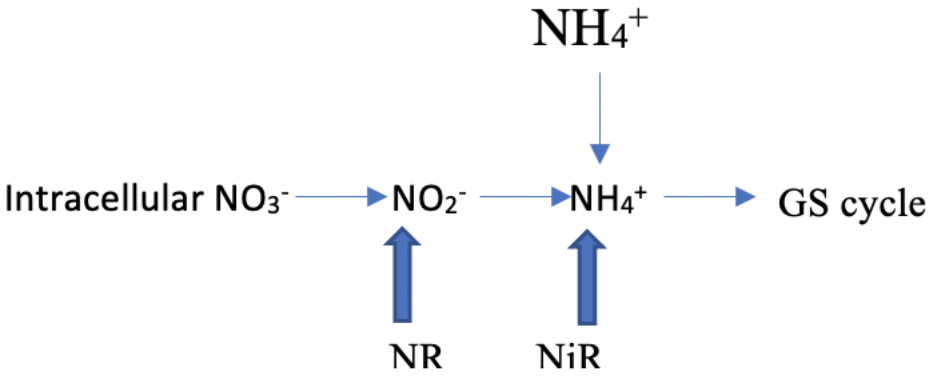

Figure 1.13.1. Nitrate reduction to ammonium using nitrate and nitrite reductases in contrast with direct ammonium assimilation via the lower energy-consuming pathway (Herrero, 2001).

This pathway can result in increased growth rates due to the shortened metabolic pathway and increased availability of energy. However, dissolved inorganic nitrogen and molecular nitrogen are often used simultaneously during the spring cyanobacterial bloom (Binhe, 1992).

1.14 Absolute and relative nutrient limitation

The concentrations of total nitrogen (TN) and total phosphorous (TP) within a reservoir is subject to the seasonal supply and demands of its flora and fauna and is therefore highly dependent upon the water chemistry and biology specific to the site.

Many variables are critical to the establishment and survival of cyanobacteria, but nitrogen (N) and phosphorus (P) primarily regulate primary production (Sommer, 1989, Litchman *et al.,* 2003). Consequently, the balance between the two nutrients may determine the dominance of one species over another. A species' ability to maximise its ability to fix nitrogen may provide the competitive advantage over other species incapable of N-fixation to survive in conditions unsuitable for most eukaryotic algae (low TN:TP) but are generally out-competed at higher levels. Redfield's TN:TP ratio of 16:1 (on a molar basis) is used as a predictor of cyanobacterial blooms, but it may be questionable under conditions where both N and P are in abundance but the TN:TP ratios are above 16; P may not be a limiting factor even during conditions where the TN:TP ratio >16:1. An alternative ratio deemed critical to cyanobacterial dominance is that of Smith's ratio, where cyanobacterial growing conditions are deemed suitable when the TN:TP ratio is <29:1 (on a molar basis). However, the use of

thresholds alone as a means of determining nutrient limitation has not been universally adopted (Litchman *et al.* 2003).

In eutrophic systems where critical nutrients are not limiting, the TN:TP ratio is a less effective predictor of cyanobacterial dominance (Paerl *et al*., 2006); The information provided by the TN:TP ratio does not provide information regarding either the N or P concentrations. Therefore, a low TN:TP ratio may indicate an N-limited reservoir, but the concentrations of P may be exceptionally high. Although the TN:TP ratio can help in the determination of the potential for cyanobacterial blooms, the ratio cannot be used without consideration of other key variables.

The importance of the TN:TP ratio with regards to the biomass of a reservoir at any given period, disregarding the importance of the season and other key factors such as temperature and pH, is dependent upon the species of phytoplankton present within the reservoir at the time of analysis. High TN:TP ratios favour the non-N_2-fixing organisms but low TN:TP ratios favour the N_2-fixing taxa. If the organisms are present and all other factors (such as temperature and pH) are favourable for growth, the taxa with the most suitable ecological traits to those specific conditions shall out-compete those lacking those traits.

1.15 Eutrophication and the impacts of increased nutrient supply

Global warming and eutrophication influence nutrient cycling within reservoirs (Zhang *et al.*, 2020). Therefore, controlling the input of P and N may be an effective method for the inhibition eutrophication (Wen *et al.*, 2020). Both P and N can be a source of eutrophication (Yogev *et al*., 2020). The amount of P and N within reservoirs will increase as a consequence of eutrophication (Van der Zee, 1988),

climate change (Dorado *et al.*, 2015), and the excessive use of nitrogen in industries such as agriculture are excelling the rate of eutrophication globally (Eiler *et al.*, 2004). Rising temperatures accompanied by an increased rainfall frequency may increase the volume of nutrient loss from agricultural land through run-off during heavy rainfall events, increasing the rate and extent of eutrophication within reservoirs (Bloomfield *et al*., 2006).

Climate change is already affecting biodiversity within the UK (Beale *et al.*, 2006). Anthropogenic activities within or near aquatic ecosystems contribute to eutrophication events (Dalu *et al.*, 2018). Eutrophication is favoured by cyanobacteria and algae, where the excessive levels of nutrients are deemed favourable for growth (Carey *et al.,* 2012).

Conditions where cyanobacteria become established within a reservoir as a consequence of eutrophication pose a significant threat to the quality of the water (Paerl *et al*., 2009).
Eutrophication and algal or cyanobacterial blooms in surface water are common within the UK and have been linked to an increase in nutrient loading (Chen *et al.,* 2018). The projected environmental forecasts suggest that potentially harmful algal and cyanobacterial species may proliferate as a consequence of climate change (Dalu *et al.*, 2018). Cyanobacteria are responsible for environmental problems associated with eutrophication and are at an evolutionary advantage during such conditions, thriving and growing at an accelerated rate, leading to sporadic dominance within a reservoir (Dalu *et al.*, 2018).
Cyanobacteria are likely to increase in most freshwater habitats in the future (Carey *et al.*, 2012), and are among the most visible indicators of eutrophication (Carvalho *et al.*, 2011).
Changes in the quality of water after eutrophication make the treatment of drinking water more difficult (Cheng *et al.*, 2003), due to the inability to completely remove taste and odour compounds such as geosmin. However, changes cannot be accurately predicted for regional climate changes (Gillett, 2005). The quality of the water is considered an indication of the suitability of the water for human consumption (Bartram *et al*., 1996), therefore; good quality must be maintained.

1.16 Climate change and impacts on reservoirs

Global climate change is expected to influence the frequency and intensity of extreme weather events, such as excessive precipitation and drought, the degree to which will be region-specific (Cann *et al*., 2013). A decrease in winter rainfall frequency and volume in southern Europe is anticipated, with an increased winter rainfall further north can be expected (Black *et al.,* 2010). Observations carried out by the Met Office (2011), showed an increase in air temperature over the UK since 1960, with the temperature rises predicted to be higher during the summer (mean >0.28°C) than in the winter (mean>0.23°C) (Brohan *et al.* 2006). The most considerable temperature changes are likely to be seen in the south of the UK (Heaviside *et al*., 2011). Higher temperatures result in a greater abundance of cyanobacteria in communities and are most evident in communities adapted to cooler temperatures, suggesting that relative temperature changes may be more significant than absolute ones (Schabhuttl *et al.,* 2013).

Annual variations are typical of rainfall volume and frequency over the UK, with no overall annual trend over England and Wales since records began in 1766 (Jenkins *et al.* 2008, Heaviside *et al.,* 2011; Alexander *et al.,* 2001). However, during extreme weather conditions, the southern UK has seen a significant increase in rainfall over the winter period, accompanied by a decrease in rainfall over the summer period (Mauraun *et al.* 2008).

Rainfall is a significant factor in the determination of the inhabitants of an ecosystem (Thornes, 2011), due to its effect upon the nutrient dynamics within the reservoir. Higher volumes and frequencies of rainfall are anticipated to increase the nutrient loading of P and N from agricultural land to the reservoirs (Jeppesen *et al.*, 2009). An increase in ammonium (NH_4^+) and dissolved reactive phosphate (DRP) accompanied by a decrease in chlorophyll-a (Chl-a) is likely during periods of high inflow from surrounding land into a reservoir (Chen *et al.*, 2018). Nitrate is expected to be diluted at first with increasing discharge before its concentration increases (Chen *et al*., 2018). Rainfall patterns and evapotranspiration are predictors of the selection across plant and animal populations throughout a reservoir (Siepielski *et al.*, 2017), each of which plays a vital role in the interaction with all other aspects of a reservoir ecosystem. Phytoplankton biomass and community composition respond to changes in nutrient loading (Dorado *et al*., 2015), therefore, variables associated with freshwater inflow are significant influences on phytoplankton dynamics (Dorado *et al.*, 2015). Changes to environmental conditions could lead to alterations in algal and cyanobacterial communities through directly affecting water chemistry. The nutritional load of a reservoir is significantly influenced by inflow following periods of heavy precipitation (Mauraun *et al.* 2008). The risk of flooding increases when rain continues to fall upon already saturated grounds. This may contribute towards the total P and N entering a water body within the UK through increased run-off from the ground, altering the nutrient dynamics within a reservoir (Cann *et al*., 2013). Flooding on saturated soil has the potential to remove P and N from the soil, carrying it into the reservoir through run-off (Hafeez *et al.*, 2019).

Persaud (2015), suggested that specific knowledge of the reservoir in question is required before reliable predictions can be made. Persaud (2015), determined that the predominant indicators and main factors determining a bloom of cyanobacteria are the water column stability, hypolimnetic TP concentration and 7-day mean wind speed (Persaud, 2015).

Research carried out by Ahn (2011), concluded that cyanobacterial blooms were highly associated with the environmental conditions three weeks before the bloom occurring. Ahn

also determined that the temperature and TON were the most significant determining factors as to whether blooms occur, with water temperature being the key factor.

1.17 Changes in nutrient supply

Climate change is increasing the worlds freshwater temperature by an average of 0.34°C/decade (0.61°F) (NASA, 2015). Water temperature significantly influences the nutrients within a reservoir, where the community structure of a given reservoir can be altered with organisms favouring the new warmer conditions, replacing the organisms that have been native to the area for centuries under colder conditions *(*Jiang *et al.,* 2014).

A rise in mean temperature can influence the metabolic pathways of organisms inhabiting the environment potentially altering the metabolic by-product (Jeppesen *et al.*, 2009). Geosmin, produced by some strains of cyanobacteria and terrestrial microorganisms (e.g., *Streptomyces*) under varying environmental conditions is detrimental to water quality due to the unfavourable earthy taste related to the compound. However, at 20°C, increasing light intensity suppresses Chl-a synthesis but raises geosmin synthesis, with the reverse occurring when the water temperature is increased to 25°C (Saadoun *et al.*, 2001).

Organism population is both directly and indirectly affected by water temperature (Rasconi *et al.,* 2015). The solubility of water during periods of warmer conditions decrease, reducing the volume of gas retained within the reservoir compared with that retained at colder water temperatures (Jeppesen *et al.,* 2009). Increased water temperature raises the energy of the oxygen molecules, leading to a loss of oxygen molecules from the water, reducing the volume of dissolved oxygen (DO) (Mauraun *et al.* 2008). Raised water temperatures also increase the rate of biological and chemical reactions, increasing the rate of by-product accumulation which indirectly increases the cycling of nutrients required for a raised metabolic rate (Jeppesen *et al.*, 2009). Consequently, a higher volume of sediment-bound nutrients may be released under a shorter timescale as a consequence of alterations to the aquatic environment such as to pH and DO, instigating and driving the establishment of cyanobacterial populations. The extent to which native species remain at a specific site is determined by their adaptation response to changes along with their ability to cohabit with recently invading non-native species favouring the altered conditions. Internal P-loading can also be a consequence of increased evapotranspiration and reduced inflow, such as that recorded during a summer period in the UK (Jeppesen *et al.*, 2009).

Studies by Bukaveckas and Crain (2002), concluded that the highest concentration of chlorophyll-a occurred in late summer (between July and October) in contrast with that during early summer (April-May). It was also noted that a transitional period occurred during mid-summer (June) resulting in a uniform concentration of chlorophyll throughout the lake. Lower flows, resulted in a high proportion of primary production closer to the inflow whereas the sites further from the inflow recorded higher primary productivity rates during periods of increased inflow (Bukaveckas *et al*., 2002).

1.18 Changes in phytoplankton and bottom community

The dynamics of cyanobacterial abundance within a reservoir are influenced by seasonal conditions. The seasonal pattern of phytoplankton is repeated on an annual basis. The Plankton Ecology Group (PEG) model emphasised the influence of grazing and nutrient upon phytoplankton communities but has since been expanded to include the influence of the microbial food web, food quality, parasitism and overwintering of key organisms and their effect upon the phytoplankton diversity and abundance (Sommer *et al.,* 2012). In addition to a response in bacterial abundance throughout the seasons to nutrient availability and environmental conditions, species abundance is also dynamic (Anneville *et al.,* 2002). This is influenced by ecophysiological traits which are influenced by geographical locations and the environment, with some traits benefiting some species during differing seasons (Wentzky *et al.,* 2020). All organisms within a reservoir are influenced by temperature and nutrient availability, the degree to which is dependent upon their physiological traits. However, the overarching influence of temperature and nutrients can be summarised to reflect the seasonal influence upon cyanobacterial and benthic communities.

The availability of organic carbon to benthic microbes during the spring period may instigate and fuel the establishment of cyanobacteria as a consequence of redox-mediated release of phosphorous from within the sediment under anoxic conditions induced by increased benthic metabolism and respiration (Eiler *et al.*, 2004). It is anticipated that warmer temperatures during the summer period fuel microbial metabolism (Jiang *et al.,* 2014) with a resulting increase in the cyanobacetrial and phytoplanktonic abundance during the mid to late summer. The growth rate of the phytoplankton and benthic communities eventually equal the rate of senescence, temporarily maintaining the abundance of cyanobacteria and

phytoplankton. However, stratification combined with the increased rate of grazing and nutrient assimilation typically leads to nutrient limitation during the late summer period, resulting in the rate of senescence overtaking that of growth.

Decreasing temperatures during early autumn reduces the rate of metabolism of the phytoplankton and benthic microbial communities, slowing the rate of nutrient release from the sediment. However, the break down of stratification (turnover) as a consequence of reduced surface water temperature results in the release of nutrients trapped within the benthic zone during the summer period as a consequence of stratification. The pulse of nutrients may lead to a second bloom (autmn bloom) of cyanobacetria. However, the colder temperatures and dfecreased length of daily sunlight suppress the metabolic activities of benthic and surface organisms, resulting in the death of phytoplankton and cyanobacteria. The cells sink to the sediment where the supply of organic carbon and phosphorous from the senesced cells shall instigate and fuel benthic microbial activity the following spring.

1.19 Implications of draw-down and re-fill

As a consequence of legal changes to the abstraction permit from the river Usk, the pumping regime at Llandegfedd is sporadic and infrequent throughout the summer period. High volumes of water are expected to enter the reservoir throughout the winter at increased and regular frequencies compared with that of the summer. Consequently, the reservoir water level is expected to experience significant annual draw-down events where the water level may decrease by up to 75% of its maximum volume (DCWW, 2016). The changes to inflow rates and frequencies are likely to result in a change in species composition (Prowse *et al.,* 1958; Talling 1980) and the sestonic biochemical composition (lipids, proteins and carbohydrates) will also likely be affected by changes to the abstraction regime (Boechat *et al.*, 2000).

Sediment exposure as a consequence of declining water levels within the reservoir alters properties of the sediment (Skinner *et al*., 2014). The fluctuating water level is expected to significantly affect internal phosphorus loading dynamics by inducing alterations to redox conditions of sediments and the aquatic pH (Aldous *et al.,* 2005; Baldwin, 1996; Baldwin *et al.*, 2000; Darke *et al.,* 1996; Lijklema, 1980; Sah *et al.,* 1989), and the microbial communities

and activity (Batzer *et al.*, 2006). Desiccation of the sediment alters its redox status and may result in a lowered P affinity (Watts, 2000). Changes in both redox potential (Eh) and pH are site-specific and can increase the rate of desorption and the bacterial process (Eggleton *et al.* 2004), thereby increasing internal P loading. An experiment by Baldwin (1996), revealed that the soluble reactive P concentrations were higher in periodically dried sediments compared to that of permanently submerged sediments as a consequence of the exposure and drying process (Baldwin, 1996).

A study by Dabrowski (2017), determined that organic-N release was lower from sediment that was constantly inundated (non-drought) relative to those experiencing a dry-wet cycle (Dabrowski *et al*. 2017). The dried sediments released a higher concentration of organic-N relative to the inundated sediments, with ammonium increasing over a period of 7-11 days. Nitrite and nitrate concentrations were initially very low but increased as NH_4^+ began to decrease (Dabrowski *et al.,* 2017).

The process of mineralisation of organic-N supplies the sediment with the highest NH_4^+ concentrations during saturated conditions. However, the cyclical desiccation of peripheral sediment of a reservoir during draw-down events could lead to inhibition of the mineralisation process, Mineralisation may also be positively related to sediment drying (Reddy *et al.*, 1975; De Groot *et al.*, 1993; Venterink *et al*., 2002; Olfs *et al*., 2004).

Bacterial activity decreases linearly with the decreasing water content of sediment (Orchard *et al.,* 1992; West *et al.,* 1992), with the drying process killing obligate anaerobic bacteria (e.g., iron and sulphur reducing bacteria) (Baldwin *et al.*, 2000; Lynch *et al.*, 1988). The death of microbes on or within the sediment results in the release of large pulses of N and P during a drying event as a consequence of microbial lysis (Qiu, 1994), with the absence of obligate anaerobic microbes resulting in the inhibition of ferric hydroxides and sulphate reduction, thereby retaining phosphate adsorbed onto ferric hydroxides. Turner, (2001), documented that bacterial lysis as a consequence of sediment desiccation released maximal phosphorus within the first 3 days of re-wetting (Turner *et al.,* 2001). Rapid environmental changes caused by short sediment drying and re-wetting cycles induce stress in microbes, resulting in death and eventually cellular lysis if the water content of the sediment falls below 10% during the drying phase (Schönbrunner *et al.,* 2012).

Draw-downs desiccate and crack exposed peripheral sediment (Cavanaugh *et al.,* 2006). Lysis

of desiccated microbial colonies with dried sediments result in the release of metabolic constituents and significantly contribute to internal P-loading concentrations (colony-size dependent) upon inundation (Mitchell *et al.*, 1998), with up to 75% of the original colony dying as a consequence of desiccation (Qiu *et al.,* 1994).

The concentrations of carbon, nitrogen and phosphate in the outer layer of the sediment can decrease 5-fold following draw-down (Skinner *et al*. 2014), accompanied by a shift from inorganic-P (before desiccation) to organic-P (following desiccation) (Skinner *et al*. 2014).
Ferrous sulphides within the sediment are oxidised to amorphous ferric (oxy)hydroxides during the drying process, with an increased surface area for P-binding and a very high affinity for phosphorus (Aldous *et al.,* 2005; Golterman, 2004). A higher degree of crystallinity of ferric (oxy)hydroxides occur as a consequence of periods of prolonged drought conditions, resulting in a decrease in binding sites for phosphorus (Baldwin, 1996; Lijklema, 1980, Schönbrunner 2012). Exposure of sediment for extended periods alters sediment composition and nutrient release rates (James *et al*. 2001).
The predicted increase in rainfall during the winter months coupled with an increase in abstraction volume is likely to result in augmented reservoir levels relative to that during the summer months, resulting in re-immersion of the previously exposed banks. Increased run-off is likely to wash nutrients stored within the exposed banks into the reservoir, potentially leading to a substantial release of phosphate to the reservoir during the inundation process (Sinke, 1992). The duration of sediment exposure directly affects the magnitude of internal phosphorus loading during re-wetting, with a higher concentration of P released to the water following more prolonged periods of sediment exposure (Suurnakki, 2015), and a significant change to concentrations of TP, Fe^{3+}, NH_4^+, NO_3^-, and NO_2^- (Suurnakki *et al*., 2015) with a significant correlation between NH_4^+ and Fe^{3+}.
Peripheral sediment disturbance during the inundation process leads to an increase in pore-water ammonium-nitrogen ($N\text{-}NH_4^+$) and soluble reactive phosphorus (SRP) release from sediments (James *et al*. 2001), altering the TN:TP ratio, changing the phytoplankton communities (Lake, 2011).

1.20 Implications of rainfall changes and pulse weather events

Climate change is predicted to raise average temperatures and alter rainfall patterns across the UK (Reichwaldt & Ghadouani, 2012). The levels of NO_3^- and NH_4^+ are anticipated to increase within reservoirs during periods of heavy rainfall as a consequence of entrapment of gaseous nitrate within the atmosphere by the rain (Jeppesen *et al.*, 2009). In addition to the TN:TP ratio, the ratio of NO_3^-: NH_4^+ (on a molar basis) also contributes to the determination of thriving phytoplankton communities and by-product generation (Riegman *et al.* 1992). High-volume inflows following heavy rainfall events have the potential to disturb established stratification, raising the levels of dissolved oxygen (DO) at the bottom of the reservoir, leading to the inhibition of further release of nutrients (Li *et al*., 2015). The restriction to nutrient release rates and quantities may result in a rapid reduction of cyanobacterial and algal biomass within the reservoir. Large storm events with an increased rainfall volume exert a long-term negative effect on cyanobacterial blooms due to increased turbulence within the water (Reichwaldt *et al.,* 2012).

The consequences of heavy rainfall following a period of drought is dependent upon the season during which the weather event occurs. Heavy rainfall during a period of drought during May is likely to instigate and fuel cyanobacterial development due to high nutrient input, at a time of increasing water temperatures, rising benthic microbial activity and leading to the early formation of an anoxic zone (Li *et al*., 2015), further fuelling cyanobacterial establishment through an increased rate of internal P-loading. However, heavy rainfall during a drought in late summer (August) can temporarily disrupt cyanobacterial blooms through increasing turbidity and introducing an influx of nitrate via inflows, temporarily restricting sediment P release. Anoxic conditions may not return to the benthic zone for several days following a summer heavy rainfall event (Li *et al.,* 2015). A period of heavy precipitation towards the end of summer (September) may disrupt the formation of cyanobacterial blooms while mixing water columns (Li *et al.,* 2015). Non-toxic strains of cyanobacteria favour low light conditions, and an increase in inorganic nutrient inflow encourages the dominance of toxic strains in cyanobacterial blooms (Ma *et al.,* 2014). In contrast, smaller rain events occurring at a regular frequency may be favourable to cyanobacteria establishment during spring/summer periods, through supplying nutrients in quantities that can be rapidly exhausted (Paul, 2008), especially if stratification remains unchanged.

Cyanobacterial toxin concentrations in reservoirs are anticipated to increase as a consequence of changes to rainfall patterns (Reichwaldt *et al.*, 2012), which will provide more favourable growth conditions for cyanobacteria.

Changes to nutrient dynamics, cyanobacterial species composition and cyanobacterial strain succession as a consequence of rainfall pattern changes are site-specific (Lehman *et al.,* 2017). Therefore, site-specific data are required to assess and mitigate the significant threat cyanobacterial blooms may pose to water quality within reservoirs.

1.21. Llandegfedd reservoir

Llandegfedd reservoir is located in south east Wales (Figure 1.21.1) and is supplied phosphorous and nitrogen through various anthropogenic and advective means including industrial (nutrients from farming and golf course via inflows, atmospheric fall-out), recreation (maintenance of recreational grounds, boating activities), and river transfer (during abstraction).

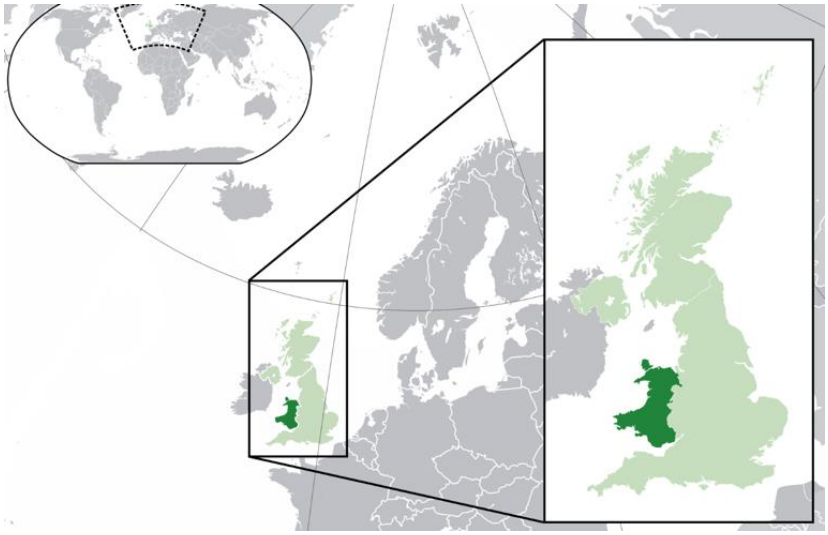

Figure 1.21.1. Llandegfedd reservoir is located in south east Wales (highlighted dark green).

An uninterrupted supply of potable water from Llandegfedd reservoir to the south-east of Wales is paramount due to the absence of an alternative source. Therefore, it is imperative that efficient water quality monitoring of Llandegfedd reservoir is established and maintained. Llandegfedd reservoir is a large (434 acres) impounding reservoir, situated in the lowlands and is a heavily modified man-made store of raw water for the supply of the majority

of south-east Wales (Figure 1.21.2). It is surrounded by agricultural land with the exception of a golf course at its north eastern point.

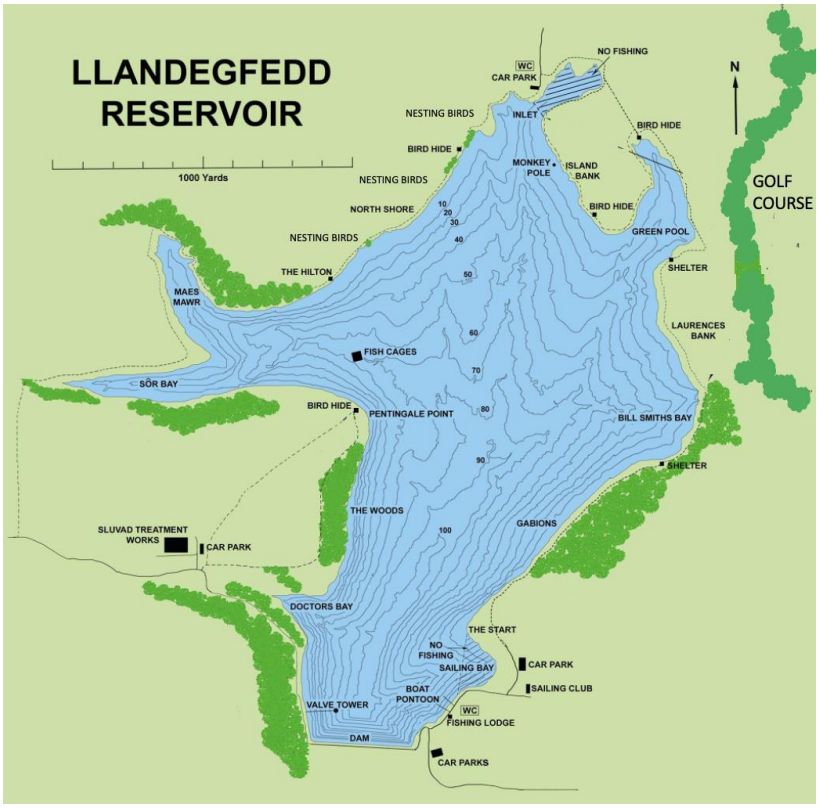

Figure 1.21.2. Llandegfedd reservoir with water depths, migratory bird nesting area and surrounding amenities highlighted (Andrew Roynon).

The reservoir depth at the inflow is relatively shallow (4m at point 4 (20ft from the northern bank when the reservoir is at maximum volume)) but increases upon progression towards the dam at its most southerly point (up to 28m at the centre (sampling point 2), and 26m at point 1 (parallel to the water tower) and 22m at sampling point 3). Summer stratification occurs annually in the southern section of the reservoir where the water is deepest, whereas regular mixing occurs in the northern section, which frequently disturbs the water during periods of active pumping.

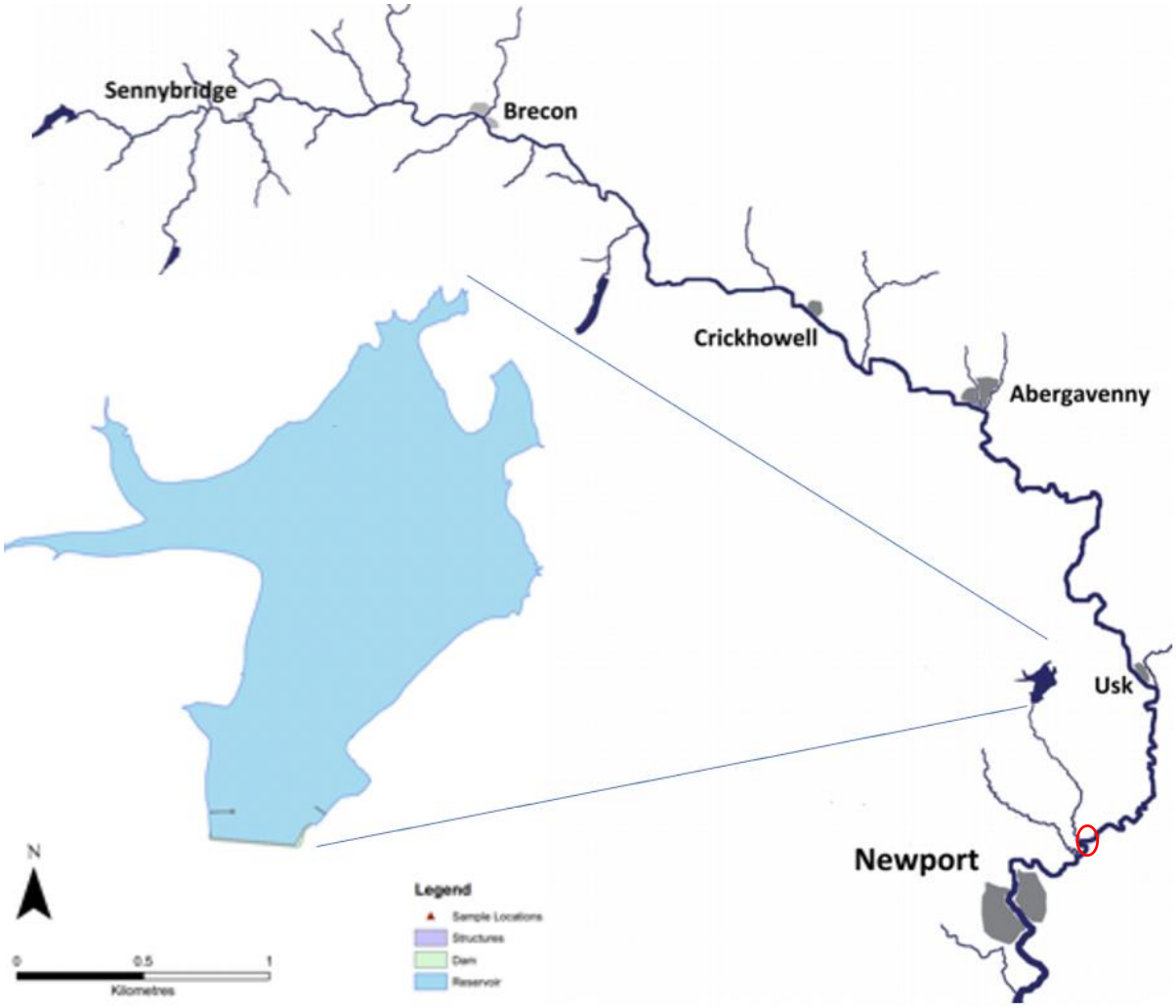

Figure 1.21.3. The River Usk and its tributaries contributing towards the water abstracted for transfer to Llandegfedd reservoir. The river abstraction point is highlighted by the red circle.

The water supplying the reservoir is actively pumped from the river Usk through incorporating the use of pumps at Prioress Mill Pumping Station situated at the rivers' side. Raw water enters the Prioress Mill Pumping Station, which was licenced to abstract up to 318Ml/day (before changes to abstraction law during January 2019), via two screens from where debris is frequently removed. The flow continues into two sumps where another screen removes any remaining smaller debris from the water. The raw water continues into two wet wells, each of which supplies five pumps that are used to pump the water through two 48" mains to Llandegfedd Reservoir.The pumps are of fixed speed and remotely controlled at the Sluvad Water Treatment Works (WTW). The raw water travels along the length of the reservoir (from north to south) before reaching the draw-off/abstraction tower.

The water is removed from the reservoir via the draw-off/abstraction tower comprised of three-tiered syphons and a compensation flow, removing the water from the base of the dam into a stream flowing away from the reservoir. When in working order, each syphon is operated using compressed air to prevent the flow of water into a selected gate, and vacuum to start the flow.The raw water is gravimetrically transferred to the Sor Pumping Station via two 36" mains where it is then actively pumped to Sluvad WTW via 48" and 42" in mains.
The WTW treating the water from Llandegfedd Reservoir is capable of removing many impurities through the incorporation of various treatment stages throughout the process. The WTW processes are explicitly designed to treat water of a quality typical of the supplying reservoir. However, some impurities, such as the by-products released by some cyanobacteria (2-Methylisoborneol (MIB) and geosmin) during cyanobacterial growth and senescence are not easily removed from the water. Approximately 30% of the compounds detrimental to taste and odour (T & O) enter distribution. Consequently, the risk of receiving customer complaints increase, resulting in financial penalties to the WTW company and loss of trust by the customers. An additional treatment step is incorporated into the water treatment process following confirmation of geosmin or 2-MIB within the treated water.

1.22 Llandegfedd Reservoir location and characteristics

The inflow from the river Usk enters the Llandegfedd Reservoir at the northern bank and is the shallowest location of the reservoir, reaching a maximum depth of 4m approximately 20' from the bank (sampling point 4) during full capacity. Consequently, thorough mixing throughout the column is expected during periods of heavy precipitation, with mixing exacerbated during times of active abstraction and inflow into the reservoir.

The greatest depths are attained at sampling points 1 and 2 (26m and 28m respectively) at full capacity. The increased depth is likely to be accompanied by reduced water mixing throughout the columns, with thermal stratification during warmer seasons leading to a substantial decrease in dissolved oxygen (DO) concentrations, chlorophyll-a (Chl-a) and pH, while an increase in total nitrogen (TN), ammonium, total phosphorus (TP) and soluble reactive phosphorus (SRP) is anticipated with depth (Brunberg *et al.*, 1992) relative to sites at shallower depths.

Run-off water enters Llandegfedd reservoir at numerous points as dictated by topography and artificial drainage and not restricted to one dedicated source of entry.

1.23 The Catchment water quality.

The quality of water abstracted for the purposes of filling Llandegfedd Reservoir has been classified as 'moderate' to 'good' by the Natural Resources Wales (NRW) as a consequence of a combination of factors including agriculture and currently unknown causes (Figure 1.23.1).

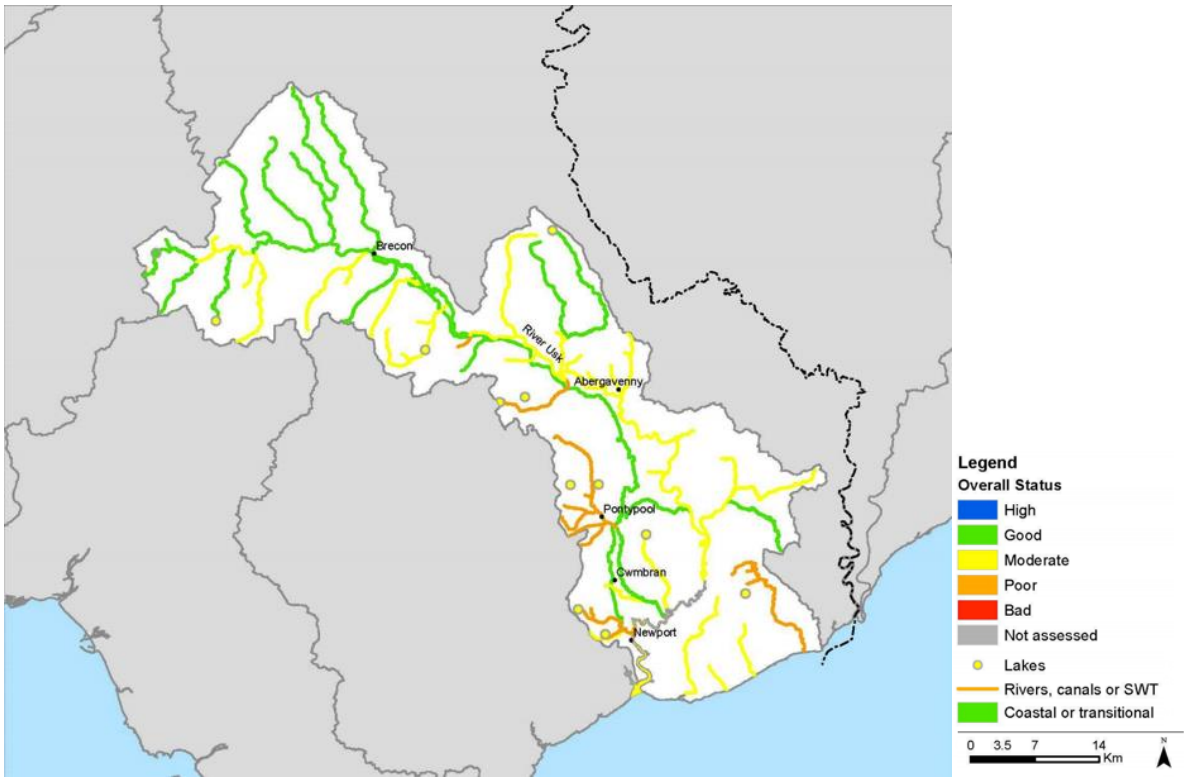

Figure 1.23.1. The water quality of the tributaries along sections of the river Usk (courtesy of the NRW, 2015).

Improved field drainage in receipt of fertiliser or those holding livestock increase the likelihood and quantity of nutrients entering reservoirs through run-off during a rainfall (Ye, 2009).Agricultural pollution is one of the major sources of aquatic pollution to the river Usk (Figure 1.23.2) and become evident in reservoirs when the phytoplanktonic response to the increased nutrient supply is rapid (Cooper, 1993).

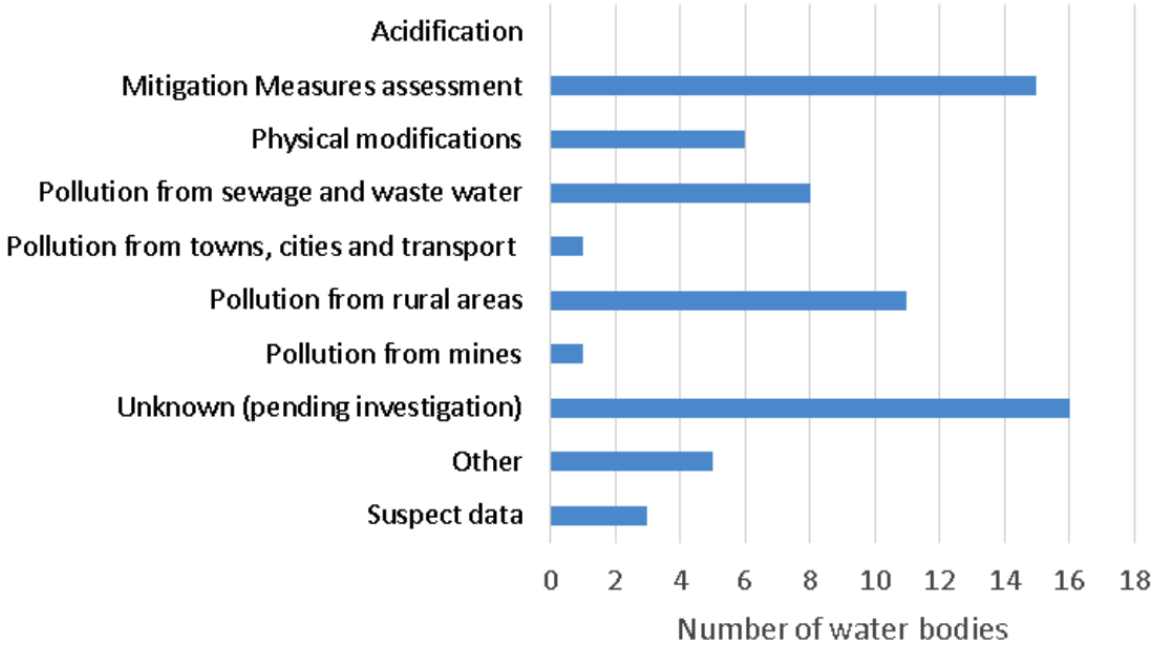

Figure 1.23.2. Reasons for not achieving allocated status' in the Usk Management (NRW, 2015).

1.24 Reservoir management and river abstraction law changes.

The abstraction depth at which the water is actively removed from the reservoir determines water quality data (Cooper, 1993). The abstraction tower at Llandegfedd Reservoir is comprised of three intake gates allowing selection of the depth at which the water is drawn. The depth selected for water removal (surface, bottom and interstitial) is adjusted to suit the climatic and water conditions, optimising the quality of the water entering the WTW, minimising water quality-enhancing treatment necessary to achieve suitable potable water. However, the ability to select the intake gate through which to abstract the water from within the reservoir has malfunctioned since the year 2000 (actual date unknown), resulting in an amalgamation of water from throughout the column entering the WTW. Therefore, the water quality data documented by DCWW from approximately the year 2000 represents that entering the WTW and not the representative water quality at specific depths at any point within the column.

Surface water nutritional load data may be diluted as a consequence of mixing with deeper water deficient in nutrients, resulting in inaccurate data modelling. Pressure increases with depth, resulting in a bias towards bottom water abstraction.

Llandegfedd Reservoir has undergone routine annual drawdowns for decades, however, following changes to the abstraction law, the water level is anticipated to reach lower levels

than previously recorded (<75% of maximum level for several months), with frequent changes to water levels expected to become an annual event (DCWW). The anticipated reduced rainfall during the warmer periods of the year is likely to coincide with the enforced reduced abstraction from the River Usk. The combined reduced precipitation and diminished abstraction from the river Usk may result in significantly lower levels of water within the Llandegfedd reservoir during the summer, potentially changing the characteristics of the reservoir.

The imposed restriction is anticipated to affect the dynamics of the reservoir through the reduced and infrequent input of freshwater, leading to a varied nutrient supply along with contrasting periods of nutrient abundance. Limitation posed upon summer-time abstraction from the River Usk when less rainfall is anticipated will likely result in a reduced nutrient inflow into the reservoir relative to that during the winter period, where rainfall frequency and volume is expected to be higher, and abstraction frequencies increased.

1.3 Thesis structure and hypotheses tested.

The thesis aims to identify limnological characteristics of Llandegfedd reservoir and determine where water quality deterioration is likely to occur under climate change predictions over a given period based on temperature and rainfall. The assessment of both historical and real-time (carried out during this study) water quality coupled with sediment data analysis was completed to determine potential characteristics of the reservoir that may increase the risk of water quality deterioration. This research will enhance knowledge concerning the nutrient dynamics within Llandegfedd Reservoir in association with amended reservoir management schemes in light of climate change.

1.3.1. Site map and sampling locations.

1.3.1.1. Historical data analysis - Chapter 2.

The data used in the historical water quality analysis were obtained at the abstraction tower at the southern point of the reservoir (Figure 1.3.1.1.1). The abstraction tower is capable of abstracting water at three levels from the reservoir, however, the ability to actively select the draw-off gate (top, centre or bottom) has been unavailable since approximately the year 2000. Therefore, all three gates were active following the year 2000.

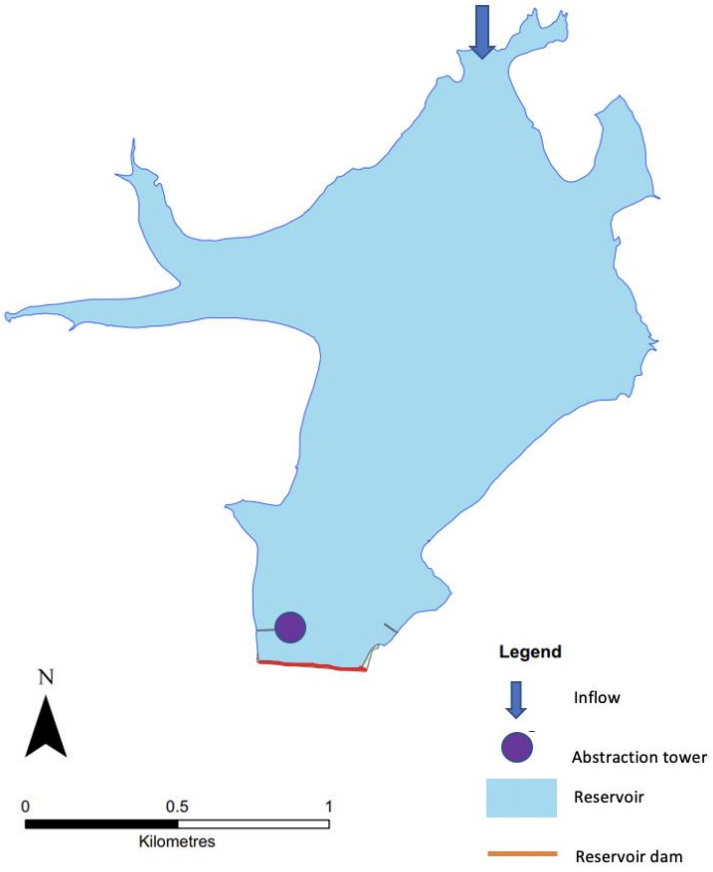

Figure 1.3.1.1.1. The location of the water quality analyser at the abstraction tower relative to the inflow at the northern point of the Llandegfedd Reservoir.

1.3.1.2. Real-time water quality analysis – Chapter 3.

Water sampling sites for the analysis of real-time data were distributed linearly from the southern to northern locations. Both the bottom and surface samples were obtained at each sampling site from site 1 to site 4 over a period of 11 months (Figure 1.3.1.2.1). The positions were maintained upon each sampling visit through employing a GPS to confirm accurate coordinates.

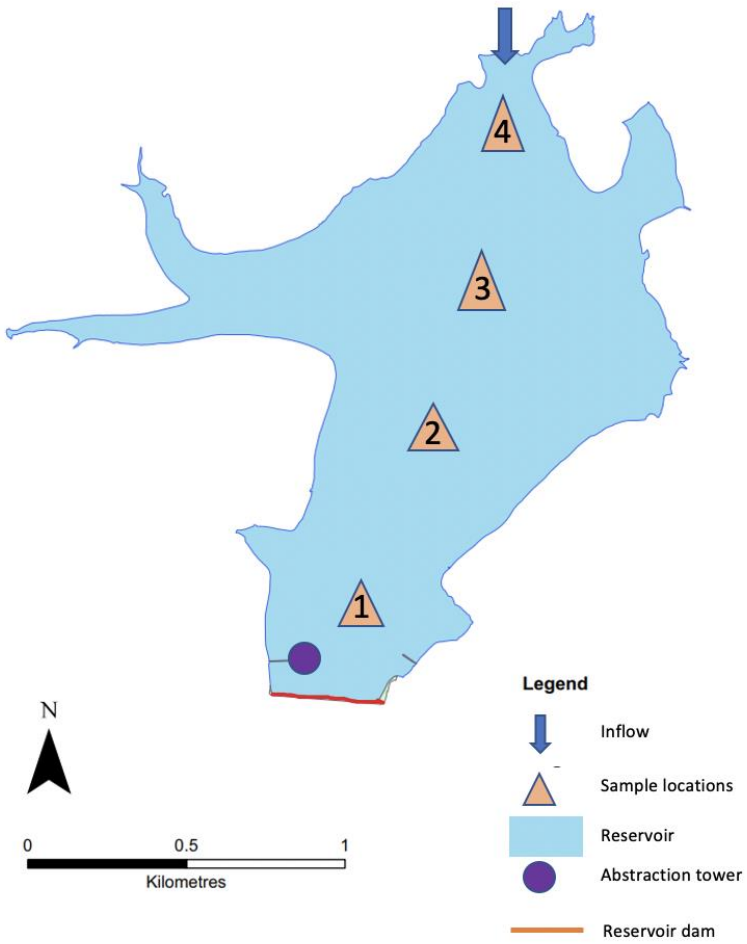

Figure 1.3.1.2.1. The water sampling locations along the transect of the Llandegfedd Reservoir.

Both sampling sites 1 and 2 were located in the southern section of the reservoir and were the sites within closest proximity to the abstraction tower. Sampling sites 3 and 4 were located within the northern section of the reservoir and were the closest in proximity to the point of river inflow at the north.

1.3.1.3. Determination of P content within several layers of sediment along the reservoir transect – Chapter 4.

Sediment cores were extracted from the reservoir at sampling points 1 through 4 as for the water sample collection for both real-time water quality analysis (Chapter 3) and the effect of rainfall upon nutrient dynamics (Chapter 5). The samples were collected During April 2016, July 2017, April 2018 and July 2018.

1.3.1.4. The effect of Extreme Weather Events upon nutrient dynamics within the reservoir – Chapter 5.

The water sampling locations used in the collection of surface and bottom samples during the time-series analysis were retained to help determine the effect of heavy rainfall and reactivation of pumping upon nutrient concentrations during a period of drought. Site 4 (the most northern site) was located within close proximity to a shallow bank constructed of predominantly loose sediment and was in contrast to that at site 1, which was surrounded by vertically assembled granite boulders.

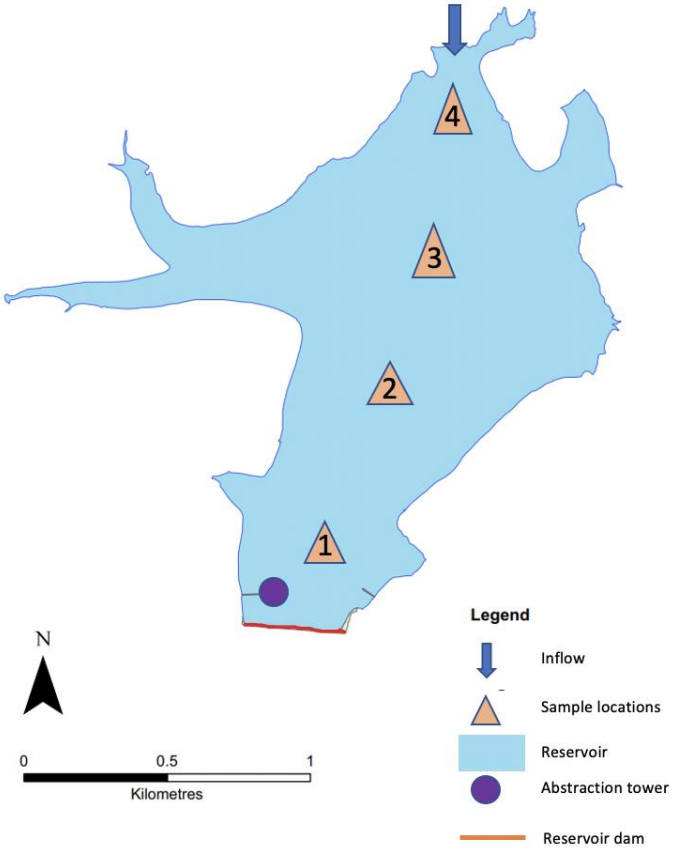

Figure 1.3.1.4.1. The water sampling locations along the transect of the Llandegfedd Reservoir.

1.4. Overarching hypotheses and sub-hypotheses investigated in this study

Throughout this study, several hypotheses shall be tested, each of which will contribute towards the understanding of the characteristics of Llandegfedd Reservoir. The aim of the thesis is to determine the resilience of Llandegfedd Reservoir to climate change and identify areas of the reservoir where direct and indirect consequences of climate change may be of a

higher risk to water quality under climatic changes. The following overarching hypotheses and sub-hypotheses are addressed under each chapter:

Chapter 2: The analysis of historical nutrient and environmental data. Overarching hypothesis: Evidence of historical climate change will not be clear through analysing the historical data due to inaccuracies within the data as a consequence of the change in abstraction method.

Sub-hypotheses:

1. Historical data will highlight the importance of establishing a suitable water sampling method in order to obtain reliable data representative of the water quality.
2. Data analysis will indicate that the reservoir level will significantly affect the concentrations of Total Phosphorous at the point of abstraction within the tower.
3. The analysis of historic rainfall data obtained over a period of a constant abstraction method will have a significant positive association with NH_4^+ and a significant negative association with NO_3^- levels.

Chapter 3: Time-series monthly nutrient and environmental analysis over an 11-month period. Overarching hypothesis: The northern sampling sites (sites 3 and 4) shall be of a higher risk to water quality as a consequence an increased volume of allochthonous P input than the southern sites (sites 1 and 2).

Sub-hypotheses:

4. Phosphorous concentrations shall be at their lowest during the winter period due to the absence or reduction in productivity and the redox effect upon internal loading.
5. There will be no significant association between P-fraction concentrations and the nutrients or environmental data.

Chapter 4: The determination of P content within the sediment. Overarching hypothesis: Sediments within a closer proximity to the pumped inflow (sampling site 4) will have greater TOC and hence enhanced benthic microbial activity.

Sub-hypotheses:

6. Labile-P concentrations will be lowest at the sediment surface and increase with sediment depth during the summer (due to a reduced redox potential).
7. Internal P loading will be greater during the summer relative to the spring period and shall be a significant source of phosphorous compared with external loading of phosphorous.

Chapter 5: Analysis of the effect of Extreme Weather Events upon nutrient dynamics within Llandegfedd reservoir. Overarching hypothesis: The nutrient content of the water within the reservoir will increase following the reactivation of pumping from the river Usk and increase further following the rainfall event.

Sub-hypotheses:

8. Nitrate will be the dominant N-fraction throughout the reservoir during the drought period, but an increase of ammonium concentrations shall be recorded following a period of heavy rainfall, particularly at site 4.
9. OP concentrations will increase as a consequence of both the active pumping and precipitation event specifically in the northern section (site 4) of the reservoir.
10. Cyanobacterial cell counts will increase in response to an inflow of nutrients.

Chapter 2: The analysis of historical nutrient and environmental data.

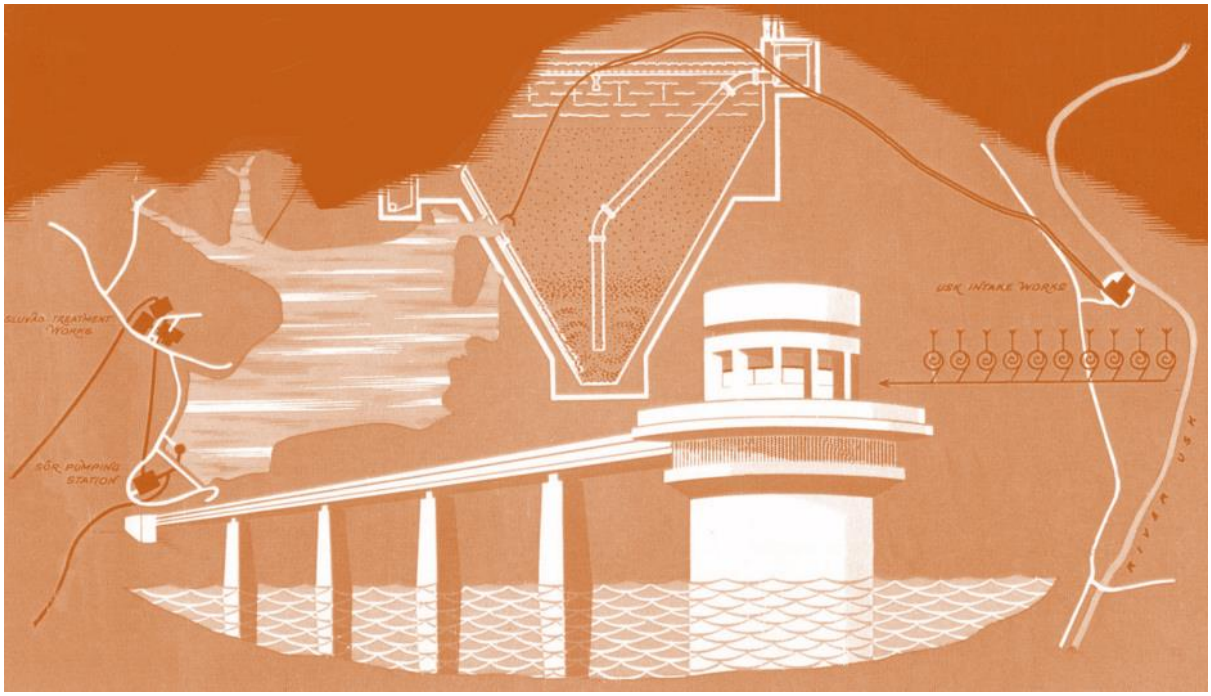

2.1. Introduction to historical data analysis – main summary of chapter

Historical water quality data of a reservoir can provide an understanding of the typical and atypical nutrient load and dynamics, hydrology and how anthropogenic influences may in turn determine the relationship between variables and factors. Historical data relating to conditions within Llandegfedd Reservoir over a 30-year period were analysed and discussed to determine whether significant associations existed between water quality parameters and meteorological variables. In addition, the consequence of the recent inability to select the abstraction gate at the abstraction tower upon the water quality data is analysed and discussed to help determine whether the modification to the abstraction process had any significant effect upon the data obtained from the water during the abstraction process.

The main findings:

- Changes to the raw water abstraction process caused by faulty mechanisms within the water tower significantly changed the quality of water abstracted from the reservoir as indicated by the data following the year 2000 relative to that before the process change.
- An increase in water temperature was not observed over the period represented by the data, indicating that climate change was not responsible for increasing water temperature nor significantly affecting the volume of rainfall during the summer nor winter between 1984 through 2016.
- Neither the water temperature nor pH data could not be relied upon as an indicator of climate change within Llandegfedd Reservoir with a malfunctioning abstraction tower.

2.1.1. The importance of historical data analysis when determining the effects of climate change upon water quality.

The analysis of historical water quality data can provide a valuable footing on which to construct an overview of water quality typically observed at Llandegfedd reservoir. Analysis of historical data can significantly contribute towards forecasting potential future water quality scenarios during a variety of meteorological (Arnell, 2006), and nutritional load conditions, using modelling techniques and the determination of associations between critical variables.

Numerous variables within a reservoir can be analysed as indicators of the effects of climate change; however, real-time data is a better indicator of water quality when the sampling and analysis is completed with a short turn-around time due to the ability of a reservoir to respond rapidly to changing conditions (Rosenzweig *et al*., 2007). The phytoplankton community structure is one of the most accurate indicators of reservoir water quality (Huisman *et al.,* 2004), with relation to real-time response to conditions of algal and cyanobacterial blooms, and response to changing environmental conditions over time (Huisman *et al.,* 2004, Johnk *et al*., 2008), water temperature (Hampton *et al.,* 2008), pH (Yan *et al*., 1996; Webster *et al*., 1996) and reservoir level (Johnk *et al.,* 2008; Rodionov 1994).

Due to the complexity of biological and chemical interactions within a reservoir ecosystem, numerous parameter measurements are required (Grant *et al.,* 1997), in order to understand the characteristics of a specific reservoir. Multivariate data analysis can highlight significant associations between water quality variables and cyanobacterial growth characteristics in drinking water reservoirs (Golshan *et al*., 2020).

The information obtained through analysis of data by sampling a reservoir is highly dependent upon the climate (Benn, 2009), and other variables including the geology and geography of the site and the fauna and flora inhabiting the reservoir (Kessel, 1977). Therefore, understanding how the factors independently and collectively influence the nutrients can improve understanding of the nutrient dynamics in real-time and better anticipate conditions within the reservoir as the conditions change.

Watershed models may be coupled with hydrodynamic models in reservoirs to improve understanding of the nutrient dynamics within a reservoir (Xu *et al*. 2007), which incorporate the complex web of interactions between biotic and abiotic nutrient dynamics (Debele *et al.* 2008). However, not all data are available retrospectively.

2.1.2. Water intake and its influence upon treated water.

A reservoir is a dynamic body of water where nutrients and water characteristics are continuously changing throughout the water column. Both natural and anthropogenic disturbances strongly influence the biodiversity and ecosystem (Huisman *et al.,* 2004) both directly and indirectly through climate change (Arnell, 2006). Dam operations significantly alter the hydrodynamics and solute transport processes within a reservoir (Carr *et al.,* 2020).

Water levels within a reservoir fluctuate in response to the inflow volume and frequency, precipitation volume and frequency, evapotranspiration and population demand. Therefore, the mode of its abstraction from the reservoir must be able to meet demand while simultaneously having a dynamic approach to minimise seasonal influences upon water quality and availability.

The Llandegfedd abstraction tower comprises three vertically aligned draw-off gates (Figure 2.1.3.1) (estimated to be at 8m, 16m and 24m deep in a total depth of 26m at sampling point 1 at full capacity) allowing draw-off regardless of water level and is located at the southern section of the reservoir. Optimum water quality is located at the surface of a reservoir (Spellman, 2000) except during periods of stratification and turn over. Abstraction towers allow water removal at the most suitable level within the water column to attain the highest quality of water throughout the seasons. However, repair and maintenance of the tower are complicated due to intakes not being readily accessible. The inability to select draw-off levels at any time during operation is of a distinct disadvantage to the water company (Spellman, 2000).

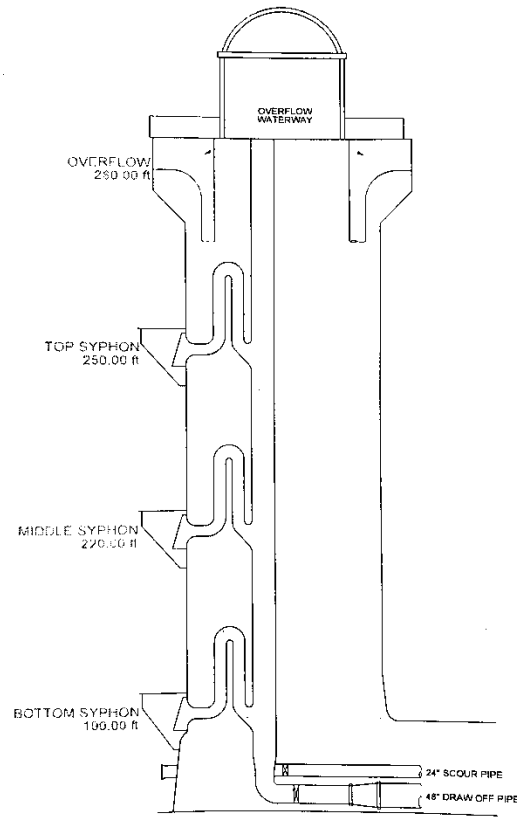

Figure 2.1.3.1. Llandegfedd reservoir valve tower (Dŵr Cymru Welsh Water).

The inability to deactivate selected syphons within the draw-off tower at Llandegfedd since between 1997 to 2000 (and continues to the present day, actual year of failure unknown) as a consequence of mechanical failure has led to the inability to select the depth from which to extract water for treatment at Sluvad WTW. The consequential continuous simultaneous syphoning of water drawn through the syphon at the top, middle and bottom gates of the reservoir result in the mixing of water from three depths of the water column. The mixed water flows through water quality analysers, generating data representing an amalgamation of the water column. This contrasts with the data obtained prior to 1997-2000 whereby water quality data represented water at individual gates within the water column at any one time. However, the selected gate was not recorded.

2.1.3. Abstraction method changes and its effect upon historical data analysis

To accurately determine reservoir water quality, the sampling method should be repeatable, and sampling location should be consistent to minimise data variability because of non-repeatable sampling processes (Chapman, 1992).

The sampling and water quality analysis location at Llandegfedd reservoir over the period of historical data collection remained unchanged. The analyser was positioned within the abstraction tower beyond the merging point of pipes from the three vertical gates

The suitability of the data recorded both pre-and-post convergence of the water levels during the year 2000 needs to be determined to optimise water quality data to reflect existing conditions within the reservoir.

Chapter 2: The analysis of historical nutrient and environmental data. Overarching hypothesis: Evidence of historical climate change will not be clear through analysing the historical data due to inaccuracies within the data as a consequence of the change in abstraction method.

Sub-hypotheses:

1. Historical data will highlight the importance of establishing a suitable water sampling method in order to obtain reliable data representative of the water quality.

2. Data analysis will indicate that the reservoir level will significantly affect the concentrations of Total Phosphorous at the point of abstraction within the tower.
3. The analysis of historic rainfall data obtained over a period of a constant abstraction method will have a significant positive association with NH_4^+ and a significant negative association with NO_3^- levels.

2.2. Sampling methods and data analysis.

2.2.1. Dŵr Cymru Welsh Water quality sampling methods.

Water samples were collected from a designated sampling tap which is housed within a protective cover at the Sluvad water treatment works. This consisted of the Raw Programme of water sampling which were analysed for historical data analysis.

The samples were collected monthly unless the sampling frequency increased as a consequence of threshold failures, increasing the sampling frequency within the month. The sampling frequency returned to a monthly frequency upon attaining satisfactory results.

Water samples were analysed at DCWW laboratories for nutrients using the Thermo Scientific Aquakem 600. To prepare the ammonia/nitrite standard stocks, the specific concentration of solution (e.g., 1ml of ammonia as N 1000mg/L and 1ml of nitrite as N 1000mg/L) was pipetted into a flask containing RO water. The flasks were inverted several times and the solution is transferred to a 100ml plastic bottle. Ammonia, phosphate, TON and nitrate stocks were prepared before hand by the supplier. A serial dilution of stocks was prepared using the solution. All samples were recorded on the DCWW LIMS system. The samples and stocks were loaded into the respective instrument following the calibration guidelines issued by the manufacturers. Dŵr Cymru Welsh Water nutrient analysis methods are presented in Appendix 1 (A1).

2.2.2. Sampling frequency.

The period of data collection used in the analyses is variable-dependent. Before 2008, sampling was sporadic and critical data for key variables including total phosphorous (TP) was absent or sparse. A comparison of historical data for some of the critical variables shall be compared pre- and post-2000 to help determine the impact of the failure of the pumping system within the draw-off tower upon the data generated by the samples. Consequently, post-2000 data reflect the inability of DCWW to select the abstraction level resulting in all

three gates remaining active simultaneously, whereas data before the year 2000 represent data acquired with the ability of gate selection. However, no records are available as to which gate was selected at any given date. No cyanobacterial data was available post-2000.

Data provided by DCWW was organised into single monthly figures through determining the mean of multiple data points for each month where applicable. The frequency of multiple data points was dependent upon water quality parameter failures and was therefore inconsistently completed.

2.2.3. Data analyses performed within this chapter

All data used within the analysis are mean/month. Data availability varied over the sampling period (Table 2.2.3.1), where some variables were represented pre-2000 only, and others post-2000 only. Therefore, no pre-and post-water mixing comparisons have been completed in these instances.

Table 2.2.3.1. Key variables included within this chapter and the period of data availability for the specific variable.

Variable	Period of data availability and analysis	Type of analyses
pH	1984-2016	- Pre-and post-2000 data analyses - LM analysis
Water temperature (°C)	1984-2016	- Pre-and post-2000 data analyses - LM analysis
Rainfall (avg./mm/month/year)	1984-2016	- Pre-and post-2000 data analyses - LM analysis
Total Nitrogen (TN) (mg L^{-1})	1984-2016	- Pre-and post-2000 data analyses - LM analysis
Total Phosphorous (TP) (mg L^{-1})	1995-2001 & 2008-2016	- Pre-and post-2000 data analyses - LM analysis
Conductivity (µs)	1984-2016	- LM analysis
Cyanobacteria (cfu/ml)	1988-1999	- Pre-and post-2000 data analyses
Chlorophyll-a (cells/ml)	1995-2009	- Pre-and post-2000 data analyses - LM analysis
NH_4^+ (mg L^{-1})	1984-2016	- Pre-and post-2000 data analyses - LM analysis
NO_3^- (mg L^{-1})	1990-2016	- Pre-and post-2000 data analyses - LM analysis
NO_3^-: NH_4^+ (mol/ml)	1990-2016	- Pre-and post-2000 data analyses

		- LM analysis
NO_2^-: NH_4^+ (mol/ml)	1990-2016	- LM analysis
TN:TP (mol/ml)	1995-2001 & 2008-2016	- Pre-and post-2000 data analyses
		- LM analysis
Reservoir level (m)	1997-2016	- LM analysis
Geosmin (ng L^{-1})	2002-2010	- LM analysis
Catchment inflow (ML/day)	1985-2015	-LM analysis

2-MIB was recorded as absent from samples or reaching the LOD (0.57ngL^{-1}) at Llandegfedd reservoir between 1984 and 2016. 2-MIB has therefore been omitted from analyses due to inflated '0' data sets. LM/GLM analyses for the pH and water temperature were completed using data from three separate sampling periods (pH data: 1984-1999 and 2000-2016; water temperature data: 1984-1999, 1984-2016 and 2000-2016) to ascertain whether the alteration to the abstraction process significantly affected associations between variables. No LM/GLM analyses were completed for continual pH data from 1984-2016 due to the interruption to its annual cycle during 2000.

For data analyses throughout the chapter, the mean value for each parameter per month was determined for each variable accompanied by the standard deviation (SD). Due to small sample sizes ($n<25$) and not normally distributed data exhibiting ties, Kendall's Tau was used to test for associations between two continuous variables and Kruskal-Wallis test to determine significant differences between sets of not normally distributed data. Where data was not normally distributed, but sample size was large ($n>25$) Spearman's rank correlation was used.

Significant associations between variables were determined using General Linear Models (normally distributed data)/Generalised Linear Models (non-normally distributed data even following transformation methods)/Linear Models (where non-normal data were successfully transformed) were completed using R studio (version 3.4.4) following the selection of independent variables demonstrating correlation with the dependent variable as determined through Principal Components Analysis (PCA) analysis using PAST (version 4.03).

Data were standardised to allow cross-variable PCA. Variables were omitted from the PCA during periods of recorded repeated '0' values. The following equation was used for the

standardisation to allow for direct data pattern comparisons between variables of differing scales:

$$(X-\mu)/\sigma$$

where X is the observation, μ is the mean and σ is the standard deviation.

Once the list of correlated variables had been determined for each dependent variable, the Shapiro-Wilks test was used to determine normality of data. Data were transformed by log, cube, square-root or Tukey's Ladder of Power where not normally distributed distributions were confirmed. Tukey's Ladder of Power selects the transformation method which maximises the Shapiro-Wilks W statistic or minimizes the Anderson-Darling A statistic, thereby producing a dataset closer to a normal distribution (Mangiafico, 2016).

The most suitable transformation method was determined through analysis of histograms and their proximity to a normal distribution using Shapiro-Wilks. Where the most efficient method of data transformation involved Tukey's ladder of power, the selected transformation mode was not indicated. Tukey's ladder of power reduces the effects of homoscedastic data leading to more accurate analysis. The Akaike Information Criterion (AIC) was used to estimate the fit of each model, with the lowest AIC value used to confirm the selection of data transformation links and models (Bozdogan, 1987; Cavanaugh, 2019).

Variables were eliminated from the model as determined by the F-test. Following removal of all unnecessary independent variables, the goodness of fit of the remaining model was tested using diagnostic plots for linear regression analysis to determine whether residuals had a non-linear pattern (Residuals vs Fitted graph), were of a normal distribution (Normal Q-Q graph), heteroscedasticity (scale location graph) and influential outliers (Residual vs Leverage plots (Cook's distance)). Following completion of the model, the data were reported using the intercept result and P value, adjusted R^2 ($^R^2$), F-test for overall model significance (Mangiafico, 2016), and model P value. Any anomalies from the diagnostic plots were reported for the final model. Furthermore, the positive/negative association of the individual parameter associations within the model with the dependent variable were reported using LM mean difference ± SE.

The key variables providing sufficient data for analysis and of prime interest within this chapter are temperature, pH, rainfall, TP, nitrate, ammonium, TN:TP (mol/ml) ratio, geosmin, chlorophyll-a, catchment inflow data and cyanobacteria.

The data are presented as a comparison of pre-2000 with post-2000 data to determine whether the tower failure significantly affected the water samples due to water mixing.

Additionally, the records for the number of cyanobacterial cells were analysed for their association with key variables at the reservoir between 1989 and 1999. Due to the distributional form of the data, along with its scale variance, Kendall's Tau was used to determine the degree of rank correlation with variables collected in real time with that of the cyanobacterial samples, and with cyanobacterial cell data which has been displaced by a month to determine whether a better association existed between real-time factors or those existing several weeks previous (displaced analysis) as per Ahn (2011). This was repeated using geosmin data as the dependent variable (data range 2008-2012).

2.3. Results.

2.3.1. Nutrient data analysis

2.3.1.1. Total Phosphorus, TP (mg L^{-1}) (1995-1999~2008-2012).

No significant difference was found between TP concentration during the summer periods or winter periods prior to and following 2000, nor winter periods pre-and post-2000 (P>0.05) (Figure 2.3.1.1.1).

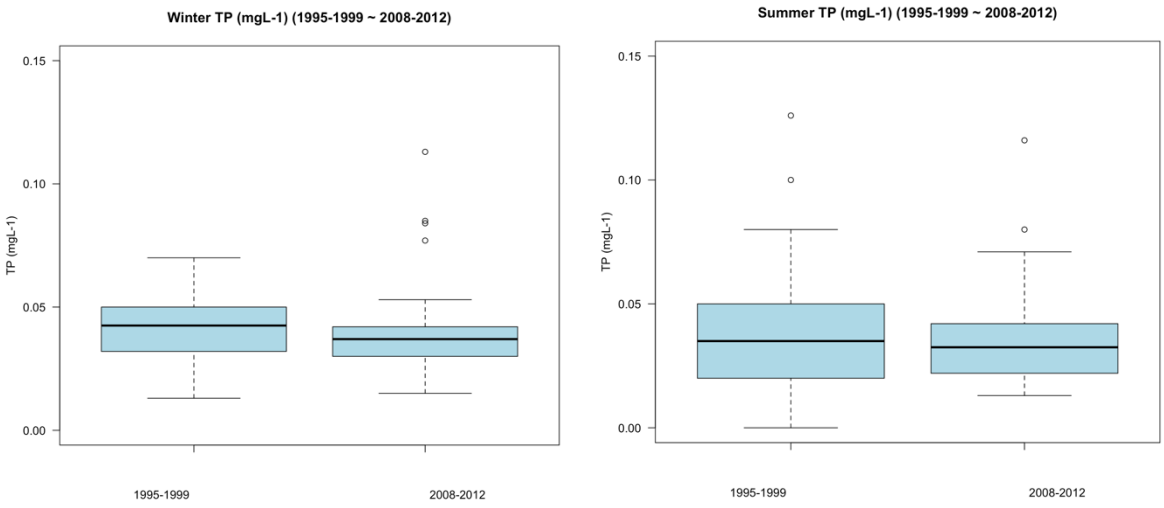

Figure 2.3.1.1.1. TP (mg L^{-1}) data during winter (left) and summer (right) periods pre-and post-2000 (median of data illustrated).

Similarly, no significant difference was determined between the mean monthly TP concentrations (mgL^{-1}) from 1995-1999 and 2008-2012 (P>0.05) (Figure 2.3.1.1.2).

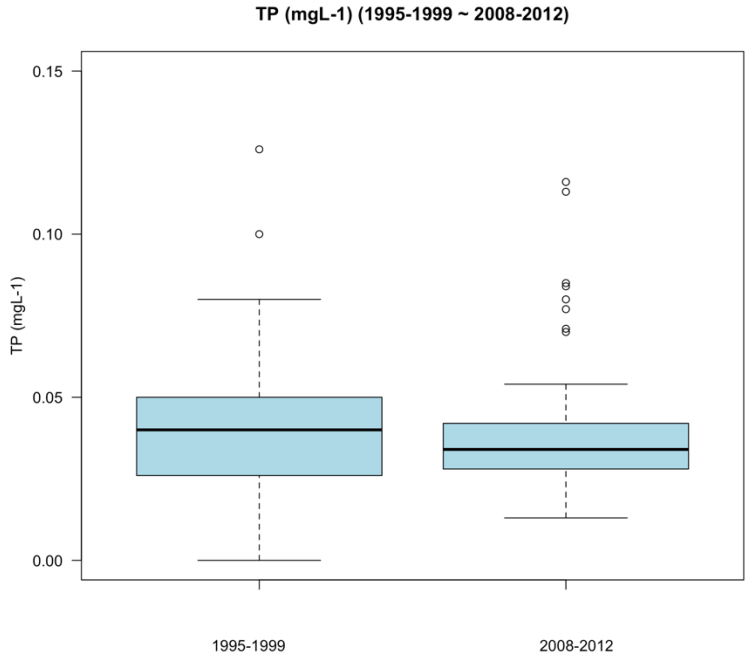

Figure 2.3.1.1.2. Mean monthly TP concentrations (mgL^{-1}) from 1995-1999 (left) and 2008-2012 (right) (median of data illustrated).

However, the average annual concentration of TP within the water samples decreased significantly (Wilcoxon signed rank test P<0.01) between 2008 ($0.053mgL^{-1}$ ± 0.028) and 2012 ($0.03mgL^{-1}$ ± 0.008) (P<0.05) with a combined average over the 5-year period of $0.039mgL^{-1}$ (± 0.022) whereas the average annual TP concentrations remained varied within the river ($0.068mgL^{-1}$ ± 0.059) (Figure 2.3.1.1.3).

No significant difference was determined between the average annual concentration of TP (mgL^{-1}) within the Usk river at the abstraction point and the concentration of TP within the reservoir between 2008-2012 (P>0.05).

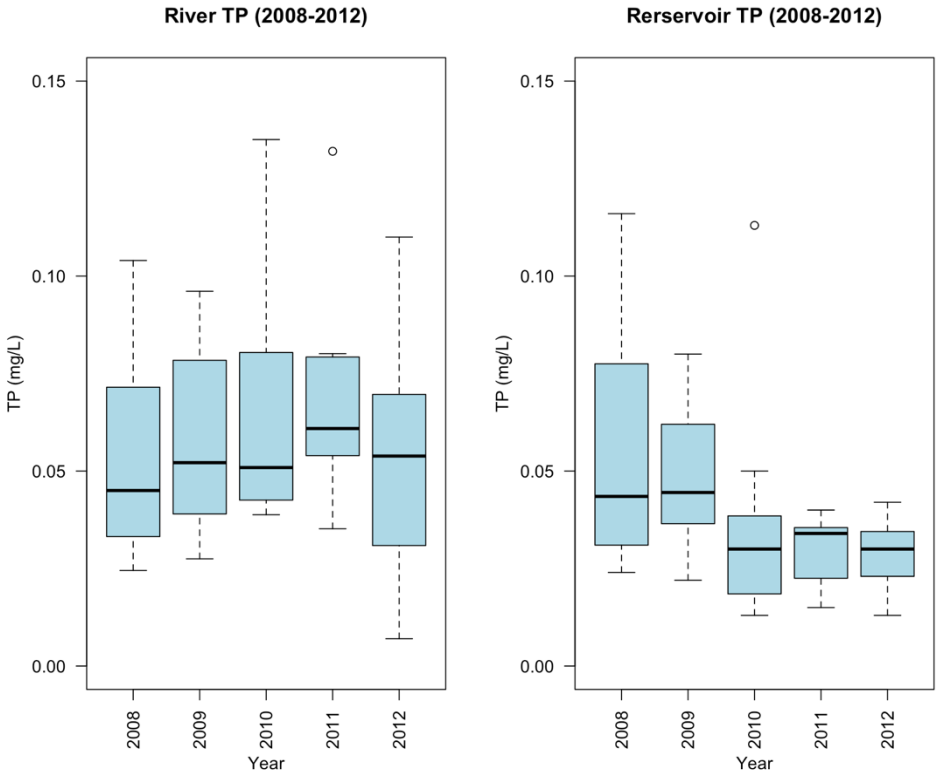

Figure 2.3.1.1.3. Mean annual TP concentrations (mg/L^{-1}) of the Usk river (left) and river reservoir (right). Usk river data sourced from the NRW.

The annual average river inflow volume into the reservoir did not vary significantly (P>0.05) between 2008-2012 (107028ML day^{-1} ± 46195.5), suggesting that inflow volume was unlikely to have been responsible for the reduction in reservoir TP concentrations post-2000 (Figure 2.3.1.1.4).

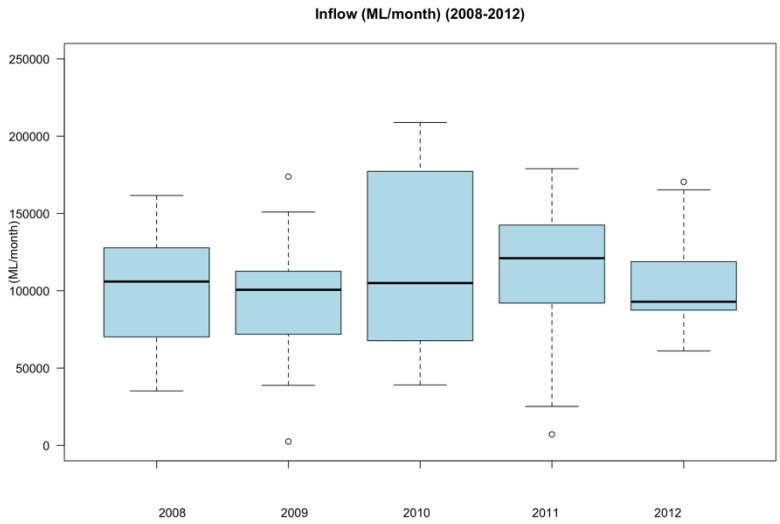

Figure 2.3.1.1.4. Average monthly annual inflow volumes from 2008-2012 (mean/ML/month/year).

2.3.1.2. Mean monthly TN (mgL^{-1}), reduced-N (mgL^{-1}) and oxidised-N (mgL^{-1}) from 1990-2009.

The concentration of NO_3^- within the reservoir post-2000 was significantly lower during both the summer ($1.53mgL^{-1} \pm 0.53$) and winter ($1.57mgL^{-1} \pm 0.39$) when compared with pre-2000 summer ($1.71mgL^{-1} \pm 0.53$) and winter ($1.82mgL^{-1} \pm 0.63$) data. The decrease in winter NO_3^- concentrations post-2000 coincided with a decrease in winter rainfall since 2000. However, a significant reduction in NO_3^- concentrations during the summer period did not correlate with the insignificant increase in rainfall volume thereby suggesting that the mode of abstraction may have been responsible for the differences in data values.

The data suggested a significant decrease in concentrations of NO_3^- pre~post-2000, but the NH_4^+ data did not indicate a significant change in concentration pre-2000 compared with post-2000 (Figure 2.3.1.2.2.), with the NH_4^+ values post-2000 ($0.036mgL^{-1} \pm 0.045$) 22% lower than those pre-2000 ($0.046mgL^{-1} \pm 0.046$) (P=0.05).

Statistical analysis confirmed a significant difference in the average annual concentrations of NO_3^- (11% decrease) (pre-2000: $1.75mgL^{-1} \pm 0.58$; post-2000 $1.55mgL^{-1} \pm 0.47$, P<0.001) and TN (9% decrease) (pre-2000 $1.57mgL^{-1} \pm 0.58$; post 2000 $1.43mgL^{-1} \pm 0.0.63$, P<0.001) when comparing data from 1990-1999 with 2000-2009.

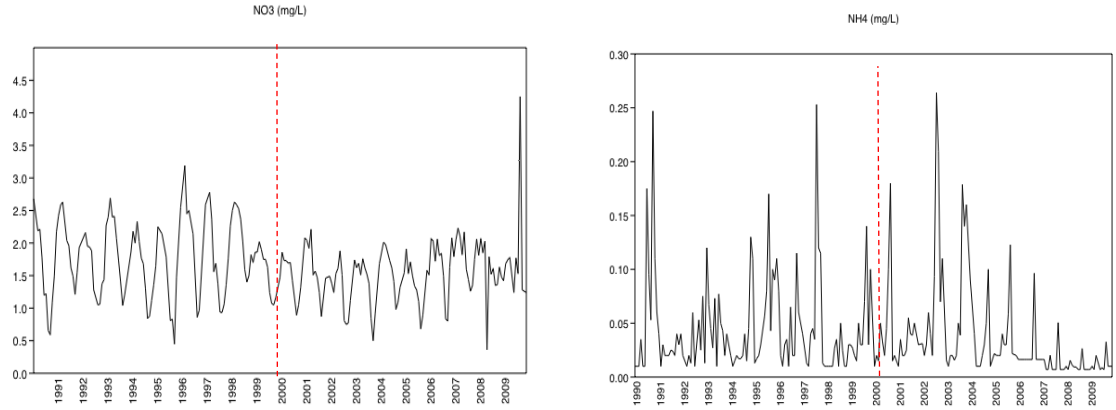

Figure 2.3.1.2.2. NO_3^- (mgL^{-1}) and NH_4^+ (mgL^{-1}) trend analyses from 1990 through 2009. The year 2000 is highlighted by the red dotted line. Data has been logged and showing a 3-point average.

The mean concentration of NO_3^- recorded annually between 2000 and 2009 (Figure 2.3.1.2.3) was 11% lower than that recorded between 1990-1999 (pre-2000: $1.75mgL^{-1} \pm 0.59$: post-

2000: 1.55mgL^{-1} ± 0.47) with the inclusion of the outlier recorded during September of 2009 (4.25mgL^{-1}).

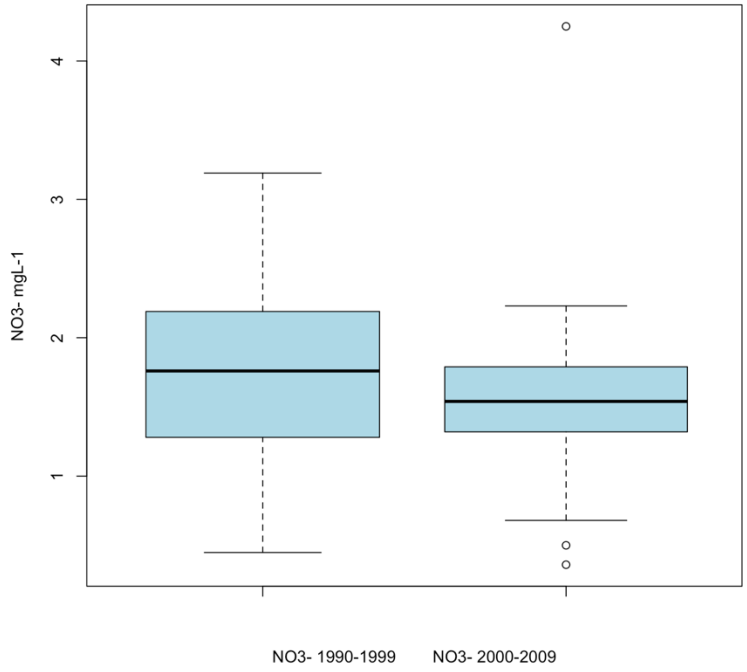

Figure 2.3.1.2.3. Average annual NO_3^- concentration (mgL^{-1}) from 1990 to 1999 and from 2000 to 2009.

Removal of the outlier further decreased the mean difference of annual NO_3^- concentrations from 2000-2009 (1.52mgL^{-1} ± 0.39), increasing the mean difference between the two periods to 13%. No Nitrate data were available throughout 2011 (Figure 2.3.1.2.4).

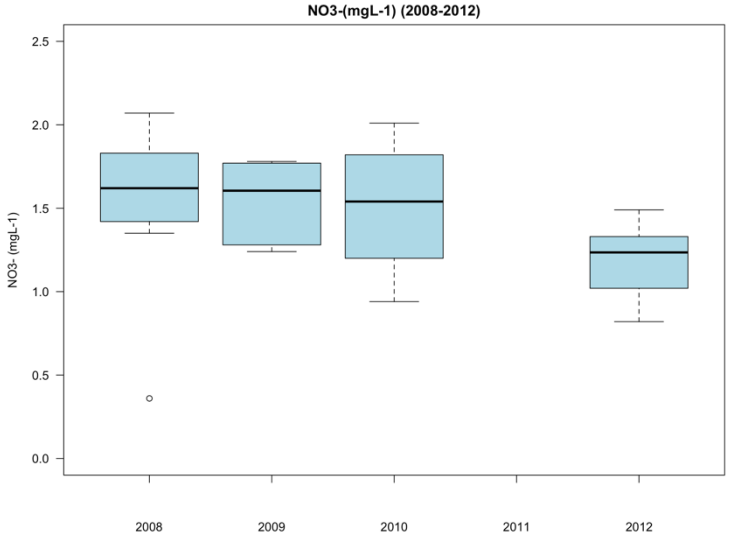

Figure 2.3.1.2.4. Annual average trend of NO_3^- from 2008 through 2012. No nitrate data was available throughout 2011.

The highest mean monthly concentration of NO_3^- between 1990-1999 was 30% higher than the highest mean monthly value recorded post-2000 (March 1996: 3.19mgL^{-1}; March 2007: 2.23mgL^{-1}) disregarding the outlier of 4.25mgL^{-1} recorded during September 2009.

NO_3^- constituted up to 99.2% (± 0.005) of the TN concentration from 2008 through 2012 while NH_4^+ constituted a mean of 0.011% (± 0.01). Therefore NO_3^- had the greatest influence upon TN concentration within the reservoir over the 2008-2012 period.

The TN:TP (mol/ml) ratio is dependent upon several factors; therefore, a non-linear relationship existed between the two variables. No significant difference was seen between the pre-and post-2000 winter or summer TN:TP ratios (mol/ml) (P>0.05 for both seasons). Similarly, no significant difference was established between seasons within the 5-year periods (Figure 2.3.1.2.5).

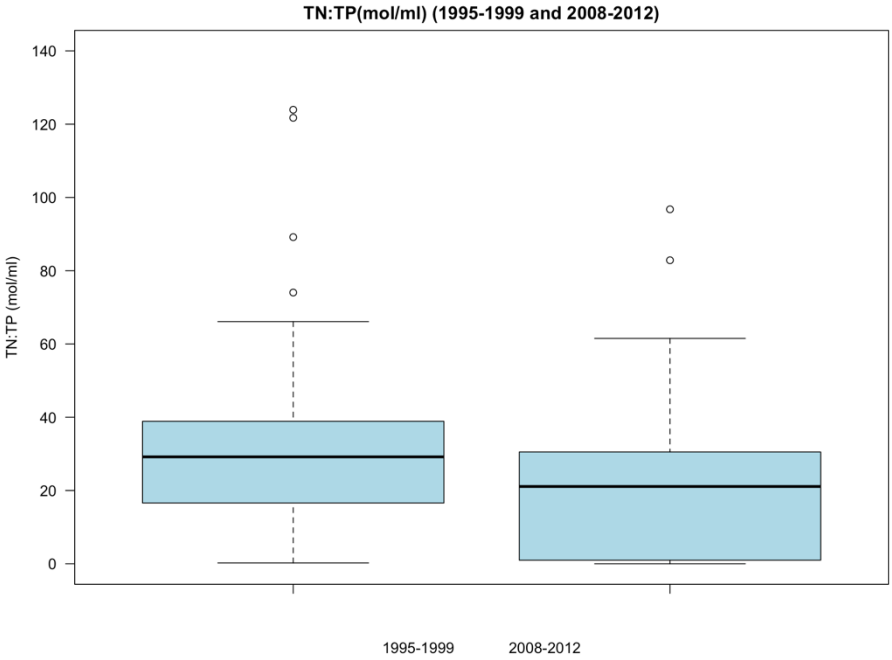

Figure 2.3.1.2.5. TN:TP (mol/ml) concentrations pre-and-post 2000.

The mean annual water samples for which the ratio was favourable to cyanobacterial growth according to the Redfield ratio (=<16:1) decreased by 12% during the summer season and by 16% during the winter season post-2000 (2008-2012) relative to the pre-2000 (1995-1999) data (Table 2.3.1.2.4). However, the mean annual water samples for which the TN:TP ratio was equal to or below Smith's ratio (=<29:1) increased by 20% during the summer periods

post-2000 but decreased by 11% during the winter season (Figure 2.3.1.2.6). Therefore, Smith's ratio was satisfied more frequently post-2000, but Redfield's ratio less frequently. The duration for which the TN:TP ratio was low and favourable to cyanobacterial establishment within the reservoir decreased for the summer and winter seasons according to Redfield's ratio (16:1) but increased during the summer and decreased during the winter as per Smith's ratio (29:1).

Table 2.3.1.2.4. The annual average duration (%) within which the reservoir TN:TP (mol/ml) ratio is within Redfield's ratio (16:1) and Smith's ratio (29:1)

Period	TN:TP =<Redfield's ratio	TN:TP =<Smith's ratio
Summer 1995-1999	32%	65%
Winter1995-1999	36%	65%
Summer 2008-2012	20%	85%
Winter 2008-2012	20%	54%

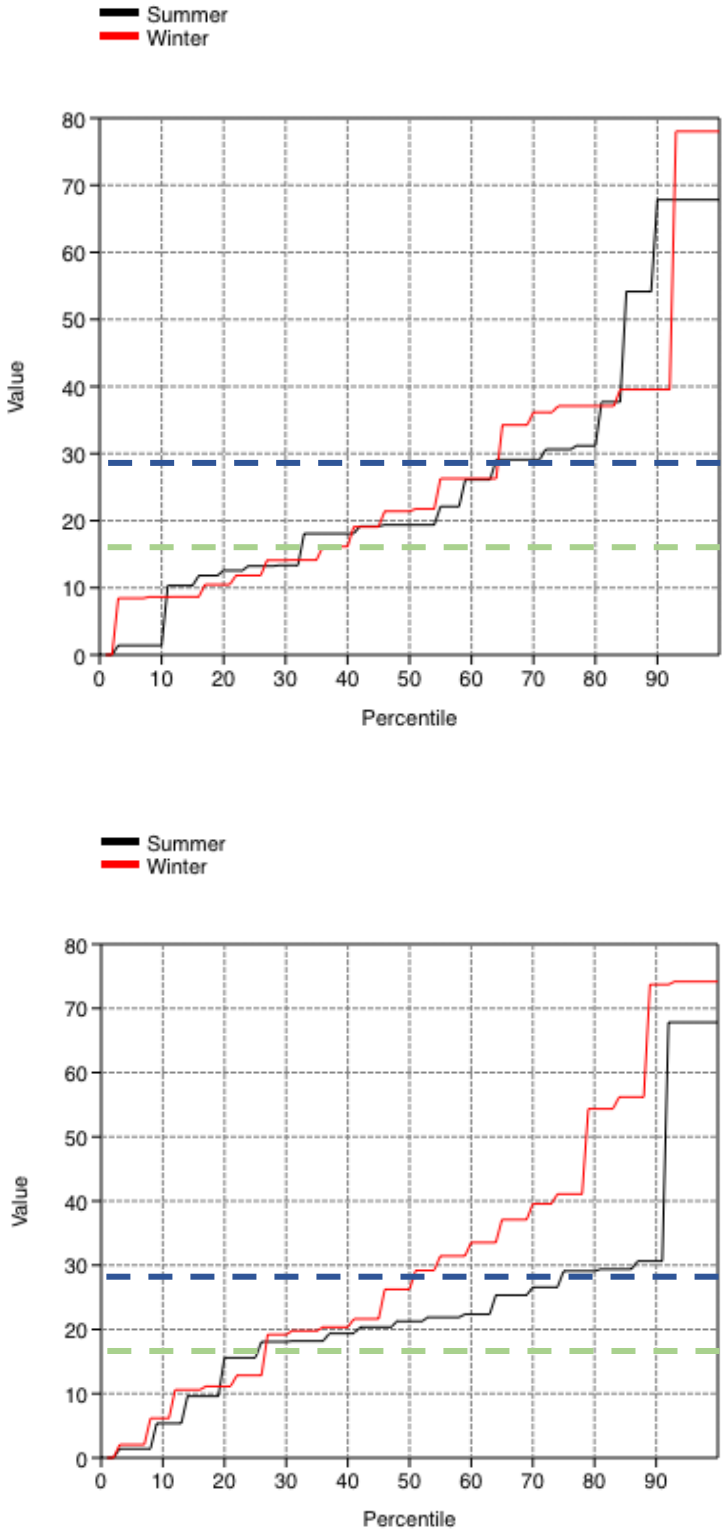

Figure 2.3.1.2.6. Summer and winter TN:TP (mol/ml) ratio of pre-2000 (1995-1999) (top) and post-2000 (2008-2012) (bottom). Green-dashed line = Redfield's ratio; Blue-dashed line = Smith's ratio)

The data indicated that TN was more influential upon the TN:TP ratio than TP (P<0.05) during the 1995-1999 sampling period (Figure 2.3.1.2.7).

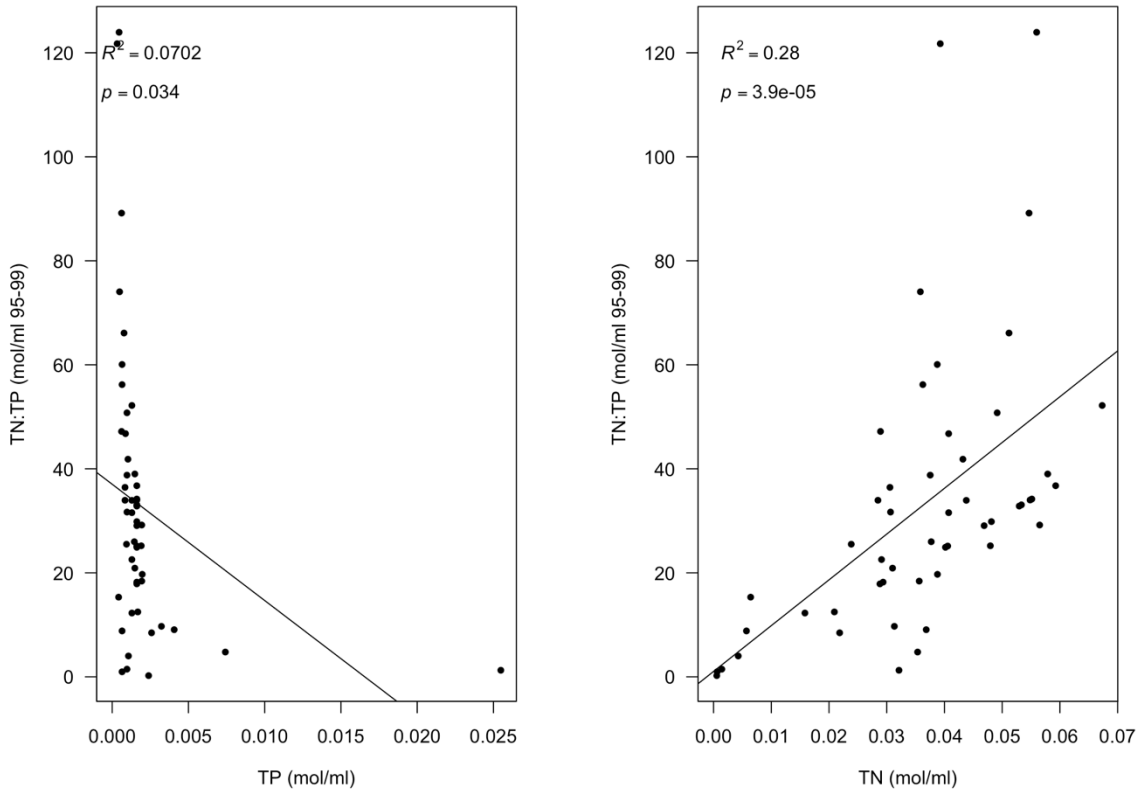

Figure 2.3.1.2.7. Correlation between TP (mol/ml) and TN (mol/ml) with TN:TP (mol/ml) (data 1995-1999).

However, both TN and TP demonstrated an increased association with the TN:TP ratio during 2008-2012 sampling period (Figure 2.3.1.2.8) than the 1995-1999 sampling period, suggesting that both the TN and TP had an increased influence upon the TN:TP ratio, with TN concentrations retaining majority of the influence.

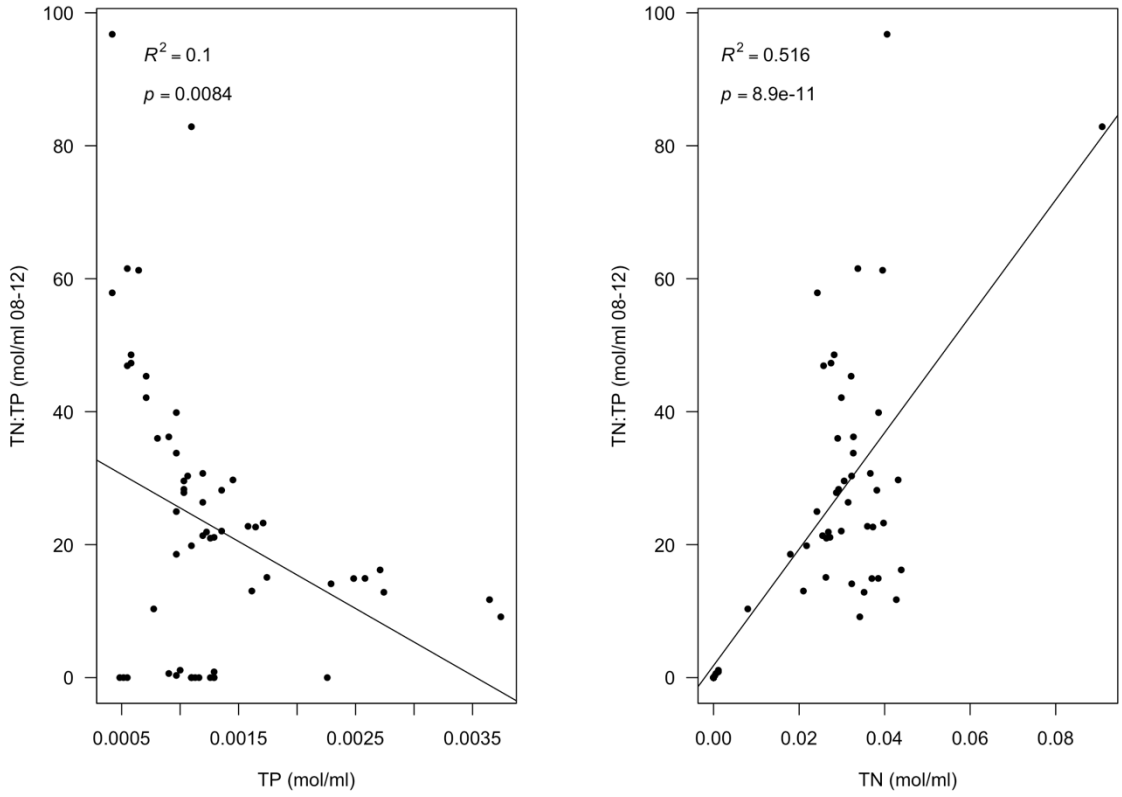

Figure 2.3.1.2.8. Correlation between TP (mol/ml) and TN (mol/ml) with TN:TP (mol/ml) (data 2008-2012).

TN concentration maintained a slight downward trend throughout 2008-2012 (Figure 2.3.1.2.9) relative to the TP concentrations. The data suggested that TP concentrations had a greater influence upon the TN:TP ratios during periods of decreased nitrate concentrations. The annual mean concentration of TP (mgL^{-1}) decreased between 2008 and 2012 by 40% from $0.05mgL^{-1}$ (± 0.03) throughout 2008 to $0.03mgL^{-1}$ (± 0.01) during 2012. Similarly, the annual mean concentration of TN (mgL^{-1}) also decreased over the 5-year period (by 25%) from $1.6mgL^{-1}$ (± 0.43) during 2008 to $1.2mgL^{-1}$ (± 0.19) during 2012.

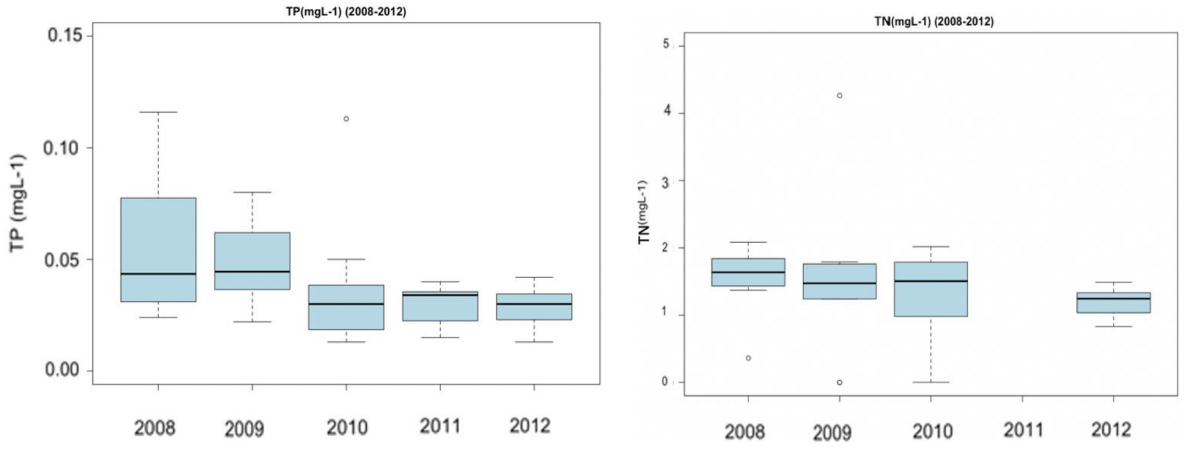

Figure 2.3.1.2.9. Annual average TP (left) and TN (right) concentrations (mgL^{-1}) from 2008-2012. No TN (mgL^{-1}) data available throughout 2011.

The decreasing NO_3^- concentration trend from 2008 through 2012 was evident within the TN (mgL^{-1}) data due to the significant contribution made by nitrate towards the TN value relative to the remaining N fractions (Figure 2.3.1.2.10).

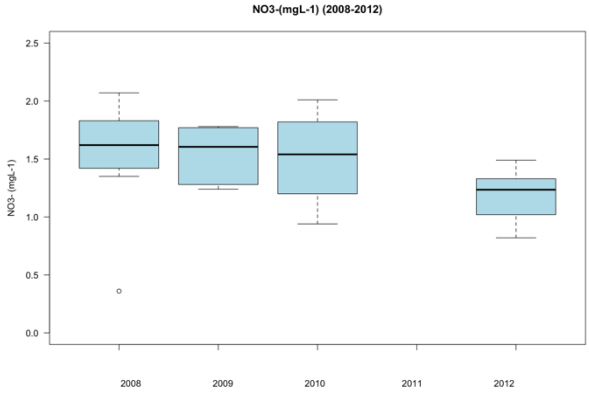

Figure 2.3.1.2.10. The decreasing annual average of NO_3^- (mgL^{-1}) from 2008 through 2012. No data was available throughout 2011.

Conversely, the annual average concentration of NH_4^+ increased by 28% between 2008 and 2012 (from 0.01mgL^{-1} ± 0.005 throughout 2008 to 0.014mgL^{-1} ± 0.006 throughout 2010), resulting in an increase in the mean annual NH_4^+ concentration contribution towards the TN (mgL^{-1}) from 2.7% (2008) to 8% during 2010 (Figure 2.3.1.2.11).

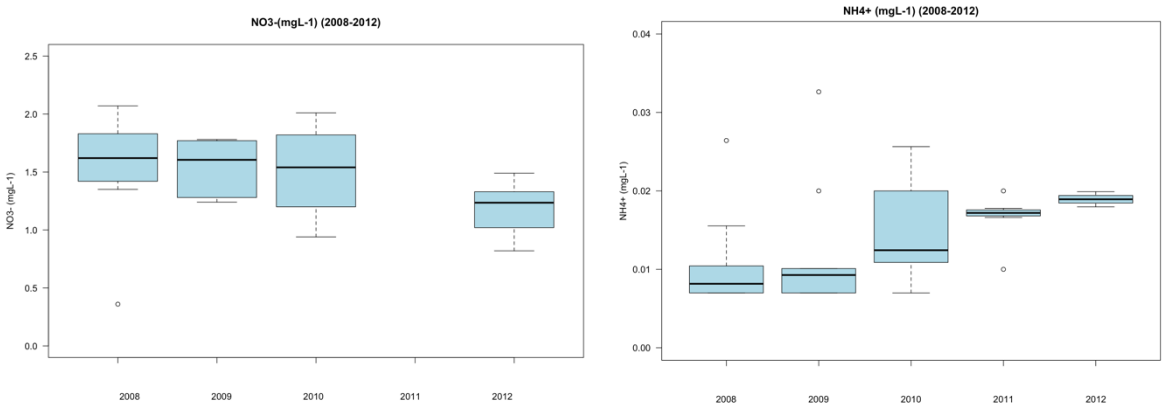

Figure 2.3.1.2.11. The annual average NO_3^- (mgL^{-1}; left) and NH_4^+ (mgL^{-1}; right) concentrations from 2008 through 2012.

The mean annual TN:TP (mol/ml) ratio (Figure 2.3.1.2.12) varied from 2008 to 2012 (311:1 ± 106), suggesting that an increase in mean annual NH_4^+ from $0.01mgL^{-1}$ (± 0.005) throughout 2008 to $0.02mgL^{-1}$ (± 0.01) throughout 2012 in conjunction with a decrease in NO_3^- and TP concentrations influenced the TN:TP ratio, with NO_3^- and TP concentrations having the greatest influence upon the ratio.

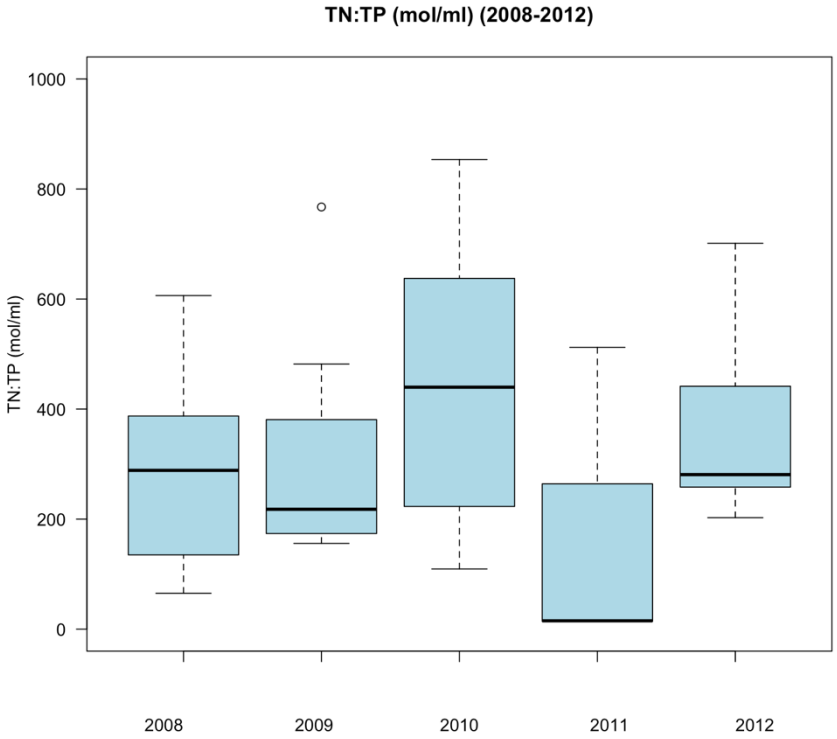

Figure 2.3.1.2.12. TN:TP (mol/ml) annual mean trend 2008-2012.

2.3.2. Environmental data

2.3.2.1. pH and water temperature water quality pre-and post-2000 (1990-1999 and 2000-2009).

A change in the mean annual cyclic pH data occurred prior to/during the year 2000 (between approximately 1997-2000, the actual date unknown) (Figure 2.3.2.1.1).

A significant difference ($P<0.001$) in the mean monthly pH of water samples collected between 1990-1999 (7.92 ± 0.29) and 2000-2009 (7.83 ± 0.19) was determined.

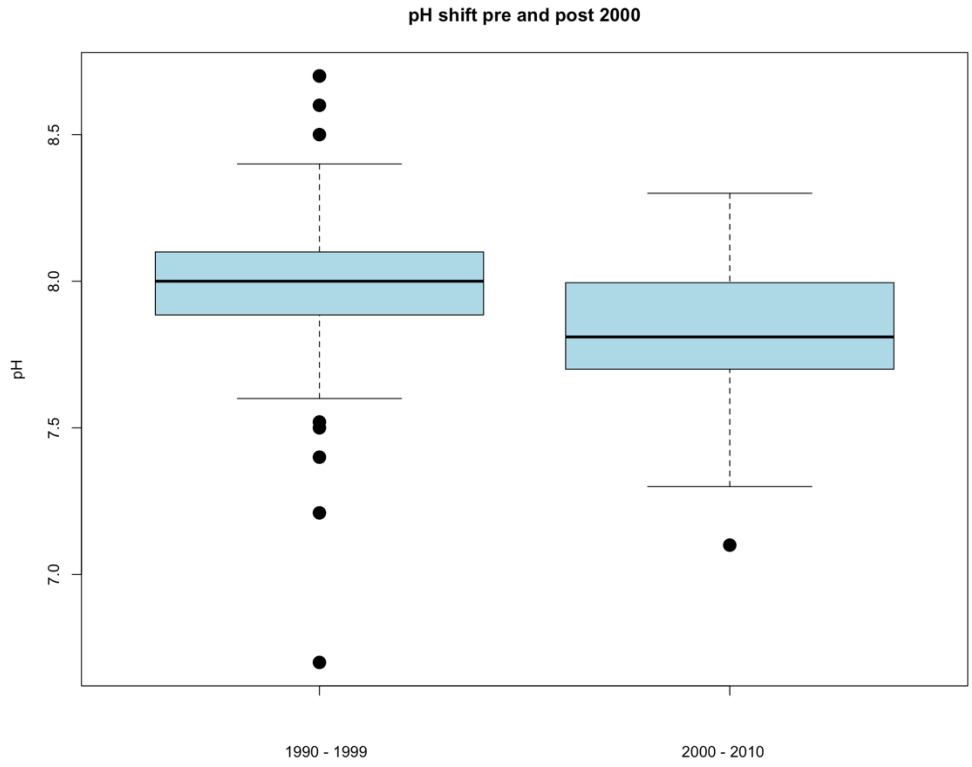

Figure 2.3.2.1.1. pH (avg./month) data from 1990-1999 (left), data from 2000-2010 (right).

Analysis of the mean monthly water temperature (°C) highlighted a significant ($P<0.001$) decline in upper temperature bandwidths of post-2000 data (2000 through 2015) compared with pre-2000 data (1985 through 1999), while the mean average monthly lower temperature range also decreased post-2000 (2000 through 2015) (10.7°C ± 3.9) relative to pre-2000 (1985 through 1999) data (9.6°C ± 3.4) (Figure 2.3.2.1.2). The change to the water temperature range was likely due to mixing of upper surface water with bottom colder water as a consequence of tower control failure which led to mixing of water from all three depths of the reservoir following the year 2000 (actual tower damage believed to be 1997-2000).

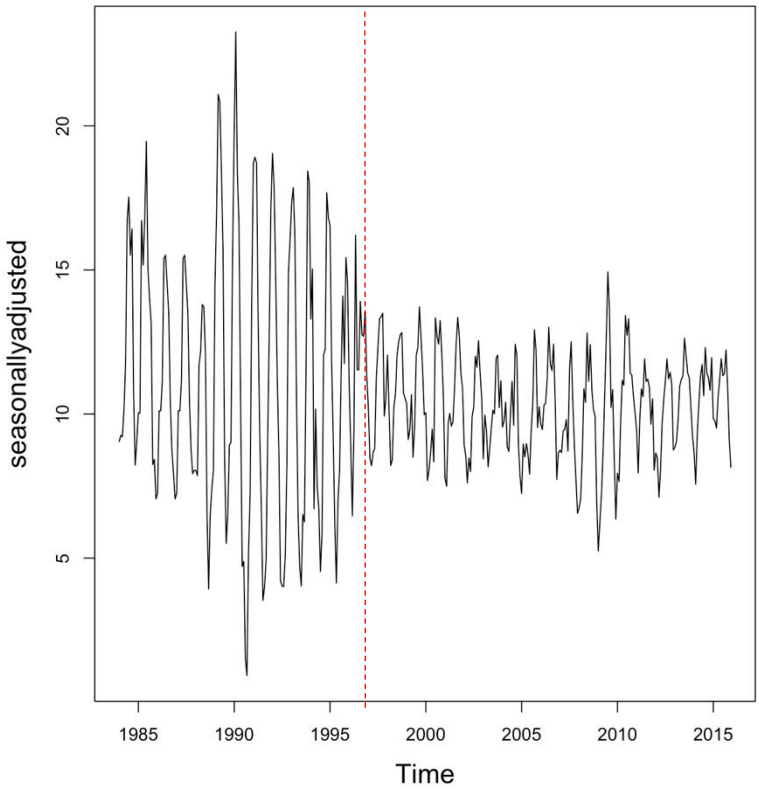

Figure 2.3.2.1.2. Seasonally adjusted model (seasonal patterns removed) of water temperature (°C) time series.

A comparison of the mean monthly pH and water temperature data from 1990 through 1999 with mean monthly data obtained from samples collected from 2000 through 2009 indicated that the pH cycle shift did not take place until during the year 2000 (Figure 2.3.2.1.3).

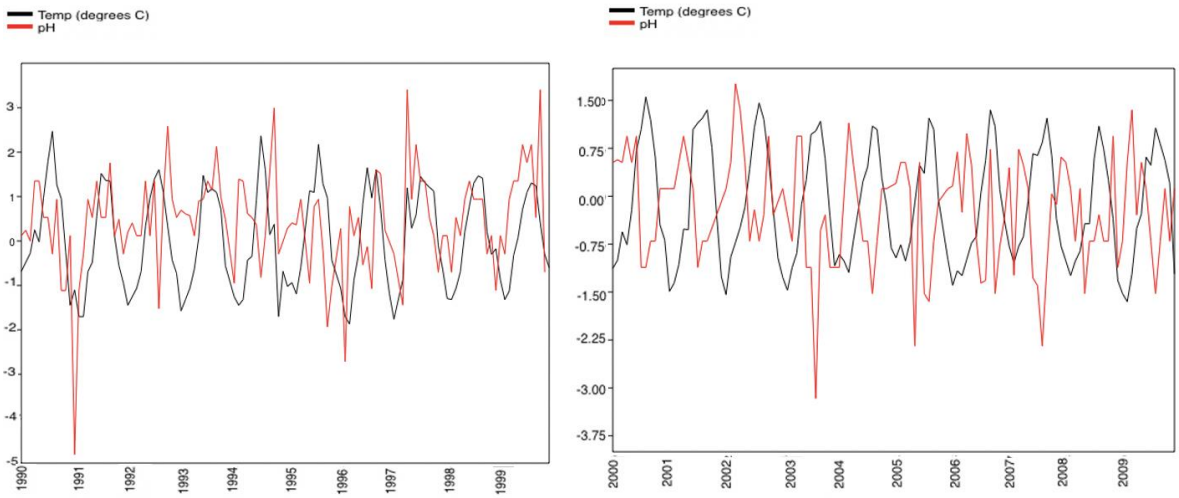

Figure 2.3.2.1.3. The pH and water temperature data (mean/month) from January 1990 through December 1999 (left), and January 2000 through December 2009 (right). Data has been standardised using the equation $(X-\mu)/\sigma$.

.

The change in the relationship between the pH values and the water temperature during approximately the year 2000 indicated to a positive relationship with water temperature pre-2000 but a negative relationship with temperature post-2000.

The data indicated to a shift in seasonal pH cycles, whereas the seasonal temperature cycle remained unchanged.

2.3.2.2. Rainfall (mm) (1990-1999 and 2000-2009).

A comparison of the pre-and-post-2000 data indicated no increase in rainfall volume during the summer periods (April-September) post-2000 (84.27mm ± 44.74) compared with pre-2000 (78.5mm ± 49.1) and no reduction during the winter (P>0.05, October-March) post-2000 (114.8mm ± 55.6) compared with pre-2000 data (115.5mm ± 59.3). Analysis of the rainfall data pre-and post-2000 indicated no significant difference between the average monthly rainfalls within seasons (Figure 2.3.2.2.1).

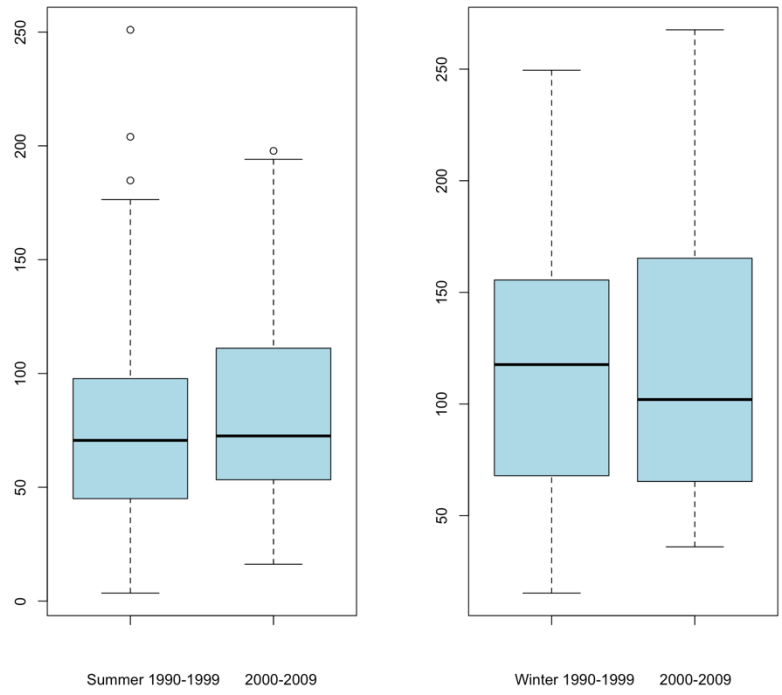

Figure 2.3.2.2.1. Summer rainfall (avg./mm/month) (left) and winter rainfall (avg./mm/month) (right) (medians).

2.3.3. Determining interaction of nutrient and environmental variables through linear models

2.3.3.1. Model addressing TP (mg L^{-1}) LM data analysis as a function.

2.3.3.1.1. TP (mg L^{-1}) data from 1995-1999.

Tukey's ladder of power was used in the transformation of not normally distributed TP data to allow for LM analysis.

LM analysis indicated that no significant association was determined for TP with any of the variables analysed.

2.3.3.1.2. TP (mg L^{-1}) LM data 2008-2012.

As TP data were not normally distributed (Shapiro-Wilks $P<0.05$), the data was transformed using Tukey's ladder of power.

Significant associations ($^{\wedge}R^2$:0.86, $F_{4,11}$:19.96, $P<0.0001$) were determined for TP (mg L^{-1}) concentration (intercept -718 ± 210, $P<0.01$) with reservoir level (m) (LM mean difference ± SE, -0.2 ± 0.07, $P< 0.05$) and Fe_3^+ (mg L^{-1}) (LM mean difference ± SE, 0.76 ± 0.2, $P<0.01$). A significant association with TN:TP (mol/ml) (LM mean difference ± SE, -0.05 ± 0.006, $P<0.0001$) indicated that TP concentrations strongly affected TN:TP (mol/ml) ratio. Finally, a significant association was determined in the model with the year in which the data set was collected (LM mean difference ± SE, 0.35 ± 0.1, $P< 0.01$) indicating that the TP ratio within the reservoir displayed a decreasing trend with the passing of each year of data.

2.3.3.2. Model addressing NH_4^+ (2008-2012) as a function.

The data distribution for NH_4^+ was heavily negatively skewed (Shapiro-Wilks: $P<0.001$) and was not successfully transformed to a normal distribution. Therefore, a GLM was used in the modelling, using the Gamma family (identity link) to determine whether an association was evident between NH_4^+ and other variables.

Following a stepwise deletion of independent variables, a weak association ($^{\wedge}R^2$:0.69, $F_{2,26}$:18. $P<0.0001$) was determined between NH_4^+ (intercept 0.0068 ± 0.003, $P<0.05$) and the NO_3^- : NH_4^+ ratio (LM mean difference ± SE, -0.0002 ± 0.00003, $P<0.0001$) and TN (mg L^{-1}) (LM mean difference ± SE, 0.55 ± 0.13, $P<0.001$) in the absence of NO_3^-.

2.3.3.3. Model addressing NO_3^- (mg L^{-1}) (2008-2012) as a function.

The NO_3^- data were not normally distributed (P<0.05) therefore the data were transformed using Tukey's ladder of power.

A weakly significant association (^R^2:0.28, $F_{2, 40}$:9.3, P<0.0005) was determined between NO_3^- (intercept 1.1 ± 0.03, P<0.0001) and NO_3^-: NH_4^+ ratio (LM mean difference ± SE, 0.001 ± 0.0004, P<0.005) and rainfall (mm) (LM mean difference ± SE, -0.0004 ± 0.0002, P<0.05). The degree of association of NH_4^+ with the NO_3^-: NH_4^+ ratio was greater than that of the association of NO_3^- with the NO_3^-: NH_4^+ ratio, suggesting the concentration of NH_4^+ had a more significant impact upon the NO_3^-: NH_4^+ ratio. However, with such a low ^ R^2 value, caution should be applied to the model.

2.3.3.4. Model addressing NO_3^-: NH_4^+ (mol/ml) (2008-2012) as a function.

The NO_3^-: NH_4^+ data were not normally distributed (P<0.05) therefore were transformed using the square root method.

The LM model for NO_3^-: NH_4^+ (mol/ml) (LM intercept 7.33 ± 0.45, P<0.0001) confirmed a significant association (^R^2:0.87, $F_{3,14}$:37.6, P<0.0001) with NO_3^- (LM mean difference ± SE, 1.9 ± 0.25, P<0.0001), geosmin and NH_4^+ (LM mean difference ± SE, -236.9 ± 23.7, P<0.0001) as independent variables. A geosmin data point was identified as an outlier using Cook's distance (24.98ngL^{-1} sampled during June 2010) indicating to the weight of the outlier upon the conclusion of the analysis. However, the geosmin data point is believed to be an accurate representation of the concentration at the time and was therefore retained within the analysis.

The data indicated to a decrease in the NO_3^-: NH_4^+ ratio during periods of increasing NH_4^+ concentration but an increase in the NO_3^-: NH_4^+ ratio during periods of raised NO_3^- concentration as expected. No significant association was determined for NO_3^-: NH_4^+ with geosmin (LM mean difference ± SE, -0.01 ± 0.02, P>0.05), but geosmin was retained within the model due to its presence decreasing the AIC from 127.8 (without geosmin) to 43.3. Its inclusion within the model was also supported by the increased ^R^2value (^R^2:0.75 without geosmin).

2.3.3.5. Model addressing TN:TP (mol/ml) as a function.

2.3.3.5.1. TN:TP (mol/ml) 1995-1999

TN:TP (mol/ml) data were not normally distributed (Shapiro-Wilks P<0.05) therefore the data were transformed for LM analysis using Tukey's ladder of power.

No significant association was determined between TN:TP (mol/ml) with any other variable analysed during their respective period (TN and TP data omitted).

2.3.3.5.2. Model addressing TN:TP (mol/ml) (2008-2012)

TN:TP data were not normally distributed (Shapiro-Wilks P<0.05), therefore, the data was transformed to allow LM analysis using Tukey's ladder of power.

No significant association was determined between TN:TP (mol/ml) with any other variable analysed during their respective period.

2.3.3.6. Model addressing pH data as a function

2.3.3.6.1. pH data (1984-1999)

No geosmin data was available for this period. Compensation flow data was insufficient in number to run the LM.

The pH data from 1984 through 1999 was not normally distributed (Shapiro-Wilks P=<0.05) and transformed using Tukey's ladder of power. A marginally significant association was determined for pH (LM intercept 609.1 ± 15.8, P<.0001) with cyanobacteria (LM mean difference ± SE, 0.006 + 0.002, P<0.05), water temperature (°C) (LM mean difference ± SE, 5.5 ± 1.4, P<0.001) and NH_4^+ (LM mean difference ± SE, -294.9 ± 102, P<0.005) (^R^2: 0.16, $F_{3,128}$:9, P<0.0001). However, with such a low ^ R^2 value, caution should be applied to the model.

2.3.3.6.2. pH post-2000 data (2000-2016)

pH data were not normally distributed (Shapiro-Wilks P=<0.05) and transformed using Tukey's ladder of power). LM analysis determined a weak association (^R^2: 0.23, $F_{1,192}$:61.3, P<0.0001) for pH (LM intercept 1732942 ± 43418, P<0.0001) with water temperature (LM mean difference ± SE, -31388 ± 4007, P<0.0001). However, with such a low ^ R^2 value, caution should be applied to the model.

The pre-and post-2000 pH ~ temperature relationship data suggested that the mode through which the water was transferred from the reservoir through to the combined network to the water quality analysers significantly and directly influenced the water quality data obtained.

2.3.3.7. Model addressing water temperature as a function

2.3.3.7.1. Water temperature 1984-2016 data

Water temperature data were not normally distributed (Shapiro-Wilks P=<0.05) and therefore was transformed for analysis using Tukey's ladder of power.

LM analysis confirmed a weak association for water temperature (°C) (LM intercept, 4.26 ± 0.12, P<0.0001) with TN (mg L^{-1}) (LM mean difference ± SE, -31 ± 4.1, P<0.0001) (^R^2: 0.18, $F_{1,236}$:55.37, P<0.0001). However, with such a low ^ R^2 value, caution should be applied to the model.

2.3.3.7.2. Water temperature 1984-1999 data

Analysis of the Water temperature data (transformed using Tukey's Ladder of Power) confirmed a significant association for water temperature (°C) (LM intercept, 4.65 ± 0.64, P<0.0001) with TN (mg L^{-1}) (LM mean difference ± SE, -48 ± 5.6, P<0.0001), conductivity (µs) (LM mean difference ± SE, 0.005 ± 0.002, P<0.05) and catchment inflow (ML/day) (LM mean difference ± SE, -0.02 ± 0.003, P<0.0001) (^R^2: 0.58, $F_{3,97}$:47.39, P<0.0001).

2.3.3.7.3. Water temperature 2000-2016 data

Water temperature data were not normally distributed and was transformed using Tukey's Ladder of Power. LM analysis for the association of water temperature (°C) (LM intercept, 12.54 ± 1.85, P<0.0001) determined a weakly significant association with reservoir level (LM mean difference ± SE, 0.05 ± 0.01, P<0.005), pH (LM mean difference ± SE, -1.29 ± 0.23, P<0.0001), NH_4^+ (LM mean difference ± SE, 4.9 ± 1.2, P<0.0005), conductivity (µs) (LM mean difference ± SE, 0.004 ± 0.001, P<0.01) and catchment inflow volume (ML/day) (LM mean difference ± SE, -0.004 ± 0.002, P<0.05) (^R^2:0.41, $F_{5,160}$: 24.4, P<0.0001).

2.3.3.8. Model addressing monthly average rainfall volume as a function

2.3.3.8.1. Mean rainfall data, 1990-1999

Rainfall data from 1990-1999 were not of a normal distribution (Shapiro-Wilks P=<0.05), therefore transformation was required to enable modelling of the data using Tukey's Ladder of Power.

No significant association was determined with any independent variable for either of the data sets.

2.3.3.8.2. Mean rainfall data: 2000-2009

Rainfall data from 2000-2009 were not of a normal distribution (Shapiro-Wilks P=<0.05), therefore, transformation was required to enable modelling of the data using Tukey's Ladder of Power.

No significant association was determined with any independent variable for either of the data sets.

2.3.4. Phytoplankton and by-product data analysis

2.3.4.1. Data analysis

2.3.4.1.1. Geosmin (ngL^{-1}), Fe_3^+ and TP, 2008-2010.

The annual average concentrations of geosmin increased by 79% between 2008-2010 (from $2.6ngL^{-1}$ ± 0.91 throughout 2008 to $24.98ngL^{-1}$ ± 7 throughout 2010) (Figure 2.3.4.1.1.1). Concurrently, the Fe_3^+ and TP concentrations within the reservoir between 2008 and 2010 decreased (Figure 2.3.4.1.1.1).

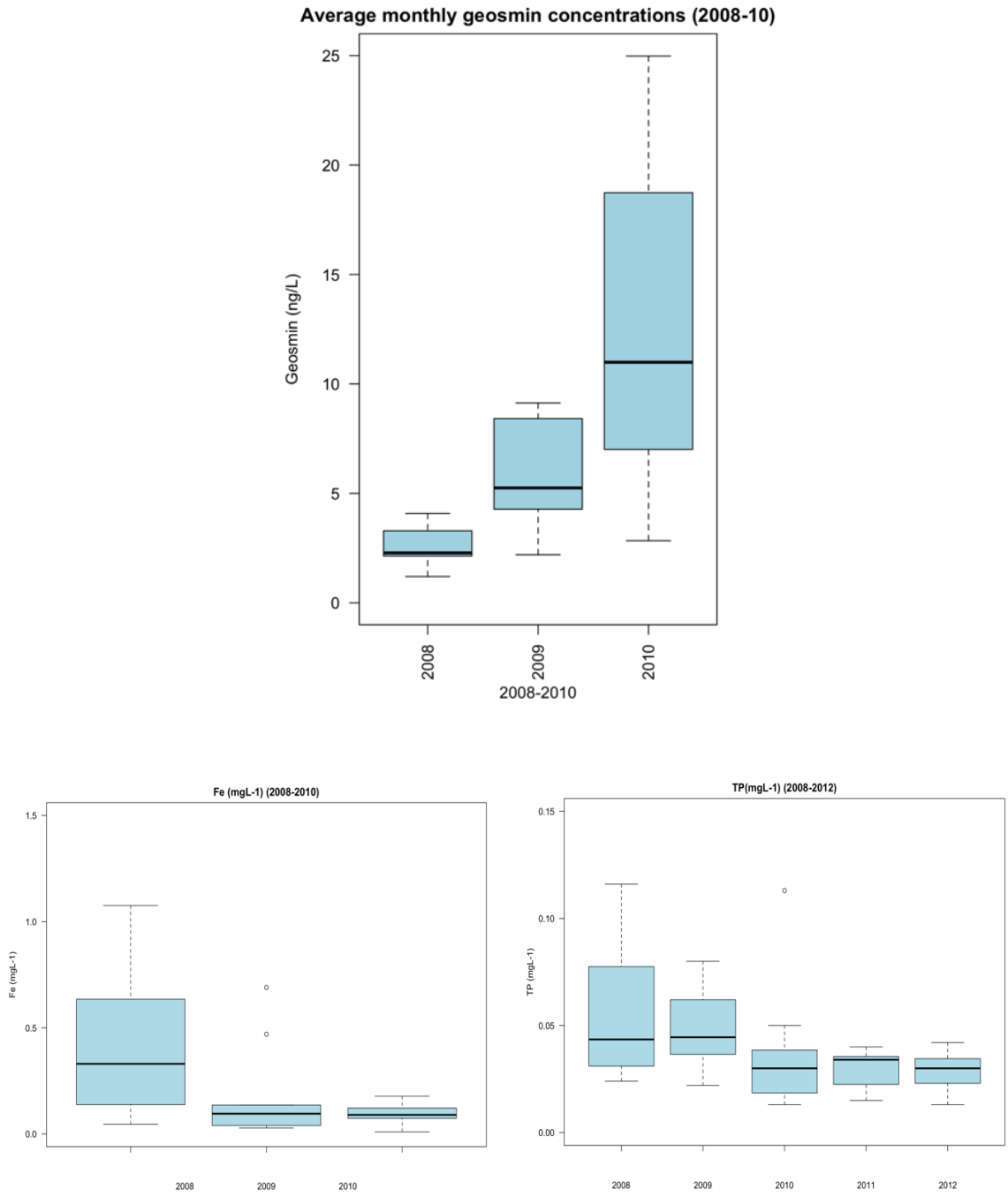

Figure 2.3.4.1.1.1. Average annual geosmin concentrations increased between 2008-2012 (ngL^{-1}) (top). Annual average Fe_3^+ (mgL^{-1}) (left) and TP (mgL^{-1}) (right) from 2008 through 2010.

The higher concentrations of geosmin during the summer of 2010 (10.8ngL^{-1} (June), 25ngL^{-1} (July) and 19ngL^{-1} (August)) occurred during a period of lower TP concentrations from June through August (0.017mgL^{-1} ± 0.004) relative to the that of the two previous summers (Figure 2.3.4.1.1.2.) of 0.076mgL^{-1} (± 0.003) and 0.046mgL^{-1} (± 0.009) for 2008 and 2009 respectively.

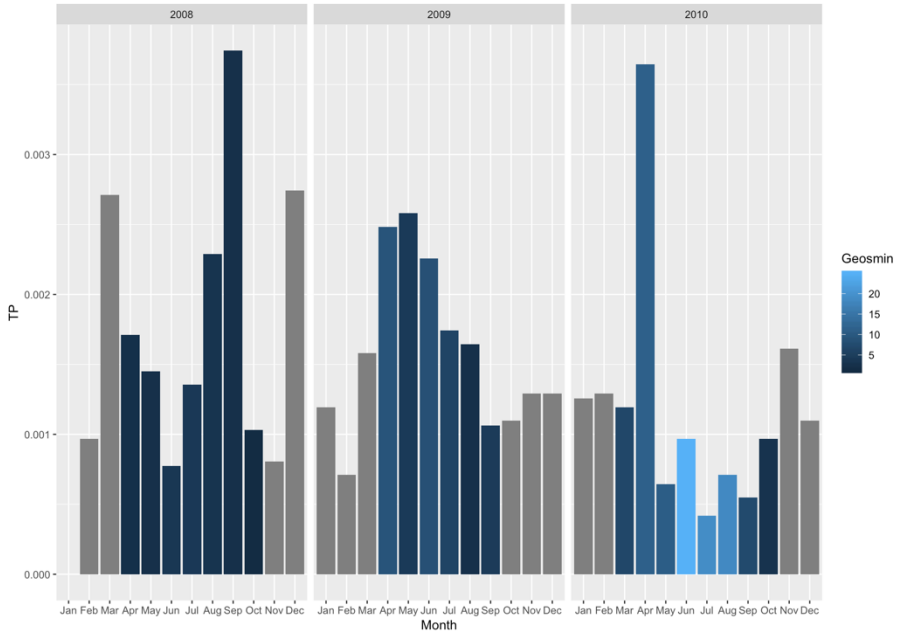

Figure 2.3.4.1.1.2. TP (mgL^{-1}) and geosmin (ngL^{-1}) concentrations from 2008 through 2010.

The data suggested that a higher concentration of TP during the spring period (April) followed by a time lag led to an increase in geosmin production.

2.3.4.1.2. Analysis of geosmin and NH_4^+ data, 2008-2010.

2010 geosmin concentrations peaked during June ($25ngL^{-1}$), July ($19ngL^{-1}$) and August ($18.4ngL^{-1}$) with concentrations of geosmin over the same period for the two previous years not exceeding $4.1ngL^{-1}$ (July 2008) and $8.4ngL^{-1}$ (June 2009).

Concurrently, the concentration of NH_4^+ during April of 2010 ($0.023mgL^{-1}$) was 11% higher than that during April of 2009 ($0.02mgL^{-1}$) and 52% higher than that during April 2008 ($0.01mgL^{-1}$).

Likewise, the concentration of NH_4^+ during May 2010 ($0.026mgL^{-1}$) was 64% higher than that recorded during May of 2008 ($0.009mgL^{-1}$) (no NH_4^+ data exists for May of 2009). In addition, the concentrations of NH_4^+ were higher during June of 2010 ($0.013mgL^{-1}$) than during June of 2008 ($0.009mgL^{-1}$) and 2009 ($0.007mgL^{-1}$) (Figure 2.3.4.1.2.1).

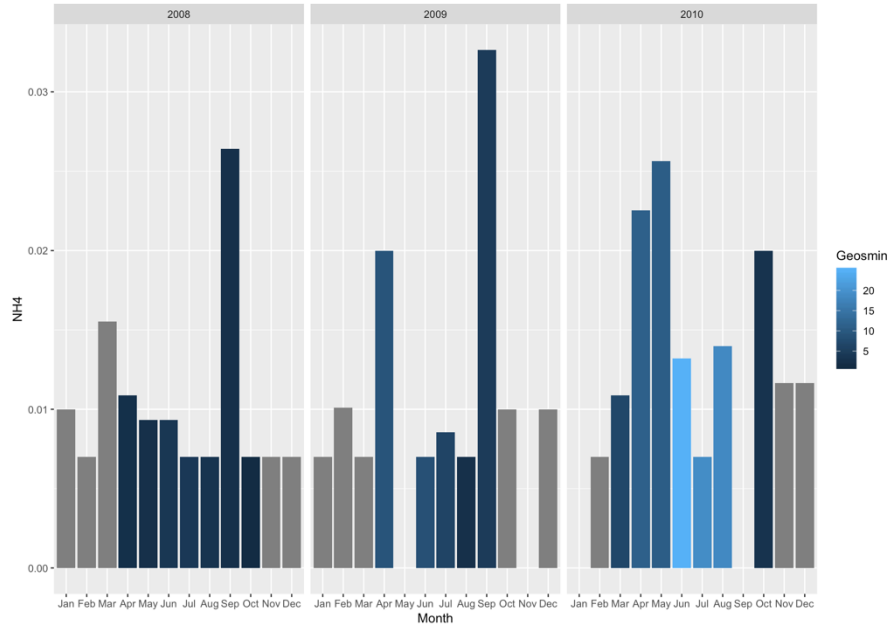

Figure 2.3.4.1.2.1. NH_4^+ (mgL^{-1}) and geosmin (ngL^{-1}) mean monthly concentrations from 2008 through 2010.

2.3.4.1.3. Analysis of geosmin and NO_3^- data

There was no significant difference in the NO_3^- concentrations during the month of June 2010 ($1.9mgL^{-1}$) compared with that during June 2008 ($1.8mgL^{-1}$) and 2009 ($1.24mgL^{-1}$) (Figure 2.3.4.1.3.1). However, the annual mean concentration of nitrate decreased significantly between 2010 and 2012 ($P<0.05$).

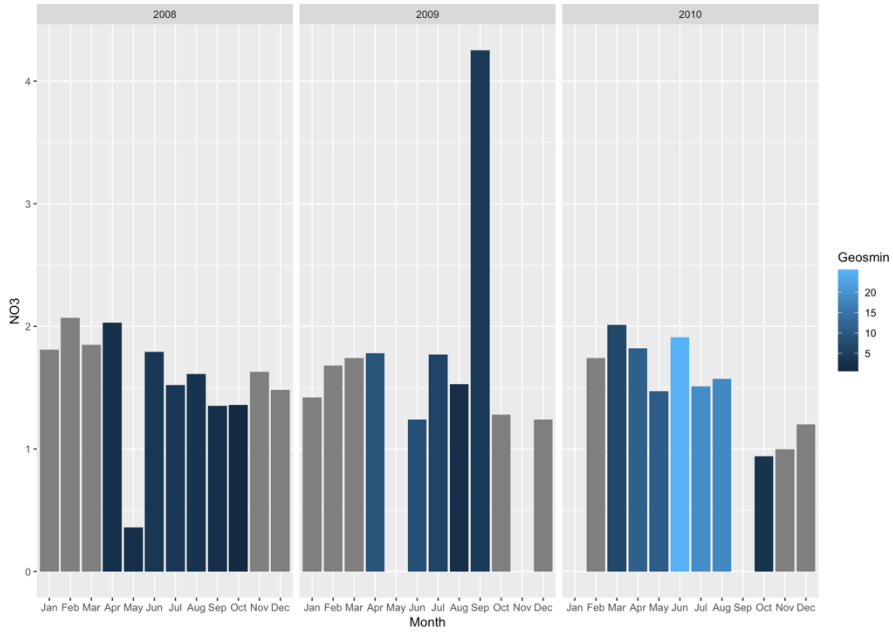

Figure 2.3.4.1.3.1. NO_3^- (mgL^{-1}) and geosmin (ngL^{-1}) average monthly concentrations from 2008 through 2010.

Low concentrations of nitrate during May 2010 preceded the increase in geosmin concentrations during June 2010 but was unlikely to have been the sole instigator of geosmin production; low nitrate concentrations during May 2008 relative to those during May 2010 did not precede raised geosmin concentrations (>15ngL^{-1}) during the associated summer months. Therefore, other factors were likely to have been a significant determinant as to whether geosmin production occurred at increased concentrations during the summer months.

2.3.4.1.4. Analysis of geosmin and the NO_3^-: NH_4^+ ratio

The NO_3^-: NH_4^+ ratio was lower during June 2010 (54:1) than during June of 2008 (72:1) and 2009 (67:1) (Figure 2.3.4.1.4.1) as a consequence of increased NH_4^+ and a reduction in NO_3^- concentrations relative to that of previous years.

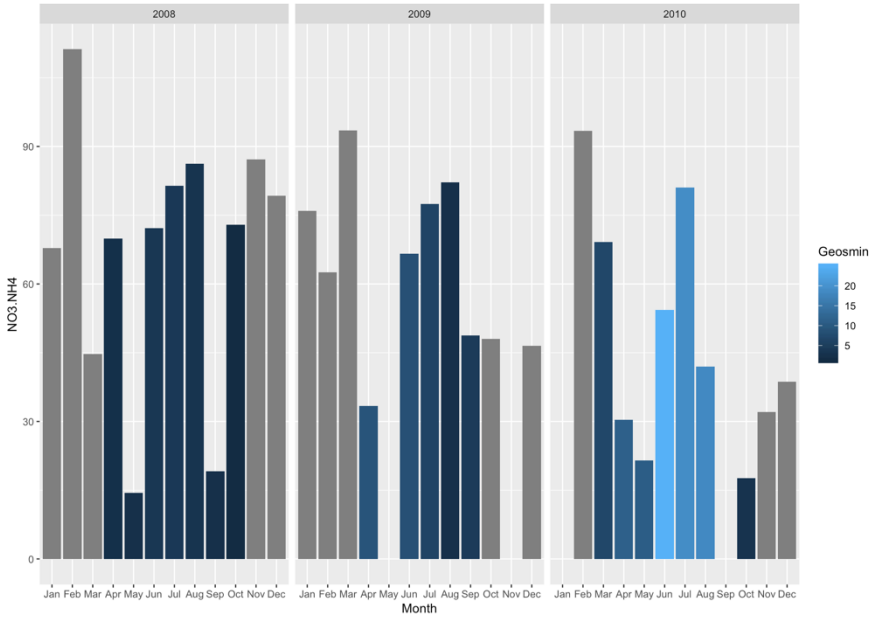

Figure 2.3.4.1.4.1. NO_3^-: NH_4^+ (mol/ml) and geosmin (ngL^{-1}) average monthly concentrations from 2008 through 2010.

The months of June through August of 2010 also recorded the highest TN:TP (mol/ml) ratios relative to the two previous years (446:1 (June), 853:1 (July) 637:1 (August) of 2010). The NH_4^+ (mgL^{-1}) increased from June 2010 (0.007mgL^{-1}) through July (0.013mgL^{-1}) and August (0.02mgL^{-1}). Similarly, the NO_3^- concentration decreased from 1.91mgL^{-1} during June to 1.51mgL^{-1} during July 2010, before increasing slightly during the August of 2010 (1.57mgL^{-1}).

However, the TP concentrations increased from June to July 2010 (0.013mgL^{-1} to 0.022mgL^{-1}), indicating to an increase in TP concentration during the summer as being key to the summer TN:TP ratios of 2010. Therefore, TP drove the TN:TP ratios and the NH_4^+ concentration drove the NO_3^-: NH_4^+ ratio.

2.3.4.1.5. Model addressing geosmin (ng L^{-1}) (2008-2010) as a function.

Geosmin data were not normally distributed (Shapiro-Wilks P<0.05) and were therefore transformed using Tukey's ladder of power for LM analyses.

No significant association was determined between geosmin and any of the variables analysed.

2.3.4.2. Chlorophyll-a 1990 to 1999 and 2000 to 2009.

2.3.4.2.1. Data analysis

Historical data indicated a decrease in the number of chlorophyll-a (µg/ml) post 2000 (figure 3.5.1) (15.12 cells/ml $^{-1}$ ± 17.3) which is significantly different from chlorophyll-a counts pre-2000 (1990-1999) (4.13µg/ml ± 3.38), (P<0.001). The chlorophyll-a count decreased in both magnitude and duration (Figure 2.3.4.2.1.1).

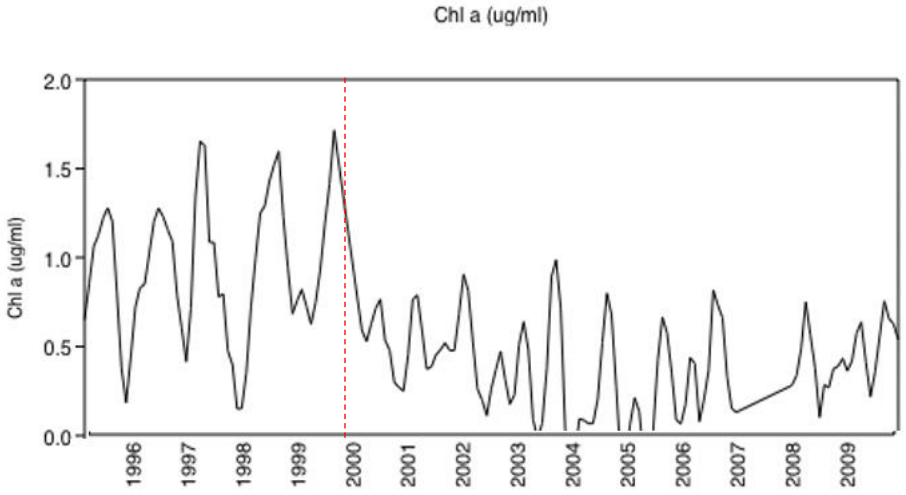

Figure 2.3.4.2.1.1. Chlorophyll-a counts pre vs post 2000.

The chlorophyll-a data suggested that the combination of water from three depths (top, middle and bottom gates) along the water column significantly negatively influenced the chlorophyll-a counts through abstracting more water from the deepest gate.

2.3.4.2.2. Model addressing chlorophyll-a (1990 to 1999) as a function.

To proceed with the LM analysis, the not normally distributed chlorophyll-a data were log-transformed. No association was determined for chlorophyll-a with the independent variables analysed.

2.3.4.3. Model addressing chlorophyll-a (2000 to 2009) as a function.

Following analysis, no association was determined for chlorophyll-a with the independent variables analysed, indicating to the dependence upon an unanalysed factor(s)/variable(s) having a greater influence upon the establishment of algae.

2.3.4.4. Analysis of cyanobacteria (cfu/ml) (1989-1999) data.

Significant differences in cyanobacterial counts were recorded between the annual total counts (cfu/ml) of 1990 and 1993 (Figure 2.3.4.4.1.1) where 27930cfu/ml (2328cfu/ml ± 4399) was the highest recorded annual total (1990) and 5855cfu/ml (488cfu/ml ± 1465) was the lowest recorded (1991).

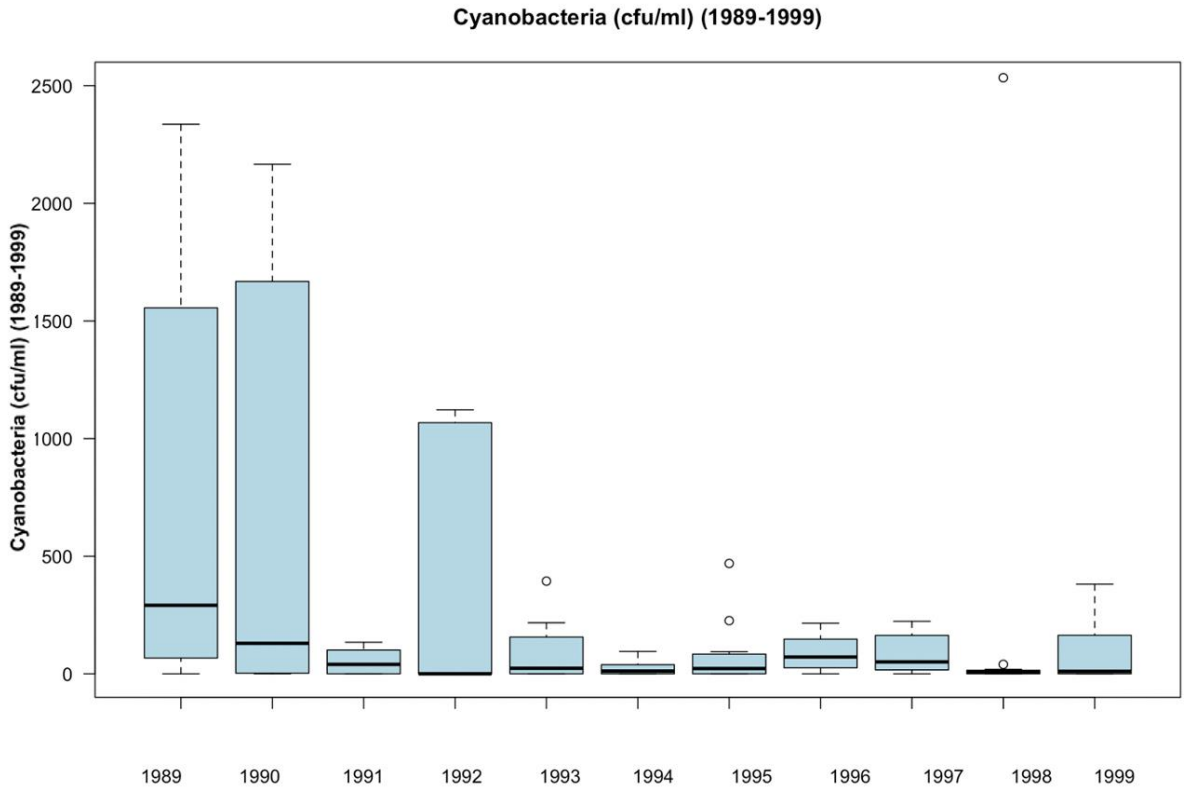

Figure 2.3.4.4.1.1. Median annual cyanobacterial count (cfu/ml) from 1989 through 1999.

Additionally, significant differences in cyanobacterial counts were identified for data between 1997 and 1998. The total number of cyanobacterial cells isolated throughout 1997 attained 12507cfu/ml (1042cfu/ml ± 2389) compared with 2637cfu/ml throughout 1998 (220 ± 698). No geosmin data were available for this time period.

2.3.4.4.2. Primary Component Analysis (PCA) of cyanobacteria data to determine correlations with other variables

Cyanobacteria data were not normally distributed and remained not normally distributed following transformation attempts using log, square-root, cube, log and Tukey's ladder of power. Consequently, GLM/LM analysis was not completed due to the high degree of skewed or absent data. Therefore, only PC analysis was completed.

PC analysis (Figure 2.3.4.4.2.1) indicated to a high cyanobacterial count in the presence of a decreased TN, TP NO_3^- concentrations and raised temperatures and pH.

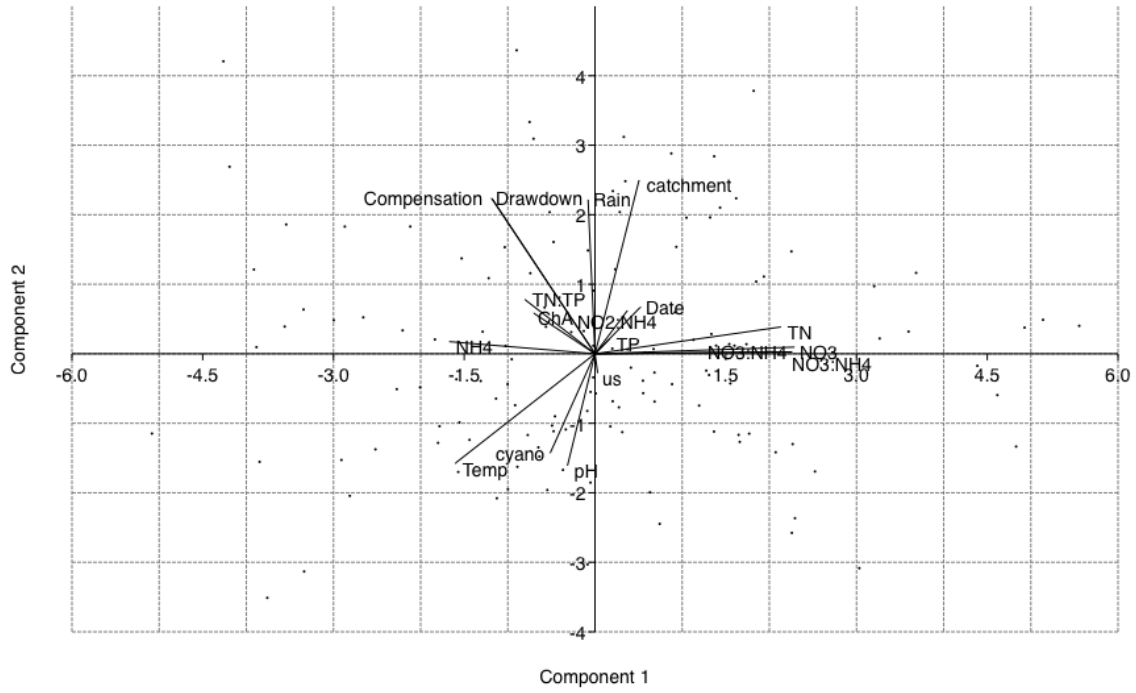

Figure 2.3.4.4.2.1. PCA plot using component 1 (24% of the variation) and component 2 (13.4% of the variation).

2.3.4.4.3. Cyanobacterial one-month displacement data (1989-1999).

The data showed a higher degree of significant association (lower P value highlighted in red) between more key variables when cyanobacterial cell numbers were analysed alongside variables collected in the displaced analysis than data analysed in real time (Table 2.3.4.4.3.1). The tau value indicated the relationship (whether positive or negative) between the two variables.

Table 2.3.4.4.3.1 Kendall's Tau ~ Cyanobacterial cell numbers. The most significant associations are highlighted in table 2.6 with p-values <=0.001 (red), the variables sharing a less significant association with p-values 0.01-0.002 (orange) and variables with the least significant association with p-values 0.05-0.02 (green). No association is highlighted in black text. No geosmin data were available.

Variable	P value (real-time)	P value (displaced analysis)
NO_3^- (mg L^{-1})	0.00007 (tau= -0.26)	0.00018 (tau= -0.25)
NO_2^- (mg L^{-1})	0.004 (tau= 0.19)	0.79 (tau= 0.01)
TN (mg L^{-1})	0.0069 (tau= -0.16)	0.003 (tau= -0.21)
TON (mg L^{-1})	0.6 (tau= -0.03)	0.026 (tau = -0.14)
NH_4^+ (mg L^{-1})	0.018 (tau= 0.15)	0.0007 (tau= 0.22)
NO_3^-: NH_4^+ (mol/ml)	0.01 (tau= -0.16)	0.0003 (tau = -0.24)
Temperature (°C)	0.00007 (tau=0.25)	0.031 (tau= 0.13)

The tau value for the relationship between cyanobacteria and correlated variables were low (≤ 0.26) indicating a weak relationship with each variable. The most significant correlations with cyanobacteria data was that with NO_3^- data both in real-time and displaced.

A negative relationship existed between cyanobacteria and NO_3^- and TN, TON and the NO_3^-: NH_4^+ ratio due to the significance of NO_3^- data upon the latter variables. However, a positive correlation was indicated between cyanobacteria and NH_4^+, with a greater correlation and higher tau value when analysing the displaced data. The data suggested that increased NH_4^+ concentrations may indicate a potential for increased cyanobacterial abundance and a decreased NO_3^-: NH_4^+ ratio during the following four weeks.

A positive correlation was determined for cyanobacterial numbers with water temperature, with a higher significance and tau value when using real-time data.

2.3.4.4.4. Cyanobacterial one-month displacement data (2001-2010).

The geosmin data showed significant correlation (Table 2.3.4.4.4.1) with environmental factors using both real time and displaced data. There was a higher correlation with real time data than displaced data but both scenarios demonstrated a negative relationship with carbon.

Table 2.3.4.4.4.1 Kendall's Tau ~ Geosmin (ngL^{-1}). The most significant associations are highlighted in table 2.6 with p-values <=0.001 (red), the variables sharing a less significant association with p-values 0.01-0.002 (orange) and variables with the least significant association with p-values 0.05-0.02 (green). Absence of a significant association is highlighted in black text.

Variable	P value (real-time)	P value (displaced analysis)
Conductivity	0.04 (tau=0.18)	0.06 (tau=0.16)
Catchment inflow	0.05 (tau=0.17)	0.2 (tau=0.1)
Reservoir level	0.001 (tau=-0.28)	4.678e-06 (tau=-0.39)
Compensation flow	0.001 (tau=-0.28)	1.346e-05 (tau=-0.37)
Chlorophyll-a	0.001 (tau=0.3)	0.3 (tau=0.08)
NO_3^-: NH_4^+	0.14 (tau=0.13)	0.008 (tau=0.23)
NH_4^+	0.2 (tau=-0.1)	0.008 (tau=-0.23)

The data suggested that the analysis of 1-month displacement data provided a significant association for geosmin with some environmental data (Reservoir level, compensation flow) than that of real-time data. The association between geosmin and NH_4^+ and the NO_3^-: NH_4^+ ratio was also more significant when analysed 1 month prior to geosmin production. However, real-time reservoir level and catchment inflow data were more significantly associated with geosmin concentrations than displaced analysis.

2.4. Discussion.

2.4.1. Overall findings

The changes to the raw water abstraction process caused by faulty mechanisms within the water tower significantly changed the quality of water abstracted from the reservoir as indicated by the data following the year 2000 relative to that before the process change. This was reflected in the significant differences in data for variables including temperature, nitrate and pH, suggesting the differences were due to the abstraction process and could not be associated with climate change. An increase in water temperature was not observed over the

period represented by the data, indicating that climate change was not responsible for increasing water temperature nor significantly affecting the volume of rainfall during the summer nor winter between 1984 through 2016. However, the reduction in temperature ranges recorded post-2000 suggested that the abstraction process following the failure of the tower was likely responsible for the changes to water temperature data recorded. Therefore, neither the water temperature nor pH data could not be relied upon as an indicator of climate change within Llandegfedd Reservoir with a malfunctioning abstraction tower.

It is likely that the cyclic decrease and inundation of the reservoir affected the TP concentration within the reservoir, but the TP concentrations were also dependent upon other variables including iron and was also dependent upon the year in which the data was accumulated.

Periods of increased rainfall volume was significantly negatively associated with nitrate concentration, but no significant association was determined for rainfall with ammonium concentrations nor the NO_3^-: NH_4^+ ratio.

2.4.2. Pre-and post-2000 data comparisons

The consequence of a faulty abstraction system at the tower within the reservoir whereby water is removed at three vertical locations simultaneously was reflected within the data.

Water abstraction before the year 2000 was active at specific gates which were selected for the water quality parameters anticipated to exert minimal impact upon filters and treatment processes. Conversely, water abstracted post-2000 was removed via all three gates simultaneously, thereby including water from all three gate depths, predominantly the bottom region.

Analyses comparing pre- with post-2000 data indicated a significant change to pH, water temperature, chlorophyll-a and nitrate variables. The data indicated that more water was likely to have been abstracted from the bottom section of the reservoir (gate 3) than from the surface (gate 1). This is due to the influence of water pressure upon the flow of water through the abstraction system.

The depth of each gate has been estimated to be 8m meters apart, with the first gate 8m below the surface of the reservoir while at full capacity. The following equation was used to determine the difference in water pressure at gate 1 and gate 3.

P=hpg

Where P=water pressure (kPa), h=depth (m), p=density of water (Kg/M^3), g=the acceleration due to Earths' gravity ($9.80m/s^2$) (Rice University).

The water pressure at the bottom gate (235.2kPa) is three times greater than that at the surface gate (78.4kPa). As flow rate increases with increased pressure, more water is removed from the reservoir via the bottom gate than the surface gate (gate 1).

The water temperature, pH, NO_3^-: NH_4^+, nitrate and chlorophyll-a data all recorded a significant decrease in values post-2000 compared to those obtained before the tower malfunction.

TP data indicated that the mixing of the water columns resulted in very little deviations from what was recorded during the period before the year 2000 compared with data following the year 2000 due to insignificant differences between the pre-and post-2000 TP concentration data. The data suggested that TP may have been uniformly distributed throughout the water column.

A reduction in TP during the summer compared with that of the winter months indicated no significant association with rainfall. Therefore, the data suggested that internal retention and release of TP was the main P-loading and storage process at Llandegfedd reservoir.

The analysis also indicated a change in the NO_3^-: NH_4^+ data pre-compared with post-2000, suggesting that the change to the abstraction process may have influenced the data. The lower ratios are preferred by cyanobacteria due to their ability to fix nitrogen, and their preference for energy-saving NH_4^+-N assimilation over energy-consuming NO_3^- (Riegman *et al.,* 1992, Hallegraeff 1993, Riegman 1995, McCarthy *et al.,* 2009, Gilbert *et al.,* 2016, Ruan *et al.*, 2017), therefore lower N concentrations are likely to result in an increased cyanobacterial bloom frequency.

A significant decrease in NO_3^- concentrations were recorded during both the summer and winter periods post 2000 compared with that before the year 2000, suggesting that changes to water abstraction methods from the reservoir may have affected recorded NO_3^- concentrations by abstracting predominantly from the bottom zone where oxygen concentrations may have been lower relative to that at the surface during periods of stratification. Beutel (2003), stated that a thermocline reduces the degree of nutrient mixing

between the hypolimnion and epilimnion, trapping nutrients within the section of the water column, with the vertical distribution of water temperature and DO concentrations significantly influencing ammonium and nitrate distribution.

NH_4^+ distribution appeared to have been more evenly distributed throughout the depths of the reservoir than nitrate as indicated by the absence of significant difference in the NH_4^+ concentration before and following the year 2000. Ubiquitous ammonium concentrations throughout a reservoir was determined by Kim *et al.,* (2006), who determined that an absence of nutrient consumption by surface-dwelling phytoplankton contributed to the accumulation of ammonium throughout the reservoir.

Nitrification and denitrification processes can significantly influence the ammonium and nitrate concentration in the surface and bottom zones, resulting in concentrations that are opposite to each other (Wall *et al*., 2005). The nitrification and ammonification process in the post-2000 data was indicated by the persistence of nitrate and ammonium (Sun *et al.*, 2018) and therefore, primary productivity was active. However, insignificant changes to the ammonium concentrations pre-and post-2000 such as those recorded at Llandegfedd Reservoir were also identified by Wall *et al.,* (2005) who determined that it may in part be due to absence of DO at the bottom zone, leading to an increase in the concentrations of ammonium released from the sediment (Wall *et al*., 2005), and due to ammonification occurring in the bottom zone.

The data suggested that NO_3^- was higher in concentration at the surface of the reservoir during both the winter and summer periods and not uniformly distributed throughout the water column; however, its detectable concentrations within the following the year 2000 during the summer period indicated the presence of oxygen in the bottom zone (Garnier *et al.,* 2000).

The air temperature and primary productivity significantly determines the water pH, the finding which were mirrored by several studies (Koinig *et al.,* 1998; Wang *et al.,* 2019). Higher CO_2 concentrations because of increased productivity decreases the pH of the water following the formation of carboxylic acid. Alternatively, the pH may remain elevated in the bottom zone due to CO_2 formation and retention following the formation of thermal stratification. A decrease in the pH as a consequence of primary production is more notable within the bottom regions, particularly during periods of stratification (Xue *et al.,* 2017), and a period of high productivity, but are typically higher at the water surface and during the

winter (reduced productivity) (Pfister *et al.,* 2019). The data indicated the abstraction of primarily surface water during the summer periods before the year 2000 where the pH trend increased during periods of primary productivity, suggesting the CO_2 escaped into the atmosphere during a period of mixing if primary production occurs close to the surface, increasing the water pH (Wang *et al*., 2019).

Data obtained following the year 2000 indicated more typical alternating pattern between pH and temperature, supporting the theory of a decreased pH during the summer period (Xue *et al*., 2017), indicating that abstraction predominantly occurred from the bottom zone where CO_2 may have been trapped due to stratification. Therefore, in the absence of abstraction depth records, it is likely that most of the abstraction through the tower before the year 2000 occurred at the surface. Additionally, water mixing following the year 2000 is likely to constitute a majority of bottom water.

The mixing of the water from all depths as a consequence of tower failure post-2000 led to a decrease in both the lower and upper-temperature range data. Miller *et al.,* (2013), determined that the aerated bottom and intermediate waters were more likely to retain gaseous by-products as a consequence of increased productivity during the summer period and the cooler temperatures compared with that at the surface. The damaged water tower directly affected the pH data, with the true pH at each gate level throughout the water column masked as a consequence of water column mixing following abstraction.

2.4.3. Nutrient and environmental data.

The historical data indicated that an insignificant change in average annual rainfall volume had occurred from 1990 through 2009.

Lower reservoir levels and lower rainfall volume/frequency resulted in increased NO_3^-, leading to a higher NO_3^- : NH_4^+ ratio and a lower potential for geosmin production. Conversely, an increase of NH_4^+ would be expected during the winter periods upon the return of the reservoir to full capacity and in periods of heavy rainfall events during the summer. The refilling process typically begins during late summer, thereby increasing the NH_4^+ concentrations during the warm season. This may instigate a higher concentration of geosmin during the autumn. LM analysis determined a weak negative association between nitrate and rainfall, indicating to the potential for the nitrate concentrations to be negatively affected by increased precipitation at Llandegfedd reservoir.

The average monthly frequency and volume of rainfall insignificantly increased since 2000. The mean volume of rain during the winter periods insignificantly decreased, and summer mean volume of rain insignificantly increased. LM analysis determined no significant association of both 1990-1999 and 2000-2009 rainfall data with any of the variables analysed which was contrary to that determined by Li *et al.,* (2015), and Reichwaldt & Ghadouani, (2012), who determined that heavy spring/summer rainfall fuelled cyanobacteria blooms within a reservoir following an increase in terrestrial-borne nutrients entrained within inflow. However, periods of heavier summer rainfall at Llandegfedd reservoir did not correlate with increased nutrients nor cyanobacterial/algal cell counts within the reservoir (Reichwaldt *et al.,* 2012).

The increase in geosmin concentrations between 2008 and 2010 during a period of decreasing TP and increasing NH_4^+ indicated the potential increased P demand by organisms within the reservoir for assimilation for the production and maintenance of cellular constituents. The increased spring NH_4^+ concentrations during 2010 relative to the spring season of the two previous years introduced the opportunity for an increased growth rate of cyanobacteria during the summer period. The decrease in NH_4^+ concentrations concurrent with increased geosmin concentrations during June 2010 indicated the senescence of a high number of cyanobacterial cells, while the continuing decreasing NH_4^+ concentration through August 2010 and continuation of a high geosmin concentration suggested that NH_4^+ assimilation was continuing alongside cyanobacterial senescence.

The data suggested that the higher concentration of NH_4^+ during the spring may have been in part due to anoxic conditions at the sediment and provided sufficient nitrogen in the form of NH_4^+, assimilation of which requires less energy by cyanobacteria than that of oxidised nitrogen (Watzer, 2019). Cavanaugh, (2006), determined that excess NH_4^+ release from N-fixing cells contributed towards the NH_4^+ concentrations within the water following cellular lysis, while Adam *et al*., (2016), concluded that the released ammonium is quickly assimilated by phytoplankton surrounding lysed cells (Adam *et al.*, 2016).

At Llandegfedd reservoir, the NH_4^+ significantly contributed towards the TN:TP ratio. A study by Cavanaugh (2006) also concluded that ammonium concentrations were significant in the determination of the TN:TP ratio and may have influenced cyanobacterial development and metabolic pathways (geosmin production) during periods of low NO_3^-: NH_4^+ ratio (during periods of raised reservoir level) (Cavanaugh, 2006). Therefore, geosmin concentrations may

be anticipated to increase during periods where the NO_3^-: NH_4^+ ratio is low, which was during periods of the reservoir is at or near its full capacity.

2.4.4. Variable associations.

LM analysis of water temperature data from 1984 through 2016 confirmed significant negative associations with TN. The data suggested that periods of higher temperatures were accompanied by decreased concentrations of nitrate in the reservoir. The analysis indicated lower concentrations of nitrate within the reservoir, likely decreased following reduction by cyanobacterial/algae, accompanied by a reduction in rainfall through the summer period may have led to a decrease in nitrate entering the reservoir through run-off.

Water temperature data from 1984 through 1999 determined a significantly negative association with TN concentration (specifically nitrate) and catchment inflow, with a positive association with conductivity. The data suggested that a reduction in nitrate concentrations were most frequently recorded during the summer period. Reservoir stratification during the summer is likely to have led to anoxic conditions within the bottom region, (potentially dominated by reduced-N), whereas surface regions are most likely to hold an increased concentration of nitrate relative to the bottom regions as a consequence of an increased availability of oxygen, leading to nitrification. Therefore, the data indicated that the most predominant depth of abstraction before the year 2000 was via the bottom gate (gate 3).

A negative association of water temperature with catchment inflow was determined during periods of increased temperatures pre-2000. This suggests that rainfall volume was lower during the summer periods before the year 2000 compared with that post-2000, which is also reflected in the rainfall data.

The analysis of water temperature from 2000 through 2016 determined a significant negative association with pH and catchment inflow, but a significant positive association with reservoir level, ammonium and conductivity. It is likely that the reservoir water abstraction method is the cause of the negative association with pH post-2000. Despite the effect of abstraction method change not altering the water temperature cycle but instead reducing the upper and lower temperature ranges, the inability to actively select abstraction depth post-2000 resulted in an increase in the volume of bottom water abstracted relative to the surface and intermediate waters. This likely skewed the water quality data post abstraction. The comparably stable method of abstraction post-2000 resulted in pH analysis of water from the

same depths, with changes to the abstraction depth seen during periods of lower reservoir levels whereby a reduced pressure from the reservoir surface resulted in an increase in water flow through the surface and intermediate gates. The absence of a significant association of water temperature with pH indicates to the frequent alternation between abstraction gates throughout the year, leading to pH values representing specific depths of water. Likewise, the positive association between water temperature and ammonium is likely due to an increase in the volume of bottom water abstraction compared with that of the other gates during periods of warmer weather. Concurrently, the negative association with catchment inflow volume indicated a reduction in precipitation during the summer period.

Despite the concentrations of TP not significantly changing as a consequence of tower failure as determined by pre-versus post-2000 association, other variables altered when comparing those from pre- and post-2000 TP data. Before the tower failure, no significant association was determined for TP with any of the variables analysed, indicating the requirement for a wider spread of variables to be studied to help determine significant influences upon the TP concentration.

However, analysis of post-2000 data (2008-2012) determined a significant relationship for TP with the year of sampling, the TN:TP ratio, Fe concentrations and reservoir level. The positive association of TP with the year of sampling suggested that the TP concentration increased with time.

The positive relationship between TP and Fe concentrations indicated the increased concentrations of Fe within the water during periods of increased P within the water. The data indicated that Fe-P release within the sediment is contributing more significantly to internal P-loading each year.

The direct negative effect of TP upon the TN:TP ratio post-2000 indicated the increased influence the TP concentration had upon the ratio compared with that prior to the year 2000 where no significant associations were determined. The molar TP concentrations were low throughout the sampling period at Llandegfedd reservoir compared with that of TN. The decreasing molar concentrations of TN post-2000 accompanied by the relatively constant TP concentrations resulted in TP having a greater influence upon the TN:TP ratio. The TN concentration likely decreased as a consequence of abstraction method change during 2000, where an increase in reduced-N was abstracted compared with oxidised-N post abstraction because of a greater majority of water abstracted being from the anoxic bottom zone. Nitrate

composed the majority of the TN (98%), therefore processes affecting the uptake of nitrate significantly affected the overall TN value. The data indicated that the ammonium had a greater influence upon the TN:TP ratio during periods of low TN:TP concentrations.

Likewise, ammonium was significantly negatively associated with NO_3^-: NH_4^+ and NO_3^-. An increase in ammonium concentration led to a decrease in the NO_3^-: NH_4^+ ratio and an increased potential for rapid cyanobacterial growth. A decrease in TON and concurrent stability in NH_4^+ suggest that less nitrification was taking place within the reservoir (De Groot *et al.,* 1993). The relatively higher cyclic NH_4^+ may indicate a continual N-reduction by bottom bacteria while a fall in N may suggest that the bank sediment-stored-N may have decreased, thereby reducing the amount of N available for oxidation.

The cyanobacterial counts displacement data association with variables such as ammonium may have indicated the development of a bloom several weeks prior to its formation, whereas other variables such as nitrate concentrations may be more relevant to the cyanobacterial bloom during real-time analyses. However, this information may be misleading due to an increased concentration of nitrate at the surface during periods of warmer weather coinciding with cyanobacterial blooms, some of which also occur at the water surface. The displaced ammonium data a month prior to a cyanobacterial bloom may indicate to ammonium assimilation during periods of the cyanobacterial growth phase.

A more significant association for geosmin with chlorophyll-a, catchment inflow volume and conductivity was determined when considering data abstracted during real-time sampling compared with that obtained several weeks prior. The data suggested that the inflow in real-time had a direct effect upon cellular lysis, thereby releasing the geosmin into the reservoir. In addition, an increase in nutrients would likely increase competition from algae, leading to an increase in chlorophyll-a.

Displaced analysis indicated lower ammonium concentrations coinciding with an increase in geosmin concentrations one month later, suggesting ammonium assimilation led to rapid cyanobacterial growth. The absence of a correlation between geosmin concentrations and cyanobacterial cells indicated their absence during periods of geosmin release, which is concurrent with cell lysis and subsequent geosmin release.

2.5. Conclusions

The hydrology of a reservoir is complex with a high degree of variability, and water levels fluctuate on an annual basis (Ford, 1990; Nowlin *et al.,* 2004), due to anthropogenic manipulation of in- and outflows.

The reliance upon water quality data obtained through sampling post reservoir abstraction led to inaccurate and misleading data for key variables including temperature, pH, nitrate, chlorophyll-a, geosmin and cyanobacteria. Data obtained prior to and following the year 2000 were misleading and did not represent conditions within the reservoir either as a whole or as sections within the water column.

Consequently, vital data for ongoing water quality analysis and prediction modelling will remain unavailable, restricting improvements to water quality management at the site. This may lead to missed opportunities to monitor water quality, decreasing the opportunity to react to a T&O event at the earliest opportunity. The information supports the hypothesis that a suitable sampling method is vital to obtain reliable data representative of the water quality at both surface and bottom sites along the transect of the reservoir. In addition, the significant positive association of the reservoir level with TP supported the hypothesis that TP concentrations increase during a period of increasing reservoir level. Therefore, higher concentrations of TP are likely to be recorded during the late summer/ autumnal seasons and is in part dependent upon the phase of reservoir refill.

An increase in the rainfall volume was associated with a decrease in the concentration of NO_3^- within the reservoir. As the rainfall is forecast to become more frequent and intense during the winter period, indications are that the NO_3^- will decrease further, resulting in a low NO_3^-: NH_4^+ ratio during the early spring. Concurrently the NH_4^+ concentrations remained insignificantly changed; therefore, the hypothesis that ammonium concentration will be significantly positively associated with increased rainfall volume must be rejected.

Geosmin production is less likely to occur during low drawdown events but may be triggered upon the return of the reservoir water level to maximum volume during the autumn or during the summer following an increase in reservoir level and periods of increased rainfall consequently leading lower NO_3^-: NH_4^+ ratios.

With the reduction in abstraction (reduced flow) anticipated at the reservoir, coupled with increased temperatures and rainfall intensities during the summer, the water quality at

Llandegfedd is likely to deteriorate through increased geosmin production and cyanobacterial dominance.

Chapter 3: Time-series monthly phosphorous, nutrient and environmental analysis over an 11-month period.

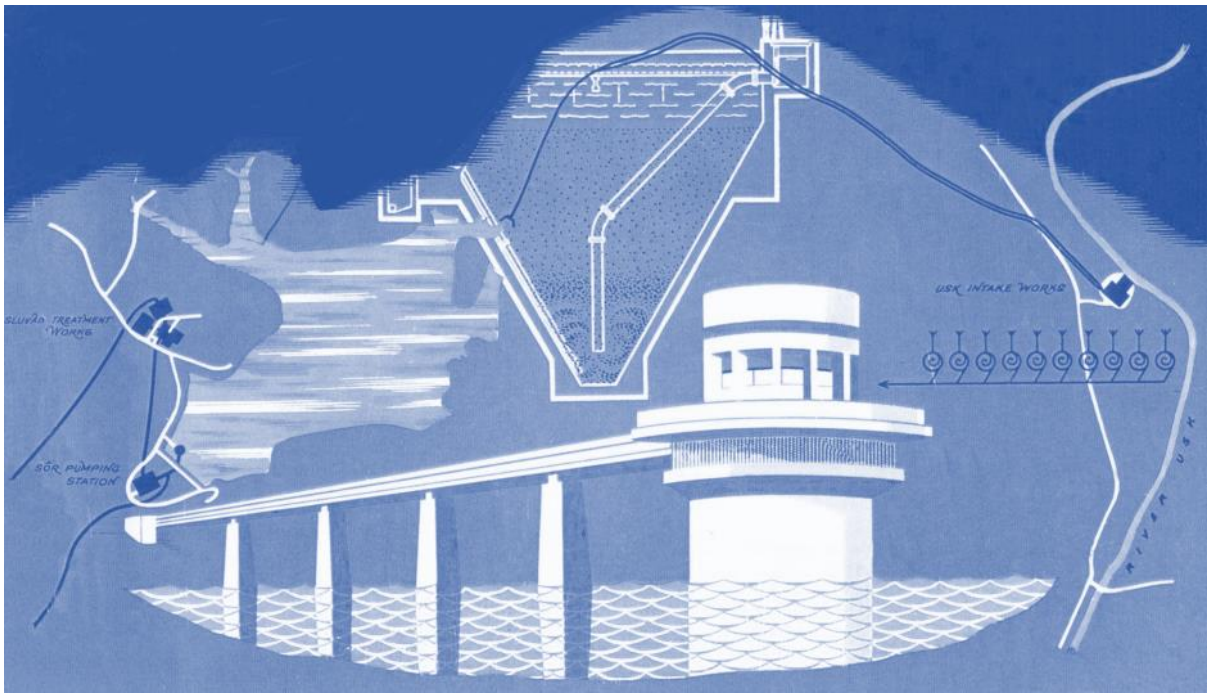

3.1. Introduction to time-series analysis of monthly sampling – main summary of chapter.

Time-series analysis of reservoir variable data can lead to production and management decisions which may result in a reduction in treatment costs and customer complaints through pre-empting potential geosmin production. Variations in inflow frequency and volume, weather and storm events, accompanied by climate change, result in uncertainty with regards to the dynamic water quality throughout the seasons (Zhang *et al.,* 2019).

Data collected over several seasons can contribute towards the forecasting of water quality within a reservoir during various environmental and inflow scenarios, further contributing towards the ability to pre-empt water quality deterioration (Majumdar and Ramesh, 1997).

This chapter focused upon the dynamics of nutrients such as phosphorous and nitrogen and their fractions in varying environmental conditions over the course of 11 months. In addition, the response of cyanobacteria and green algae to the nutrients and changing conditions were assessed, along with the effect of meteorological conditions upon characteristics of the reservoir.

The main findings of the chapter:

- AHP was the predominant fraction of P throughout the reservoir over the 11-month sampling period.
- Site B4 Recorded the highest concentration of AHP during January, organic-P and OP during February and the P-fractions consisted of condensed -P during May, June and August. Both the bottom and surface sites recorded the highest TP concentrations during August.
- Geosmin was detected within the reservoir throughout the 11-month sampling period with the highest concentrations detected during May, indicating to the spring as being the period of highest taste and odour (T&O) failure risk to DCWW.

3.1.1. P-fractions and their interaction withing the reservoir.

P concentrations within a reservoir vary throughout the year in response to seasonal parameters and are also dependent upon the interaction with aquatic organisms, environmental conditions and anthropogenic activities. Typically, three P-fractions are of interest during nutrient analysis in reservoirs; AHP (Acid Hydrolysable Phosphorous), organic

P (Org-P) and orthophosphate (OP (PO_4^{3-})). P-fractions are interlinked, but not all fractions are instantly available for uptake by biota (Moore, 1994).

The P can either be retained within cyanobacteria as a form of luxury uptake (condensed-P), become temporarily or permanently bound to the sediment, hydrolysed by cyanobacteria producing APase (Petterson, 1998; Moore, 1994), or released following bacterial lysis. P release from organic matter during its degradation can promote phytoplankton growth, increasing phytoplankton biomass and depleting DO concentrations (Yu *et al.,* 2020). The determination of AP activity can indicate the degree of P limitation.

Organic phosphorus concentrations decrease with depth during warmer periods, indicating that degradation of the organic matter occurs during the process of deposition (Yu *et al*., 2020).

Acid Hydrolysable Phosphorous (AHP) is a fraction of potentially bioavailable P following its hydrolysis by naturally occurring substances and environmental conditions (Boström *et al.,* 1988). AHP comprises OP and condensed-P, (polyphosphates, and metaphosphates), formed by condensation of two or more OP groups.

Orthophosphate is a fraction of P readily available for assimilation by cyanobacteria. Orthophosphate is available by release from lysed bacterial cells, internal P loading, run-off into reservoirs carrying excess fertiliser from land and through the hydrolysis of polyphosphates. The phosphorus released from cyanobacteria during the death phase is one of the most critical steps in the lake P-biogeochemical cycle (Zhang *et al.,* 2018).

Condensed phosphates are the most abundant fraction of phosphates in natural waters (Boström *et al.,* 1988). Some microorganisms capable of luxury P uptake can store orthophosphate as polyphosphate (She *et al.*, 2019) in conditions of excess P, therefore the real-time concentration of orthophosphate within the reservoir may not accurately reflect the risk of a cyanobacterial bloom.

The ability to store poly-P is coupled with the ability to hydrolyse poly-P during periods of P-deficiency, providing a competitive advantage during periods of P-limitation and allowing growth to continue (Ma *et al.,* 2016), during periods of P-limitation within the reservoir.

The water level at the Llandegfedd reservoir is governed by several factors, all of which vary throughout the year. The principal drivers in determining water level are public demand and water abstraction volumes and frequencies. Typically, water demand increases as a response

to rising temperatures during the summer period. Conversely, the abstraction law prevents or severely limits the volume and frequency of abstraction from the River Usk during the summer period. The combination of supply restrictions and public demand during the summer months leads to a reduction in the water level. Consequently, greater areas of sediment are exposed at the periphery, and water retention time is increased.

3.1.2. *Ammonium transformations within a reservoir*

Nitrogen fractions are dynamic within a reservoir in response to prevailing water quality conditions and microbiological species present (Figure 3.1.2.1).

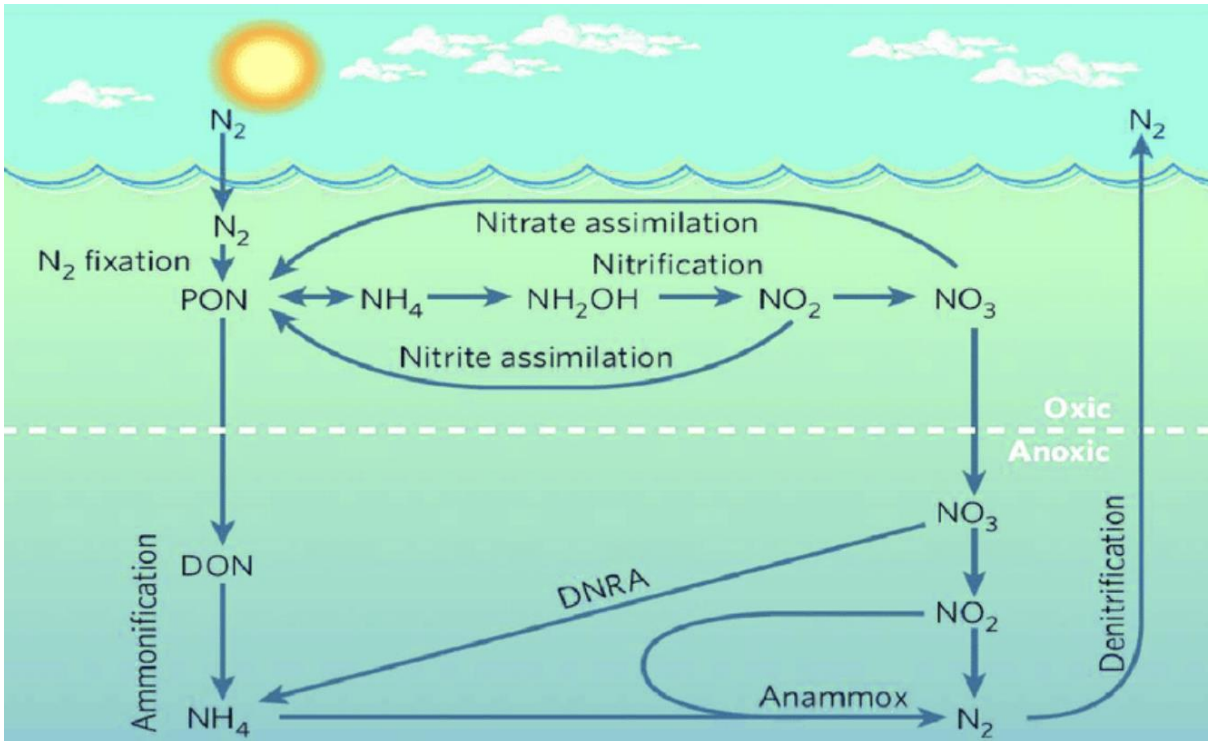

Figure 3.1.2.1. Oxic and anoxic processes of nitrogen fraction cycle (Winkel, 2013).

Ammonium may be made available to phytoplankton through several pathways. Conditions at the sediment-water interface is critical in the release of ammonium from the sediment. The conversion of nitrate to ammonium increases with decreasing redox potential (Kaspar *et al.,* 1981). Anoxic conditions may lead to the release of ammonium from within the sediment as a consequence of a change to the redox conditions. Ammonium can build up within the sediment following the loss or absence of biological nitrification and a decrease in ammonium assimilation by anaerobic microorganisms (Beutel, 2006). The rise in ammonium

concentrations may further fuel benthic microbial activity or instigate a second cyanobacterial bloom within the surface water following turnover during late summer/early autumn.

3.1.3. Aim of this chapter.

In this chapter, the water characteristics (Table 3.2.5.1.) at Llandegfedd reservoir were addressed over a sampling period of 11 months at four surface and bottom sites from the southern to the northern section of the reservoir in addition to cross-site analyses for each month of sampling. The P-fraction concentrations were used to determine water quality status of the reservoir.

This chapter addresses the following overarching and sub-hypotheses:

Overarching hypothesis: The northern sampling sites (sites 3 and 4) shall be of a higher risk to water quality as a consequence an increased volume of allochthonous P input than the southern sites (sites 1 and 2).

Sub-hypotheses:

1. Phosphorous concentrations shall be at their lowest during the winter period.
2. There will be no significant association between P-fraction concentrations and the nutrients or environmental data.

3.1.4. Environmental conditions of site during the study period.

The study period of January 2018 through November 2018 saw extreme dry conditions through the months of May, June and July where high daily air temperatures were maintained (>20˚C) (source: Met Office).

Precipitation was lower during the month of June 2018 than recorded during 2017 and 2016 (source: Met Office). However, no significant differences were observed in total rainfall nor temperature between years (2016-2018).

No significant difference was recorded in the reservoir level between years. However, Maximum reservoir level for 2018 was attained during March and began to fall during April. Conversely, maximum reservoir level for 2016 was attained during the month of April and maintained through until July.

3.2 materials and methods

3.2.1 Sampling methods

Water column samples were collected on a fortnightly basis throughout 2018, except where weather conditions prevented access to the reservoir (March through April). Surface samples were collected at four sites along the transect of the reservoir and bottom water samples were collected using a Van Dorn depth sampler at between 0.5-1 m from the bottom. An EXO Sonde (handheld model 4P Sonde SN 16J104715, pH probe (SN 16J104328), ODO probe (16J103539), turbidity probe (SN 16J102916), CT probe (SN 16J104738), depth (SN 16J102280)) was used at each location to predetermine the depth. Samples were returned to the laboratory for P analysis (Cardiff University) and nutrient and environmental (pH, reduced N, oxidised N, conductivity, cyanobacteria data, green algae data and turbidity) analysis (DCWW). Data collected by the Sonde (pH, temperature, depth, DO and turbidity) were uploaded by DCWW (Appendix 1).

Water samples were analysed at DCWW laboratories for nutrients using the Thermo Scientific Aquakem 600. To prepare the ammonia/nitrite standard stocks, the specific concentration of solution (e.g., 1ml of ammonia as N 1000mg/L and 1ml of nitrite as N 1000mg/L) was pipetted into a flask containing RO water. The flasks were inverted several times and the solution is transferred to a 100ml plastic bottle. Ammonia, phosphate, TON and nitrate stocks were prepared before hand by the supplier. A serial dilution of stocks was prepared using the solution. All samples were recorded on the DCWW LIMS system. The samples and stocks were loaded into the respective instrument following the calibration guidelines issued by the manufacturers. Dŵr Cymru Welsh Water nutrient analysis methods are presented in Appendix 1 (A1).

3.2.2. P fraction analysis.

Unfiltered samples were analysed for orthophosphate (OP), total phosphorus (TP) and acid hydrolysable phosphorus (AHP). When necessary, samples were frozen for storage in acid washed and triple-rinsed polypropylene bottles. The Orthophosphate (OP), Total Phosphate (TP) and Acid Hydrolysable Phosphate (AHP) were analysed on the day proceeding sample collection. The method is presented in Appendix 6 (A6).

3.2.2.1 Orthophosphate (OP)

OP concentration was determined using the ascorbic acid method (APHA, 1995). Ammonium molybdate and potassium antimonyl tartrate react in an acidified medium with orthophosphate to form phosphomolybdic acid. This is reduced with ascorbic acid to form molybdenum blue with the absorbance at 880 nm used to quantify the concentration using a standard curve constructed from a 4-level serial dilution of 10μM potassium di-hydrogen orthophosphate (KH_2PO_4) diluted 1 in 100ml to produce a standard from which a four-fold serial dilution was created and run on a Cary 60 UV-Vis spectrophotometer (Agilent). Reagent 1 (Ammonium molybdate and potassium antimonyl tartrate) was made through adding 10 ml sulphuric acid (250ml of Sulphuric acid (5N) (2.5M) = 35ml conc H_2SO_4 + 215ml distilled water), with 6ml of ammonium molybdate solution (1g in 25ml distilled water) and 0.1ml of Potassium antimonyl tartrate solution (1.325g Potassium antimonyl tartrate solution in 25ml distilled water).

Reagent 2 (Ascorbic acid) was created through adding 4.2g ascorbic acid in 500ml distilled water and labelled 'Reagent 2'.

Following the creation of the reagents, 6 blanks were run and the instrument set at auto zero, with lowest blank in position 1 and first 5 samples. Following setup, 0.8ml of each sample was added to a cuvette followed by 0.1ml reagent 1 and 0.1ml reagent 2. The results were read at 880nm and recorded.

3.2.2.2. Total Phosphorous (TP)

TP was analysed using persulphate digestion (APHA, 1995). Soluble and insoluble condensed phosphates and organic and inorganic phosphorus species are hydrolysed to OP by the breaking of C-O-P and C-P bonds. A thoroughly mixed sample of 20 ml unfiltered site water was boiled gently for 30 minutes with addition of 0.16 g ammonium persulphate and 0.4 ml sulphuric acid solution. After cooling and neutralisation with sodium hydroxide the OP concentration was determined as before.

3.2.2.3. Acid Hydrolysable Phosphorous (AHP)

AHP concentration was determined after hydrolysis with sulphuric and nitric acids. This is a measurement of condensed phosphates and some organic phosphate compounds. A strong acid solution created through diluting 75ml H_2SO_4 to 150ml in distilled water. 1ml HNO_3 was added and diluted to 250ml. Secondly, 6N Sodium Hydroxide was prepared through adding 24g in 100ml of distilled water. 5ml of each raw sample was diluted in 15ml distilled water and followed by the addition of 1 drop phenolphthalein indicator. On occasions where the sample turned red, concentrated acid solution was added until the colour cleared. 0.3ml concentrated acid solution was then added to each sample in excess. The samples and solutions were then boiled gently for 90 minutes with foil on each tube containing a small hole. The samples were then cooled and neutralised to a faint pink colour with NaOH solution (0.4ml approximately). The samples then underwent colourimetric analysis as for Orthophosphate.

AHP concentration was determined by deducting the OP concentration obtained without acid hydrolysis. The concentration of condensed phosphate was determined using the following equation:

Condensed phosphates = Acid Hydrolysable Phosphorous - Orthophosphate

(Hach, doc TE365)

AHP data was used in all analyses in lieu of Condensed P data due to the inability to differentiate between condensed P fractions.

3.2.2.4. Organic Phosphorous (Org-P)

Organic phosphorus (Org-P) concentration was determined by difference by deducting the OP and AHP concentrations from the TP concentration.

3.2.3. Alkaline Phosphatase Activity (APA)

Alkaline Phosphatase Activity (APA) (method presented in Appendix 7 (A7)) was measured using a modification of the method of Hernandez and Fernandez (1994) and Hernandez and

Whitton (1996) (Whitton, pers. comm.). A 45ml water sample was aliquoted into a 50ml conical flask. pH was adjusted to pH 8.0 or pH 10.3 by the addition of 4 ml of buffer solution (final concentration 50mM). Two buffer solutions were used, N-2-hydroxyethylpiperazine-N-2-ethanesulphonic acid (HEPES) adjusted with sodium hydroxide to pH 8.0 and glycine and sodium hydroxide for pH 10.3. Assays were carried out at both pH 8.0 and pH 10.3 as the former represented the site pH whilst the latter is the standard pH used for APA assay (Whitton, pers. comm.). The substrate was added in the form of 1 ml of p-nitrophenyl phosphate (*p*NPP) solution (final concentration 100 mM). *p*NPP solution consisted of one tablet of *p*NPP dissolved in 10 ml of the appropriate buffer solution. Flasks were sealed leaving a small headspace and incubated at 20 °C in a darkened rotary shaker at 100 rpm for 60 minutes. The assays were terminated after 60 minutes by addition of 5 M sodium hydroxide to increase the pH above 12. Samples were then filtered through Whatman GF/F paper and the absorbance read at 405 nm using the Cary 60 UV-Vis spectrophotometer. Samples were blanked against assays with 45 ml ultra-high purity (UHP) water replacing the site water sample. Activities were calculated as mmol *p*NPP hydrolysed mg^{-1} Chl a h^{-1} using a standard curve of *p*NPP. APA data are presented in Appendix 3h (A3h). APA PCA data are presented in Appendix 3i (A3i).

3.2.4. Data analyses in this chapter.

Site-specific P-fraction concentration analyses over an 11-month period and cross-site bi-monthly analysis of all sites were completed and discussed separately. Statistical analyses of N and P fraction molar ratios were completed for each site over an 11-month period and cross-site monthly analysis of all sites were completed. Site-specific nutrient concentrations and environmental data analyses were completed along with bi-monthly/monthly analyses of all sites.

For data analyses throughout the chapter, the mean value for each parameter per month was determined for each variable accompanied by the standard deviation (SD). Due to small sample sizes ($n<25$) and not normally distributed data exhibiting ties, Kendall's Tau was used to test for associations between two continuous variables and Kruskal-Wallis test to determine significant differences between sets of not normally distributed data. Where data was not normally distributed, but sample size was large ($n>25$) Spearman's rank correlation was used.

Significant associations between variables were determined using General Linear Models (normally distributed data)/Generalised Linear Models (non-normally distributed data even following transformation methods)/Linear Models (where non-normal data were successfully transformed) were completed using R studio (version 3.4.4) following the selection of independent variables demonstrating correlation with the dependent variable as determined through Principal Components Analysis (PCA) analysis using PAST (version 4.03).

Data were standardised to allow cross-variable PCA. Variables were omitted from the PCA during periods of recorded repeated '0' values. The following equation was used for the standardisation to allow for direct data pattern comparisons between variables of differing scales:

$$(X-\mu)/\sigma$$

where X is the observation, μ is the mean and σ is the standard deviation.

Once the list of correlated variables had been determined for each dependent variable, the Shapiro-Wilks test was used to determine normality of data. Data were transformed by log, cube, square-root or Tukey's Ladder of Power where not normally distributed distributions were confirmed. The most suitable transformation method was determined through analysis of histograms and their proximity to a normal distribution using Shapiro-Wilks. Where the most efficient method of data transformation involved Tukey's ladder of power, the selected transformation mode was not indicated. Tukey's ladder of power reduces the effects of homoscedastic data leading to more accurate analysis. The Akaike Information Criterion (AIC) was used to estimate the fit of each model, with the lowest AIC value used to confirm the selection of data transformation links and models (Bozdogan, 1987; Cavanaugh, 2019).

Variables were eliminated from the model as determined by the F-test. Following removal of all unnecessary independent variables, the goodness of fit of the remaining model was tested using diagnostic plots for linear regression analysis to determine whether residuals had a non-linear pattern (Residuals vs Fitted graph), were of a normal distribution (Normal Q-Q graph), heteroscedasticity (scale location graph) and influential outliers (Residual vs Leverage plots (Cook's distance)). Following completion of the model, the data were reported using the intercept result and P value, adjusted R^2 ($^R^2$), F-test for overall model significance (Mangiafico,

2016), and model P value. Any anomalies from the diagnostic plots were reported for the final model. Furthermore, the positive/negative association of the individual parameter associations within the model with the dependent variable were reported using LM mean difference ± SE.

Model analyses are presented in Appendix 3b (A3b) and Appendix 3e (A3e). Parameters analysed as part of PCA or GLM/LM analyses alongside P data (OP, Organic-P, TP and AHP) were dissolved Fe, dissolved Mn, *Dolichospermum*, Green algae, *Aphanizomenon*, Total Oxidised Nitrogen (TON), Nitrate (NO_3^-), Nitrite (NO_2^-), ammonium (NH_4^+), turbidity (ntu), pH and geosmin. Nutrient and environment data tables are presented in Appendix 3c (A3c) and Appendix 3f (A3f) with molar data in Appendix 3g (A3g). Nutrient PCA data are presented in Appendix 3a (A3a) and Appendix 3d (A3d). Monthly analyses were completed for each site and are listed in appendix 8.

3.2.5. Site-specific data analysis.

No data were available for the month of September at site B4 due to the high degree of turbidity caused by volatile weather which in turn led to extreme conditions within the reservoir. Additionally, no data were available for October at site B4 due to the low reservoir levels exposing the sediment close to the B4 sampling site. Consequently, only a surface sample was taken during October (sampling site T4).

2-MIB was not included in the analysis in this chapter due to its infrequent and insignificant volumes recorded at each site throughout the sampling period.

Cyanobacteria are recorded as “Blue Green Algae” during the analysis of water stratification. Four variables were sampled during stratification data sampling using the EXO Sonde along the depth of each site during August: temperature (°C), pH, Blue Green Algae count (BGA) (cells/ml) and turbidity (ntu). DO data were not available during August. DCWW water analysis methods are displayed in Appendix 1.

3.2.6. Cross-site monthly modelling.

No statistical analyses were carried out on data from January 2018 through April 2018 due to unavailability of suitable data through low to no detection of P across majority of the sites or unsampled periods (March and April). Data analysis for the month of January is restricted to PCA due to the degree of '0' inflated data and very low values, therefore no modelling could be completed. Variables analysed in all models are listed in Table 3.2.6.1. On occasions where certain variables were omitted from analyses, these have been specified when discussing the relevant month/site. Not normally distributed dependent data were transformed prior to LM analysis. Transformation was determined through applying various transformation approaches (cube, log, square-root or Tukey's Ladder of Power), the most suitable of which was determined by the lowest AIC (Akaike Information Criterion). The transformation method applied is specified in each case.

Where parametric and not normally distributed data were analysed using GLM, the most suitable family (Gamma for not normally distributed data where possible, Gaussian for parametric data) and link (inverse, identity, log) were also determined by the lowest AIC.

Table 3.2.6.1. Independent variables analysed for associations with dependent factors, unless otherwise stated. Not all variables were available for each sampling point on each sampling date.

Variable	
pH	NH_3^+ (mg L^{-1})
Temperature (°C)	NO_3^-: NH_4^+ (mol/ml)
Rainfall (mm)	NO_2^- (mg L^{-1})
Total Nitrogen (TN) (mg L^{-1})	Organic P (OrgP) (mg L^{-1})
Total Phosphorous (TP) (mg L^{-1})	Organic Carbon (mg L^{-1})
Conductivity (µs)	Orthophosphate (PO_4^-) (OP) (mg L^{-1})
Oscillatoria (cfu/ml)	Acid Hydrolysable Phosphorous (AHP) (mg L^{-1})
Fe_3^+ (mg L^{-1})	Turbidity (ntu)
NH_4^+ (mg L^{-1})	Green algae (cells/ml)
NO_3^- (mg L^{-1})	Geosmin (ng L^{-1})
TN:TP (mol/ml)	Mn (mg L^{-1})

Heatmaps were used to illustrate the concentration variations of TP, AHP, OP ad Organic P across the transect of the reservoir throughout the chapter. Higher concentrations are represented by darker shades of colour, where no colour represents no P present, or P present below the LOD.

3.3. Results

3.3.1.1. Overview of the annual mean P-fraction data at each of the four sampling sites.

Overall, TP data varied across all sites over the 11-month sampling period (Figure 3.3.1.1.1). AHP accounted for the majority of TP (>50%) over the 11-months at each site within the reservoir, the portion of which was OP and Con-P varied with the seasons. Periods of raised Con-P concentrations indicated a risk of an increase in OP under changing water quality conditions. No significant differences were found between the concentrations of P-fractions (OP, AHP and Org-P) (Kruskal-Wallis P>0.05) at any of the sampling sites or between sampling sites.

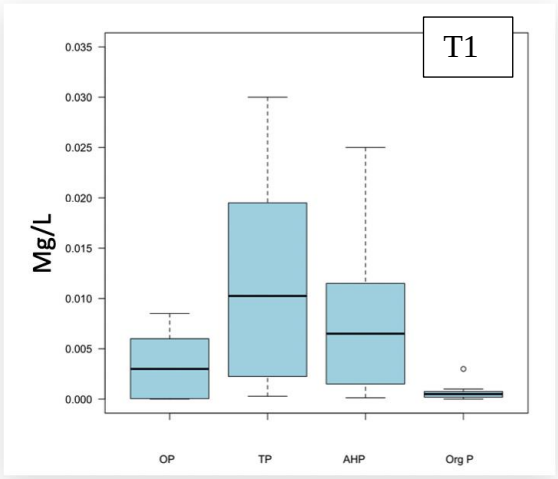

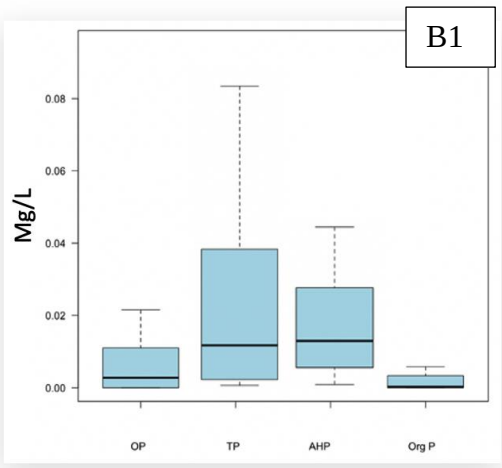

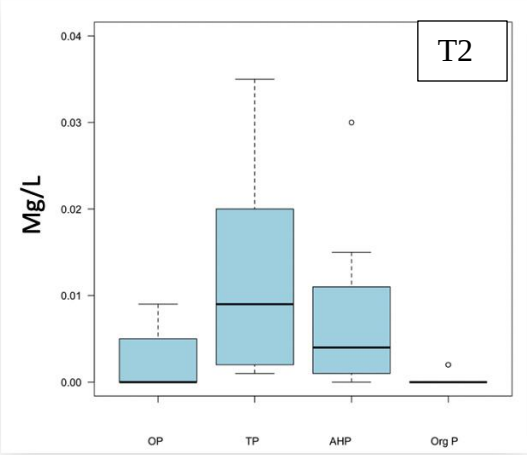
T2
Mg/L
0.04
0.03
0.02
0.01
0.00
OP
TP
AHP
Org P

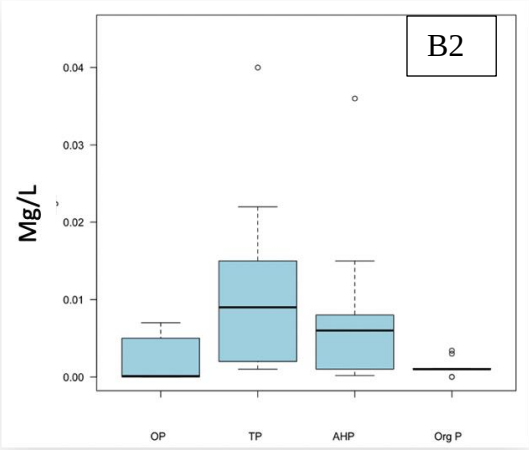
B2
Mg/L
0.04
0.03
0.02
0.01
0.00
OP
TP
AHP
Org P

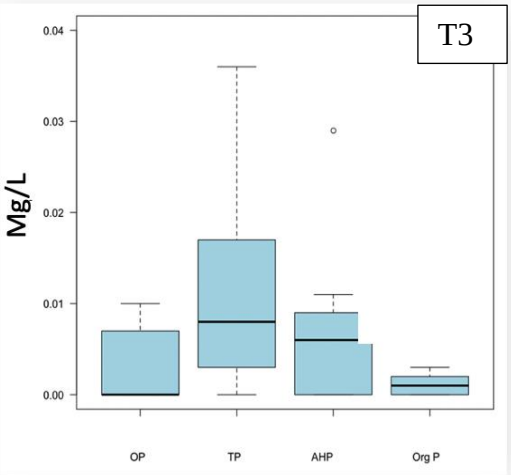
T3
Mg/L
0.04
0.03
0.02
0.01
0.00
OP
TP
AHP
Org P

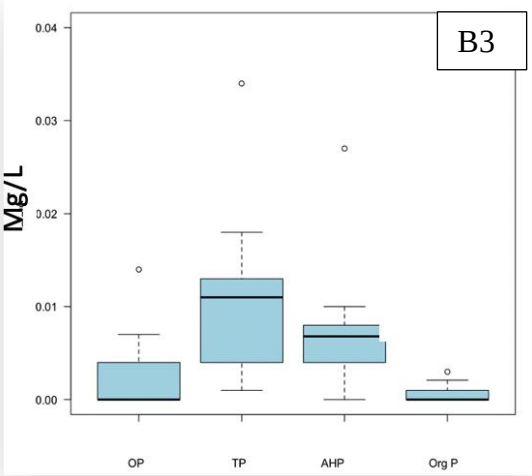
B3
Mg/L
0.04
0.03
0.02
0.01
0.00
OP
TP
AHP
Org P

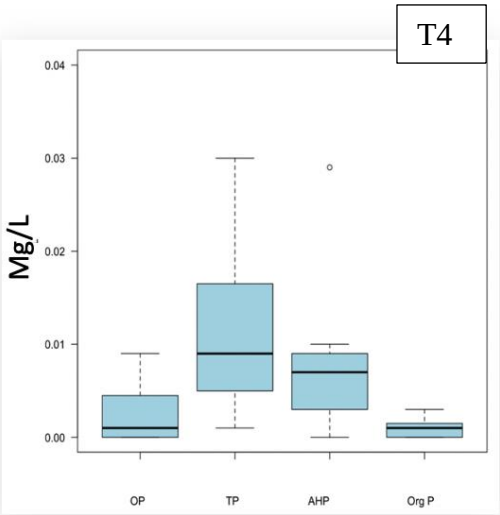
T4
Mg/L
0.04
0.03
0.02
0.01
0.00
OP
TP
AHP
Org P

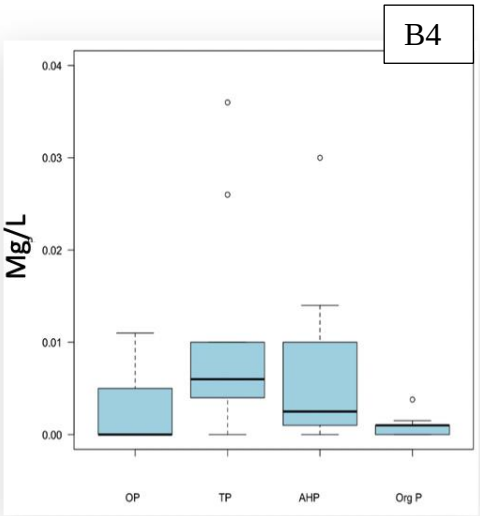
B4
Mg/L
0.04
0.03
0.02
0.01
0.00
OP
TP
AHP
Org P

Figure 3.3.1.1.1. P-fraction distribution (mgL^{-1}) with minimum, first quartile, median, third quartile, maximum and outlying data points for all sites throughout the 2018 sampling period. No significant difference was determined between the concentrations of P-fractions. Please note different Y axis values for site 1.

3.3.1.2. Mean annual Total Phosphorous (TP) concentrations across surface and bottom sampling sites

TP at all sites increased to the maximum recorded concentrations over the 11-month sampling period during the month of May at each site with the exception of site B4, where a TP peak was recorded during the July (Figure 3.3.1.2.1). TP concentrations decreased during the autumn and winter periods and were also low during the January-February relative to spring/summer concentrations for each site. A decreasing TP trend during the summer period was followed by an increase in TP concentrations at 3 of the 4 surface sites, and one bottom site (B3).

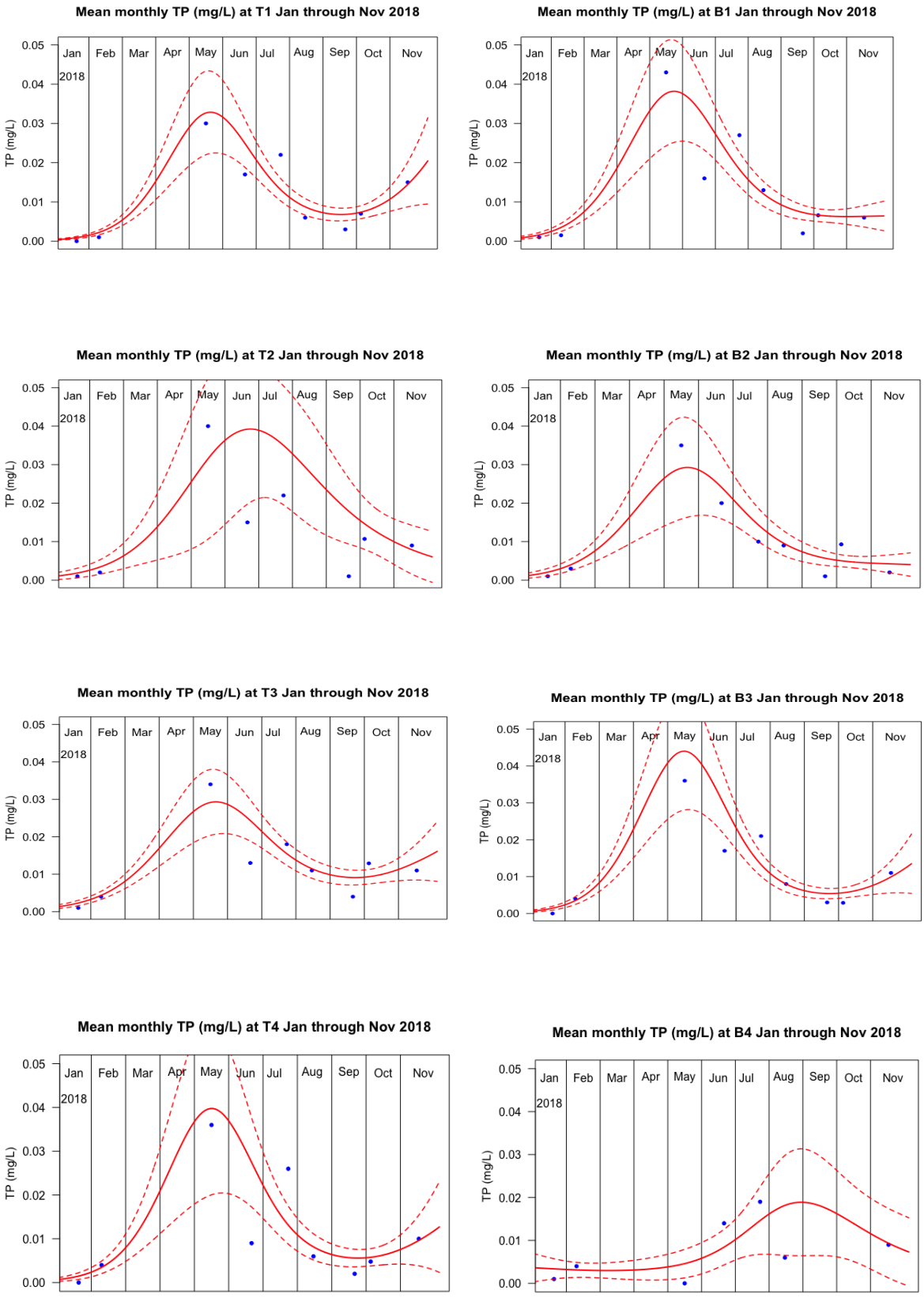

Figure 3.3.1.2.1. Total phosphorous (TP) concentrations (mgL^{-1}) with 95% C.I. in surface and bottom water samples at all eight sampling sites of the reservoir throughout 2018.

3.3.1.3. Mean annual Orthophosphate (OP) concentrations across surface and bottom sampling sites

Orthophosphate concentrations (Figure 3.3.1.3.1) contributed towards a maximum of 27% of the mean annual TP (sites B2 and T3) and peaked between June and July but remained undetected during the winter months (January – February) at most sites with the exception of site B4.

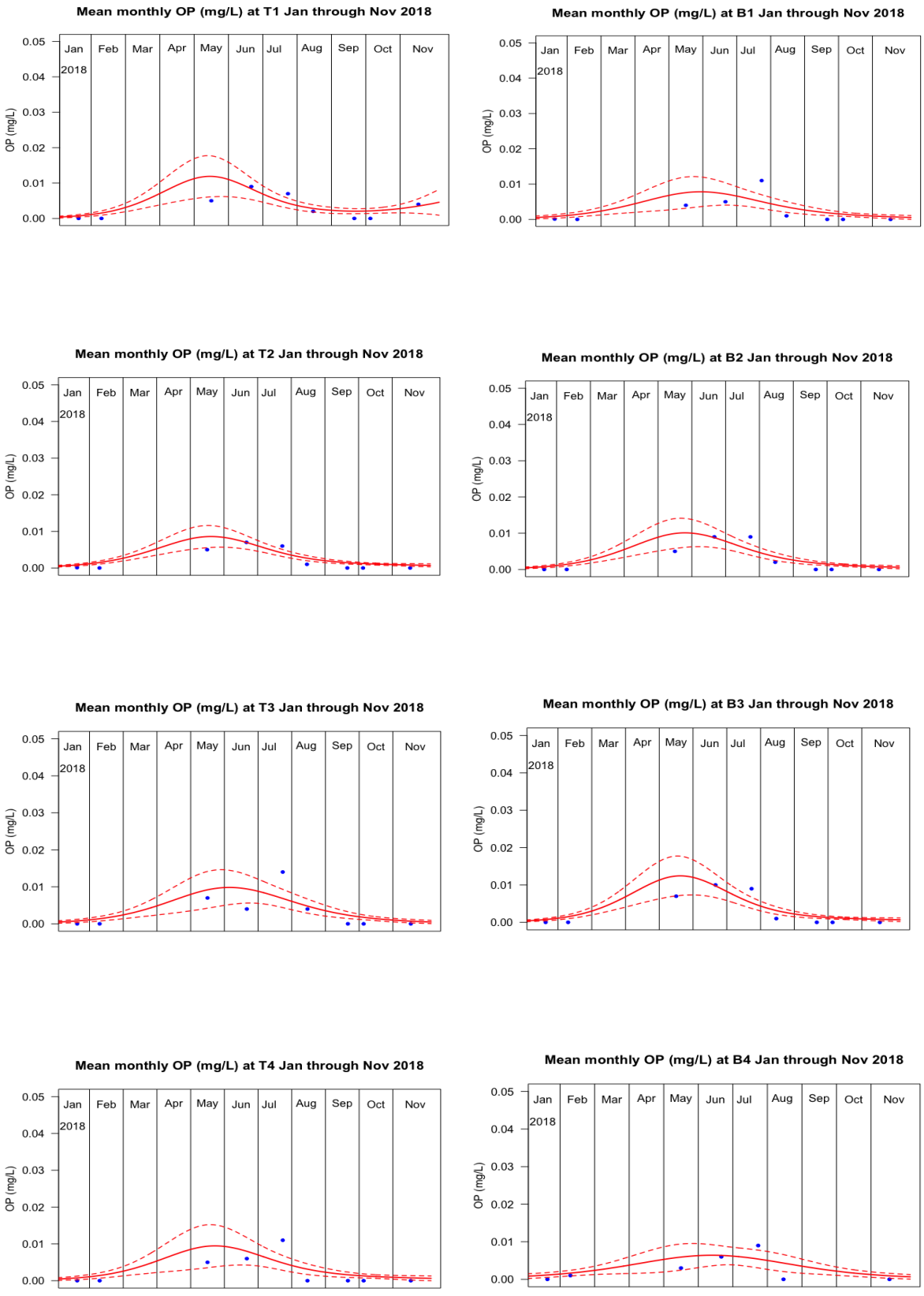

Figure 3.3.1.3.1. Orthophosphate (OP) concentrations (mgL^{-1}) with 95% C.I. in surface and bottom water samples at all eight sampling sites of the reservoir throughout 2018.

3.3.1.4. Mean annual Acid Hydrolysable Phosphorous (AHP) across surface and bottom sampling sites

AHP was the most dominant fraction of TP (>50%) throughout the reservoir over the 11-month sampling period with the exception of site T2 (mean AHP: 46%), with site B2 recording the highest percentage of mean annual AHP (78%). AHP peaked during May for each site and was lowest during the winter period (January and February) and late summer (August through September) at sites 1 through 3. Surface and bottom site 4 decreased during June.

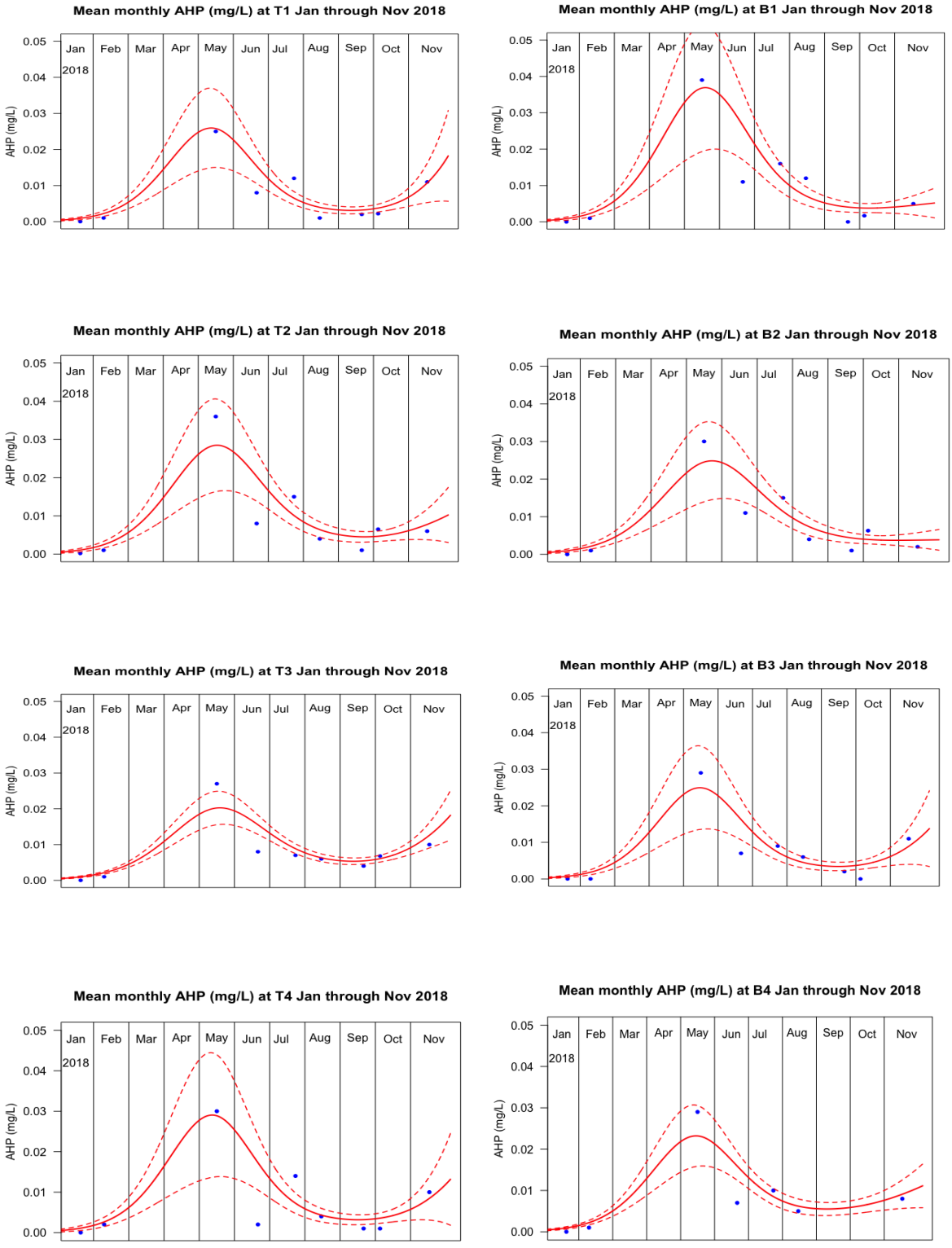

Figure 3.3.1.4.1. Acid Hydrolysable Phosphate (AHP) concentrations (mgL^{-1}) with 95% C.I. in surface and bottom water samples at all eight sampling sites of the reservoir throughout 2018.

3.3.1.5. Mean annual Organic-P (Org-P) concentrations across the surface and bottom sampling sites

Organic-P concentrations remained low throughout the 11-month sampling period at all sites relative to concentrations of OP and AHP fraction concentrations (=<12% mean annual TP). Organic-P concentrations peaked during February or October (site-dependent) with the exception of site B2 where org-P was detected during the months of May and August only.

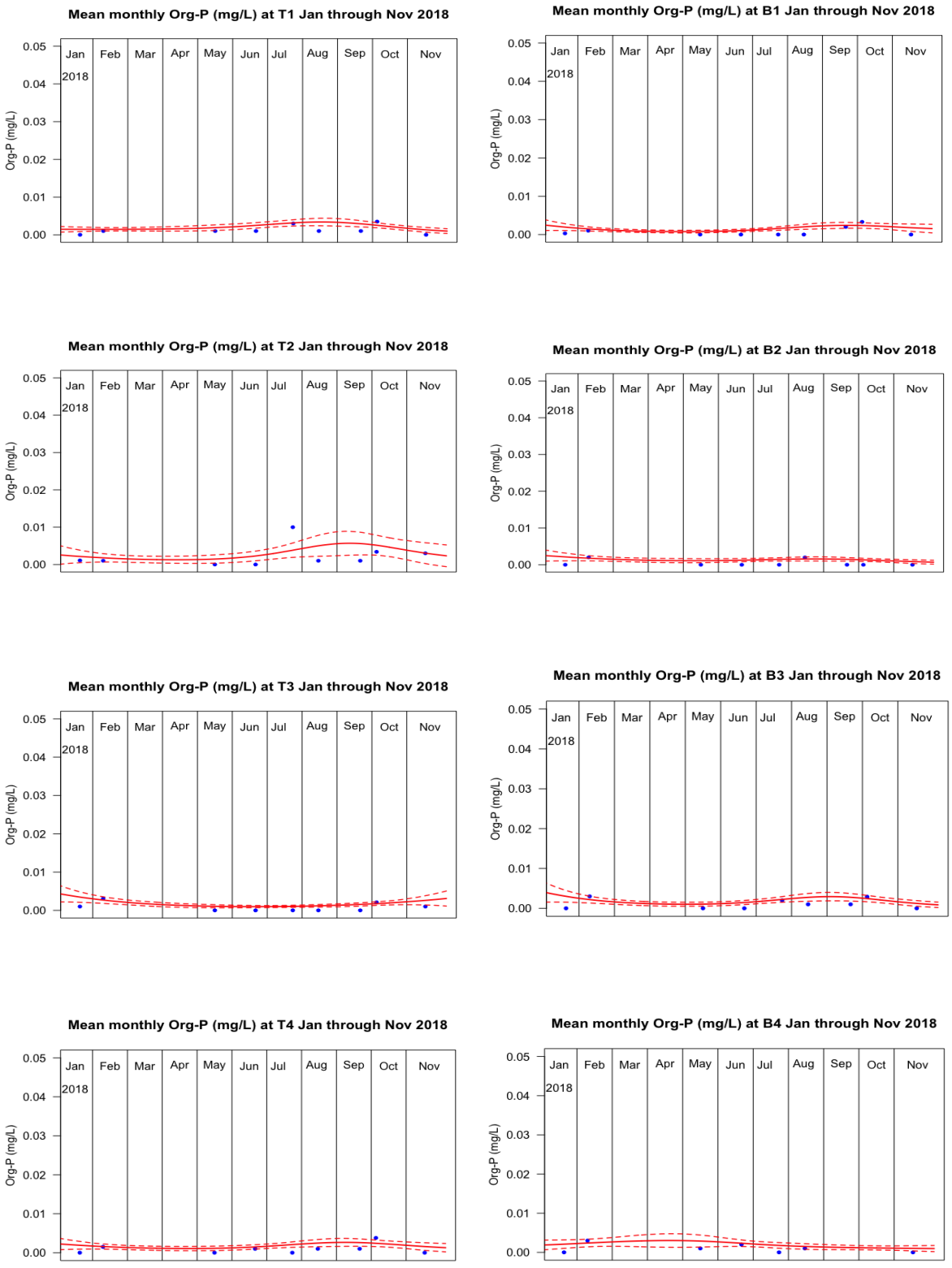

Figure 3.3.1.5.1. Organic Phosphate (Org-P) concentrations (mgL^{-1}) with 95% C.I. in surface and bottom water samples at all eight sampling sites of the reservoir throughout 2018.

3.3.2. The mean annual N-fraction molar ratios across the surface and bottom sampling sites.

The NO_3^-: NH_4^+ ratio reached its highest during February at every site 126:1. However, the ratio decreased by May throughout the reservoir (between 3:1 and 10:1 with the exception of site T4, where ammonium concentrations were three times that of nitrate during May (Figure 3.3.2.1). The NO_3^-: NH_4^+ ratios increased at most sites (bottom sites 2 through 4 and surface site 4) during the late summer period. Site B2 recorded the highest NO_3^-: NH_4^+ ratio increase during the summer (71:1 during August).

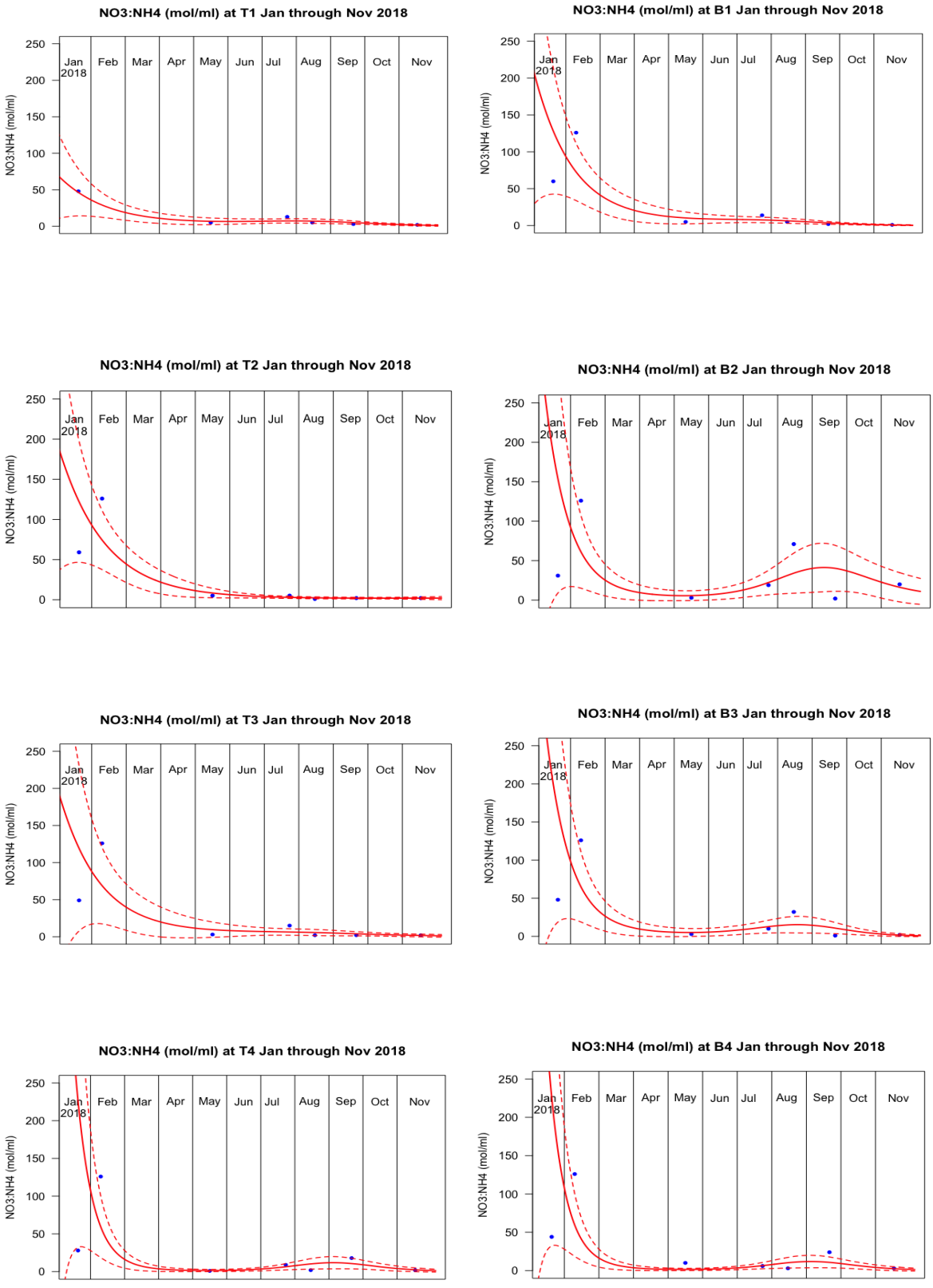

Figure 3.3.2.1. NO_3^-: NH_4^+ molar ratio with 95% C.I. in surface and bottom water samples at all eight sampling sites of the reservoir throughout 2018.

3.3.3. APA concentrations at surface and bottom sampling sites

3.3.3.1. APA data analysis 9th July

Under sustained drought conditions (no precipitation nor active inflow for >6 weeks at the Llandegfedd reservoir site), site B3 indicated having the greatest degree of phosphorous limitation (TP 0.008 mgL^{-1} ± 0.006) and data variability (16.13 µmoles *p*NPP/ µg Chl a / h ± 26.47) of all sites sampled (Figure 3.3.3.1.1). Surface site 4 (T4) indicated as being the least phosphorous limited (0.93 µmoles *p*NPP / µg Chl a / h ± 0.35) with TP at site T4 supporting the data through recording the highest TP (0.013 mgL^{-1} ± 0.01) of all sites. No cyanobacteria were detected at any site on the 9th July, suggesting lysis of cells and release of AP.

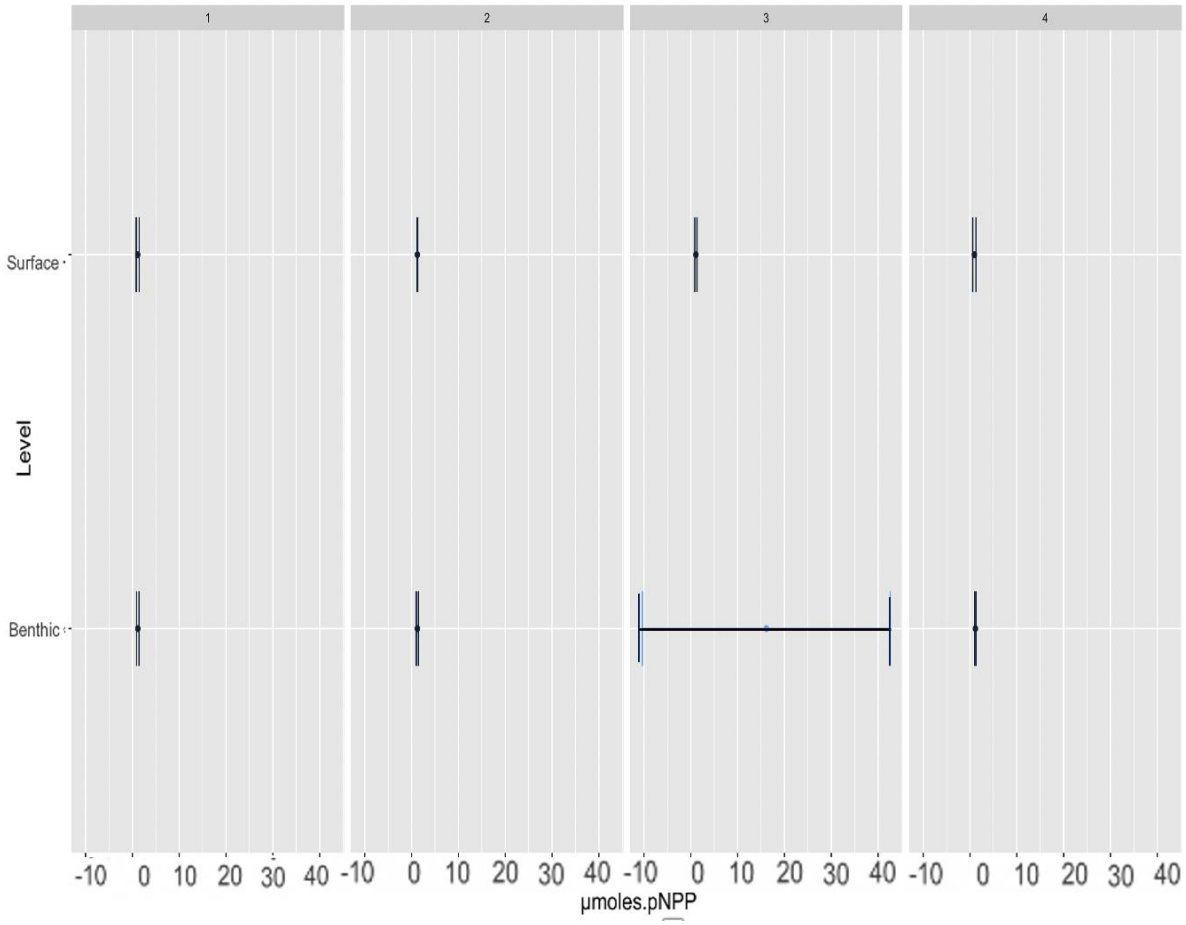

Figure 3.3.3.1.1. Mean µmoles *p*NPP / µg Chl a / h (± SD) data 9th July. Data variability was low throughout the rseervoir with the exception of benthic sample at site 3.

The high *p*NPP concentration recorded at site B3 correlated with an absence of OP and low AHP concentrations (0.001mgL^{-1}) at the site. The majority of the P isolated at site B3 was

comprised of organic P. No correlation was determined between the *p*NPP concentrations and OP nor AHP at any of the sites (P>0.05).

3.3.3.2. APA data analysis 23rd July

The site with the greatest P limitation and data variability on the 23rd July was site B4 (2.55 µmoles *p*NPP / µg Chl a / h ± 2.98) (Figure 3.3.3.2.1) and was reflected by recording the lowest TP concentration throughout the reservoir (0.016 mgL^{-1} ± 0.006). The lowest degree of P limitation was identified at site B2 (0.74 µmoles *p*NPP / µg Chl a / h ± 0.15) however, the TP concentrations were not the highest recorded of all sites. Overall, the *p*NPP concentrations decreased across the reservoir by between 94% (site B3) and 10% (site T4) relative to concentrations recorded on the 9th July, suggesting an increase in P availability at site B3 (from 0.008 mgL^{-1} ± 0.006 to 0.018 mgL^{-1} ± 0.002).

An increase in *p*NPP was observed at sites B1 and T4, indicating an increase in P limitation at these sites since July 9th (Figure 3.3.4.2.1), and this was reflected in the OP concentrations (B1: July 9th 0.007 mgL^{-1} ± 0.005; 23rd July 0.012 mgL^{-1} ± 0.007 mgL^{-1} ± 0; T4: July 9th 0.001 mgL^{-1} ± 0; 23rd July 0.016).

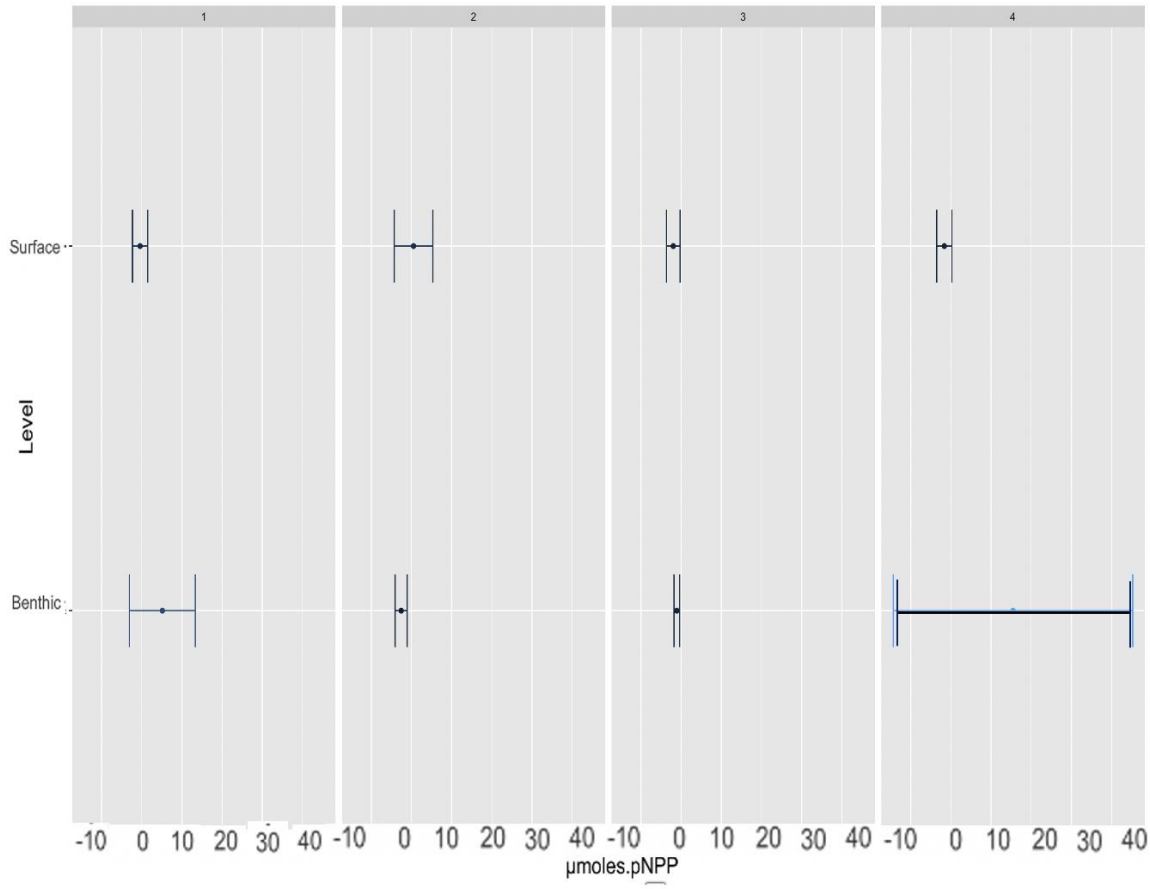

Figure 3.3.3.2.1. Mean µmoles *p*NPP / µg Chl a / h (± SD) data 23rd July. Data variability increased at most sites relative to that on July 9th. Benthic sample of site 4 demonstrated the greatest degree of data variability.

The low variation in *p*NPP concentrations between sites (1.17 (µmoles *p*NPP / µg Chl a / h ± SE 0.57) mirror the low variation in OP concentrations (0.01mgL^{-1} ± SE 0.004) between sites on the 23rd July. No correlation was determined between the *p*NPP concentrations and OP nor AHP at any of the sites (P>0.05).

3.3.3.3. APA data analysis 31st July

Following 4 days of precipitation (27th July-30th July), the concentration of *p*NPP on the 31st July decreased across the reservoir indicating to an increase in P availability with the exception of sites B1 and T3, with T3 recording a high level of *p*NPP and data variability (24.5 µmoles *p*NPP / µg Chl a / h ± 42.5) relative to data obtained on 9th July and 23rd July (Figure 3.3.3.3.1). The data indicated no P limitation at either bottom or surface of sites 4 or 2.

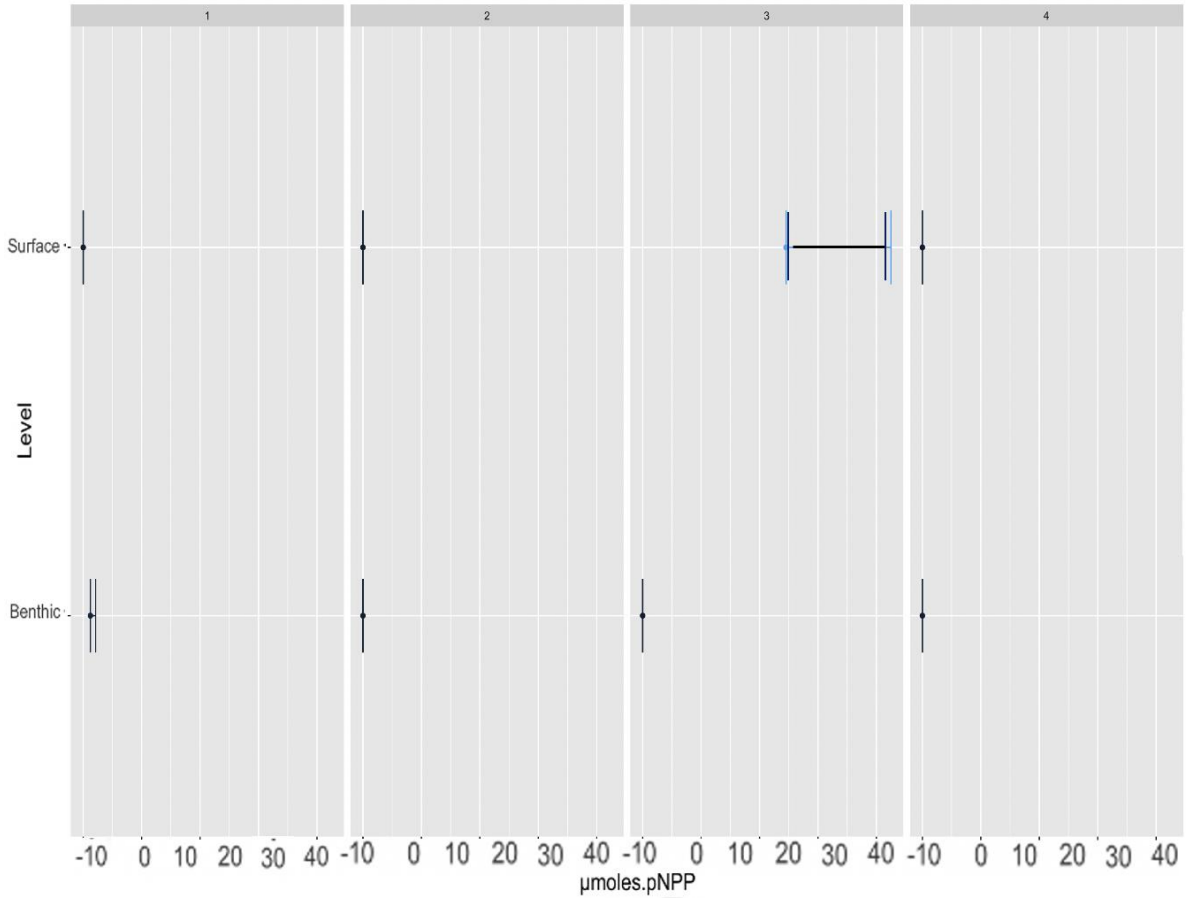

Figure 3.3.3.3.1. Mean µmoles *p*NPP / µg Chl a / h (± SD) data 31st July. Data variability was low relative to that recorded on July 23rd. The surface sample at site 3 demonstrated the highest degree of data variability.

The low *p*NPP concentrations across the majority of the sites were recorded with increased concentrations of OP. No correlation was determined between the *p*NPP concentrations and OP nor AHP at any of the sites (P>0.05).

3.3.3.4. APA data analysis 3rd August

Samples collected four days following the end of the precipitation event (3rd August), *p*NPP concentrations indicated P limitation at all surface sites, with the greatest degree of P-limitation at site T3; however, the data displayed a high degree of variability (12.93 µmoles pNPP / µg Chl a / h ± 18.25) (Figure 3.3.3.4.1). The *p*NPP concentrations decreased at site B1 by 50% (from 1.23 (± 2.13) µmoles *p*NPP / µg Chl a / h on the 31st July to 0.6 µmoles *p*NPP / µg Chl a / h (± 17.56)); however, OP concentrations decreased from 0.014 mgL^{-1} (± 0.002) on 31st July to 0 mgL^{-1} on 3rd August.

Similarly, *p*NPP concentrations decreased by 47% at site T3 during the same period (from 24.5 µmoles *p*NPP / µg Chl a / h (± 42.5) on the 31st July to 12.9 µmoles *p*NPP / µg Chl a / h (± 18.25) on the 3rd August). A decrease in OP was also recorded at site T3 over the same period (from 0.016 mgL^{-1} ± 0 to 0.007 mgL^{-1} ± 0.008).

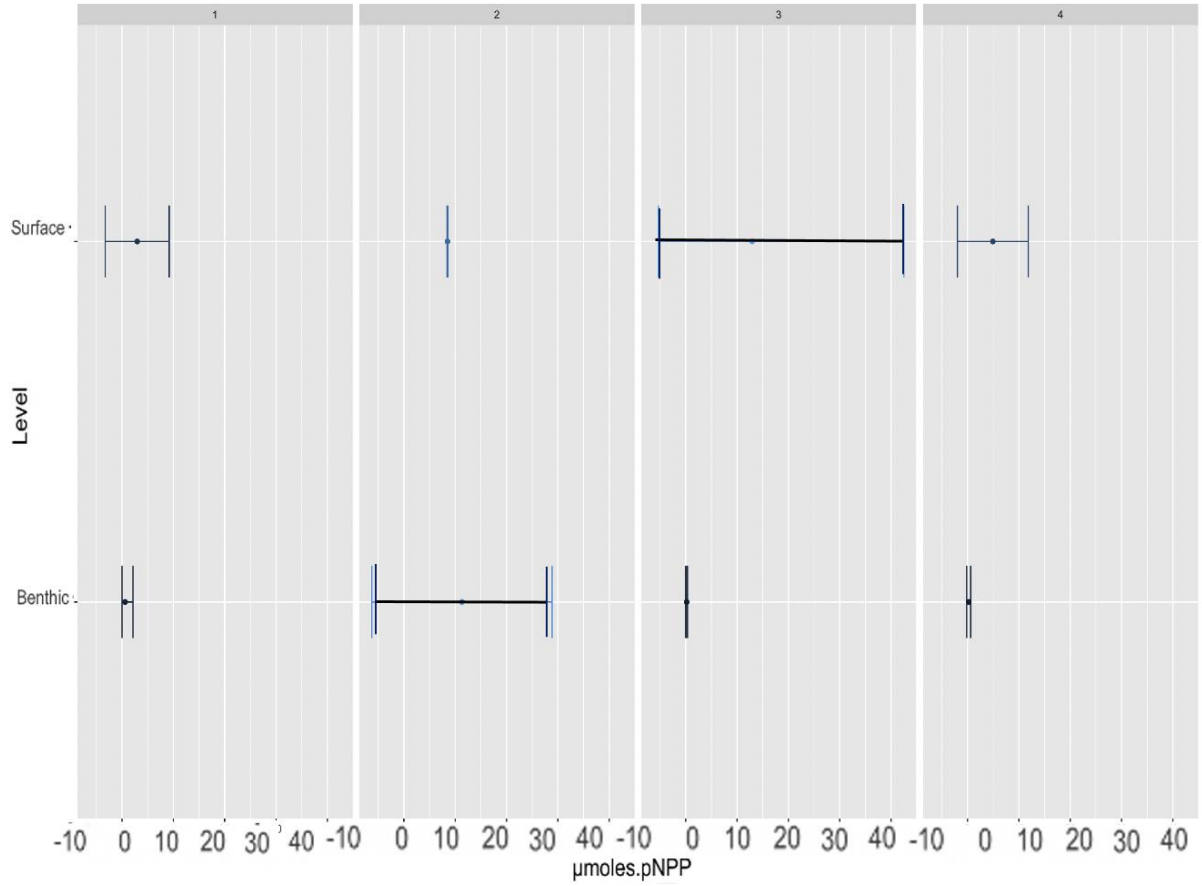

Figure 3.3.3.4.1. Mean µmoles *p*NPP / µg Chl a / h (± SD) data 3rd August. The highest degree of data variability was recirded at the surface of site 3, similar to that recorded on July 31st.

No correlation was determined between the *p*NPP concentrations and OP nor AHP at any of the sites.

3.3.3.5. APA data analysis 20th August

The *p*NPP concentrations decreased to 0 µmoles *p*NPP / µg Chl a / h (Figure 3.3.3.5.1) between the period of 3rd August to the 20th August across all sites with the exception of site B2 (0.11 µmoles *p*NPP / µg Chl a / h ± 0.09) where a decrease in pNPP concentration of 98.7% was observed. The undetected/ low concentration of *p*NPP across all sites reflected the higher concentrations of OP and AHP across the sites on the 20th August relative to the

concentrations recorded on August 3rd, with the exception of site T4, where no OP nor AHP was recorded. The data indicated very little P limitation within the reservoir on 20th August (mean OP concentrations from 0.001 mgL^{-1} (sites T3, B3 and B4) to 0.004 mgL^{-1} (site B2), site T4 excluded).

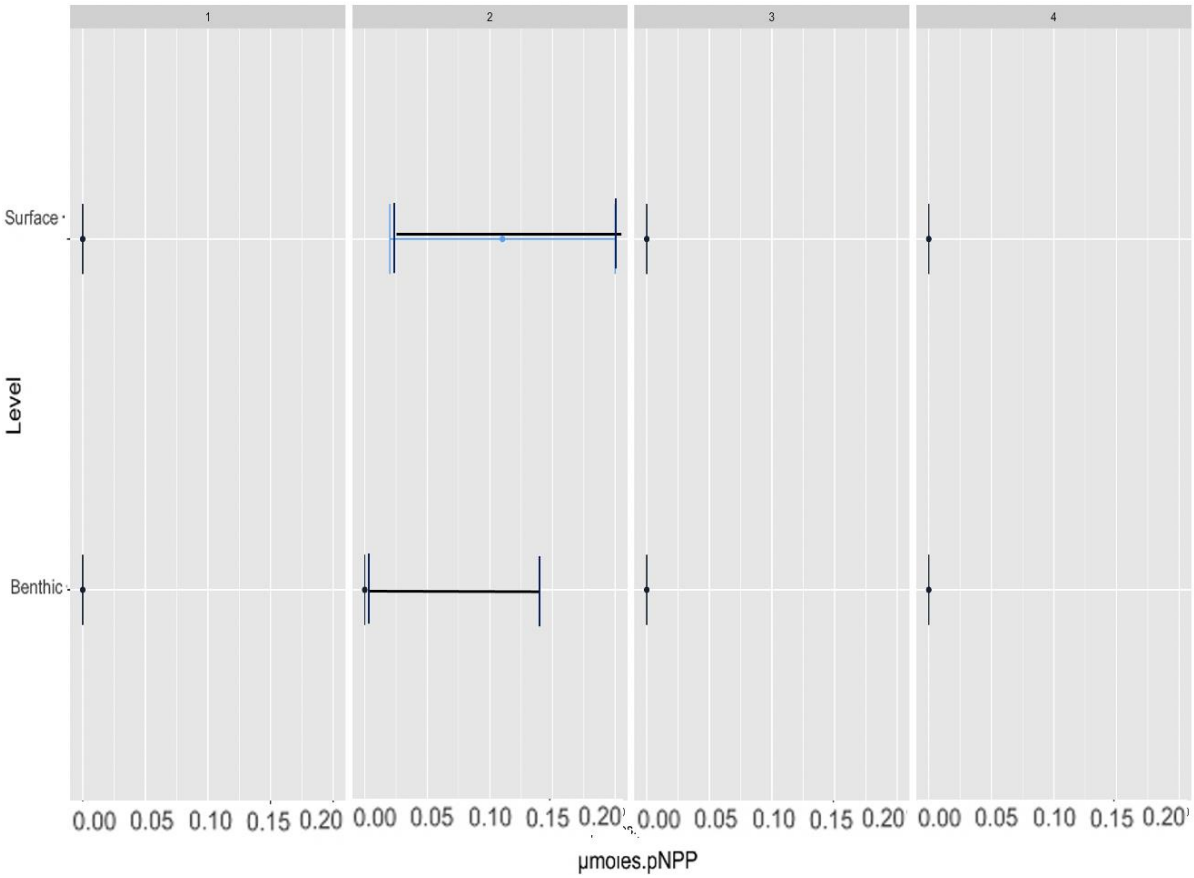

Figure 3.3.3.5.1. Mean µmoles *p*NPP / µg Chl a / h (± SD) data 20th August. Data variability was low throughout the sampling points with the exception of the surface sample at site2.

3.3.4. Nutrient and environmental data analysis.

The concentration of nitrate was highest during the end of winter (February: 1.3mgL^{-1} across the sites) but decreased at all sites during May (0.015 mgL^{-1} to 0.017 mgL^{-1}). However, nitrate concentrations increased towards the end of May (0.97 mgL^{-1} to 1.1 mgL^{-1}) with oscillating concentrations through the remainder of the sampling period (Figure 3.3.4.1). July recorded the highest nitrate concentrations and continued to increase during a drought in the spring and summer. Concentrations decreased during August following a period of heavy rainfall.

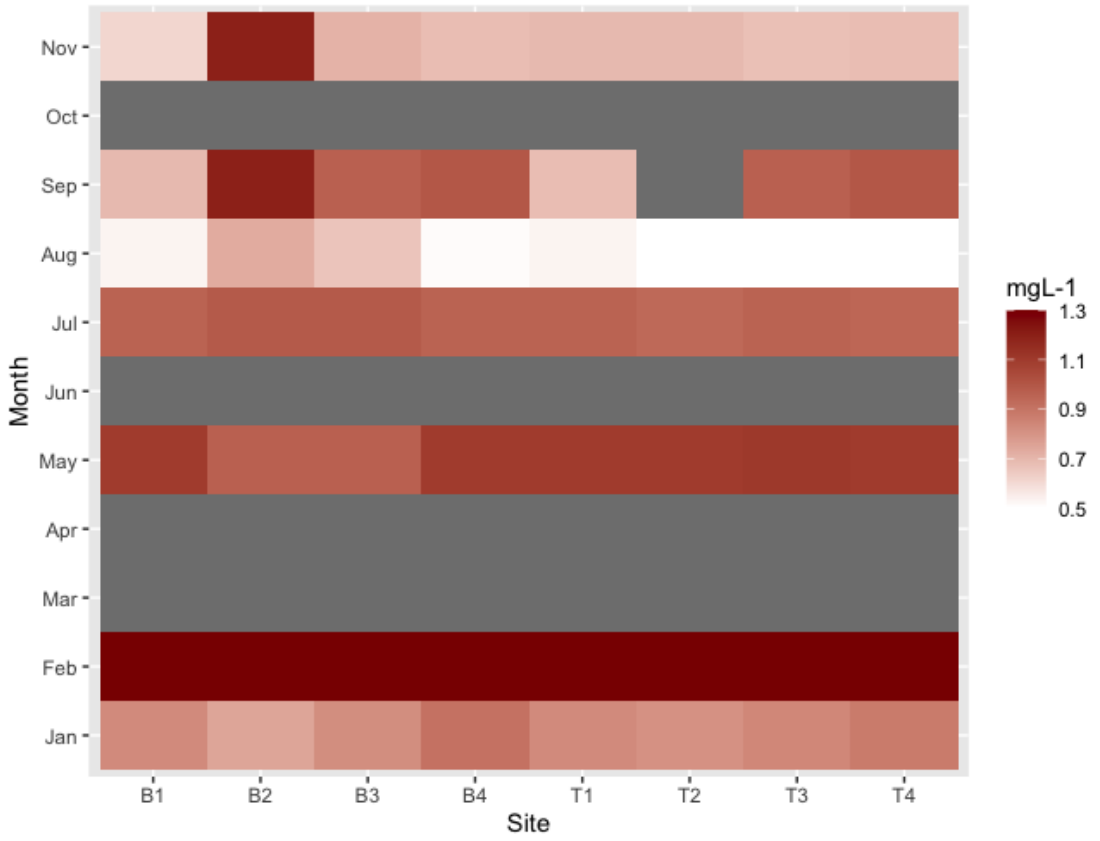

Figure 3.3.541. Mean monthly nitrate concentrations (mgL^{-1}) at each surface and bottom sampling site over the 11-month sampling period. Grey squares represent the absence of data.

Ammonium concentrations were low throughout the reservoir over the sampling period relative to that of nitrate (Figure 3.3.4.2). Ammonium concentrations increased as the seasons progressed, peaking during November for each site (0.72 mgL^{-1} to 0.29 mgL^{-1}) with the exception of site B2 where the highest ammonium concentration was recorded during the May (0.068 mgL^{-1}).

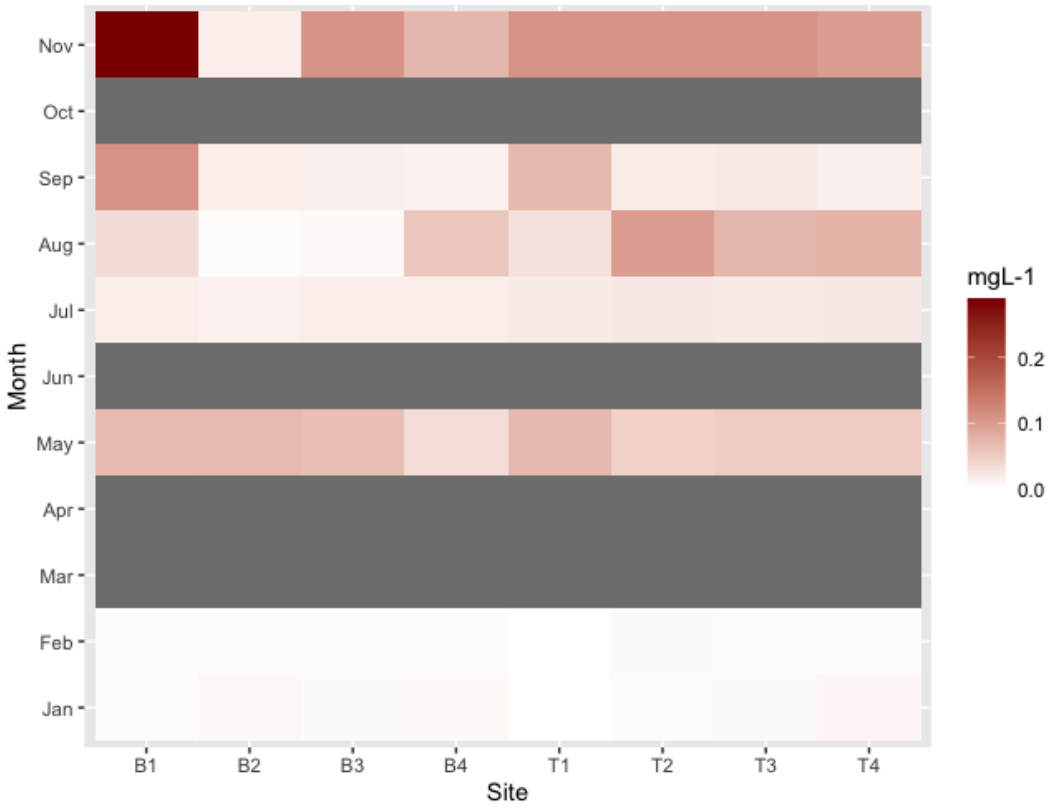

Figure 3.3.4.2. Mean monthly ammonium concentrations (mgL^{-1}) at each surface and bottom sampling site over the 11-month sampling period. Grey squares represent the absence of data. (

Cyanobacteria were isolated at the reservoir during August only for all sites with the exceptions of sites B4 and T2, where cyanobacteria were also detected during May (Figure 3.3.4.3). Bottom sites 2 and 3 recorded no cyanobacteria throughout the 11-month sampling period.

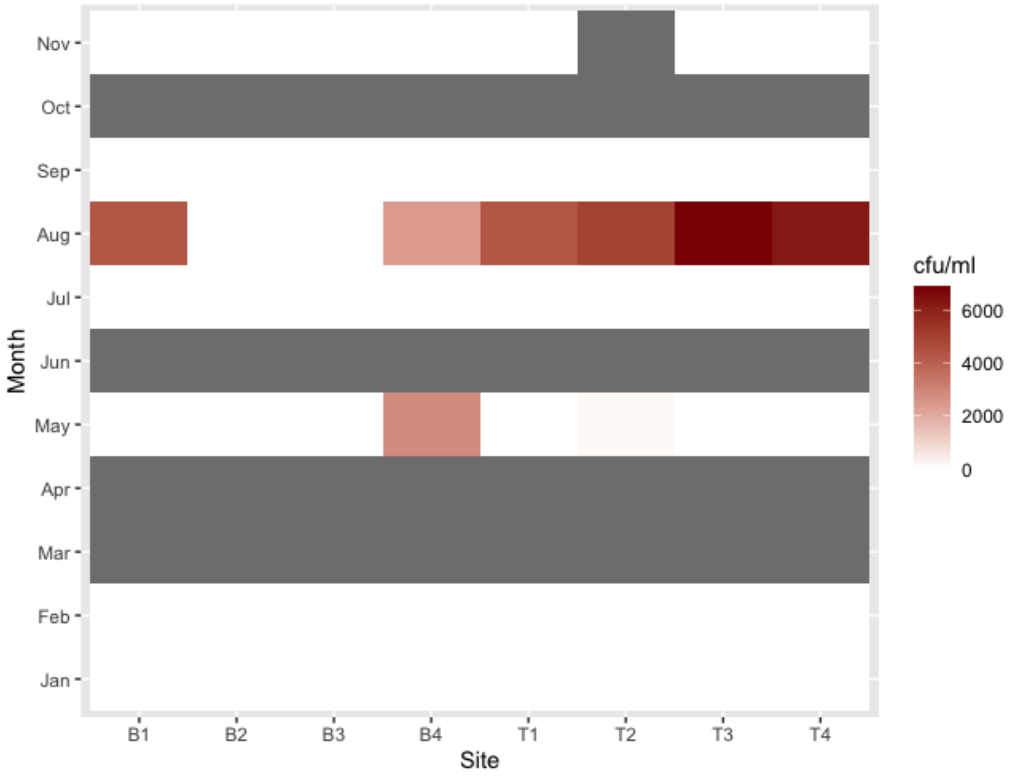

Figure 3.3.4.3. Mean monthly cyanobacterial abundance (cfu/ml) at each surface and bottom sampling site over the 11-month sampling period. Grey squares represent the absence of data.

Geosmin was isolated at each site during the 11-month sampling period and peaked during May (5ngL^{-1}) at site B4 (Figure 3.3.4.4). May recorded the highest concentrations of geosmin at all sites with the exception of sites B1 (1.5ngL^{-1}) during June and February, B2 (2ngL^{-1}) during July and site B3 (0.9ngL^{-1}) during August. The distribution of geosmin (Shapiro-Wilks $P<0.05$) and cyanobacterial counts (Shapiro-Wilks $P<0.005$) between the surface and bottom sites between May and September were significantly different (Kruskal Wallace $P<0.05$), however, geosmin concentrations were insignificantly different between the surface and bottom sites from October to November.

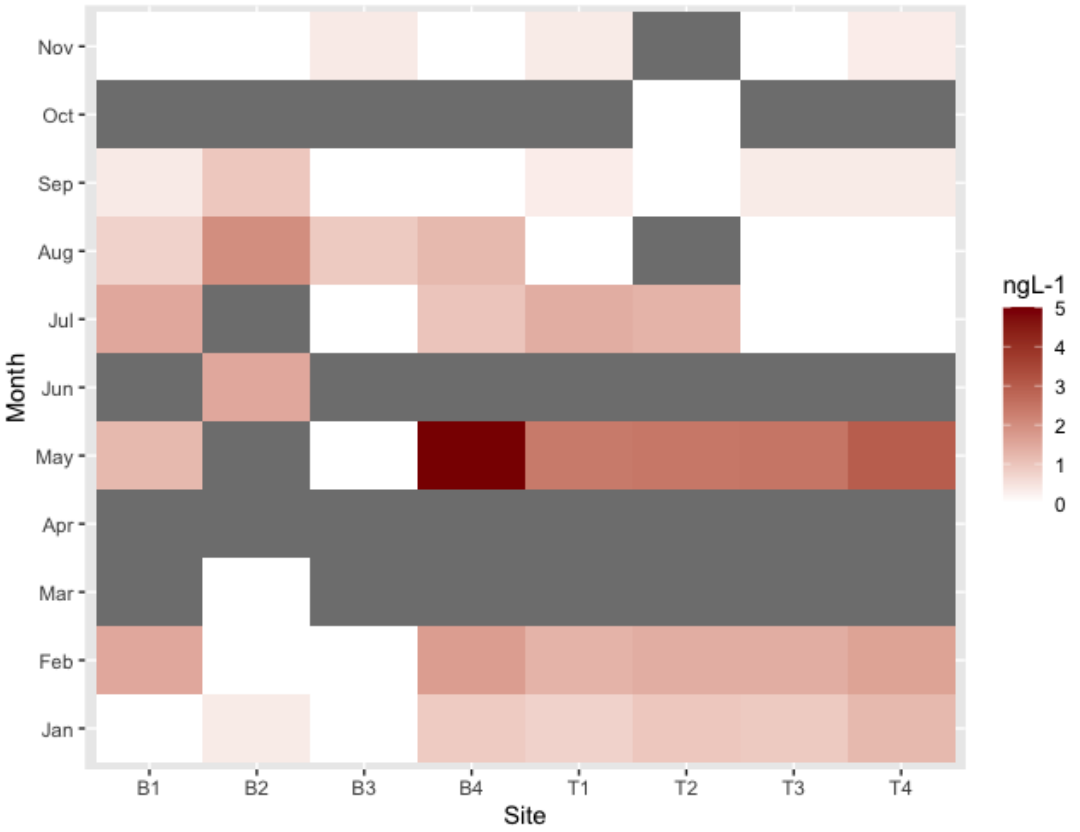

Figure 3.3.4.4. Mean monthly geosmin concentrations (ngL^{-1}) at each surface and bottom sampling site over the 11-month sampling period. Grey squares represent the absence of data.

3.3.5. General, generalised and linear modelling of data over the 11-month period.

3.3.5.1. Model addressing P-fractions with water quality and environmental variables at sampling site B4: January – November 2018.

PCA determined that OP, TP and AHP were positively correlated with one-another, however, Organic-P was not correlated with other P-fractions (Figure 3.3.5.1.1).

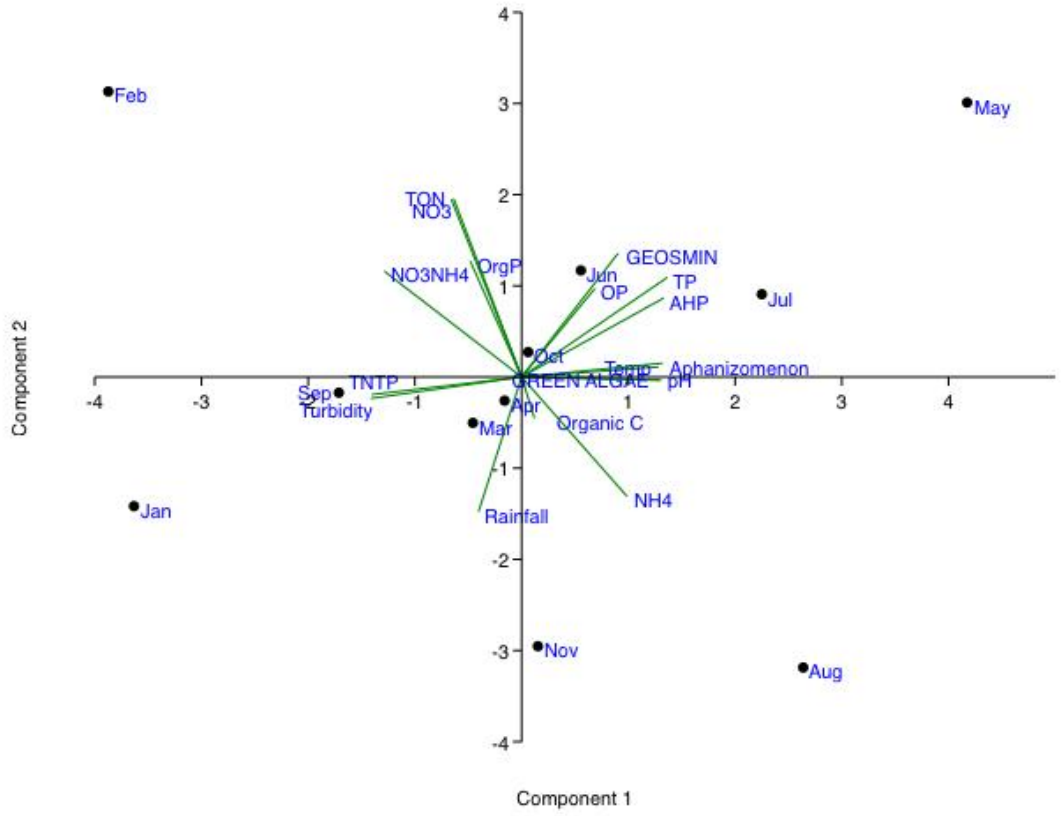

Figure 3.3.5.1.1. PCA of B4 data obtained over the 11-month sampling period using PC1 and PC2. The occurrence of high rainfall volume and turbidity were not correlated with an increase in the N fractions.

The variables determined to be correlated with P-fractions using the PCA are listed in Table 3.3.5.1.1. The variables included in the modelling varied between the P-fractions due to the absence of correlation of organic-P with any of the other P-fractions.

Table 3.3.5.1.1. Variables included within the LM/GLM analyses as independent variables

Variables correlating with respective P-fractions	
OP, AHP & TP	Organic-P
Geosmin (ng L^{-1})	NH_4^+ (mg L^{-1})
Aphanizomenon (cfu/ml)	Organic C (mg L^{-1})
Temperature (°C)	Green algae (cells/ml)
Rainfall (mm)	pH
Turbidity (ntu)	NO_3^-: NH_4^+ molar ratio

TN:TP molar ratio	TN (mg L^{-1})
	NO_3^- (mg L^{-1})
	Oscillatoria (cfu/ml)

TP data were parametric whereas AHP, OP and Org-P data were not normally distributed. Untransformed non-normally distributed data demonstrated no significant association with the variables. TP data were analysed using a General Linear Model and the Gaussian family (inverse link).

AHP data were prepared for analysis using the square root transformation. Both the Org-P and the OP data were transformed through cubing the data.

No significant association was determined for TP, OP, Org-P nor AHP with any of the variables analysed.

No significant association was determined for TP, OP, Org-P nor AHP fractions with any of the variables analysed at any of the four surface or bottom sites (1 through 4) over the 11-month sampling period.

3.3.5.2. Models addressing APA activity (µmoles pNPP (µg Chl a / h) July 9th).

3.3.5.2.1. pNPP activity data obtained on July 9th

The variables displaying correlation with *p*NPP activity are listed in Table 3.3.5.2.1.1. following PC analysis using PC1 and PC2.

Table 3.3.5.2.1.1. Variables included LM analyses with *p*NPP

Geosmin (ng L^{-1})
AHP (mg L^{-1})
TP (mg L^{-1})
Turbidity (ntu)
Organic P (mg L^{-1})
TN (mg L^{-1})
pH
TN:TP molar ratio
Temperature

The *p*NPP data was not normally distributed so were transformed using Tukey's Ladder of Power.

No significant association was determined for *p*NPP with any of the variables. Furthermore, no significant association was determined for pNPP concentration with any variables sampled on the 23rd July, 31st July, 3rd August or the 20th August.

3.3.6.2. Model addressing P-fraction data at each sampling site obtained on 14th and 29th May.

3.3.6.2.1. P-fraction model based on data obtained by sampling on May 14th.

PCA determined that OP, TP and AHP were positively correlated with one-another, however, Org-P data were not correlated with other P-fractions (Table 3.3.6.2.1.1).

Table 3.3.6.2.1.1. Variables determined by PCA for model addressing P-fraction data

OP, AHP & TP	Organic-P
Geosmin (ng L^{-1})	NH_4^+ (mg L^{-1})
Aphanizomenon (cfu/ml)	Organic C (mg L^{-1})
Temperature (°C)	Green algae(cells/ml)
Rainfall (mm)	pH
Turbidity (ntu)	NO_3^-: NH_4^+ molar ratio
TN:TP molar ratio	TN (mg L^{-1})
	NO_3^- (mg L^{-1})
	Oscillatoria (cfu/ml)

Both OP and AHP data exhibited a normal distribution (Shapiro-Wilks P>0.05), therefore the Gaussian family (log link) was used in the GLM analysis. However, neither TP nor geosmin data exhibited a normal distribution and remained skewed following transformation attempts. Therefore, the data were analysed using Gamma family (inverse link) as a Generalised Linear model. Untransformed non-normally distributed data demonstrated no significant association with the variables.

No significant association was determined between TP, OP nor AHP concentrations with any of the variables analysed on the 14th May.

3.3.6.2.2. P-fraction model based on data obtained by sampling on May 29th.

PCA determined that OP, TP and AHP were positively correlated with one-another, however, Org-P was not correlated with other P-fractions (Table 3.3.8.2.2.1).

Table 3.3.8.2.2.1. Variables determined by PCA for model addressing P-fraction data

OP, AHP & TP	Organic-P
NO_3^-: NH_4^+ molar ratio	Geosmin (ng L^{-1})
Aphanizomenon (cfu/ml)	NO_3^- (mg L^{-1})
Organic C (mg L^{-1})	TN (mg L^{-1})
NH_4^+ (mg L^{-1})	pH
Temperature (°C)	Turbidity (ntu)
Rainfall (mm)	TN:TP molar ratio
	Green algae (cell/ml)
	Oscillatoria (cfu/ml)

The OP data displayed a normal distribution (Shapiro-Wilks P>0.05), whereas data for AHP, TP, Org-P and geosmin did not (Shapiro-Wilks P<0.05). TP was transformed using Tukey's ladder of power to create a normal distribution. Untransformed non-normally distributed data demonstrated no significant association with the variables using Gaussian family (Identity link).

No significant association was determined for any P-fractions nor geosmin with any variables analysed on the 29th May.

No significant associations were determined for any of the P-fractions with any of the nutrient or environmental variables over the 11-month sampling period. Untransformed non-normally distributed data demonstrated no significant association with the variables using Gaussian family (Identity link).

3.3.7. Peak TP and geosmin concentration spatial and temporal distribution.

Geosmin concentrations varied throughout the seasons and between sites, with the highest concentrations attained at each site during May with the exception of sites B1 (February and July; 1.5ngL^{-1}) and B3 (August; 0.9ngL^{-1}) (Table 3.3.7.1).

Table 3.3.7.1. Geosmin concentrations (ngL^{-1}, mean/month) in surface and bottom water samples at sites along the reservoir between January 2018 and November 2018. The highest geosmin concentrations highlighted in red.

Site	Jan	Feb	Mar	Apr	May	Jun	Jul	Aug	Sep	Oct	Nov
T1	0.75	1.3			**2.4**		1.4	0	0.31		0.34
B1	0	**1.5**			1.2		**1.5**	0.75	0.36		0
T2	0.94	1.4			**2.45**		1.3	0	0		0.34
B2	0	0			**1.5**		2	0.94	0		0
T3	0.9	1.4			**2.5**		0	0	0.34		0
B3	0	0			0		0	**0.9**	0		0.36
T4	1.2	1.6			**3**		0	0	0.34		0.31
B4	0.88	1.7			**5**		1	1.2	0		0

Each site recorded its peak TP ($0.051mgL^{-1}$ ± 0.007) and AHP ($0.04mgL^{-1}$ ± 0.006) concentration during May (Table 3.3.7.2), with the highest at site B2 ($0.057mgL^{-1}$) and the lowest concentrations at $0.04mgL^{-1}$ (T1). The highest OP values ($0.015mgL^{-1}$ ± 0.0009) recorded during July ($0.016mgL^{-1}$) with the exception of site T2, where its OP peaked during May. Organic P ($0.006mgL^{-1}$ ± 0.002) most often reached its highest concentration during summer/autumn, however, organic P peaked during February at sites T3 ($0.005mgL^{-1}$) and B4 ($0.006mgL^{-1}$).

Table 3.3.7.2. Orthophosphate (OP), Total Phosphorous (TP), Acid Hydrolysable Phosphorous (AHP) and Organic Phosphorous (Org-P) concentrations (mgL^{-1}, mean/month) in surface and bottom water samples at sites along the reservoir between January and November 2018. Grey squares indicate an absence of data. Peak annual P-fraction concentrations are highlighted by their respective colour.

	Jan	Feb	Mar	Apr	May		Jun	Jul		Aug	Sep	Oct	Nov
T1					0.034	0.04		0.016	0.009				
B1					0.047	0.055		0.014				0.0033	
T2					0.046	0.014	0.056					0.0034	
B2					0.043	0.057		0.016		0.003			
T3		0.005			0.03	0.043		0.016					
B3					0.04	0.055		0.016	0.007				
T4					0.046	0.055		0.016				0.0038	
B4		0.006			0.035	0.043		0.015					

Acid Hydrolysable Phosphate

Organic P

Orthophosphate

Total P

3.3.8. pH and temperature stratification data

3.3.8.1. Data recorded on August 3rd 2018.

3.3.8.1.1. Sampling Site 1.

The temperature decreased from the surface (21.9°C) steadily to a depth of 11.34m (18.62°C) before attaining its lowest temperature at the bottom level of 15.6°C. A thermocline extended from 0.36m deep through the column to a depth of 11.43m, where the temperature decreased sharply from 18.75°C to 15.6°C (Figure 3.3.8.1.1.1). Therefore, the bottom level recorded temperatures sufficient for microbial activity (Pomeroy, 1991). The pH increased from the surface to a depth of 0.7m at site 1, where the higher pH was maintained to a depth of 1.7m. The sharp decline in pH to the bottom layer indicated primary productivity through the production of carbonic acid.

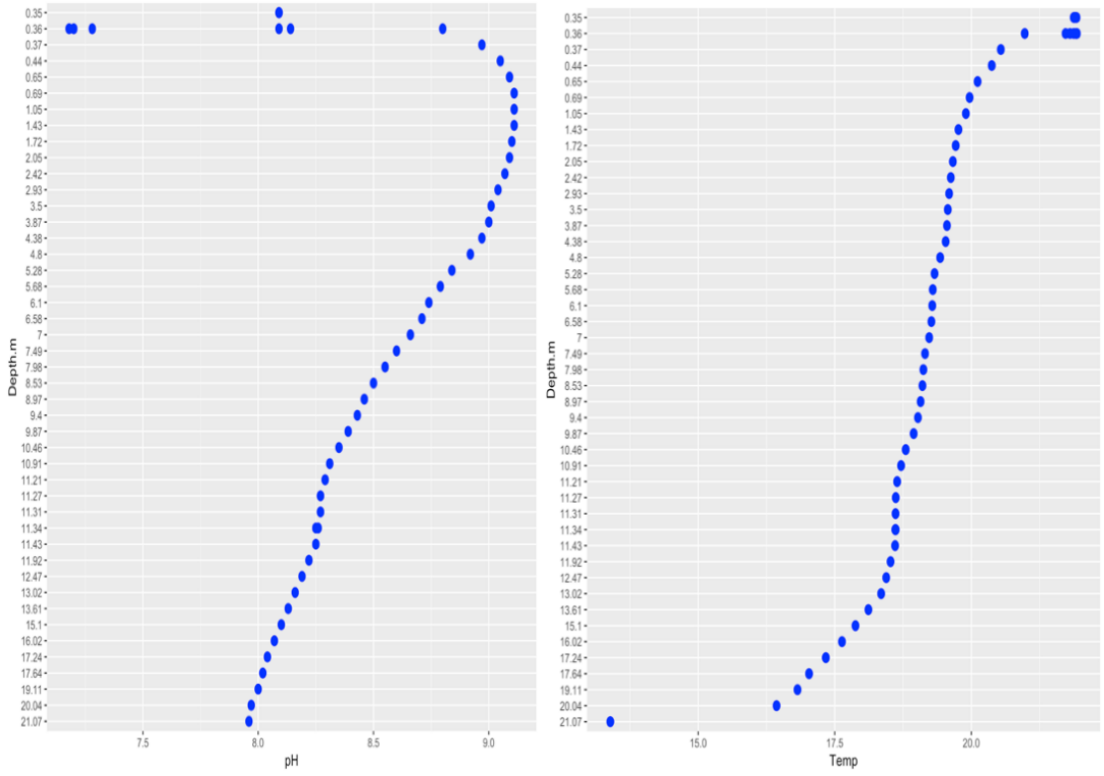

Figure 3.3.8.1.1.1. pH (left) and Temperature (°C) (right)profile for site 1 on August 3rd 2018.

3.3.8.1.2. Sampling site 2

The pH increased with depth to 3.3m and the temperature decreased, marking the start of the thermocline (Figure 3.3.8.1.2.1). A discrepancy of 3.8°C was recorded between the

surface and bottom water accompanied by a pH difference of 6.7, with the highest pH recorded (8.7) at a depth of 3.3m.

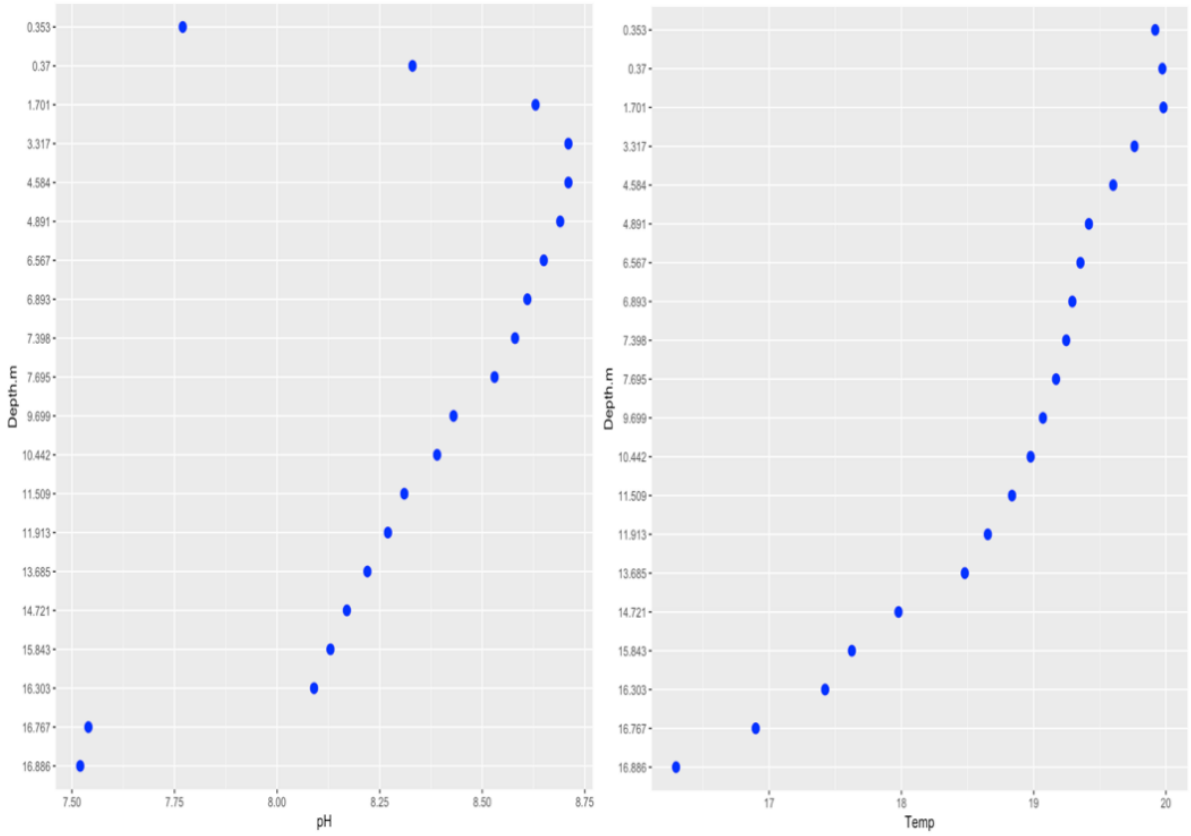

Figure 3.3.8.1.2.1. pH (left) and temperature (°C) (right) profiles of sampling site 2 during August.

3.3.8.1.3. Sampling site 3

The thermocline started at a depth of 0.62m where the temperature dropped from 21.3°C at a depth of 0.36m to 21°C, coinciding with an increase in pH from 7.45 at a depth of 0.36m to 7.7 (Figure 3.3.8.1.3.1).

At a depth of 5m, the temperature stabilised at 18.5°C. The pH was at its highest (8.49) at a depth of 4.26m but declined sharply (7.6) at a depth of 5m, where it continued to decrease until attaining pH6.5 at the bottom water.

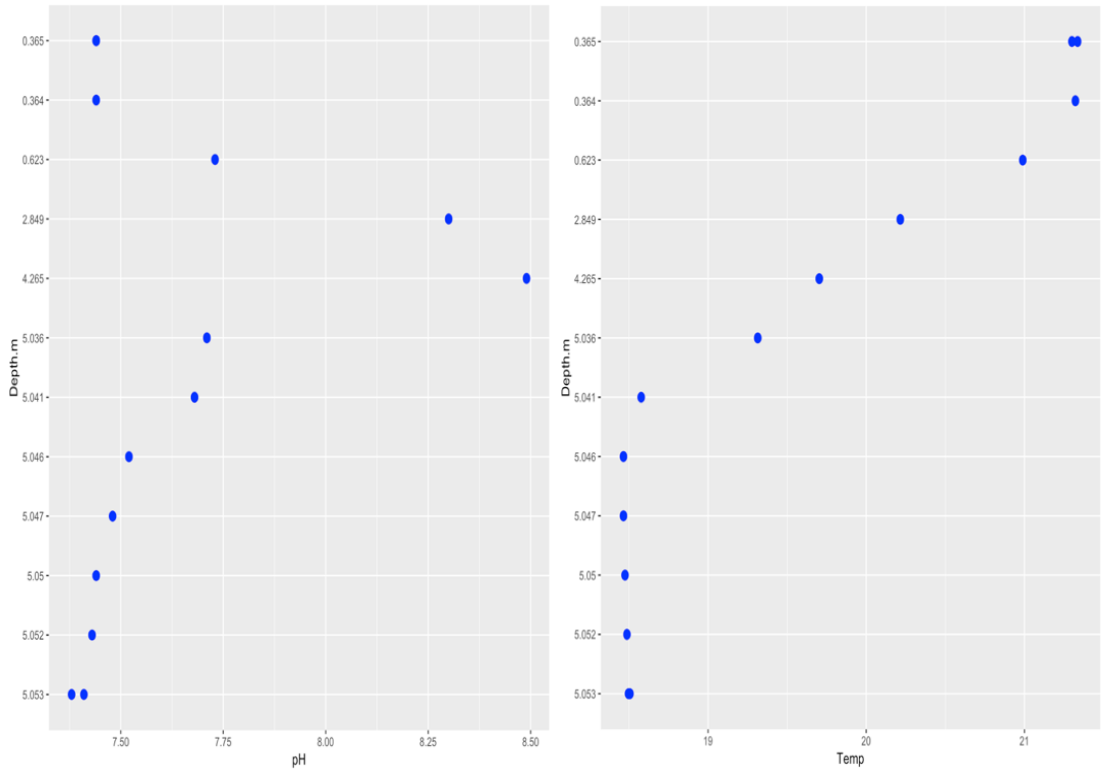

Figure 3.3.8.1.3.1. pH (left) and temperature (°C) (right) profiles of sampling site 3 during August.

3.3.8.1.4 Sampling point 4.

The temperature started to decrease at a depth of 0.353m from 22.8°C to 21.4°C, at which point the pH increased from 7 to 7.54, attaining its highest pH (8.7) at a depth of 1.4m. The pH decreased sharply at a depth of 1.73m to 7.8, attaining its lowest pH of 7.4 at a depth of 2.13m. A difference of 2.5°C was recorded between the surface and bottom water (Figure 3.3.8.1.4.1).

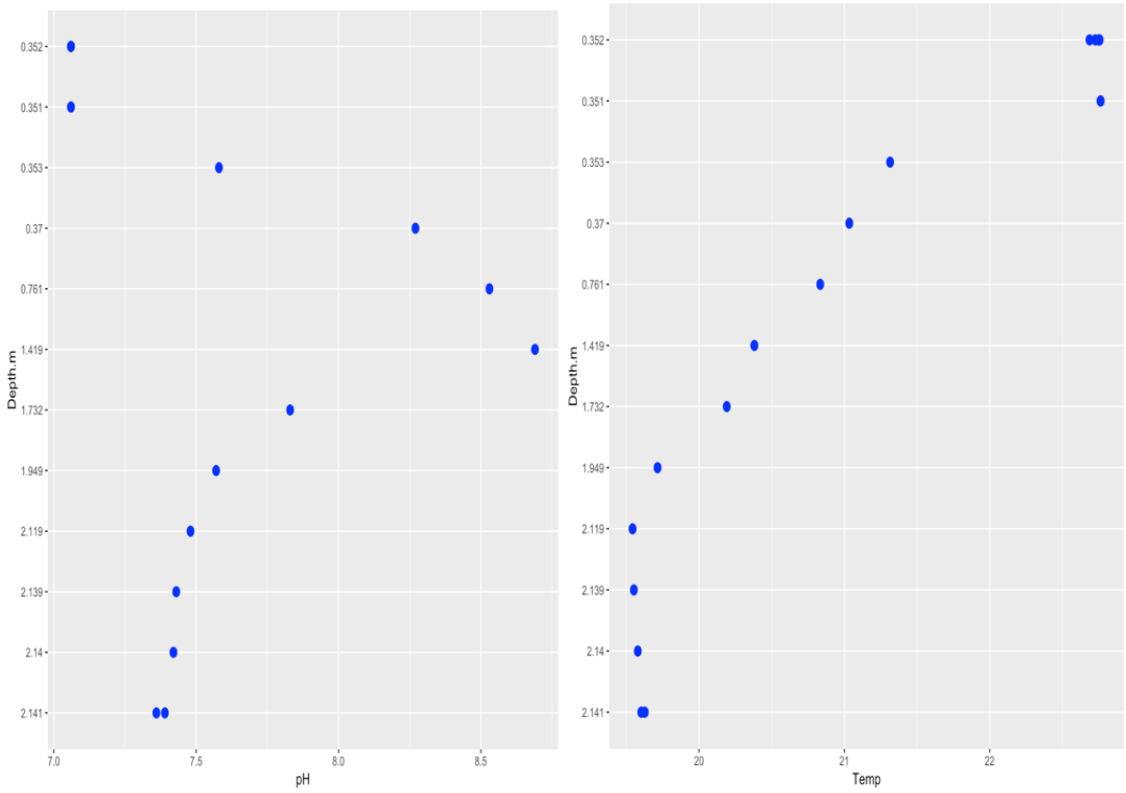

Figure 3.3.8.1.4.1. pH (left) and temperature (°C) (right) profiles of sampling site 4 during August.

3.3.8.2. Data recorded on 12th November

3.3.8.2.1. Sampling Site 1.

The temperature profile data for site 1 (Figure 3.3.8.2.1.1) indicated the absence of stratification and a thermocline. The surface temperature (10.5°C) insignificantly decreased at the bottom level by 0.1°C (to 10.4°C), indicating that the water had mixed throughout the column. A significant decrease in temperature was recorded throughout the depth of the reservoir at site 1 compared with that recorded during August (24°C at the surface, 16°C at the bottom level).

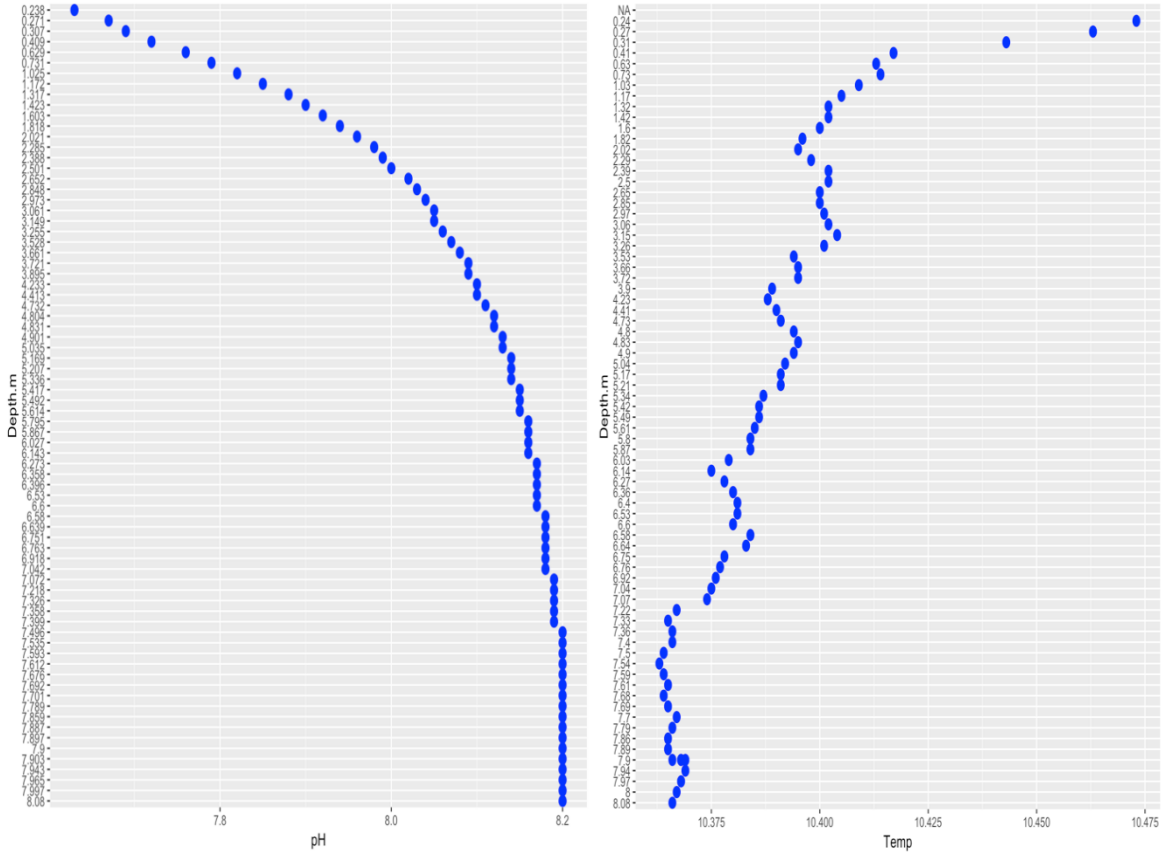

Figure 3.3.8.2.1.1. pH (left) and temperature (°C) (right) profiles of sampling site 1 during November.

The pH range at site 1 increased from the surface (7.6) to 8.2 at the bottom level (figure 3.3.8.2.1.2) indicating to primary productivity at the sediment surface.

3.3.8.2.2. Sampling site 2

The temperature data suggested that the water throughout the water column had undergone mixing. The surface temperature (10.4°C) decreased by 3% to its lowest temperature (10.1°C) at 18.2m, (Figure 3.3.8.2.2.1), indicating to an absence of a thermocline.

The pH profile through the water column showed a decrease in pH by 8% from the surface (8.5) to the bottom region (7.8), indicating to active or recently active primary production.

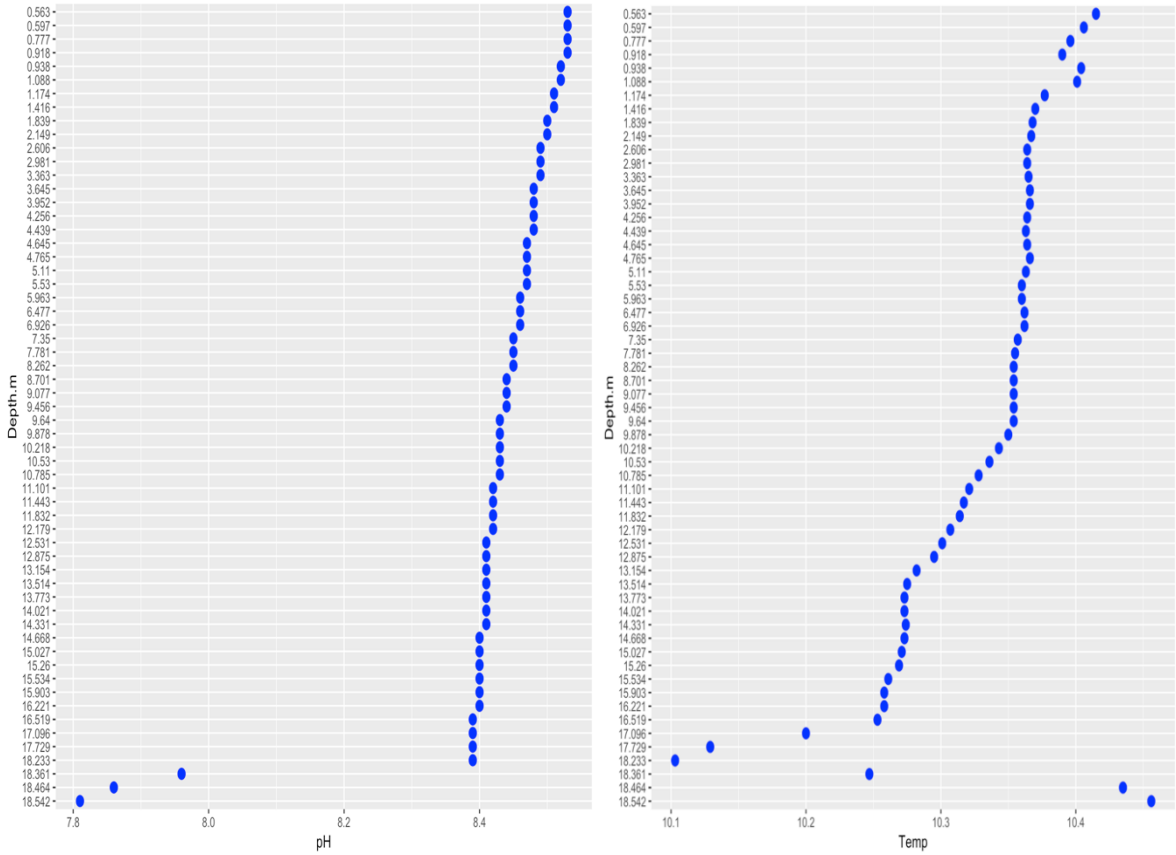

Figure 3.3.8.2.2.1. pH (left) and temperature (°C) (right) profiles of sampling site 2 during November.

3.3.8.2.3. Sampling site 3.

No thermocline was evident at site 3 during November. The temperature discrepancy between the surface to the bottom level was only 0.5% where the temperature reached 10.4°C at the surface and 10.3°C at the bottom level (Figure 3.3.8.2.3.1).

Site 3 displayed a uniform pH profile with only a 0.5% variation over the depth of the site. There was a reduction in pH at the bottom layer (to 7.96pH) compared with that at the surface (8.33pH).

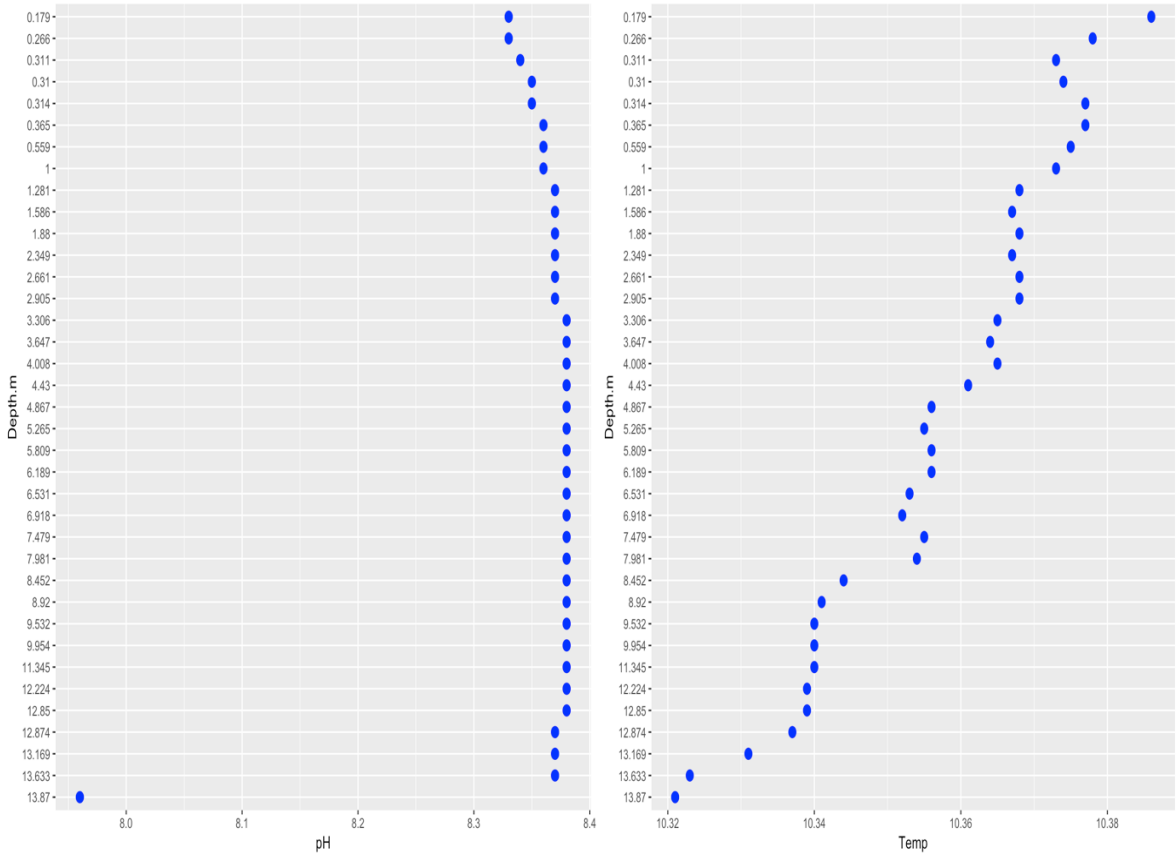

Figure 3.3.8.2.3.1. pH (left) and temperature (°C) (right) profiles of sampling site 3 during November.

3.3.8.2.4. Sampling site 4.

The temperature at site 4 during November showed a small degree of variation with depth (10.3°C ± 0.08) (Figure 3.3.8.2.4.1).

The temperature increased from a depth of 1m from 10.1°C to 10.2°C and continued to increase until a depth of 3m was reached (10.4°C). The data indicated a cooling of the water at the surface, and no thermocline was present. Site 4 was the shallowest of all sites (3.65m during November 2018) and as such, the water throughout the column at this site was more susceptible to external meteorological changes.

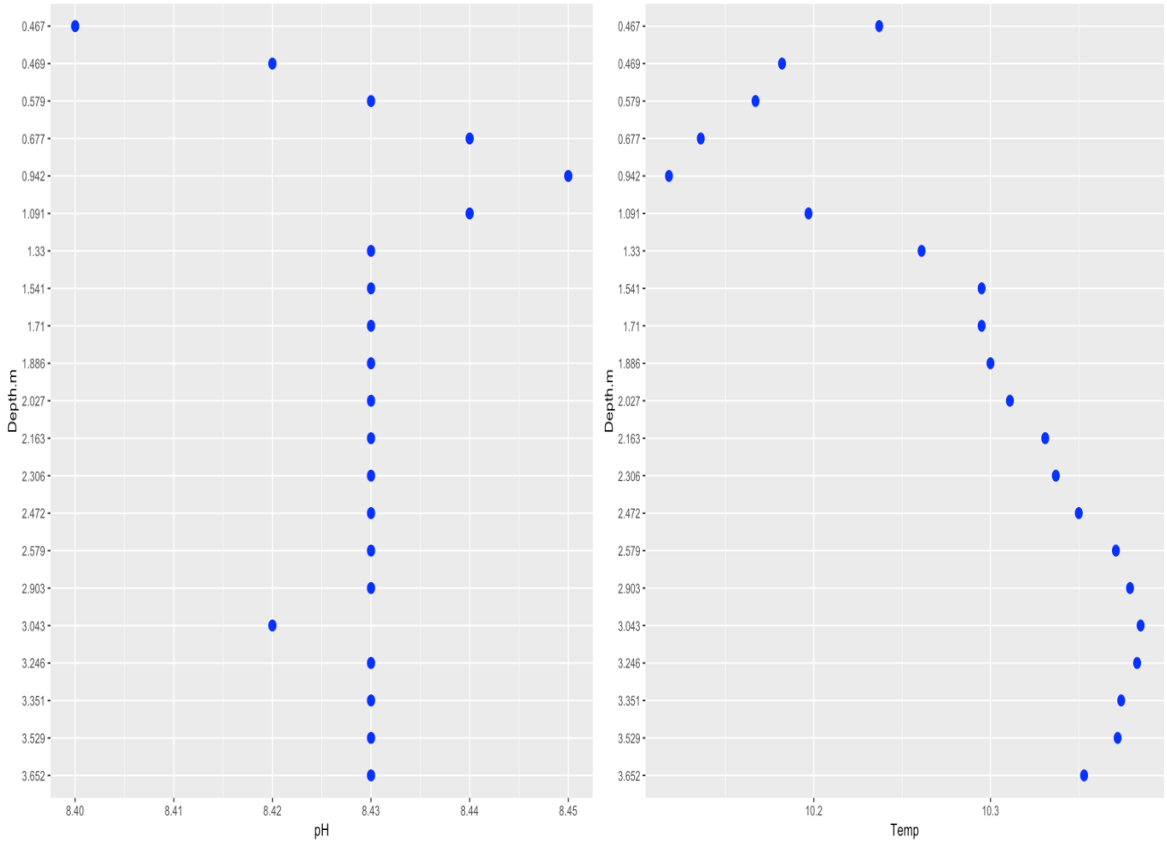

Figure 3.3.8.2.4.1 pH (left) and temperature (°C) (right) profiles of sampling site 4 during November.

There was a small degree of variation in pH (8.4 ± 0.01) at the surface of the reservoir at site 4 during November, indicating a stable and mixed column of water.

3.4. Discussion.

3.4.1. Main findings

AHP was the predominant fraction of P throughout the reservoir over the 11-month sampling period. OP was detected more frequently and at higher concentrations throughout the reservoir during the summer relative to the winter period, whereas organic-P was undetected or sporadically detected throughout the spring/summer period but detected more frequently and reliably during the autumn/winter periods. Site 4 was most at risk of increased organic-P concentrations throughout the year potentially as a consequence of a combination of factors including its proximity to the inflow, shallow characteristics and periphery constructed of loose sediment. Site B4 Recorded the highest concentration of AHP during January, organic-P and OP during February and the P-fractions consisted of condensed -P during May, June and

August. Both the bottom and surface sites recorded the highest TP concentrations during August.

The month of May was the period identified as being as a higher risk of cyanobacterial blooms as a consequence of low TN:TP ratios relative to TN:TP concentrations during any other month during which sampling took place. Cyanobacterial bloom risks were also greater during the spring/summer season in response to lower NO_3^-: NH_4^+ ratios throughout the reservoir. Both the TN:TP and NO_3^-: NH_4^+ ratios were most frequently determined by the concentrations of nitrate due to its significant contribution towards the ratios relative to that of ammonium. However, the TN:TP ratio was mostly determined by the P concentrations, and the NO_3^-: NH_4^+ ratio mostly determined by the ammonium concentrations during periods of lower ratios.

Geosmin was detected within the reservoir throughout the 11-month sampling period with the highest concentrations detected during May, indicating to the spring as being the period of highest taste and odour (T&O) failure risk to DCWW.

Stratification was recorded during the summer period (August), however, no significant difference in nutrient or environmental variables were identified between the surface and bottom sites during water sampling using the depth sampler. The reservoir had undergone mixing by November. APA analysis indicated P-limitation within the reservoir during early July during a dry period, but decreased pNPP concentrations following a period of heavy rain towards the end of July were recorded, indicating to an increase in P availability. However, P-limitation was evident during early August but undetected pNPP at the end of August indicated the absence of P-limitation.

3.4.2. General discussion

3.4.2.1. Phosphorous fractions data throughout the reservoir over the 11-month sampling period.

TP levels as low as 0.005mgL^{-1} are enough to maintain eutrophication (EPA). TP concentrations 0.01 - 0.03 mgL^{-1} suggested that P contamination was not an existing issue at the time of sampling, but the potential for eutrophication existed in the reservoir (Osis, 1986). Peak TP concentrations within the reservoir (0.057mgL^{-1}) exceeded concentrations deemed capable of sustaining cyanobacterial growth by the EPA (0.005mgL^{-1}) indicating a level of P that may potentially lead to eutrophication under changing climatic conditions.

UKTAG are a group of experts advising the government on environmental and conservational legislation. UKTAG reports define conditions deemed suitable for the support of healthy communities of aquatic plants and animals. Guidance and advice proposed by the UKTAG group are set using standards deemed appropriate for water quality classification by expert members of the UKTAG group (UKTAG, 2008). The status of a waterbody (e.g., good, bad etc.) is determined by the frequency a particular body of water meets or falls below thresholds set for specific variables. The thresholds are determined by UKTAG and are dependent upon the purpose of the waterbody (e.g., drinking, watersports) (UKTAG, 2008).

Llandegfedd reservoir was categorised as having a 'bad' status at sampling sites 1, 2 and 3 (>15m) on May 2nd with TP concentrations exceeding 0.048mgL^{-1} (UKTAG, 2016) at 4 of the 6 sites. During the same sampling period, the shallower site 4 (3-15m, UKTAG, 2016) also fell into the 'bad' category with the surface sample exceeding the threshold of 0.04mgL^{-1}.

Therefore, Llandegfedd reservoir achieved its worst water quality rating (bad) with regards to P concentration during the month of May, which also recorded low rainfall volume (50mm) and warm water temperatures (=>19°C). The presence of cyanobacteria and algae accompanied by an increase in ammonium concentrations relative to that during February, suggested that primary productivity was active within the reservoir during May, which is indicative of deteriorating water quality, with increased microbial metabolic activity during warmer conditions (Tian *et al.,* 2012). The limited rainfall during May could have eliminated inflows transporting nitrate from the land and oxidising the sediment which may have increased P-sorption (Wang *et al*. 2008), fuelling internal P-release within the reservoir.

Llandegfedd reservoir was categorised as being of a 'high' water quality status with regards to P concentration on 45% of sampling occasions (TP<0.008mgL^{-1}) over the 11-month sampling period (UKTAG, 2016). The 'High' status applied to all sampling sites during January, February and September, and to most sites in June, early July and late August. The depletion of P reserves by phytoplankton within the reservoir during warmer periods may have led to the 'High' water quality status being achieved (Carey *et al*., 2012). Therefore, high water quality with respect to potential eutrophication does not reflect the overall water quality of a reservoir.

The P concentration throughout the reservoir achieved a 'Good' status (TP = 0.0081-0.012mgL^{-1}) on 13% of the sampling occasions, with all occurring during and post-June, with

most sites (>4 out of 8 sites) registering as 'Good' at the beginning of August and during November.

The 'Moderate' status (TP= 0.0121 – 0.024mgL^{-1}) was achieved upon 15% of the sampling occurrences, with the majority of sites falling under this category at the beginning of August and during November. However, a 'Poor' status (TP=0.024 – 0.048mgL^{-1}) was achieved at most of the sampling sites (>4 out of 8 sites) on 29% of occasions during early May, increasing in frequency until early June. Each site achieved the 'Poor' status on July 31st after several days of precipitation following weeks of drought. The TP concentrations were insignificantly different between sites and depth of samples.

TP concentrations within lakes and reservoirs are known to fluctuate with the seasons and through the years in response to changes in the environment (Jeppeson, 2009). Bowman *et al.,* (1993), determined that the rate of eutrophication is increasing in parts of the UK, with particular reference to Lough Derg reservoir, Ireland, where mean annual TP concentrations were 43μgL^{-1} and considered to represent a high concentration of TP. Lough Derg reservoir would have been considered to be of an oligotrophic status with this concentration of P (OECD, 1982). Likewise, research by Spear *et al.,* (2018), indicated a maximum concentration of TP at Alderfren Broad, Hatchmere and Mere Mere water bodies of between 63μgL^{-1} and 89μgL^{-1}, with mean TP concentrations peaking during the winter at 82μgL^{-1} (Alderfen Broad) and at 124μgL^{-1} (Alderfen Broad) during the summer. Llandegfedd mean TP peaked at 0.057mgL^{-1} (± 0.004) (57μgL^{-1}) which was recorded during May, indicating that the TP at Llandegfedd reservoir is typically lower than that recorded at any of the three British sites studied by Spear during 2018.

Of the P-fractions, AHP was the most common throughout the sampling period, indicating a potential for an increase in the bioavailability of P under changing environmental conditions. Studies by Bostrom, (1988), also determined that the majority of bioavailable P within freshwater was AHP, a small portion of which was OP, with the remainder comprising condensed-P with the potential to become bioavailable under changing water conditions. The potentially available condensed-P was absent from all sites during January with the exception of bottom sites 2 and 4. However, the percentage of condensed-P increased by February to contribute 100% of the potentially bioavailable P to the reservoir, predominantly at the southern section of the reservoir, with pH >8 at each sampling site.

Levels of condensed-P during the middle of May were similar to those of OP. The pH remained between 8.2-8.4 at all sites. A high pH at the sediment/water interface may trigger orthophosphate (PO_4^{3-}) release from aerobic sediments by OH^- exchange with PO_4^{3-} bound to surfaces of metal oxides-hydroxides (Xie, 2012). The absence of inflow during May suggested that an increase in OP during the spring may have been a consequence of internal loading. The decrease in OP at the end of May concomitant with an increase in cyanobacteria, geosmin and condensed P suggested that cyanobacteria were assimilating OP at an increased rate relative to that during February. A rapid rate of cyanobacterial cellular lysis during a period of exponential growth in the presence of increased nutrient concentrations may have led to an increase in release of geosmin and condensed P to the water during a period of high pH (pH=>8.2).

Condensed-P concentrations increased throughout the reservoir over June and represented 100% of TP at sites B1, B4 and T3. Condensed-P concentrations declined through July and were absent at sampling points 3 and 4 by the end of July, indicating to a change to the aquatic environment which may have led to the hydrolysis of condensed P at the northern sampling points. However, the pH throughout the reservoir remained high (7.9-8.9), indicating to an increase in condensed-P as a consequence of the lysis of P-storing phytoplankton. Also, the short period of heavy precipitation at the end of July may have contributed towards the influx of inorganic-P from the surrounding agricultural land. Run-off events following periods of heavy rainfall can contribute up to 90% AHP to a reservoir (Sharpley, 1993), with bioavailable particulate P comprising 10-90% of particulate P transported into a reservoir in run-off (Sharpley, 1993). Tian *et al.,* (2012), documented that the effect of phosphorus availability on cyanobacterial abundance becomes evident in warm periods compared with that during colder temperature (Tian *et al.,* 2012), due to increased microbial metabolism at higher temperatures. Bacteria respond to nutrients at a faster rate in warmer temperatures due to an increase in available energy (Carey *et al*., 2012). Therefore, microbes achieve a faster rate of growth during warmer periods due to the ability of the cells to metabolise nutrients at a faster rate.

The OP concentrations decreased, and the pH increased (8-8.6) during early August, coinciding with an increase in condensed-P concentrations throughout the reservoir with the exception of site T3 where OP was the predominant fraction of P. Site T3 also recorded the

lowest pH of all sites (7.9), suggesting that pH changes within the reservoir influenced the condensed-P concentrations.

The concentration of condensed-P increased throughout the reservoir through autumn and into winter. Concomitantly, OP concentrations were below detection limit throughout the reservoir during September through November with the exception of low concentrations at site T1 during November. The pH decreased throughout the reservoir during September (7.9-8.2), with the lower pH retained through November. OP concentrations increased to equal/surpass AHP concentrations at the end of June through early July at most sites. The concentrations of condensed-P (AHP) excluding OP occupied the majority of TP.

Three peaks in OP concentrations were recorded across all sites over a period of 3 months (early May, early June and mid to end of July). Cyanobacteria shared a negative correlation with OP during May, indicating to the depletion of OP due to assimilation, but were only recorded at bottom site 4 during late July (23rd) in the absence of any recorded OP. A negative association was determined for OP with geosmin during July indicating to the absence of cyanobacteria at the majority of sites (7/8) due to senescence (Gomes *et al.,* 2012). OP remained low following August throughout the reservoir (<0.007mgL^{-1}), indicating a limited availability for phytoplankton growth.

Organic-P was the least frequently detected P-fraction throughout the 11-month period, being absent from May through September with the exception of July 9th where organic-P was isolated at six of the eight sites and attained its highest concentration of the sampling period (<0.009mgL^{-1}). Spear *et al.,* (2018), determined that OP was most likely to be detected within a reservoir throughout each of the four seasons in the UK, but organic-P was most likely to be detected during the autumn and winter seasons in the UK only. Although data from Llandegfedd indicated sporadic detection of organic-P throughout all seasons, the organic-P was most frequently recorded during the winter and autumnal seasons, supporting the findings made by Spear *et al.,* (2018). Yu, (2020), determined that increased rates of eutrophication were concomitant with increased concentrations of Organic phosphorus. Therefore, the relatively low organic-P concentrations at Llandegfedd reservoir suggest a low risk of eutrophication during the sampling period of 2018.

3.4.2.2. APase activity during the summer period and P-fraction concentrations.

APase activity varied from July through August with an increase in activity at most sites on August 3rd compared with that throughout July. The increase in activity coincided with an increase in organic-P, high cyanobacterial cell counts (2400 cfu/ml – 6900 cfu/ml) and low concentrations of P_i indicating active hydrolysis of organic-P. The recycled P load may be increased by up 22% by the hydrolysis of organic-P upon initiation of alkaline phosphatase which releases hydrolysed condensed-P in phytoplankton and cyanobacteria to the water (Feng *et al*., 2018).

A decrease in APase activity during July was accompanied by an increase in OP concentrations, indicating to the sufficient volume of OP for cyanobacterial growth during the drought period with APase activity no longer required, indicating a reduction in cyanobacterial stress (Pandey, 2011). Low internal and external P concentrations induce the production and secretion of APase, which is repressed when P concentrations return to sufficient levels for growth and metabolism (Zhou, 2015).

An increase in free APase is positively linked to an increase in cyanobacterial stress and mortality (Baltar *et al.,* 2019). Therefore, an increase in the concentration of APase on August 3rd coinciding with an increase in organic-P, predominantly at the surface sites in the absence of geosmin but the presence of cyanobacteria indicated the detection of cellular APase activity in living cyanobacteria. However, cyanobacteria were not identified at any of the bottom sites on August 3rd using depth sampling techniques, data which was supported by the detection of geosmin, indicating cellular lysis. Conversely, the Sonde identified the presence of cyanobacteria at all four sites. Therefore, bottom APase activity on August 3rd may have been indicative of both free and cellular bound APase. Zhou, (2015), determined that a reduction in APase may also be a consequence of increased water turbulence, such as that likely during the period of heavy rainfall. However, a decrease in APase was not recorded on 3rd August, suggesting that the rainfall recorded at the end of July did not induce turbulent conditions sufficient to decrease APase concentrations.

3.4.2.3. TN:TP and NO_3^-: NH_4^+ molar ratios throughout the reservoir over the 11-month sampling period.

The TP concentrations were low throughout the reservoir relative to the concentrations of TN, leading to TN:TP ratios frequently exceeding 29:1 (Smith's ratio) over the 11-month

sampling period. TN:TP ratios ranged from 14:1 during May to 699:1 during February (January omitted due to absence of P), indicating a high degree of nutrient variability within the reservoir over an 11-month period.

The mean monthly TN:TP ratios were greater than that of Smiths ratio at >4 sites during January, February, early July, August, September and November. However, the ratio remained between that of Redfield and Smith (16:1 – 29:1) throughout May at 7 of 8 sites and late July for 3 of the 8 sites, indicating an increased risk of cyanobacterial establishment during the spring and following an extended period of dry warm weather. The NO_3^-: NH_4^+ ratio remained low relative to the TN:TP ratio for the majority of the 11-month period (May through November), indicating to the potential for rapid cyanobacterial growth throughout the warmer seasons. The month of May also recorded the lowest TN:TP ratio for all sites (as low as 16:1 at T2 and B1) with the exception of site T4, where the lowest TN:TP ratio was recorded during July (31:1) and remained above Smith's ratio (29:1) over the sampling period. Likewise, the NO_3^-: NH_4^+ ratio was low during May, predominantly a consequence of raised ammonium concentrations as opposed to decreased nitrate. The decreased TN:TP ratio was predominantly due to the increase in TP concentrations as opposed to a large nitrate concentration decrease. The lowest NO_3^-: NH_4^+ ratios were recorded during the autumn at site T3.

All sites recorded a high TN:TP ratio (>100:1) during January and February (where data present) with the exception of site B1 (27:1), and NO_3^-: NH_4^+ ratios remained high at all sites relative to TN:TP ratios, indicating a low potential for rapid cyanobacterial growth. However, both the TN:TP and NO_3^-: NH_4^+ ratio decreased during May, with the NO_3^-: NH_4^+ ratios decreasing to 10:1 or below throughout the reservoir. The NO_3^-: NH_4^+ ratio became negative at site T4 during May, with ammonium concentrations three times greater than that of nitrate. The data suggested that surface site 4 was of a greater risk of rapid cyanobacterial growth during May than any other site. The decreased TN:TP ratio at the surface sites and B4 was concomitant with geosmin detection at the sites during mid-May. Geosmin was recorded at all southerly sites (1 & 2) but was highest at site B4 and concomitant with the highest count of cyanobacteria at the end of May. The TN:TP ratios had increased above Smith's ratio by early July, with the highest ratios recorded at sites B2, T3 and B4 indicating to an increase in nitrate following a rise in recorded P from June. The increase in NO_3^-: NH_4^+ ratio suggested that nitrate was the predominant cause of the TN:TP increase during early July.

The end of July recorded a TN:TP ratio equal to or below Smith's ratio at each site, with the ratio falling below Redfield's ratio at bottom site 1. The data suggested that the prolonged dry conditions become favourable to cyanobacterial growth at most sites with the exception of site B2 where the NO_3^-: NH_4^+ ratio was significantly higher than that recorded at any other site. The TN:TP ratios decreased at most sites during early August relative to that at the end of July due to a decrease in TN and an increase in TP concentrations. The NO_3^-: NH_4^+ ratio was low (<5:1) throughout the reservoir with the exception of sites B2 and B3, suggesting that the mid-transect bottom sites were the least likely sites to record rapid cyanobacterial growth relative to all other sites.

The TN:TP ratios were very high (>100:1) during September throughout the reservoir; however, the NO_3^-: NH_4^+ ratio was low (=<2:1) at each sampling point with the exception of site B4, indicating to its susceptibility to decreased ammonium during late summer. The absence of both geosmin and cyanobacteria at B4 suggested that the 10-fold decrease in ammonium accompanied by a smaller decrease in nitrate concentrations relative to other sites may have been a consequence of changes to the sediment or microbial communities at the northern site. The increase in nitrate concentrations was primarily responsible for the increase in both the TN:TP and NO_3^- : NH_4^+ ratios. The TN:TP concentrations decreased during November from those in September. TN:TP ratio at site B2 remained high during November (214:1) relative to all other sites (=<88:1 and a low as 35:1 (B1)). The NO_3^-: NH_4^+ ratio remained low (=<3:1) throughout the reservoir with the exception of site B2 (20:1).

The increased concentration of ammonium at surface sites compared with bottom sites during mid-summer indicated a reduction of N at the surface where high counts of cyanobacteria were isolated. Higher concentrations of ammonium were detected at all four bottom sites on the 3rd of August and were concurrent with the detection of cyanobacteria whilst using the Sonde. Also, potentially anoxic conditions in the bottom zone on 3rd August may have led to the release of ammonium from the sediment (Su *et al*., 2019).

Nitrate concentrations decreased throughout the reservoir following a period of precipitation at the end of July. The data indicated the precipitation as the cause of the increase in nitrates throughout the reservoir, and an increase in nitrate reduction as a cause of a decrease in nitrate concentration (by up to 50%) on the 3rd of August. Wang *et al.,* (2008) determined that an increase in NO_3^- concentrations as a result of nitrate entering the reservoir entrained within inflow raises the PO_4^{3-} sorption capabilities of surface sediment through maintaining

the oxidised state of Fe_3^+. Conversely, NO_3^- also stimulates the growth of iron-reducing bacteria in anoxic conditions, potentially increasing the rate of P release to the water (Jensen *Model addressing significant associations of independent variables with dependent variables.*, 1992). Therefore, N-fraction data analysis may contribute towards understanding the potential for both the periods of increased P-sorption and increased microbial activity within a reservoir.

A study into nitrogen retention in a reservoir by Liu *et al*., (2019), determined that an increase in nitrate (and therefore TN) concentrations were recorded throughout the reservoir during periods of warmer weather under conditions of decreased wind velocity, supporting the data obtained from Llandegfedd reservoir. Likewise, Liu also determined that ammonium concentrations were elevated over the same period but differed from nitrate fluctuations through remaining at an increased concentration for a longer period into the colder seasons.

3.4.2.4. Geosmin concentrations throughout the reservoir over the 11-month sampling period.

Geosmin concentrations remained low (<6ngL^{-1}) throughout the sampling period, with the highest concentrations recorded during May (5ngL^{-1} at site B4). Nutrients, particularly P and N, contribute towards the regulation of geosmin production in cyanobacteria (Zhang *et al.,* 2019), especially during mixed, warm periods (Clercin *et al.,* 2019). Espinosa *et al.,* (2020), determined that geosmin production by cyanobacteria is most likely to occur during periods of low TN:TP ratios, particularly when the concentrations of orthophosphate decrease (Espinosa *et al*., 2020), indicating a period of rapid growth. The TN:TP ratio reached its lowest at most sites during May which was accompanied by peak geosmin concentrations at most of the sites, concurring with what was documented by Espinosa *et al.,* (2020). However, OP concentrations were also at their highest during May, suggesting that P was not a limiting factor during the month of May at Llandegfedd reservoir.

Environmental conditions may also influence geosmin production by cyanobacteria (Li *et al.,* 2012), with light intensity (Blevins *et al.,* 1995), and water flow (Juttner *et al.*, 2007), being among the most critical environmental factors (Elosegi *et al.*, 2013). Increased light intensity can contribute towards the risk of geosmin production (Saadoun *et al.,* 2001), therefore climate change may exacerbate geosmin-producing conditions within the UK (Elosegi *et al.*, 2013). Therefore, the potential for geosmin production at Llandegfedd reservoir may have been fuelled by the increased light intensity during the May relative to that during the winter

periods. Juttner and Watson, (2007), determined that the risk of geosmin production within a reservoir increased at locations closer to a dam relative to other locations within the reservoir due to the reduction in flow leading to less turbulent conditions (Juttner *et al.*, 2007). However, geosmin concentrations were higher at the sites furthest from the dam, potentially exacerbated by the inflow of nutrients within close proximity to the northern sites.

Research by Vilalta *et al.,* (2003), into the ecological factors that co-occur with geosmin production determined that the highest concentrations of geosmin in a European lake occurred between January and May in the presence of *Oscillatoria spp*. of cyanobacteria, which concurred with the data obtained at Llandegfedd reservoir.

3.4.2.5. Model addressing significant associations of independent variables with dependent variables.

Analysis of the data concluded that no significant association was determined for any P fraction with any of the variables analysed, suggesting that variables beyond the scope of this project may be smore ignificantly influencing the P within the reservoir.

Stratification occurred at all four sites by August, suggesting limited nutrient availability at the bottom sites. Yu *et al.*, (2020), determined that anoxic benthic zones may lead to enhanced P release during organic matter degradation, fuelling phytoplankton growth and a more severe DO depletion (Yu *et al.*, 2020). However, despite a thermocline being evident in the stratification data on August 3rd, a decrease in P was recorded in the bottom waters relative to the P concentrations during July, suggesting P depletion following assimilation.

However, rainfall can disturb the structure of a thermocline and lead to mixing throughout the water column. Rain disturbs the bottom and surface water, potentially leading to growth inhibition of algae and cyanobacteria (Weng *et al.*, 2019), through suppressing sediment P-release. Therefore, the rainfall recorded at the end of July may have contributed towards the decrease in bottom water P concentrations on the 3rd August.

During stratification, pH decreased with depth at all four sites indicating primary production, thereby supporting the detection of cyanobacteria when using the Sonde.

However, no evidence of a thermocline remained during November, suggesting that mixing of the water column had occurred. The mixing coincided with an increase of OP throughout the reservoir, but no cyanobacterial bloom was recorded during the autumn.

Thermal stratification and the mixing process as a consequence of stratification breakdown disrupts the nutrient dynamics within a reservoir (Pu *et al*., 2020). Despite a significant difference between surface and bottom geosmin and cyanobacterial concentrations from May through September, the absence of a significant difference in environmental and nutrient parameters suggested a ubiquitous water column with the absence of nutrient restrictions as a consequence of stratification during the summer period. However, nutrients may be entering the surface of the reservoir through inflow or run-off during periods of rainfall where it may have been retained by the thermocline, providing conditions insignificantly different from those in the bottom regions.

Stratification can frequently explain the temporal and spatial distribution of cyanobacteria (Golshan *et al*., 2020), and pH (Dong *et al.,* 2013), within a reservoir. The hypolimnion restricts the volume of gaseous exchange with the atmosphere during periods of stratification relative to the gas exchange when the water column is mixed (Pu *et al.,* 2020), leading to the potential for anoxic conditions and an increase in sediment-P release. However, no significant differences between TP concentrations of the bottom and surface waters were recorded on August 3rd at any of the sites sampled.

3.5. Conclusion

Following completion of the data analyses, two of the three hypotheses need to be retained; The P concentrations were at their lowest during the winter period and there were no significant associations between P-fraction concentrations and the nutrients or environmental data.

With regards to the third hypothesis stating that 'higher P concentrations shall be recorded at site 4 relative to that at any other site', the data indicated that the highest mean annual TP concentrations were isolated at site 2 (specifically T2). Also, neither the surface or bottom samples of site 4 recorded the highest or lowest mean annual OP, AHP or Organic-P over the 11-month sampling period. Therefore, data led to the rejection of the hypothesis anticipating higher concentrations at site 4 relative to that at any other site. However, monthly analysis of P-fraction data indicated site 4 (bottom and surface) as being the highest risk site of cyanobacterial growth during the summer period due to high OP concentrations relative to all other sites, and during the spring under changing reservoir conditions, during which, condensed-P may be hydrolysed to OP.

Llandegfedd reservoir mainly attained a 'High' status of water quality with regards to P concentration more frequently than any other status throughout the 11-month sampling period. Llandegfedd reservoir was at an increased risk of eutrophication as a consequence of raised P concentrations, particularly during May, during which it was deemed to be of a 'bad' quality (UKTAG). The high concentration of condensed phosphates relative to other P fractions highlighted the potential for an increased risk of internal P loading during periods of environmental changes resulting in a decrease in water pH, where the condensed P may be hydrolysed to OP. The pH at Llandegfedd reservoir was predominantly >7.5 as indicated by the domination of condensed-P but was prone to a decrease in pH during periods of primary productivity, with the potential for hydrolysis of condensed-P to orthophosphate, thereby increasing the immediately bioavailable load of P within the reservoir.

The TN:TP ratios frequently recorded below the ratio recommended by Smith, (1982), for suitable cyanobacterial growth, with the greatest risk during, but not limited to May. The low NO_3^-: NH_4^+ molar ratios throughout the spring and summer seasons suggested Llandegfedd Reservoir was at frequent risk of rapid cyanobacterial growth and therefore, geosmin production.

The northern half of the reservoir was a higher risk of cyanobacterial bloom during mid to late summer as indicated by a decrease in condensed-P and a simultaneous increase in OP.

Organic-P was more prevalent during the autumnal and winter seasons, indicating that inactivity of APase and reduction/absence of microbial activity throughout the reservoir during colder seasons, but APase activity increased during the spring/summer season, thereby increasing OP availability and a greater risk of cyanobacterial blooms.

Llandegfedd reservoir undergoes a period of stratification on at least one occasion a year, the establishment of which affects the distribution of nutrients within the reservoir. However, benthic bacteria are more influential upon the nutrient distribution throughout the water column than stratification (Pu *et al.,* 2020), suggesting that further analysis of benthic biota may further our understanding of Llandegfedd reservoir and its nutrient dynamics.

Chapter 4: Spatial and temporal variation in sediment Phosphorus fractions in Llandegfedd Reservoir

4.1. Chapter summary

The sediment of reservoirs pose a threat to water quality through eutrophication of the water as a consequence of internal loading. The phosphorus (P) release mechanisms are reservoir specific (Søndergaard *et al.,* 2003), the rate of which can be accelerated or decelerated either directly or indirectly through changes to various environmental factors including pH changes (Hupfer *et al.,* 2004), as a consequence of microbial activity, redox changes (Vepraskas *et al.,* 2016), and climatic conditions (Kragh *et al*., 2017), each of which has the potential to change rapidly within a reservoir environment.

In this chapter, P-fraction data collected from sediment samples at various depths at different period of the year at four sampling points along the transect of the reservoir are discussed. In addition, P-fraction concentration data at each depth sampled are analysed with water quality variables to help determine whether significant associations exist between the variables.

In addition, the Total Organic Carbon (TOC) is discussed to help to determine the potential risk of microbially-mediated P release. Analysis is completed to determine whether TOC concentrations are significantly associated with P concentrations.

Main findings of this chapter:

- Llandegfedd reservoir demonstrated dynamic P-binding properties through the sediment layers over the sampling period along with changes to sediment composition that may have altered the conditions under which enhanced sediment-P dissolution occurred.
- Site 4 was at the highest risk of cyanobacterial establishment of all sampling sites due to its proximity to an allochthonous nutrient supply and its shallow characteristics. Therefore, site 4 may pose a higher risk to water quality degradation as a consequence of climate change relative to all other sampling sites. Internal nutrient loading may lead to eutrophication of Llandegfedd Reservoir

4.1.1. Sediment disturbance impact upon P-release.

Hydrodynamic conditions such as stratification, bioturbation and sedimentation events in the overlying water of the sediment control the changes in redox conditions (Jensen *et al.,* 1992). Repeated resuspension of sediment particles and microorganisms within the sediment induces dynamic changes from aerobic and anaerobic conditions (Gerhardt *et al.,*

2005), changing the chemical properties that may move phosphorous and other nutrients to the water (Eggleton *et al.,* 2004). The sediment P concentrations are typically lower in shallow water (< 0.1 m) relative to sediments from deeper locations within a reservoir, suggesting that P is depleted at a higher rate in shallower areas of a reservoir (relative to sediments within deeper areas) due to frequent sediment suspension during storms (Kragh *et al.,* 2017).

4.1.2. Fe-P and Ca-P within sediment

Higher rates of primary productivity in either the benthic zone or the water column are associated with reducing conditions which are associated with an increase dissolution rate of Fe-P and Ca-P, further fuelling decomposition processes (Paudel *et al*., 2017).

Phosphorous can be loosely bound to sediment (labile-P) or bound to iron (Fe-P) or calcium (Ca-P) complexes which can be easily dissolved depending upon the water conditions. The organic P fraction are most frequently omitted from biogeochemical cycling but support the long-term burial of P within the sediment (Hartzell *et al.,* 2010); however, labile-P, Fe-P and Ca-P undergo frequent cycling from within the sediment to the water column depending upon the prevailing conditions. Therefore, the conditions under which the P becomes dissociated into the water is dependent upon the metal to which the P is bound (Gomez *et al.,* 1999).

4.1.3. Internal P loading

Changes in the oxygen status of overlying water in anaerobic conditions may fuel an increase in internal P loading from the sediment (Moore *et al.,* 1998), which is considered to be both a P source and P sink, changing from one status to the other depending upon the conditions of the overlying water (Liu *et al.*, 2016).

A variety of conditions at the sediment surface can lead to an increase in internal P loading rate and volume. Changes to the redox potential (Jensen *et al.,* 1992), at the sediment surface as a consequence of anaerobic conditions may increase P concentrations in the water (Watts, 2000), fuelling cyanobacterial establishment through releasing nutrients from the sediment. In addition, changes to the pH and redox potential at the sediment surface can increase the rate of internal P loading and bacterial degradation (Eggleton *et al.,* 2004), with a high pH positively influencing the rate of nitrogen and phosphorus release (Hou *et al*.,

2013). Redox conditions >100 mV are recorded when oxidised conditions are prevalent; however, the conditions become reducing when redox conditions are <100 mV (Miao *et al.,* 2006). When the conditions are oxidising, the concentration of free electrons within the water decrease, leading to a reduction in the rate and volume of internal P loading due to an increase in P binding to the metals within the sediment (Christophoridis, 2006).

4.1.4. The importance of internal loading within a reservoir.

Phosphorous is one of the drivers of primary production within a reservoir and is often deemed to be the critical nutrient in the control of cyanobacterial blooms (Schindler *et al.,* 2016). Orthophosphate is the P-fraction required by autotrophs for assimilation, leading to the excessive production of algae and cyanobacteria (Correll, 1998), potentially leading to deterioration in the water quality. Information acquired regarding the sediment chemical P-fraction concentrations may help understand whether the sediment acts as a source or sink of P (Sahin, 2012), with the concentration of phosphate bound to iron and calcium being the most informative (Perrone *et al.,* 2008).

Net phosphorous removal from the water by the sediment decreases with increasing depth (Stumm, 1983), and the overall quantity of P release from sediment in deeper regions being very small relative to that of other fluxes (Stumm, 1973), due to a decrease in parameters that influence sediment P release such as microbial-induced redox changes and wind-induced sediment disturbance. Internal P loading may limit or disrupt attempts to improve water quality within the reservoir (Søndergaard *et al*., 2003). Analysis of the different P-fractions within reservoir sediment is an efficient method of determining the extent to which sediment P concentrations affect lake eutrophication (Perrone *et al.,* 2008). Phosphorous stored within the sediment can be released from a depth of 20cm within the sediment (Søndergaard *et al*., 2003); therefore, data regarding the phosphorous-fraction concentrations through the sediment depth are required to understand the risk of internal loading within a reservoir. Analysis of inflow and outflow of P can increase the understanding of P loading within the reservoir.

4.15. Hypotheses addressed in this chapter

In this chapter the following overarching hypothesis and subhypotheses shall be addressed: Overarching hypothesis: Sediments within a closer proximity to the pumped inflow (sampling site 4) will have greater TOC and hence enhanced benthic microbial activity.

Sub-hypotheses:

1. Labile-P concentrations will be lowest at the sediment surface and increase with sediment depth during the summer (due to a reduced redox potential).
2. Internal P loading will be greater during the summer relative to the spring period. Internal loading will be a significant source of phosphorous compared with external loading of phosphorous.

4.2. Sampling sites and method

4.2.1. Sediment sampling processes

Sediment cores were collected in triplicate up to 15 cm length (internal diameter 7.5 cm) at each site on four occasions over two years with the first sample taken during April 2016 and subsequent samples collected during July 2017, April 2018 and July 2018. The cores were obtained using a cylinder attached to a cord to help prevent loss of the instrument at depth. The base of the corer was plugged following loss of weight upon the cord, thereby triggering the movement of the plug over the base of the corer, locking the sediment core within the cylinder.

Due to the unavailability of the corer for the July 2018 sampling date, sediment samples were collected using a mechanical grab. The weight of the instrument insured sufficient sediment was recovered at depth to represent samples at 1-3cm and 13-15cm depth section of each core. However, no analysis was carried out for samples between depths of 4-12cm.

Cores were stored vertically and returned to the laboratory. Overlying water was carefully siphoned off and on initial sampling dates tested for orthophosphate. Cores were sectioned into 3 cm depth intervals and stored in sealed plastic containers at 4 °C. After gentle mixing

of core sections, sub-samples were taken for analysis for organic carbon content and sequential fractional analysis for phosphorus and mineral ion concentrations.

4.2.2. Sediment TOC analysis methods

Percentage moisture content (wt / wt) was analysed by loss of weight on drying at 80°C for 24 hours. The dried samples were then incinerated at 550°C in a muffle furnace for one hour to determine the percentage ash free dry weight (wt / dw).

4.2.3. Ion chromatography analysis of iron and manganese ionic concentrations

Samples of sediment pressed into a powder were covered with an x-ray transparent Prolene film and were analysed by portable x-ray fluorescence (pXRF) at Cardiff University using an Olympus Delta Pro pXRF system with a Rh tube anode. Freeze-dried sediment sub-samples of depths 0-3cm, 4-6cm and 7-9cm were analysed for iron and manganese ion concentrations in Geochem mode using a total count time of 40 seconds. High purity silica powder was used to determine a blank and calibration was based on a series of certified reference materials made up of contaminated soils, crushed rocks and crushed ores (NIST 2710a, KC1, UM1, HV1 and SU1a). Raw results were exported in csv format into Excel for further processing. No data were available for samples collected during April 2016.

4.2.4. Sequential phosphorus fractionation

Sediment samples equivalent to 1.0g dry weight were analysed for labile phosphorus, iron-bound phosphorus and calcium-bound phosphorus using sequential extractions in ammonium chloride (1M, pH 7), sodium hydroxide (0.1M) and hydrochloric acid (0.5M) following the method of Hieltjes and Lijklema (1980) which removed labile P, Fe/Al bound and Ca bound-P respectively. The method can be seen in Appendix 6.

After neutralising and centrifugation, samples were measured for orthophosphate using the ascorbic acid method (APHA, 1995).

4.2.5. Statistical analysis

For data analyses throughout the chapter, the mean value for each parameter per month was determined for each variable accompanied by the standard deviation (SD). Due to small sample sizes (n<25) and not normally distributed data exhibiting ties, Kendall's Tau was used to test for associations between two continuous variables and Kruskal-Wallis test to determine significant differences between sets of not normally distributed data. Where data was not normally distributed, but sample size was large (n>25) Spearman's rank correlation was used.

Significant associations between variables were determined using General Linear Models (normally distributed data)/Generalised Linear Models (non-normally distributed data even following transformation methods)/Linear Models (where non-normal data were successfully transformed) were completed using R studio (version 3.4.4) following the selection of independent variables demonstrating correlation with the dependent variable as determined through Principal Components Analysis (PCA) analysis using PAST (version 4.03).

Data were standardised to allow cross-variable PCA. Variables were omitted from the PCA during periods of recorded repeated '0' values. The following equation was used for the standardisation to allow for direct data pattern comparisons between variables of differing scales:

$$(X-\mu)/\sigma$$

where X is the observation, μ is the mean and σ is the standard deviation.

Once the list of correlated variables had been determined for each dependent variable, the Shapiro-Wilks test was used to determine normality of data. Data were transformed by log, cube, square-root or Tukey's Ladder of Power where not normally distributed distributions were confirmed. The most suitable transformation method was determined through analysis of histograms and their proximity to a normal distribution using Shapiro-Wilks. Where the most efficient method of data transformation involved Tukey's ladder of power, the selected transformation mode was not indicated. Tukey's ladder of power reduces the effects of homoscedastic data leading to more accurate analysis. The Akaike Information Criterion (AIC)

was used to estimate the fit of each model, with the lowest AIC value used to confirm the selection of data transformation links and models (Bozdogan, 1987; Cavanaugh, 2019). Variables were eliminated from the model as determined by the F-test. Following removal of all unnecessary independent variables, the goodness of fit of the remaining model was tested using diagnostic plots for linear regression analysis to determine whether residuals had a non-linear pattern (Residuals vs Fitted graph), were of a normal distribution (Normal Q-Q graph), heteroscedasticity (scale location graph) and influential outliers (Residual vs Leverage plots (Cook's distance)). Following completion of the model, the data were reported using the intercept result and P value, adjusted R^2 (^R^2), F-test for overall model significance (Mangiafico, 2016), and model P value. Any anomalies from the diagnostic plots were reported for the final model. Furthermore, the positive/negative association of the individual parameter associations within the model with the dependent variable were reported using LM mean difference ± SE.

Due to small sample sizes (n<25) and not normally distributed data displaying blocks, Friedman's test was used in the place of a 2-way ANOVA to determine significant associations between sediment depth and site with P concentration. Standard deviation, mean, standard error, median and quartile data were determined for each variable (P-fractions, Total Organic Carbon (TOC) and ion data). LM/GLM analyses were completed for 2016 P-fraction data using only P-fraction, sampling site, sediment layer and TOC data from due to the absence of other data. GLM/LM analyses for 2017 and April 2018 data included the P-fraction data, Sampling site, Sediment layer, TOC data, and ion data in the analyses (sediment derived data Table 4.2.5.1). Due to the small number for variables for the 2016 and 2017 GLM/LM analyses, no PCA was used to determine the most suitable independent variables for the analyses. Data are presented in Appendix 4 (A4). PCA was used to determine the most suitable variable s for the GLM/LM analyses of the July 2018 data.

July 2018 data was analysed using GLM/LM incorporating P-fraction data, TOC data, ion data and water quality data collected on the same sampling date as one another.

Table 4.2.5.1. Variables sampled on July 9th alongside sediment collection at Llandegfedd Reservoir used in GLM/LM analyses of sediment-derived data of July 2018.

Sediment-derived data	Water quality data
Mn (mg/g)	pH
Fe (mg/g)	Turbidity (ntu)
Fe-P (mg/g)	Organic C (mgL^{-1})
Ca-P (mg/g)	TN (mgL)
TOC (mg/g)	NO_3^- (mgL^{-1})
Labile-P (mg/g)	NH_4^+ (mgL^{-1})
Site	Cyanobacteria (cfu/ml)
Sediment layer	Green algae (cells/ml)
	Geosmin (ngL^{-1})

4.2.6. Mass balance analysis of internal P loading

Sediment P-fraction data obtained from cores during May and August 2018 were used to obtain an understanding of the internal P loading risk during summer relative to spring at Llandegfedd reservoir.

Mass balance followed the Vollenweider (1968) input - output model:-

$$V \frac{dP(t)}{dt} = Mi(t) - Mo(t) - Sed(t)$$

where V = volume (m^3)

dP(t)/dt = change in mean lake phosphorus concentration (g m^{-3} $month^{-1}$)

Mi(t) = external loading per unit time at time t (g $month^{-1}$)

Mo(t) = outflow loading per unit time at time t (g $month^{-1}$)

Sed(t) = amount of phosphorus per unit time stored in the sediment (g $month^{-1}$)

The term Sed(t) is the flux of phosphorus to the sediment or, if negative, the internal loading to the reservoir from the sediment. Sed(t) can be normalised per unit area (Sed(t) / Ao) describing the retention of phosphorus by the sediment on an aerial basis. Alternatively, the retention coefficient R and the apparent settling coefficient (s) can be determined as follows:-

$$R = Sed(t) / Mi(t) \text{ and } s = Sed(t) / (V.P_L^m)$$

where P_L^m = the average monthly phosphorus concentration.

Sed(t) is dependent upon the sediment type, redox conditions among other factors controlling phosphorus transfer across the sediment. The retention coefficient (R) is the proportion of the external phosphorus loading lost to the sediment. The apparent settling rate (s) is the proportion of the phosphorus lost from the water column by sedimentation and is a sinking rate according to Stoke's law.

4.3 Results

4.3.1 Bound-P cross-period analysis

4.3.1.1.1. Mean Fe-P fraction concentrations between April 2016 and July 2018

Fe-P (mg/g) concentrations were low throughout the reservoir during April 2016 (mean: 0.47mg/g ± SE 0.09) relative to that recorded throughout the reservoir from July 2017 through August 2018 (74.53mg/g ± SE 11.29), with an increase across all sediment layers between April 2016 and July 2018 of 99.99%.

Despite an increase in Fe-P throughout the sediment depths during April 2018 (115.42mg/g ± 20.43) relative to that during July 2017 (19.03mg/g ± 2.77), the variability of the April 2018 data were high (Figure 4.3.1.1.1.1).

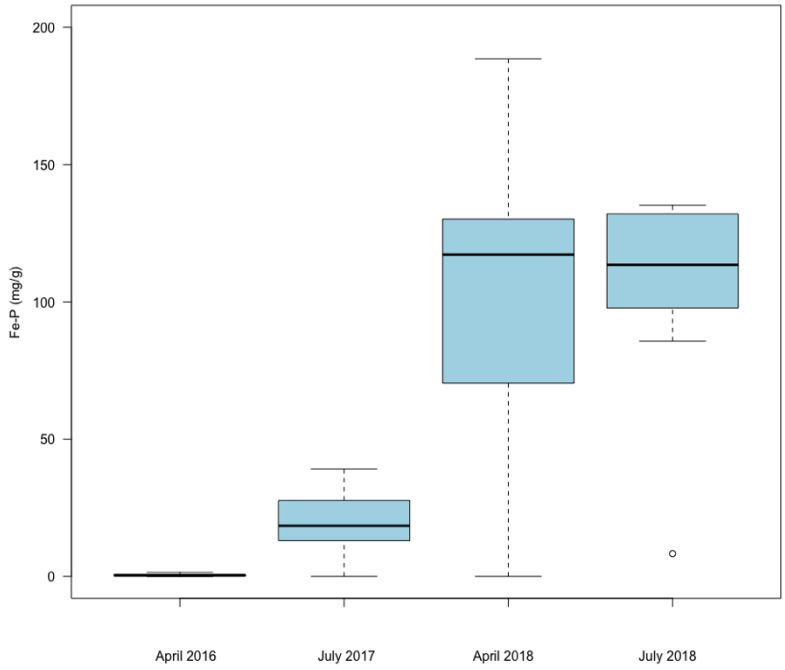

Figure 4.3.1.1.1.1. Fe-P concentrations (mg/g), median and quartiles) during sampling sessions during April 2016, July 2017, April 2018 and July 2018.

Site 2 recorded an increase in Fe-P concentrations throughout the sediment depth (mean 0.36mg/g ± SE 0.008) relative to that at site 1 (0.01mg/g ± SE 0.008) with the highest concentration isolated at layer 5 (0.45mg/g ± 0.06). However, the Fe-P concentrations at site 3 throughout the sediment depth was higher (1.06mg/g ± SE 0.14) than that throughout site 2, although the difference was insignificant (P>0.05). The concentration of Fe-P increased with depth at site 3, with the highest concentration attained at layer 5 (1.49mg/g ± SD 0.18).

Mean Fe-P during July 2018 (103.77mg/g ± 41.86) was insignificantly higher than the mean during April 2018 but the data exhibited a decrease in variability (115.42mg/g ± 84.4).

4.3.1.1.2. Mean surface sample concentrations of Fe-P fractions.

Fe-P was detected at low levels (0.031mg/g ± SE 0.16) throughout the surface samples (layer 1) of the reservoir during April 2016 (Table 4.3.1.1.2.1), with no Fe-P detected at surface of site 1. The concentration of Fe-P across the surface sediment (layer 1) of the reservoir during April 2018 (102.72mg/g ± SE 27.5) was greater than that recorded during July 2017 (22.7mg/g ± SE 3.15), indicating an increase in sediment-P surface deposition over the 9-month period

by 78%, with the greatest increase (84%) in Fe-P concentrations (from mean 30mg/g ± 23.88 to mean 188.54mg/g ± 42.23) at surface site 3 (Figure 5.3.1.1.2.1).

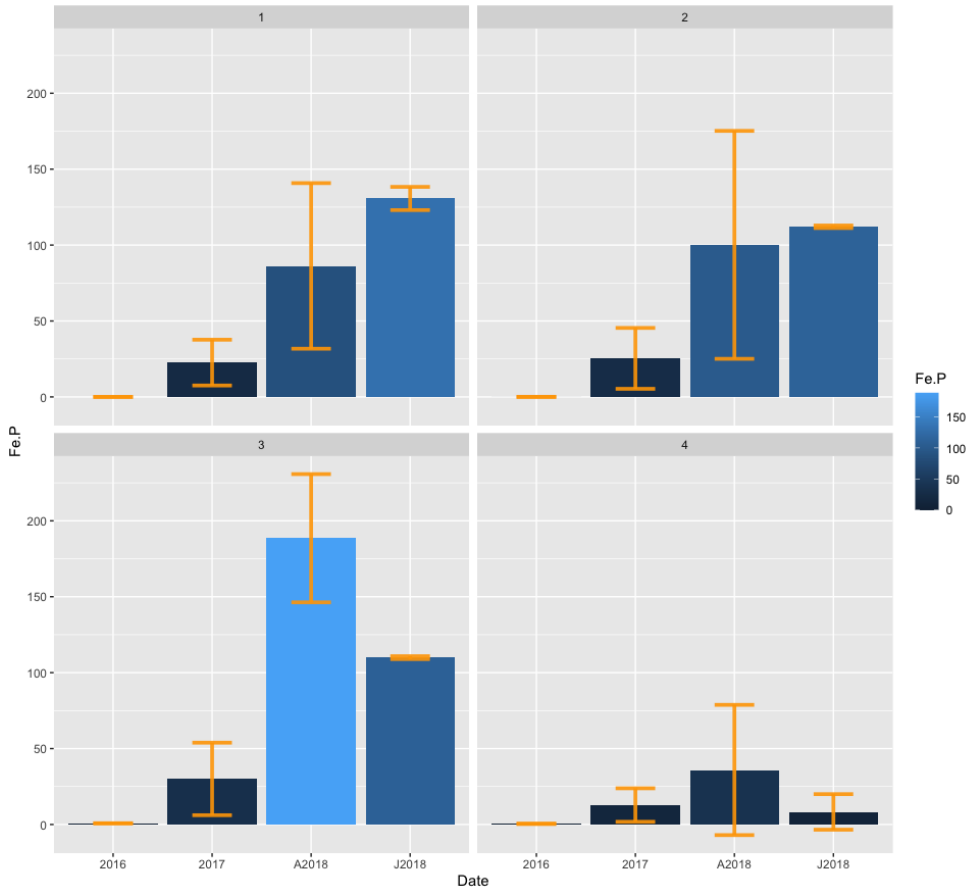

Figure 4.3.1.1.2.1. Mean Fe-P (mg/g ± SE) at surface sediments (layer 1) at sampling sites 1,2,3 and 4 during April 2016, July 2017, April 2018 and July 2018.

However, the surface samples of all sites recorded a reduced Fe-P binding capacity during July 2018 compared with that during April 2018, suggesting an increased risk of internal P loading throughout the reservoir.

4.3.1.1.3. Mean Fe-P concentrations (mg/g) during April 2016

The concentrations of Fe-P at site 4 were of a low variability through the sediment layers (combined sample mean 0.47mg/g ± SE 0.006), indicating a constant rate of P deposition (Figure 4.3.1.1.3.1.) relative to that of the other sites.

Fe-P was undetected at site in the surface layer (layer1) through layer 4, suggesting a lower Fe surface for P-binding relative to that at all other sites.

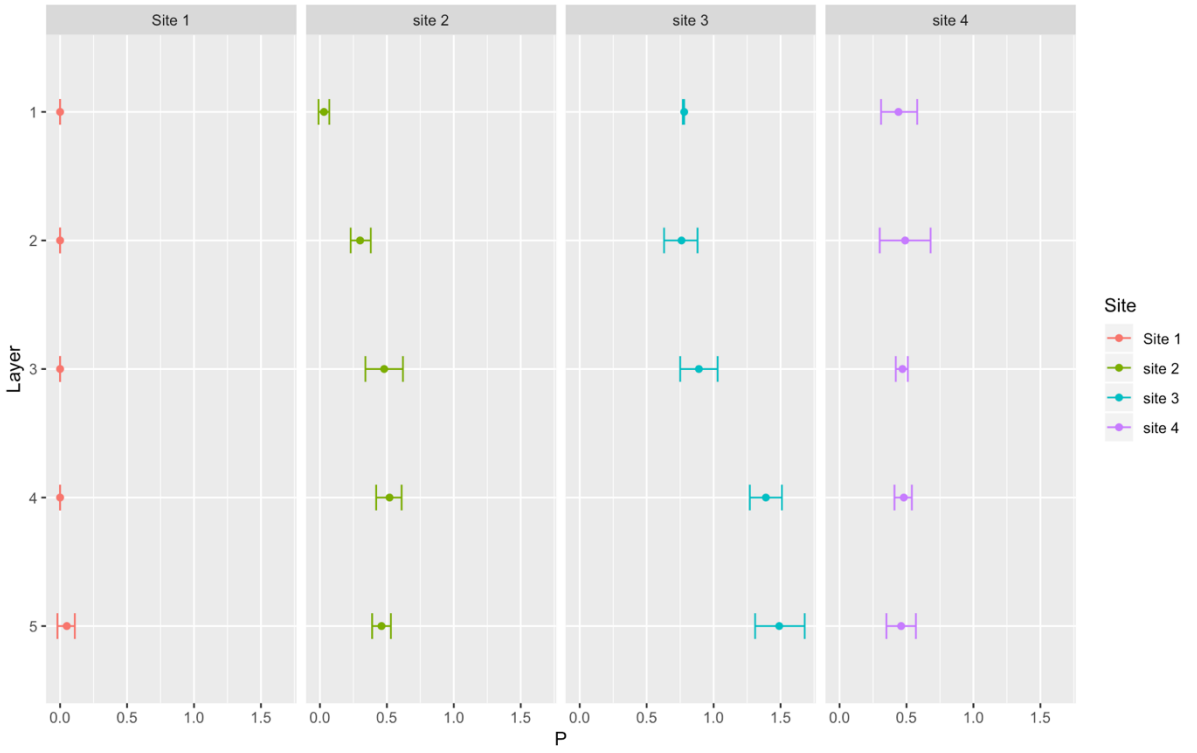

Figure 4.3.1.1.3.1. Fe-P (mg/g) in April 2016 (mean ± SD) for sites 1, 2, 3 and 4 throughout the sediment layers. Layer 1 represents the top 0-3cm, layer 2 represents 4-6cm, layer 3 represents 7-9cm, layer 4 represents 10-12cm and layer 5 represents 13-15cm of sediment depth.

4.3.1.1.4. Mean Fe-P concentrations (mg/g) during July 2017

Fe-P concentrations significantly increased (P<0.0001) at all surface sites relative to that recorded during April 2016, with an increase in surface Fe-P concentrations by 99.99%. Site 1 recorded 18.34mg/g (± SE 5.08), with the highest concentration of Fe-P detected in the second layer of sediment (32.23mg/g ± SD 2.23). The concentration of Fe-P of site 2 was greater than that isolated at site 1 (16.71 ± SE 3.41), with the highest concentration isolated at the surface (25.38mg/g ± SD 20.05).

Site 3 recorded the highest Fe-P surface concentration (30mg/g ± SD 23.88) of all four sites, with the highest concentrations of each layer thereafter recording the highest Fe-P concentrations of any site. The highest concentration was detected within layer 3 of site 3 (39.19mg/g ± SD 9.65), indicating a high risk of internal P loading at site 3 relative to all other sites (Figure 4.3.1.1.4.1) if the sediment were to be scoured to a depth of 7cm. The Fe-P concentrations decreased with increasing sediment depth at site three after the surface layer, with the fourth layer recording the lowest Fe-P concentrations of all layers at site 3.

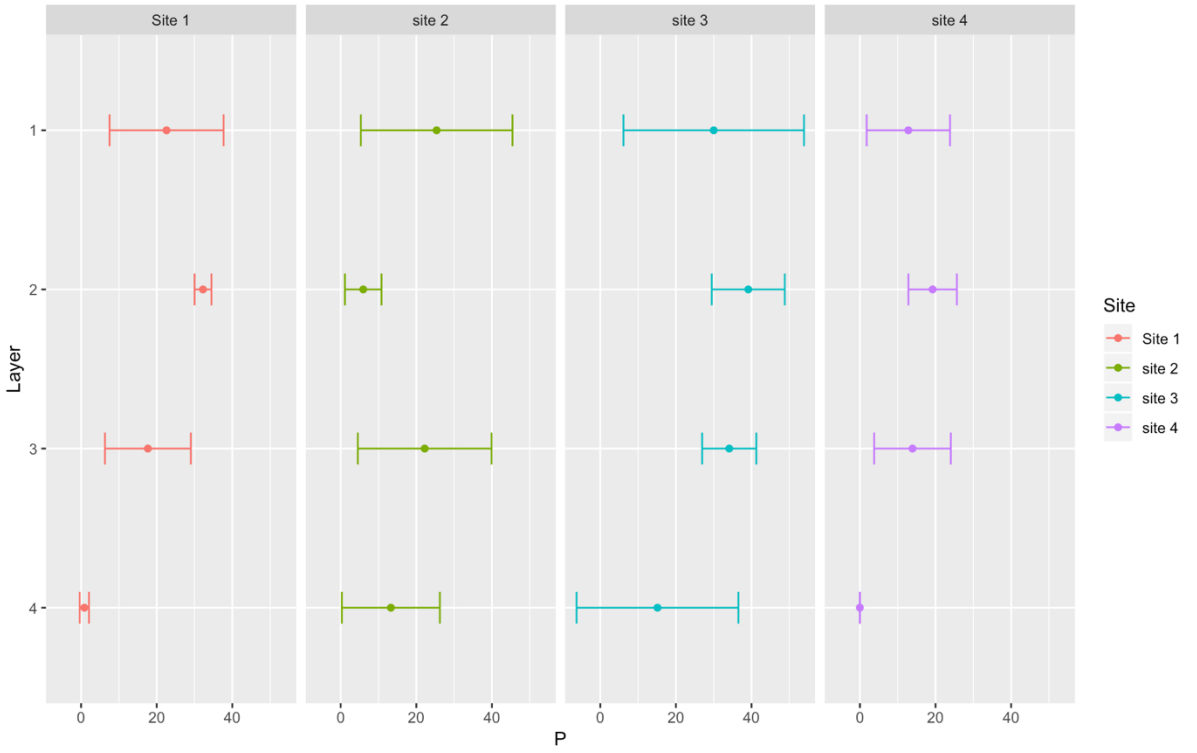

Figure 4.3.1.1.4.1. Fe-P (mg/g) in July 2017 (mean ± SD) for sites 1, 2, 3 and 4 throughout the sediment layers. Layer 1 represents the top 0-3cm, layer 2 represents 4-6cm, layer 3 represents 7-9cm, layer 4 represents 10-12cm of sediment depth.

The concentrations of Fe-P at site four was the lowest of all sites sampled (11.49mg/g ± SE 3.16), with no Fe-P isolated in the fourth layer of sediment. The lower concentrations of Fe-P throughout the sediment depth relative to all other sites suggests that site 4 has the lowest risk for internal P loading.

4.3.1.1.5. Mean Fe-P concentrations (mg/g) during April 2018.

Site 3 recorded the highest surface Fe-P concentration of all four sites (188.54mg/g ± 42.23), with the lowest Fe-P concentration recorded at site 4 (35.9mg/g + 42.89). However, the mean concentrations of Fe-P within the second layer at site 4 are the highest of all sites (374.43 ± 524.36), however, the large SD indicated the not normally distributed nature of the data.

The second layer of sediment (4-6cm depth) contained the highest Fe-P concentrations within the southern section of the reservoir (site 1 & 2), indicating an increase in the risk of internal P loading under conditions causing sediment disturbance at the southern section of the reservoir. However, site 3 poses the highest immediate risk of internal P loading due to the

high Fe-P concentrations within the uppermost surface layer (Figure 4.3.1.1.5.1).

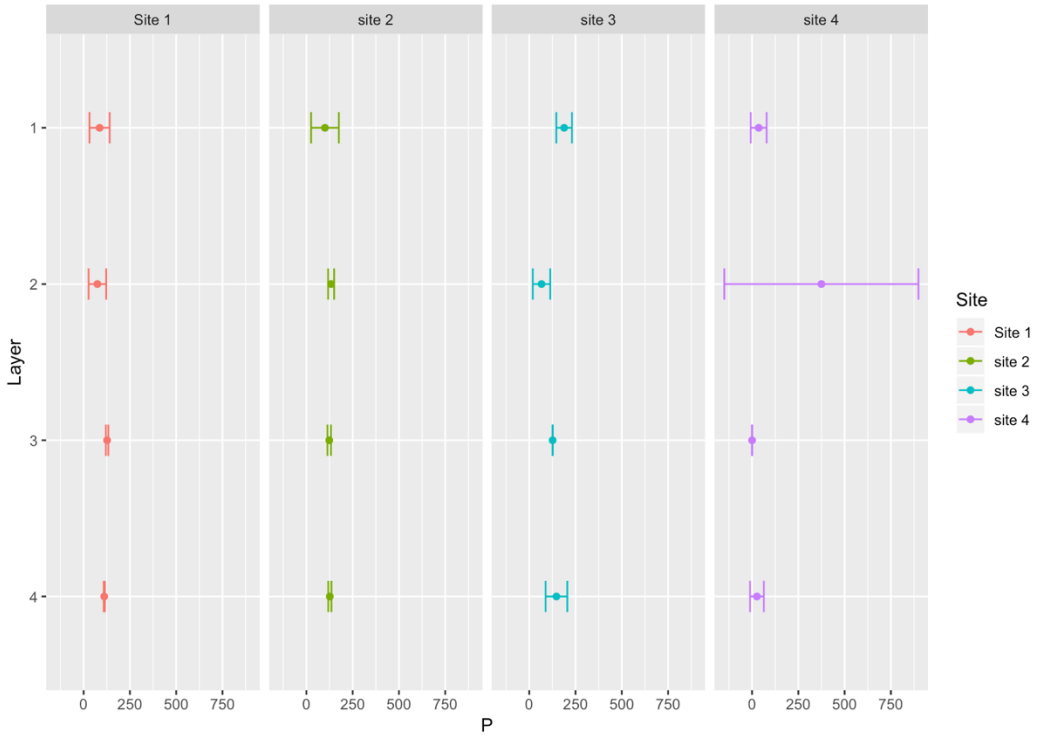

Figure 4.3.1.1.5.1. Fe-P (mg/g) in April 2018 (mean ± SD) for sites 1, 2, 3 and 4 throughout the sediment layers. Layer 1 represents the top 0-3cm, layer 2 represents 4-6cm, layer 3 represents 7-9cm and layer 4 represents 10-12cm of sediment depth.

4.3.1.1.6. Mean Fe-P concentrations (mg/g) during July 2018.

The sediment surface layer of the southern sites (sites 1 & 2) recorded the highest concentration of Fe-P throughout the reservoir, with site 1 recording the highest (130.69mg/g ± 7.64) and therefore posing the greatest risk of internal P loading. The sediment-bound P at surface site 4 posed the lowest risk (8.28mg/g ± 11.7).

All mean Fe-P concentrations within the bottom (fifth) layer were high (117.31mg/g ± SE 9.95) suggesting a high degree of P retention within the sediment (Figure 4.3.1.1.6.1). However, the mean Fe-P (mg/g) within the surface layer was also high (91.22mg/g ± SE 26.98), indicating a high potential of internal P loading.

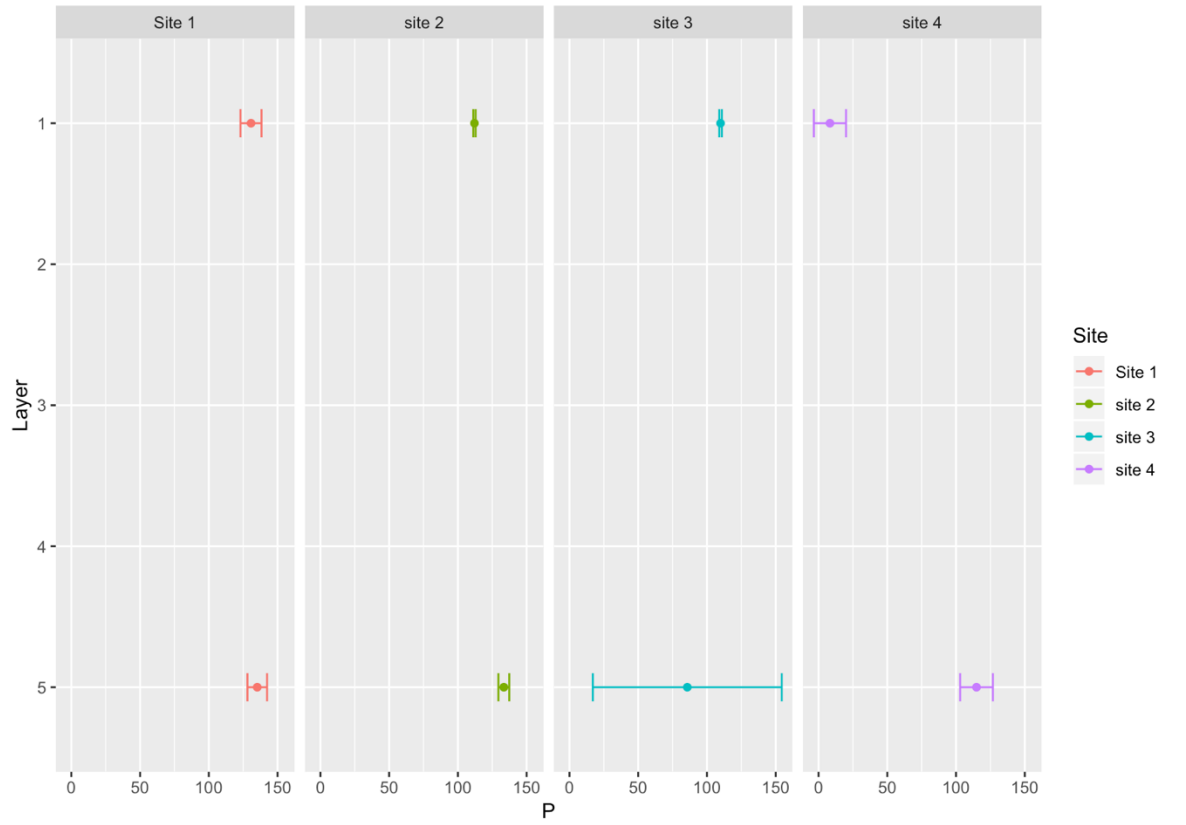

Figure 4.3.1.1.6.1. Mean Fe-P (mg/g) in July 2018 (mean ± SD) for sites 1, 2, 3 and 4 throughout the sediment layers. Layer 1 represents the top 0-3cm and layer 5 represents the bottom 13cm-15cm.

4.3.1.2.1. Mean Ca-P fraction concentrations between April 2016 and July 2018

Ca-P concentrations were low and recorded a low degree of variability over April 2016 through April 2018 (mean 11.1mg/g ± SE 1.84) compared with that during July 2018 (mean 37.6mg/g ± SE 10.93). An increase in Ca-P concentrations throughout the sediment depth by 65% was recorded during July 2018 compared with that during April for all sediment depths throughout the reservoir (Figure 4.3.1.2.1), with Ca-P concentrations throughout 2016 recording the lowest combined mean concentration (6.69mg/g ± SE 0.67).

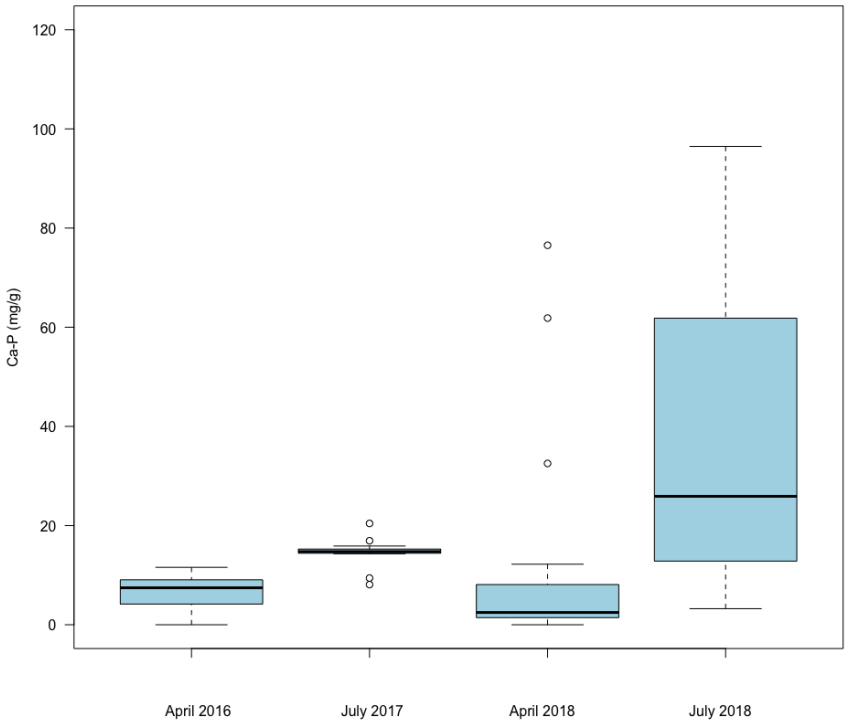

Figure 4.3.1.2.1.1. Ca-P concentrations (mean mg/g, median and quartiles) during sampling sessions during April 2016, July 2017, April 2018 and July 2018.

4.3.1.2.2. Surface sediment mean Ca-P concentration (mg/g)

Surface sediment Ca-P content increased at site 4 during July 2018 more than that recorded for any other site during the same sampling period (Figure 4.3.1.2.2.1), however, the variation within the data was large relative to the mean (71.18mg/g ± 87.81).

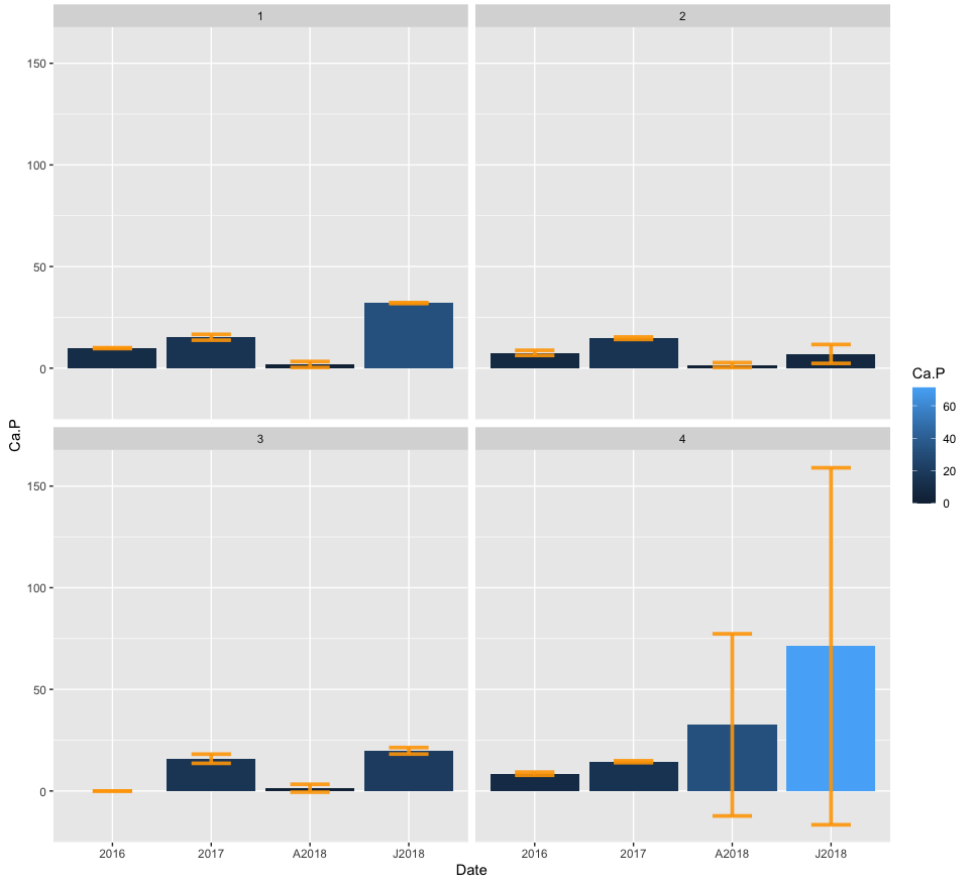

Figure 4.3.1.2.2.1. Ca-P (mg/g ± SE) at surface sediments (layer 1) at sampling sites 1, 2, 3 and 4 during April 2016, July 2017, April 2018 and July 2018.

4.3.1.2.3. Mean Ca-P concentrations (mg/g) during April 2016.

The concentrations of Ca-P varied throughout the reservoir (6.79mg/g ± SE 0.67) with the highest surface Ca-P concentrations detected at site 1 (9.84mg/g ± 0.19).

The southern section of the reservoir (sites 1 & 2) recorded higher concentrations of Ca-P throughout the sediment depths and were of a very similar concentration (site 1: 9.07mg/g ± SE 0.67; site 2: 9.04 ± SE 0.55) compared with that of the northern section (site 3: 2.74mg/g ± SE 0.61; site 4: 6.32mg/g ± SE 0.68).

The concentrations of Ca-P increased during July 2018 (32.03mg/g ± 0.23) at surface sample of site 4, indicating this site to have the highest P-binding capacity (Figure 4.3.1.2.3.1). No Ca-P was isolated at surface sediment of site 3, however, the concentration increased with depth. Site 3 contained the lowest concentration of Ca-P throughout the sediment depth with the exception of layer 3 where the Ca-P concentration was greater than that isolated within layer

3 at site 4 (4.39mg/g ± 6.21 and 3.94mg/g ± 2.47 respectively. The high SD relative to the low mean throughout layers 2, 3, 4 and 5 of site 3 indicate the extent of not normally distributed data.

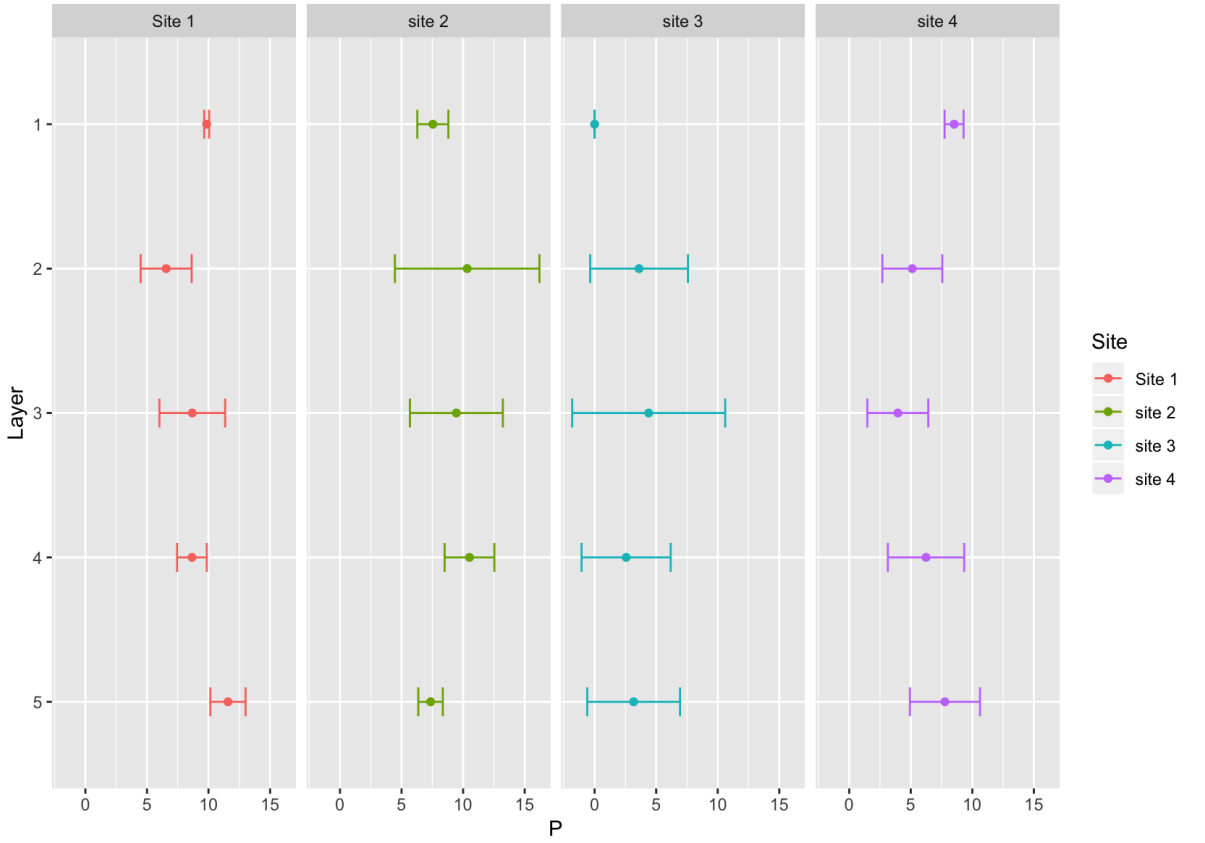

Figure 4.3.1.2.3.1. Ca-P (mg/g) in April 2016 (mean ± SD) for sites 1, 2, 3, 4 and 5 throughout the sediment layers. Layer 1 represents the top 0-3cm, layer 2 represents 4-6cm, layer 3 represents 7-9cm, layer 4 represents 10-12cm and layer 5 represents 13-15cm of sediment depth.

4.3.1.2.4. Mean Ca-P concentrations (mg/g) during July 2017.

High concentrations of Ca-P were isolated (14.59mg/g ± SE 0.66) at each site during July 2017, with Ca-P detected within every sediment layer at each site.

The highest concentration of sediment surface Ca-P was isolated at site 1 (15.21mg/g ± 1.44) however, the Ca-P concentrations across all sediment surfaces (15.06mg/g ± SE 0.27) were insignificantly different (P>0.05). The concentration of Ca-P was maintained throughout the depth of the sediment, with the lowest concentration within layer 4 of site 4 (8.09mg/g ± 9.06) and the highest within layer 3 of site 1 (20.43mg/g ± 6.26). The largest degree of

variance was recorded at site 1 (layer 3), site 3 (layer 4) and site 4 (layer 4) (Figure 4.3.1.2.4.1).

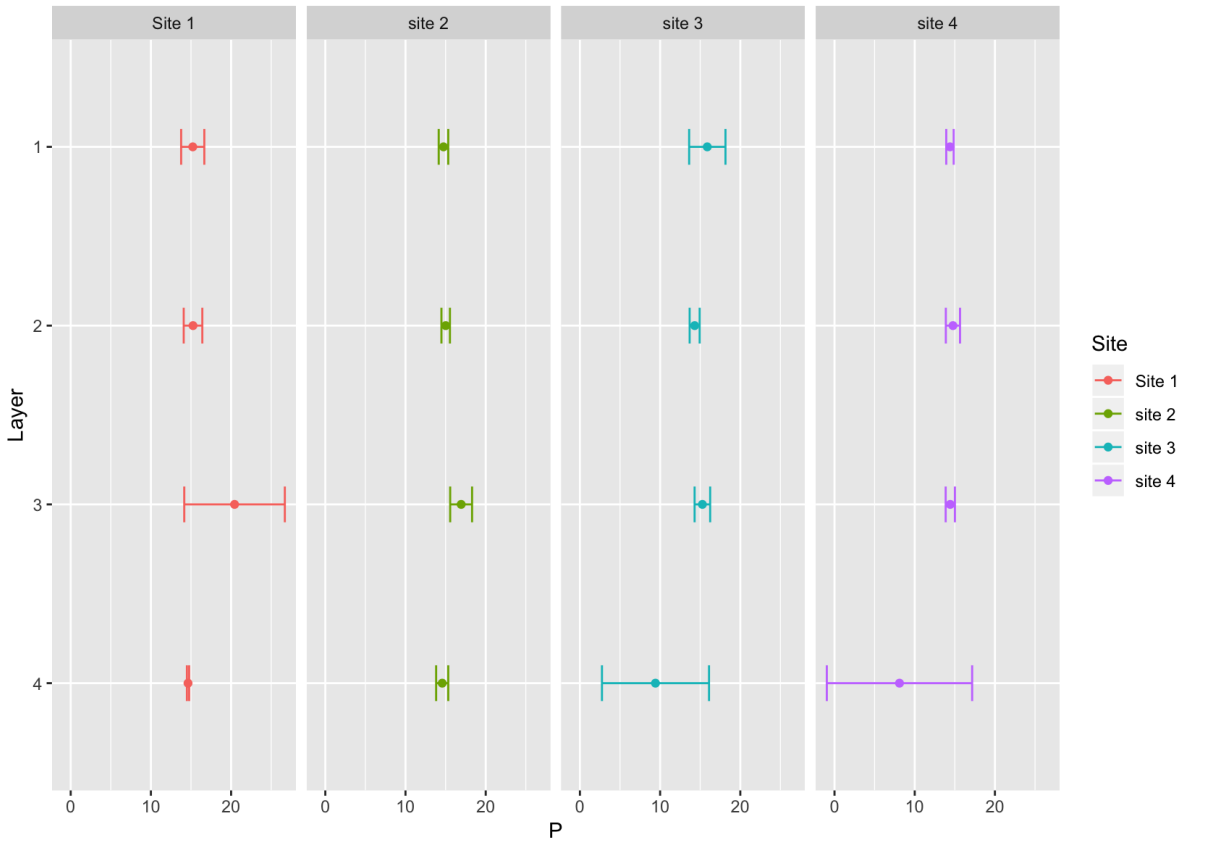

Figure 4.3.1.2.4.1. Ca-P (mg/g) in July 2017 (mean ± SD) for sites 1, 2, 3 and 4 throughout the sediment layers. Layer 1 represents the top 0-3cm, layer 2 represents 4-6cm, layer 3 represents 7-9cm, layer 4 represents 10-12cm of sediment depth.

4.3.1.2.5. Mean Ca-P concentrations (mg/g) during April 2018.

Ca-P concentrations were significantly different ($P<0.05$) within the surface layer of site (32.53mg/g ± 44.8) compared with that of all other sites (1.58 ± SE 0.1). However, the Ca-P concentrations were low within layer 2 at each site (2.99mg/g ± SE 0.5) and layer 3 at each site (1.17mg/g ± 0.4), suggesting that the permanent P-binding capacity of the sediment had recently been low.

The Ca-P content of each site (Figure 4.3.1.2.5.1) increased in layer 4 (50.2mg/g ± SE 15.88) relative to that in layers 2 and 3, with the exception of site 2, where the concentration remained low (3.52mg/g ± 4.28), with the highest Ca-P concentration isolated at site 3 (76.53mg/g ± 104.66).

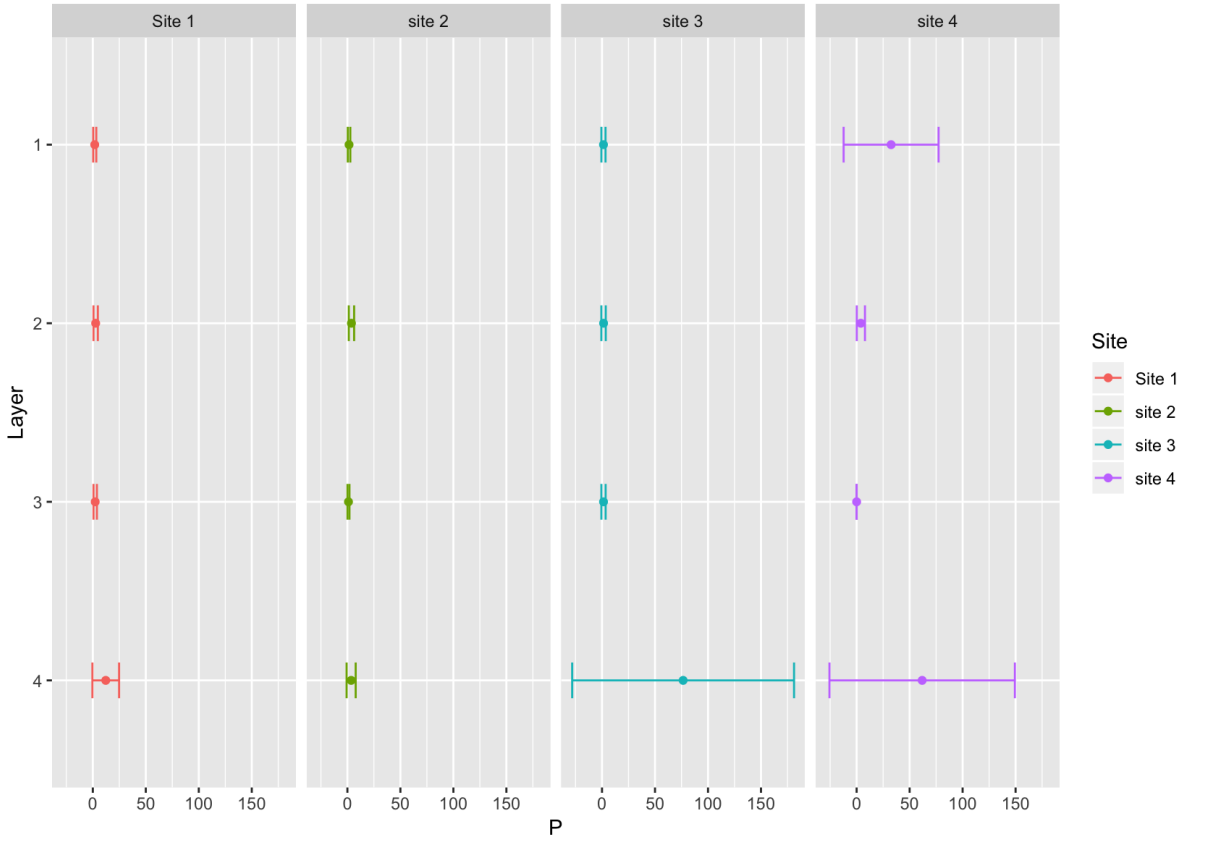

Figure 4.3.1.2.5.1. Ca-P (mg/g) in April 2018 (mean ± SD) for sites 1, 2, 3 and 4 throughout the sediment layers. Layer 1 represents the top 0-3cm, layer 2 represents 4-6cm, layer 3 represents 7-9cm and layer 4 represents 10-12cm of sediment depth.

4.3.1.2.6. Mean Ca-P concentrations (mg/g) during July 2018.

The Ca-P concentrations throughout the sediment surface were variable throughout the reservoir (32.49mg/g ± 12.01), with repeatability of layer 1 at site 4 having the greatest degree of variability (71.18mg/g ± 87.81) (Figure 4.3.1.2.6.1).

The lowest concentration of surface Ca-P was isolated at site 2 (7mg/g ± 4.64) with the highest isolated at site 4 (71.18mg/g ± 87.81). The Ca-P within the bottom layer (layer 5) was greater than that within the surface sediment of the southern sites but lower than those of the northern sites. The highest Ca-P concentration within the bottom layers (96.46mg/g ± 76.32) was isolated at site 2.

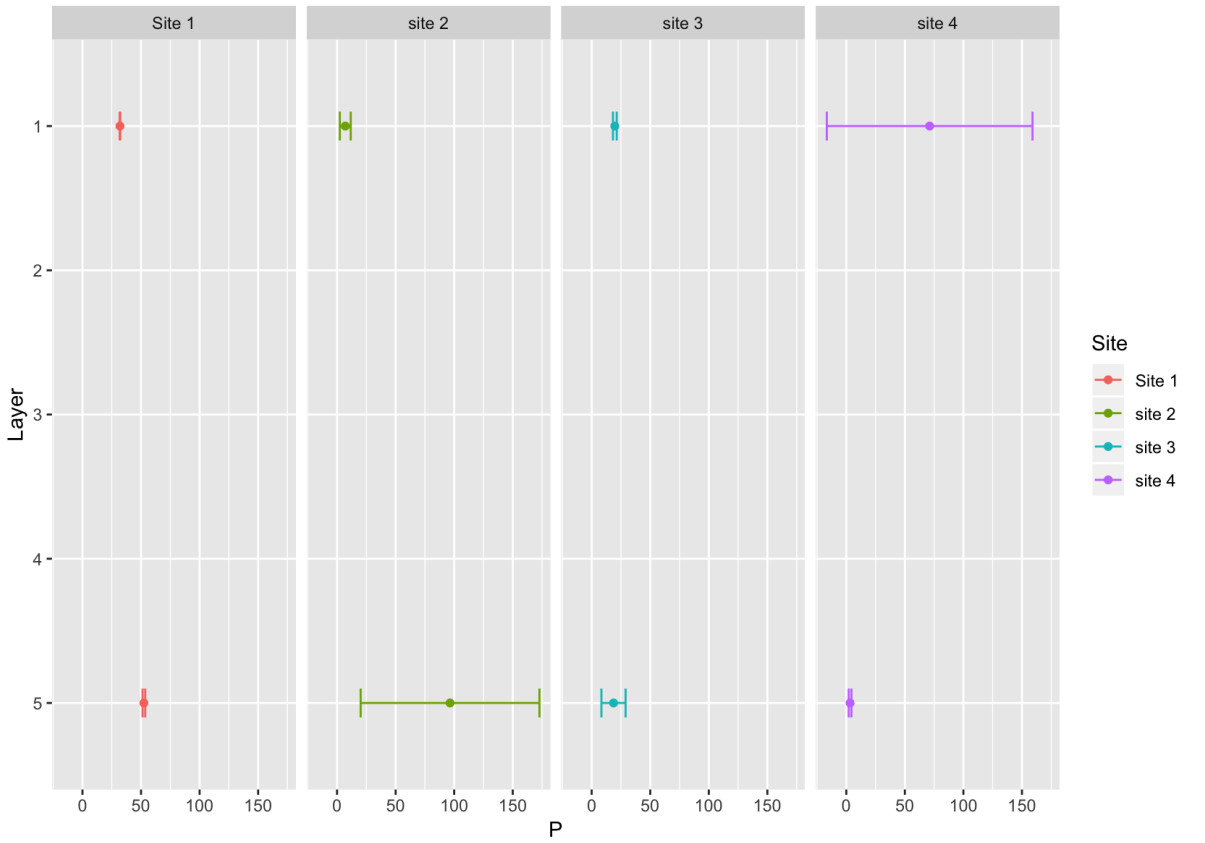

Figure 4.3.1.2.6.1. Ca-P (mg/g) in July 2018 (mean ± SD) for sites 1, 2, 3 and 4 throughout the sediment layers. Layer 1 represents the top 0-3cm and layer 5 represents the bottom 13cm-15cm.

4.3.1.3.1. Mean Labile-P fraction concentrations between April 2016 and July 2018

Labile-P concentrations remained low throughout sediment across the reservoir (mean 20.03mg/g ± SE 5.52) over the sampling period (April 2016 through July 2018), with the highest recorded mean concentrations recorded during July 2017.

The highest concentrations of labile-P were recorded during July 2017 (12.89mg/g ± 0.35), with the date recording the next highest labile-P concentrations in July 2018 (27.44mg/g ± SE 21.48) (Figure 4.3.1.3.1.1).

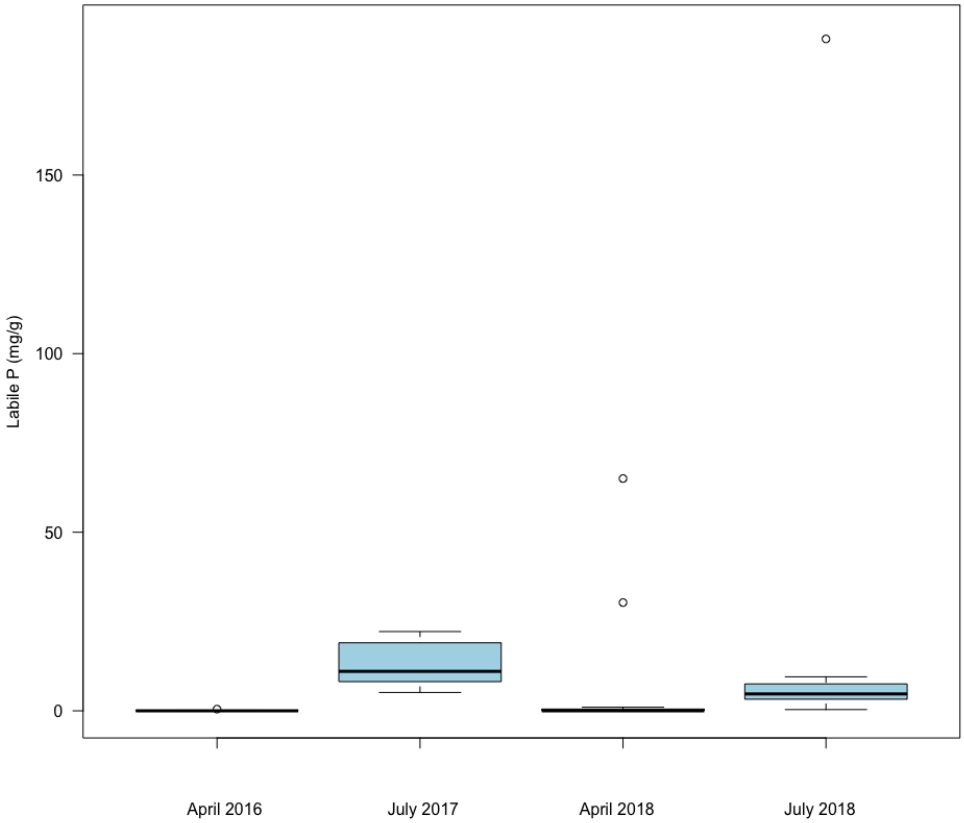

Figure 4.3.1.3.1.1. La-P concentrations (mean mg/g, median and quartiles) during sampling sessions during April 2016, July 2017, April 2018 and July 2018.

4.3.1.3.2. Mean La-P surface concentrations (mg/g) between April 2016 and July 2018.

The greatest increase in surface labile-P concentrations was recorded within surface sediment of site 4 during July 2018 (188.11mg/g ± 1.62) (Figure 4.3.1.3.2.1).

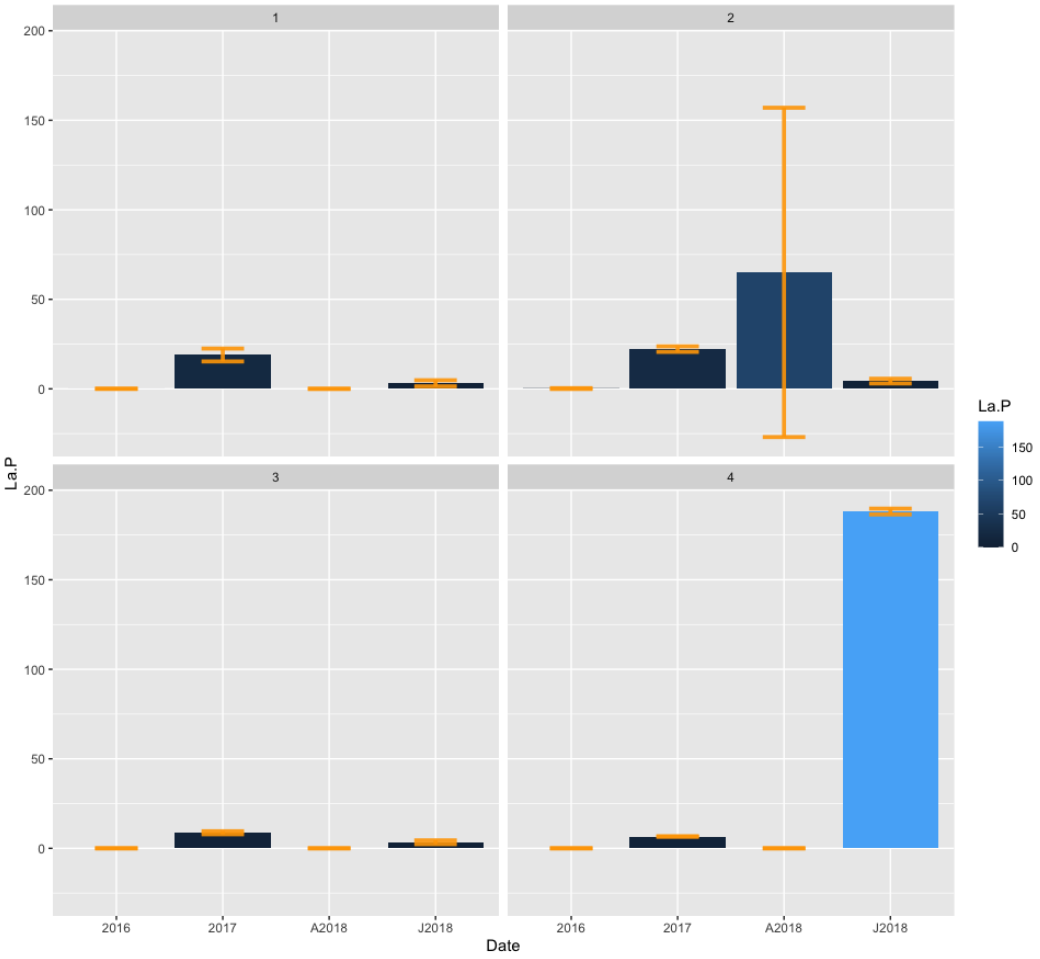

Figure 4.3.1.3.2.1. La-P (mg/g ± SE) at surface sediments (layer 1) at sampling sites 1, 2, 3 and 4 during April 2016, July 2017, April 2018 and July 2018.

4.3.1.3.3. Mean Labile-P concentrations (mg/g) during April 2016.

The concentrations of labile P throughout the sediment depths of each sampling site of the reservoir was low (0.05mg/g ± 0.023). Ca-P was absent from every layer at the northern section of the reservoir but isolated within each layer at the southern sites with the exception of layer 3 of site 1.

The highest surface La-P concentrations were isolated at site 2 (0.16mg/g ± 0.23) relative to site 1 (0.017mg/g ± 0.012). The concentrations of La-P varied (Figure 4.3.1.3.3.1) over the sediment depth at site 1 (0.04mg/g ± SE 0.015) and site 2 (0.17mg/g ± SE 0.06)

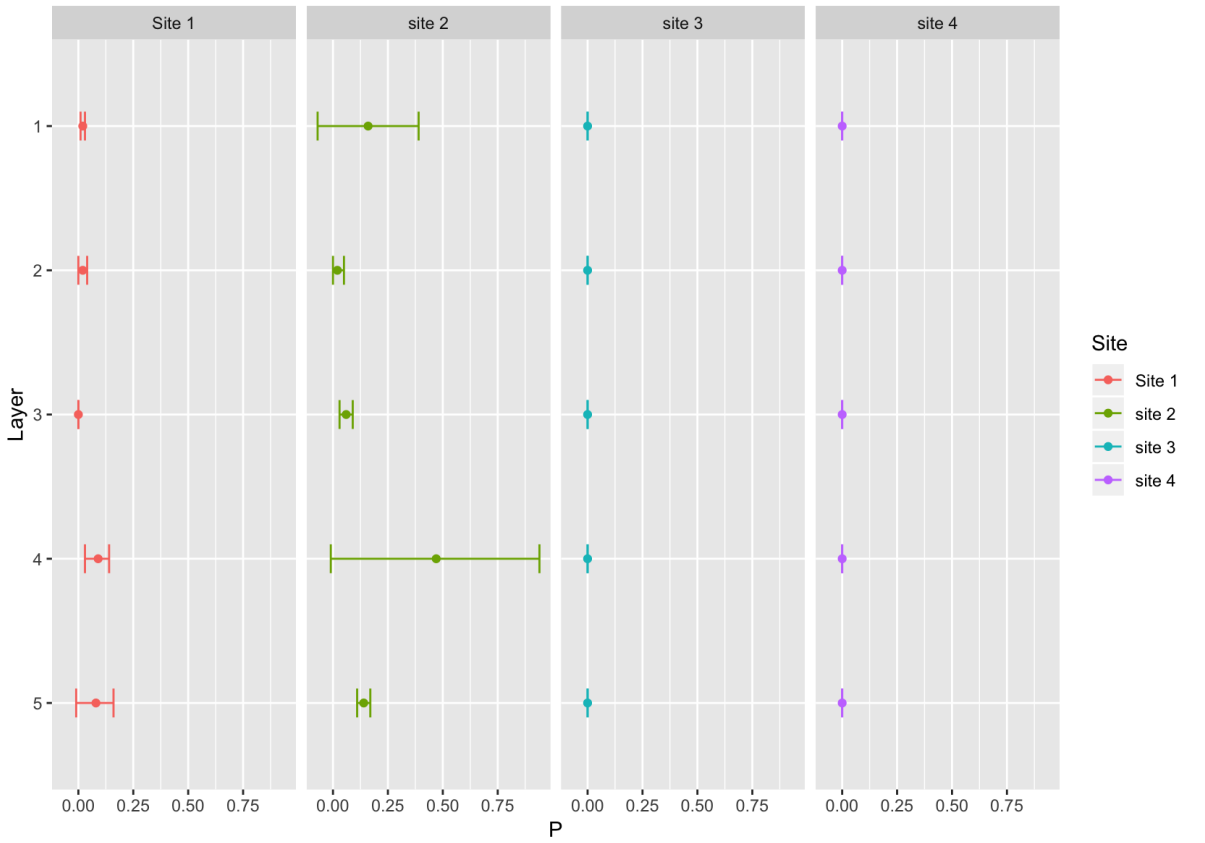

Figure 4.3.1.3.3.1. La-P (mg/g) concentrations (mean ± SD) in sediment samples at site 1, 2, 3 and 4 during April 2016. Layer 1 represents the top 0-3cm, layer 2 represents 4-6cm, layer 3 represents 7-9cm, layer 4 represents 10-12cm and layer 5 represents 13-15cm of sediment depth.

4.3.1.3.4. Mean Labile-P concentrations (mg/g) during July 2017.

The concentrations of labile P were 56% higher within the surface sediments of the southern sites (20.54mg/g ± SE 1.16) compared with that of the northern sites (7.65mg/g ± SE 0.74), with the highest concentrations isolated at site 2 (22.19mg/g ± 1.54).

The lowest La-P concentrations were isolated at site 4 at each sediment layer, indicating that P was permanently sediment-bound at this site (Figure 4.3.1.3.4.1).

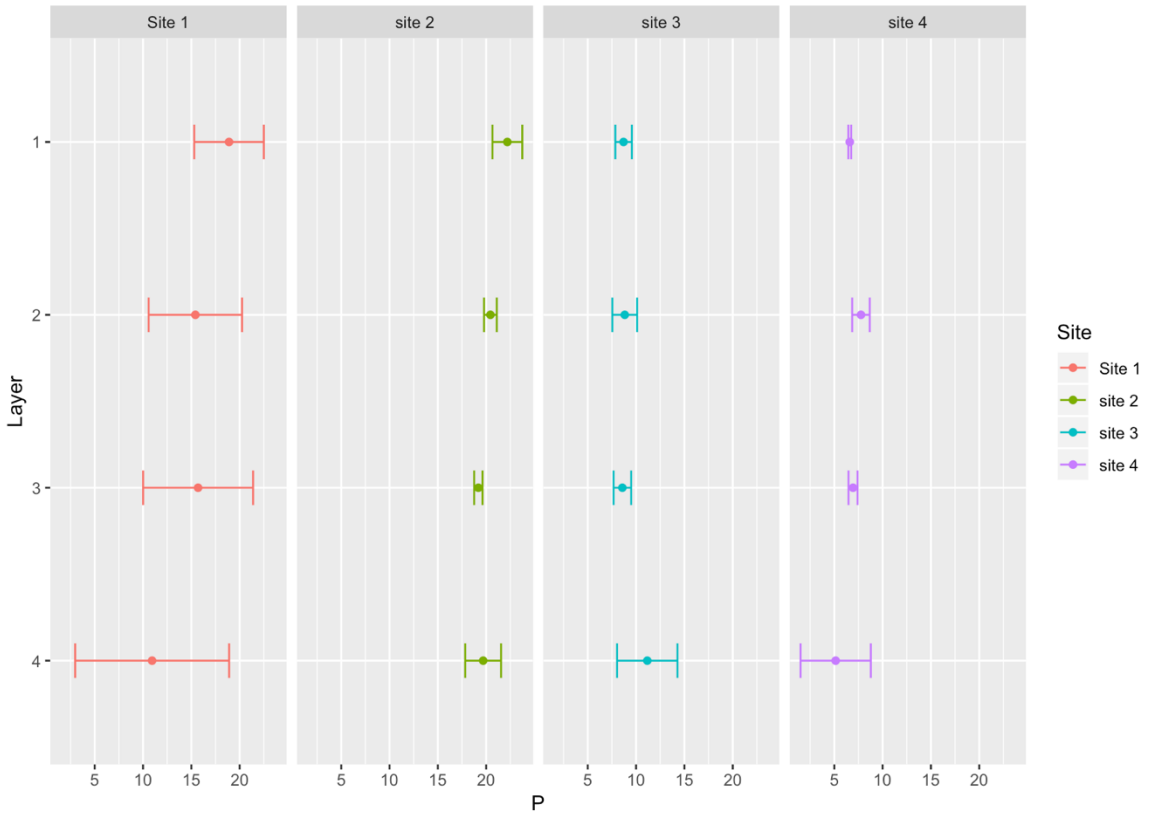

Figure 4.3.1.3.4.1. La-P (mg/g) in July 2017 (mean ± SD) for sites 1, 2, 3 and 4 throughout the sediment layers. Layer 1 represents the top 0-3cm, layer 2 represents 4-6cm, layer 3 represents 7-9cm, layer 4 represents 10-12cm of sediment depth.

4.3.1.3.5. Mean Labile-P concentrations (mg/g) during April 2018.

The concentrations of labile-P throughout the reservoir during April 2018 were low (6.08mg/g ± SE 4.21), with the highest concentration isolated within the surface layer of site 2 (65.03mg/g ± 91.97).

No Ca-P was detected within any sediment layer at site 4 and only very low concentrations (0.98mg/g ± 1.39) detected throughout the sediment layers at site 1.

The variability of the surface sample of site was high (Figure 4.3.1.3.5.1) indicating the sporadic culmination of Ca-P within the sediment.

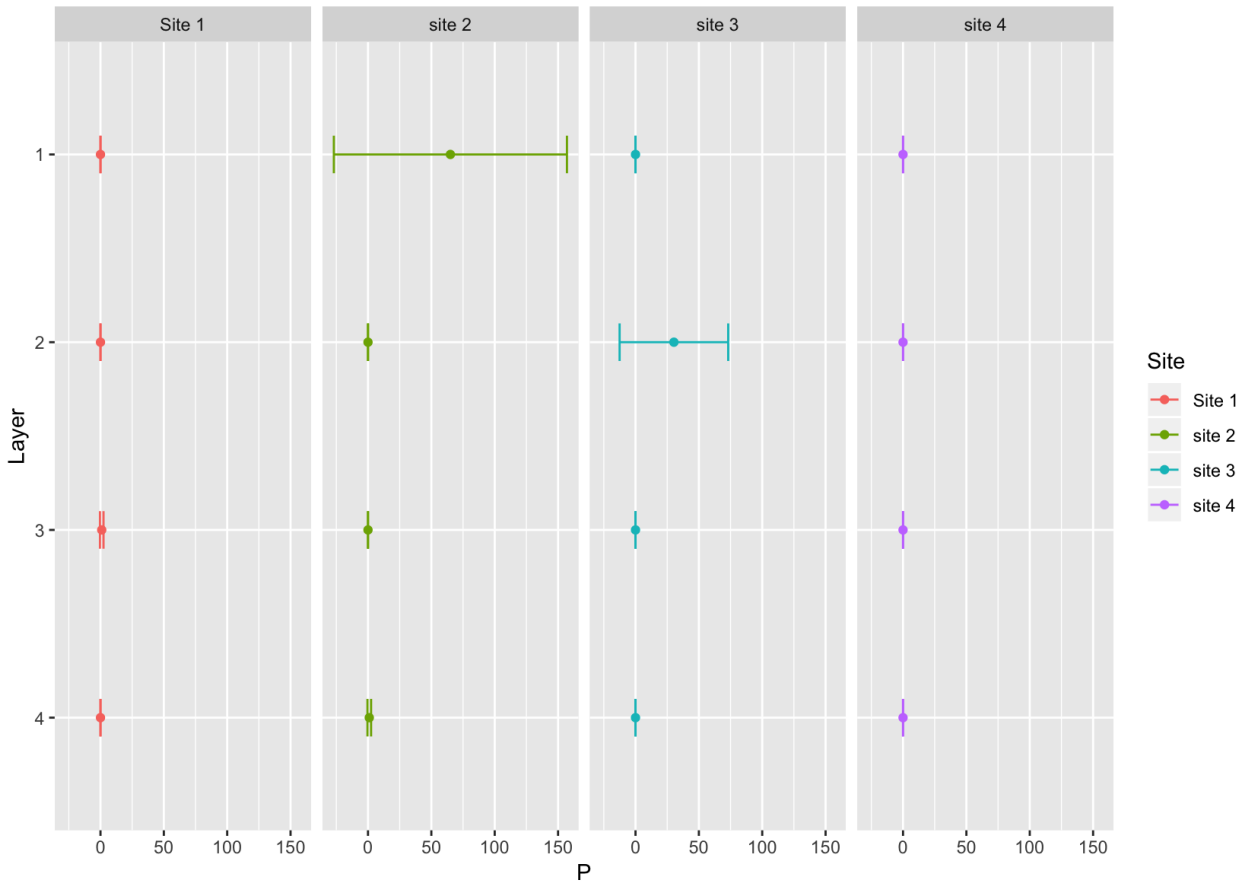

Figure 4.3.1.3.5.1. La-P (mg/g) in April 2018 (mean ± SD) for sites 1, 2, 3 and 4 throughout the sediment layers. Layer 1 represents the top 0-3cm, layer 2 represents 4-6cm, layer 3 represents 7-9cm and layer 4 represents 10-12cm of sediment depth.

4.3.1.3.6. Mean Labile-P July concentrations (mg/g) during 2018.

Labile P concentrations were low (3.6mg/g ± SE 0.3) within the surface samples of sites 1, 2 and 3, however, the concentrations were high (188.1 mg/g ± 1.61) within the surface samples of site 4.

Labile-P concentrations were low (5.14mg/g ± SE 1.13) within all bottom layers (layer 5), with layer 5 of site 4 recording the lowest concentrations of labile-P (0.34g/mg ± 0.24). The mean concentrations of each layer demonstrated a low degree of variability between samples (Figure 4.3.1.3.6.1).

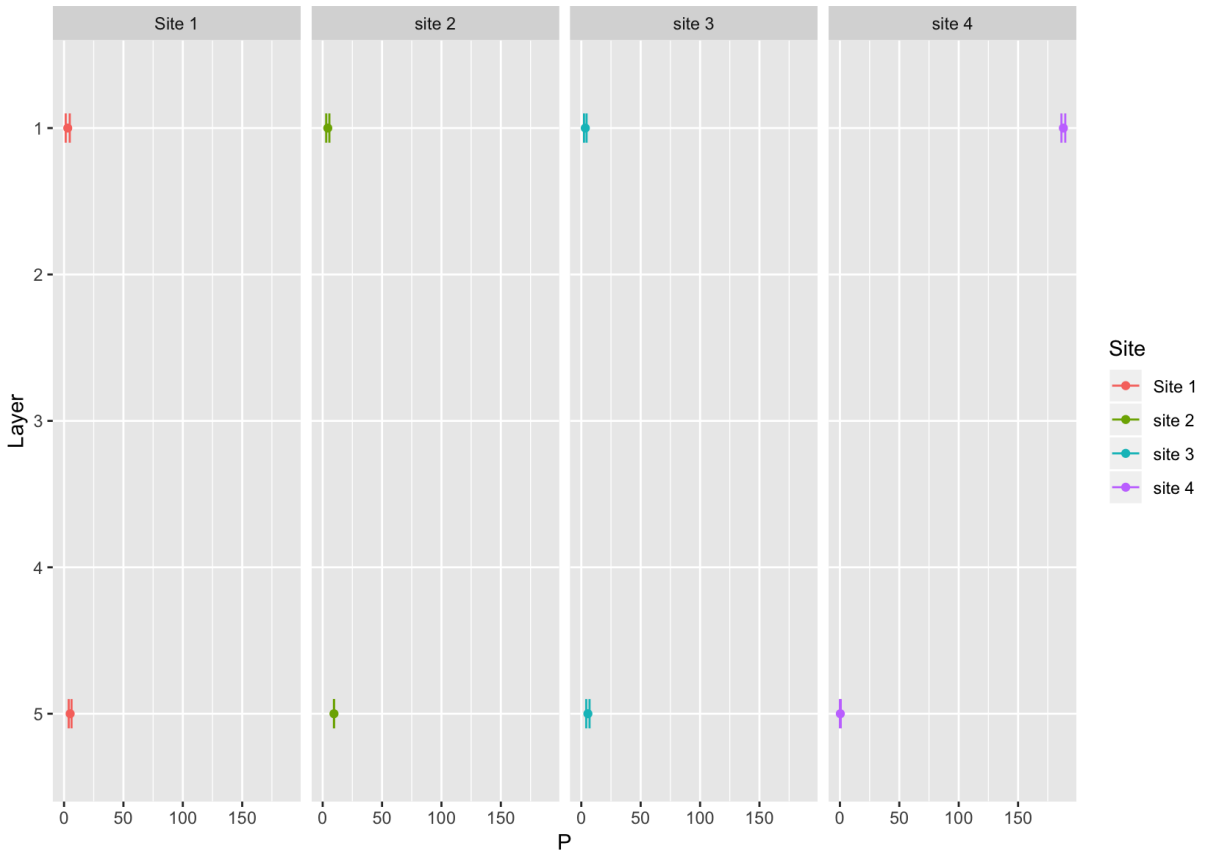

Figure 4.3.1.3.6.1. La-P (mg/g) in July 2018 (mean ± SD) for sites 1, 2, 3 and 4 throughout the sediment layers. Layer 1 represents the top 0-3cm and layer 5 represents the bottom 13cm-15cm.

4.3.2.1. Mean Total Organic Carbon (TOC) concentrations between April 2016 and July 2018

The mean TOC concentrations (mg/g) across the 0cm to 15cm sediment depth decreased over the sampling period from April 2016 through July 2018 by 45% along the transect of the reservoir from 7.6mg/g (± 1.33) (April 2016) to 4.19mg/g (± 0.5) (July 2018).

The degree of data variability was greatest in samples obtained during July 2017 (Figure 4.3.2.1.1), with the mean TOC concentration of 11.23 ± SE 4.56. The samples with the greatest degree of variation were recorded at surface site 1 (26.08mg/g ± 23.28) and surface sample of site 4 (76.35mg/g ± 96.65).

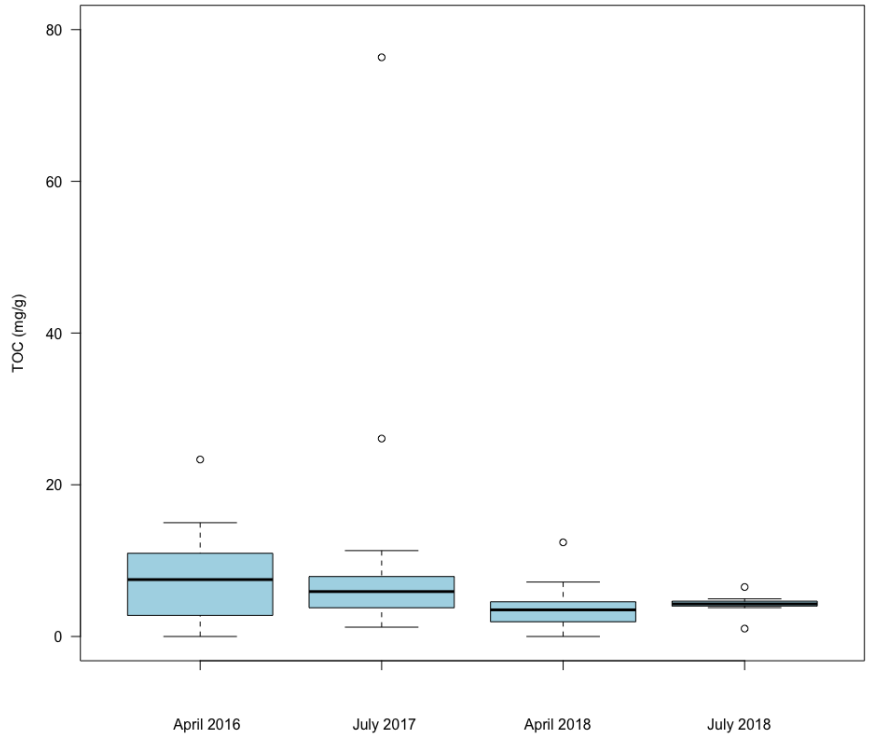

Figure 4.3.2.1.1. TOC concentrations (median and quartiles) during sampling sessions during April 2016, July 2017, April 2018 and July 2018.

4.3.2.2. Mean TOC (mg/g) in surface sediment (0-3cm).

Of the surface sediment, site 2 recorded the greatest TOC concentration during July 2017 (Figure 4.3.2.2.1) with concentrations averaging 765mg/g (± 96.6), however the variation is data was large.

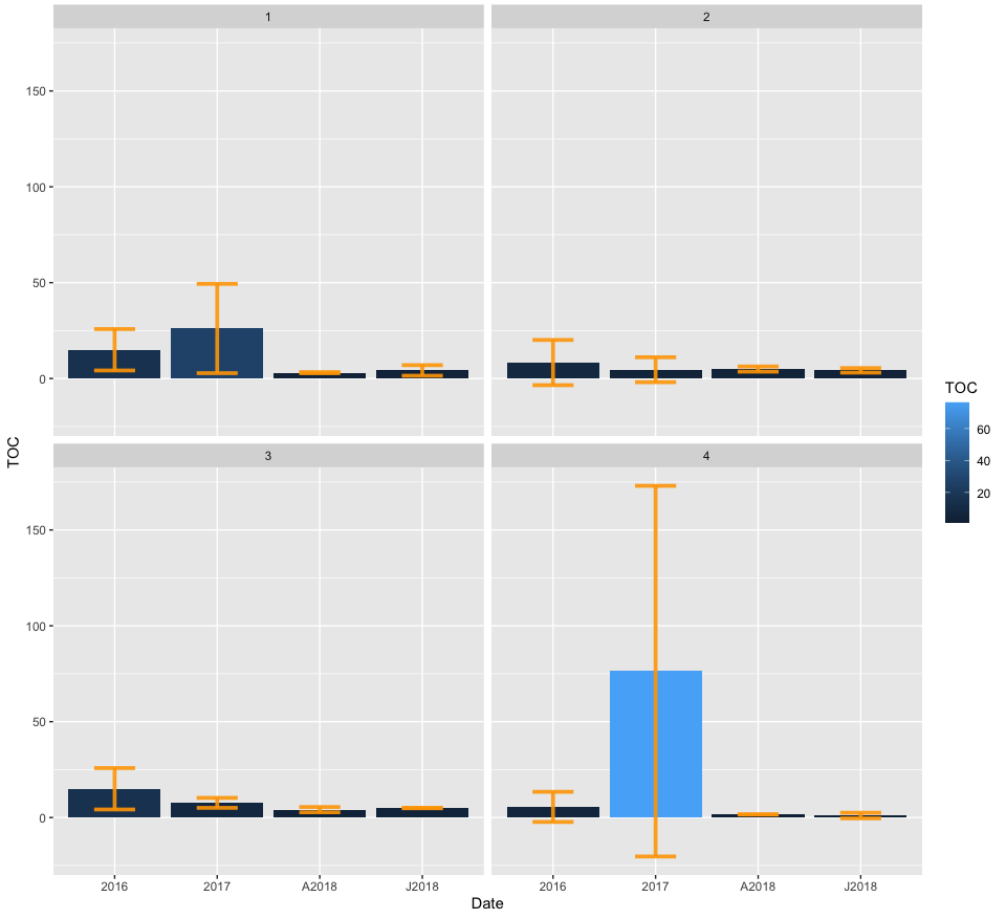

4.3.2.2.1. TOC (mg/g ± at surface sediments (layer 1) at sampling sites 1,2,3 and 4 during April 2016, July 2017, April 2018 and July 2018.

The concentrations of TOC were lower throughout 2018 (3.52mg/g ± SE 0.49), indicating a decrease in carbon settlement.

4.3.2.3. Mean total organic carbon (mg/g) April 2016.

Concentrations of TOC were variable across the surface of the reservoir, with the highest concentrations isolated at site 1 15mg/g ± 10.8), however, the difference between the concentrations of TOC at site 1 and site 2 (14.99 ± 10.8) were insignificant.

The lowest concentrations of TOC within layer 1 of the samples was isolated at site 4 (5.55mg/g ± 7.85), however, site 4 was the only site to record the detection of TOC within each of the 5 layers of sediment (9.06mg/g ± SE 1.29).

The TOC concentrations decreased at each site within layer 2 of the sediment with the exception of site 4, where the TOC concentrations increased (12.22mg/g ± 8.74). No TOC was

isolated within layers 2 nor 3 of site 3, indicating a reduction in primary productivity activity at this site upon disturbance to the sediment to between 4cm to 9cm in depth.

The highest TOC concentration within layer 5 was recorded at site 3 (23.22mg/g ± 2.35) indicating the reduction in primary productivity activity likely at this site over the sedimentation process (Figure 4.3.2.3.1).

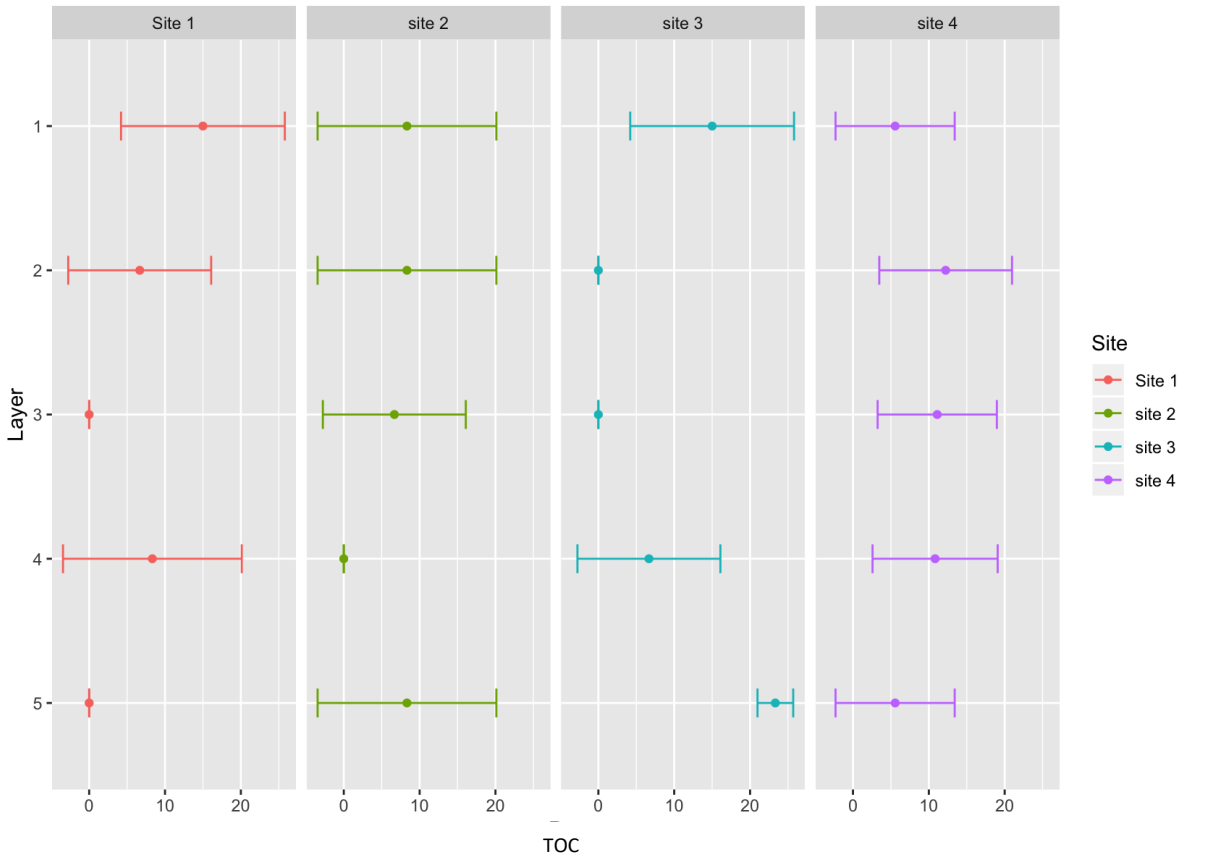

Table 4.3.2.3.1. TOC (mg/g) concentrations (mean ± SD) in sediment samples at sites 1, 2, 3 and 4 during April 2016. Layer 1 represents the top 0-3cm, layer 2 represents 4-6cm, layer 3 represents 7-9cm, layer 4 represents 10-12cm and layer 5 represents 13-15cm of sediment depth.

4.3.2.4. Mean total organic carbon (mg/g) July 2017.

TOC concentration was highest (76.35mg/g ± 96.65) at surface site 4 (Layer 1) relative to any other sites sampled during July 2017 (6.89mg/g ± SE 1.46), however, mean TOC isolated in sediment layers 2,3 and 4 of site 4 were significantly lower (<0.005; 5.58mg/g ± SE 0.69) that that isolated within layer 1.

Surface samples of sites 2 (4.59mg/g ± 6.5) and 3 (7.65mg/g ± 2.6) contained relatively low concentrations of TOC compared with that of sites 1 (26.08 ± 23.27) and 4, however, layers 2 (11.32mg/g ± 1.95) and 3 (8.15mg/g ± 5.38) of site 3 contained the highest TOC concentrations of any other site (layer 2 of sites 1,2 and 4: mean 4.11mg/g ± SE 0.62; layer 3 of sites 1,2 and 4: mean 4.36mg/g ± SE 1.28). Data variability was greatest at layer 1 of site 4 (Figure 4.3.2.4.1)

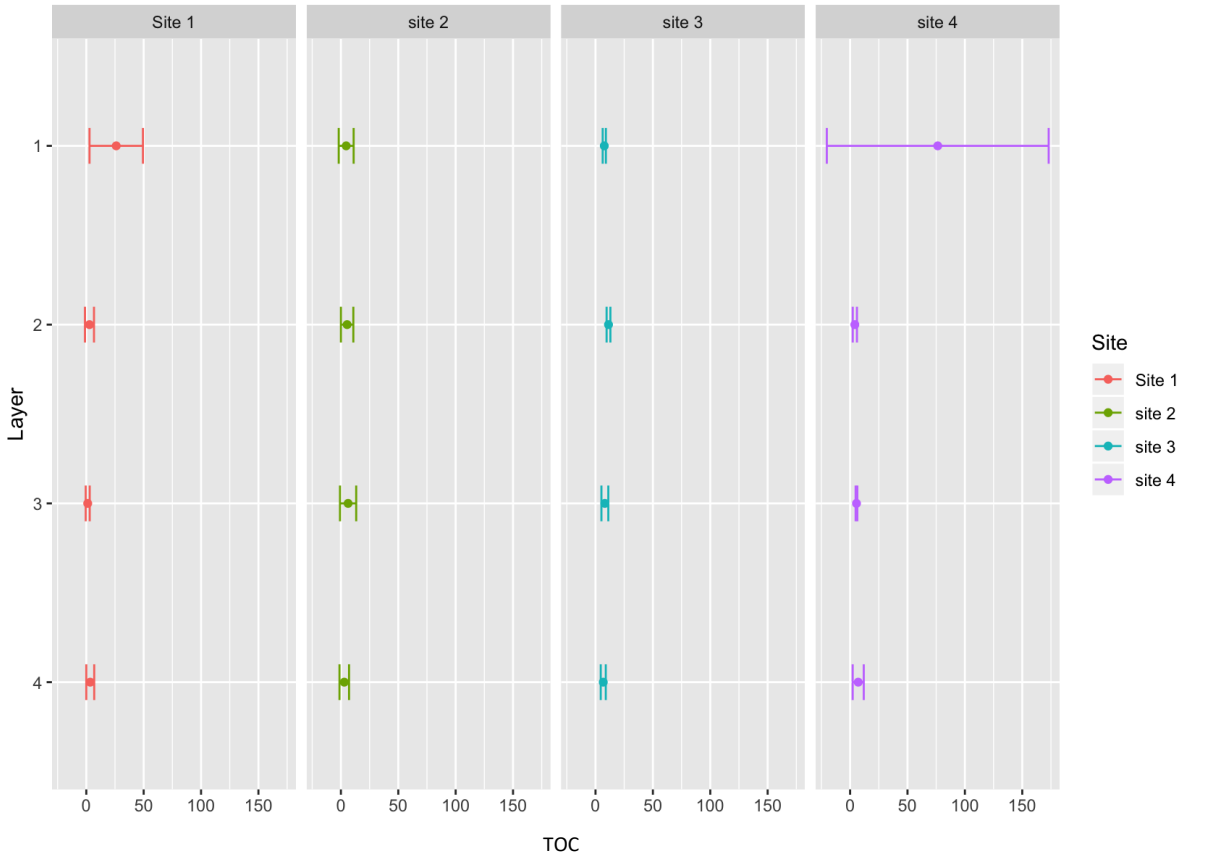

Figure 4.3.2.4.1. TOC (mg/g) in July 2017 (mean ± SD) for sites 1, 2, 3 and 4 throughout the sediment layers. Layer 1 represents the top 0-3cm, layer 2 represents 4-6cm, layer 3 represents 7-9cm, layer 4 represents 10-12cm of sediment depth.

4.3.2.5. Mean total organic carbon (mg/g) April 2018.

The concentration of TOC within the surface samples at each of the sites was low (3.42mg/g ± SE 0.62) relative to that isolated at layer 2 of site 1 (12.41mg/g ± 13.32). The data suggested a greater risk of microbial activity induced as a consequence of release of organic C following sediment disturbance is likely at site 2.

The TOC concentrations were lowest at site 4 at each layer relative to that at sites 1, 2 and 3, suggesting that site 4 posed the lowest risk of inducing bottom microbial activity. Layer 2 of site 1 recorded the highest concentrations of TOC (12.41mg/g + 13.32) but also recorded a large SD (Figure 4.3.2.5.1).

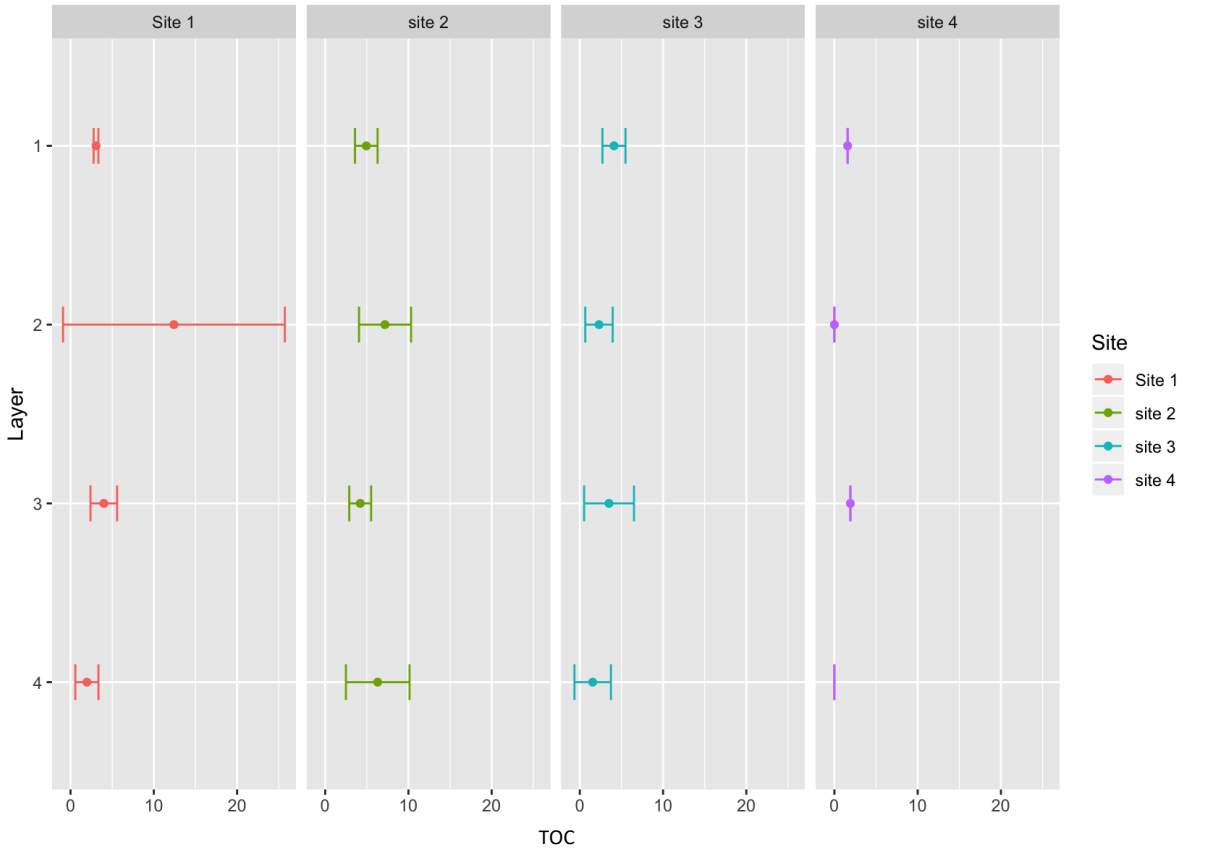

Figure 4.3.2.5.1. TOC (mg/g) in April 2018 (mean ± SD) for sites 1, 2, 3 and 4 throughout the sediment layers. Layer 1 represents the top 0-3cm, layer 2 represents 4-6cm, layer 3 represents 7-9cm and layer 4 represents 10-12cm of sediment depth.

4.3.2.6. Mean total organic carbon (mg/g) July 2018.

The mean concentrations of TOC within the surface samples of sites 1, 2 and 3 increased with a south to north progression along the reservoir, however, the variability within repeated measures increased.

The lowest risk of benthic microbial activity during July 2018 was at sampling 4 which recorded the lowest TOC (1.04mg/g ± 1.43). Sediment disturbance to a depth of between 13cm and 15cm may have induced or supported further bottom microbial activity through

the exposure of higher concentrations of TOC within layer 5 at each site relative to that isolated within the first layer along the transect of the reservoir (Figure 4.3.2.6.1).

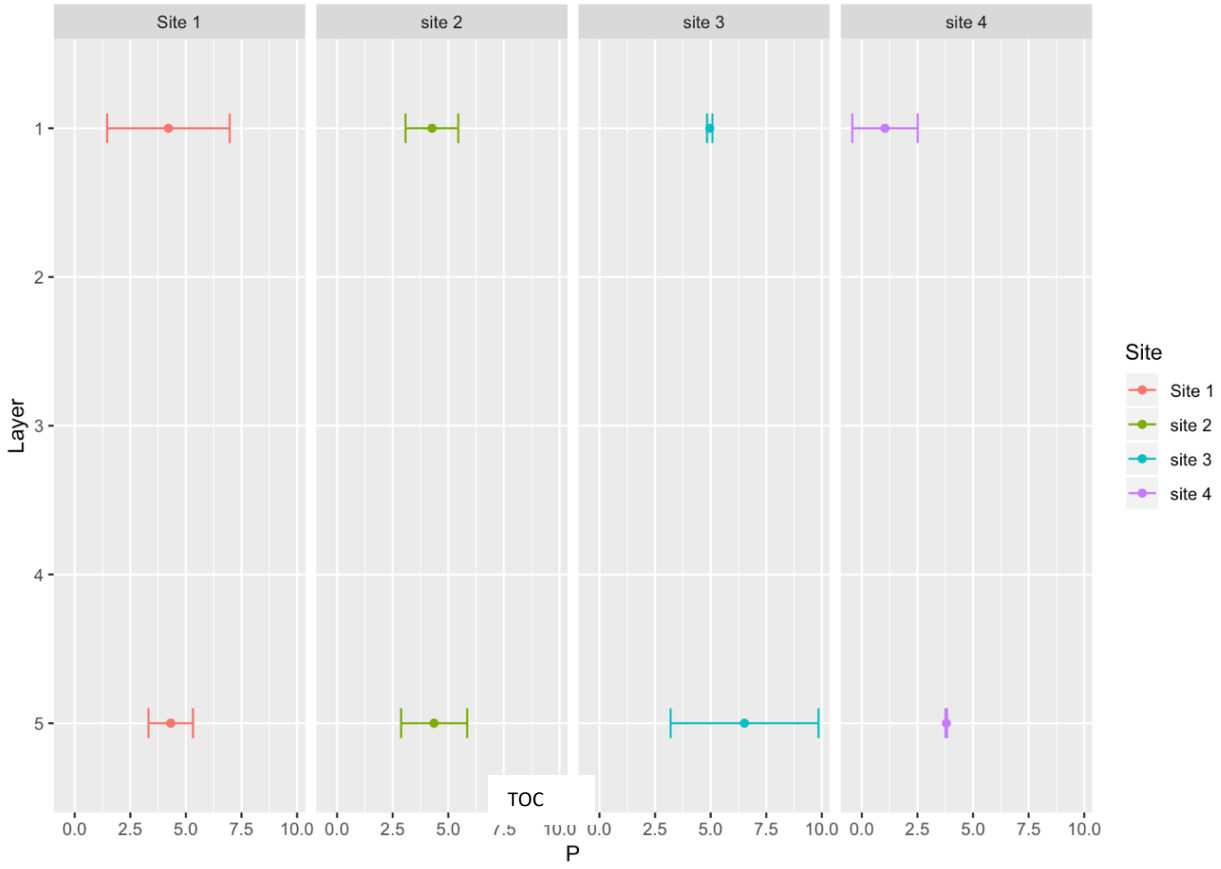

Figure 4.3.2.6.1. TOC (mg/g) in July 2018 (mean ± SD) for sites 1, 2, 3 and 4 throughout the sediment layers. Layer 1 represents the top 0-3cm and layer 5 represents the bottom 13cm-15cm.

4.3.3. Mean Fe-P: Ca-P molar ratios throughout the sediment layers at each site from April 2016 through July 2018.

Fe-P: Ca-P ratios were analysed to determine the ratios over the 2016 through 2018 sampling period (Table 4.3.3.1).

Sample analysis of data obtained during April 2016 indicated that 89% of the samples were likely to release a greater concentration of P under acidic conditions. However, a significant change to the Fe-P: Ca-P ratio occured by July 2017 resulting in only 38% of all sediment samples likely to release an increased concentration of P under acidic conditions.

The samples obtained during April 2018 indicated that an increase in Fe-P was recorded throughout the reservoir since July 2017 resulting in only 20% of the sediment samples likely

to release an increase cioncentration of P in acidic conditions, with the trend of an increased risk of internal P release under alkaline conditions continuing into July 2018 with just 13%.

Table 4.3.3.1. Fe-P: Ca-P molar ratio throughout the sediment layers for each sampling site during April 2016 through July 2018. Greater P release likely in acidic conditions highlighted in red; greater P release in alkaline conditions highlighted in blue.

Site	Layer	April 2016	July 2017	April 2018	July 2018
1	1	0	0.13:1	4.1:1	8.6:1
	2	0	4.5:1	2.4:1	
	3	0	1.8:1	0.21:1	
	4	0	0.12:1	0.79:1	
	5	0.01:1			5.4:1
2	1	0.01:1	3.6:1	5.7:1	1.38:1
	2	0.06:1	0.84:1	73.8:1	
	3	0.11:1	2.7:1	10.7:1	
	4	0.1:1	0.08:1	3.1:1	
	5	0.13:1			2.9:1
3	1		0.17:1	0.50	11.7:1
	2	0.44:1	5.7:1	95.6:1	
	3	0.42:1	4.7:1	188.7:1	
	4	1.14:1	3.3:1	0.17:1	
	5	0.99:1			9.6:1
4	1	0.11:1	1.8:1	2.3:1	0.25:1
	2	0.2:1	2.7:1	8.2:1	
	3	0.25:1	0.08:1		
	4	0.16:1	0	0.9:1	
	5	0.12:1			3.1:1

A 65% increase in Ca-P concentration was recorded throughout the reservoir between April 2018 (13mg/g ± 23.4) and July 2018 (37.6mg/g ± 32.3) (Figure 4.3.3.2), indicating the potential shift from alkaline-activated P release to acid-activiated P release. However, the ratios were not low enough during August 2018 to suggest that acidic conditions would instigate internal P-release over alkaline conditions.

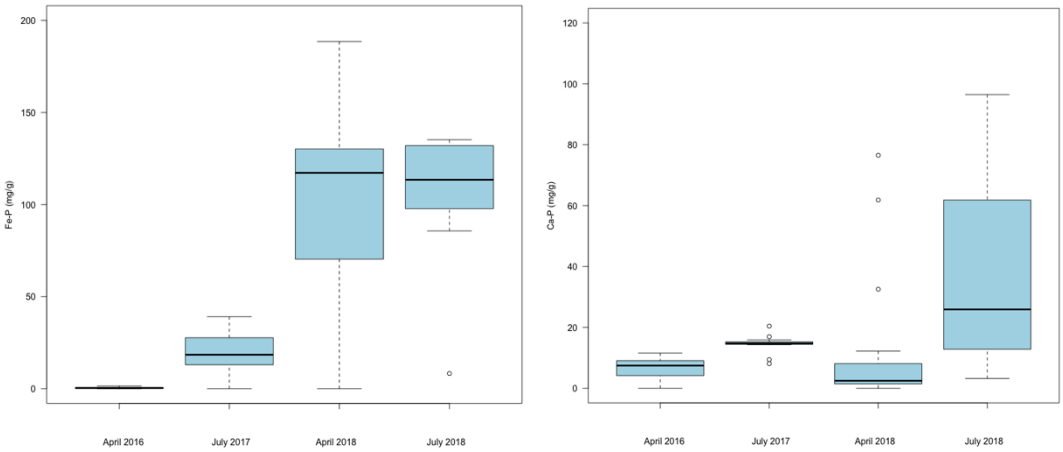

Figure 4.3.3.2. Fe-P and Ca-P concentrations (mean mg/g, median and quartiles) during sampling sessions during April 2016, July 2017, April 2018 and July 2018.

The greatest change to the Fe-P:Ca-P ratio occurred between April 2016 and July 2017 where a mean increase in Fe-P concentrations throughout the reservoir from 0.47mg/g (± 0.43) to 19.03mg/g (± 11.4) was recorded, which coincided with an increase in mean Ca-P concentrations (from 6.69mg/g (± 3) to 14.6mg/g (±2.7)). However, Fe-P recorded a greater increase in concentration (99.8%) than Ca-P (55%).

The period of greatest increase in Fe-P concentrations coincided with a period of greatest increase in labile P concentrations (2016-2017), indicating the release of P to solution as a consequence of Fe-P dissolution (Figure 4.3.3.3).

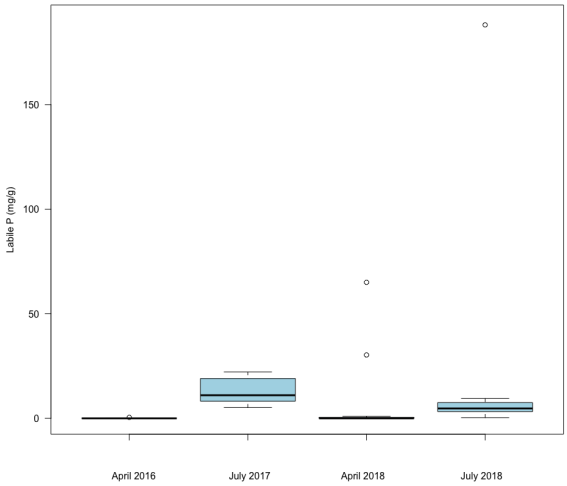

Figure 4.3.3.3. La-P concentrations (mean mg/g, median and quartiles) during sampling sessions during April 2016, July 2017, April 2018 and July 2018.

Of the surface samples, site 3 retained an Fe-P:Ca-P <0.5 until July 2018, with the surface samples of all sites indicating alkaline conditions instigating a greater P release with the exception of site 4 (0.25:1).

An increase in Fe-P concentration was recorded at the surface samples at the southern section the reservoir during July 2018 (Figure 4.3.3.4) relative to that during April 2016. However, the Fe-P concentrstaions decreased from April 2018 to July 2018 at the northern section of the rseercoir (sites 3 and 4)

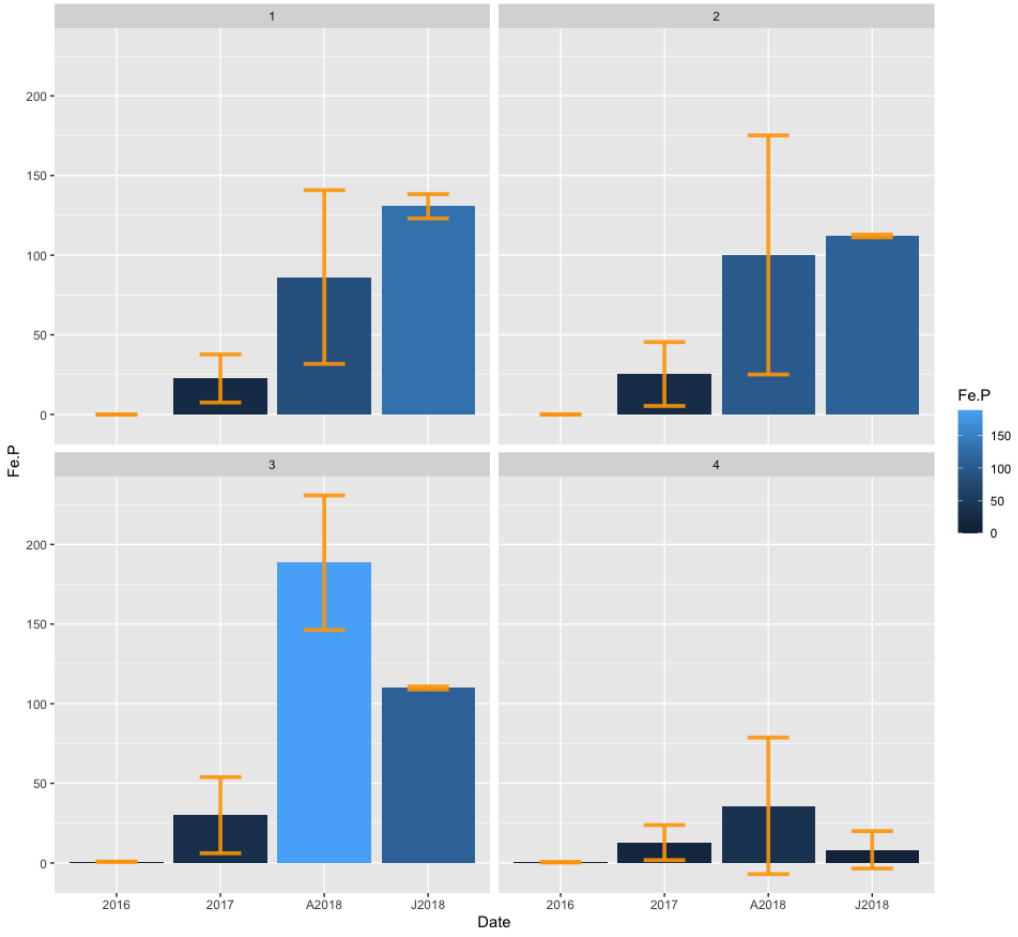

Figure 4.3.3.4. Fe-P (mg/g ± SE) at surface sediments (layer 1) at sampling sites 1, 2, 3 and 4 during April 2016, July 2017, April 2018 and July 2018.

4.3.4 Ion chromatography data July 2017, April 2017 and July 2018

4.3.4.1. Fe and Mn ion July 2017

Mean Fe concentrations were significantly higher in concentrations than mean Mn concentrations (99.9%) throughout the top three layers of sediment (0-9cm).

The concentration of Fe was highest at site 2 (51.53mg/g ± SE 1.64) within layer 2 (53.93mg/g ± 0.2) relative to all other sites at the reservoir, however, the difference between mean Fe (mg/g) at site 2 and mean Fe concentrations at site 2 (48.16mg/g ± SE 1.43) was insignificant (>0.05).

The mean Fe concentrations were significantly lower (P<0.05) at site 3 (43.03mg/g ± 0.37) relative to sites 1 and 2, and mean Fe concentrations were significantly lower (P<0.05) at site 4 (31.59mg/g ± 2.32) than mean Fe concentrations at site 3. The data indicated a reduction in Fe concentrations from the southern to the northern sections of the reservoir (Figure 4.3.4.1.1).

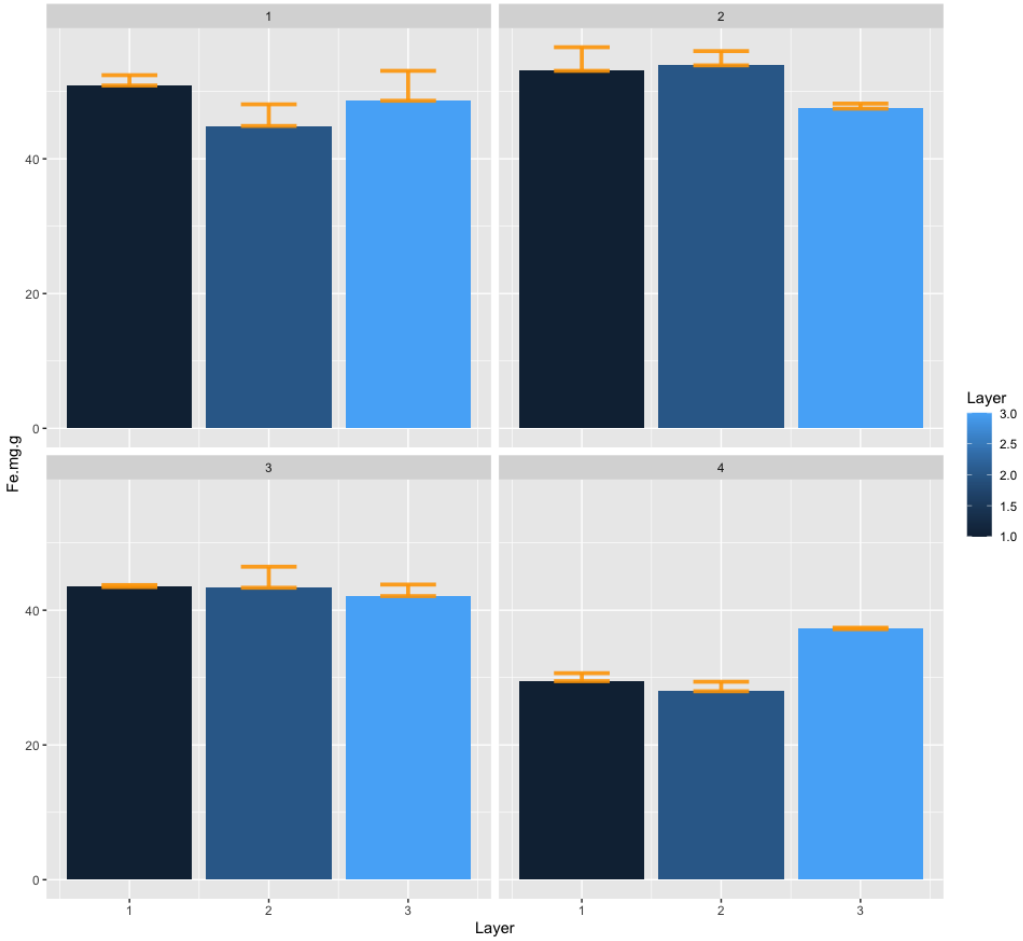

Figure 4.3.4.1.1. Mean ± SE Fe ion concentration (mg/g) throughout layer 1 (0-3cm), layer 2 (4-6cm and layer 3 (7-9cm) of sediment at sample point 1, 2, 3and 4 during July 2017.

The highest concentrations of Fe at each site were isolated within the surface sediment (layer 1) at sites 1 and 3 (50.93mg/g ± 0.14; 43.56mg/g ± 0.01 respectively). The highest Fe concentrations at sites 2 (53.93mg/g ± 0.2) and 4 (37.23mg/g ± 0.01) were isolated within layers 2 (4-6cm depth) and 3 of the sediment (7-9cm depth) respectively (Figure 4.3.4.1.2).

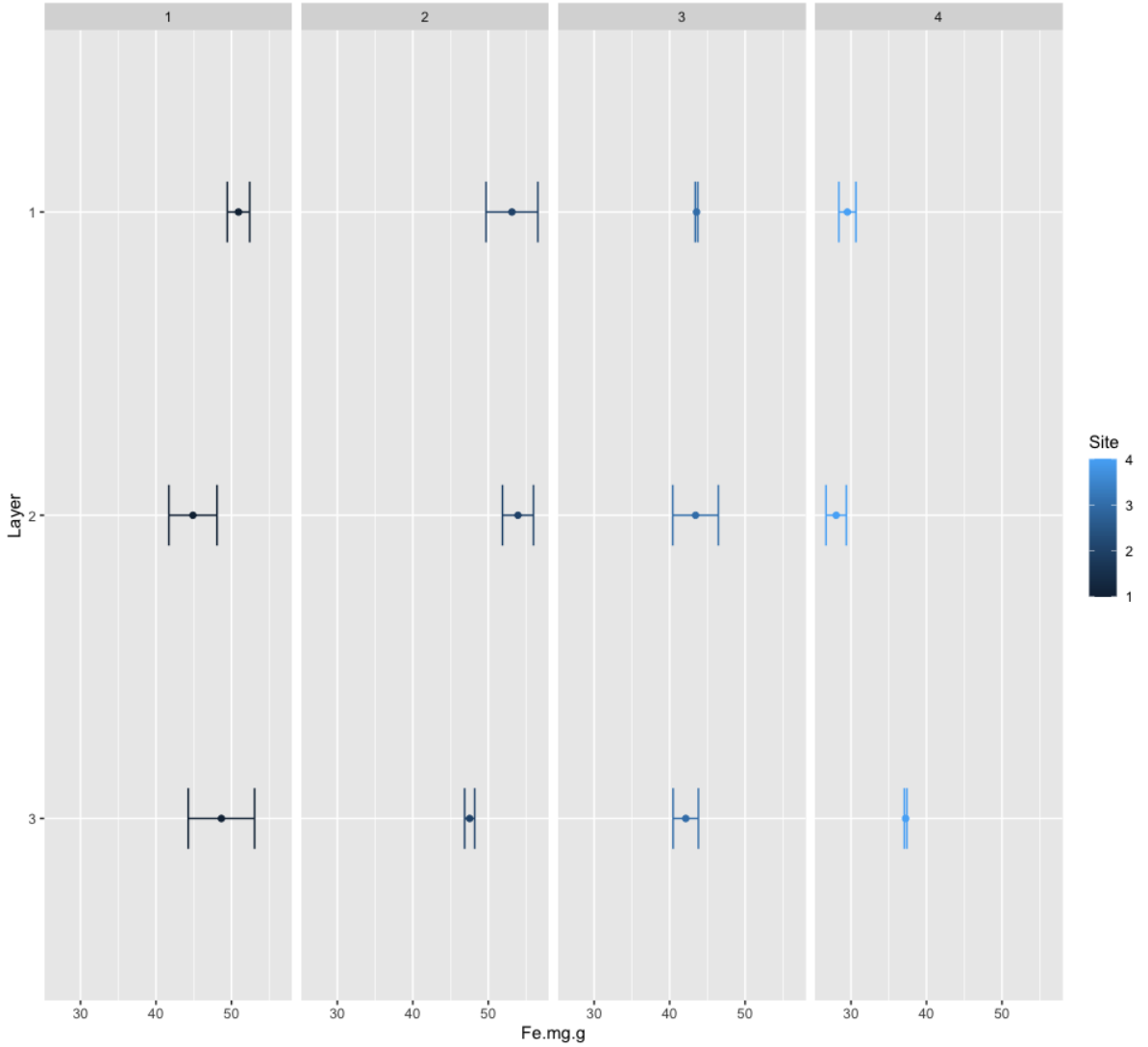

Figure 4.3.4.1.2. Fe mean concentrations ± SD throughout the top three layers of sediment at each site during July 2017. Layer 1 represents the top 0-3cm, layer 2 represents 4-6cm, layer 3 represents 7-9cm of sediment depth.

Mn decreased in mean concentration throughout the sediment depth from the southerly sampling points to the northerly sampling points (Figure 4.3.4.1.3), with the highest mean isolated within the surface layer at sites 1 and 3 (0.996mg/g ± 0.05 and 0.819mg/g ± 0.13 respectively).

The highest concentration of Mn at sites 2 and 4 were recorded within sediment layers 2 (0.98mg/g ± 0.08) and 3 (0.73mg/g ± 0.05) respectively.

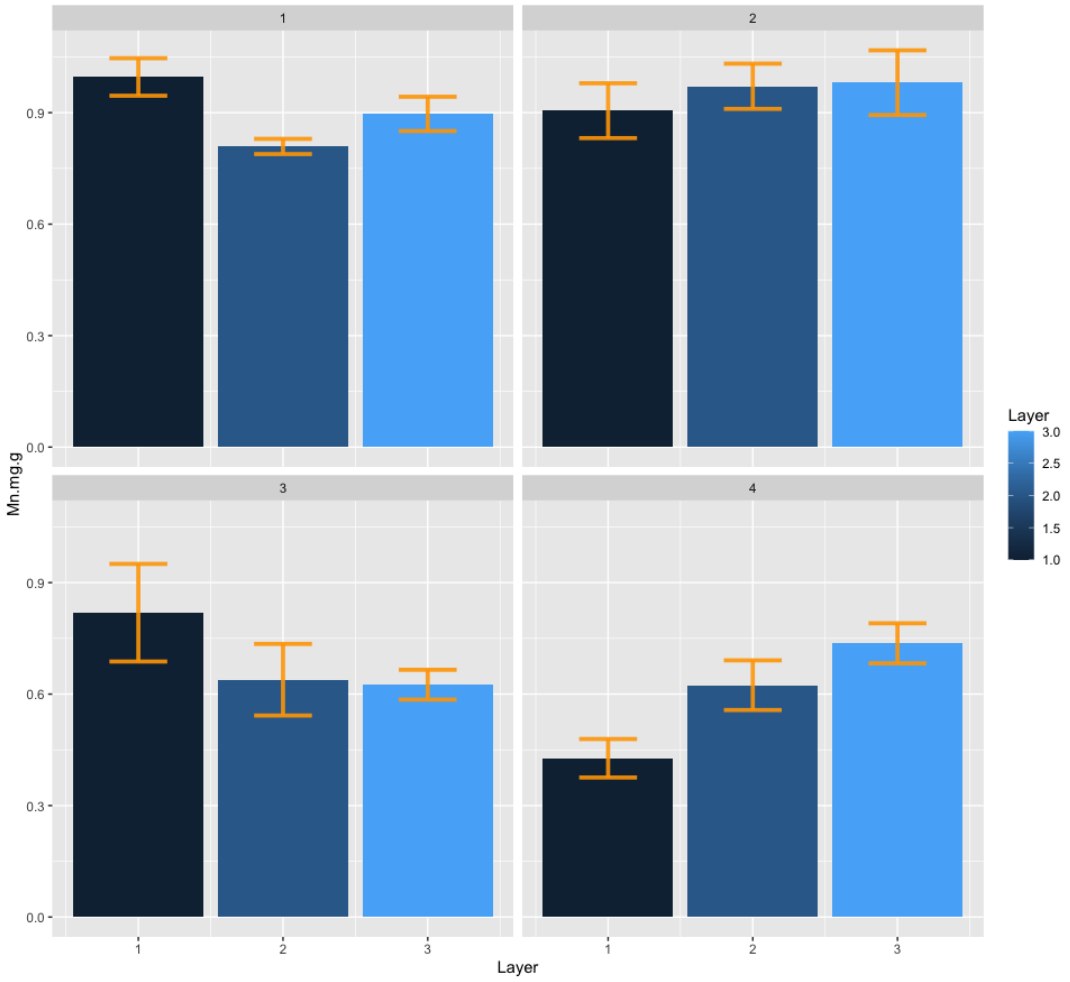

Figure 4.3.4.1.3. Mean ± SE Mn ion concentration (mg/g) throughout layer 1 (0-3cm), layer 2 (4-6cm and layer 3 (7-9cm) of sediment at sample point 1, 2, 3and 4 during July 2017.

An increasing trend in mean Mn ion concentration was observed at sites 2 and 4 (Figure 4.3.4.1.4) with sediment depth, whereas a decreasing trend in Mn+ concentrations was recorded through the sediment layers at site 3.

Sampling site 3 (surface layer) recorded the greatest degree in data variation (0.819mg/g ± 0.13).

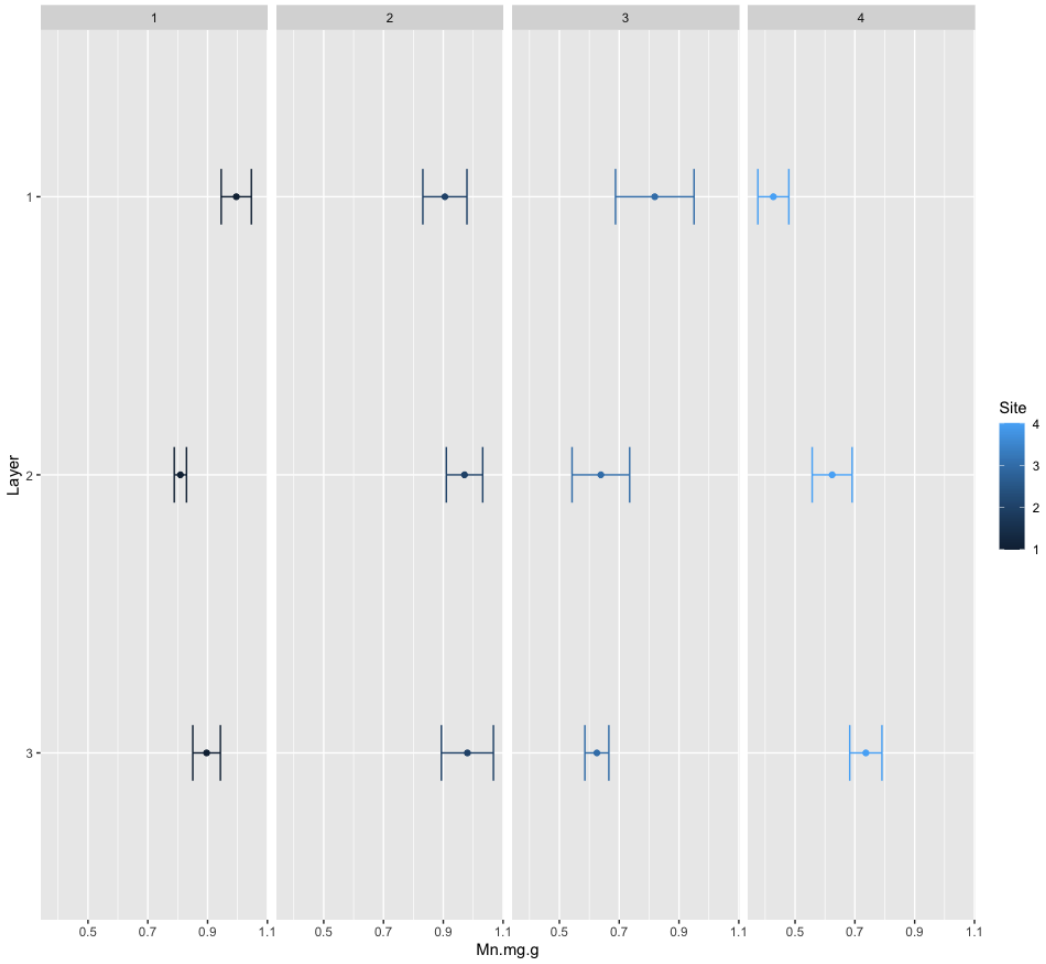

Figure 4.3.4.1.4. Mn mean concentrations ± SD throughout the top three layers of sediment at each site during July 2017. Layer 1 represents the top 0-3cm, layer 2 represents 4-6cm, layer 3 represents 7-9cm of sediment depth.

4.3.4.2. Fe and Mn ion April 2018

The Fe ion concentrations were higher across the reservoir (46.89mg/g ± SE 1.6) throughout the sediment depths relative to that of mean Mn concentrations (0.94mg/g ± SE 0.09) (Table 4.3.4.2.1) throughout the sediment depths.

The highest concentration of Fe was isolated at the surface (layer1) at sites 1 (51.9mg/g ± 3.31) and 2 (53.03mg/g ± 1.43). However, layer 2 recorded the highest Fe concentrations of site 3. The unavailability of data beyond layer 1 and site 4 prevented further comparison at this site (Figure 4.3.4.2.1).

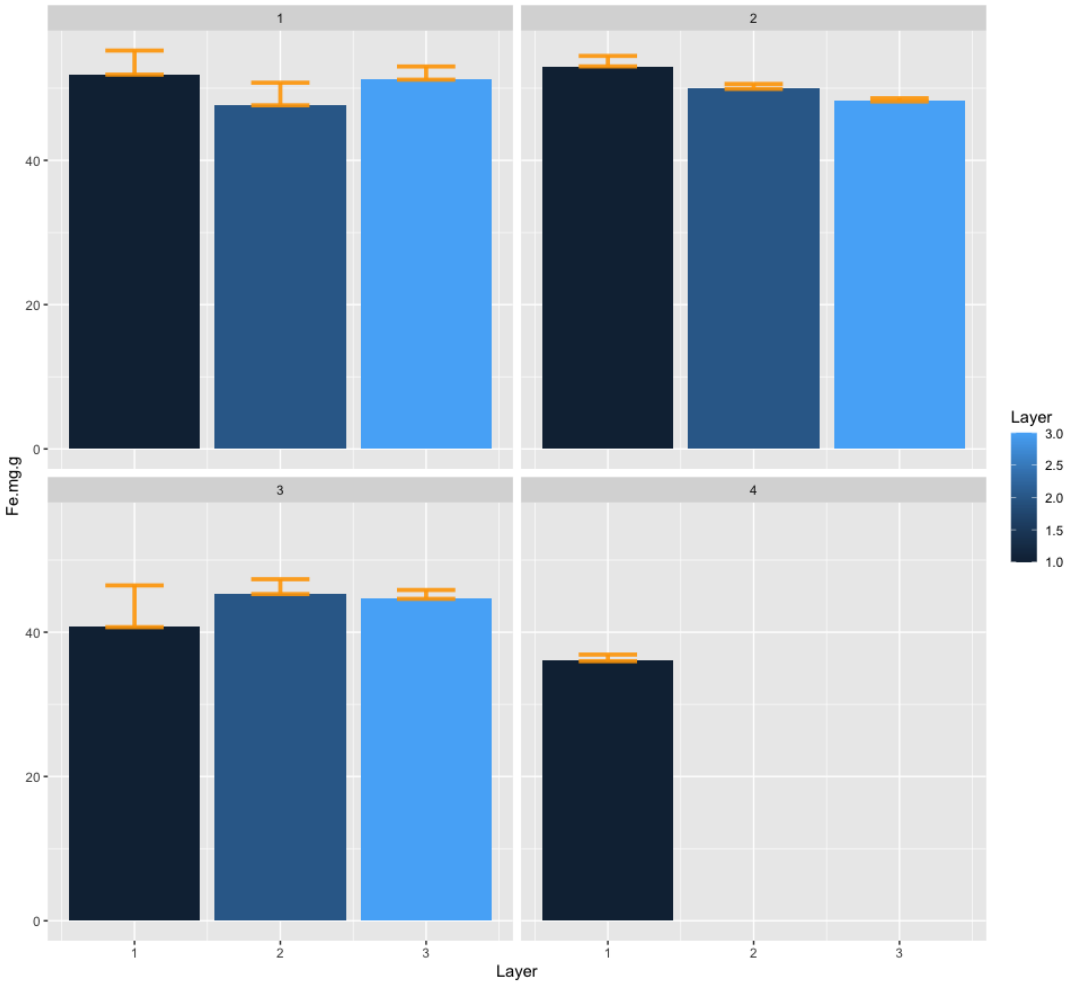

Figure 4.3.4.2.1. Mean ± SE Fe ion concentration (mg/g) throughout layer 1 (0-3cm), layer 2 (4-6cm) and layer 3 (7-9cm) of sediment at sample point 1, 2, 3 and 4 during April 2018.

The greatest degree of variation was recorded at surface site 3 (40.77mg/g ± 5.7), with layer 3 of site 2 recording the lowest degree of data variation (48.26mg/g ± 0.33) (Figure 4.3.4.2.2).

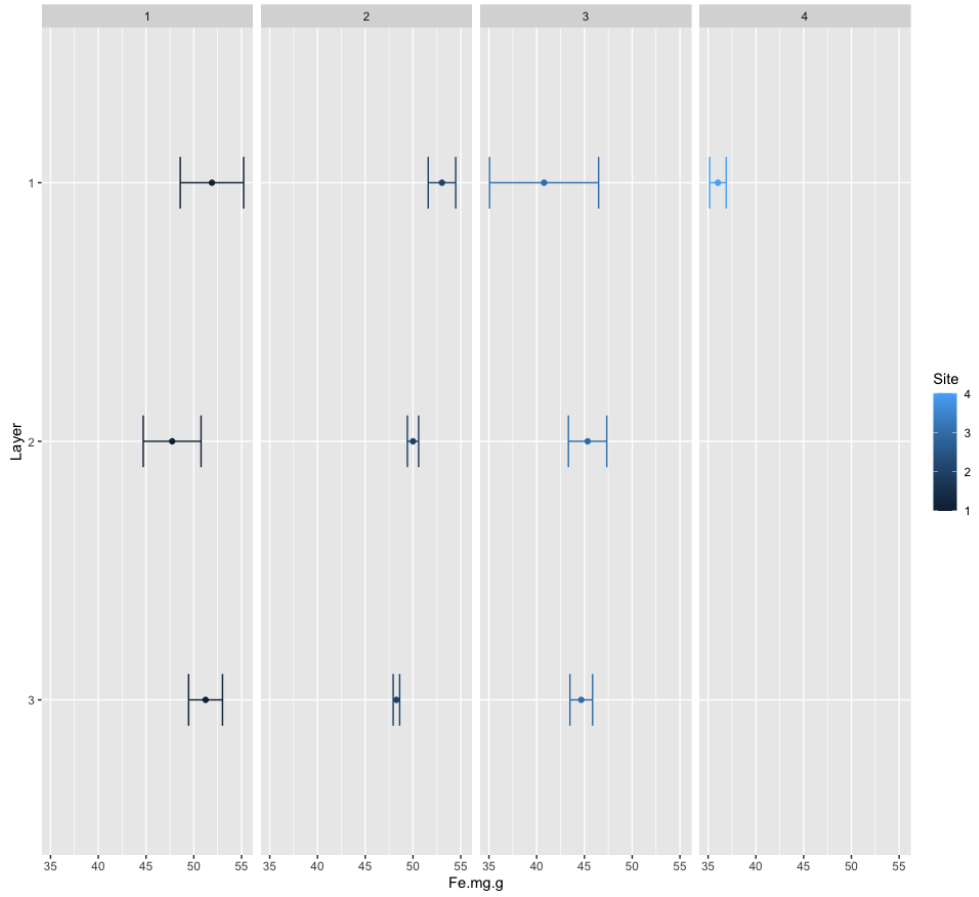

Figure 4.3.4.2.2. Fe mean concentrations ± SD throughout the top three layers of sediment at each site during April 2018. Layer 1 represents the top 0-3cm, layer 2 represents 4-6cm, layer 3 represents 7-9cm of sediment depth.

An increasing trend in Mn concentrations was recorded at site 2 (Figure 4.3.4.2.3), with layer 3 recording the highest concentartions (1.24mg/g ± 0.1). Of sites 1 and 3, the surface layer contained the highest mean Mn concentrations (1.53mg/g ± 0.01 site 1; 0.89mg/g ± 0.07 site 3). The lowest Mn concentration was recorded at surface site 4 (0.5mg/g ± 0.04).

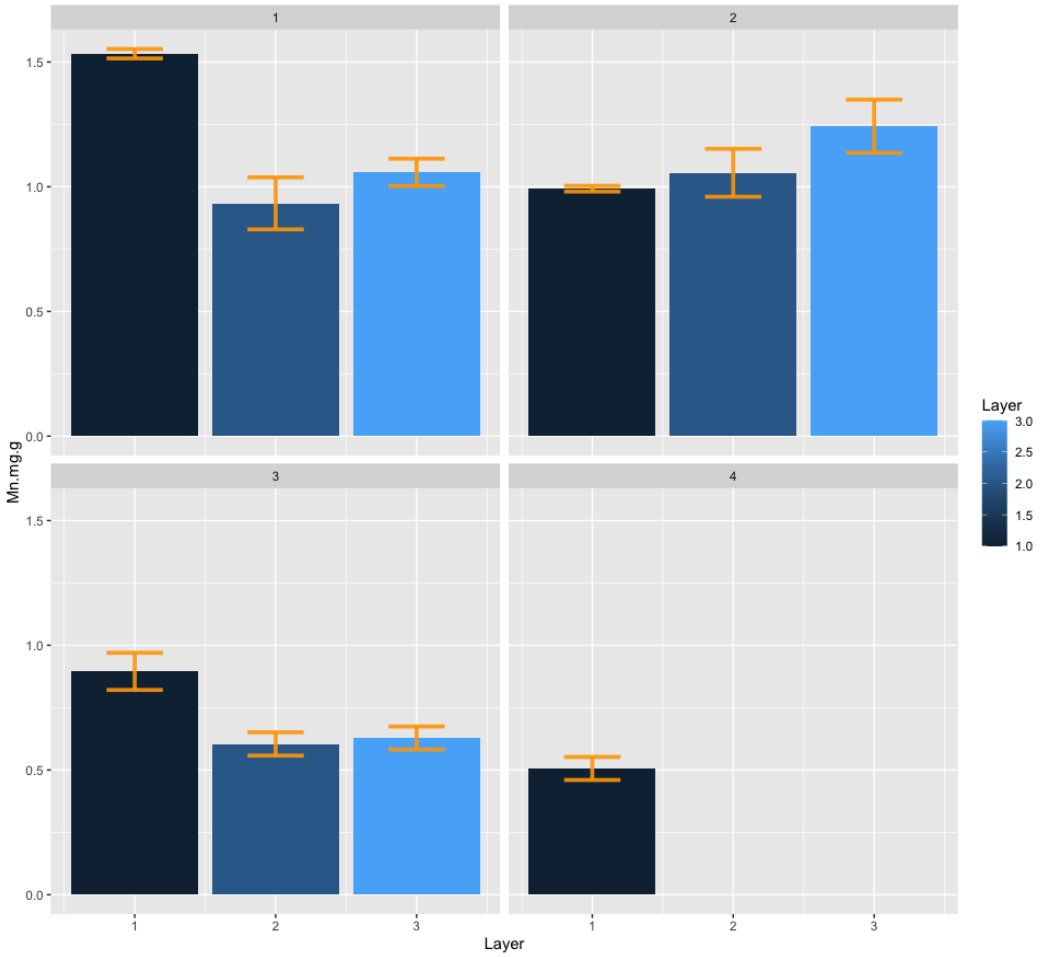

Figure 4.3.4.2.3. Mean ± SE Mn ion concentration (mg/g) throughout layer 1 (0-3cm), layer 2 (4-6cm and layer 3 (7-9cm) of sediment at sample point 1, 2, 3and 4 during April 2018.

The greatest degree of variation within the data was recorded at site 1, layer 2 where the data varied by 10% (0.93mg/g ± 0.1), 8.5% at site 2, layer 2 (1.05mg/g ± 0.09) and 8% at site 2 layer 3 (0.62mg/g ± 0.04) (Figure 4.3.4.2.4).

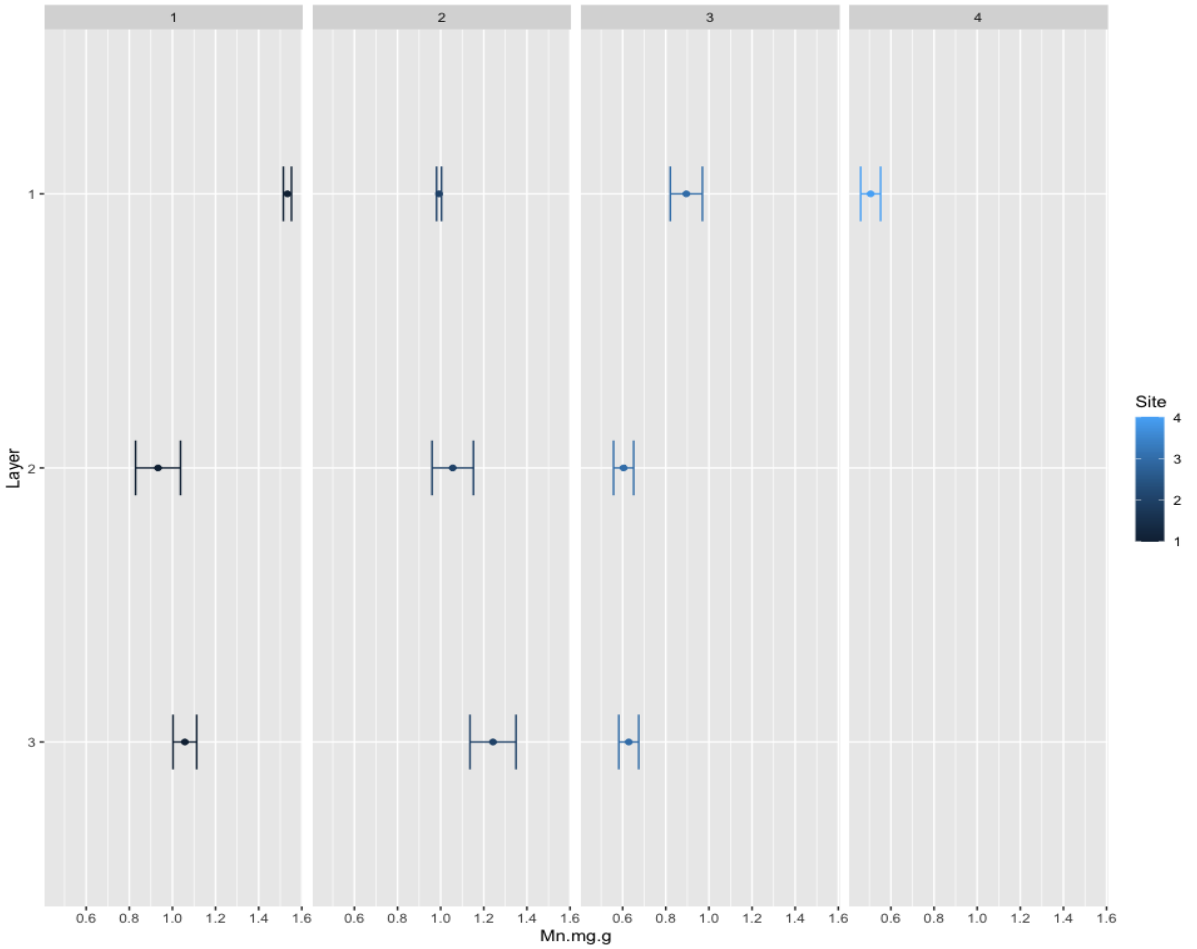

Figure 4.3.4.2.4. Mn mean concentrations ± SD throughout the top three layers of sediment at each site during April 2018. Layer 1 represents the top 0-3cm, layer 2 represents 4-6cm, layer 3 represents 7-9cm of sediment depth.

4.3.4.3. Fe and Mn ions July 2018

The highest mean concentration of Fe was isoalted at site 1 (62.2mg/g ± 1.13) during July 2018, with mean Fe concentrations across the sediment surface along the transect of the reservoir showing small degree of variation (49.15mg/g ± SE 6.51).

The lowest mean concentration of Fe (31.44mg/g ± 0.4) was isolated at site 4 (Figure 4.3.4.3.1), with an increase in mean concentrations recorded along the progeression of the reservoir from northern to southern sites.

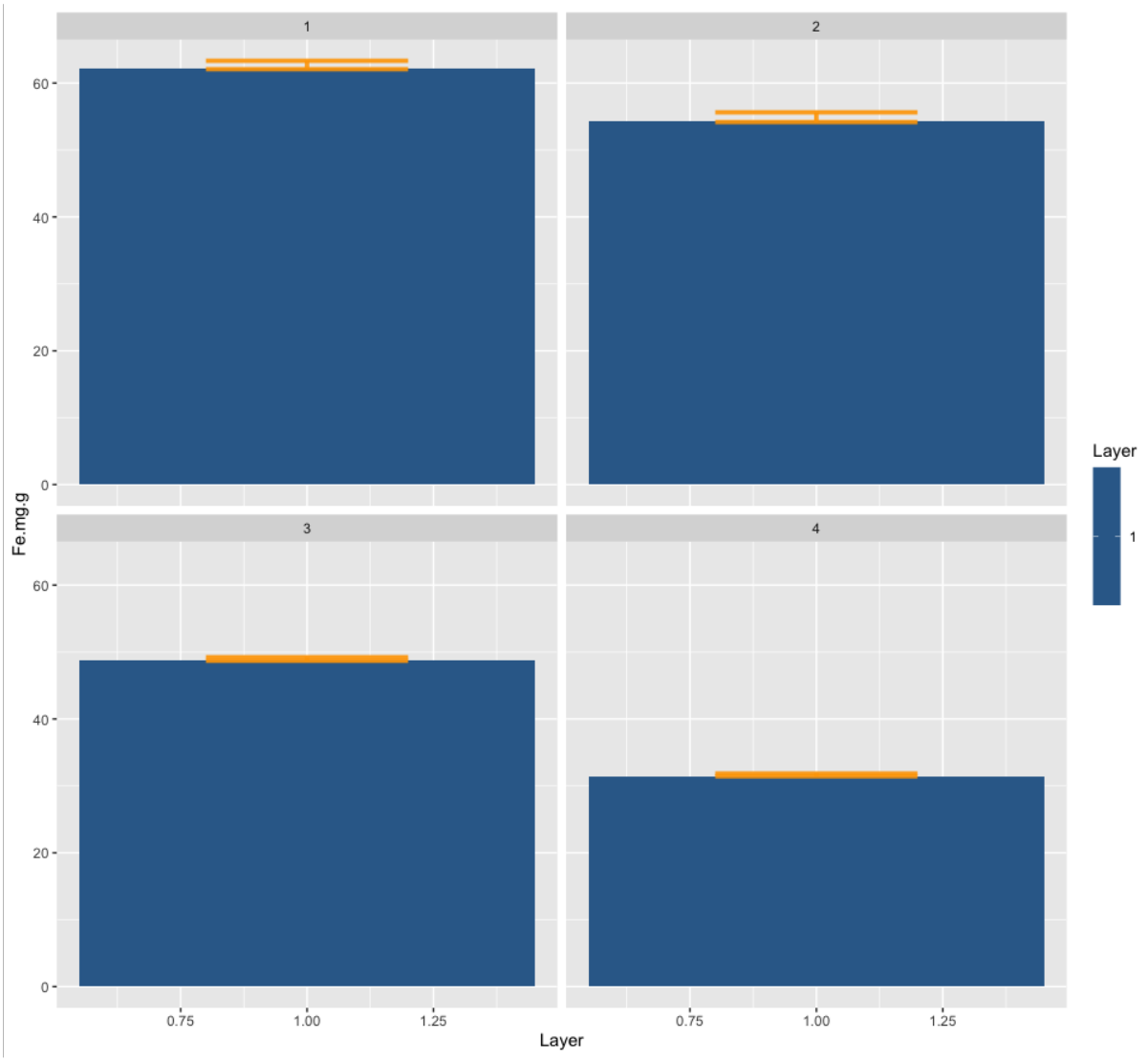

Figure 4.3.4.3.1. Mean ± SE Fe ion concentration (mg/g) throughout layer 1 (0-3cm) of sediment at sample point 1, 2, 3and 4 during April 2018.

Mean Mn concentartions decreased from the southern surface layer to the northern surface layer, with an insignificant difference in Mn content of layer 1 at site1 andlayer 1 at site 2 (P>0.05). However, a significant difference in Mn content (Figure 4.3.4.3.2) was recorded at surface sediment of site 4 (0.35mg/g ± 0.01) relative to that within surface sediments of sites 1, 2 and 3 (0.93mg/g ± SE 0.05).

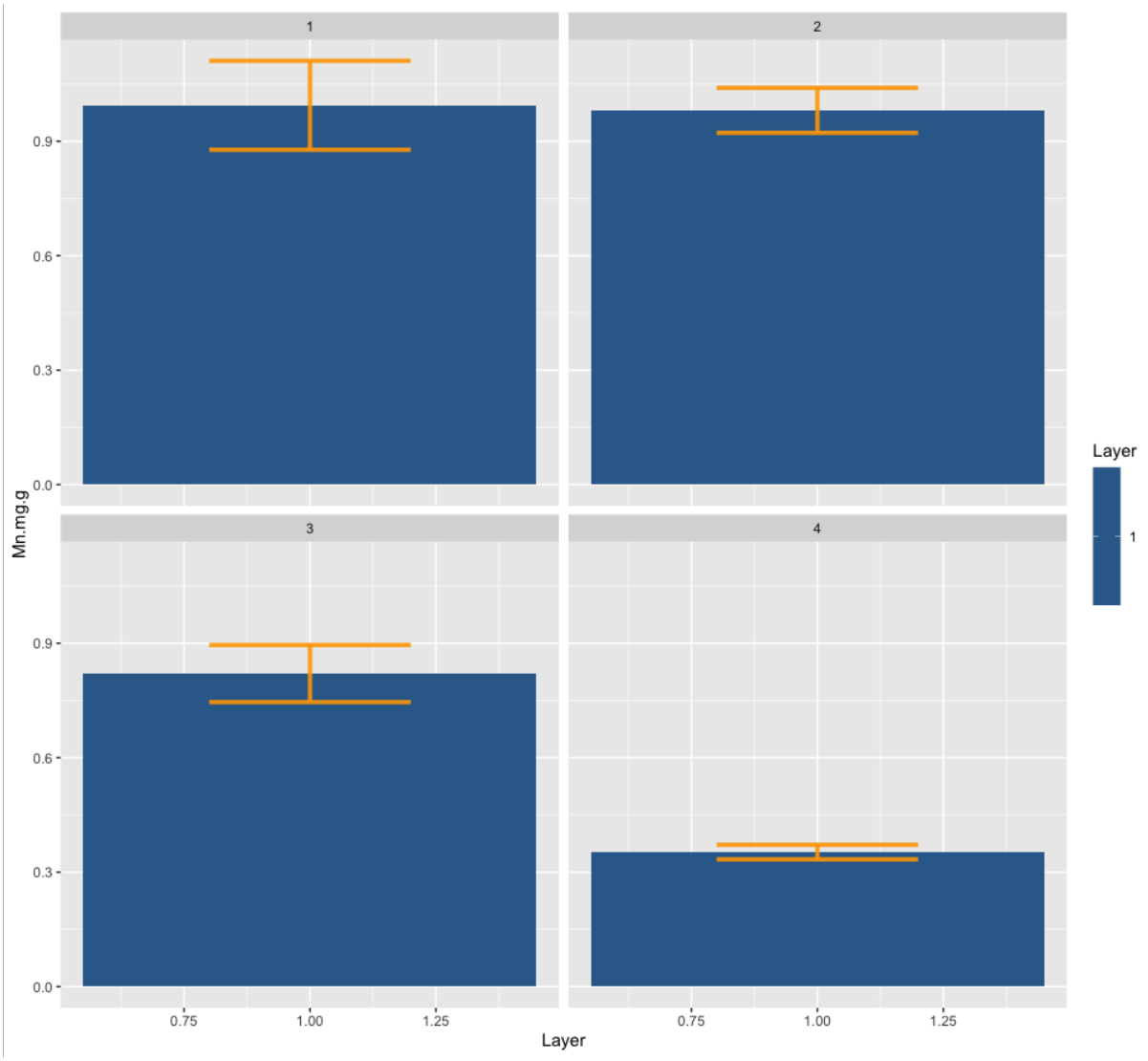

Figure 4.3.4.3.2. Mean ± SE Mn ion concentration (mg/g) throughout layer 1 (0-3cm) of sediment at sample

4.3.5. Across-site modelling of P-fractions, TOC and ion data from April 2016 through July 2018.

4.3.5.1. Mean collective P-fraction and TOC concentrations GLM/LM analyses throughout the sediment depths and transect of the reservoir during April 2016.

Fe-P data were not normally distributed and was transformed using the square root method. Fe-P (2016) was transformed using the square root method. A significant association (^R^2: 0.35, $F_{1,18}$:11.42; P<0.005) was determined for collective mean Fe-P (LM intercept, 1.1 ± 0.17, P<0.0001) with collective mean Ca-P data (LM mean difference ± SE, -0.07 ± 0.02, P<0.005).

Ca-P data were parametric, therefore GLM analyses was completed using gaussian family (identity link). A significant association (^R^2**:** 0.45, $F_{1,18}$:16.6; P<0.0001) was determined for Ca-P data (LM intercept, 9.15 ± 0.77, P<0.0001) with Fe-P data (LM mean difference ± SE, -4.97 ± 1.22, P<0.0001).

No significant associations were determined for labile-P or TOC with any of the variables analysed.

4.3.5.2. Mean collective P-fraction, TOC and ion concentrations model analyses throughout the sediment depths and transect of the reservoir during July 2017

Labile-P data were parametric, therefore GLM analyses were completed with a gaussian family (identity link). A significant association was determined (^R^2**:** 0.72, $F_{1,10}$:26.6; P<0.0005) was determined for Labile-P concentrations (LM intercept, -9.0 ± 4.4, P=0.06) with Mn concentrations (LM mean difference ± SE, 2683 ± 5.48, P<0.0005).

Mn data were parametric therefore analysis was completed using GLM (Gaussian family, inverse link). A significant association was determined (^R^2**:** 0.4, $F_{1,10}$:8.3; P<0.05) for Mn concentrations (LM intercept, 2.69 ± 0.34, P<0.0001) with Fe concentrations (LM mean difference ± SE, -0.03 ± 0.007, P<0.005).

Fe data were parametric therefore analysis was completed using GLM (Gaussian family, identity link). A significant association (^R^2**:** 0.83, $F_{3,8}$:19.6; P<0.0005) was determined for Fe data (LM intercept, 48.16 ± 1.96, P<0.0001) with sampling site 4 (LM mean difference ± SE, -16.56 ± 2.78, P<0.0005) with the inclusion of sites 2 and 3 in the model, with which no significant association was determined individually.

No significant associations were determined for Ca-P, Fe-P or TOC with any of the variables analysed.

4.3.5.3. Mean collective P-fraction, TOC and ion concentrations model analyses throughout the sediment depths and transect of the reservoir during April 2018.

Ca-P data were not normally distributed and was transformed using Tukey's Ladder of Power.

A significant association (^R^2: 0.88, $F_{4,5}$:17.7; P<0.005) was determined for Ca-P data (LM intercept, 1.29 ± 1.03, P>0.05) with sampling site 4 (LM mean difference ± SE, 0.32 ± 1.03, P<0.05) with the inclusion of Fe^+ in the model, with which, Ca-P concentrations had no individual significant association. The mean Fe concentration (36mg/g ± 0.86) skewed the data due to its low mean concentration relative to that at all other sites (48.1mg/g ± 3.96), however, the data did not breach Cook's distance, suggesting the datapoint did not significantly affect the analysis.

Mn data were parametric therefore GLM analyses were completed using the Gaussian family (inverse link). A significant association (^R^2: 0.97, $F_{6,3}$:51.29; P<0.01) was determined for Mn (LM intercept, -4.27 ± 0.73, P>0.01) with Fe (LM mean difference ± SE, 0.08 ± 0.01, P<0.01), TOC (LM mean difference ± SE, 0.06 ± 0.007, P<0.005), Layer (LM mean difference ± SE, 0.14 ± 0.02, P<0.01), Site 1 (LM mean difference ± SE, 0.09 ± 0.03, P=0.07), Site 3 (LM mean difference ± SE, 1.37 ± 0.13, P<0.005) and Site 4 (LM mean difference ± SE, 2.81 ± 0.3, P<0.005).

Fe data were parametric, therefore GLM analyses were completed using Gaussian family (inverse link). A significant association was determined for mean Fe concentrations (^R^2: 0.99, $F_{3,6}$:2.2+04; P<0.0001) with Site 3 (LM intercept, -0.14 ± 0.04, P<0.05) and Site 4 (LM mean difference ± SE, -0.33 ± 0.07, P<0.005).

No significant associations were determined for Fe-P or TOC with any of the variables analysed. Labile-P was excluded from LM analyses due to '0' inflated data.

4.3.5.4. Mean collective P-fraction, TOC and ion concentrations model analyses throughout the sediment depths and length of the reservoir during July 2018.

PCA was used to determine the most suitable variables as independent variables in GLM/LM analyses with sediment data (Table 4.3.5.4.1).

Table 4.3.5.4.1. The dependent sediment variables and their independent water quality variables.

Fe-P	Ca-P	La-P	TOC	Mn	Fe
Fe (mg/g)	Organic C (mg/g)	Fe (mg/g)	Fe (mg/g)	Fe-P (mg/g)	Fe-P (mg/g)

Bottom NO_3^- (mg/g)	Bottom pH	Bottom NO_3^- (mg/g)	Bottom NO_3^- (mg/g)	Bottom NO_3^- (mg/g)	Bottom NO_3^- (mg/g)
Surface Green algae (cells/ml)	Bottom geosmin	Surface Green algae (cells/ml)	Surface Green algae (cells/ml)	Surface Green algae (cells/ml)	Surface Green algae (cells/ml)
Mn (mg/g)	pH	Mn (mg/g)	Mn (mg/g)	Fe (mg/g)	Mn (mg/g)
NO_3^- (mg/g)	Geosmin (ngL^{-1})	NO_3^- (mg/g)	NO_3^- (mg/g)	NO_3^- (mg/g)	NO_3^- (mg/g)
TOC (mg/g)	Bottom TN (mg/g)	TOC (mg/g)	Fe-P (mg/g)	TOC (mg/g)	TOC (mg/g)
La-P (mg/g)	TN (mg/g)	Fe-P (mg/g)	La-P (mg/g)	La-P (mg/g)	La-P (mg/g)
NH_4^+ (mg/g)	Bottom NH4 (mg/g)	NH_4^+ (mg/g)	NH_4^+ (mg/g)	NH_4^+ (mg/g)	NH_4^+ (mg/g)
Bottom Green algae Turbidity (ntu)	Bottom turbidity (ntu)	Bottom Green algae Turbidity (ntu)	Bottom Green algae Turbidity (ntu)	Bottom Green algae Turbidity (ntu)	Bottom Green algae Turbidity (ntu)

Mean Fe-P data were not normally distributed; however, the data could not be transformed to become parametric. Therefore, the data were analysed for significant associations using GLM with Gamma family (identity link). A significant association (^R^2**:** 0.98, $F_{2,5}$:229.7; P<0.0001) was determined for Fe-P (LM intercept, 192.4 ± 25, P<0.0001) with TOC (LM mean difference ± SE, -15.2 ± 4.9, P<0.05) and Labile-P (LM mean difference ± SE, -0.89 ± 0.1, P<0.0001).

Mean TOC was of a parametric distribution, therefore a GLM analyses was completed using Gaussian family (log link). A significant association (^R^2**:** 0.98, $F_{3,4}$:219.6; P<0.0001) was determined for TOC (LM intercept, 2.24 ± 0.26, P<0.005) with Fe-P (LM mean difference ± SE, -0.007 ± 0.002, P<0.05), labile-P (LM mean difference ± SE, -0.01 ± 0.002, P<0.05) with the inclusion of surface green algae counts in the absence of individual significant association with green algae.

No significant associations were determined for Ca-P, Labile-P, Mn or Fe with any of the variables analysed.

4.3.6. Mass balance of TP within Llandegfedd Reservoir during the month of May and August 2018.

Mass balance data for the whole of the reservoir during May and for the month of August are indicated a low influx of P from the sediment (Table 4.3.6.1).

Table 4.3.6.1. Mass balance data calculated for the whole reservoir during May and August, 2018 (P_L^m = average monthly water TP concentration, Pin = external TP point source loading, Pout = output TP load, Sed = sedimentation flux, R = retention coefficient, s = apparent settling rate)

Month	**P_L^m mg l^{-1}**	**Pin kg P $month^{-1}$**	**Pout kg P $month^{-1}$**	**Sed kg P $month^{-1}$**	**R**	**s $month^{-1}$**
May	0.038	0.14	0.13	0.66	4.71	17.3
August	0.018	0.01	0.1	-0.85	-85	-47.2

The data indicated P influxes being introduced to the reservoir through external loading as opposed to internal release from the sediment during both May and August. However, a greater influx of P from the sediment was detected during the month of August relative to that during May.

4.4. Discussion summary

Llandegfedd reservoir demonstrated dynamic P-binding properties through the sediment layers over the sampling period along with changes to sediment composition that may have altered the conditions under which enhanced sediment-P dissolution occurred. Such changes to the sediment were localised and did not occur simultaneously throughout the reservoir, indicating the unpredictability of the conditions under which phosphorous may be retained or released at various locations throughout the reservoir.

Site 4 was at the highest risk of cyanobacterial establishment of all sampling sites due to its proximity to an allochthonous nutrient supply and its shallow characteristics. The shallower depth of water allows maximisation of conditions such as light penetration and sediment disturbance which may exacerbate and fuel cyanobacterial establishment and sediment nutrient release. Therefore, site 4 may pose a higher risk to water quality degradation as a

consequence of climate change relative to all other sampling sites. Internal nutrient loading may lead to eutrophication of Llandegfedd Reservoir

4.4.1. Phosphorous and TOC concentrations

4.4.1.1. Did the data suggest evidence of internal loading?

Fe-P concentrations within the deeper layers of the sediment during April 2018 were lower at site 4 relative to that of all other sites, suggesting a greater degree of historical P dissociation and internal loading, which may have been caused by the influence of factors other than redox conditions for sediment P release (Jensen *et al.,* 1992), such as meteorological/hydrological conditions.

Fe-P: Ca-P ratios at Llandegfedd reservoir shifted over the sampling period of April 2016 to July 2018, with the greatest shift taking place between April 2016 and July 2017. The resulting shift in ratios suggested a change in conditions that may have fuelled internal P-loading throughout the reservoir over the sampling period, with alkaline conditions most likely to have released sediment P during 2018. Huang *et al.,* (2015), determined that more P was released under acidic conditions where the Fe-P: Ca-P ratio is <0.5 within the sediment. Conversely, sediment ratios of Fe-P:Ca-P >0.5 released more P at alkaline conditions (Huang *et al.,* 2015).

The data suggested all sites were oligotrophic by July 2018 with the exception of site 4, where the surface samples recorded a higher concentration of Ca-P relative to that of Fe-P (Huang *et al.,* 2015). Therefore, site 4 was of a eutrophic status during July 2018. Research by Re *et al.,* (2018), assessing the water quality within different lakes concluded that a decrease in P concentrations within overlying bottom water was due to an increase in Ca-P binding which made the P unavailable for biological assimilation and internal loading (Koschel *et al.,* 1983).

Internal loading due to sediment disturbance at site 4 was less likely to induce benthic microbial activity compared with the risks at other sites, where the concentrations of TOC were higher. Li *et al.,* (2019), determined that the sediment of a shallower section of a lake may photo-release sediment-bound nutrients during resuspension. Rydin (2000) determined that high concentrations of organic-C at the sediment surface indicated recent sedimentation processes; therefore, the data indicated a low volume of detritus settled over the 2017-2018 winter period, suggesting a low algal/cyanobacterial abundance during the previous growing

season. Gonsiorczyk *et al.,* (1998), determined that the mobilisation of recently sedimented organic-C drives P release in a eutrophic reservoir.

A significant negative association was determiend for Fe-P concentrations with Ca-P concentrations during April 2016. The data suggested that the Fe-P may have dissociated at sites where Ca-P remained in higher concentrations due to its insensitivity to redox conditions (Kufel *et al.* 2013), and was therefore a period of internal-P loading.

During July 2018, a significant negative association was determined for Fe-P with Labile-P and TOC concentrations, indicating Fe-P was an internal source of P during the summer period of 2018 and anaerobic conditions prevailed at the bottom water which may have led to lower redox conditions and subsequent Fe-P dissolution. However, the mass balance calculations determined low internal loading volumes within the rseervoir during August 2018, albeit raised relative to that during the spring.

The negative association of Fe-P with TOC concentrations suggested active mineralisation of TOC during periods of raised concentrations of Labile-P, indicating the release of Fe-bound P during a period of high benthic microbial activity and P availability to fuel algal and cyanobacterial establishment. Site 4 potentially offered optimum conditions for cyanobacterial development due to its shallow nature leading to increased light penetration and regular sediment mixing, increasing the potential for internal nutrient loading (Nixdorf *et al.,* 1995).

4.4.1.2. Was there evidence for an increased risk of internal loading under changing climatic or hydrologic conditions?

The Fe-P concentrations in the sediment surface throughout the reservoir during July 2017 were significantly greater than those isolated at the surface throughout the reservoir during A significant increase in the potential for internal P loading was identified at each site with the exception of site 4 where Fe-P remained lower. Howell, (2010), determined that low concentrations of phosphorous within sediment was indicative of a large particle size which was in contrast to that of a clay sediment, where the smaller particles were able to retain the phosphorous. Therefore, site 4 was at highest risk of P assimilation due to the increased potential for sediment disturbance as a consequence of wave action, pumped inflow and disturbance during a period of heavy rainfall under conditions of decreased active pumping during a period of drought.

4.4.1.3. Was there evidence of sediment P concentrations affecting water P limitation?

Ca-P concentrations were evenly distrubuted throughout the surface layers of the sediment of the reservoir during July 2017 suggesting an increased potential for permanent P-binding relative to that during April 2016 and that the Ca-binding capacity had been maintained over the previous 12cm sedimentation process, contributing towards the limitation of internal loading.

During April 2018, the surface sediment of site 4 contained the highest concentration of Ca-P, indicating an increased capacity for permanent P-binding relative to that at all other sites and a decreased likelihood of P dissociation to the water. The higher Ca-P concentrations at the surface of site 4 relative to that isolated within layers 1, 2 and 3 indicated a change in Ca concentrations within the reservoir, resulting in a greater P-binding capacity at site 4 during April 2018 than that available during earlier sedimentation periods.

Analysis of the data obtained during April 2016 indicated that all sites, with the exception of site 3, recorded a higher Ca-P concentration than Fe-P concentration at the sediment surface, suggesting eutrophic conditions within the reservoir. However, the sediment surface of sites 1, 2 and 4 recorded higher concentrations of Fe-P than Ca-P during July 2017, indicating a largely oligotrophic reservoir. Gonsiorczyk *et al.,* (1998), determined that the element to which P is bound varies in concentrations through the sediment depth; increased concentrations of Fe-P and Mn-P in oligotrophic reservoirs are typically located at the sediment surface relative to that of the Ca-P concentrations, however the converse applies in eutrophic reservoirs where Ca-P concentrations are higher at the sediment surface than either the Fe-P or Mn-P concentrations.

Significant negative associations were determined during July 2017 for Labile-P with the Mn ion and for the Fe ion with the Mn ion, suggesting that P may have become dissociated from the potentially higher Fe pool relative to the Mn pool within the sediment.

Mass balance analysis determined that very little internal loading occurred during spring 2018, indicating external sources were the predominant P source during spring. However it is likely that low concentrations of O during the summer relative to early spring may be a consequence of assimilation by cyanobacteria and algae. Therefore, it may be difficult to conclude whether P concentrations within the water are a consequence of sediment release or microbial assimilation/ senescence and lysis.

Mass balance analysis also determined a greater quantity of P released from the sediment during late summer relative to that during the spring, indicating a higher risk of primary production and conditions more favourable to sediment P release during the summer period (Søndergaard *et al.,* 2003), supporting the hypothesis that internal P loading was higher during the summer relative to the spring. However, the rate of internal P loading was so low that it is likely that the external loading of P occurred at a higher rate, therefore, the hypothesis stating that internal loading of P will be a significant source of P must be rejected.

4.4.1.4. Was there evidence of spatial patterns in phosphorous and TOC concentrations?

Fe-P concentrations were homogenous through the sediment layers at site 4 during April 2016 relative to that at all other sites indictating a constant rate of P sedimentation and P-binding characteristics of the sediment at site 4 (Howell, 2010). Its location within close proximity to the pumped inflow and its shallow water increased the risk of sediment disturbance; however, the Fe-P concentrations during April 2018 of all other sites were higher at a sediment depth of between 4-6cm suggesting a change in sediment binding properties over the sedimentation process from that indicative of an oligotrophic reservoir (increased Fe-P concentrations retained within layers 4-6cm) to that indicative of a eutrophic reservoir (by the decreased surface Fe-P concentrations) (Carey, 2011).

Ca-P levels were higher throughout the sediment depths in the southern section of the reservoir during April 2016 compared with that of the northern section, with site 1 recording the highest surface concentrations of Ca-P. The data indicated the southern section as containing more permanently bound P than the northern section, reducing the likelihood of internal P loading due to the insensitivity of the Ca-P complex to changing redox conditions (Kufel *et al.,* 2013).

Conversely, during July 2018, the lowest surface Ca-P concentrations were isolated at site 2 with the highest Ca-P concentrations within its bottom sediment layer. Ca-P concentrations increased at site 4 and decreased at site 2 over the sedimentation period, with site 4 being the most likely site to retain P at the sediment surface once bound to Ca.

Labile-P was low within the surface sediment of the southern sites (sites 1 and 2) but increased with sediment depth during April 2016. Labile-P was absent throughout the sediment depth up to 15cm at the northern sites (sites 3 and 4) presenting a decreased risk of etutrophication during April 2016 and indicative of P-disocciation during previous summer

periods. He *et al.,* (2011), determined that shallower sections of a lake where sunlight is able to penetrate to the sediment may result in a decrease in labile-P within the sediment due to UV breaking down phosphate-humic acid complexes. The increasing labile-P concentration with sediment depth at sites 1 and 2 indicated P-dissociation through the sediment depth where anoxic conditions prevailed.

Sediment surface labile-P concentrations during July 2017 were highest in the southern section of the reservoir compared with that of the northern section indicating a lower rate of P dissolution at the deeper sites 1 and 2 compared with 3 and 4. The increased concentrations of labile-P within the surface sediment of sites 1 and 2 may have been in part due to redox mediated P release occurring during a period of stratification, resulting in dissociated P remaining trapped in the benthic zone during the summer and not released until turn over during the autumn (Forsberg, 1989).

Deep layers along the transect of the reservoir recorded very low concentrations of TOC which indicated a low potential for microbial activity as a consequence of sediment disturbance which was unlikely at sites 1 and 3 compared with that at site 4. Søndergaard *et al.,* (2003), determined that Increased water mixing and wave-induced sediment disturbance in shallow sections of a reservoir may increase microbial activity and organic degradation, releasing more nutrients to the water relative to sediments at greater depths and therefore, protected from wind or wave-induced suspension events.

During July 2018, the surface TOC increased from site 1 through site 3, highlighting the dynamics of settlement over the sediment surface. Site 4 recorded the lowest TOC concentrations, suggesting that the organic-C was either carried southerly by the inflow or assimilated at a greater rate relative to that at any other site. Therefore, site 4 did not record the highest concentration of TOC throughout the sampling period as anticipated, nullifying the hypothesis.

The highest concentrations of the Mn and Fe ions and thefeore, P dissociation and transient P-binding capacity during July 2017 were recorded at surface sites 1 and 3, whereas that at sites 2 and 4 were recorded deeper within their respective sediment layers suggesting a greater potential for P-binding to Fe and Mn at sites 1 and 3. Conversely, deeper layers of sediment at sites 2 and 4 held a greater potenatial for P-binding. The change from the oxidised to reduced status (and vice versa) may be directly associated with the oxygen concentration

within the water (Skoog *et al.,* 1996). Therefore, the data indicated sampling sites 1 and 3 having been depleted of oxygen during July 2017, resulting in an icrease of ion concentrations within the sediment following the reduction of the Fe and Mn ions.

During July 2017, the Mn ion concentration was determined to have a significant negative association with Fe ions, TOC concentrations and the sampling sites. The data indicated a decrease in Mn ion concentrations from the southern to the northern sites (sites 1 to 4) suggesting that the redox conditions along the length of the reservoir varied. The northern sites (sites 3 and 4) may have been less likely to bind P using Mn during July 2017 than the southern sites (sites 1 and 2). Consequently, the data hgighlighted the dynamic characteristoics of TOC and P-fraction distribution between sites and seasons.

4.5. Conclusions

The hypothesis stating that the concentration of labile-P will be lowest at the sediment surface could not be accepted throughout the sampling period due to variations in P-fraction concentrations across the sampling sites and through the sediment depths.

Overall, P dissolution was greater within the surface sediment throughout the reservoir, but a potential existed for P dissolution from within the deeper layers of the sediment (Søndergaard *et al*., 2003), which was most likely to occur at site 4 where sediment disturbance was also at an increased risk. Additionally, the northern sites (sites 3 and 4) were less likely to transiently bind P in the sediment than the southern sites due to the lower concentrations of available ions within the sediment and were therefore at a relatively increased risk to water quality deterioration through cyanobacterial establishment. Higher concentrations of labile P and Ca-P in the northern section relative to the southern ection coupled with the ion concentration differences indicated that the sediment at the northern sites contained less metals available for P binding, leading to the labile P and permanently bound Ca-P fractions dominating at the sites.

A conversion from a sediment representative of a eutrophic reservoir to sediment more typical of an oligotrophic reservoir occurred by July 2018 with the exception of site 4 which remained eutrophic and simultaneously recorded the lowest TOC concentrations of all sites, further suggesting site 4 to be at an increased risk of a higher rate of internal loading that may fuel cyanobacterial activity relative to all other sites.

An increase in water temperature due to climate change may increase the mineralisation rate of TOC along with the rate of P-dissolution from anaerobic environments. This in turn may potentially feed the cyanobacterial cycle through the spring and summer periods. Milder winters may also induce an earlier cycle of primary productivity, lengthening the cyanobacterial window of dominance throughout the reservoir. Analysis of the deeper water samples analysed in Chapter 3 indicated warmer temperatures at depth, increasing the risk of water quality degradation as a consequence of increased benthic microbial activity. Consequently, water quality deterioration may occur at Llandegfedd Reservoir as a consequence of climate change, with site 4 being the highest risk of triggering and maintaining poor water quality.

The sediment is a dynamic component of the reservoir with characteristics and environmental conditions frequently changing. The sediment characteristics were not uniform throughout its depth or along the transect of the reservoir but consisted of frequently changing properties. Therefore, ongoing sampling of the sediment at numerous locations within the reservoir may provide an improved understanding of the role site-specific sediment plays in the internal loading of P.

Chapter 5: Analysis of the effect of Extreme Weather Events upon nutrient dynamics within Llandegfedd Reservoir

5.1. Introduction to the chapter.

Extreme weather events describe episodes of extreme weather or conditions unusual to that climate, negatively impacting natural systems or societies, and is defined using some metric to characterise the meteorology or its impacts (Stott *et al.,* 2013). The global air temperature is anticipated to increase by an average of 1.5°C by 2081-2100 relative to the average global temperature between 1981-2000 (IPCC). It is also anticipated that the average annual rainfall will be significantly higher in some regions, significantly lower in other region and some regions unchanged by 2081-2100 relative to that recorded between 1981-2000 (IPCC). As climate change progresses, alteration to the rainfall and temperature patterns lead to uncharacteristic storm events within a given region, which are anticipated to become more frequent (Walter *et al*., 2018). The direct and indirect consequences of climate change upon a reservoir are site dependent and the extreme event taking place (heavy rainfall or heatwave etc.) are region and season dependent (Grimay *et al*., 2009). Therefore, different extreme weather events will affect the reservoir in different ways. This chapter focuses upon the effect of a short period (four days) of heavy rainfall in comparison with active pumping of water following several weeks of drought and high temperatures upon the concentrations of phosphorous, nitrogen, water quality and algal and cyanobacterial establishment at Llandegfedd Reservoir.

Main findings of this chapter:

- Drought conditions recorded the presence of Org-P and high nitrate levels but lower concentrations of ammonium, OP and AHP, resulting in high NO_3^-: NH_4^+ and TN:TP ratios. No cyanobacteria nor green algae were detected.
- The onset of pumping decreased both NO_3^-: NH_4^+ and TN:TP ratios due to a decrease in nitrate. Org-P was also undetected throughout the reservoir but an increase in ammonium, OP and AHP (and therefore TP) concentrations were recorded.
- Geosmin concentrations were predominantly detected at the bottom sites during the drought period and four days following the rain. Geosmin concentrations decreased following activation of pumping but increased following the rain.

5.1.1. The impact of climate change upon internal nutrient release and external loading.

The geomorphology and hydrodynamics of a reservoir in part determine the response of the water quality to climatic events. Water density principally determines the hydrodynamics of a reservoir, which in turn is determined by water temperature and turbidity as a consequence of sediment disturbance (Marti *et al.,* 2011; Rueda *et al.,* 2007).

External loading as a result of increased inflow volumes transport sediment carrying with it particulate nitrogen and phosphorus into reservoirs (Huang *et al.,* 2014b; Atkins et al., 2001), including condensed phosphorus from surrounding agricultural land (Sharpley, 1993). In contrast, drought conditions lead to a reduced volume of water retained within reservoirs as a consequence of minimal or absence of inflow, which concentrates nutrients within the reservoir stored nutrient pools (sediment and water column).

An inflow as a consequence of a period of heavy rainfall during a period of drought can decrease the rate of, or temporarily inhibit, internal nutrient loading within a reservoir. The oxygen mixing with the de-oxygenated bottom layer as a part of the inflow process, temporarily destabilises the water column (Li *et al.,* 2015), and alters bottom redox conditions. However, the degree to which nutrient release is disrupted partly depends upon the depth of the reservoir, bathymetry and water temperature (Li *et al.*, 2015). The heavier density of the colder inflow water compared with the lower density of the warmer surface waters of the reservoir allow the inflow to continue in a downwards trajectory towards the bottom zone of the reservoir (Huang *et al.*, 2014). The increased DO at the bottom layer raises the P-binding capabilities of the sediment (Boström *et al*. 1988), decreasing the rate of internal loading.

During long periods of P-deprivation, cyanobacteria excrete APase to catalyse the degradation of organic phosphate into biologically available inorganic phosphate (Stihl *et al*., 2001), making poly-P a highly variable P-pool which can be released from the sediment (Hupfer *et al.*, 2004), into the water following its release from decaying phytoplankton by alkaline phosphatase activities (Ma *et al.*, 2016). Therefore, poly-P concentrations indicate the proportion of P that may become bioavailable in changing pH and water temperature conditions anticipated as a consequence of climate change.

Oscillating redox conditions are favoured by poly-P- accumulating organisms (Kortstee *et al*. 1994). Micro zones within the sediment containing oxygen or nitrate are niches for poly-P-storing bacteria (Hupfer *et al.*, 2004). Nitrate in the absence of oxygen restricts the release of poly-P because denitrifying bacteria substantially decrease the supply of organic substrates (Kortstee *et al*. 1994), and store poly-P themselves (Barak *et al.,* 2000).

Dissolved oxygen stratification significantly affects the nitrogen cycle (Su *et al.,* 2019). Phytoplankton have a significant influence upon the N-fractions in the epilimnion, with organic-N typically being the most dominant fraction. Release of N from the sediment can contribute up to 85% of hypolimnetic N (Su *et al*., 2019). Disruption to stratified water of a reservoir as a consequence of a heavy rainfall event may alter the N-fraction distribution throughout the water column (Su *et al*., 2019), thereby changing water quality throughout the reservoir.

5.1.2. Hypotheses addressed in this chapter

In this chapter, the overarching hypothesis and sub-hypotheses were tested: Overarching hypothesis: The nutrient content of the water within the reservoir will increase following the reactivation of pumping from the river Usk and increase further following the rainfall event.
Sub-hypotheses:

1. Nitrate will be the dominant N-fraction throughout the reservoir during the drought period, but an increase of ammonium concentrations shall be recorded following a period of heavy rainfall, particularly at site 4.
2. OP concentrations will increase as a consequence of both the active pumping and precipitation event specifically in the northern section (site 4) of the reservoir.
3. Cyanobacterial cell counts will increase in response to an inflow of nutrients.

5.2. Sampling methods and data analysis.

5.2.1. Water sampling methods.

Surface and bottom water samples were collected in triplicate at each site during drought conditions in the absence of inflow (July 9th), during drought conditions following the onset

of active pumping from the river Usk (July 23rd), one day post cessation of 4 days of rainfall (July 31st) and four days post cessation of rainfall event (August 3rd) (Figure 5.2.1.1).
Surface water samples were collected at four sites along the transect of the reservoir and bottom water samples were collected using a Van Dorn depth sampler at between 0.5-1 m from the bottom. An EXO Sonde (handheld model 4P Sonde SN 16J104715, pH probe (SN 16J104328), ODO probe (16J103539), turbidity probe (SN 16J102916), CT probe (SN 16J104738), depth (SN 16J102280)) was used at each location to predetermine the depth. Samples were returned to the laboratory for P analysis (Cardiff University) and other nutrient analysis (DCWW).

Water samples collected on the 31st July were solely analysed for P fractions due to the unavailability of DCWW laboratory for completion of further analysis.
The reservoir level decreased in depth from 25m to 23.5m at the tower between the 9th July and the 3rd August 2018. No active abstraction from the river Usk to the reservoir had taken place for a minimum of 1 month previous to, during or following the onset of heavy rainfall (27th July 2018). An average of 8.4mm of rain was recorded during the month of June, but 46mm fell during the wet period at the end of July (27th through 30th). The weather data was collated from a station based in Cardiff and supplied by the Met office (https://www.metoffice.gov.uk/pub/data/weather/uk/climate/stationdata/cardiffdata.txt).

5.2.1.1. Nutrient and environmental analysis.

Water samples were analysed at DCWW laboratories for nutrients using the Thermo Scientific Aquakem 600. To prepare the ammonia/nitrite standard stocks, the specific concentration of solution (e.g., 1ml of ammonia as N 1000mg/L and 1ml of nitrite as N 1000mg/L) was pipetted into a flask containing RO water. The flasks were inverted several times and the solution is transferred to a 100ml plastic bottle. Ammonia, phosphate, TON and nitrate stocks were prepared before hand by the supplier. A serial dilution of stocks was prepared using the solution. All samples were recorded on the DCWW LIMS system. The samples and stocks were loaded into the respective instrument following the calibration guidelines issued by the manufacturers. Dŵr Cymru Welsh Water nutrient analysis methods are presented in Appendix 1 (A1).

5.2.1.2. P-fraction analysis

The P data (TP, OP, AHP and organic-P) were obtained through following the same methods as those stated in Chapter 3. OP concentration was determined using the ascorbic acid method (APHA, 1995), TP was analysed using persulphate digestion (APHA, 1995) and AHP concentration was determined after hydrolysis with sulphuric and nitric acids.

Organic phosphorus (Org-P) concentration was determined by difference by deducting the OP and AHP concentrations from the TP concentration. Data are presented in Appendix 5 (A5).

5.2.2. Statistical analyses

For data analyses throughout the chapter, the mean value for each parameter per month was determined for each variable accompanied by the standard deviation (SD). The Wilcoxon-signed rank test was used to determine whether any significant differences existed between two variables. Due to small sample sizes ($n<25$) and not normally distributed data exhibiting ties, Kendall's Tau was used to test for associations between two continuous variables and Kruskal-Wallis test to determine significant differences between sets of not normally distributed data. Where data was not normally distributed, but sample size was large ($n>25$) Spearman's rank correlation was used.

Significant associations between variables were determined using General Linear Models (normally distributed data)/Generalised Linear Models (non-normally distributed data even following transformation methods)/Linear Models (where non-normal data were successfully transformed) were completed using R studio (version 3.4.4) following the selection of independent variables demonstrating correlation with the dependent variable as determined through Principal Components Analysis (PCA) analysis using PAST (version 4.03).

Data were standardised to allow cross-variable PCA (Table 5.2.2.1). Variables were omitted from the PCA during periods of recorded repeated '0' values. The following equation was used for the standardisation to allow for direct data pattern comparisons between variables of differing scales:

$$(X-\mu)/\sigma$$

where X is the observation, μ is the mean and σ is the standard deviation.

Once the list of correlated variables had been determined for each dependent variable, the Shapiro-Wilks test was used to determine normality of data. Data were transformed by log, cube, square-root or Tukey's Ladder of Power where not normally distributed distributions were confirmed. The most suitable transformation method was determined through analysis of histograms and their proximity to a normal distribution using Shapiro-Wilks. Where the most efficient method of data transformation involved Tukey's ladder of power, the selected transformation mode was not indicated. Tukey's ladder of power reduces the effects of homoscedastic data leading to more accurate analysis. The Akaike Information Criterion (AIC) was used to estimate the fit of each model, with the lowest AIC value used to confirm the selection of data transformation links and models (Bozdogan, 1987; Cavanaugh, 2019).
Variables were eliminated from the model as determined by the F-test. Following removal of all unnecessary independent variables, the goodness of fit of the remaining model was tested using diagnostic plots for linear regression analysis to determine whether residuals had a non-linear pattern (Residuals vs Fitted graph), were of a normal distribution (Normal Q-Q graph), heteroscedasticity (scale location graph) and influential outliers (Residual vs Leverage plots (Cook's distance)). Following completion of the model, the data were reported using the intercept result and P value, adjusted R^2 (^R^2), F-test for overall model significance (Mangiafico, 2016), and model P value. Any anomalies from the diagnostic plots were reported for the final model. Furthermore, the positive/negative association of the individual parameter associations within the model with the dependent variable were reported using LM mean difference ± SE.

Table 5.2.2.1. Variables used in PCA to determine suitability for GLM/LM analyses with P fractions.

Geosmin (ngL^{-1})	Chlorophyll a (ugL^{-1})
pH	Turbidity (ntu)
NH_4^- (mgL^{-1})	NO_3^- (mgL^{-1})
Green Algae (cells/ml)	Rainfall (mm)
TN (mgL^{-1})	*Oscillatoria* (cfu/ml)
Aphanizomenon (cfu/ml)	Temperature °C

Heat maps were used to illustrate the concentration variations of TP, AHP, OP ad Organic-P across the transect of the reservoir. Variable concentration density graphs are used to illustrate the density of concentrations throughout the chapter. Higher concentrations are represented by darker shades of colour, where no colour represents no P nor its fractions present, or P present below the LOD. References made to 'northern sites' represent site 3 and 4, whereas reference made to the 'southern sites' represent sites 1 and 2.

5.3. Results.

5.3.1. Analysis of P-fraction data obtained before, during and after the rainfall event.

5.3.1.1.1. Orthophosphate (OP) (mgL^{-1}) site concentrations over the course of the EWE.

OP declined to concentrations of =<0.002mgL^{-1} (± 0.002) during the drought period (9th July), with the exception of site B1 which recorded the highest OP concentration (0.007mgL^{-1}). At site B3 OP was below the Limit of Detection (LoD) throughout this period (Table 5.3.1.1.1.1). Higher OP concentrations (0.003 mgL^{-1} ± 0.002) were observed at the southern section (sampling sites 3 and 4 near to pumped inflow) of the reservoir relative to that in the northern section (0.001 mgL^{-1} ± 0.0007).

During the onset of active pumping into the reservoir (23rd July), the concentrations of OP increased at all sites (0.01 mgL^{-1} ± .003), with site 4 recording the greatest increase (by 0.11 mgL^{-1} at the surface and by 0.015mgL^{-1} at the bottom zone). Site T1 recorded the least increase in OP concentration (0.003) since July 9th and the lowest concentration of all sites on July 23rd (0.004 mgL^{-1}) (Figure 5.3.1.1.1.1) of all sites. The northern sites (sites 3 and 4) recorded the higher concentrations of OP (0.013 mgL^{-1} ± 0.002) following the onset of pumping compared with the southern half of the reservoir (0.008 mgL^{-1} ± 0.003), however, the difference was insignificant.

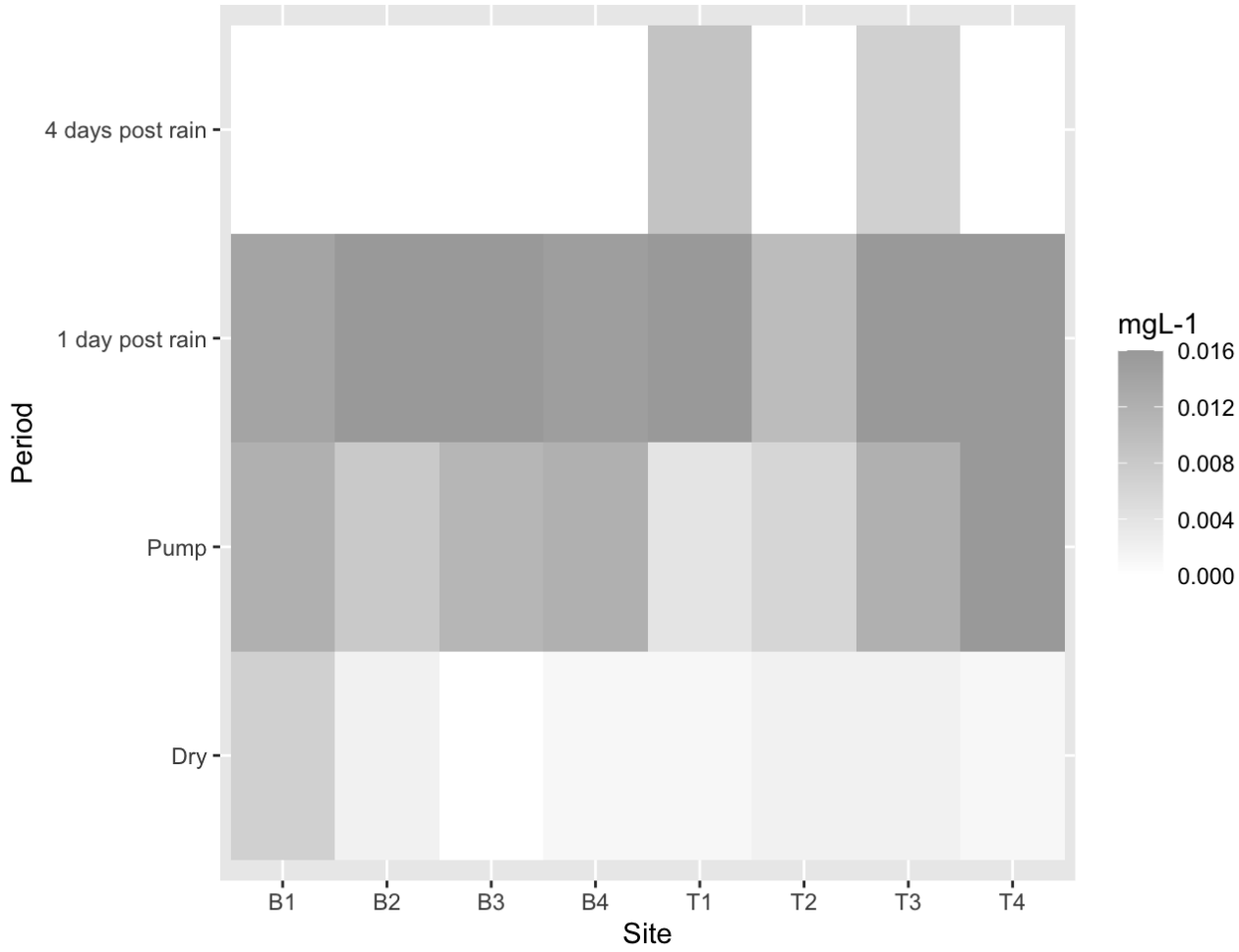

Figure 5.3.1.1.1.1. OP concentrations over the drought and EWE sampling period. Key: B=Bottom; T=Top, 1, 2, 3, 4 = site reference. Dry= during drought period with no inflow; Pump = during drought period and active pumping of water into reservoir; 1-day post rain= 4 days of rain event ceased and pumping ongoing; 4 days post rain= 4 days following cessation of rain event and pumping ongoing.

The highest concentrations of OP recorded over the sampling period (0.015 mgL^{-1} ± 0.002) occurred across the reservoir one day following cessation of the EWE (July 31st), where an increase in concentration in OP of between 20% (site B4) and 75% (Site T1) was recorded (0.015 mgL^{-1} ± 0.001 throughout the reservoir) relative to drought concentrations, but no change to OP concentrations were recorded at site T4 (0.016 mgL^{-1}). The highest concentrations of OP were detected at the northern sites (0.016 ± 0) compared with sites 1 & 2 at the southern section of the reservoir (0.014 ± 0), however, the difference was insignificant.

The concentrations of OP became undetectable 4 days post cessation of heavy rainfall (August 31st) at all sites with the exception of sites T1 (0.001 mgL^{-1} ± 0) and T3 (0.007 mgL^{-1} ± 0.008),

highlighting the rapid depletion of OP following the rain event and the absence or change in the conditions of the OP source. The Mean concentration of OP within the reservoir during the dry period (0.002 mgL^{-1} ± 0.002) was significantly lower than OP detected following the onset of pumping during the dry period (0.01 mgL^{-1} ± 0.003) (W=2, df=15, P<0.005), which were significantly higher that OP concentrations four days post rainfall (0.001 mgL^{-1} ± 0.002) (W=2, df=15, P<0.005).

5.3.1.2.1. Acid hydrolysable phosphate (AHP) (mgL^{-1}) site concentrations over the course of the EWE.

AHP concentrations were low (=<0.01 mgL^{-1}) throughout the reservoir during the drought period (0.003 mgL^{-1} ± 0.003), with the highest concentration isolated at site T4 (0.01 mgL^{-1} ± 0.01) and undetected at sites T1 and T3. AHP concentrations were insignificant higher in the northern half of the reservoir (0.003 mgL^{-1} ± 0.004) than in the southern half (0.002 mgL^{-1} ± 0.001) during the drought.

AHP concentrations increased after the onset of active pumping (0.011 mgL^{-1} ± 0.005) by between 9% (site T4) to 100% (sites T1 and T3) compared with that during the drought period. The southern half of the reservoir recorded higher concentrations (0.015 mgL^{-1} ± 0.003) of AHP compared with that of the northern half (0.007 mgL^{-1} ± 0.002) following active pumping during the dry period. AHP concentrations increased further throughout the reservoir (0.023 mgL^{-1} ± .004) following the cessation of rainfall (July 31st) by between 16% (site B1) and 78% (site B4), with the southern sites retaining a higher concentration of AHP (0.026 ± 0.002) relative to the northern sites (3 & 4) (0.02 mgL^{-1} ± 0.002), however, the difference was insignificant (Figure 5.3.1.2.1.1).

Four days following the cessation of rainfall, AHP concentrations decreased at each site (0.008 mgL^{-1} ± 0.015) by between 81% (site B2) and 50% (site B3), with site 2 recording the greatest decrease in concentrations (combined surface and bottom concentrations by 78%). The northern section recorded a higher concentration of AHP (0.009 mgL^{-1} ± 0.0005) than the southern half of the reservoir (0.008 mgL^{-1} ± 0.001) four days following cessation of the rainfall, however, the difference was insignificant.

Despite lower concentrations across the reservoir 4 days post cessation of rainfall, AHP concentrations remained higher than those recorded during the drought conditions at every site with the exception of site T4, where the concentration was 9% lower (0.009 mgL^{-1} four

days post rainfall, 0.01 mgL^{-1} during drought conditions).

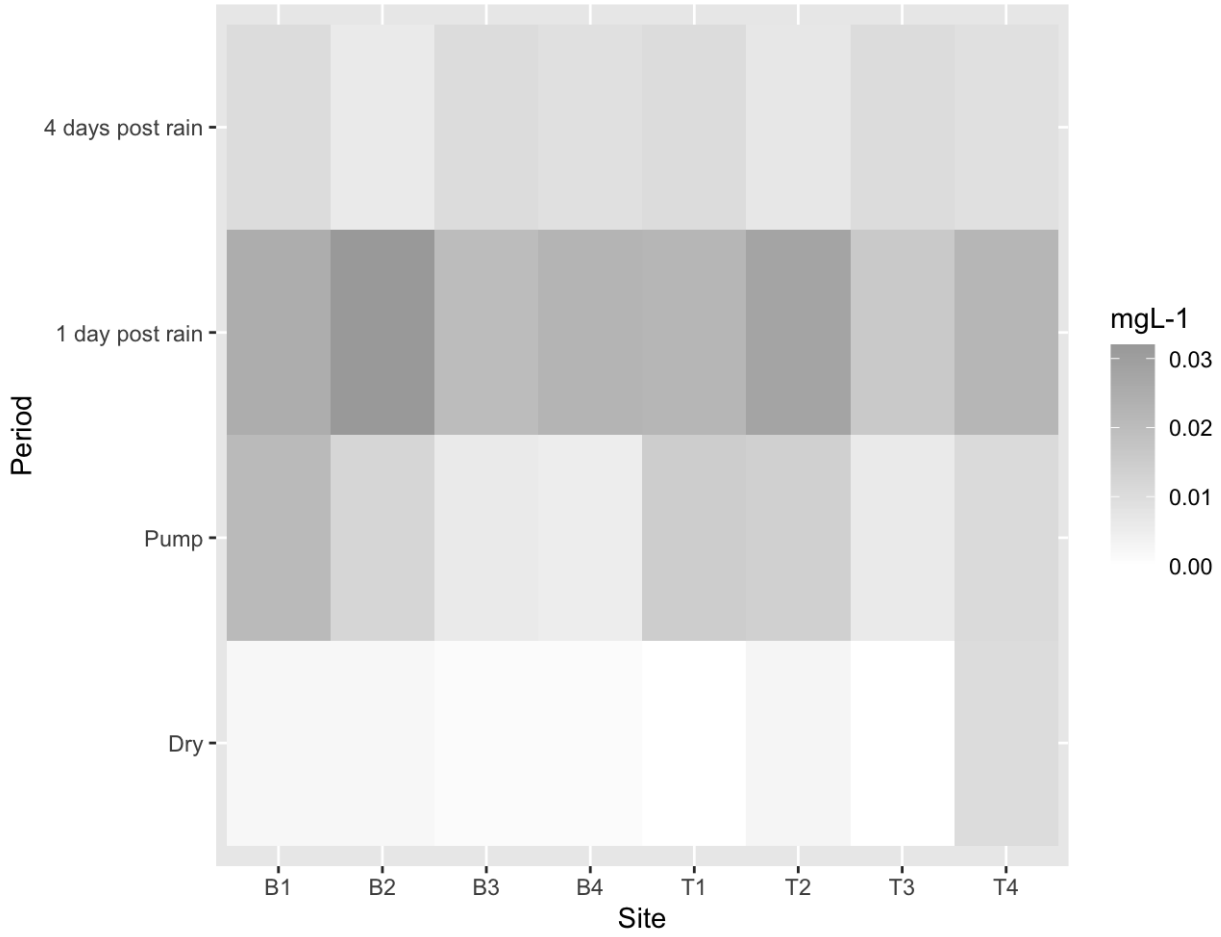

Figure 5.3.1.2.1.1. AHP concentrations over the drought and EWE sampling period. Key: B=Bottom; T=Top, 1, 2, 3, 4 = site reference. Dry= during drought period with no inflow; Pump = during drought period and active pumping of water into reservoir; 1-day post rain= 4 days of rain event ceased and pumping ongoing; 4 days post rain= 4 days following cessation of rain event and pumping ongoing.

Mean AHP concentrations throughout the reservoir during the dry period (0.002 mgL^{-1} ± 0.003) were significantly (88%) lower (W=3, df=15, P<0.001) than that following the initiation of pumping (0.011 mgL^{-1} ± 0.005). However, the AHP concentrations 4 days following cessation of the rainfall event were not significantly different to those following reactivation of pumping (W=23, df=15, P>0.05).

5.3.1.3.1. Organic-P concentrations (mgL^{-1}) over the course of the EWE.

During drought conditions (July 9th), Org-P was detected throughout the reservoir at low concentrations (=<0.009 mgL^{-1}) with exception to sites B4 and B2. The highest concentration of Org-P was isolated in the southern section (sites 1 and 2) of the reservoir (0.003 mgL^{-1} ±

0.003) relative to the northern section (sites 3 and 4) of the reservoir (0.002 mgL^{-1} ± 0.002). The highest concentrations of Org-P were isolated at sites T1 and B3 (0.009 mgL^{-1} and 0.007 mgL^{-1} respectively). However, Org-P became undetected at every site during the onset of active pumping (July 23rd).

Organic P remained undetected at all sites one day post cessation of EWE (Figure 5.3.1.3.1.1) but concentrations increased 4 days post EWE at sites B2 (0.003 mgL^{-1}) and T2 (0.002 mgL^{-1}).

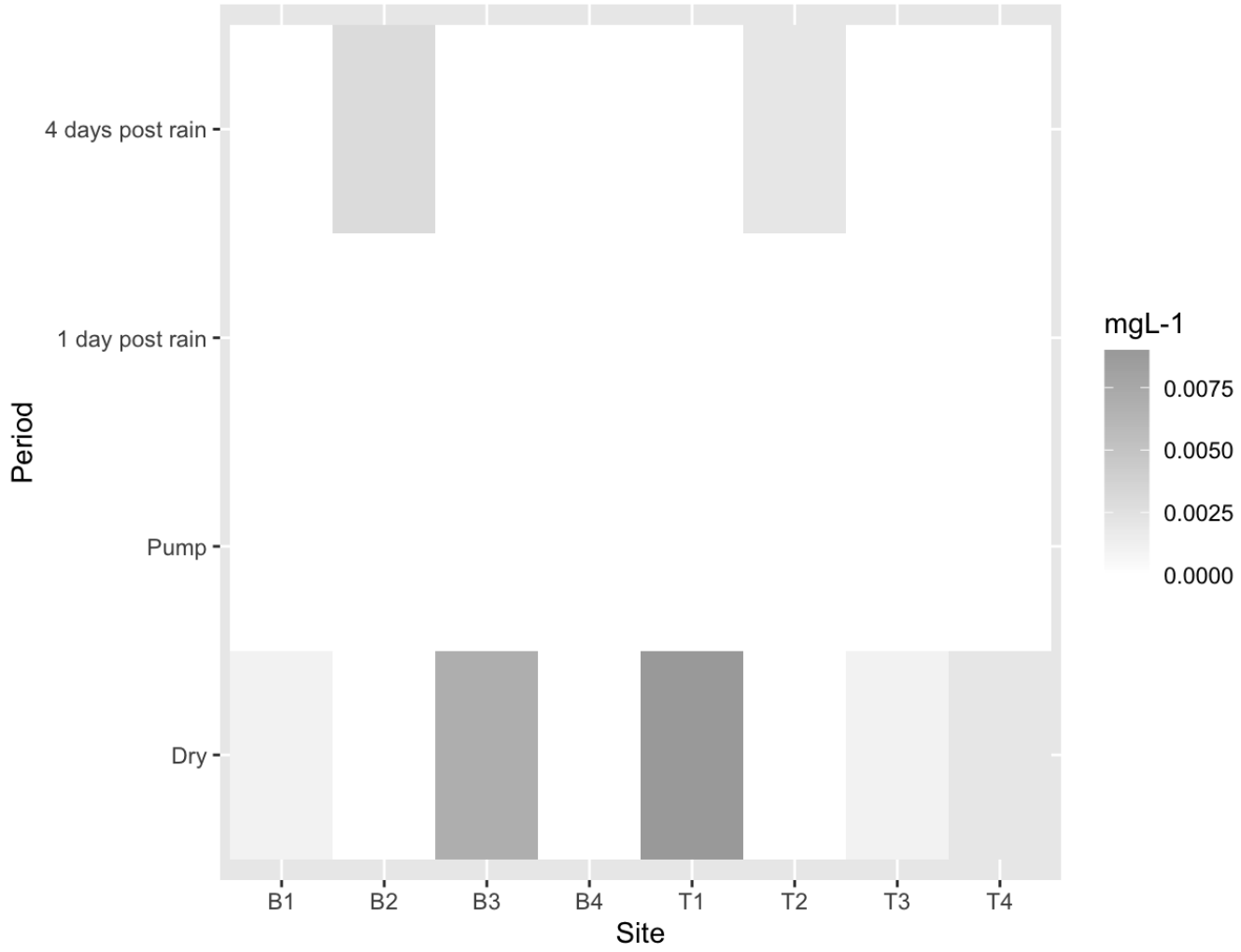

Figure 5.3.1.3.1.1. Org-P concentrations over the drought and EWE sampling period. Key: B=Bottom; T=Top, 1, 2, 3, 4 = site reference. Dry= during drought period with no inflow; Pump = during drought period and active pumping of water into reservoir; 1-day post rain= 4 days of rain event ceased and pumping ongoing; 4 days post rain= 4 days following cessation of rain event and pumping ongoing.

5.3.1.4.1. Total P (mgL^{-1}) concentrations over the course of the EWE.

TP varied throughout the EWE sampling event indicating the positive influence of inflow upon the P concentrations. TP was at its lowest during the drought period (0.007 mgL^{-1} ± 0.003) at

all sampling sites with the exception of site T4 (0.013 mgL^{-1}).

A significant difference was determined for TP concentrations between sampling sites (W:0; df, 15; P<0.005) following the onset of pumping compared with that during the drought period (absence of inflow), with the highest TP concentrations isolated at site T4 and the lowest at B4 (Figure 5.3.1.4.1.1) following the onset of active pumping. The southern half of the reservoir retained a higher concentration of TP (0.02 mgL^{-1} ± 0.005) compared with that of the northern half (0.019 mgL^{-1} ± 0.003), however, the difference was insignificant.

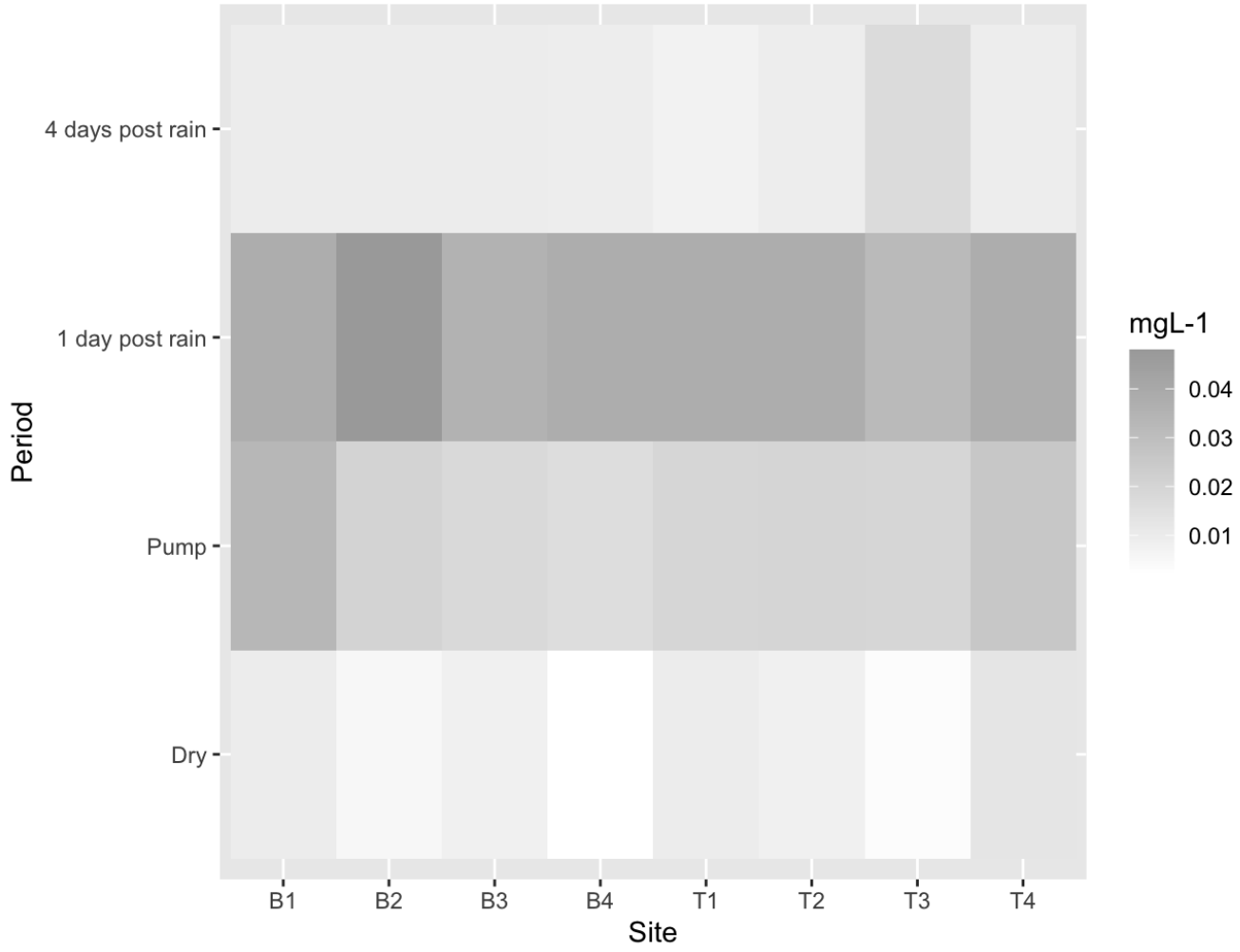

Figure 5.3.1.4.1.1. TP concentrations over the drought and EWE sampling period. Key: B=Bottom; T=Top, 1, 2, 3, 4 = site reference. Dry= during drought period with no inflow; Pump = during drought period and active pumping of water into reservoir; 1-day post rain= 4 days of rain event ceased and pumping ongoing; 4 days post rain= 4 days following cessation of rain event and pumping ongoing.

The greatest TP concentrations were recorded across the reservoir one day post cessation of the rainfall event (0.038mgL^{-1} ± SD 0.004), with the highest concentrations recorded at site

B2 (0.048 mgL^{-1}), indicating that a rainfall event introduced additional P into the reservoir to the active pumping from the river Usk. The southern section of the reservoir maintained a higher TP concentration (0.04 mgL^{-1} ± 0.004) than that of the northern section of the reservoir (0.036mgL^{-1} ± 0.002) one day following cessation of the rainfall event, however, the difference was insignificant (P>0.05).

Four days post cessation of rainfall event, the TP concentrations fell throughout the reservoir (0.01mgL^{-1} ± 0.002), with the highest concentrations recorded at site T3 (0.017mgL^{-1}) and the lowest (0.009mgL^{-1}) at surface and bottom site 4. The southern half of the reservoir a lower TP concentration (0.009mgL^{-1} ± 0.001) relative to that of the northern half (0.01mgL^{-1} ± 0.003), though the difference was insignificant.

5.3.1.5.1. Potentially bioavailable P (Con-P) concentrations over the course of the EWE.

AHP data revealed that condensed P concentrations increased over the sampling period at all sites indicating to a rise the contribution of potentially bioavailable P from drought conditions (undetected at B1 and B2, 12% of TP at T3) to 4 days post rain during active pumping (60%-100% of TP at all sites) (Table 5.3.1.5.1.1).

Condensed-P diminished or remained undetected at all surface and bottom sites in the norther section (sites 3 &4) at the onset of pumping whilst simultaneously increasing at all southern sites.

Table 5.3.1.5.1.1. Condensed-P (Con-P), concentrations (mean mgL^{-1} and as % of TP) in surface and bottom water samples at sites along the reservoir during the dry, active pumping, active pumping with rain, and active pumping no rain events of summer 2018.

Con P	Site	No pumping, no rain (9th July)	Active pumping, no rain (23rd July)	Active pumping and 1-day post rain (31st July)	Active pumping, 4 days post rain (3rd August)
mgL^{-1}	T1	0	0.011	0.006	0.009
	B1	0	0.009	0.011	0.01
	T2	0.001	0.008	0.018	0.007
	B2	0	0.004	0.016	0.006
	T3	0	0	0	0.003
	B3	0.001	0	0.004	0.01
	T4	0.009	0	0.006	0.009
	B4	0	0	0.008	0.009
As % of TP	T1	0	57.89	15.79	86.5

B1	0	27.27	28.95	100
T2	12.5	40	47.37	77.78
B2	0	19.05	33.33	60
T3	0	0	0	17.65
B3	12.5	0	11.11	100
T4	69.23	0	15.79	100
B4	0	0	21.05	100

One day post cessation of rainfall (31st July), Con-P concentrations increased at all sites with the exception of T1 (decreased by 73%) and remained undetected at site T3. However, four days post cessation of rainfall and during active pumping, the biggest increase in condensed P concentrations at each site throughout the reservoir was recorded, with condensed-P representing all potentially bioavailable P at site 4, B1 and B3, and between 60% and 86% at all other sites with the exception of site T3, where only 17.65% of TP was recorded as condensed-P.

5.3.1.6.1. Cross site analyses of P-fraction concentrations over the course of the EWE.

The most dominant P fraction during the drought conditions was that of organic P which constituted 38% of all P fractions, with AHP and OP constituting 32% and 26% respectively (Figure 5.3.1.6.1.1).

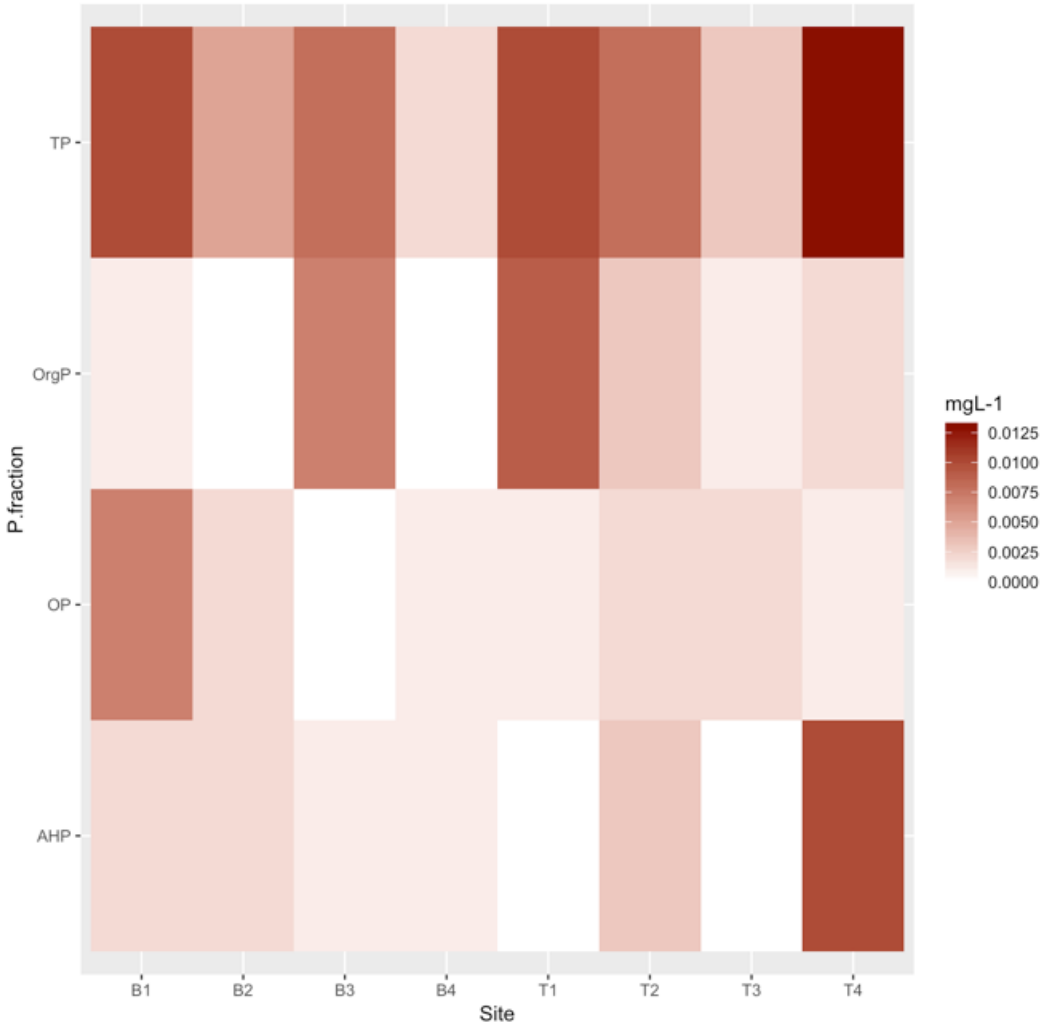

Figure 5.3.1.6.1.1. Drought period July 9th. Key: B=Bottom; T=Top, 1, 2, 3, 4 = site reference.

However, upon the onset of active pumping into the reservoir from the river Usk, AHP concentrations increased to constitute 78% of all P fractions, of which 21% was as OP (Figure 5.3.1.6.1.2). Organic-P was below the LoD in the sampled sites on July 23rd.

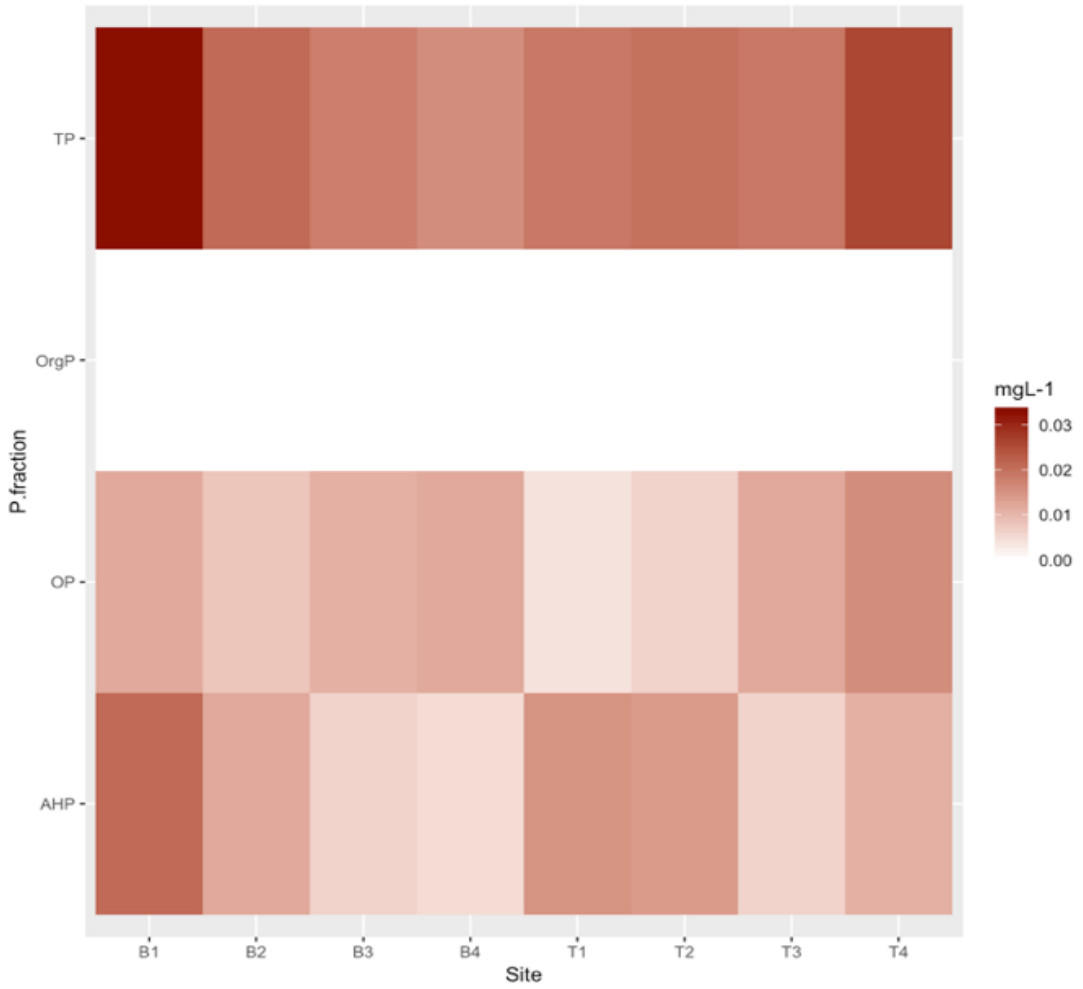

Figure 5.3.1.6.1.2. At onset of active pumping July 23rd. Key: B=Bottom; T=Top, 1, 2, 3, 4 = site reference.

One day post cessation of EWE (July 31st), AHP remained the most common P fraction throughout the reservoir (61%), of which 39% was OP. Organic P remained undetected at any site (Figure 5.3.1.6.1.3).

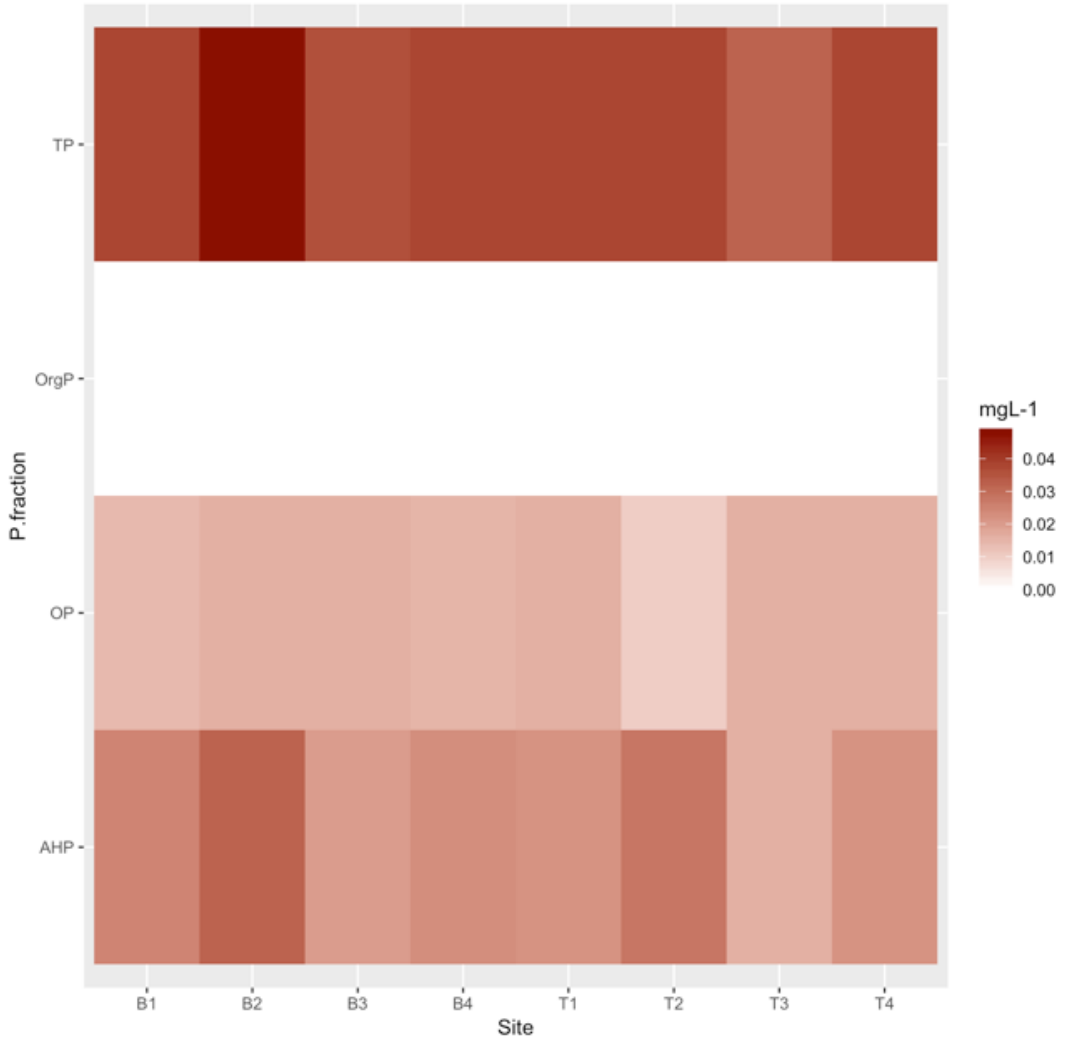

Figure 5.3.1.6.1.3. 1-day post rainfall event July 31st. Key: B=Bottom; T=Top, 1, 2, 3, 4 = site reference.

However, four days following cessation of the rainfall event (Figure 5.3.1.6.1.4)., organic P was detected at site 2 (surface and bottom) whilst OP was undetected at all sites with the exception of sites T1 and T3, where low concentrations (0.001mgL^{-1} and 0.007mgL^{-1} respectively) were isolated. The greatest fraction of TP was of AHP (71%), with only low concentrations of OP and organic-P detected (8% and 6% respectively), indicating to the dominance of potentially bioavailable condensed P throughout the reservoir.

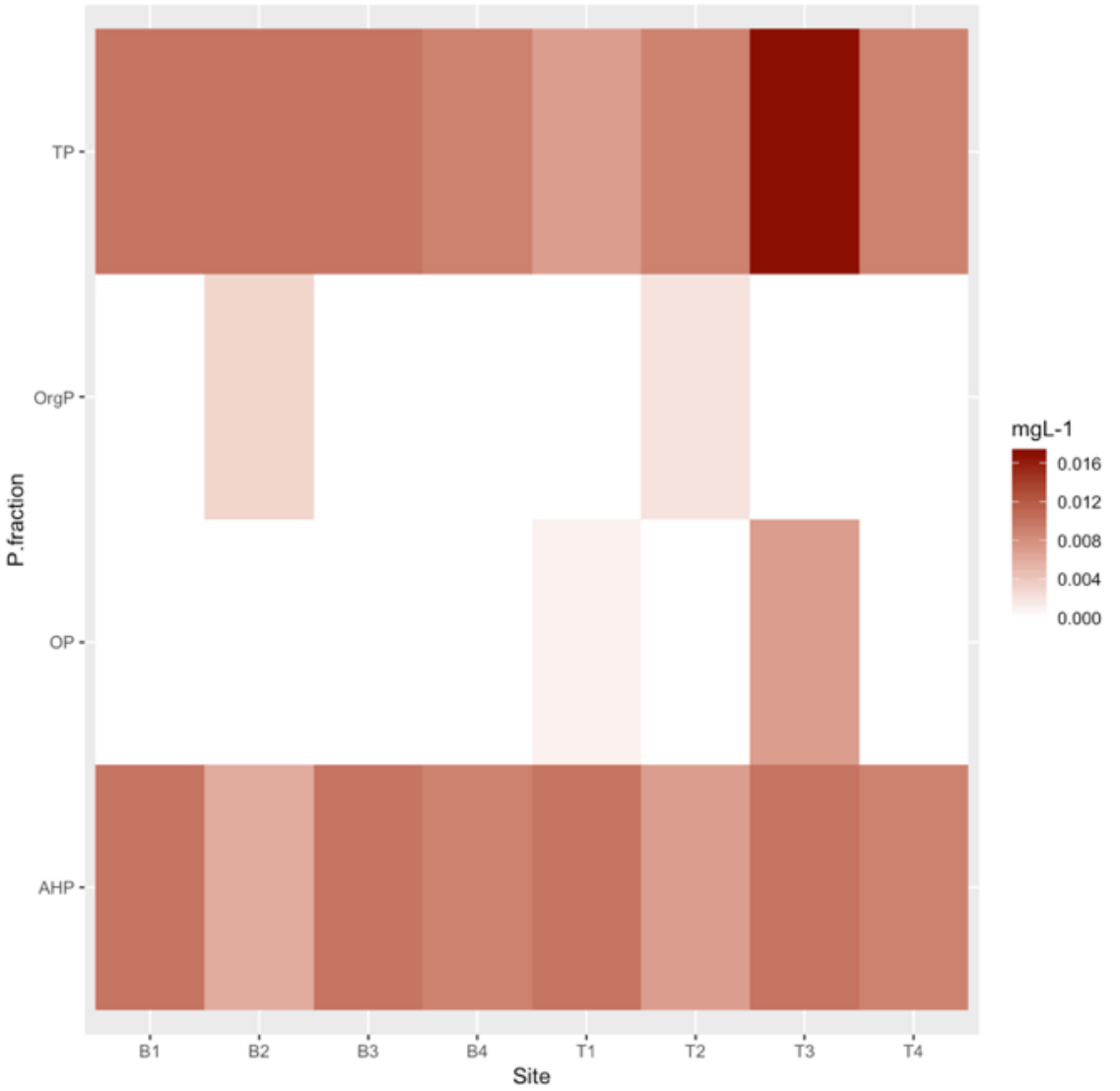

Figure 5.3.1.6.1.4. Four days post rainfall event August 3rd (bottom right). Key: B=Bottom; T=Top, 1, 2, 3, 4 = site reference.

However, four days following cessation of the rainfall event, organic P was detected at site 2 (surface and bottom) whilst OP was undetected at all sites with the exception of sites T1 and T3, where low concentrations (0.001mgL^{-1} and 0.007mgL^{-1} respectively) were isolated. The greatest fraction of TP was of AHP (71%), with only low concentrations of OP and organic-P detected (8% and 6% respectively), indicating to the dominance of potentially bioavailable condensed P throughout the reservoir.

5.3.1.7. Oxidised and Reduced N data analysis over the course of the EWE.

5.3.1.7.1.1. Oxidised N data analysis.

The concentrations of NO_3^- varied throughout the reservoir over the sampling period, with

the highest concentrations isolated during the drought period.

Nitrate was uniformly distributed along the reservoir surface and bottom region, with the bottom regions attaining higher nitrate concentrations (0.98 mgL^{-1} ± 0.012) relative to that at the surface (0.95 mgL^{-1} ± 0.008).

NO_3^- concentrations decreased by a mean of 23% throughout the reservoir following the initiation of active pumping (from a mean of 0.97mgL^{-1} to 0.75mgL^{-1}) in the absence of rainfall compared with concentrations during the drought period, but the concentrations were evenly distributed between surface and bottom samples (0.75mgL^{-1} ± 0.07). Similarly, the distribution of nitrate along the transect of the reservoir remained insignificantly different between the southern sites (0.76mgL^{-1} ± 0.07) and the northern sites (0.74mgL^{-1} ± 0.068).

A further decrease in nitrate concentrations occurred throughout the reservoir by a mean of 23% four days following the cessation of the precipitation event (August 3rd) (Figure 5.3.1.7.1.1.1) predominantly from the surface sites (0.5mgL^{-1} ± 0.012) compared with that of the bottom sites (0.65mgL^{-1} ± 0.08). However, the northern half (sites 3 and 4) of the reservoir recorded a higher concentration of nitrate following the rainfall (0.615 mgL^{-1} ± 0.1) relative to the northern half (0.54 mgL^{-1} ± 0.06). However, the difference was not significant.

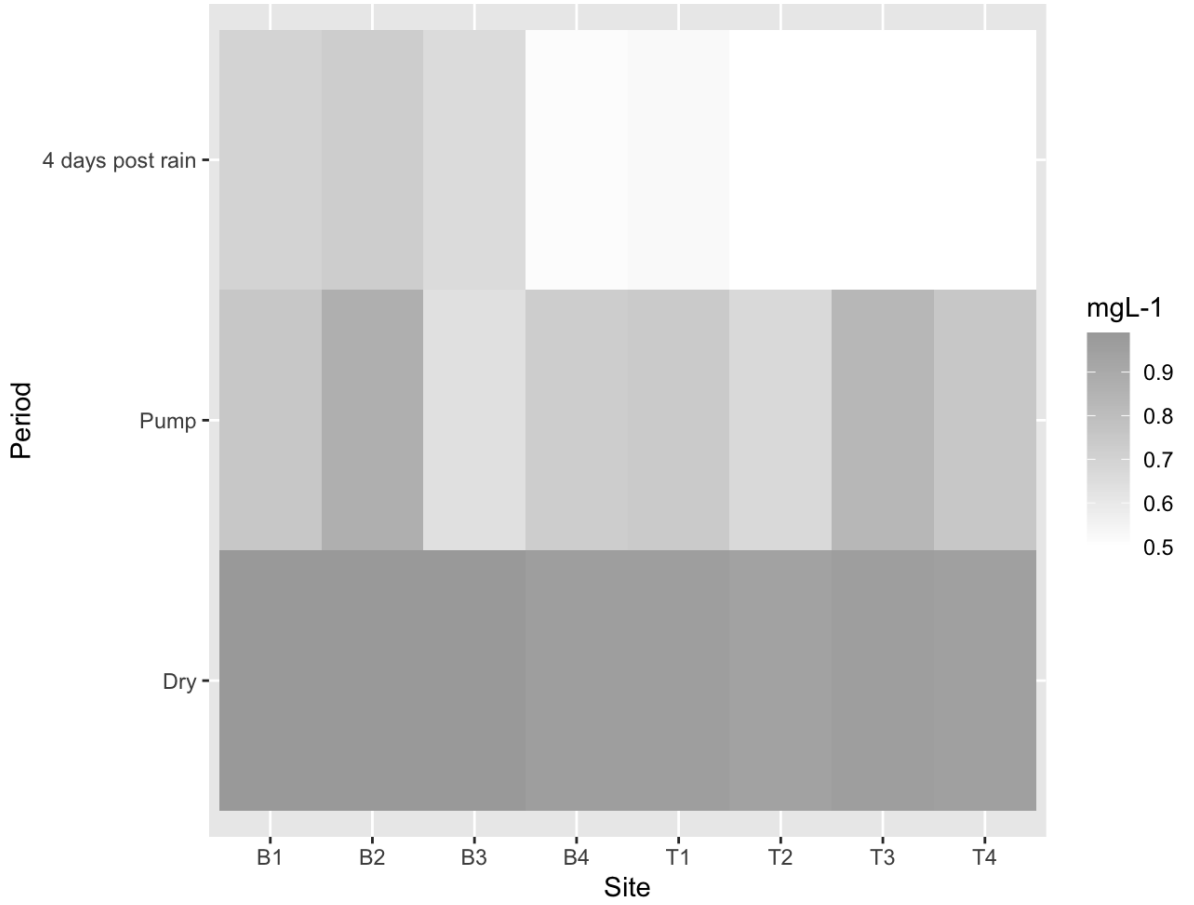

5.3.1.7.1.1.1. NO_3^- concentrations during the dry period (9th July), during pumping only (23rd July) and 4 days following the precipitation event (3rd August) (mgL^{-1}). Key: B=Bottom; T=Top, 1, 2, 3, 4 = site reference. Dry= during drought period with no inflow; Pump = during drought period and active pumping of water into reservoir; 4 days post rain= 4 days following cessation of rain event and pumping ongoing.

The bottom regions retained the majority of the nitrate four days following the rain event, with concentrations being on average 22% higher in the bottom region than at the surface.

5.3.1.7.2.1. Reduced N over the course of the EWE.

The concentrations of NH_4^+ varied throughout the reservoir over the sampling period, indicating an influence of inflow upon ammonium within the reservoir. Higher concentrations of ammonium were recorded at the surface sites ($0.019mgL^{-1} \pm 0.001$) relative to the bottom sites ($0.013mgL^{-1} \pm 0.004$) during the drought period, with the highest concentrations recorded in the northern half of the reservoir ($0.018mgL^{-1} \pm 0.001$) compared with that of the southern half ($0.014mgL^{-1} \pm 0.005$).

The highest concentration of ammonium (0.021mgL^{-1}) was recorded at site T2 during the drought (Figure 5.3.1.7.2.1.1), where the highest concentration of ammonium was retained over the course of EWE sampling.

A mean NH_4^+ concentration increase of 60% was recorded throughout the reservoir following the initiation of pumping (from a mean of 0.017mgL^{-1} (± 0.004) during drought to 0.042mgL^{-1} (± 0.027) following the onset of active pumping).

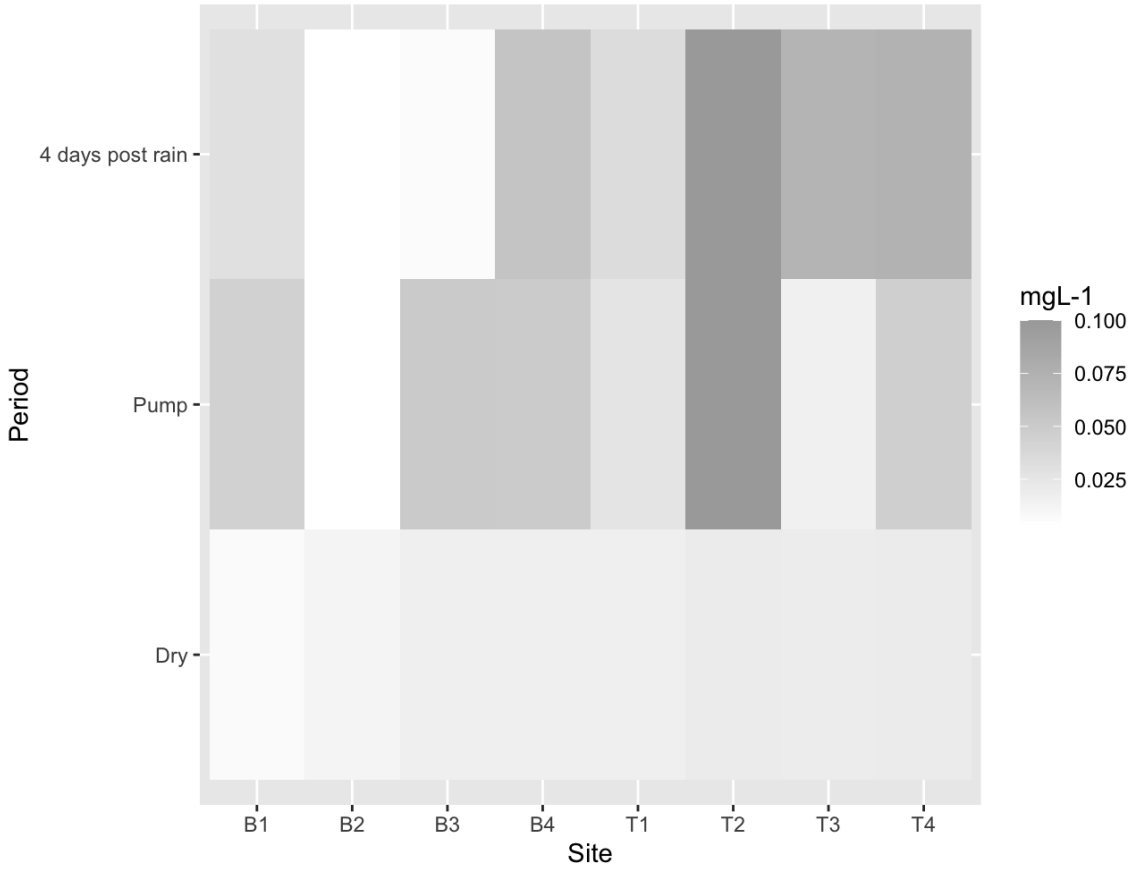

5.3.1.7.2.1.1. Ammonium concentrations during the dry period (9th July), during active pumping only (23rd July) and 4 days following the precipitation event during active pumping (3rd August) (mgL^{-1}). Key: B=Bottom; T=Top, 1, 2, 3, 4 = site reference. Dry= during drought period with no inflow; Pump = during drought period and active pumping of water into reservoir; 4 days post rain= 4 days following cessation of rain event and pumping ongoing.

The introduction of water into the reservoir through active pumping raised the ammonium concentrations by between 84% (B1) and 37% (T1) at each sampling site with the exception of sites B2 and T3, where a decrease was recorded (77% and 16% respectively). An insignificant difference in ammonium concentration distribution was recorded vertically

(surface sites 0.04 mgL^{-1} ± 0.03; bottom sites 0.037mgL^{-1} ± 0.019) or along the transect of the reservoir (southern sites 0.043mgL^{-1} ± 0.03; northern sites 0.04mgL^{-1} ± .014), indicating to an even distribution throughout the reservoir.

The concentrations of ammonium increased further by an average of 11% four days following the cessation of rainfall (to 0.047mgL^{-1} ± 0.032) across all sites 4 days post cessation of rainfall with the exception of sites B1, B2 and B3, where a decrease of 88% was observed at site B3 (to 0.006mgL^{-1}), site B2 concentrations remained unchanged (0.003mgL^{-1}) and by 30% at site B1 (to 0.031mgL^{-1}). The surface sites recorded a significantly higher ($P<0.05$) concentration of ammonium (0.07mgL^{-1} ± 0.02) compared to that at the bottom sites (0.024mgL^{-1} ± 0.02), however no significant difference was recorded between the ammonium concentrations at the northern half of the reservoir (0.05mgL^{-1} ± 0.02) and the southern half of the reservoir (0.042mgL^{-1} ± 0.03).

5.3.1.8.1. TN:TP molar ratio over the course of the EWE.

The TN:TP ratios were at their highest during the drought period (79:1 ± 58) relative to the ratio during active pumping while dry (22:1 ± 5) and active pumping 4 days post cessation of rainfall event (41:1 ± 8). The highest ratio during the drought period attained a ratio of 167:1 at site T3, with the lowest ratio recorded at site T4 (42:1). Following the activation of pumping, the TN:TP ratios decreased across the reservoir with the lowest ratio recorded at site B1 (13:1) and the highest at site B4 (29:1).

Every site recorded a ratio below that of Smiths ratio, and 1 site recorded a ratio lower than that of Redfield, indicating to suitable growing conditions for cyanobacteria (Figure 5.3.1.8.1.1).

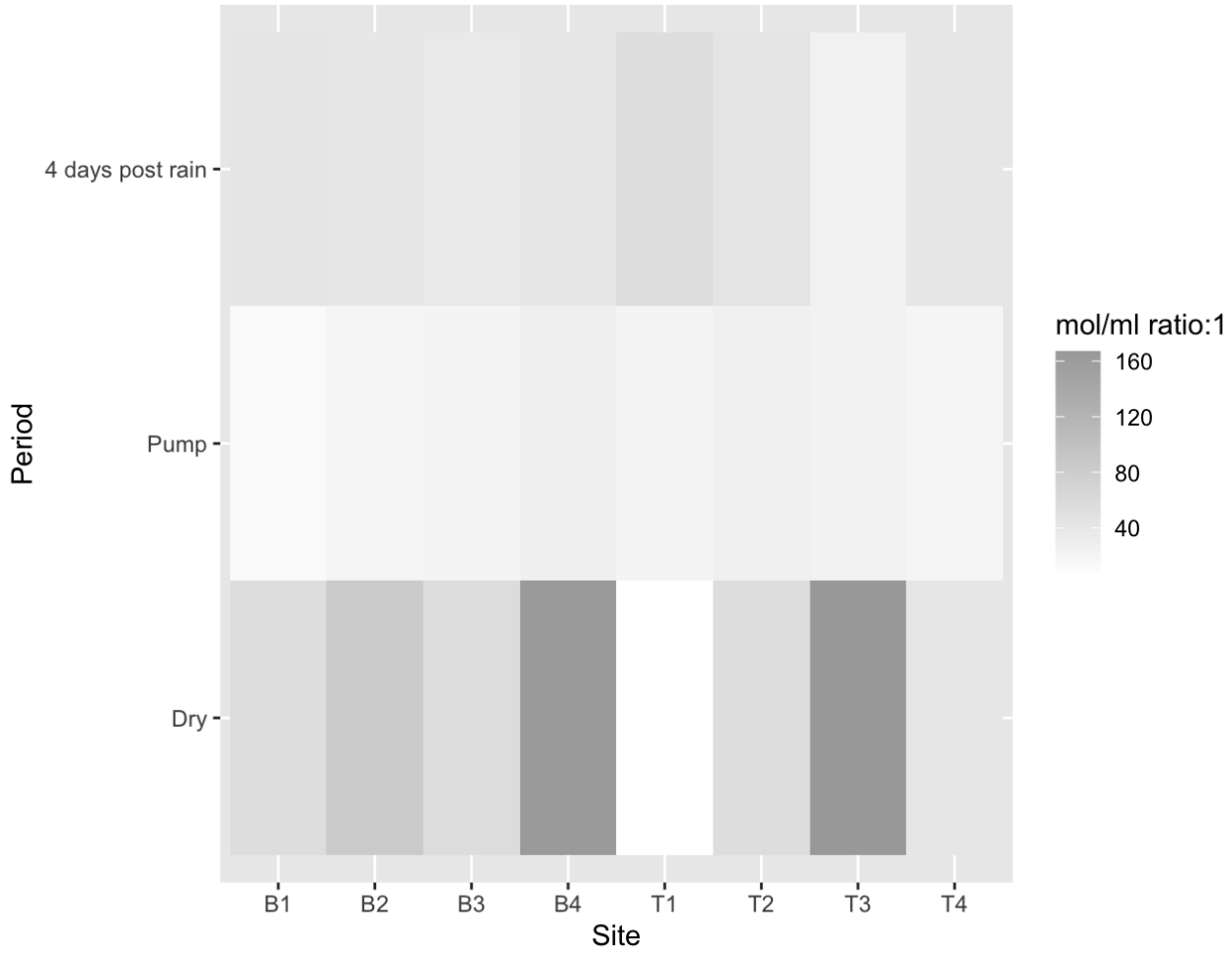

5.3.1.8.1.1. TN:TP molar ratios during the dry period (9th July) and during active pumping (3rd August) and 4 days following the precipitation event during active pumping (3rd August) (mgL^{-1}). Key: B=Bottom; T=Top, 1, 2, 3, 4 = site reference. Dry= during drought period with no inflow; Pump = during drought period and active pumping of water into reservoir; 4 days post rain= 4 days following cessation of rain event and pumping ongoing.

The highest ratios during the drought period were recorded at the northern section (108:1 ± 68; sites 3 and 4) and were significantly higher than those at the southern section (50:1 ± 33). Despite the northern section retaining the highest TN:TP ratios following initiation of the pumping, the difference in ratios were insignificant (Southern section; 21:1 ± 6; Northern section; 23:1 ± 4).

Four days post the rainfall event, the TN:TP ratios (41:1 ± 8) increased from those prior to the rain event but remained lower than those during the drought period. The TN:TP ratios were higher at the southern section (46:1 ± 6) than at the northern section (36:1 ± 8).

5.3.1.9.1. NO_3^-: NH_4^+ molar ratio over the course of the EWE.

The reduction in NO_3^- concentrations (mgL^{-1}) during a period of increased NH_4^+ concentrations (mgL^{-1}) resulted in a lower NO_3^-: NH_4^+ ratio across all sampling sites with the exception of site B2 which recorded an increase in NO_3^-:NH_4^+ ratio from 22:1 during the dry period (9th July) to 71:1 following four days following the rain (3rd August). The onset of active pumping in the absence of rainfall increased the ratio to 84:1. Additionally, sites B1 and B3 recorded an increase in NO_3^-: NH_4^+ ratio following the precipitation event, with B3 recording the higher ratio (32:1). The lowest NO_3^-: NH_4^+ ratio during the dry period was recorded at sites T2 and T4 (13:1), with the highest at site B1 (41:1). The ratio was insignificantly different between the surface samples (14:1 ± 1) and the bottom samples (15:1 ± 6), and the northern half (15:1 ± 1) and the southern half of the reservoir (14:1 ± 6). Active pumping before the onset of the precipitation event led to an increase in the NO_3^-: NH_4^+ ratio at site B2 to 84:1 from 22:1 recorded on the 9th July, with all other sites having recorded a decrease in ratio with the exception of site T3, where the ratio increased to 15:1 (Figure 5.3.1.9.1.1). However, a significant difference was determined in the ratios between the southern (32:1(mol/ml) ± SE 25) and the northern half of the reservoir (9:1 ± SE 3.5) and similarly between the surface sites (10:1 ± SE 3.6) and the bottom sites of the reservoir (31:1 ± SE 25.7).

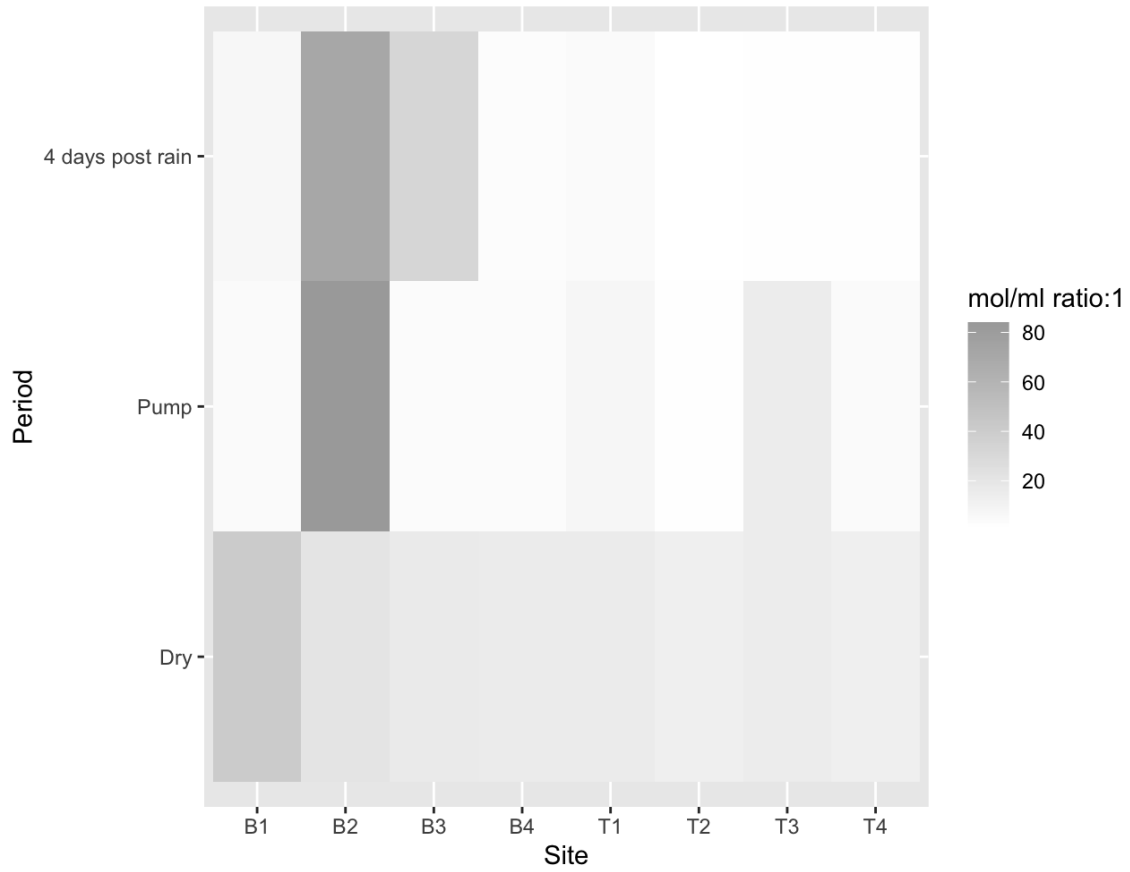

Figure 5.3.1.9.1.1. NO_3^-:NH_4^+ (mol/ml) ratio distribution at each sampling site of the reservoir during dry, active pumping and dry and active pumping following a precipitation event. Key: B=Bottom; T=Top, 1, 2, 3, 4 = site reference. Dry= during drought period with no inflow; Pump = during drought period and active pumping of water into reservoir; 4 days post rain= 4 days following cessation of rain event and pumping ongoing.

Four days following the cessation of rainfall, the NO_3^-: NH_4^+ ratios decreased to 1:1 at site T2, and 2:1 at sites T3 and T4, with all other sites recording a ratio of <8:1 with the exception of sites B2 and B3, where ratios of 71:1 and 32:1 were recorded respectively. The lower NO_3^-: NH_4^+ ratios were isolated at the northern section (10:1 ± 12) relative to the southern section of the reservoir (21:1 ± 28) and the surface sites (2:1 ± 1) relative to the bottom site samples (28:1 ± 27).

5.3.1.10. Algae and geosmin response over the course of the EWE.

5.3.1.10.1. Geosmin concentration data analysis

Geosmin concentrations remained below the DCWW failure threshold (6 ngL^{-1}) throughout the drought sampling period. The highest concentrations were isolated at the southern sites during the drought period and were absent from the northern sites with the exception of site

B4 (1ngL-1).

The onset of active pumping during the drought period coincided with a reduction in geosmin concentrations throughout the reservoir, with concentrations peaking at 0.44 ngL^{-1} at site T4. Four days following cessation of precipitation and during active pumping, the geosmin was restricted to the bottom sites, with B4 recording the highest concentration (1.2 ngL^{-1}) (Figure 5.3.1.10.1.1).

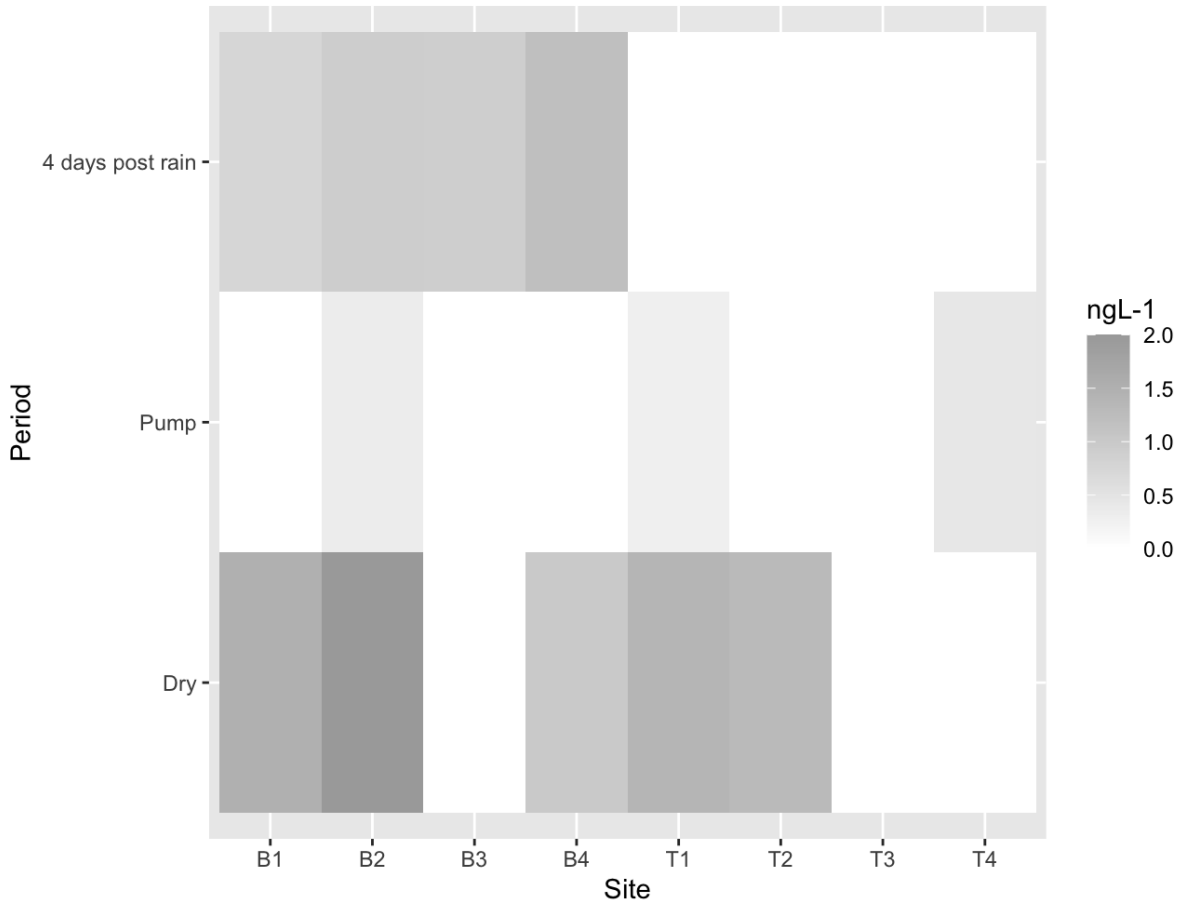

Figure 5.3.1.10.1.1. Geosmin (ngL^{-1}) distribution and concentration at each sampling site of the reservoir during dry, active pumping and dry and active pumping following a precipitation event. Key: B=Bottom; T=Top, 1, 2, 3, 4 = site reference. Dry= during drought period with no inflow; Pump = during drought period and active pumping of water into reservoir; 4 days post rain= 4 days following cessation of rain event and pumping ongoing.

5.3.1.11. *Cyanobacteria cell counts (cfu/ml) (colony forming units /ml) and distribution.*

Cyanobacteria were undetected at all sampling sites during the drought period indicating to unfavourable growth conditions.

Following the initiation of pumping during the dry period, *Oscillatoria* were the only species identified at all bottom water sites and the surface water at site 1 (2660cfu/ml ± 882) (Figure 5.3.1.11.1). Four days following cessation of the rainfall event and during continuation of pumping, no cyanobacteria were detected at the bottom sampling sites, however, an increased count of *Oscillatoria* had been recorded at all surface sites (4400 cfu/ml to 6900 cfu/ml)

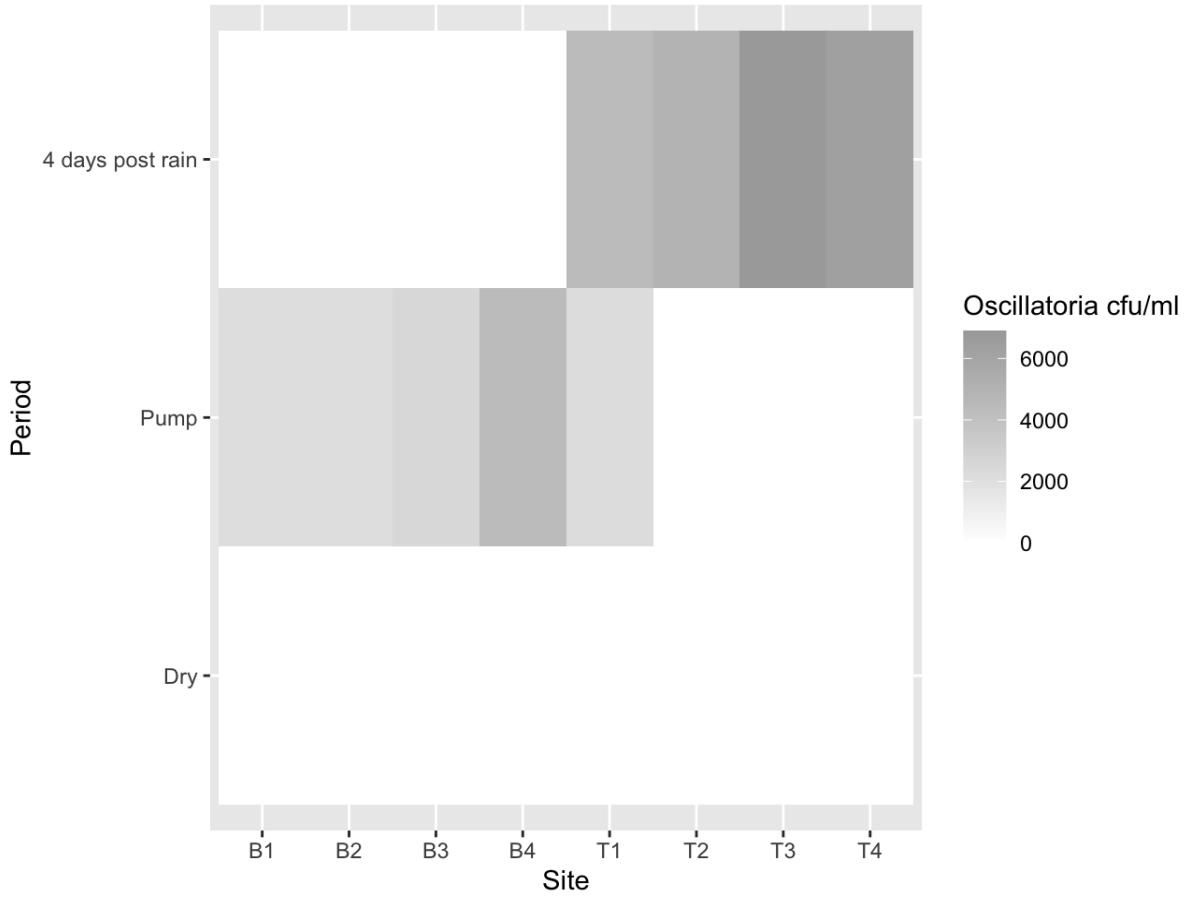

Figure 5.3.1.11.1. *Oscillatoria* count (cfu/ml) and distribution at each sampling site of the reservoir during the dry, active pumping and dry and active pumping following a precipitation event.

5.3.1.12. Green algae (cells/ml) cell count and distribution.

Green algae were isolated at three of the four surface sites at low numbers (190cells/ml to 240cells/ml) during the drought period, and at bottom site 4 (B4 (48cells/ml).

Green algae were recorded at all sites with particularly high cell number in the northern section of the reservoir (1700cells/ml at T3 and 5500cells/ml at B4) following the initiation of pumping during the dry period (Figure 5.3.1.12.1), with the majority of the establishment at the southern sites.

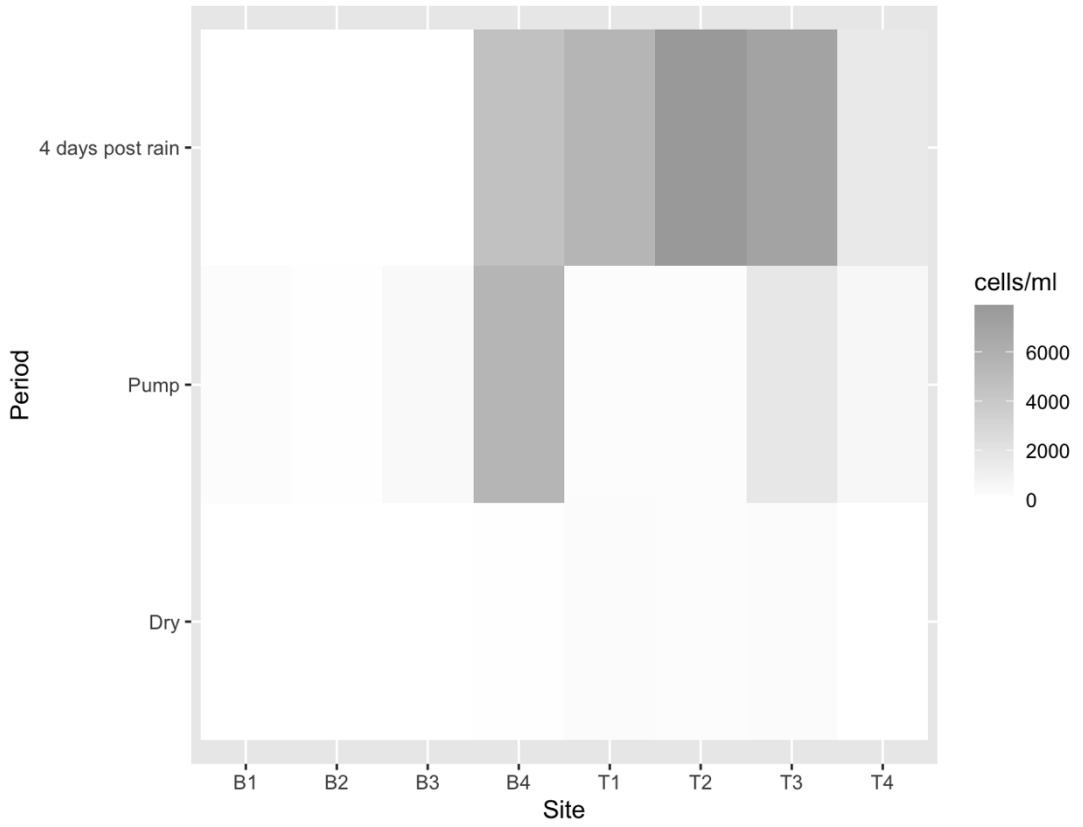

Figure 5.3.1.12.1. Green algae count and distribution at each sampling site of the reservoir during the dry, active pumping and dry and active pumping following a precipitation event.

Four days following cessation of rainfall, green algae were isolated at the same sites as those recorded during the drought period, with bottom site 4 being the only bottom site to record the presence of green algae (4600cells/ml).

5.3.2. Determination of variable association using General(ised) or Linear Modelling.

5.3.2.1. Model applied to P-fraction and variable data obtained July 9th

Water quality parameters such as temperature, pH, carbon, total nitrogen (TN), total phosphorus (TP), ammonium (NH_4^+), nitrate (NO_3^-), orthophosphate (OP) are deemed to be among the most critical factors when determining water quality (Dorado *et al.*, 2015; Wang *et al.,* 2002),

In addition to P fraction data, the data of the variables used in the GLM/LM analyses representing conditions within the reservoir on July 9th are listed in Table 5.3.2.1.1.

Table 5.3.2.1.1. The concentrations of critical variables in the determination of water quality across the reservoir on 9th July. Fe concentrations remained below the LOD at each site.

Site	Rainfall (mm/month)	Temp (°C)	pH	Turbidity (ntu)	Organic C (mg/L)	TN (mg/L)	NO_3^- (mg/L)	NH_4^+ (mg/L)	*Aphanizomenon/ Oscillatoria* (cfu/ml)	Green algae (cells/ml)	Geosmin (ng/L)
T1	46	25.4	8.9	1.2	2.4	0.99	0.96	0.017	0	240	1.4
B1	46	25.4	8.9	0.78	2.7	0.97	0.99	0.007	0	0	1.5
T2	46	25.4	8.9	1.1	2.6	0.99	0.94	0.021	0	190	1.3
B2	46	25.4	8.9	0.93	2.6	0.98	0.99	0.013	0	0	2
T3	46	25.4	7.9	1.1	2.3	1	0.96	0.019	0	240	0
B3	46	25.4	8	1.4	2.6	1	0.99	0.017	0	0	0
T4	46	25.4	7.9	1.5	2.5	1	0.95	0.021	0	0	0
B4	46	25.4	8.9	1.4	2.6	0.99	0.96	0.017	0	48	1

PCA determined the suitable variables for GLM/LM analyses with independent variables (Table 5.3.2.1.2).

Table 5.3.2.1.2. The dependent variables analyse with their respective independent variables as determined by PCA.

Geosmin (ngL^{-1})	NH_4^+	NO_3^-	Organic C ($mg\ L^{-1}$)	OP & TP	Organic P and AHP
TN:TP (mol/ml)	Green algae	Green algae	TN:TP (mol/ml)	Temperature (°C)	Geosmin ($ng\ L^{-1}$)
pH	Temperature	Temperature	pH	NO_3^-: NH_4^+ (mol/ml)	NO_3^- ($mg\ L^{-1}$)
Turbidity	Rainfall	Rainfall	Turbidity	Rainfall (mm)	TN ($mg\ L^{-1}$)
TN ($mg\ L^{-1}$)	NO_3^-: NH_4^+	NO_3^-: NH_4^+	TN (mol/ml)	NH_4^+ ($mg\ L^{-1}$)	pH
OrgP ($mg\ L^{-1}$)	OP ($mg\ L^{-1}$)	OP	OrgP ($mg\ L^{-1}$)	Green algae (cells/ml)	Turbidity (ntu)
AHP ($mg\ L^{-1}$)	NO_3^-	NH_4^+	AHP ($mg\ L^{-1}$)		TN:TP (mol/ml)
Org C ($mg\ L^{-1}$)	TP ($mg\ L^{-1}$)	TP	Geosmin ($ng\ L^{-1}$)		

Geosmin, Org-C, NH_4^+ and NO_3^- data were of a normal distribution, therefore a GLM was completed using Gaussian family (inverse link for all four independent variables). TP and Organic P were normally distributed, therefore GLM analyses were completed using the Gaussian family, log link (TP) and identity link (Organic P). OP and AHP not normally distributed data (Shapiro-Wilks $P<0.05$). OP was transformed using Tukey's ladder of power. AHP was transformed using cubic method.

A significant association (^R^2:0.8, $F_{1,6}$:63.7. P<0.001) for NH_4^+ (GLM intercept 0.002 ± -0.001, P<0.0001) with NO_3^-: NH_4^+ ratio (GLM mean difference ± SE, 0.0004 ± 0.00005, P<0.0001). No significant association was determined for NO_3^- with the NO_3^-: NH_4^+ ratio, and no other significant associations were determined.

5.3.2.2. Model applied to P-fraction and variable data obtained July 23rd

In addition to P fraction data, the data of the variables used in the GLM/LM analyses representing conditions within the reservoir on July 9th are listed in Table 5.3.2.2.1

Table 5.3.2.2.1 The concentrations of critical variables in the determination of water quality across the reservoir on 23rd July. Fe, pH, organic C and turbidity data were unavailable.

Site	Rainfall (mm/month)	Temp (°C)	TN (mg/L)	NO_3^- (mg/L)	NH_4^+ (mg/L)	*Oscillatoria* (cfu/ml)	Green algae (cells/ml)	Geosmin (ng/L)
T1	46	25.4	0.99	0.79	0.74	2200	150	0.3
B1	46	25.4	0.97	0.81	0.76	2100	190	0
T2	46	25.4	0.99	0.7	0.67	0	140	0
B2	46	25.4	0.98	0.88	0.87	2100	86	0.34
T3	46	25.4	1	0.91	0.83	0	1700	0
B3	46	25.4	1	0.68	0.64	2500	430	0
T4	46	25.4	1	0.81	0.76	0	520	0.44
B4	46	25.4	0.99	0.75	0.73	4400	5500	0

PCA determined the suitable variables for GLM/LM analyses with independent variables (Table 5.3.2.2.2).

Table 5.3.2.2.2. The dependent variables analyse with their respective independent variables a s determined by PCA. Organic P was absent from all samples on July 23rd.

Geosmin (ngL-1)	NH_4^+	NO_3^-	TP & AHP (mg L^{-1})	OP (mg L^{-1})
Oscillatoria (cfu/ml)	*Oscillatoria* (cfu/ml)	*Oscillatoria* (cfu/ml)	*Oscillatoria* (cfu/ml)	Rainfall (mm)
Green algae (cells/ml)	Green algae (cells/ml)	Green algae (cells/ml)	Green algae (cells/ml)	Temperature (°C)
NO_3^-: NH_4^+ (mol/ml)	NO_3^-: NH_4^+ (mol/ml)	NO_3^-: NH_4^+ (mol/ml)	NO_3^-: NH_4^+ (mol/ml)	
NH_4^+ (mg L^{-1})	Geosmin (ng L^{-1})	Geosmin (ng L^{-1})	Geosmin (ng L^{-1})	

NO_3^- (mg L^{-1})	NO_3^- (mg L^{-1})	NH_4^+ (mg L^{-1})	NO_3^- (mg L^{-1})	
TP (mg L^{-1})	TP (mg L^{-1})	TP (mg L^{-1})	NH_4^+ (mg L^{-1})	
OP (mg L^{-1})	OP (mg L^{-1})	OP (mg L^{-1})		

All P fraction data were not normally distributed and were transformed for analyses using Tukey's Ladder of Power. The N fraction data was parametric and analysed using GLM (Gaussian family, identity link (NH_4^+), inverse (NO_3^-)).

Geosmin data was not normally distributed and remained not normally distributed following transformation attempts. Therefore, the data was analysed using a GLM (Gamma family, inverse link).

A significant association (^R^2:0.91, $F_{1,6}$:6.8. P<0.0005) was determined for NH_4^+ (GLM intercept, 0.03 ± 0.08, P=0.7) with NO_3^- (GLM mean difference ± SE, 0.9 ± 0.1, P<0.0005).

No significant associations were determined for any other variables.

5.3.2.3. Model applied to P-fraction and variable data obtained August 3rd

In addition to P fraction data, the data of the variables used in the GLM/LM analyses representing conditions within the reservoir on July 9th are listed in Table 5.3.2.3.1.

Table 5.3.2.3.1. The concentrations of critical variables in the determination of water quality across the reservoir on August 3rd.

Site	Rainfall (mm/month)	Temp (°C)	pH	Turbidity (ntu)	Organic C (mg/L)	TN (mg/L)	NO_3^- (mg/L)	NH_4^+ (mg/L)	*Oscillatoria* (cfu/ml)	*Aphanizomenon* (cfu/ml)	Green algae (cells/ml)	Geosmin (ng/L)
T1	129.8	21.4	8.5	1.1	2.3	0.58	0.53	0.034	4400	0	5500	0
B1	129.8	21.4	8.6	1	2.1	0.74	0.7	0.031	0	0	0	0.75
T2	129.8	21.4	8.6	1.2	2.4	0.48	0.5	0.1	5000	0	7900	0
B2	129.8	21.4	8.6	1.4	2	0.75	0.73	0.003	0	0	0	0.94
T3	129.8	21.4	7.9	2.6	2.4	0.48	0.5	0.072	6900	0	7000	0
B3	129.8	21.4	7.8	4.1	2.1	0.71	0.66	0.006	0	0	0	0.9
T4	129.8	21.4	8	1.2	2.4	0.51	0.5	0.075	6300	0	1600	0
B4	129.8	21.4	8.6	1.8	2.6	0.56	0.51	0.056	0	2400	4600	1.2

PCA determined the suitable variables for GLM/LM analyses with independent variables (Table 5.3.2.3.2).

Table 5.3.2.3.2. The dependent variables analyse with their respective independent variables a s determined by PCA.

Geosmin (ngL^{-1})	NH_4^+	NO_3^-	Organic-C ($mg\ L^{-1}$)	Org-P, AHP, OP & TP
Green algae (cells/ml)	Green algae (cells/ml)	Green algae (cells/ml)	Green algae (cells/ml)	*Oscillatoria* (cfu/ml)
NO_3^- ($mg\ L^{-1}$)	NO_3^- ($mg\ L^{-1}$)	NH_4^+ ($mg\ L^{-1}$)	TN ($mg\ L^{-1}$)	pH
Rainfall (mm)	Rainfall (mm)	Rainfall (mm)	NH_4^+ ($mg\ L^{-1}$)	NO_3^-: NH_4^+ (mol/ml)
TN:TP (mol/ml)	TN:TP (mol/ml)	TN:TP (mol/ml)	Rainfall (mm)	*Aphanizomenon* (cfu/ml)
NH_4^+ ($mg\ L^{-1}$)	Geosmin ($ng\ L^{-1}$)	Geosmin ($ng\ L^{-1}$)	TN:TP (mol/ml)	Temperature (°C)
Org-C ($mg\ L^{-1}$)	Org-C ($mg\ L^{-1}$)	Org-C ($mg\ L^{-1}$)	Geosmin ($ng\ L^{-1}$)	
			NO_3^- ($mg\ L^{-1}$)	

Organic-C and NH_4^+ were of a normal distribution, therefore a GLM was completed using Gaussian family (identity link) for both independent variables. Geosmin data were not normally distributed and could not be transformed to a normal distribution using Tukey's ladder of power, square root, cube transformations nor logging the data. Therefore, geosmin was analysed using GLM (Gamma family (inverse link). NO_3^-, OP and AHP demonstrated not normally distributed (Shapiro-Wilks $P<0.05$). NO_3^- and OP were transformed using Tukey's ladder of power. AHP was transformed using cubic method. TP and Organic P were normally distributed, therefore GLM analyses were completed using the Gaussian family, log link (TP) and identity link (Organic-P). No significant associations were determined for any of the independent variables with those analysed.

A significant association (^R^2:0.8, $F_{1,6}$:31.2. $P<0.005$) was determined for organic-C (GLM intercept 3.36 ± 0.19, $P<0.001$) with NO_3^- (GLM mean difference ± SE, -1.86 ± 0.33, $P<0.005$). No other significant associations were determined for any of the variables analysed.

5.4. Discussion

5.4.1. Discussion Summary

Drought conditions recorded the presence of Org-P and high nitrate levels but lower concentrations of ammonium, OP and AHP, resulting in high NO_3^-:NH_4^+ and TN:TP ratios. No cyanobacteria nor green algae were detected. The onset of pumping decreased both ratios

due to a decrease in nitrate. Org-P was also undetected throughout the reservoir but an increase in ammonium, OP and AHP (and therefore TP) concentrations were recorded. Cyanobacteria were detected at the bottom sites only, but green algae were detected at multiple sites. Four days post rain recorded a slight increase in TN:TP ratios, ammonium and Org-P concentrations, but a further decrease in nitrate. Cyanobacteria and green algae were detected at the surface sites only.

Geosmin concentrations were predominantly detected at the bottom sites during the drought period and four days following the rain. Geosmin concentrations decreased following activation of pumping but increased following the rain.

5.4.2. Main discussion

5.4.2.1. P-fraction concentration response to EWE

The southern section (sites 1 and 2) of the reservoir recorded the higher concentrations of OP relative to the northern sites (sites 3 and 4) during the drought period. Following active pumping from the river, OP concentrations increased and attained a higher concentration in the north of the reservoir compared with that in the south, possibly due to sediment disturbance as a result of inflow and introduction of OP from the river. Svendsen and Kronvang (1993) determined that resuspension of sediment resulted in an increase in P released to the water, a situation that may have occurred at the northern banks of Llandegfedd reservoir during a storm due to the bank characteristics. Vadas (2006) determined that the majority of P enters the reservoir from soil during a few intense storms, indicating that a steady rainfall volume is less effective at leaching P into the reservoir than periods of heavy isolated rainfall events. The data obtained 1-day post heavy rainfall event indicated to the bottom site 1 (B1) as recording the greatest increase in TP concentrations of all sites sampled. However, the surface site 4 (T4) recorded the second highest TP concentration, sugges`ting that nutrient inflow from the surrounding banks may have occurred during an increase in run-off.

Post rainfall, the northern section of the reservoir retained a higher OP concentration relative to that of the south. However, the difference in concentrations was not as stark as those following the onset of pumping, indicating a greater influence of pumping upon the OP concentrations and distribution within the reservoir than rainfall. The northern section (sites 3 and 4) retained a higher AHP concentration during the drought period.

Conversely, the southern section (sites 1 and 2) recorded the higher AHP concentrations relative to the northern section following the onset of pumping. The data suggested that physiological characteristics of the reservoir (pH, temperature) may have been influenced by the environment to increase the AHP concentrations at the northern sites as a consequence of pumping. The southern sites also retained a higher AHP concentration relative to that of the northern sites following the rainfall event; however, the difference was insignificant. Four days post cessation of rainfall the AHP concentrations returned to pre-drought distribution whereby the southern half retained the higher AHP concentration. The lower P concentrations during drought periods may have provided a competitive edge to cyanobacterial species capable of luxury P storage, potentially leading to cyanobacterial proliferation, however, no cyanobacteria were detected during the drought period (early July). Increased TP was likely the consequence of a combination of run-off from heavy rainfall, sediment disturbance at the periphery where banks remained exposed, and demand at site 1, leading to active water disturbance in the sediment immediately surrounding the abstraction tower. Kragh *et al.,* (2017), determined that the retention of lower reservoir levels during summer periods at times of extreme weather events increased P loss by enhancing both sediment resuspension and hydraulic flushing. Additionally, water retention time is likely to be longer during the summer periods compared with that during the winter, potentially leading to an increase in P sediment release during the summer (Kragh *et al.,* 2017). P distribution variations were divided along the transect of the reservoir (north to south) whereas TN concentrations were divided by sample depth (surface to bottom).

5.4.2.2. N-fraction response to EWE

The bottom retained the higher NO_3^- concentrations during the drought period relative to the surface sites. The initiation of pumping decreased nitrate concentrations and even distribution of NO_3^- between the surface and bottom, northern and southern sections (sites 1 and 2) of the reservoir. However, the southern section of the reservoir recorded higher concentrations of NO_3^- than the northern section 4 days post-rain. Lee *et al.,* (2011), concluded that the concentration of pollutants such as NO_3^- carried by run-off during heavy rain depended highly upon the length of dry period beforehand and the intensity of the rainfall. The dry period before the rainfall event lasted approximately 12 weeks; therefore, the concentrations of pollutants recorded represent a period of run-off following an extreme

weather event in the UK, however, the data suggested a decrease in nitrate occurred following the rainfall event, but ammonium concentrations increased. Research by Cooney *et al.,* (2018), studying the effect of heavy run-off events upon nutrient dynamics within the Great Lakes determined that a period of heavy rainfall led to the introduction of ammonium into the lakes, significantly increasing its concentrations relative to that before the storm events. However, such a significant increase in nitrate was not recorded. Chen *et al*., (2018), determined that ammonium and dissolved reactive phosphate (DRP) increased following a period of heavy rainfall accompanied by a decrease in chlorophyll-a (Chl-a) and nitrate. Nitrate concentrations decreased as a consequence of dilution but increased soon after. The ammonium was of a higher concentration at the surface and northern sites during the drought period but cyamobacetria were undetected throughout the reservoir. The onset of active pumping increased the concentration of ammonium throughout the reservoir, which may lead to an increase in cyanobacterial growth and the production of geosmin. Four days post rainfall the ammonium concentrations were significantly higher at the surface of the reservoir relative to the bottom region. However, nitrate was distributed uniformly along the transect of the reservoir.

5.4.2.3. N-fraction ratio response to EWE

The increased frequency of lower NO_3^-: NH_4^+ ratios negatively correlated with geosmin concentration, indicating a phase of exponential cyanobacterial growth duirng periods of lower NO_3^-: NH_4^+ ratios. Raised NO_3^-: NH_4^+ ratios during the drought period suggested a decreased potential of geosmin production relative to that detected during a period of lower ratios following active inflow into the reservoir. NH_4^+ is sorbed to negatively charged clay particles and soil organic matter. The positive charge prevents NH_4^+ from being washed out of the soil (or leached) by rainfall. In contrast, the negatively charged NO_3^- is not held by soil particles and so can be washed out of the soil, leading to nitrate enrichment of the reservoir. The NO_3^-: NH_4^+ ratio was evenly distributed throughout the reservoir during the drought period, but the lower ratios were isolated following pump activation in the northern and surface samples, indicating to a higher risk of geosmin production at the sites. This was maintained following the cessation of the rainfall event. NO_3^-: NH_4^+ ratio was consistently highest at B2, but B3 also recorded a high ratio following the rainfall event, suggesting bottom sites 2 & 3 of being the site least at risk of geosmin production. A decrease in OP following

heavy precipitation suggests assimilation by cyanobacteria while the decrease in NO_3^- and concomitant increase in NH_4^+ is indicative of nitrate reduction during cyanobacterial growth. The resultant lower NO_3^-: NH_4^+ in the presence of high energy allows for growth at an increased rate, leading to the use of the secondary metabolic pathway, producing geosmin as a by-product. Songmin, (2017), determined that ammonium is washed from the land into water during the first run-off of a storm event, with nitrate concentrations remaining low in the run-off. However, nitrate concentrations in run-off waters increased during subsequent run-off into water, indicating to an initial decrease in the NO_3^-: NH_4^+ ratio followed by an increase in the NO_3^-: NH_4^+ ratio.

5.4.2.4. Geosmin distribution and concentrations is response to the EWE.

Lower NO_3^-: NH_4^+ ratio likely contributed towards the increase in geosmin levels recorded following the rain event (an increase in geosmin of 53% from 0.68ngL^{-1} to 1.44ngL^{-1}). Geosmin concentrations remained low during the drought (<6ngL^{-1}) and were predominantly isolated to the southern sites (sites 1 and 2). The activation of pumping resulted in the decrease of geosmin across the reservoir, indicating to the reduction in cyanobacterial senescence. However, four days post-cessation of rainfall, geosmin was detected at very low concentrations but restricted to the bottom sites, indicating to a period of rapid growth and a period of senescence at the bottom region.

Stanos *et al.,* (2015), determined that the stability of a cyanobacterial bloom can be affected by wind speed and heavy rain, with an increase in both wind and rain volume potentially forcing cyanobacteria and their metabolic by-products deeper into the water column. This can increase the risk of taste and odour complaints to water companies due to a higher potential for uptake of geosmin during abstraction via the bottom intake, especially during a period of faulty abstraction with bias towards the bottom water (Gonzalez-Piana *et al.*, 2018). In the event of an increase in extreme weather events, Llandegfedd Reservoir may be subject to increasing frequencies of geosmin production, leading to a rise in the number and frequency of customer taste and odour complaints.

5.4.2.5. Cyanobacterial response to the EWE.

The heavy rainfall following a period of drought and pumped water into an impounding reservoir at Llandegfedd resulted in a decrease in NO_3^- concentrations (0.99mgL^{-1} prior to the

rain to 1mgL^{-1} following the rain) and increased NH_4^+ concentrations leading to a lower NO_3^-: NH_4^+. Cyanobacteria opt for the lower energy-consuming pathway of N-assimilation (Riegman *et al.,* 1992, Hallegraeff 1993, Riegman 1995, McCarthy *et al*., 2009, Glibert *et al,.* 2016, Ruan *et al.*, 2017, Watzer, 2019), thereby selecting N- NH_4^+assimilation. The pathway may lead to an increase in cyanobacterial growth rate and an increase in the by-product geosmin and AHP release during a period of mineralisation in the bottom water. An increase in available P following precipitation and pumping into the reservoir reduced P limitation in cyanobacterial cells, deactivating the APase enzyme. The rise observed is geosmin concentration at site B3 from 0.68ngL^{-1} during drought conditions to 1.44ngL^{-1} following a week of heavy rain, accompanied by an increase in water temperature of 2.5°C indicated a rise in primary productivity within the reservoir following the rain at site B3.

Oscillatoria were the only species of cyanobacteria identified at the reservoir over the EWE sampling period.

No cyanobacteria were isolated during the drought period, suggesting that unfavourable conditions were presented for cyanobacterial growth in the absence of an inflow. However, the activation of pumps resulted in the isolation of cyanobacteria predominantly at the bottom sites, with the northern site four being of highest risk of greater cyanobacterial densities.

Four days following cessation of precipitation resulted in the absence of cyanobacteria at all bottom sites, but increased counts at all surface sites. The detection of geosmin at all bottom sites was concurrent with the absence of cyanobacteria. Ho *et al*., (2019), determined that the effect of precipitation upon cyanobacetrial establishment could not be proven; depite run-off introducing an increase in nutrients to the reservoir which is favourable to cyanobacteria, he found that heavy precipitation drove greater flushing, decreasing the nutrients within the reservoir.

5.4.2.6. The response of green algae to the EWE.

Surface sites were more at risk of green algae establishment during the drought period but proliferated throughout the reservoir following initiation of pumping. The southern sites (sites 1 and 2) recorded the highest concentration of green algae following activation of pumping. The detection of green algae at bottom site four, while it remained undetected at

all other bottom sites, may be due to the shallow nature of the site. Light can penetrate to the sediment at site 4, particularly during periods of drought where the reservoir level is low. Four days following cessation of rainfall, green algae was detected at all sites previously identified as being occupied during drought conditions, albeit at higher numbers. A significant association was determined for ammonium with NO_3^-: NH_4^+ molar ratio, but no association was determined for NO_3^- with the NO_3^-: NH_4^+ ratio during the drought period. The data indicated to ammonium exerting a greater influence upon the ratio than the concentration of NO_3^-.

5.4.2.7. Significant associations determined through modelling variable data.

A significantly positive association was determined for NH_4^+ with NO_3^- following the initiation of pumping. A significantly negative association was determined for organic C with NO_3^- four days post-cessation of rainfall. The concentration of nitrate decreased as a consequence of rainfall; however, the concentration of organic C increased. The organic C likely increased as a consequence of inflow, where terrestrially-sourced C was washed into the reservoir via inflow.

5.5. Conclusion.

The drought period resulted in the southern section (sites 1 and 2) of the reservoir being at increased risk of cyanobacterial establishment and geosmin production as a consequence of the increased OP, AHP and ammonium concentrations relative to that of the northern section (sites 3 and 4).

However, the activation of pumping increased the cyanobacterial establishment and geosmin risk at the northern section (sites 3 and 4) through decreasing the NO_3^-: NH_4^+ ratio, particularly at the surface sites and site 4 (bottom and surface). The data supported the hypothesis that nitrate dominated during the drought conditions but ammonium increased while nitrate decreased following the activation of pumping and rainfall event.

Drought conditions did not create ideal cyanobacterial growing conditions throughout the reservoir. Site 4 closest to the inflow was the site of highest risk of cyanobacterial establishment upon activation of pumps during a drought period, but the surface sites became highest at risk of cyanobacterial establishment four days following cessation of the rainfall event. The active pumping following a drought event had a more significant effect

upon bioavailable P and potentially bioavailable P throughout the reservoir than the rainfall event, indicating that the hypothesis that both the return of active pumping and heavy rainfall have an equal effect upon the P concentrations must be rejected.

The southern half of the reservoir was more likely to record higher concentrations of condensed-P as opposed to the bioavailable OP, but the converse was true for the northern section (sites 3 & 4), supporting the hypothesis that bioavailable P concentrations will increase following the precipitation event specifically in the northern section (site 4) of the reservoir.

The cyanobacterial counts increased within the reservoir following activation of pumping, but predoninanty in the bottom water. However, a period of rainfall resulted in the detection of cyanobacterial cells predominantly in the surface waters. The data supported the hypothesis of an increase in cyanobacetrial counts as a consequence of inflow into the reservoir, therefore, the hypothesis may be accepted.

Heavy rainfall events could lead to very high nutrient input into the reservoir due to erosion from the surrounding bare steep northern banks, and the particulate matter may contribute to most nutrient inputs (Huang *et al.*, 2014). High levels of suspended solids, attributed to inputs from tributaries, may inhibit light penetration and thus have a considerable impact on cyanobacteria (Woldeab *et al*., 2018), and may force cyanobacterial blooms away from the tributary to the more settled section, often nearest the dam and therefore, abstraction tower.

Chapter 6: General discussion

6.1. Chapter summary.

Llandegfedd Reservoir consists of a dynamic body of water which is subject to influences by the climate and its surrounding environment, the extent to which is in part determined by the characteristics of its water supply (inflows and run-off) and sediment. Overall, data analyses highlighted the northern section (sites 3 and 4) of the reservoir as being the highest risk of algal and cyanobacterial activity due to its shallow characteristics and its proximity to the inflow and susceptibility to nutrient inflow entrained within run-off during and following periods of heavy rain. This was reflected in the nutrient concentrations detected within both the sediment and water data under varying environmental conditions and seasons. The method of water abstraction significantly affected the quality of water removed for treatment. This was indicated by the significant difference in the mean monthly concentrations of some nutrients (e.g., nitrate) prior to the method change relative to that following the change to the abstraction method. The data suggested changes to the abstraction method resulted in a bias towards abstraction of the bottom water.

A review of the analyses of reservoir variables and their dynamics directly or indirectly affecting water quality may result in a change to the existing methods of reservoir management by DCWW. In this chapter, the rejection or acceptance of the sub-hypotheses in the course of answering the overarching hypotheses, sub hypotheses are discussed, and information attained through the analyses of the water and sediment data in the previous chapters are reviewed to help determine the characteristics of Llandegfedd reservoir and more importantly, its resilience to the predicted change in climate.

6.2. Main discussion of overarching and sub-hypotheses

To help determine whether the first hypothesis relating to the historical data analysis is to be accepted or rejected, the sub-hypotheses are discussed.

6.2.1. Overarching hypothesis: *Evidence of historical climate change will not be clear through analysing the historical data due to inaccuracies within the data as a consequence of the change in abstraction method.*

Analysis of historical data (Chapter 2: Nutrient data analysis) determined significant differences between data sets within some variables critical in the analysis of risk of water deterioration (e.g., nitrate), when compared prior to and following changes to the abstraction

method. The data indicated the depth of abstraction and mixing of water from throughout the column (with bias towards the bottom water) had a significant effect upon the quality of the water extracted for treatment.

Research completed by Amikhani *et al.,* (2016), assessing the water quality of outflow from a reservoir using multiple (two) outflow options versus one continuous and unchangeable outflow determined that water quality was enhanced when selecting for outflows based upon real-time reservoir conditions relative to that where the outflow depth was constant.

Research by Azadi *et al.,* (2018), assessing the risk to reservoir water quality under climate change projections determined that nutrient loading will likely affect different water depths under varying seasonal conditions, with the ability to actively select the depth of water abstracted for treatment a clear advantage to minimising treatment costs and water quality breaches. Therefore, the data were not suitable for purposes beyond the scope of determining the water quality of that abstracted for treatment and therefore cannot provide guidance relating to the true conditions within the reservoir. Therefore, water quality data obtained using water quality monitors located within the abstraction tower are not representative of a specific water depth while the abstraction instruments continue to malfunction. Also, the reliance upon a single point for water quality monitoring cannot indicate the water quality across the whole of the reservoir. Consequently, a single point of water quality analysis may result in poor reservoir management decisions due to the inability to understand conditions throughout the wider reservoir.

6.2.1.1. Sub-hypothesis 1: Historical data will highlight the importance of establishing a suitable water sampling method in order to obtain reliable data representative of the water quality.

Analysis of the historical data (Chapter 2: Nutrient data analysis) indicated a significant decrease in nitrate concentrations during both the summer and winter months post-2000 relative to that pre-2000, suggesting that the changes to the abstraction method significantly affected the data collected post 2000 with bias towards water quality analysis of the bottom water. Concurrently, the relatively constant ammonium concentrations also highlighted by the change to abstraction method may have presented an increased risk of geosmin production as a consequence of assimilation of ammonium over nitrate in the bottom water.

The data also indicated the phosphorous concentrations were not significantly affected by the change in abstraction method as a consequence of tower malfunction, suggesting that the phosphorous distribution throughout the water column was ubiquitous. This was supported by the analysis of TP concentrations of the mean annual bottom and surface sites throughout the 2018 real-time sampling period which indicated no significant difference in the concentrations of mean annual TP, OP nor AHP between the bottom and surface sites.

The data highlighted a potential for masking water quality deterioration following to the failure of abstraction tower through amalgamating water from three depths, neutralising some of the variable data. Also, bias towards analysis of the deeper water may prevent an understanding of the water quality throughout the rest of the column, presenting opportunities for missed risk management/mitigation. Therefore, sub-hypothesis 1 can be accepted.

6.2.1.2. Sub-hypothesis 2: Data analysis will indicate that the reservoir level will significantly affect the concentrations of Total Phosphorous at the point of abstraction within the tower.

The analysis of historical data determined a significant positive association for reservoir level with the TP concentrations, leading to the acceptance of sub-hypothesis 2. The data indicated a lower TP concentration at the point of abstraction during periods of a lower reservoir level relative to that during periods of an increased reservoir level. Decaying organic matter situated at the exposed periphery of the reservoir during periods of low water volume is incorporated into the water upon rewetting (Hupfer *et al.,* 2003). Therefore, nutrient concentrations including phosphorous may increase during the refilling process of the reservoir. The positive relationship between P concentration and reservoir level was identified by Heron (1960). Heron researched the seasonal nutrient cycles within lakes and determined that a rise in phosphorous concentrations strongly correlated with a rise in water level as a consequence of phosphorous from lysed microbial cells within the desiccated sediment becoming entrained within the rising water. Therefore, influences upon P concentrations within the reservoir are not restricted to anaerobic internal loading or external loading through entrainment during a period of heavy rainfall.

The intensity of the drying and re-wetting cycles of the sediment is expected to intensify as a consequence of climate change (IPCC, 2014), due to longer periods of warmer summers interspersed with a decrease in frequency of rainfall. The duration of sediment exposure and

the consequential drying effect significantly affects the nutrients leached into the reservoir during the rewetting process (Khan, 2019). The potential for increased frequencies of short periods of heavy summer rain also as a consequence of climate change, increases the risk of nutrient loading due to entrainment of the nutrients within the run-off. The data indicated that Llandegfedd Reservoir may be susceptible to an increase in TP concentrations if climate change progresses as predicted.

6.2.1.3. Sub-hypothesis: The analysis of historic rainfall data obtained over a period of a constant abstraction method will have a significant positive association with NH_4^+ and a significant negative association with NO_3^- levels.

Data analysis determined a significant negative association between the nitrate concentrations and rainfall volume which may have been due to dilution of the water within the reservoir. However, no significant association was determined for NH_4^+ with rainfall. Therefore, the sub-hypothesis can be partly rejected. Historical data analysis also determined that raised nitrate concentrations were negatively associated with rainfall volume, positively associated with the NO_3^-: NH_4^+ ratio, but no significant association was determined for rainfall with ammonium concentrations.

The ammonium concentrations may have been maintained by denitrifying bacteria and bacteria responsible for DNRA (Dissimilatory Nitrate Reduction to Ammonium) (oxidation of organic matter using nitrate as the electron acceptor) (An *et al.,* 2002). Both denitrifying and DNRA bacteria compete for nitrate in the bottom zone resulting in a decrease in nitrate (An *et al.,* 2002); however, denitrifying bacteria convert nitrate to N_2 but nitrate ammonifying bacteria reduce the nitrate to ammonium, maintaining or increasing the ammonium concentrations and potentially decreasing the NO_3^-: NH_4^+ ratio.

Arce *et al.,* (2018), researched the consequence of a drying and rainfall events upon the nitrogen concentrations within water. It was determined that nitrate concentrations increased during periods of drought and was concomitant with a decrease in ammonium. Similarly, the rainfall event was strongly correlated with an increase in ammonium and concurrent decrease in nitrate concentrations. However, Acre *et al.,* (2018), concluded that such increases in the nitrogen-fraction concentrations only occurred following a long period of drought (minimum of 6 weeks). Therefore, the risk of water quality deterioration within Llandegfedd reservoir may increase as a consequence of the predicted meteorological

changes due to climate change, with water conditions becoming more favourable to cyanobacterial establishment.

Following a review of the sub-hypotheses, the overarching hypothesis was accepted. The analysis of the data concluded that evidence of historical climate change within the water quality data could not be determined in part as a consequence of the effect of the change to the abstraction method upon the water quality data recorded. In addition, significant associations were determined between meteorological conditions and nutrient concentrations within the reservoir over periods of a continuation in abstraction method, with data indicating to a risk of water quality deterioration at Llandegfedd reservoir due to climate change. The data suggested that improvement to the water quality monitoring and abstraction methods are required to help decrease the risk of water quality degradation as a consequence of climate change through an improved reservoir management approach.

6.2.2. Overarching hypothesis: The northern sampling sites (sites 3 and 4) shall be of a higher risk to water quality as a consequence an increased volume of allochthonous P input than the southern sites (sites 1 and 2).

The site of the inflow at the northern bank introduced nutrients to the reservoir directly from the river Usk and likely increased the rate of internal nutrient loading through sediment disturbance of unprotected banks in the inflow channel. Therefore, site 4 was at the highest risk of algal and cyanobacterial establishment (Makarewicz *et al.,* 2012), due to the multiple channels of nutrient loading. This was reflected in the organic-P (Chapter 3) which was not ubiquitous throughout the reservoir during 2018. A higher concentration of organic-P at the northern sites (3 and 4) relative to the southern sites (1 and 2) suggested an increased risk of cyanobacterial establishment at the bottom of northern sites. The data was indicative of a sink for organic-P at the northern section (sites 3 and 4) of the reservoir, where higher sediment organic-P deposition rates may have occurred over the 2018 sampling period, leading to the acceptance of the overarching hypothesis. However, a low rate of internal P loading within the reservoir during both the spring and summer months indicated the majority of the phosphorous within the reservoir was likely derived from an allochthonous source. Therefore, Llandegfedd reservoir was susceptible to the influence of phosphorous derived from the catchment. Changes induced by climate change upon catchment

management, activities and use may deleteriously affect water quality within Llandegfedd reservoir.

6.2.2.1. *Sub-hypothesis: Phosphorous concentrations shall be at their lowest during the winter period.*

Total phosphorous concentrations were lower during the winter period (January through March and October through December) relative to that during the summer period (April through September) throughout the reservoir, leading to the acceptance of the sub-hypothesis. Water phosphorous concentrations increased during the summer as a consequence of environmental and biological stimuli such as warmer temperatures and increased benthic microbial activity.

Filbrun *et al.,* (2012), researched the influence of seasons upon the phosphorous dynamics within Grand Lake St. Marys, Ohio. Filbrun determined a correlation between phosphorous concentrations within the lake and the seasons, changes to the P concentrations between the winter and summer periods due to its main supply changing from internal loading during the summer to a predominantly tributary-fed supply during the winter.

The source of phosphorous may change in response to the seasons from autochthonous during the spring to allochthonous later in the summer period during periods of extreme weather events. Therefore, an increased risk of water quality degradation may be present within Llandegfedd reservoir during the summer season as a consequence of an increased concentration of phosphorous and a raised microbial metabolic rate in response to the warmer conditions.

6.2.2.2. Sub-hypothesis 2: There will be no significant association between P-fraction concentrations and the nutrients or environmental data.

Data analysis indicated no significant association between P-fraction concentrations and the nutrient or environmental data, leading to the acceptance of the sub-hypothesis. The concentrations of phosphorous within the water column is dependent upon both allochthonous and autochthonous sources. The phosphorous stored within Llandegfedd reservoir is likely to have derived predominantly from an allochthonous source as indicated by the mass balance calculations and plays a significant role in determining the P concentrations of the water (Richey, 1979).

The progression of climate warming is increasing the volume of allochthonous phosphorous into reservoirs worldwide (Frey *et al.,* 2005; Haaland *et al.,* 2010; Vonk *et al.,* 2015), amplifying the risk of increasing the allochthonous phosphorous load within Llandegfedd reservoir. Allochthonous sources of phosphorous are variable in frequency and concentration (Xie *et al.*, 2014), with the travel time from its source to the reservoir dependant upon numerous variables including slope of route travelled (Fu *et al.,* 2016), the intensity and duration of the rainfall event (Zhang *et al.,* 2018), and types and use of the encompassing land (Tiwari *et al.,* 2010). Therefore, the meteorological data having been obtained several miles from the reservoir coupled with the exclusion of data representing details of the catchment topography decreases the likelihood of determining a significant association between phosphorous concentrations and meteorological conditions. In addition, there is a delay between the external loading of phosphorous and the detection of the consequent increase in phosphorous concentrations within the hypolimnion (Nürnberg *et al.,* 2004).

The internal release of phosphorous from the sediment is not a process that begins and stops abruptly, for example, in the presence of oxygenated water entering the benthic zone following a deluge of cold rain during a period of stratification (Söndergaard *et al.,* 2002), highlighting the overlapping processes of phosphorous sediment release/ allochthonous input. Nitrate in bottom waters prevent or limit the volume of P released from the sediment (Anderson, 1982). The absence of a significant association between TP with nitrate indicated the insignificant effect of bottom water nitrogen upon internal P loading.

The concentration of phosphorous introduced into a reservoir from an allochthonous source may be independent of the conditions within the reservoir or localised meteorological conditions, particularly when internal P loading has been determined to be low. The absence of a significant correlation between P concentration data and meteorological or nutrient data indicated the presence of influences not measured or included within this thesis, highlighting the complexity of the phosphorous cycle. Consequently, improving the water quality monitoring methods at Llandegfedd reservoir through an increased sampling frequency and number of sampling sites throughout the reservoir would likely not provide an accurate model for phosphorous concentration prediction.

Following a review of the sub-hypotheses, the overarching hypothesis was accepted. Site 4 was indicated as being closer to an allochthonous source of phosphorous relative to all other

sites indicating to the pumped inflow and rainwater run-off as the predominant route for allochthonous P loading. Consequently, the northern sites (sites 3 and 4) were of a higher risk of water quality deterioration than the southern (sites 1 and 2) sampling sites. The increased risk of nutrient inflow and deposition at site 4 may decrease the resilience of Llandegfedd reservoir to climate change, potentially resulting in changes to the water quality at the site.

6.2.3. *Overarching hypothesis: Sediments within a closer proximity to the pumped inflow (sampling site 4) will have greater TOC and hence enhanced benthic microbial activity.*

TOC was least likely to be detected at sampling site 4 relative to any other sampling site, with the southern sites (sites 1 and 2) being locations where the highest concentrations of C were detected. The detection of lower concentrations of TOC and P-fractions at site 4 relative to that at any other sampling site indicated an increase in C and P assimilation and therefore, an increased susceptibility to cyanobacterial and algal growth and establishment during the summer period in the absence of turbidity induced by active inflow at the northern point of the reservoir contributing towards sediment resuspension (Padisák *et al.*, 2003). Additionally, the increased TOC concentrations at sites 1 through 3 may have been due to anaerobic bottom conditions which decrease mineralisation of C by up to 50% relative to that in aerobic conditions (Isidorova *et al*. 2016), which may have been prevalent at site 4 due to the Its shallower water which may have increased oxygen penetration at the sediment surface as a consequence of sediment disturbance.

Most of the annual P leaching from the soil surrounding a reservoir occurs during a few, intense storms (Vadas, 2006). Mobilised sediment entering a reservoir is a pollutant due to its association with the suspension of solids within the water column (Lenzi *et al.,* 2000).

Sediment redistribution as a result of inflow within an artificial landscape differs from that of a natural landscape due to controlled inflow velocities and frequencies (Tang *et al.,* 2016).

There is an increased proportion of finer particles within the substrate at the peripheral banks at the northern section of Llandegfedd reservoir (as indicated by the absence of granite boulders and the presence of sandy deposits) relative to that of the southern section, the latter which is surrounded by granite boulders. Therefore, bank instability through episodic inflows caused by abstraction and periods of heavy precipitation increases the potential for sediment redistribution in the northern section of the reservoir (Odhiambo, 2014). Rainfall volumes and inflow volumes are positively correlated (Ran *et al.,* 2012); consequently,

precipitation fuels run-off volume and frequency (Cantón *et al.,* 2011). Therefore, the northern sites (sites 3 and 4) are most at risk from the effects of run-off upon the water quality relative to the southern sites.

6.2.3.1. Sub-hypothesis: Labile-P concentrations will be lowest at the sediment surface and increase with sediment depth during the summer (due to a reduced redox potential).

The concentration of labile-P through the sediment profiles disagreed with the sub-hypothesis, with the majority of the profiles demonstrating no change to labile-P concentration with depth or a decrease in labile-P with sediment depth. However, the labile-p concentration gradients at each sampling site were infrequently repeatedly recorded during subsequent sediment profiling. However, research by Lyde *et al.,* (2013), determined that the majority of labile P was detected in the deeper profiles of the sediment due to an increased rate of mineralisation and anoxic conditions resulting in an increased concentration of labile-P, a profile which was recorded occasionally at Llandegfedd reservoir. Consequently, the sub-hypothesis can be rejected due to the unrepeatability of the sediment conditions.

6.2.3.2. Sub-hypothesis: Internal P loading will be greater during the summer relative to the spring period. Internal loading will be a significant source of phosphorous compared with external loading of phosphorous.

Mass balance calculations determined that a greater degree of internal loading occurred during the summer relative to that during the spring. This was also documented by Goedkoop *et al.,* (2000), who determined that the sediment phosphorous varied significantly from spring to summer as a consequence of raised benthic microbial activity following senescence of a springtime diatom bloom. Söndergaard *et al.,* (2005), determined that shallow sections of lakes respond differently to external loading relative to deeper sections of the lake through responding quicker to meteorological changes and changes within the environment. However, the phosphorous movement from the sediment to the water is lake specific with the greatest P-influx occurring over many episodes through the summer period (Søndergaard *et al.,* 2003), and not isolated as one large pulse of P release. Therefore, the frequency of monitoring can impact significantly on the mass balance data.

Both seasons exhibited a low degree of internal P loading, indicating a low risk of P dissociation from the sediment to the water, suggesting an external source of P was the predominant source of P to the Llandegfedd Reservoir. Therefore, the sub-hypothesis can be rejected.

Following a review of the sub-hypotheses, the overarching hypothesis can be rejected. Despite sampling site 4 not concurring with the overarching hypothesis through recording lower TOC concentrations relative to other sampling sites, it is anticipated that the cause of the lower TOC concentrations may have been due to raised microbial activity. Therefore, site 4 may be subject to enhanced microbial activity which may be evident in the lower concentrations of TOC relative to other sampling sites.

Labile-P concentrations were lower in the sediment surface at the northern sites indicating a greater degree of dissociation and assimilation. However, the labile-P concentrations were highest at sampling site 4 during July 2018. This highlighted the criticality of sampling frequency due to the fast-changing conditions particularly within the shallower locations.

6.2.4. Overarching hypothesis: The nutrient content of the water within the reservoir will increase following the reactivation of pumping from the river Usk and increase further following the rainfall event.

The EWE (Extreme Weather Event) data indicated the dry conditions during May 2018 through end July of 2018 led to an increase of organic-P throughout the majority of the reservoir, providing a source of nutrients for processes essential to primary productivity. Sediment labile-P concentrations were higher during the July sampling periods than during the April sampling periods on all sampling occasions, indicating conditions within the reservoir changing between the spring and mid summer in favour of increased internal P release (Jensen, *et al.*, 1992). However, organic-P was not detected following the reactivation of pumping or following the rainfall during the dry period in the presence of cyanobacteria and algae, indicating to an increased rate of mineralisation and assimilation in the bottom water where the majority of the cyanobacteria were detected.

In addition to nutrient availability increasing the risk of bottom primary productivity in the north of the reservoir, increased light attenuation may fuel bottom cyanobacterial development at the shallower sample site 4 (Karlsson *et al.*,2009). Conversely, increased

concentrations of organic material following a storm event in the shallower zone may reduce light penetration, decreasing the rate of primary productivity and increasing organic burial to the sediment (Tanabe *et al.,* 2019).

Following the rainfall event, OP concentrations diminished through the majority of the reservoir whereas condensed-P concentrations increased, particularly at the northern sites (sites 3 and 4), indicating to exhaustion of OP and a change to the pH from that prior to and following the activation of pumping and the rainfall events. The pH data indicated the northern sites (sites 3 and 4) were of an increased susceptibility to pH changes and were therefore more likely to experience hydrolysis of condensed-P to OP and its reversion than the southern sites, increasing the risk of primary productivity. The unpredictability of the response to the storm event at site 4 may increase the risk of water quality deterioration, decreasing the resilience of the reservoir to possible future climate change scenarios. Consequently, the overarching hypothesis can be accepted due to the increase in concentrations of some key nutrients (e.g., organic-P, sediment labile-P, ammonium) following the rainfall event.

6.2.4.1. Sub-hypothesis: Nitrate will be the dominant N-fraction throughout the reservoir during the drought period, but an increase of ammonium concentrations shall be recorded following a period of heavy rainfall, particularly at site 4.

Data analysis from the Extreme Weather Event (EWE) of 2018 (Chapter 5) suggested that nitrate concentrations were higher than ammonium concentrations during the drought, resulting in a high NO_3^-: NH_4^+ ratio and a negative nitrate: rainfall correlation, leading to acceptance of the sub-hypothesis. The raised nitrate concentrations relative to the ammonium is favoured by denitrifying and DNRA bacteria and nitrate can be assimilated by algae and cyanobacteria during a period of active growth. The nitrate: ammonium ratio decreased following the onset of the pumping and rainfall event as a consequence of nitrate concentration decrease and simultaneous ammonium concentration increase. The increase in ammonium concentrations following the EWE suggested that ammonium may have been carried into the reservoir via run-off through entrainment or released from the sediment as a consequence of stratification destabilisation by the inflow of colder water. Additionally, an inflow of nutrients during the pumping and rainfall events may have fuelled benthic primary

production of ammonifying bacteria, increasing the concentrations of ammonium and simultaneously decreasing the nitrate concentrations within the reservoir.

The data indicated an increased susceptibility of Llandegfedd reservoir to water quality degradation during the summer period in the event of reactivation of pumped inflow and summertime rainfall.

6.2.4.2. Sub-hypothesis: OP concentrations will increase as a consequence of both the active pumping and precipitation event specifically in the northern section (site 4) of the reservoir.

The concentrations of OP in the water samples during the drought period of 2018 (Chapter 5) were higher at the southern section (sites 1 and 2) relative to the northern section of the reservoir indicating to a higher risk of primary production at the southern sampling points and increased assimilation in the northern sites. In addition, the sediment surface samples of the northern sites recorded a decrease in the concentrations of Fe-P from April 2018 to July 2018, also suggesting that OP assimilation was greater at sites 3 and 4 than at sites 1 and 2, but the potential for cyanobacterial establishment remained higher due to continued nutrient availability at sites 1 and 2.

Ockenden *et al.,* (2016), researched the effect of climate change upon nutrient transfer in head-water catchments. It was determined that greater than 80% of the phosphorous within the water was derived from a terrestrial source, transported to the water entrained within run-off as a consequence of a period of heavy summertime rainfall. Therefore, it is likely that the increased P concentration was terrestrially derived. The water OP and condensed-P concentrations increased in the northern section (sites 3 and 4) of the reservoir following the activation of pumping during the drought period, indicating to OP and AHP input from a river source and potential sediment P release as a consequence of disturbance during inflow.

Nitrate may suppress internal loading through oxygenating the sediment. Lower P concentrations were determined during the drought period coinciding with higher nitrate concentrations relative to that following the activation of pumping and rainfall event. Nitrate concentrations decreased following the reactivation of pumping while both OP and cyanobacterial abundance increased. Ma *et al.,* (2021), researched the effect of nitrate concentrations upon internal sediment P release: nitrate may reduce sediment P release through providing oxygen to the sediment or promote sediment P release through fuelling cyanobacterial metabolism leading to oxygen depletion. Ma *et al.,* concluded that the P

release inhibition effect of nitrate decreased, while sediment P release increased under conditions of higher nitrate concentrations due to an increased rate of cyanobacterial metabolism (Søndergaard *et al.,* 2021). Therefore, the low P concentrations during the drought period may have been due to the high nitrate concentrations relative to that before the reactivation of pumping or the EWE.

Despite a further increase in the OP concentrations following the rainfall event, the reactivation of a pumped inflow had a more significant effect upon the OP concentrations than that recorded following the rainfall event, indicating to a greater risk of cyanobacterial establishment during summertime pumping than that anticipated as a consequence of summer-time rainfall following a period of drought. However, it is unknown whether a reversal in incidences (an EWE prior to reactivation of pumping during a drought period) would yield similar results. Sediment consisting of higher proportions of finer substrate undergoes sedimentation during the dry season (Tang *et al.,* 2016), when the proportion of sediment erosion is greater in areas subsurface relative to exposed banks. Sediment consisting predominantly of larger particles undergo sedimentation during the wet season (Tang *et al.,* 2016). Therefore, the forecasted longer periods of drier weather during the summer may increase the deposition of a finer substrate at the exposed periphery, resulting in decreased bank stability at the north of the reservoir (Odhiambo, 2014), and an increase in the volume of unstable sediment liable to redeposition during heavy deluges (Frey *et al.,* 2015).

The force of the water entering the reservoir at the northern banks during periods of active pumping has damaged the peripheral bank through visibly stripping vast quantities of sediment, continually exposing new sections of sediment. The exposed sediment may be actively carried into the reservoir with the flow of water. The finer sediment at the northern banks of the reservoir is more likely to be eroded by the water upon entry via the inflow (Odhiambo, 2014). Its resuspension may contribute to the majority of the phosphorous of a reservoir (Svendsen *et al*., 1993). A land devoid of foliage such as the exposed northern banks of Llandegfedd reservoir during periods of reduced volume may contribute more towards run-off volumes (Pope *et al.,* 2014).

A lower reservoir level during the July resulted in the northern section of the reservoir (sites 3 and 4) being immersed in shallower depths of water relative to periods of higher reservoir levels and were therefore more likely to be influenced by meteorological conditions than

deeper sites (Rydin, 2000). Shallower areas of the reservoir (site 4) had a higher risk of rainfall-generated run-off oxygenating the sediment layer and were more likely to be exposed to a higher pH (Wetzel, 2001)), potentially resulting in an increase in sediment-P dissolution (Hudon *et al.,* 2000; Wetzel, 2001) and condensed-P hydrolysis.

The increased rate of P assimilation as indicated by the sediment data coupled with raised OP concentrations following the resumption of inflows and a potential for an increased frequency of AHP hydrolysis as a consequence of meteorologically induced water pH changes may lead to an increase in bioavailable P. This may further fuel cyanobacterial establishment, particularly at site 4. Therefore, the sub-hypothesis can be accepted.

6.2.4.3. Sub-hypothesis: Cyanobacterial cell counts will increase in response to an inflow of nutrients.

The data obtained during the Extreme Weather Event (EWE) analysis of 2018 (Chapter 5) indicated that cyanobacteria became established at all four bottom regions following the onset of pumping, while the low concentration and infrequent occurrence of detectable geosmin relative to that prior to reactivation of pumped inflow suggested that cyanobacterial lysis as a consequence of increased turbidity did not occur. Therefore, the sub-hypothesis can be accepted.

High inflow volume as a consequence of heavy rainfall or active pumping may lead to a reduction in the variety and density of algal communities through increasing water turbidity, with cyanobacterial species capable of buoyancy control (Anabaena, Aphanizomenon and Microcystis) most likely to survive through the turbulent conditions (Karp-Boss *et al*. 1996).

Research by Vidal *et al*., (2011), focussed upon the significance of a river inflow upon the water quality of a reservoir. It was determined that the inflow of a river into a reservoir during the summer period instigated an algal bloom predominantly due to the nutritional concentrations as opposed to a consequence of sediment disturbance upon entry into the reservoir.

Geosmin production is most likely during/following periods of increased ammonium concentrations (Perkins *et al.,* 2019). Geosmin concentrations were high during the dry period relative to that following reactivation of the pumps suggesting recent cyanobacterial growth and senescence, and ammonium concentrations were low during the dry period relative to

concentrations following pump reactivation. Therefore, the decrease in geosmin predominantly in the bottom sites following the activation of pumped inflow have may have been due to an increase in ammonium within the reservoir at six of the eight sites providing a source of nutrients to sustain cyanobacterial growth. Consequently, the death phase of cyanobacteria during periods of lower ammonium as indicated by the detection of geosmin (during the dry period) may have been slowed by the increase ammonium concentrations, leading to a decrease in geosmin concentrations.

The increase in ammonium concentrations and concomitant decrease in the NO_3^-:NH_4^+ ratio during the reactivation of pumped inflow but prior to the rainfall event may have led to a rise in the number of cyanobacterial cells in the bottom waters of the reservoir. Water sampling following reactivation of the pumped inflow and the rainfall event may have detected the geosmin in the bottom waters released during the cyanobacterial death phase following a successful period of rapid growth. The decrease in ammonium concentrations across the bottom sites with the exception of site B4 (the bottom of the most northern sampling site) four days post rainfall event, coupled with an increase in the TN:TP ratio and geosmin may have been a consequence of the decrease in cyanobacterial cell numbers.

The data analyses indicated to the susceptibility of Llandegfedd reservoir to water quality deterioration during a period of drought and following an Extreme Weather Event. The drought period introduced opportunity for nitrate assimilation by algae and cyanobacteria while conversely, an increase in ammonium concentrations following the EWE increased the risk of a taste and odour event as a consequence of a lower NO_3^-:NH_4^+ ratio.

The increase in phosphorous and ammonium following the reactivation of active pumping and the rainfall event led to the acceptance of the overarching hypothesis. However, the biggest increases occurred following the reactivation of pumping. The data highlighted the importance of water quality sampling during/following an event leading to inflow into the reservoir, regardless of its source and the susceptibility of Llandegfedd reservoir to water quality deterioration under changing climatic conditions.

6.3 Recommendations for increasing the resilience of Llandegfedd Reservoir to the consequences of climate change and improving reservoir management.

Reservoirs are subject to seasonal and annual meteorological changes resulting in a dynamic algal and cyanobacterial population which may continue to evolve as a consequence of the progression of climate change. The nutrient concentration and balance within a reservoir are site dependent but are susceptible to change irrespective of its location. Climate change is anticipated to be a global event therefore, all reservoirs are at risk of a deteriorating water quality due to drier, warmer summers interspersed with more frequent extreme weather events. The consequential deterioration in water quality will be dependent upon the resilience of the reservoir to changes induced by climate change. Resilience to change will be dependent upon the individual characteristics of the reservoir including its location and catchment characteristics, geology, nutrient dynamics and management.

Based on the Llandegfedd reservoir data analyses completed within this thesis, I would recommend the following steps to increase reservoir resilience to water quality deterioration as a consequence of the predicted climate change:

- The data of historically abstracted water cannot be used as a reliable indicator of past climate change due to the change in the abstraction method. The analysis of reservoir water quality can indicate a risk of deterioration and the depth at which the sample was abstracted contributes of the water analysed contributes towards understanding the risk to water quality degradation. The depth at which the water was abstracted (surface, middle or bottom water) pre-2000 (before the gate selection failure) was not recorded. Therefore, water quality data cannot be assigned to a specific depth. Data collected post-2000 was not representative of water quality of a specified depth due to mixing of the water prior to analysis. Therefore, it is recommended that the gate selection facility within the abstraction tower is repaired and the depth at which abstraction occurs are recorded in order to obtain real time water quality data at a specified depth within the water column at the point of abstraction.
- Nutrients may travel southwards from the inflow, increasing the risk of cyanobacterial establishment along the transect of the reservoir. The influence of the nutrients and water quality upon the southern section of the reservoir decrease with increasing distance from the northern banks (Howell *et al.,* 2014). Therefore, changes to the water quality at sites 3 and 4 favouring cyanobacterial and algal development

resulting in the production of taste and odour metabolites may negatively influence water quality along the length of the reservoir (Yurista *et al*., 2012), particularly during periods of drought, but may not be detected by the existing water quality monitoring method within the abstraction tower at the most southern point of the reservoir. Regular water sampling at the surface, middle and bottom of the water column along the transect of the reservoir would be recommended to improve understanding of the characteristics specific to Llandegfedd Reservoir. This would improve reservoir management through obtaining sufficient data that may lead to the development of predictive models based on real-time depth-related sampling. Also, regular real-time monitoring along the transect of the reservoir may lead to improved water treatment processes through the early detection of conditions indicative of the potential for metabolite production and eventually taste and odour degradation within the abstracted water.

- Conditions within the sediment are transient and require frequent ongoing sediment sampling and analysis in order to understand P-fraction concentrations, changes and dissemination risks at various locations throughout the reservoir throughout the seasons. In addition to improving the understanding of real-time water quality risks within the reservoir, data obtained from regular sediment sampling and analysis may contribute towards the development of a prediction model, enabling DCWW to anticipate periods of increased P-dissemination risks and identify sections within the reservoir that may pose the highest risk of cyanobacterial or algal activity. This may lead to the early detection of conditions indicative of a higher taste and odour risk.
- Sediment disturbance increases the risk of nutrient release to the reservoir during periods of extreme weather events or as a consequence of turbulence during active pumping. The placement of large granite boulders (Figure 6.3.1) along the inflow path of the reservoir may decrease the severity of sediment disturbance and bank erosion while helping to retain the inflow bank structure during a period of active pumping. Increasing the inflow path bank stability may decrease the volume of nutrients released to the reservoir resulting from sediment disturbance and reduce the rate of bank erosion, helping to maintain the integrity of the reservoir.

Figure 6.3.1. Example of granite boulders placed to protect unstable banking from erosion (Alamy stock photo).

- The consequence of an influx of nutrients during/following a period of increased run-off from rainfall is a factor that should be anticipated when designing and maintaining a reservoir (Howell *et al.,* 2014). Where the reservoir design cannot be altered to mitigate run-off volumes, increased sampling frequencies of the higher risk section (sampling site 4) would be advised, which would allow reservoir management to be aware of periods of increased nutrient input in real-time. This would contribute towards more efficient reservoir management regimes and more accurate data for predictive modelling to help better predict situations that may lead to water quality deterioration.
- Extreme weather events increase the risk of taste and odour metabolite production through decreasing the NO_3^-: NH_4^+ ratio. The development of an effective model to predict periods of increased taste and odour risks would require a flexible reservoir management programme incorporating the ability to adjust sampling frequency as defined by the season and meteorological forecast. Increasing the sampling frequency would decrease the risk of taste and odour customer complaints through allowing early detection of the conditions which may lead to cyanobacterial metabolite production. Consequently, the Water Treatment Works would optimise the treatment process to the changing water conditions.

6.4 Overarching Conclusion

Data obtained from the analysis of abstracted water at Llandegfedd reservoir tower is not suitable for the analysis of historical climate change. The inability to actively select the gate through which to abstract the water for treatment decreases the water quality entering the treatment works. This may potentially lead to costly treatment processes, an increase in the volume of chemicals used in the treatment process and a higher rate of process disruption due to an increased frequency of filter blinding (blocking).

Phosphorous concentrations at Llandegfedd reservoir varied with the season and were low throughout the reservoir over the 11-month sampling period relative to that of TN. The greatest risk of cyanobacterial blooms within the reservoir with respect to phosphorous concentrations was recorded during May, where the water quality was deemed to be 'bad' as a consequence of phosphorous concentrations (UKTAG, 2016).

Potentially bioavailable-P (AHP) was the dominant P-fraction over the 11-month sampling period and was particularly high relative to OP and organic-P fractions during February and early summer of 2018. However, an increase in pH throughout the reservoir during the spring and summer period, likely as a consequence of primary productivity, had the potential to lead to the hydrolysis of condensed-P to OP, further fuelling cyanobacterial activity throughout the summer. The northern section of the reservoir (sampling sites 3 and 4) was at a higher risk of algae and cyanobacterial development due to an increased risk of OP availability relative to the southern section through a higher concentration of AHP and a varied pH distribution following a period of pumping and rainfall (Hudon *et al.,* 2000).

The sediment Fe-P: Ca-P ratio suggested that site 4 retained a eutrophic status during July 2018 and the site least likely to bind P to the sediment, while simultaneously most likely to have P dissociate. Mass balance analysis during April 2018 indicated to very little P being released from the sediment throughout the reservoir indicating low benthic cyanobacterial activity. Likewise, despite a low volume of internal P release during the summer, the data indicated to internal P release as not being a high risk at Llandegfedd reservoir during 2018, with the reservoir displaying oligotrophic characteristics. Therefore, P was the limiting nutrient at Llandegfedd reservoir.

P-fraction data obtained during the analysis of the effect of drought and inflow upon water quality (Chapter 5) indicated a susceptibility of Llandegfedd reservoir to changes in the dominant P-fractions and distributions throughout the water column and along its transect

as a consequence of nutrient inflow, changes to water pH and microbial senescence during an extreme weather event (EWE). Therefore, extreme weather conditions are likely to lead to water quality deterioration within Llandegfedd reservoir.

A reduction in rainfall frequency through the summer period may increase nitrate concentrations within the reservoir, fuelling algal and cyanobacterial growth and potentially increasing internal P release. Therefore, periods of heavy rainfall during the summer periods, particularly following a period of warm, dry weather, may require an increased rate of water quality monitoring in order to determine whether conditions are more likely to lead to geosmin production as a consequence of a lower NO_3^-:NH_4^+ ratio.

With the current water quality monitoring process retained to the abstraction tower, there is a risk of water quality deterioration within the reservoir going unnoticed until poor water quality is abstracted for treatment. Llandegfedd reservoir is susceptible to changes in the nutrient balance with conditions favouring cyanobacterial establishment as climate change progresses. A reservoir management programme incorporating regular sampling along the transect and through the water column of the reservoir and flexible sampling regimes would improve awareness of decreasing water quality prior to its abstraction, enabling DCWW to optimise treatment processes. Also, catchment management would decrease the risk of allochthonous nutrient transport, limiting water quality deterioration as climate change progresses.

6.5 Further research

6.5.1. Variables affecting water quality not discussed in this thesis.

The reservoir characteristics are not solely bound to the characteristics within the reservoir periphery. The frequent fluctuation of the reservoir level constantly expands and contracts the volume of the internal environment, resulting in variations in nutrient and organism contributions to the reservoir dynamics.

Additionally, the transport of nutrients and organisms from surrounding land during run-off, and anthropological manipulation of the land and interactions with the reservoir through water sport activities have the potential to introduce invasive species to the reservoir which may have a negative impact on overall water quality.

Analysis of a limited dataset obtained following the tower malfunction event indicated a downward trend in phosphorous concentrations between 2008 and 2012, suggesting that

either the source of phosphorous or its sink had been altered. However, the data was bias to the representation of phosphorous concentrations in the bottom water due to the mode of water abstraction and water quality data collection. In addition, the low frequency of significant associations between nutrients and the environmental factors analysed indicated other significant variables affecting the nutrient concentrations and distribution that were not analysed.

References.

Adam, B., Klawonn, I., Sveden, J. B., Bergkvist, J., Nahar, N., Walve, J., Ploug, H. 2016. N2-fixation, ammonium release and N-transfer to the microbial and classical food web within a plankton community. ISME J, 10(2), 450-459. doi:10.1038/ismej.2015.126

Adrian, R., O'Reilly, C. M., Zagaese, H., Baines, S. B., Hessen, D. O., Keller, W., Livingstone, D. M., Sommuraga, R., Straile, D., Van Donk, E., Weyhenmever, G. A., Winder, M. 2009. Lakes as sentinels of climate change. Association for the Sciences of Limnology and Oceanography 54(6). Pp 2283-2297.

Allen, J. F., Thake, B., Martin, W. F. 2019. Nitrogenase Inhibition Limited Oxygenation of Earth's Proterozoic Atmosphere. Trends Plant Sci, 24(11), 1022-1031. doi:10.1016/j.tplants.2019.07.007

Allhoff, K. T., Drossel, B. 2016. Biodiversity and ecosystem functioning in evolving food webs. Philos Trans R Soc Lond B Biol Sci, 371(1694). doi:10.1098/rstb.2015.0281

Amirkhani, M., Bozorg-Haddad, O., Fallah-Mehdipour, F., Loáiciga, A. 2016. Multi objective reservoir operation for water quality optimization. Journal of irrigation and drainage Engineering. Vol. 142:12.

Ammar, R., Kazpard, V., El Samrani, A. G., Amacha, N., Saad, Z., Chou, L. 2017. Hydrodynamic influence on reservoir sustainability in semi-arid climate: A physicochemical and environmental isotopic study. J Environmental Management, 197, 571-581. doi:10.1016/j.jenvman.2017.04.030

An, S., Gardner, W. S. 2002. Dissimilatory nitrate reduction to ammonium (DNRA) as a nitrogen link, versus denitrification as a sink in a shallow estuary (Laguna Madre/Baffin Bay, Texas). MEPS. 237; 41-50.

Ahn, C, Y., Oh, H. M., Park, Y. S. 2011. Evaluation of environmental factors on cyanobacterial bloom in eutrophic reservoir using neural networks. 47 (3). pp495-503.

Anneville, O., Souissi, S., Ibanez, F., Ginot, V., Druart, J. C., & Angeli, N. (2002). Temporal mapping of phytoplankton assemblages in Lake Geneva: Annual and interannual changes in their patterns of succession. *Limnology and* Oceanography, **47**, 1355– 1366.

Arnell, N. W., Reynard, N. S. 1996. The effects of climate change due to global warming on river flows in Great Britain. Journal of Hydrology. 183:397-424

Arce, M, I., Schiller, D. V., Bengtsson, M. M., Hinze, C., Chung, H., Alves., J. E., Urich, T., Singer, G. 2018. Drying and Rainfall Shape the Structure and Functioning of Nitrifying Microbial Communities in Riverbed Sediments. Frontiers in Microbiology.

Atkins, R., Rose, T., Brown, R. S., Robb, M. 2001. The Microcystis cyanobacteria bloom in the Swan River-February 2000. Water Science Technology, 43(9), 107-114.

Arnott, D.L., Vanni, M.J., 1996. Nitrogen and phosphorus recycling by the zebra mussel (*Dreissena polymorpha*) in the western basin of Lake Erie. Can. J. Fish. Aquatic Science 659, 646–659.

Auer, M.T., Tomlinson, L.M., Higgins, S.N., Malkin, S.Y., Howell, E.T., Bootsma, H.A., 2010. Great Lakes Cladophora in the 21st century: same algae—different ecosystem. Journal of Great Lakes Researsh. 36:248–255. https://doi.org/10.1016/j.jglr.2010.03.001.

Azadi, F., Ashofteh, P., Loáiciga, H. A. 2018. Reservoir water quality projections under Climate Change Conditions. Water resource management. 33, 401-421.

Baltar, F., De Corte, D., Yokokawa, T. 2019. Bacterial Stress and Mortality may be a Source of Cell-free Enzymatic Activity in the Marine Environment. Microbes in Environment, 34(1), 83-88. doi:10.1264/jsme2.ME18123

Baptista, M. S., Vasconcelos, M. T. 2006. Cyanobacteria metal interactions: requirements, toxicity, and ecological implications. Crit Rev Microbiol, 32(3), 127-137. doi:10.1080/10408410600822934

Barnum, T. R., Drake, J. M., Colon-Gaud, C., Rugenski, A. T., Frauendorf, T. C., Connelly, S., Pringle, C. M. 2015. Evidence for the persistence of food web structure after amphibian extirpation in a Neotropical stream. Ecology, 96(8), 2106-2116. doi:10.1890/14-1526.1

Bar-Yosef, Y., Sukenik, A., Hadas, O., Viner-Mozzini, Y., Kaplan, A. 2010. Enslavement in the water body by toxic *Aphanizomenon ovalisporum*, inducing alkaline phosphatase in phytoplanktons. Current Biology 20, 1557–1561.

Beale, C. M., Burfield, I. J., Sim, I. M., Rebecca, G. W., Pearce-Higgins, J. W., Grant, M. C. 2006. Climate change may account for the decline in British ring ouzels *Turdus torquatus*. J Animal Ecology, 75(3), 826-835. doi:10.1111/j.1365-2656.2006.01102.

Beutel, M.W. 2003. Hypolimnetic anoxia and sediment oxygen demand in California drinking water reservoirs. Lake. Reserv. Manage. 19, 208–221.

Binhe, G., Alexander, V. 1987. Dissolved nitrogen uptake by cyanobacterial bloom (*Anabaena flo-aquae*) in a subarctic lake. Applied and environmental biology, pp 422-430.

Black, E., Brayshaw, D. J., Rambeau, C. M. 2010. Past, present and future precipitation in the Middle East: insights from models and observations. Philos Trans A Math Phys Eng Sci, 368(1931), 5173-5184. doi:10.1098/rsta.2010.0199

Blevins, W. T., Schrader, K. K., Saadoun, I. 1995. Comparative physiology of geosmin production by *Streptomyces-halstedii* and *Anabaena* Sp. Water Sci. Technol. 31, 127–133.

Bloomfield, J. P., Williams, R. J., Gooddy, D. C., Cape, J. N., Guha, P. 2006. Impacts of climate change on the fate and behaviour of pesticides in surface and groundwater--A UK perspective. Sci Total Environ, 369(1-3), 163-177. doi:10.1016/j.scitotenv.2006.05.019

Boechat, I. G., Giani, A. 2000. Factors affecting biochemical composition of seston in an eutrophic reservoir (Pampulha Reservoir, Belo Horizonte, MG). Rev Bras Biol, 60(1), 63-71.

Bonito, G., Benucci, G. M. N., Hameed, K., Weighill, D., Jones, P., Chen, K. H., Vilgalys, R. 2019. Fungal-Bacterial Networks in the Populus Rhizobiome Are Impacted by Soil Properties and Host Genotype. Front Microbiol, 10, 481. doi:10.3389/fmicb.2019.00481

Bowman, J, J. McGarrigle, M, L., Clabby, K. J. 1993. Lough Derg. An investigation of eutrophication and its causes. Environmental research unit, Dublin.

Bozdogan, H. Model selection and Akaike's Information Criterion (AIC): The general theory and its analytical extensions. Psychometrika, 52: 345-370.

Briland, J. F., Jacquet, S., Flinois, C., Avois-Jacquet, C., Maisonnette, C., Leberre, B., Humbert, J. F. 2005. Variations in the microcystin production of *Planktothrix rubescens* (cyanobacteria) assessed from a four-year survey of Lac du Bourget (France) and from laboratory experiments. Microb Ecol, 50(3), 418-428. doi:10.1007/s00248-005-0186-z

Bullerjahn, G. S., McKay, R. M., Davis, T. W., Baker, D. B., Boyer, G. L., D'Anglada, L. V., Wilhelm, S. W. 2016. Global solutions to regional problems: Collecting global expertise to address the problem of harmful cyanobacterial blooms. A Lake Erie case study. Harmful Algae, 54, 223-238. doi:10.1016/j.hal.2016.01.003

Briland, R. D., Stone, J. P., Manubolu, M., Lee, J., Ludsin, S. A. 2020. Cyanobacterial blooms modify food web structure and interactions in western Lake Erie. Harmful Algae, 92, 101586. doi:10.1016/j.hal.2019.03.004

Burdon, F. J., McIntosh, A. R., Harding, J. S. 2020. Mechanisms of trophic niche compression: Evidence from landscape disturbance. J Anim Ecol, 89(3), 730-744. doi:10.1111/1365-2656.13142

Burford, M. A., Davis, T. W., Orr, P. T., Sinha, R., Willis, A., Neilan, B. A. 2014. Nutrient-related changes in the toxicity of field blooms of the cyanobacterium, *Cylindrospermopsis raciborskii*. FEMS Microbiol Ecol, 89(1), 135-148. doi:10.1111/1574-6941.12341

Cao, X., Wang, Y., He, J., Luo, X., & Zheng, Z. (2016). Phosphorus mobility among sediments, water and cyanobacteria enhanced by cyanobacteria blooms in eutrophic Lake Dianchi. *Environ Pollut, 219*, 580-587. doi:10.1016/j.envpol.2016.06.017

Carpenter, S, R., Caraco, N. F., Corell, D. L., Howarth, R. W., Sharpley, A. N., Smith, V. H. 1998. Nonpoint pollution of surface water with phosphorous and nitrogen. Ecol.Applic. 8:559-568.

Camargo, J. A., Alonso, A. 2006. Ecological and toxicological effects of inorganic nitrogen pollution in aquatic ecosystems: A global assessment. Environ Int, 32(6), 831-849. doi:10.1016/j.envint.2006.05.002

Cangelosi, R., Goriely, A. 2007. Component retention in principal component analysis with application to cDNA microarray data. Biol. Direct. 2:2. doi: 10.1186/1745-6150-2-2

Cao, X., Wang, Y., He, J., Luo, X., Zheng, Z. 2016. Phosphorus mobility among sediments, water and cyanobacteria enhanced by cyanobacteria blooms in eutrophic Lake Dianchi. Environ Pollut, 219, 580-587. doi:10.1016/j.envpol.2016.06.017

Carman, R., Edlund, G., Damberg, C. 2000. Distribution of organic and inorganic phosphorus compounds in marine and lacustrine sediments: A 31P NMR study. Chem. Geol. 163: 101–114.

Carr, M. K., Sadeghian, A., Lindenschmidt, K. E., Rinke, K., Morales-Marin, L. 2020. Impacts of Varying Dam Outflow Elevations on Water Temperature, Dissolved Oxygen, and Nutrient Distributions in a Large Prairie Reservoir. Environ Eng Sci, 37(1), 78-97. doi:10.1089/ees.2019.0146

Carey, C. C., Ibelings, B. W., Hoffmann, E. P., Hamilton, D. P., Brookes, J. D. 2012. Eco-physiological adaptations that favour freshwater cyanobacteria in a changing climate. Water Res, 46(5), 1394-1407. doi:10.1016/j.watres.2011.12.016

Carvalho, L., Miller nee Ferguson, C. A., Scott, E. M., Codd, G. A., Davies, P. S., Tyler, A. N. 2011. Cyanobacterial blooms: statistical models describing risk factors for national-scale lake assessment and lake management. Sci Total Environ, 409(24), 5353-5358. doi:10.1016/j.scitotenv.2011.09.030

Cavanaugh, J. C., Richardson, W. B., Strauss, E. A., Bartsch, L. A. 2006. Nitrogen dynamics in sediment during water level manipulation on the Upper Mississippi River. River Research and Applications, 22(6), 651-666. doi:10.1002/rra.926

Cavanaugh, J. E., Neath, A. A. 2019. The Akaike Information Criterion: Background, derivation, properties, application, interpretation and refinements. WIREs, 3:11.

Chen, N., Mo, Q., Kuo, Y. M., Su, Y., Zhong, Y. 2018. Hydrochemical controls on reservoir nutrient and phytoplankton dynamics under storms. Sci Total Environ, 619-620, 301-310. doi:10.1016/j.scitotenv.2017.09.216

Cheng, W. P., Chi, F. H. 2003. Influence of eutrophication on the coagulation efficiency in reservoir water. Chemosphere, 53(7), 773-778. doi:10.1016/S0045-6535(03)00510-1

Chien, Y. C., Wu, S. C., Wu, J. T. 2009. Identification of physical parameters controlling the dominance of algal species in a subtropical reservoir. Water Sci Technol, 60(7), 1779-1786. doi:10.2166/wst.2009.541

Chu, Z., Jin, X., Yang, B., Zeng, Q. Buoyancy regulation of *Microcystis flosaquae* during phosphorus-limited and nitrogen-limited growth. J Plankton Res. 2007; 29(9):739–745

Clercin, N. A., Druschel, G. K. 2019. Influence of Environmental Factors on the Production of MIB and Geosmin Metabolites by Bacteria in a Eutrophic Reservoir. Water Resources research. 55:7. 5413-5430.

Cooney, E. M., McKinney, P., Sterner, R., Small, G. E., Minor, E. C. 2018. Tale of Two Storms: Impact of Extreme Rain Events on the Biogeochemistry of Lake Superior. Vol 123:5. pp1719-1731.

Cooper, C. M. 1993. Biological Effects of Agriculturally Derived Surface Water Pollutants on Aquatic Systems—A Review. Journal of Environmental Quality, 22(3), 402-408. doi:10.2134/jeq1993.00472425002200030003x

Correll, D. L. 1998. The role of phosphorous in the eutrophication of receiving waters: A review. Journal of Envrion. Qual. 27: 261-266.

Crossetti, L. O., Bicudo, D. C., Bicudo, C. E., Bini, L. M. 2008. Phytoplankton biodiversity changes in a shallow tropical reservoir during the hypertrophication process. Braz J Biol, 68(4 Suppl), 1061-1067.

Dabrowski, J., Baldwin, D. S., Dabrowski, J. M., Hill, L., Shadung, J. 2017. Impact of temporary desiccation on the mobility of nutrients and metals from sediments of Loskop Reservoir, Olifants River. Water SA, 43(1). doi:10.4314/wsa.v43i1.02

Dalu, T., Wasserman, R. J. 2018. Cyanobacteria dynamics in a small tropical reservoir: Understanding spatio-temporal variability and influence of environmental variables. Sci Total Environ, 643, 835-841. doi:10.1016/j.scitotenv.2018.06.256

Davies, J.-M., Hecky, R.E., 2005. Initial measurements of bottom photosynthesis and respiration in Lake Erie. J. Great Lakes Res. 31:195–207. https://doi.org/10.1016/S0380- 1330(05)70314-2.

Dolman, A. M., Rucker, J., Pick, F. R., Fastner, J., Rohrlack, T., Mischke, U., Wiedner, C. 2012. Cyanobacteria and cyanotoxins: the influence of nitrogen versus phosphorus. PLoS One, 7(6), e38757. doi:10.1371/journal.pone.0038757

Dong, C. Y., Yu, Z. M., Wu, Z. X., Wu, C. J. 2013. Study on seasonal characteristics of thermal stratification in lacustrine zone of Lake Qiandao. Huan Jing Ke Xue, 34(7), 2574-2581.

Dorado, S., Booe, T., Steichen, J., McInnes, A. S., Windham, R., Shepard, A., Quigg, A. 2015. Towards an Understanding of the Interactions between Freshwater Inflows and Phytoplankton Communities in a Subtropical Estuary in the Gulf of Mexico. PLoS One, 10(7), e0130931. doi:10.1371/journal.pone.0130931

Drath, M., Kloft, N., Batschauer, A., Marin, K., Novak, J., Forchhammer, K. (2008). Ammonia triggers photodamage of photosystem II in the cyanobacterium Synechocystis sp. strain PCC 6803. Plant Physiol, 147(1), 206-215. doi:10.1104/pp.108.117218

Eggleton, J., Thomas, K. V. 2004. A review of factors affecting the release and bioavailability of contaminants during sediment disturbance events. Environment International, 30(7), 973-980. doi:https://doi.org/10.1016/j.envint.2004.03.001

Elosegi, A., Sabater, S. 2013. Effects of hydromorphological impacts on river ecosystem functioning: a review and suggestions for assessing ecological impacts. Hydrobiologia 712, 129–143.

Espinosa, C., Abril, M., Gausch, H., Pou, N., Proia, L., Ricart, M., Ordeix, M., Llenas, L. 2020. Water Flow and Light Availability Influence on Intracellular Geosmin Production in River Biofilms. Aquatic Microbiology.

Feng, W., Wu, F., He, Z., Song, F., Zhu, Y., Giesy, J. P., Sun, F. 2018. Simulated bioavailability of phosphorus from aquatic macrophytes and phytoplankton by aqueous suspension and incubation with alkaline phosphatase. Sci Total Environ, 616-617, 1431-1439. doi:10.1016/j.scitotenv.2017.10.172

Forsberg, C. 1989. Importance of sediments in understanding nutrient cycling in lakes. Hydrobiologia, 176(177), 263–277.

Francis, C. A., Beman, J. M., Kuypers, M. M. M. 2007. New processes and players in the nitrogen cycle: the microbial ecology of anaerobic and archaeal ammonia oxidation. The ISME Journal 1: 19-27

Frey, K. E., Smith, L. C. 2005. Amplified carbon release from vast West Siberian peatlands by 2100. Geophys. Res. Lett. 32, 1–4.

Fu, X.; Zhang, L.; Wang, X. 2016. The effect of slope length on sediment yield by rainfall impact under different land use types. Water Resour. 43, 478–485.

Ghaffar, S., Stevenson, R. J., & Khan, Z. 2017. Effect of phosphorus stress on *Microcystis aeruginosa* growth and phosphorus uptake. PLoS One, 12(3), e0174349. doi:10.1371/journal.pone.0174349

Gillett, N. P. 2005. Climate modelling: Northern Hemisphere circulation. Nature, 437(7058), 496. doi:10.1038/437496a

Golshan, A., Evans, C., Geary, P., Morrow, A., Maeder, M., Tauler, R. 2020. Patterns of cyanobacterial abundance in a major drinking water reservoir: what 3 years of comprehensive monitoring data reveals? Environ Monit Assess, 192(2), 113. doi:10.1007/s10661-020-8090-z

Gomes, L. N., Oliveira, S. M., Giani, A., von Sperling, E. 2012. Association between biotic and abiotic parameters and the occurrence of cyanobacteria in a Brazilian reservoir. Environ Monit Assess, 184(8), 4635-4645. doi:10.1007/s10661-011-2291-4

Gomez, E., Durillon, C., Rofes, G. Picot, B. 1999. Phosphate adsorption and release from sediments of brackish lagoons: pH, O_2 and loading influence. Water Research,33, 2437– 2447.

Gonsiorczyk, T., Casper, P., Koschel, R. 1998. Phosphorus-binding forms in the sediment of an oligotrophic and a eutrophic hardwater lake of the Baltic Lake District (Germany). Water science and Technology. 37:3; 51-58.

Gonzalez-Piana, M., Piccardo, A., Ferrer, C., Brena, B., Pirez, M., Fabian, D., Chalar, G. 2018. Effects of Wind Mixing in a Stratified Water Column on Toxic Cyanobacteria and Microcystin-LR Distribution in a Subtropical Reservoir. Bull Environ Contam Toxicol, 101(5), 611-616. doi:10.1007/s00128-018-2446-x

Grant, W. E., Pedersen, E. K., Marin, S. L. 1997. Ecology and natural resource management: Systems analysis and simulation, 373Chichester, (GB)

Grey, M., Henry, C. 2002. Phosphorus and nitrogen runoff from a forested watershed fertilized with biosolids. J Environ Qual, 31(3), 926-936. doi:10.2134/jeq2002.9260

Guedes, I. A., Pacheco, A. B. F., Vilar, M. C. P., Mello, M. M., Marinho, M. M., Lurling, M., Azevedo, S. 2019. Intraspecific variability in response to phosphorus depleted conditions in the cyanobacteria *Microcystis aeruginosa* and *Raphidiopsis raciborskii*. Harmful Algae, 86, 96-105. doi:10.1016/j.hal.2019.03.006

Haaland, S., Hongve, D., Laudon, H., Riise, G., Vogt, R. D. 2010. Quantifying the Drivers of the Increasing Coloured Organic Matter in Boreal Surface Waters. Environ. Sci. Technol. 44, 2975–2980

Hafeez, F., Zafar, N., Nazir, R., Javeed, H. M. R., Rizwan, M., Faridullah, Iqbal, A. 2019. Assessment of flood-induced changes in soil heavy metal and nutrient status in Rajanpur, Pakistan. Environ Monit Assess, 191(4), 234. doi:10.1007/s10661-019-7371-x

Haggard, B.E., Stanley, E.H., Storm, D.E., 2005. Nutrient retention in a point-source enriched stream. J. North Am. Benthol. Soc. 24, 29–47.

Harold, F. M. 1962. Depletion and replenishment of the inorganic polyphosphate pool in Neurospora crassa. J Bacteriol, 83, 1047-1057.

Harris, T., Smith, V., Graham, J., Van de Waal, D., Tedesco, L., Clercin, N. 2016. Combined effects of nitrogen to phosphorus and nitrate to ammonia ratios on cyanobacterial metabolite concentrations in eutrophic Midwestern USA reservoirs. Inland Waters, 6(2), 199-210. doi:10.5268/iw-6.2.938

He, Z., Olk, D. C., Cade-Menun, B. J. 2011. Forms and lability of phosphorus in humic acid fractions of Hord silt loam soil. Soil Science Society of America, 75; pp. 1712-1722

Hecky, R., Smith, R.E.H., Barton, D.R., Guildford, S.J., Taylor, W.D., Charlton, M.N., Howell, E. T. 2004. The nearshore phosphorus shunt: a consequence of ecosystem engineering by *dreissenids* in the Laurentian Great Lakes. Can. J. Fish. Aquat. Sci. 1293:1285–1293. https://doi.org/10.1139/F04-065.

Heron, J. 1960. The seasonal variation of phosphate, silicate and nitrate in waters of the English Lake District. Freshwater Biological association. 338-345.

Higgins, S.N., Hecky, R.E., Guildford, S.J., 2006. Environmental controls of Cladophora growth dynamics in eastern Lake Erie: application of the Cladophora growth model (CGM). J. Great Lakes Res. 32:629–644. https://doi.org/10.3394/0380-1330(2006)32.

Higgins, S.N., Malkin, S.Y., Todd Howell, E., Guildford, S.J., Campbell, L., Hiriart-Baer, V., Hecky, R.E., 2008. An ecological review of *Cladophora glomerata* (Chlorophyta) in the Laurentian Great Lakes. J. Phycol. 44:839–854. https://doi.org/10.1111/j.1529-8817.2008.00538.x.

Higgins, S.N., Pennuto, C.M., Howell, E.T., Lewis, T.W., Makarewicz, J.C., 2012. Urban influences on Cladophora blooms in Lake Ontario. J. Great Lakes Res. 38:116–123. https:// doi.org/10.1016/j.jglr.2011.11.017.

Horst, G. P., Sarnelle, O., White, J. D., Hamilton, S. K., Kaul, R. B., Bressie, J. D. 2014. Nitrogen availability increases the toxin quota of a harmful cyanobacterium, *Microcystis aeruginosa.* Water Res, 54, 188-198. doi:10.1016/j.watres.2014.01.063

Hou, D., He, J., Lu, C., Sun, Y., Zhang, F., Otgonbayar, K. 2013. Effects of environmental factors on nutrients release at sediment-water interface and assessment of trophic status for a typical shallow lake, northwest China. Scientific World Journal, 716342. doi:10.1155/2013/716342

Huang, T., Li, X., Rijnaarts, H., Grotenhuis, T., Ma, W., Sun, X., Xu, J. 2014. Effects of storm runoff on the thermal regime and water quality of a deep, stratified reservoir in a temperate monsoon zone, in Northwest China. Sci Total Environ, 485-486, 820-827. doi:10.1016/j.scitotenv.2014.01.008

Howell, J. 2010. The distribution of phosphorous within sediment and water downstream from a sewage treatment works. Bioscience Horizons. 2:3. Pages 112-123.

Howell, E.T., Barton, D.R., Fietsch, C.-L., Kaltenecker, G., 2014. Fine-scale nutrient enrichment and water quality on the rural shores of Southeast Lake Huron. J. Great Lakes Res. 40:126–140. https://doi.org/10.1016/j.jglr.2013.12.009.

Hou, D., He, J., Lu, C., Sun, Y., Zhang, F., & Otgonbayar, K. (2013). Effects of environmental factors on nutrients release at sediment-water interface and assessment of trophic status for a typical shallow lake, northwest China. *ScientificWorldJournal, 2013*, 716342. doi:10.1155/2013/716342

Huang, Q., Wang, Z., Wang, C., Wang, S., Jin, X. 2015. Phosphorous release in response to pH variation in the lake sediments with different ratios of iron-bound P to calcium-bound P. Chemical speciation and Bioavailability. 17:2, 55-61.

Hudon, C., Lalonde, S., Gagnon, P., 2000. Ranking the effects of site exposure, plant growth form, water depth, and transparency on aquatic plant biomass. Can. J. Fish. Aquat. Sci. 57:31–42. https://doi.org/10.1139/f99-232

Hupfer, M., Ruübe, B., Schmeider, P. 2004. Origin and diagenesis of polyphosphate in lake sediments: A 31P‡NMR study. Limnology and Oceanography. Vol 49; 1. pp1-10.

IPCC (2014). Climate Change 2014: Synthesis Report: Contribution of Working Groups I, II and III to the Fifth Assessment Report of the Intergovernmental Panel on Climate Change [Core Writing Team], eds R.K. Pachauri and L.A. Meyer. Geneva: IPCC, 151.

Isidorova, A., Bravo, A. G., Riise, G., Bouchait, s., Björn, E. S., Sobek, S. 2016. The effect of lake browning and respiration mode on the burial and fate of carbon in the sediment of two boreal lakes. Journal of Geophysical Research: Bio-geosciences 121: 233–245

Isidorova, A., Mendonca, R., Sobek, S. 2019. Reduced Mineralization of Terrestrial OC in Anoxic Sediment Suggests Enhanced Burial Efficiency in Reservoirs Compared to Other Depositional Environments. J Geophys Res Biogeosci, 124(3), 678-688. doi:10.1029/2018JG004823

Jacobson L, Halmann M. Polyphosphate metabolism in the blue-green alga *Microcystis aeruginosa*. J Plankton Res. 1982; 4(3):481–488

Jensen, H. S., Andersen, F. Ø. 1992. Importance of temperature, nitrate, and pH for phosphate release from aerobic sediments of four shallow, eutrophic lakes. Limnol. Oceanogr. 37: 577–589.

Jensen, H. S., Kristensen, P., Jeppesen, E., Skytthe, A. 1992. Iron:phosphorus ratio in surface sediment as an indicator of phosphate release from aerobic sediments in shallow lakes. Hydrobiologia, 235(1), 731-743. doi:10.1007/bf00026261

Jeppesen, E., Kronvang, B., Meerhoff, M., Sondergaard, M., Hansen, K. M., Andersen, H. E., Olesen, J. E. 2009. Climate change effects on runoff, catchment phosphorus loading and lake ecological state, and potential adaptations. J Environ Qual, 38(5), 1930-1941. doi:10.2134/jeq2008.0113

Jiang, Z., Liu, J., Chen, J., Chen, Q., Yan, X., Xuan, J., Zeng, J. 2014. Responses of summer phytoplankton community to drastic environmental changes in the Changjiang (Yangtze River) estuary during the past 50 years. Water Res, 54, 1-11. doi:10.1016/j.watres.2014.01.032

Jin, J., Wells, S. A., Liu, D., Yang, G., Zhu, S., Ma, J., Yang, Z. 2019. Effects of water level fluctuation on thermal stratification in a typical tributary bay of Three Gorges Reservoir, China. PeerJ, 7, e6925. doi:10.7717/peerj.6925

Jüttner, F., Watson, S. B. 2007. Biochemical and ecological control of geosmin and 2-Methylisoborneol in source waters. Appl. Environ. Microbiol. 73, 4395–4406.

Karlsson, J., Byström, P., Ask, J. 2009. Light limitation of nutrient-poor lake ecosystems. Nature 460, 506–509

Kaspar,H. F., Tiedje, J. M. & Firestoner,. B. (1981). Denitrification and dissimilatory nitrate reduction to ammonium in digested sludge. Canadi- an Journal of'Microbiology 27,878-885.

Kessel, M. 1977. Identification of a phosphorus-containing storage granule in the cyanobacterium plectonema boryanum by electron microscope x-ray microanalysis. J Bacteriol, 129(3), 1502-1505.

Khan, S. U., Hooda, P. S., Blackwell, M. S. A., Busquets, R. 2019. Microbial Biomass Responses to Soil Drying-Rewetting and Phosphorus Leaching. Front. Environ. Sci.

Kornberg, A. 1999. Inorganic polyphosphate: a molecule of many functions. Prog Mol Subcell Biol, 23, 1-18. doi:10.1007/978-3-642-58444-2_1

Koschel, R.; Bemmdorf, J.; Proft, G.; Recknagel, F. 1983. Calcite precipitation as a natural control mechanism of eutrophication. Arch. für Hydrobiol. 98, 380–408.

Koski-Vahala, J., Hartikainen, H., Tallberg, P. 2001. Phosphorus mobilization from various sediment pools in response to increased pH and silicate concentration. J Environ Qual, 30(2), 546-552.

Kragh, T., Sand-Jensen, K., Petersen, K., Kristensen, E. 2017. Fast phosphorus loss by sediment resuspension in a re-established shallow lake on former agricultural fields. Ecological Engineering, 108, 2-9. doi:10.1016/j.ecoleng.2017.07.026

Lapota, M., Tandyrak, R., Parszuto, K., Augustyniak, Grochowska, J, Plachta, A. 2019. External loading of phosphorous in deep, stratified lake affected with drainage water. Erath and Environmental science. Vol 221.

Lehman, P. W., Kurobe, T., Lesmeister, S., Baxa, D., Tung, A., Teh, S. J. 2017. Impacts of the 2014 severe drought on the *Microcystis* bloom in San Francisco Estuary. Harmful Algae, 63, 94-108. doi:10.1016/j.hal.2017.01.011

Lenzi, M.A., Marchi, L. 2000. Suspended sediment load during floods in a small stream of the Dolomites (northeastern Italy). Catena 39: 267–282.

Li, J., Zhang, J., Huang, W., Kong, F., Li, Y., Xi, M., Zheng, Z. 2016. Comparative bioavailability of ammonium, nitrate, nitrite and urea to typically harmful cyanobacterium *Microcystis aeruginosa*. Mar Pollut Bull, 110(1), 93-98. doi:10.1016/j.marpolbul.2016.06.077

Li, S., Wang, C., Qin, H., Li, Y., Zheng, J., Peng, C., Li, D. 2016. Influence of phosphorus availability on the community structure and physiology of cultured biofilms. J Environ Sci (China), 42, 19-31. doi:10.1016/j.jes.2015.08.005

Li, X., Huang, T., Ma, W., Sun, X., Zhang, H. 2015. Effects of rainfall patterns on water quality in a stratified reservoir subject to eutrophication: Implications for management. Sci Total Environ, 521-522, 27-36. doi:10.1016/j.scitotenv.2015.03.062

Li, X., Guo, M., Duan, X., Zhao, J., Hua, Y., Zhou, Y., Liu, G., Dionysiou, D. 2019. Distribution of organic phosphorus species in sediment profiles of shallow lakes and its effect on photo-release of phosphate during sediment resuspension. Environmental International, vol:130.

Li, Z., House, J., Burch, M. D., Hobson, P., Yang, M., An, W. 2012. Earthy odour compounds production and loss in three cyanobacterial cultures. Water Res. 46, 5165–5173.

Liu, J., Luo, X., Zhang, N., Wu, Y. 2016. Phosphorus released from sediment of Dianchi Lake and its effect on growth of *Microcystis aeruginosa*. Environ Sci Pollut Res Int, 23(16), 16321-16328. doi:10.1007/s11356-016-6816-9

Lowe, R.L., Pillsbury, R.W., 1995. Shifts in bottom algal community structure and function following the appearance of zebra mussels (*Dreissena polymorpha*) in Saginaw Bay, Lake Huron. J. Great Lakes Res. 558–566.

Lyde, T. A. S., Daouda, M., Dieudonné, Z. N., Ousmane, B., Moctar, B. L. 2013. Eutrophication, sediment Phosphorus fractionation and short-term mobility study in the surface and under profile sediment of a water dam. J. Appl. Sci. Environ. Manage. Vol. 17 (4) 517-526.

Ma, J., Brookes, J. D., Qin, B., Paerl, H. W., Gao, G., Wu, P., Niu, H. 2014. Environmental factors controlling colony formation in blooms of the cyanobacteria *Microcystis* spp. in Lake Taihu, China. Harmful Algae, 31, 136-142. doi:10.1016/j.hal.2013.10.016

Ma, T., Chen, Q., Gui, M., Li, C., Ni, J. 2016. Simultaneous denitrification and phosphorus removal by Agrobacterium sp. LAD9 under varying oxygen concentration. Appl Microbiol Biotechnol, 100(7), 3337-3346. doi:10.1007/s00253-015-7217-6

Ma, Z., Niu, Y., Xie, P., Chen, J., Tao, M., Deng, X. 2013. Off-flavor compounds from decaying cyanobacterial blooms of Lake Taihu. J Environ Sci (China), 25(3), 495-501.

Ma, S., Wang, H., Wang, H., Zhang, M., Li, Y, Bian, S, Liang, X, Søndergaard, M., Jeppesen, E. 2021. Effect of nitrate on phosphorous release from lake sediments: a three-month mesocosm experiment. Vol: 194. DO: 10.1016/j.watres.2021.116894

Majumdar, P. P., Ramesh, T. S. V. 1997. Real-time reservoir operation for irrigation. Water Resources research. Vol. 33:5. 1157-1164.

Makarewicz, J.C., Howell, E.T., 2012. The Lake Ontario Nearshore study: introduction and summary. J. Great Lakes Res. 38:2–9. https://doi.org/10.1016/j.jglr.2012.07.006.

Mangiafico, S. S. 2016. Summary and analysis of extension program evaluation in R, version 1.18.8.

rcompanion.org/handbook/.(Pdfversion:rcompanion.org/documents/RHandbookProgramEvaluation.pdf.)

Martin, P., Dyhrman, S. T., Lomas, M. W., Poulton, N. J., Van Mooy, B. A. 2014. Accumulation and enhanced cycling of polyphosphate by *Sargasso* Sea plankton in response to low phosphorus. Proc Natl Acad Sci U S A, 111(22), 8089-8094. doi:10.1073/pnas.1321719111

Mjelde, M.; Ballot, A.; Swe, T.; Eriksen, T.E.; Nesheim, I.; Aung, T.T. 2017. Integrated Water Resources Management in Myanmar. Assessing ecological status in Inlay Lake. Preliminary Report. 7163-2017, Norwegian Institute for Water Research; p. 76.

Miller, S. R., Longley, R., Hutchins, P. R., Bauersachs, T. 2020. Cellular Innovation of the Cyanobacterial Heterocyst by the Adaptive Loss of Plasticity. Curr Biol, 30(2), 344-350 e344. doi:10.1016/j.cub.2019.11.056

Miller, T. R., Beversdorf, L., Chaston, S. D., McMahon, K. D. 2013. Spatiotemporal molecular analysis of cyanobacteria blooms reveals *Microcystis--Aphanizomenon* interactions. PLoS One, 8(9), e74933. doi:10.1371/journal.pone.0074933

Miller, T. R., Beversdorf, L. J., Weirich, C. A., Bartlett, S. L. 2017. Cyanobacterial Toxins of the Laurentian Great Lakes, Their Toxicological Effects, and Numerical Limits in Drinking Water. Mar Drugs, 15(6). doi:10.3390/md15060160

Mistry, D., Powles, N. 2013. The relative hydrolytic reactivities of pyrophosphites and pyrophosphates. Org. Biomol. Chem. 11, 5727-5733.

Mohanty, A. K., Bramha, S. N., Satpathy, K. K., Padhi, R. K., Panigrahi, S. N., Kumar, S. B., Sarkar, S. K., Prasad, M. V. R. 2016. Geochemical distribution of forms of phosphorus in marine sediment of Bay of Bengal, southeast coast of India. Indian Journal of Geo Marine Sciences Vol. 47 (06), June 2018, pp. 1132-1141

Moore, P. A., Reddy, K. R., Fisher, M. M. 1998. Phosphorus Flux between Sediment and Overlying Water in Lake Okeechobee, Florida: Spatial and Temporal Variations. Journal of Environmental Quality, 27, 1428-1439. doi:10.2134/jeq1998.00472425002700060020x

Murphy, C. A., Arismendi, I., Taylor, G. A., Johnson, S. L. 2019. Evidence for lasting alterations to aquatic food webs with short-duration reservoir draining. PLoS One, 14(2), e0211870. doi:10.1371/journal.pone.0211870

Mustapha, M. K. 2009. Influence of watershed activities on the water quality and fish assemblages of a tropical African reservoir. Rev Biol Trop, 57(3), 707-719. doi:10.15517/rbt.v57i3.5486

Nixdorf, B. Deneke, R. 1995. Why very shallow lakes are more successful opposing reduced nutrient loads. Hydrobiologica, 342, 269-284.

Ockenden, C., Deasy, C. E., Benskin, CMcWH, Beven, K. J., Burke, S., Collins, A. L., Evans, R., Falloon, P. D., Forber, K. J., Hiscock, K. M., Hollaway, M. J., Kahana, R., Macloed, C. J. A., Reaney, S. M., Snell, M. A., Villamizar, M. L., Wearing, C., Withers, P. J. A., Haygarth, P. M. 2016. Changing climate and nutrient transfers: Evidence from high temporal resolution concentration-flow dynamics in headwater catchments. Science of the total Environment. Vol 548 – 549. Pp 325-339.

Olsen, B. K., Chislock, M. F., Wilson, A. E. 2016. Eutrophication mediates a common off-flavor compound, 2-methylisoborneol, in a drinking water reservoir. Water Res, 92, 228-234. doi:10.1016/j.watres.2016.01.058

Otten, T. G., Graham, J. L., Harris, T. D., Dreher, T. W. 2016. Elucidation of Taste- and Odor-Producing Bacteria and Toxigenic Cyanobacteria in a Midwestern Drinking Water Supply Reservoir by Shotgun Metagenomic Analysis. Appl Environ Microbiol, 82(17), 5410-5420. doi:10.1128/AEM.01334-16

Owens, P.N., Walling, D.E. 2002. The phosphorus content of fluvial sediment in rural and industrialized river basins. Water Res. 36: 685–701.

Osis, V. J. 1986. Water, water everywhere. Second Revised Edition. Extension Marine Education Specialist and Associate Professor Oregon State University.

Ozersky, T., Malkin, S.Y., Barton, D.R., Hecky, R.E. 2009. Dreissenid phosphorus excretion can sustain C. glomerata growth along a portion of Lake Ontario shoreline. J. Great Lakes Res. 35:321–328. https://doi.org/10.1016/j.jglr.2009.05.001.

Padisák, J., Reynolds, C. 2003. Shallow lakes: the absolute, the relative, the functional and the pragmatic. Hydrobiologia, vol. 506-509, p. 1-11

Pall, P., Aina, T., Stone, D. A., Stott, P. A., Nozawa, T., Hilberts, A. G., Allen, M. R. 2011. Anthropogenic greenhouse gas contribution to flood risk in England and Wales in autumn 2000. Nature, 470(7334), 382-385. doi:10.1038/nature09762

Paudel, B., Weston, N., O'Connor, J., Sutter, L., Velinsky, D. 2017. Phosphorus Dynamics in the Water Column and Sediments of Barnegat Bay, New Jersey. Journal of Coastal research (78(10078)):60:69.

Paul, V. J. 2008. Global warming and cyanobacterial harmful algal blooms. Adv Exp Med Biol, 619, 239-257. doi:10.1007/978-0-387-75865-7_11

Perkins, R. G., Slavin, E. I., Andrade, T. M. C., Blenkinsopp, C., Pearson, P., Froggatt, T., Godwin, G., Parslow, J., Hurley, S., Luckwell, R., Wain, D. J. 2019. Managing taste and odour metabolite production in drinking water reservoirs: The importance of ammonium as a key nutrient trigger. Journal of Environmental Management; 244. Pp 276-284.

Perrone, U.; Facchinelli, A.; Sacchi, E. 2008. Phosphorus dynamics in a small eutrophic Italian lake. Water Air. Soil Pollut. 189, 335–351.

Persaud, A. D., Paterson, A. M., Dillon, P. J., Winter, J. G., Palmer, M., Somers, K. M. 2015. Forecasting cyanobacteria dominance in Canadian temperate lakes. J Environ Manage, 151, 343-352. doi:10.1016/j.jenvman.2015.01.009

Pfister, C. A., Altabet, M. A., Weigel, B. L. 2019. Kelp beds and their local effects on seawater chemistry, productivity, and microbial communities. Ecology, 100(10), e02798. doi:10.1002/ecy.2798

Poikane, S., Kelly, M. G., Salas Herrero, F., Pitt, J. A., Jarvie, H. P., Claussen, U., Phillips, G. 2019. Nutrient criteria for surface waters under the European Water Framework Directive: Current state-of-the-art, challenges and future outlook. Sci Total Environ, 695, 133888. doi:10.1016/j.scitotenv.2019.133888

Pomeroy, L. R., Wiebe, W. J., Deibel, D., Thompson, R. J., Rowe, G. T., Pakulski, J. D. 1991. Bacterial responses to temperature and substrate concentration during the Newfoundland spring bloom. Marine ecology progress series. Vol 75:143-159.

Pope, I. C., Odhiambo, B. K. 2014. Soil erosion and sediment fluxes analysis: a watershed study of the Ni Reservoir, Spotsylvania County, VA, USA. Environ Monit Assess, 186(3), 1719-1733. doi:10.1007/s10661-013-3488-5

Qiu, Y., Tian, S., Gu, L., Hildreth, M., Zhou, R. 2019. Identification of surface polysaccharides in akinetes, heterocysts and vegetative cells of *Anabaena cylindrica* using fluorescein-labeled lectins. Arch Microbiol, 201(1), 17-25. doi:10.1007/s00203-018-1565-4

Ramcharan CW, DK Padilla, Si Dodson. 1992. Models to predict potential occurrence and density of the zebra mussel *Dreissena-polymorpha*. Canadian Journal of Fisheries and Aquatic Sciences. 49:12 (2611-2620)

Rasconi, S., Gall, A., Winter, K., Kainz, M. J. 2015. Increasing Water Temperature Triggers Dominance of Small Freshwater Plankton. PLoS One, 10(10), e0140449. doi:10.1371/journal.pone.0140449

Raven, J. A., 2010. Cyanotoxins: a posion that frees phosphate. Current Biology, Vol 20;19

Re, V.; Thin, M.M.; Setti, M.; Comizzoli, S.; Sacchi, E. 2018. Present status and future criticalities evidenced by an integrated assessment of water resources quality at catchment scale: The case of Inle Lake (Southern Shan state, Myanmar). Appl. Geochem. 92, 82–93

Reichwaldt, E. S., Ghadouani, A. 2012. Effects of rainfall patterns on toxic cyanobacterial blooms in a changing climate: between simplistic scenarios and complex dynamics. Water Res, 46(5), 1372-1393. doi:10.1016/j.watres.2011.11.052

Richie, E. R., Wissmar, R. C. 1979. Sources and Influences of Allochthonous Inputs on the Productivity of a Subalpine Lake. Ecology, Vol. 60:2. Pp 318-328.

Saadoun, I. M. K., Schrader, K. K., Blevins, W. T. 2001. Environmental and nutritional factors affecting geosmin synthesis by *Anabaena* sp. Water Res. 35, 1209–1218.

Sahin, Y.; Demirak, A.; Keskin, F. 2012. Phosphorus fractions and its potential release in the sediments of Koycegiz Lake, Turkey. Ponds, 6, 139–153.

Santos, R. M., Saggio, A. A., Silva, T. L., Negreiros, N. F., Rocha, O. 2015. Short-term thermal stratification and partial overturning events in a warm polymictic reservoir: effects on distribution of phytoplankton community. Braz J Biol, 75(1), 19-29. doi:10.1590/1519-6984.05313

Saygõ-Başbuğ, Y., Demirkalp, F. Y. 2004. Orimary production in shallow eutrophic Yenicaga Lake (BOLU, TURKEY). Fresenius Environmental Bulletin. Volume 13;2. Limnol. Oceanogr., 27: 1101-1112

Schabhuttl, S., Hingsamer, P., Weigelhofer, G., Hein, T., Weigert, A., Striebel, M. 2013. Temperature and species richness effects in phytoplankton communities. Oecologia, 171(2), 527-536. doi:10.1007/s00442-012-2419-4

Schindler, D. W., Carpenter, S. R., Chapra, S. C., Hecky, R. E., Orihel, D. M. 2016. Reducing phosphorous to curb lake eutrophication is a success. Environ. Sci. Tegnol. 50, 17, 8923–8929

Schoffelen, N. J., Mohr, W., Ferdelman, T. G., Duerschlag, J., Littmann, S., Ploug, H., Kuypers, M. M. M. 2019. Phosphate availability affects fixed nitrogen transfer from diazotrophs to their epibionts. ISME J, 13(11), 2701-2713. doi:10.1038/s41396-019-0453-5

Selim, K. A., Ermilova, E., Forchhammer, K. 2020. From cyanobacteria to Archaeplastida: new evolutionary insights into PII signalling in the plant kingdom. New Phytol. doi:10.1111/nph.16492

Semenov, A. V., Elsas, J. D., Glandorf, D. C., Schilthuizen, M., Boer, W. F. 2013. The use of statistical tools in field testing of putative effects of genetically modified plants on nontarget organisms. Ecol Evol, 3(8), 2739-2750. doi:10.1002/ece3.640

Sharpley, A. N. 1993. An Innovative Approach to Estimate Bioavailable Phosphorus in Agricultural Runoff Using Iron Oxide—Impregnated Paper. Journal of Environ. Qual. 22:597-601.

She, C. X., Wang, J., Su, Y. P., Lin, W. Z., Lan, R. F., Liu, J. X., Lin, J. 2019. Community characteristics of polyphosphate accumulating organisms in the heart sediment of three reservoirs in Fujian Province, China. Ying Yong Sheng Tai Xue Bao, 30(7), 2393-2403. doi:10.13287/j.1001-9332.201907.026

Siepielski, A. M., Morrissey, M. B., Buoro, M., Carlson, S. M., Caruso, C. M., Clegg, S. M., MacColl, A. D. 2017. Precipitation drives global variation in natural selection. Science, 355(6328), 959-962. doi:10.1126/science.aag2773

Skoog, A., Hall, P.O.J., Hulth, S., Paxéus, N., Rutgers van der Loeff, M., Westerlund, S., 1996. Early diagenetic production and sediment–water exchange of fluorescent dissolved organic matter in the coastal environment. Geochimica et Cosmochimica Acta 60, 3619–3629.

Smith, V.H. 1982. The nitrogen and phosphorus dependence of algae in lakes: an empirical and theoretical analysis. Limnol. Oceanogr., 27: 1101-1112.

Sommer, U., Adrian, R., Domis, L. S., Elser, J. J., Gaedke, U., Ibelings, B., Jeppesen, E., Lurling, M., Molinero, J. C., Mooij, W. M., Donk, E., Winder, M. 2012. Beyond the plankton ecology group (PEG) model: mechanisms driving plankton succession. Annual review of ecology, evolution and systematics. Vol:43; 429-448.

Søndergaard, M., J. P. Jensen, E. Jeppesen, P. H. Moller 2002, Seasonal dynamics in the concentrations and retention of phosphorus in shallow Danish lakes after reduced loading, Aquat. Ecosyst. Health Manage., 5, 19–29.

Søndergaard, M., Jensen, J. P., Jeppesen, E. 2003. Role of sediment and internal loading of phosphorus in shallow lakes. Hydrobiologia, 506(1), 135-145. doi:10.1023/B:HYDR.0000008611.12704.dd

Søndergaard, M., Jensen, J. P., Jeppesen, E. 2005. Seasonal response of nutrients to reduced phosphorus loading in 12 Danish lakes. Freshwater Biology; 50:10. 1605-1615.

Songmin, L., Xialoing, A., Bin, Q., Jiansheng, L., Jiamin, T. 2017. First flush charachteristics of rainfall run-off from a paddy field in the Taihu Lake watershed, China. Environ Sci Pollut Res Int.

Spears, B.M., Andrews, C., Banin, L., Carvalho, L., Cole, S., De Ville, M., Gunn, I.D.M., Ives, S., Lawlor, A., Leaf, S., Lofts, S., Maberly, S.C., Madgwick, G., May, L., Moore, A., Pitt, J., Smith, R., Waters, K., Watt, J., Winfield, I.J, Woods, H. 2018. Assessment of sediment phosphorus capping to control nutrient concentrations in English lakes. Environment Agency. Project number: SC120064/R9

Spellman, F. R., Drinan, J., Drinan, J. E. 2000. The drinking water handbook. Pp65

Stott PA, Allen M, Christidis N, Dole R, Hoerling M, Huntingford C, Pall P, Perlwitz J, Stone D. 2013. Attribution of weather and climate-related extreme events. In: Monograph: 'Climate Science for Serving Society: Research, Modelling and Prediction Priorities.' Position Paper for WCRP OSC. Accepted as part of monograph of position papers. Dordrecht, Netherlands: Springer; 307–337.

Strayer DL, J Powell, P Ambrose, LC Smith, ML Pace, DT Fischer. 1996. Arrival, spread, and early dynamics of a zebra mussel (*Dreissena polymorpha*) population in the Hudson River estuary. Can. J. Fish. Aquat. Sci. Vol. 1144 53.

Stumm, W. 1983. Significance of phosphorous in lakes and coastal water sediments and benthos. Limnology, 2nd edition. Saunders College publishing, Philadelphia. Page 129

Su, X., He, Q., Mao, Y., Chen, Y., Hu, Z. 2019. Dissolved oxygen stratification changes nitrogen speciation and transformation in a stratified lake. Environ Sci Pollut Res Int, 26(3), 2898-2907. doi:10.1007/s11356-018-3716-1

Sun, X. J., Qin, B. Q., Zhu, G. W., Zhang, Z. P. 2007. Effect of wind-induced wave on concentration of colloidal nutrient and phytoplankton in Lake Taihu. Huan Jing Ke Xue, 28(3), 506-511.

Sun, X., Zhu, G. W., Da, W. Y., Yu, M. L., Yang, W. B., Zhu, M. Y., Li, H. Y. 2018. Thermal Stratification and Its Impacts on Water Quality in Shahe Reservoir, Liyang, China. Huan Jing Ke Xue, 39(6), 2632-2640. doi:10.13227/j.hjkx.201710223

Sutherland, R.A. 2000. Bed sediment-associated trace metals in an urban stream, Oahu, Hawaii. Environ. Geol. 39: 611–627.

Suurnakki, S., Gomez-Saez, G. V., Rantala-Ylinen, A., Jokela, J., Fewer, D. P., Sivonen, K. 2015. Identification of geosmin and 2-methylisoborneol in cyanobacteria and molecular detection methods for the producers of these compounds. Water Res, 68, 56-66. doi:10.1016/j.watres.2014.09.037

Svendsen, L.M., Kronvang, B. 1993. Retention of nitrogen and phosphorus in a Danish lowland river system: Implications for the export from watershed. Hydrobiologia 251: 123–135.

Tanabe, Y., Hori, M., Mizuno, A.N. 2019. Light quality determines primary production in nutrient-poor small lakes. Sci Rep 9, 4639.

Tang, Q., Bao, Y., He, X., Fu, B., Collins, A. L., Zhang, X. 2016. Flow regulation manipulates contemporary seasonal sedimentary dynamics in the reservoir fluctuation zone of the Three Gorges Reservoir, China. Sci Total Environ, 548-549, 410-420. doi:10.1016/j.scitotenv.2015.12.158

Tian, C., Peil, H., Hu, W., Xie, J. 2012. Variation of cyanobacteria with different environmental conditions in Nansi Lake, China. J Environ Sci (China), 24(8), 1394-1402.

Tiwari, K.R.; Sitaula, B.K.; Bajracharya, R.M.; Borresen, T. 2010. Effects of soil and crop management practices on yields, income and nutrients losses from upland farming systems in the Middle Mountains region of Nepal. Nutr. Cycl. Agroecosys. 86, 241–253.

Tu, L., Jarosch, K. A., Schneider, T., Grosjean, M. 2019. Phosphorus fractions in sediments and their relevance for historical lake eutrophication in the Ponte Tresa basin (Lake Lugano, Switzerland) since 1959. Sci Total Environ, 685, 806-817. doi:10.1016/j.scitotenv.2019.06.243

UKTAG. 2008. UK Technical Advisory Group on the water framework directive. UK environmental standards and conditions (Phase 1).

Vadas, P. A., Krogstad, T., Sharpley, A. N. 2006. Modelling Phosphorus Transfer between Labile and Nonlabile Soil Pools: Updating the EPIC Model. SOIL SCIENCE SIOCIETY OF AMEFRICA(70), 736–743.

Vidal, J., Marcé, R., Serra, T., Colomer, J., Rueda, F., Casamitjana, X., 2011. Localized algal blooms induced by river inflows in a canyon type reservoir. Aquatic Sciences, 74; 315-327.

Vilalta, E, Guasch, H, Munoz, I., Navarro, E., Romani, A, M., Valero, F., Rodriguez, J, J., Alcaraz, R., Sabater, S. 2003. Ecological factors that co-occur with geosmin production by bottom cyanobacteria. The case of the Llobregat river. Algological studies; 109:1. pp 579-592.

Vonk, J. E. 2015. Reviews and Syntheses: Effects of permafrost thaw on arctic aquatic ecosystems. Biogeosciences Discuss. 12, 10719–10815

Wang, M., Xu, X., Wu, Z., Zhang, X., Sun, P., Wen, Y., Tong, Y. 2019. Seasonal Pattern of Nutrient Limitation in a Eutrophic Lake and Quantitative Analysis of the Impacts from Internal Nutrient Cycling. Environ Sci Technol, 53(23), 13675-13686. doi:10.1021/acs.est.9b04266

Wang, S., Zhang, S. S., Xu, Y., Guan, Z. Y., Yang, Z. J., Liu, D. F., Ma, J. 2019. Relationship Between the Vertical Distribution of Nutrients and Bacterial Community Structures in Sediment Interstitial Waters of Stratified Reservoirs with Different Water Temperatures. Huan Jing Ke Xue, 40(6), 2753-2763. doi:10.13227/j.hjkx.201811116

Wang, X., Parkpian, P., Fujimoto, N., Ruchirawat, K. M., DeLaune, R. D., Jugsujinda, A. 2002. Environmental conditions associating microcystins production to *Microcystis aeruginosa* in a reservoir of Thailand. J Environ Sci Health A Tox Hazard Subst Environ Eng, 37(7), 1181-1207.

Watts, C. J. 2000. Seasonal phosphorus release from exposed, re-inundated littoral sediments of two Australian reservoirs. Hydrobiologia, 431(1), 27-39. doi:10.1023/a:1004098120517

Wen, S., Zhong, J., Li, X., Liu, C., Yin, H., Li, D., Fan, C. 2020. Does external phosphorus loading diminish the effect of sediment dredging on internal phosphorus loading? An in-situ simulation study. J Hazard Mater, 394, 122548. doi:10.1016/j.jhazmat.2020.122548

Weng, C. S., Liu, D. F., Zhang, J. L., Gong, C., Shen, X. Z. 2019. Influence of Rainfall on the in situ Growth of Dominant Algae Species in Xiangxi River. Huan Jing Ke Xue, 40(7), 3108-3117. doi:10.13227/j.hjkx.201811235

Wentzky, V. C., Tittel, J., Jager, C. G., Bruggeman, J., Rinke, K. 2020. Seasonal successional of functional traits in phytoplankton communities and their interaction with trophic state. Journal of Ecology. Vol 108:4. 1649-1663.

Weston, N.B.; Dixon R.E., Joye, S.B., 2006. Ramifications of increased salinity in tidal freshwater sediments: Geochemistry and microbial pathways of organic matter mineralization. Journal of Geophysical Research, 111(G1)

Wetzel, R.G. 2001. Limnology: lake and river ecosystems. 3'd Edition. Academic Press, San Diego, CA

Whittier, TR. Ringold, P. L., Herlihy, A. T., Pierson, S. M. 2008. A calcium-based invasion risk assessment for zebra and quagga mussels (*Dreissena* spp). Frontiers in Ecology. 6(4); 180-184.

Williamson, T. J., Cross, W. F., Benstead, J. P., Gislason, G. M., Hood, J. M., Huryn, A. D., Welter, J. R. 2016. Warming alters coupled carbon and nutrient cycles in experimental streams. Glob Chang Biol, 22(6), 2152-2164. doi:10.1111/gcb.13205

Winkel, M. 2013. Chemolithotrophic and chemoheterotrophic microorganisms in sedimented and rock-hosted hydrothermal systems. Thesis.

Woldeab, B., Beyene, A., Ambelu, A., Buffam, I., Mereta, S. T. 2018. Seasonal and spatial variation of reservoir water quality in the southwest of Ethiopia. Environ Monit Assess, 190(3), 163. doi:10.1007/s10661-018-6527-4

Xiao, L. W., Zhu, B. 2017. Impacts of Environmental Conditions on the Soaking Release of Nitrogen and Phosphorus from *Cynodon dactylon* (Linn.) Pers. in the Water-level Fluctuation Zone of the Three Gorges Reservoir Region. Huan Jing Ke Xue, 38(11), 4580-4588. doi:10.13227/j.hjkx.201703195

Xiao, Y., Li, Z., Li, C., Zhang, Z., Guo, J. 2016. Effect of Small-Scale Turbulence on the Physiology and Morphology of Two Bloom-Forming Cyanobacteria. PLoS One, 11(12), e0168925. doi:10.1371/journal.pone.0168925

Xie, S.; Mo, M.; Tu, A.; Liu, Y. 2014. Characteristics of vertical runoff output on red-soil slope under natural rainfall condition. Trans. Chin. Soc. Agric. Eng. 30, 132–138.

Xue, Y., Yu, Z., Chen, H., Yang, J. R., Liu, M., Liu, L., Yang, J. 2017. Cyanobacterial bloom significantly boosts hypolimnelic anammox bacterial abundance in a subtropical stratified reservoir. FEMS Microbiol Ecol, 93(10). doi:10.1093/femsec/fix118

Yang, Z., Zhang, M., Shi, X., Kong, F., Ma, R., Yu, Y. 2016. Nutrient reduction magnifies the impact of extreme weather on cyanobacterial bloom formation in large shallow Lake Taihu (China). Water Res, 103, 302-310. doi:10.1016/j.watres.2016.07.047

Yogev, U., Vogler, M., Nir, O., Londong, J., Gross, A. 2020. Phosphorous recovery from a novel recirculating aquaculture system followed by its sustainable reuse as a fertilizer. Sci Total Environ, 722, 137949. doi:10.1016/j.scitotenv.2020.137949

Amano, Y., Machida, M., Tatsumoto, H., George, D., Berk, S., Taki, K. 2008. Prediction of Microcystis Blooms Based on TN:TP Ratio and Lake Origin. The Scientific World JOURNAL (2008) 8, 558-572

Yu, J., Chen, J., Zeng, Y., Lu, Y., Chen, Q. 2020. Carbon and phosphorus transformation during the deposition of particulate matter in the large deep reservoir. J Environ Manage, 265, 110514. doi:10.1016/j.jenvman.2020.110514

Yu, Z., Yang, J., Amalfitano, S., Yu, X., Liu, L. 2014. Effects of water stratification and mixing on microbial community structure in a subtropical deep reservoir. Sci Rep, 4, 5821. doi:10.1038/srep05821

Yurista, P.M., Kelly, J.R., Miller, S.E., Van Alstine, J.D., 2012. Water quality and plankton in the United States nearshore waters of Lake Huron. Environ. Manag. 50:664–678.

Zhai, S., Yang, L., Hu, W. 2009. Observations of atmospheric nitrogen and phosphorus deposition during the period of algal bloom formation in northern Lake Taihu, China. Environ Manage, 44(3), 542-551. doi:10.1007/s00267-009-9334-4

Zhang, P., Kuramae, A., van Leeuwen, C. H. A., Velthuis, M., van Donk, E., Xu, J., Bakker, E. S. 2020. Interactive Effects of Rising Temperature and Nutrient Enrichment on Aquatic Plant Growth, Stoichiometry, and Palatability. Front Plant Sci, 11, 58. doi:10.3389/fpls.2020.00058

Zhang, S., Wang, W., Zhang, K., Xu, P., Lu, Y. 2018. Phosphorus release from cyanobacterial blooms during their decline period in eutrophic Dianchi Lake, China. Environ Sci Pollut Res Int, 25(14), 13579-13588. doi:10.1007/s11356-018-1517-1

Zhang, T., Li, L., Zheng, L., Song, L. 2019. Effects of nutritional factors on the geosmin production of *Lyngbya kuetzingii* UTEX 1547 (*Oscillatoriales*, Cyanobacteria). Phycologica vol 56:2. 221-229.

Zheng, Y., Mi, W., Bi, Y., Hu, Z. 2017. The response of phosphorus uptake strategies of *Microcystis aeruginosa* to hydrodynamics fluctuations. Environ Sci Pollut Res Int, 24(10), 9251-9258. doi:10.1007/s11356-017-8502-y

Zhou, Q., Zhang, Y., Lin, D., Shan, K., Luo, Y., Zhao, L., Song, L. 2016. The relationships of meteorological factors and nutrient levels with phytoplankton biomass in a shallow eutrophic lake dominated by cyanobacteria, Lake Dianchi from 1991 to 2013. Environ Sci Pollut Res Int, 23(15), 15616-15626. doi:10.1007/s11356-016-6748-4

Zhou, X., Chen, N., Yan, Z., Duan, S. 2016. Warming increases nutrient mobilization and gaseous nitrogen removal from sediments across cascade reservoirs. Environ Pollut, 219, 490-500. doi:10.1016/j.envpol.2016.05.060

Zhang, R.; Li, M.; Yuan, X.; Pan, Z. 2018. Influence of rainfall intensity and slope on suspended solids and phosphorus losses in runoff. Environ. Sci. Pollut. Res. 26, 1–13

Zhang, X., Liu, P., Xu, C. Y., Cheng, L., He, S. 2019. Real-time reservoir flood control operation for cascade reservoirs using a two-stage flood risk analysis method. Journal of Hydrology. Vol. 557.

Appendix 1: Dŵr Cymru Welsh Water quality analytical methods

Training Required:	**Read and Comprehend**	**Effective Date:**	**08/03/2017**
Reviewed By:	**Marta Glabska**	**Issue Number:**	**016**
Approved By:	**Sumit Yadav**	**Issue Date:**	**08/03/2017**
Associated Documents:	**LPS003, 046, 051, 074, 099, 117, 135 LPF006, 096, 132, 147, 173, 174, 294, 306 ,334, 337,LPF132-LPM036**		

Record of Change

Issue	Issue Date	Record of Change
016	08/03/2017	Section 13.0: Calibration check to be analysed after each calibration.

1.0 Title

Determination of Nutrients in potable waters by Aquakem 600.

2.0 Scope

The method details the procedure in the quantitative determination of ammonia, total oxidized nitrogen (TON), nitrite, chloride, phosphate, sulphate and silicate in potable waters using the Thermo Scientific Aquakem 600.
Potable waters are analysed for nutrients using this method for concentrations over the following concentration ranges:

Analyte	Range	PCV Values
Ammonia-N	**0.003 – 0.6 mg/L**	**0.388 mg/l as N**
TON-N	**0.48 - 60 mg/L**	**11.29mg/l as N**
Nitrite-N	**0.0045 – 0.6 mg/L**	**0.152 mg/l as N**
Chloride	**3.1 – 300 mg/L**	**250 mg/l**
Phosphate	**0.03 – 1.2 mg/L**	**n/a**
Sulphate	**2.7 – 300 mg/L**	**250 mg/l**
Silica as SiO_2	**0.19 – 20 mg/L**	**n/a**

3.0 Principle of method

Nutrient concentrations are measured by either measuring colour metrically or turbid metrically.
The analytical method of measurement is dependent upon the reaction between the analyte within the sample and the reagents. Sulphates react with the reagent to produce an insoluble precipitate which is measured turbid metrically.
All other determinants produce a coloured complex when reacted with the reagents.
At a predetermined wavelength the intensity of the coloured or turbid sample solution is proportional to the concentration of the analyte within the sample.
When a monochromatic light is focused upon the sample, in the form of a homogeneous medium, an amount of the focused light is absorbed by the sample, the remainder of the light, which is not absorbed, is transmitted and measured by a detector within the instrument.
The ratio of the incident light to the transmitted light is referred to as the absorbance.
Analysis follows the principle of Beer-Lambert's Law which states that: A = ECL
Where A = Absorbance, E = Molar Extinction Coefficient, C = Concentration and L = Light Path.

It is noted from Beer-Lamberts Law that concentration is proportional to absorbance. Using calibration standards of known analyte concentrations, the instrument can be accurately calibrated to identify the absorbance of standard concentrations.
The Aquakem 600 measures the samples absorbance values against those of the calibration standards and correctly determines the sample's analyte concentration.

4.0 Definitions

Chemistry Reverse Osmosis (RO) Water – water produced by a reverse osmosis water purification system capable of producing water which will have a conductivity of ≤**2**\µS/cm and a TOC of <20 ppb.

5.0 Safety and COSHH

Refer to: "Risk Assessment Aquakem 600 Nutrients" within the Risk Assessment folder in the Inorganic section of the shared drive.
Sodium Nitrite May intensify fire. Toxic if swallowed. Very toxic to aquatic life.

6.0 Reagents & Materials

All reagents must be of analytical grade unless otherwise stated.
All reagents, used as purchased, must be discarded by the manufacturer's expiry date.

- Sodium Nitrite.
- Anhydrous Sodium Hexaflourosilicate.

Temperature and time must be recorded in **LPF334** when drying a reagent in the oven.

RO water. All blanks, standards and sample dilutions are prepared from this water source.
It should be drawn fresh on day of use.
Check the log **LPF189** to confirm that the RO water has passed its daily check for this day.

Standards and AQCs should be sourced from two separate suppliers and should be prepared by two separate analysts. If this is not possible two separate batches should be used.
Calibration standards and/or AQC solutions are, wherever possible, prepared from traceable Reference Material or certified Reference material.
If calibration standard or AQC standard is not traceable follow the procedure **LPS117** for statistical analysis to show they are fit for purpose.

6.1 Preparation of Calibration Standards

Complete all relevant calibration standard logs following preparation in **LPF132** STD, AQC, ISTD & Reagent Preparation Log. The paper copy is kept by the instrument.
AQC's should be made in Quality lab. Separate pipettes and glassware should be used to prepare calibration standards and AQCs.
All purchased standards should have the opened date, expiry date and initials of analyst opening the solution written on the container.

Standards and AQCs prepared in the lab must be clearly labeled with the date prepared and the expiry date followed by initials of an analyst who prepared the solution and a unique Laboratory Number.
Calibration check is calibration **standard 3** analysed as a sample against the calibration.
Calibrations blanks need to be drawn fresh on day of use.

6.2 Ammonia as N 1000 mg/L Standard Stock

Commercially available Certified Stock Standard should be used.

6.3 Nitrite as N 1000 mg/L Standard Stock

Commercially available Certified Stock Standard should be used.

6.4 Ammonia/Nitrite 10 mg/L Intermediate Standard

Into a 100 ml volumetric flask containing approximately 50 ml of RO water, using a pipette transfer 1 ml of Ammonia as N 1000 mg/L Stock Standard (6.2) and 1 ml of Nitrite as N 1000 mg/L Standard Stock (6.3). Invert the flask several times to ensure mixing and make up to the mark RO water. Transfer to a 100 ml plastic bottle. Label the bottle with the analyst's initials, date of preparation and expiry and unique laboratory number.
Stored between 3±2°C the solution is stable for **one week**.

6.5 Ammonia/Nitrite Working Standards (Sep MIXA-1 to 6)

Into six 100 ml volumetric flasks containing approximately 40 ml of RO water, using an appropriate calibrated pipette transfer the following volumes of Ammonia/Nitrite 10 mg/L Intermediate B Standard:

Standard	Volume of Ammonia/Nitrite 10 mg/L Intermediate Standard (ml)	Concentration of Standards (mg/L)
1	1	0.1
2	2	0.2
3	3	0.3
4	4	0.4
5	5	0.5
6	6	0.6

Invert the flasks several times to ensure mixing and make up to the mark RO water. Transfer to a 125 ml plastic bottles.
Label the bottles with the analyst's initials, date of preparation and expiry and unique laboratory number.
Stored between 3±2°C, the solutions are stable for **one week**.

6.6 Total Oxidised Nitrogen (TON) as N, Nitrate – Nitrogen 1000 mg/L Standard Stock

Commercially available Certified Stock Standard should be used.

6.7 Chloride 10,000 mg/L Standard Stock

Commercially available Certified Stock Standard should be used.

6.8 TON/Chloride Working Standards (Sep MixB-1 to 6)

Into six 100 ml volumetric flasks containing approximately 40 ml of RO water, using an appropriate calibrated pipette transfer the following volumes of TON as N 1000 mg/l Standard Stock and Chloride 10,000 mg/L Standard Stock:

Standard	Volume of TON as N 1000 mg/l Stock (ml)	TON Conc. (mg/L)	Volume of Chloride 10,000 mg/l Standard Stock (ml)	Chloride Conc. (mg/L)
1	1	10	0.3	30
2	2	20	0.7	70
3	3	30	1.5	150
4	4	40	2.0	200
5	5	50	2.5	250
6	6	60	3.0	300

Invert the flasks several times to ensure mixing and make up to the mark RO water. Transfer to a 125 ml plastic bottles.
Label the bottles with the analyst's initials, date of preparation and expiry and unique laboratory number.
Stored between 3±2°C, the solutions are stable for **one week.**

6.9 Sulphate 10,000 mg/L Standard Stock

Commercially available Certified Stock Standard should be used.

6.10 Silicate as SiO_2 1000 mg/L Standard Stock

Using previously dried (at 110°C +/- 5°C for at least 2h) analytical grade Anhydrous Silicate, dissolve 1.57 grams ± 0.015 grams in approximately 250 ml of RO water in a 500 ml .volumetric flask.
Allow to dissolve then invert the flask several times to ensure mixing and make up to the mark with RO water. Transfer the solution to a plastic 500 ml bottle.
Label the bottle with the analyst's initials, date of preparation and expiry and unique laboratory number. Stored between 3±2°C, the solution is stable for **six month**s.
Commercially available stock standard can also be used to prepare working Standards (MIX-1 to 6).

6.11 Sulphate/Silicate Working Standards (MIX-1 to 6)

Into six 100 ml volumetric flasks containing approximately 40 ml of RO water, using an appropriate calibrated pipette transfer the following volumes of Silicate as SiO_2 1000 mg/L or Silica 1000 mg/l Certified Stock Standard and Sulphate 10,000 mg/L Certified Standard Stock:

Standard	Volume of Silicate 1000 mg Stock Standard (ml)	Silicate Conc. (mg/L)	Volume of Sulphate 10,000 mg/L Standard Stock (ml)	Sulphate Conc. (mg/L)
1	0.2	2	0.3	30
2	0.5	5	0.7	70
3	1.0	10	1.5	150
4	1.5	15	2.0	200
5	2.0	20	2.5	250

6	-	-	3.0	300

Invert the flasks several times to ensure mixing and make up to the mark RO water. Transfer to a 125ml plastic bottle. Label the bottles with the analyst's initials, date of preparation and expiry and unique laboratory number. Stored between 3±2°C, the solution is stable for **one week.**

6.12 Phosphate as P 1000 mg/L Standard Stock

Commercially available Certified Stock Standard should be used.

6.13 Phosphate 10 mg/L Intermediate Standard

Into a 100 ml volumetric flask containing approximately 50 ml of RO water, transfer with a calibrated pipette 1ml of Phosphate as P 1000 mg/L Standard Stock Solution (6.12).
Invert the flask several times to ensure mixing and make up to the mark RO water. Transfer to a 125 ml plastic bottle.
Label the bottle with the analyst's initials and date of preparation and expiry and unique laboratory number.
Stored between 3±2°C, the solution is stable for **one week**.

6.14 Phosphate as P Working Standards (PO4-1 to 5)

Into a 100 ml volumetric flasks containing approximately 40 ml of RO water, using a calibrated pipettes transfer the following volumes of Phosphate 10mg/L Intermediate Standard (6.13).

Standard	Volume of Phosphate as P 10 mg/L Intermediate B Standard (ml)	Phosphate Conc. (ug/L)
1	**1**	**100**
2	**2**	**200**
3	**4**	**400**
4	**8**	**800**
5	**12**	**1200**

Invert the flasks several times to ensure mixing and make up to the mark RO water. Transfer to a 125ml plastic bottles.
Label the bottles with the analyst's initials and date of preparation and expiry and unique laboratory number.
Stored between 3±2°C, the solutions are stable for **one week.**

6.15 Reagents

Analyst must complete **LPF132** STD, AQC, ISTD & Reagent Preparation Log for manually prepared reagents and update **LPF337** for reagents poured daily. **LPF306** Inorganics stock standard and Inventory must be completed when reagents are installed into the instrument.
All reagents stability data is taken from the Certificates of Performance provided by the supplier (Thermo Fisher Scientific). When reagents are not in use they are to be stored between 3±2°C.
Ammonia 1 KR108 – stable on board for 1 day.
Ammonia 2 KR109 – stable on board for 5 days.

TON 1 KR103 – stable on board for 1 day.
TON 2 KR104 – stable on board for 5 days.
TON 3 KR105 – stable on board for 5 days.
Nitrite KR105 – stable on board for 5 days.
Chloride KR101 – stable on board for 5 days.
Phosphate 1 KR106 – stable on board for 5 days.
Phosphate 2 KR107 – stable on board for 5 days.
Sulphate KR102 – stable on board for 5 days. (Alternatively see Sulphate reagent preparation below).
Silica 1 109-1140 - stable on board for 5 days.
Silica 2 109-1150 –stable on board for 5 days.
Silica 3 109-1160 –stable on board for 5 days.

Sulphate Reagent preparation

Dissolve 0.25g (± 0.0025 g) of gelatine in 300ml of warm RO water in a 1000ml beaker. Use a magnetic hot plate stirrer to ensure that all gelatine is dissolved.
Turn off hot place and then add 10.0g (± 0.10 g) of Barium Chloride and 10.0g (± 0.10 g) of Sodium Chloride.
Stir until dissolved. Transfer into a 1000ml volumetric flask using a funnel. Using a calibrated 10ml pipette carefully add 5ml of concentrated hydrochloric acid.
Invert the flask several times to ensure mixing and make up to the mark with RO water. Transfer to a 1000ml plastic bottle.
Label the bottle with the analyst's initials, date of preparation and expiry and unique laboratory number.
Stored between 3±2°C, the solution is stable for **six months** but poured fresh daily as the reagent vial does not have a barcode that contains installation date.

6.16 Analytical Quality Controls (AQC)

Standards and AQCs should be sourced from two separate suppliers and should be prepared by two separate analysts. If this is not possible two separate batches should be used.
Calibration standards and/or AQC solutions are, wherever possible, prepared from traceable Reference Material or certified Reference material.
If calibration standard or AQC standard is not traceable follow the procedure **LPS117** for statistical analysis to show they are fit for purpose.
AQC's should be made in Quality lab. Separate pipettes and glassware should be used to prepare calibration standards and AQCs. All purchased standards should have the opened date, expiry date and initials of analyst opening the solution written on the container.
Standards and AQCs prepared in the lab must be clearly labeled with the date prepared and the expiry date followed by initials of an analyst who prepared the solution and a unique Laboratory Number.
Complete all relevant AQC standard logs following preparation in **LPF132** STD, AQC, ISTD & Reagent Preparation Log.

6.17 Ammonia as N 10 mg/L AQC Stock

Commercially available Certified Stock Standard should be used.

6.18 Nitrite as N 100 mg/L AQC Stock

Using previously dried (at 110°C +/- 5°C for at least 2h) analytical grade Sodium Nitrite, dissolve 0.493 g ± 0.004 g in approximately 400 ml of RO water in a 1000 ml. volumetric flask.

Allow to dissolve and invert the flask several times to ensure mixing and make up to the mark with RO water.

Transfer the solution to a plastic 1000 ml bottle. Label the bottle with the analyst's initials, date of preparation and expiry and unique laboratory number.

Stored between 3±2°C, the solution is stable for **one month**. **Commercially available stock standard can also be used.**

6.19 Nitrite 10 mg/L Intermediate AQC

Into a 100 ml volumetric flask containing approximately 40 ml of RO water, using a 10 ml pipette, transfer 10 ml of Nitrite as N 100 mg/L AQC Stock. Invert the flask several times to ensure mixing and make up to the mark RO water. Transfer to a 125 ml plastic bottle. Label the bottle with the analyst's initials, date of preparation and expiry and unique laboratory number. Stored between 3±2°C, the solution is stable for **one week**.

6.20 Ammonia 0.4 mg/L AQC Working Solution

Into a 100ml volumetric flask containing approximately 40 ml of RO water using an appropriate calibrated pipette transfer 4 ml of Ammonia 10 mg/L AQC Stock. Invert several times to ensure mixing. Make up to the mark using RO water. Transfer to a 125 ml plastic bottle. Label the bottle with the analyst's initials, date of preparation and expiry and unique laboratory number. Stored between 3±2°C, the solution is stable for **one week**.

6.21 Nitrite 0.12 mg/L AQC Working Solution

Into a 100ml volumetric flask containing approximately 40 ml of RO water using appropriate pipette transfer 1.2ml of Nitrite 10 mg/L Intermediate AQC Invert several times to ensure mixing. Make up to the mark using RO water. Transfer to a 125 ml plastic bottle. Label the bottle with the analyst's initials, date of preparation and expiry and unique laboratory number. Stored between 3±2°C, the solution is stable for **one week**.

6.22 Total Oxidised Nitrogen (TON), Nitrate as N, 10,000 mg/L AQC Stock

Commercially available Certified Stock Standard should be used.

6.23 TON 50 mg/L AQC Working Solution

Using an appropriate calibrated pipette transfer 0.5 ml of Total Oxidised Nitrogen (TON) as N, 10,000 mg/L AQC Stock into a 100 ml volumetric flask containing approximately 40 ml of RO water. Invert the flask several times to ensure mixing. Make up to the mark using RO water.

Transfer to a 125 ml plastic bottle. Label the bottle with the analyst's initials, date of preparation and expiry and unique laboratory number.

Stored between 3±2°C, the solution is stable for **one week.**

6.24 Chloride 10,000 mg/L AQC Stock

Commercially available Certified Stock Standard should be used.

6.25 Chloride 250 mg/L AQC Working solution

Using a calibrated pipette transfer 5ml of Chloride 10,000 mg/L AQC Stock into a 200 ml volumetric flask containing approximately 40 ml of RO water.

Invert the flask several times to ensure mixing. Make up to the mark using RO water.
Transfer to a 250 ml plastic bottle. Label the bottle with the analyst's initials, date of preparation and expiry and unique laboratory number.
Stored between 3±2°C, the solution is stable for **one month.**

6.26 **Sulphate 10,000 mg/L AQC Stock**

Commercially available Certified Stock Standard should be used.

6.27 **Silicate as SiO_2 1000 mg/L AQC Stock**

Using previously dried (at 110°C +/- 5°C for at least 2h) analytical grade Anhydrous Silicate, dissolve 1.57 g ± 0.015 g in approximately 250 ml of RO water in a 500 ml volumetric flask.
Allow to dissolve then invert the flask several times to ensure mixing and make up to the mark with RO water. Transfer to plastic bottle.
Label the bottle with the analyst's initials, date of preparation and expiry and unique laboratory number.
Stored between 3±2°C, the solution is stable for **six months**.
Commercially available stock standard can also be used.

6.28 **Silicate as SiO_2 100 mg/L Intermediate A AQC**

Into a 250 ml volumetric flask containing approximately 150 ml of RO water, using a calibrated pipette, transfer 25 ml of Silicate as SiO_2 1000 mg/L AQC Stock.
Invert the flask several times to ensure mixing and make up to the mark RO water. Transfer to plastic bottle.
Label the bottle with the analyst's initials, date of preparation and expiry and unique laboratory number.
Stored between 3±2°C, the solution is stable for **one month**.
Commercially available stock standard can also be used.

6.29 **Silicate 4mg/L & Sulphate 250mg/L AQC Working Solution**

Using an appropriate calibrated pipette, transfer 8.0 ml of the Silicate as SiO_2 100 mg/L **Intermediate A** AQC into a 200 ml volumetric flask containing approximately 40 ml of RO water and 5 ml of Sulphate 10,000mg/L AQC Stock.
Invert several times to ensure mixing. Make up to the mark using RO water.
Transfer to a 250 ml plastic bottle. Label the bottle with the analyst's initials, date of preparation and expiry and unique laboratory number. Stored between 3±2°C, the solution is stable for **one month.**

6.30 **Phosphate as P 1000 mg/L AQC Stock**

Commercially available Certified Stock Standard should be used.

6.31 **Phosphate as P 10 mg/L Intermediate AQC**

Into a 100 ml volumetric flask containing approximately 40 ml of RO water, using a calibrated pipette transfer 1 ml of Phosphate as P 1000 mg/L AQC Stock. Invert the flask several times to ensure mixing and make up to the mark RO water. Transfer to a 100 ml plastic bottle. Label the bottle with the analyst's initials, date of preparation and expiry and unique laboratory number. Stored between 3±2°C, the solution is stable for **one week**.

6.32 **Phosphate as P 0.5 mg/L AQC Working Solution**

With an appropriate calibrated transfer 12.5 ml of the Phosphate as P 10 mg/L Intermediate AQC into a 250ml volumetric flask containing approximately 40 ml of RO water. Invert several times to ensure mixing. Make up to the mark using RO

water. Transfer to a 250ml plastic bottle. Label the bottle with the analyst's initials, date of preparation and expiry and unique laboratory number.
Stored between 3±2°C, the solution is stable for **one week.**

7.0 Interference

Total Oxidized Nitrogen (TON)

No interferences identified.

Ammonia

Magnesium forming a precipitate of magnesium hydroxide at high pH values (>12). The reagent is used to prevent this interference and the method should tolerate magnesium at concentrations normally found in most non-saline waters.

Phosphate

Silica forms a pale blue complex which absorbs at 880 nm. This interference is insignificant, as to produce a positive 1 mg/L error in orthophosphate would require a silica concentration of approximately 4000 mg/L. The determination is sensitive to variations in acid concentrations, the higher the acidity, the lower and the sensitivity.

Sulphate

Turbid/highly coloured samples may interfere. Not applicable for the sample type.

Silica

If the pH of the samples falls outside ph units 2-10 and the sample is buffered, the required silicomolybdate complex may not be formed under the conditions of this method. Not applicable for the sample type.

8.0 Apparatus and Equipment

- Thermo Scientific Aquakem 600.
- Assorted volumetric glassware – To be of grade B or better.
- Calibrated 1, 5 & 10ml pipettes.
- Aquakem cuvettes.
- 2ml sample cups.
- 4ml sample cups.
- Calibrated balance.
- 10 ml Opaque sample tubes.

9.0 Sampling collection, preservation and handling

Samples are collected in 1 litre bottles.

If analysis cannot be undertaken immediately, samples should be stored at the following temperature until the day of analysis.

- 3+-2°C (Chemistry).

Allow samples to settle at room temperature before undertaking analysis.
Based on stability testing, this analysis shall be completed within 9 days from date of sampling.
Following analysis the samples should be placed back in storage.

10.0 Service & Maintenance

Instrument is under annual service contract via manufacturer.

Maintenance and Best Practice:

a. Leave DI water in the container used as rinse to degas overnight.
b. Wash needles and water reservoirs daily.
c. Do not use cold reagents straight from the fridge. Allow them to warm up for approximately 20 min before use.
d. Do not over-fill the sample tubes/cups with the liquid.
e. While performing **standby** use washing solution neat on the Monday and the dilute it throughout the week.

11.0 Calibration

Automatic Pipettes

The automatic pipettes are calibrated annually by a UKAS accredited company.
Daily calibration checks are carried out and recorded on **LPF096**.

Balances

Balances are calibrated every 12 months by a UKAS accredited company.
Daily calibration checks are carried out and recorded on **LPF006**.
Please refer to procedure **LPS003** Balances – Calibration and In-house monitoring of analytical and top pan balances.

Calibration of the instrument

Prior to any samples analysis the instrument must be calibrated;
Remove the working calibration standards from the refrigerator and allow 20 minutes for the working standards to warm.
Open the window of the sample lid (purple) and remove the lid when the green light appears.
Remove any 4 ml cups from the top of the wheel.
Pour out the calibration blanks drawn fresh each day for each required determinant and place into their desired position. The positions are labelled as below:

S0 – AMMONIA	**S4 – CHLORIDE**
S1 – PHOSPHATE	**S5 – SULPHATE**
S2 – NITRITE	**S9 – SILICA**
S3 – TON	

Replace the lid and close the window.
Select two racks (for example racks 1 and 2) and pour out the standards in to 4 ml cups as shown below.

Rack 1 Position	Calibration Standard	Rack 2 Position	Calibration Standard

1	**Sep Mix A Cal Std 1**	**1**	**MIX Std 1**
2	**Sep Mix A Cal Std 2**	**2**	**MIX Std 2**
3	**Sep Mix A Cal Std 3**	**3**	**MIX Std 3**
4	**Sep Mix A Cal Std 4**	**4**	**MIX Std 4**
5	**Sep Mix A Cal Std 5**	**5**	**MIX Std 5**
6	**Sep Mix A Cal Std 6**	**6**	**MIX Std 6**
7	**Sep Mix B Cal Std 1**	**7**	**PO4 Std 1**
8	**Sep Mix B Cal Std 2**	**8**	**PO4 Std 2**
9	**Sep Mix B Cal Std 3**	**9**	**PO4 Std 3**
10	**Sep Mix B Cal Std 4**	**10**	**PO4 Std 4**
11	**Sep Mix B Cal Std 5**	**11**	**PO4 Std 5**
12	**Sep Mix B Cal Std 6**	**12**	**Empty**
13	**Empty**	**12**	**Empty**
14	**Empty**	**14**	**Empty**

Once a rack of standards is complete, ensure that the green light is on, and open the rack door in front of the sample carousel. Place the rack inside and onto the metal dowels.

Make sure the rack is firmly place into position. Slide the door closed.

The main screen will indicate which rack has been entered. Select the rack by clicking on the rack icon. Enter the calibration standard identity from the drop down list for every position.

The calibration identities are as below:

Standard	**NH_4**	**NO_2**	**TON**	**Cl**	**SO_4**	**Si**	**PO**
1	**Sep Mix A-1**	**Sep Mix A-1**	**Sep Mix B-1**	**Sep Mix B-1**	**MIX-1**	**MIX-1**	**PO4 - 1**
2	**Sep Mix A-2**	**Sep Mix A-2**	**Sep Mix B-2**	**Sep Mix B-2**	**MIX-2**	**MIX-2**	**PO4 - 2**
3	**Sep Mix A-3**	**Sep Mix A-3**	**Sep Mix B-3**	**Sep Mix B-3**	**MIX-3**	**MIX-3**	**PO4 – 3**
4	**Sep Mix A-4**	**Sep Mix A-4**	**Sep Mix B-4**	**Sep Mix B-4**	**MIX-4**	**MIX-4**	**PO4 – 4**
5	**Sep Mix A-5**	**Sep Mix A-5**	**Sep Mix B-5**	**Sep Mix B-5**	**MIX-5**	**MIX-5**	**PO4 - 5**
6	**Sep Mix A-6**	**Sep Mix A-6**	**Sep Mix B-6**	**Sep Mix B-6**	**MIX-6**	**-**	**-**

Select “Main” followed by F6 “Calibration/QC Selection”. Select the appropriate calibration tests from the list below:

1. Ammonia NH_4 Sep
2. Nitrite NO_2 Sep
3. TON TON Sep
4. Chloride Cl Sep
5. Sulphate SO_4 MIX
6. Silica Si MIX
7. Phosphate PO_4 CAL

Select F1 ‘’Calibrate’’ than calibration status will change to pending.

Select “Main” and press the green <I> start button next to the “Home” button on the keypad.
Remember the instrument will not proceed until this button is pressed.
The standards are analysed in duplication.
The instrument then produces a calibration slope calculated from the measured concentration and the desired concentration.
Calibration coefficient need to be greater than 0.998 and recorded **on LPF294**.
Complete any system suitability requirements for the calibration, the mean of the duplicated second standard responses should meet the criteria **LPF173**.
The calculated concentration of the blank standard 0 should be within twice the LOD.
If the result is outside 2 X LOD the run must be rejected and an investigation into the cause must be undertaken.
The calibration must have an R^2 as stated on **LPF173** or greater. The duplicated standards should show good duplication.
If the calibration is not acceptable, print it out and on it explain why it has been rejected.
Keep the calibration, as it will form part of the final report.
Repeat any failed calibrations by selecting “Recalibrate” F6.
Accepted calibrations are printed and stored with any run information.
Calibration Check should meet the criteria and must be recorded on **LPF174**.

12.0 Quality Control

The results for the AQC are plotted on Shewart charts which are maintained via CSOLS software.
For use of this software please refer to procedure **LPS135**.
The following rules are applied to the charts:

- 2 out of 3 2S.
- 3S.
- Nine consecutive points on the same side as the mean.
- Six consecutive points increasing or decreasing.

In addition to the AQC chart rules the following are also applied as part of quality control:

- Blank.
- Calibration/drift Check.
- System suitability.

Rule breaches are investigated as per **LPS074** Analytical Quality Control – Chemistry & Sampling.
For trending issues or in the event of significant issues a larger scale investigation may be required and will be documented through procedure **LPS046.**
For any sample result above PCV follow **LPS051**
A batch consists of no more than **19** samples.
Complete all daily and monthly maintenance records.
Record in the system suitability check logs the following:

1. Second standards response mean (System suitability check).Ensure the response is between the set limits.

2. The coefficient of det. Ensuring this is between set limits.
3. The calibration standard zero is less than twice the LOD.
4. The calibration check is between the set limits.
5. The blank sample is less than twice the LOD

Analyst can use an AQC prepared from non-traceable standard if the comparison test has been carried out following **LPS117**. Other option in section 6.38 does not require any comparison test if analyst chooses to use an AQC made from traceable material.
Record all AQC data on the AQC charts on CSOLS.
Record any issues in the Instrument Diary.
In order for the associated samples to be accepted, the calibration must have an R^2 as stated on **LPF294** or greater.
If the R^2 is not acceptable then results cannot be accepted and the instrument must be recalibrated before analysis can be continued.

13.0 Procedure

Daily Start-Up Procedure

Turn on the monitor. If the system requires a password to enter the software enter the following: "Klab1sUPER", and click on the Aquakem icon on the desktop.
Slide out the storage compartments in the middle of the instrument and check the waste water container is empty. If it is not then pour remaining liquid down the sinks within the laboratory.
Check the cuvettes waste container is not full. If this is full then remove and seal up as instructed on the cardboard box and dispose of in the correct procedure.
Remove the supply water tank which is labelled "H_2O" and refill with deionised water. (Use a trolley to carry the water containers). The deionised water used as wash should be left overnight to degas before use.
On the right hand side of the instrument slide the reagent window lid (coloured orange)
open. Wait for the green light to appear.

NOTE: NEVER ATTEMPT TO PLACE FINGERS WITHIN THE INSTRUMENT WHILE THE RED LIGHT IS ON. THE RED LIGHT INDICATES THE INSTRUMENT IS STILL MOVING.

Once it has turned green remove the lid (the analyst may have to open the main hood of the instrument to do this), then remove the reagent carousel inside.
With some blue paper remove any condensation from within the chamber.
Replace carousel and lid and slide the window closed.
Ensure there are no warning messages requiring any maintenance flagged up on the monitor screen.
If everything is okay, select "More" F8 and "Instruction Actions" F2using the mouse, or touch screen feature. Select "Perform Water Wash" F6 and select "OK".
The instrument will then perform a water wash which will purge the system of any air bubbles.
Perform this wash three times.
Once the instrument has completed the water wash the instrument must perform a "Start Up". To do this, select "Start Up" F1 on the main page.

The instrument will inform you of any expired reagents, press ok to this. The instrument will then ask if you would like to perform a start-up, press ok.
If the instrument performs a successful start-up it will indicate this by showing a "Ready" message in blue in the top left hand corner of the screen.
If this does not occur consult an experienced analyst.
During the start up the instrument will perform a water blank on the supply deionised water.
To check the blank results press "More" F8, "Instrument Actions" F2, "More" F8 and "Check Water Blank" F1.
Initially this page shows the blank absorbance values for the lowest wavelength, 340 nm. Press "Show All" F5 and all the results for each of the wavelengths are superimposed on the screen.
To ensure the deionised supply water is not contaminated the absorbance values for should fall within +/- 2 mA.
If this is not the case, than select "Instrument Actions" F1 and "Perform Water Blank" F1.
Allow the instrument to perform the function and check water blanks again.
If the problem persists consult an experienced analyst.
Select "Main" in the top left hand corner.
This will take the analyst back to the home page. Select "Reagents" to the left of the "Main" icon.
The page indicates the position and condition of the reagents.
The key in the bottom left hand corner indicates whether a reagent is empty (red), expired (purple) or is low in volume (yellow).
To remove any reagents which are outside of stability or empty, simply select the reagent position on the screen either by touch or by using the mouse.
Select "Remove Reagent" F3, slides the window of the reagent lid open until the green light is displayed.
The green light indicates the reagent carousel has stopped moving and will not move again until the reagent lid window is closed.
Remove the reagent from the carousel and close the lid. Open a new reagent bottle and complete the reagent log (**LPF132 or LPF306**).
Again select the position on the screen in which the reagent is to be placed.
Select "Insert Reagent" F2 and a library list of reagents will appear, select the appropriate description and press "OK".
Slide the reagent window open and wait for the green light to appear, then insert the reagent and close the window.
The instrument will identify the reagent lot number by scanning the barcode on the bottle.
The positions of the reagents within the carousel are:

Reagent Carousel positions		
1 TON 3.	**3 TON 1.**	**4 Chloride**
6 Silica 1.	**7 Silica 2.**	**8 Silica 3.**
15 Sulphate.	**24 TON 2.**	**30 Phosphate 1.**
31 Phosphate 2.	**40 Ammonia 1.**	**41 Ammonia 2.**
44 RO Water.		

Sample Preparation and Analysis

Label all tubes with the DCWW LIMS sample ID number with a permanent marker pen.

This will aid the analyst during pouring of samples and reduce the risk of incorrect sample analysis.

Invert the sample bottle to ensure a homogenous solution.

Check the sample bottle ID number with the number of the tube.

Rinse the 10 ml opaque analysis tube with the sample to remove contamination and pour into a waste container.

Fill the tube to approximately three quarters with the sample and place into its allocated segment position. Each run should include:

- Wash at the start.
- Calibration check after each calibration (Working Calibration Standard 3: Sep Mix A-3, Sep Mix B-3, Mix-3, PO_4-3)
- Blank RO water sample (poured out at the same time as samples are racked up)
- Nineteen samples
- AQC sample (poured out at the same time as samples are racked up)

When the samples have been poured out they can be loaded into the instrument.

Ensuring that the segment loading door green light is on, slides open the door. Load the segment into the loading bay making certain the segment is positioned securely on the metal positioning dowels and close the door. The segment loading door light will turn red.

Complete the loading of the remaining segments by following the process again.

When all the segments are loaded into the instrument the analyst should press the main icon on the monitor screen. This will take the software back to the main screen, if not already on the main page. Select the "Sample Disk Info" above the list of segments. This will show the samples and segments within the instrument.

Check the sample disk info against the sample numbers on the worksheet.

Once the analyst is satisfied the samples are in the correct positions press the green <I> start button on the keypad.

Confirmation of Results

During and following the analysis the results will be shown on the sample results page.

All results can be checked by the analyst either during the analysis or once the analysis is complete. The drop down menu at the top of the results screen will allow the analyst to view the results of all completed determinants.

Check the calibration checks, blanks and AQCs are acceptable. If any system suitability check and/or quality controls do not meet the set requirements then follow the correct quality procedures.

Samples analysis can be repeated if necessary by highlighting the sample in the list of results and selecting "More" F8, and "Rerun Selected" F3.

Any results which exceed the Prescribed Concentration Value (PCV) must be logged on the correct PCV breach document (**LPF147**).

On completion of the analysis the analyst should print out the "Sample Disk Info" and the results.
Combine this data with the calibration data and staple. On the cover page (Sample Disk Info) the analyst is required to date the run, add sample worksheet information, AQC batch information and the analyst's initials.
The run data then follows the archive procedure.
All AQCs are then plotted on the determinants Shewart Quality Control graph.

14.0 Calculations

No manual calculation is required in the method however, the results generated as N by the instrument for all Nitrogen species can be converted by using the conversion factors below.
Ammonium as NH_4: Ammonium as NH_4 is calculated by multiplying the instrument result as N with the factor of 1.286. This factor is applied in LIMS.
Where the result for Ammonium as N is less than the LOD, the calculated result is reported in a less than '<' entry.
Nitrite as NO_2: Nitrite as NO_2 is calculated by multiplying the instrument result as N with the factor of 3.286. The factor is applied in QDB.
Where the value for Nitrite as N is less than the LOD, the calculated value is reported in a less than '<' entry.
Total Oxidised Nitrogen (TON) as NO_3: Total Oxidised Nitrogen (TON) **as NO_3** is calculated by multiplying the instrument result as N with the factor of 4.428.
The factor is applied in QDB. If the value for TON as N is less than the LOD, the calculated value is reported in a less than '<' entry.
Nitrate as NO_3: Nitrate as NO_3 is calculated by subtracting NO_2 as N from TON as N then multiplying the resulting value with the factor of 4.428. NO_3 as N is calculated in LIMS and the factor is applied in QDB.
Where the result for Nitrite as N is less than the LOD and TON as N is less than the LOD, the Nitrate as NO_3 is reported in a less than '<' entry after applying the conversion factor below.
In an instance where either NO_2 as N or TON as N value is less than LOD, the calculated value is reported in a less than '<' entry.
Nitrate/Nitrite ratio: Nitrate/Nitrite ratio is defined in "Guidelines for drinking-water quality, second edition, volume 2" as the sum of ratios of the concentration of each component to its guideline value.
Therefore, Nitrate/Nitrite ratio is calculated by dividing the Nitrate value by 11.29 and dividing the Nitrite value by 0.913 then adding the two resulting values together.
Where the result for Nitrite as N is less than the LOD and NO_3 as N is less than the LOD, the calculated Nitrate/Nitrite ratio is reported in a less than '<' entry.

This calculation is applied in LIMS.

Ammonium as N to NH_4 = N*1.286

Nitrite as N to NO_2 = N*3.286

Nitrate as N to NO_3 = (TON as N-NO_2 as N)*4.428

TON as N to TON as NO_3 = N*4.428

Nitrate/Nitrite ratio = (NO_3 as N/11.29) + (NO_2 as N/0.913)

15.0 Recording and Reporting of Results

All hand written results should be written in blue or black ink.
All results are recorded and authorised into LIMS in two significant figures and in accordance with the DCWW procedure.
Results are reported into LIMS according to LIMS procedure **LPS099.**

16.0 References

Thermo Scientific Aquakem 600 manual.
Guidelines for drinking-water quality, second edition, volume 2.

17.0 Appendix 1: Method Validation

A complete set of the validation data is maintained on the Infozone.
The location of this information is: **08 Validation data.**
Within this storage location a summary is available by test.

18.0 Appendix 2 – Performance Data

Parameter	Equipment	Limit of Detection			Reporting Limit	
		Target % of PCV	Actual	Units		
Chloride	KONE1	10	3.002	mg/l	3.1	mg/l
Ammonium	KONE1	10	0.0030	mg/l	0.0030	mg/l
TON	KONE1	10	0.476	mg/l	0.48	mg/l
Nitrite	KONE1	10	0.00448	mg/l	0.0045	mg/l
Sulphate	KONE1	10	2.669	mg/l	2.7	mg/l
Phosphate	KONE1	10	0.029	mg/l	0.03	mg/l
Silicate	KONE1	10	0.185	mg/L	0.19	mg/L

19.0 Appendix 3 – System Suitability

System Suitability Checks

All data is recorded onto the relevant documents.
Each analytical run should comply with the following system suitability checks:

- The correlation coefficient for each calibration should be in accordance with **LPF173.**
- The calibration second standard absorbance should fall between the set limits.
- The calibration check should comply with set limits.
- The blank samples should not exceed set limits.

20.0 Appendix 4 – Method Training

Only fully trained staff are permitted to perform this procedure.
Details of training can be found on the Infozone.
The location of this information is:
05. Laboratory Quality Spreadsheets – 10 - DCWW Glaslyn & Bretton Training Matrix

21.0 Appendix 5 – Measurement of Uncertainty

An estimation of the Uncertainty of Measurement is maintained on the Infozone.
The location of this information is: **08 Validation data – uncertainty of Measurement – Chemistry.** Within this storage location a summary is available by test.

22.0 Appendix 6 – Risk Assessment

The associated risk assessment for this procedure is maintained on the Infozone.
The location of this information is: **12. Health & Safety.**

Appendix 2: Primary Component Analysis of data (Chapter 2)

A2.1 TP (mg L^{-1}) LM data 1995-1999.
Primary Component Analysis (PCA) was completed including all variables where data was available between 2008-2012 (Figure A2.1.1).

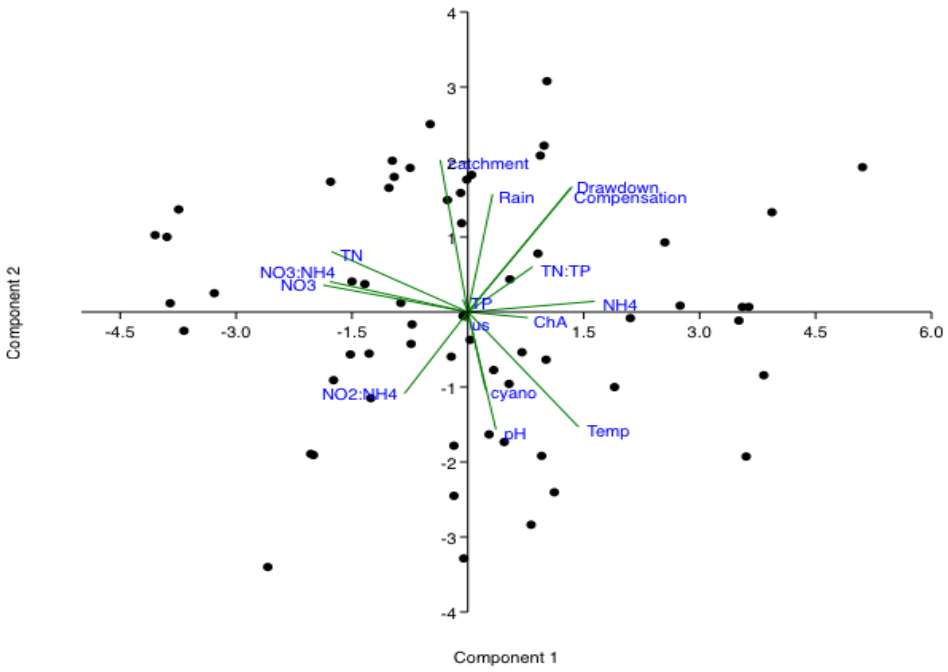

Figure A2.1.1. PCA for all variables 1995-1999. PC1 and PC2 represented 27.47% and 14.73% of the data variation respectively.

The variables demonstrating correlation with TP over the 1995-1999 sampling period were included in the LM analysis (Table A2.1.1)

Table A2.1.1. variables in LM analysis

Variables
TN:TP (mol/ml)
Rainfall (mm)
Compensation volume (ML/day)
Reservoir level (m)
NH_4^+ (mg L^{-1})
NO_2^-: NH_4^+ (mol/ml)

A2.2. TP (mg L^{-1}) LM data 2008-2012.
Primary Component Analysis (PCA) was completed including all variables where data was available between 2008-2012 (Figure A2.2.1).

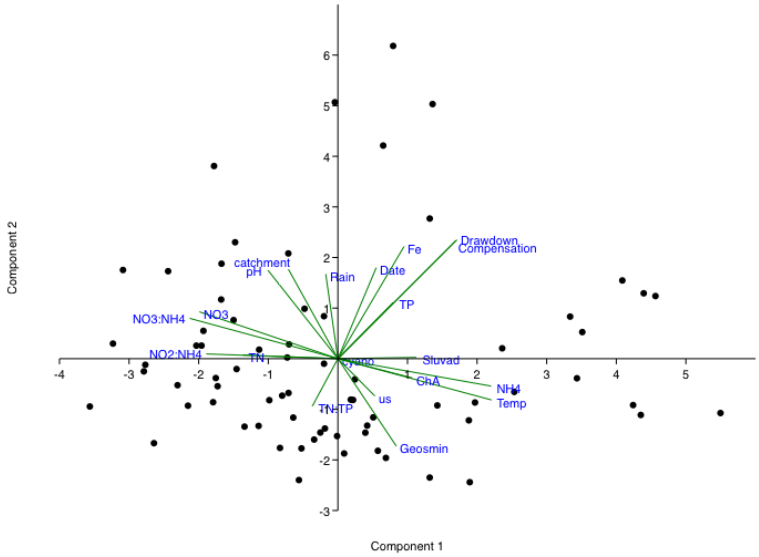

Figure A2.2.1. PCA for all variables 2008-2012. PC1 and PC2 represented 22.12% and 16.32% of the data variation respectively.

The variables demonstrating correlation with TP over the 2008-2012 sampling period were included in the LM analysis (Table A2.2.1).

Table A2.2.1. variables in LM analysis

Variables
Reservoir level (m)
Compensation volume (ML/day)
TN:TP (mol/ml)
Fe_{3}^{+} (mg L^{-1})
Date (year)

A2.3. LM analysis of NH_4^+ (2008-2012)

Primary Component Analysis (PCA) was completed including all variables where data was available between 2008-2012 (Figure A2.3.1).

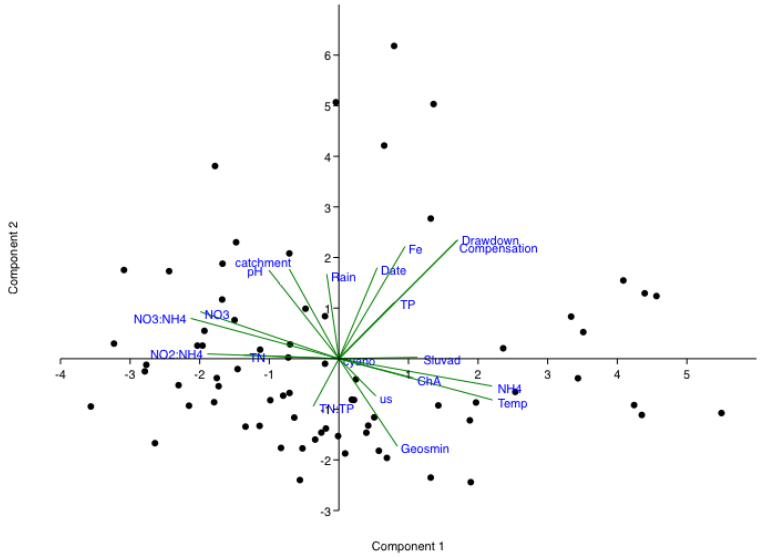

Figure A2.3.1. PCA for all variables 2008-2012. PC1 and PC2 represented 22.12% and 16.32% of the data variation respectively.

The variables demonstrating correlation with NH_4^+ over the 2008-2012 sampling period were included in the LM analysis (Table A2.3.1).

Table A2.3.1. variables in LM analysis

Variables
Water temperature (°C)
Geosmin (ng L^{-1})
Chlorophyll-a (cells/ml)
Conductivity (µs)
Cyanobacteria (cfu/ml)
Catchment inflow (ML/day)
pH
NO_3^- (mg L^{-1})
NO_3^-: NH_4^+ (mol/ml)
NO_2^-: NH_4^+ (mol/ml)
Rainfall (mm)
TN (mg L^{-1})

A2.4. LM analysis NO_3^- (mg L^{-1}) (2008-2012).

Primary Component Analysis (PCA) was completed including all variables where data was available between 2008-2012 (Figure A2.4.1).

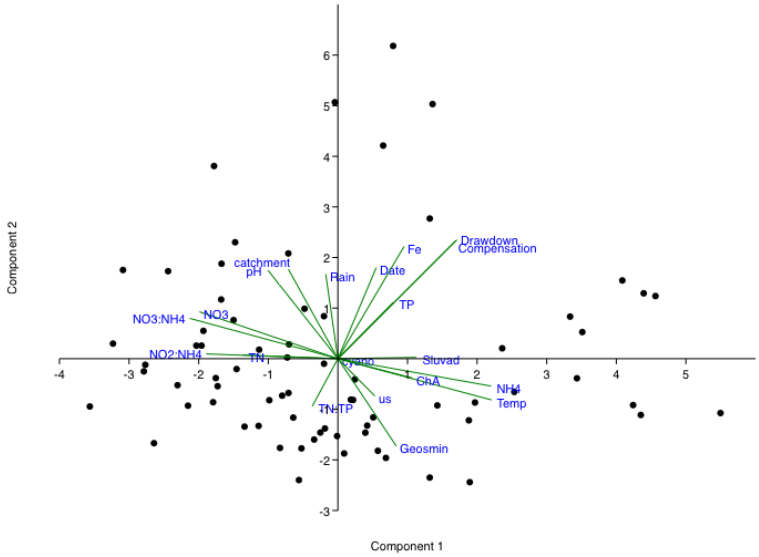

Figure A2.4.1 PCA for all variables 2008-2012. PC1 and PC2 represented 22.12% and 16.32% of the data variation respectively.

The variables demonstrating correlation with NO_3^- over the 2008-2012 sampling period were included in the LM analysis (Table A2.4.1).

Table A2.4.1. variables in LM analysis

Variables
Water temperature (°C)
Geosmin (ng L^{-1})
Chlorophyll-a (cells/ml)
Conductivity (µs)
Cyanobacteria (cfu/ml)
Catchment inflow (ML/day)
pH
NH_4^+ (mg L^{-1})
NO_3^-: NH_4^+ (mol/ml)
NO_2^-: NH_4^+ (mol/ml)
Rainfall (mm)
TN (mg L^{-1})

A2.5. LM analysis NO_3^-: NH_4^+ (mol/ml) (2008-2012)

Primary Component Analysis (PCA) was completed including all variables where data was available between 2008-2012 (Figure A2.5.1).

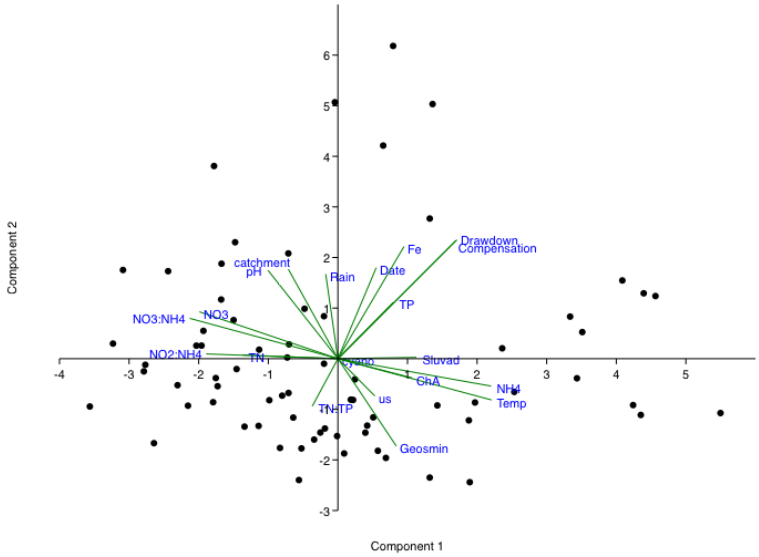

Figure A2.5.1. PCA for all variables 2008-2012. PC1 and PC2 represented 22.12% and 16.32% of the data variation respectively.

The variables demonstrating correlation with NO_3^-: NH_4^+ (mol/ml) over the 2008-2012 sampling period were included in the LM analysis (Table A2.5.1).

Table A2.5.1. variables in LM analysis

Variables
Water temperature (°C)
Geosmin (ng L^{-1})
Chlorophyll-a (cells/ml)
Conductivity (µs)
Cyanobacteria (cfu/ml)
Catchment inflow (ML/day)
pH
NH_4^+ (mg L^{-1})
NO_3^- (mg L^{-1})
NO_2^-: NH_4^+ (mol/ml)
Rainfall (mm)
TN (mg L^{-1})

A2.6. Primary Component Analysis (PCA) was completed including all variables where data was available between 1995-1999 (Figure A2.6.1).

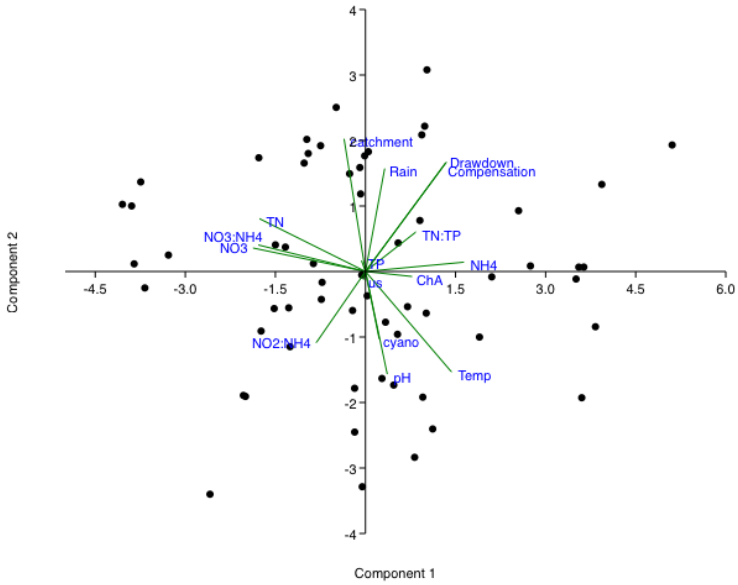

Figure A2.6.1. PCA for all variables 2008-2012. PC1 and PC2 represented 27.47% and 14.73% of the data variation respectively.

The variables demonstrating correlation with TN:TP (mol/ml) over the 1995-1999 sampling period were included in the LM analysis (Table A2.6.1).

Table 2A2.6.1 variables in LM analysis

Variables
TP (mg L^{-1})
Reservoir level (m)
Compensation flow (ML/day)
Rainfall (mm)
NH_4^+ (mg L^{-1})
NO_3^-: NH_4^+ (mol/ml)
TN:TP (mol/ml)

A2.7. LM analysis of TN:TP (mol/ml) (2008-2012)

Primary Component Analysis (PCA) was completed including all variables where data was available between 1995-1999 (Figure A2.7.1).

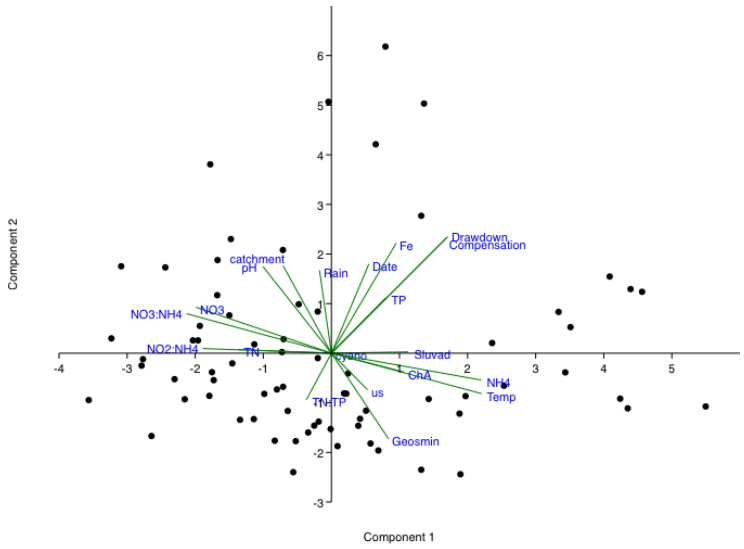

Figure A2.7.1. PCA for all variables 2008-2012. PC1 and PC2 represented 22.12% and 16.32% of the data variation respectively.

The variables demonstrating correlation with TN:TP (mol/ml) over the 2008-2012 sampling period were included in the LM analysis (Table A2.7.1).

Table A2.7.1. variables in LM analysis

Variables
Compensation flow (ML/day)
Reservoir level (m)
Date (year)
TP (mg L^{-1})
Fe_{3}^{+} (mg L^{-1})

A2.8. pH data (1984-1999)

Primary Component Analysis (PCA) was completed including all variables where data was available between 1984-1999 (Figure A2.8.1).

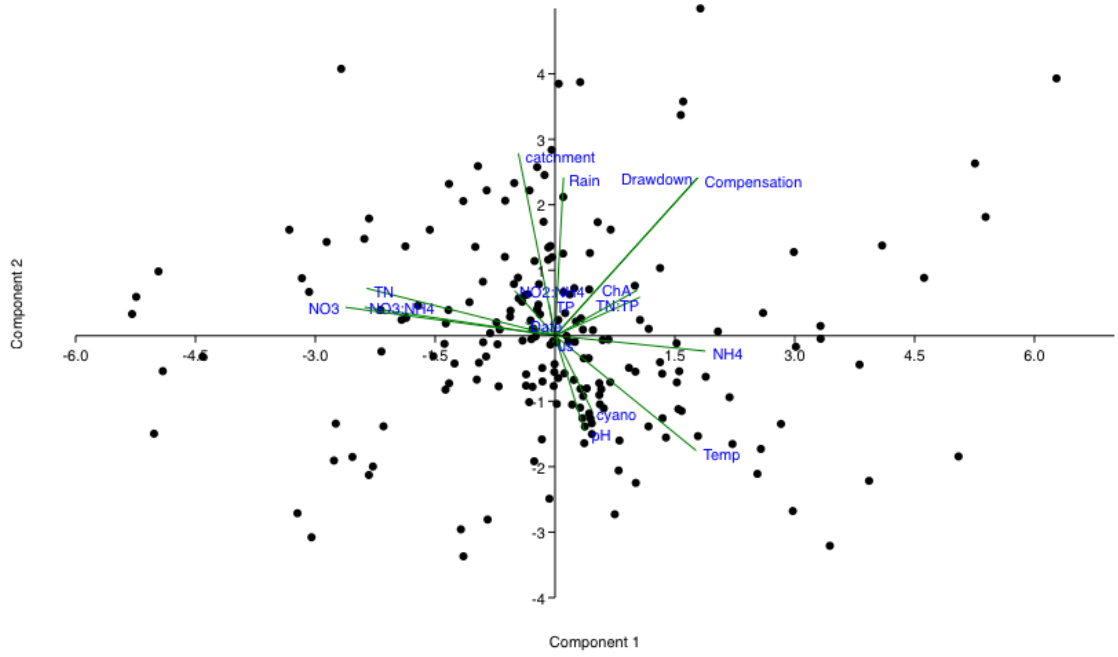

Figure A2.8.1. PCA for all variables 1984-1999. PC1 and PC2 represented 20.55% and 12.92% of the data variation respectively.

The variables demonstrating correlation with pH over the 1984-1999 sampling period were included in the LM analysis (Table A2.8.1).

Table A2.8.1. variables included in LM analysis

Variables
Cyanobacteria (cfu/ml)
Water temperature (°C)
NH_4^+ (mg L^{-1})
Conductivity (µm)
TN (mgL^{-1})
NO_3^-: NH_4^+(mol/ml)
NO_3^-
NO_2^-
Catchment inflow (ML/day)

A2.9. pH post-2000 data (2000-2016)

Primary Component Analysis (PCA) was completed including all variables where data was available between 2000-2016 (Figure A2.9.1).

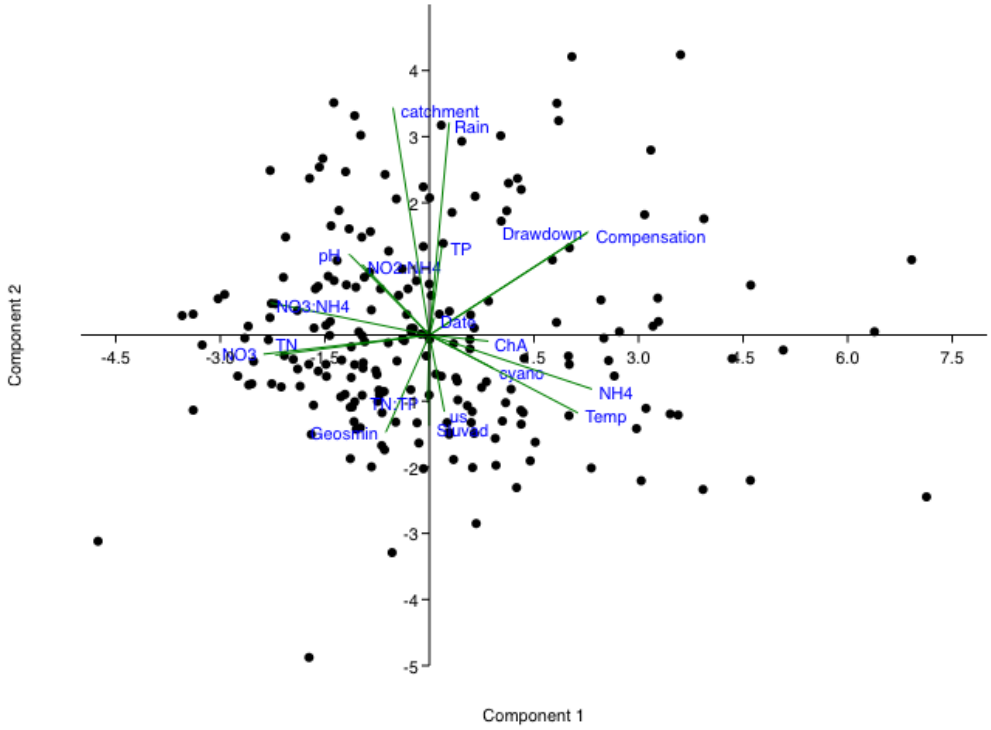

Figure A2.9.1. PCA for all variables 2000-2016. PC1 and PC2 represented 19.84% and 11.5% of the data variation respectively.

The variables demonstrating correlation with pH over the 2000-2016 sampling period were included in the LM analysis (Table A2.9.1)

Table 2.3.3.6.2.1. variables omitted from LM analysis

Variables
NO_2^-: NH_4^+ (mol/ml)
Reservoir level (m)
NO_3^-: NH_4^+ (mol/ml)
Catchment inflow (ML/day)
Water temperature (°C)
NH_4^+ (mg L^{-1})
Cyanobacteria (cfu/ml)
Conductivity (µs)
Chlorophyll-a (cells/ml)

A2.10. Water temperature 1984-2016 data

Primary Component Analysis (PCA) was completed including all variables where data was available between 1984-2016 (Figure A2.10.1).

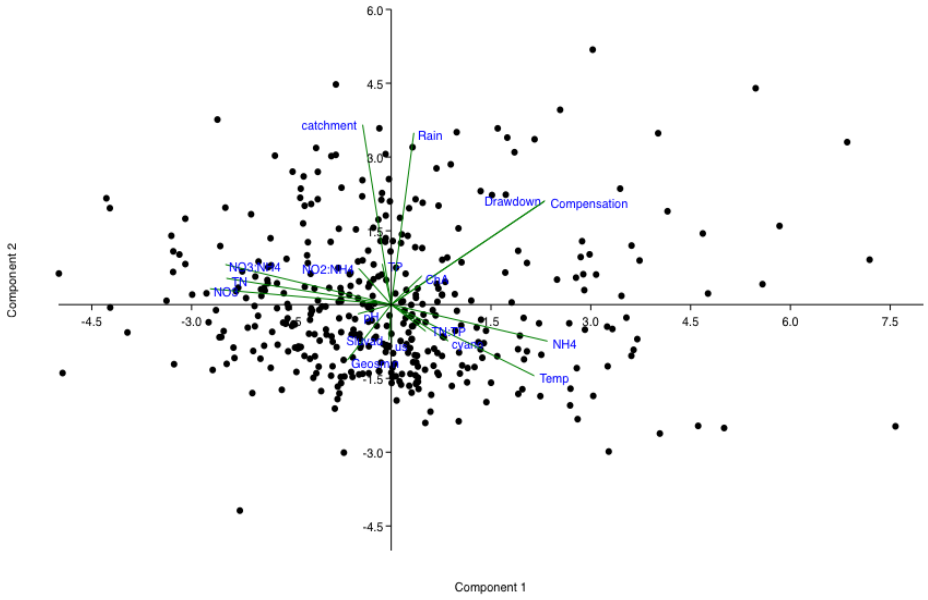

Figure A2.10.1. PCA for all variables 2000-2016. PC1 and PC2 represented 18.93% and 11.25% of the data variation respectively.

The variables that demonstrated correlation with water temperature over the 1984-2016 sampling period were included in the LM analysis (Table A2.10.1)

Table 2A2.10.1. variables LM analysis

Variables
NH_4^+ (mg L^{-1})
TN:TP (mol/ml)
Cyanobacteria (cfu/ml)
Conductivity (µs)
NO_2^-: NH_4^+ (mol/ml)
Catchment inflow
NO_3^-: NH_4^+ (mol/ml)
NO_3^- (mg L^{-1})
TN (mg L^{-1})

A2.11. Water temperature 1984-1999 data

Primary Component Analysis (PCA) was completed including all variables where data was available between 1984-1999 (Figure A2.11.1).

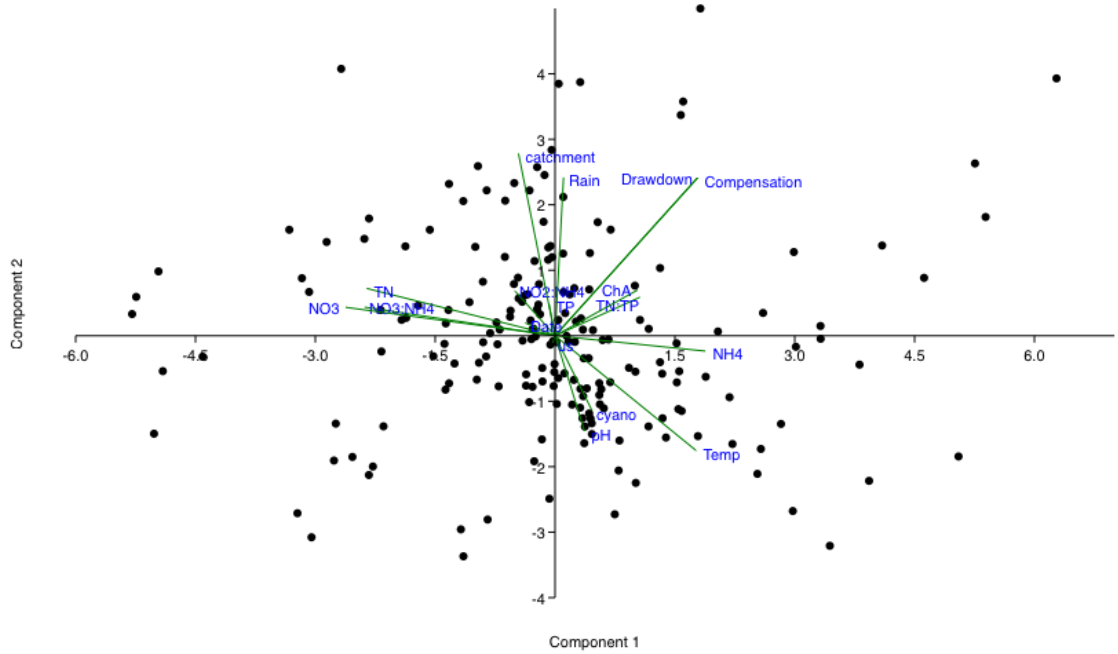

Figure A2.11.1. PCA for all variables 1984-1999. PC1 and PC2 represented 20.55% and 12.92% of the data variation respectively.

The variables that demonstrated correlation with water temperature over the 1984-1999 sampling period were included in the LM analysis (Table A2.11.1)

Table A2.11.1. variables in LM analysis

Variables
Cyanobacteria (cfu/ml)
pH
NH_4^+ (mg L^{-1})
Conductivity (µs)
TN (mgL^{-1})
NO_3^-: NH_4^+ (mol/ml)
NO_3^-
NO_2^-
Catchment inflow (ML/day)

A2.12. Water temperature (°C) 2000-2016 data

Primary Component Analysis (PCA) was completed including all variables where data was available between 2000-2016 (Figure A2.12.1).

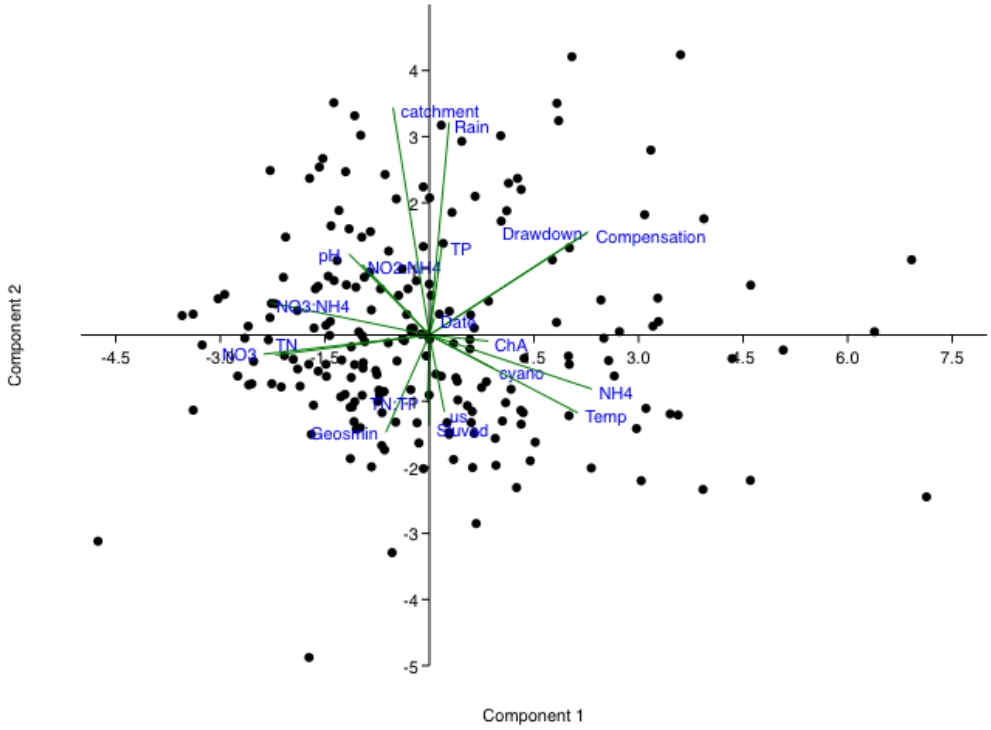

Figure A2.12.1. PCA for all variables 2000-2016. PC1 and PC2 represented 19.84% and 11.5% of the data variation respectively.

The variables that demonstrated correlation with water temperature over the 2000-2016 sampling period were included in the LM analysis (Table A2.12.1)

Table A2.12.1. variables in LM analysis

Variables
NO_2^-: NH_4^+ (mol/ml)
Reservoir level (m)
NO_3^-: NH_4^+ (mol/ml)
Catchment inflow (ML/day)
Water temperature (°C)
NH_4^+ (mg L^{-1})
Cyanobacteria (cfu/ml)
Conductivity (µs)
Chlorophyll-a (cells/ml)

A2.13. Mean rainfall data: 1990-1999

Primary Component Analysis (PCA) was completed including all variables where data was available between 1990-1999 (Figure A2.13.1).

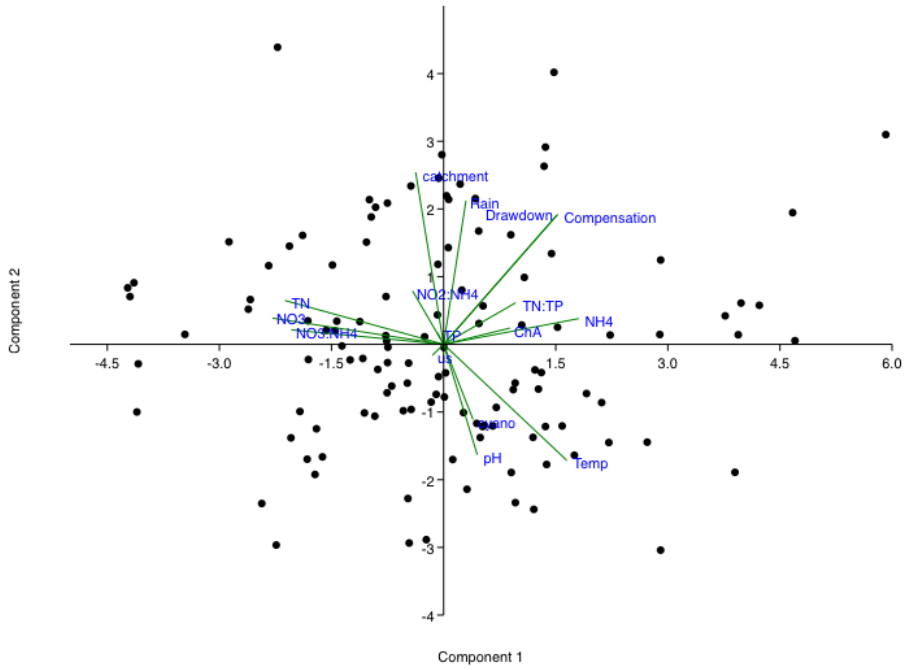

Figure A2.13.1. PCA for all variables 1990-1999. PC1 and PC2 represented 23.52% and 14.32% of the data variation respectively.

The variables that demonstrated correlation with water temperature over the 1990-1999 sampling period were included in the LM analysis (Table A2.13.1)

Table A2.13.1. variables in LM analysis

Variables
Reservoir level (m)
TN:TP (mol/ml)
NH_4^+ (mg L^{-1})
Chlorophyll-a (cells/ml)
TP (mg L^{-1})
Conductivity (µs)

A2.14. Mean rainfall data: 2000-2009

Primary Component Analysis (PCA) was completed including all variables where data was available between 2000-2016 (Figure A2.14.1).

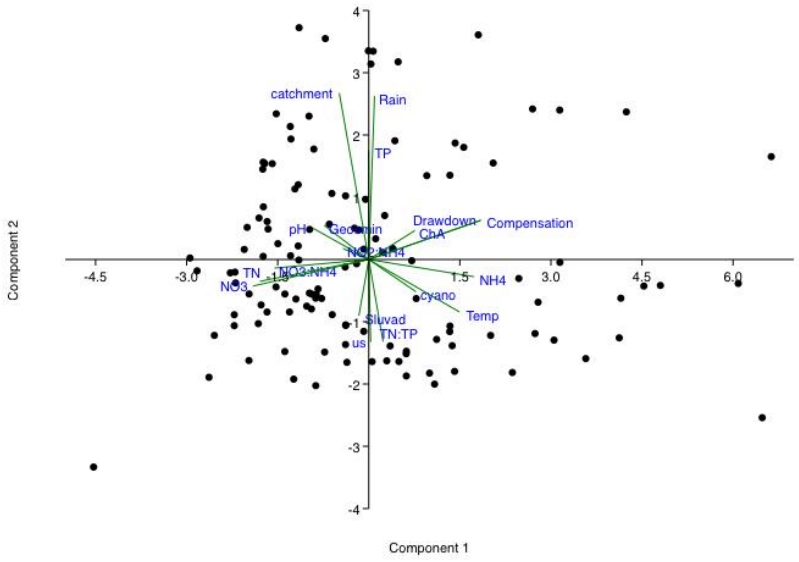

Figure A2.14.1. PCA for all variables 2000-2009. PC1 and PC2 represented 23.12% and 12.31% of the data variation respectively.

The variables that demonstrated correlation with water temperature over the 2000-2009 sampling period were included in the LM analysis (Table A2.14.1)

Table A2.14.1 variables in LM analysis

Variables
TP (mg L^{-1})
Reservoir level (m)
Chlorophyll-a (cells/ml)
Compensation volume (ML/day)
NO_2^-: NH_4^+ (mol/ml)
TN (mg L^{-1})
NO_3^- (mg L^{-1})
NO_3^-: NH_4^+ (mol/ml)
Conductivity (µs)

A2.15.1. Geosmin (ng L^{-1}) LM analysis (2008-2010).

Primary Component Analysis (PCA) was completed including all variables where data was available between 2008-2010 (Figure 2A2.15.1

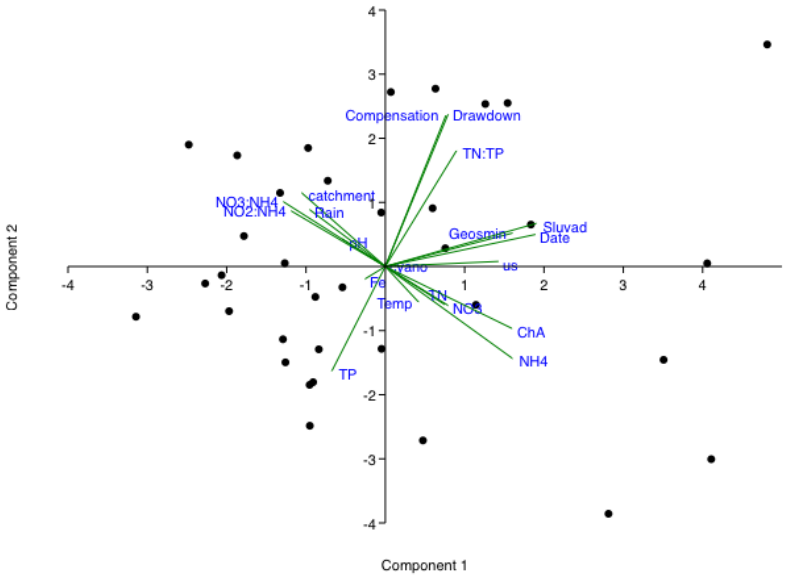

Figure A2.15.1. PCA for all variables 2008-2010. PC1 and PC2 represented 19.91% and 16.23% of the data variation respectively.

The variables that demonstrated correlation with geosmin over the 2008-2010 sampling period were included in the LM analysis (Table A2.15.1)

Table A2.15.1. Variables in LM analysis

Variables
Water temperature (°C)
TP (mg L^{-1})
Fe (mg L^{-1})
Reservoir volume (m)
Compensation flow (ML/day)
Conductivity (µs)
Date (year)
TN:TP (mol/ml)

A2.16. Chlorophyll-a 1990 to 1999.

Primary Component Analysis (PCA) was completed including all variables where data was available between 1990-1999 (Figure A2.16.1).

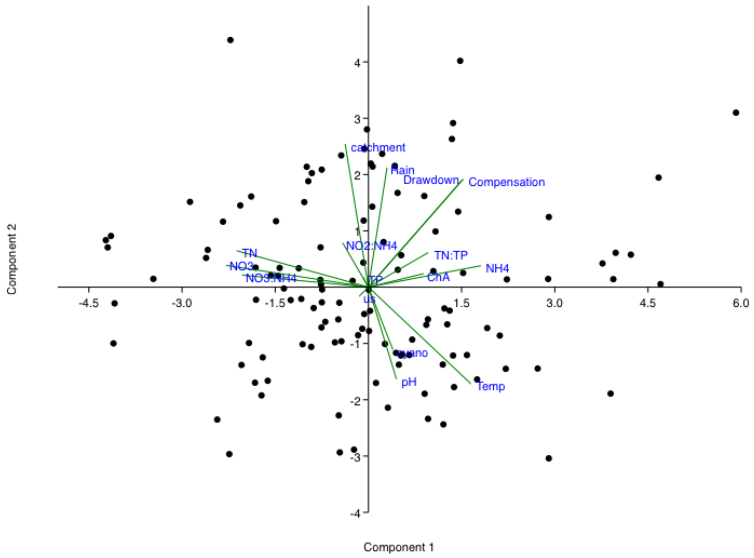

Figure A2.16.1 PCA for all variables 1990-1999. PC1 and PC2 represented 23.52% and 14.32% of the data variation respectively.

The variables that demonstrated correlation with chlorophyll-a over the 1990-1999 sampling period were included in the LM analysis (Table A2.16.1)

Table A2.16.1 Variables in LM analysis

Variables
Conductivity (µs)
Rainfall (mm)
Reservoir level (m)
Compensation flow (ML/day)
TN:TP (mol/ml)
NH_4^+ (mg L^{-1})
TP (mg L^{-1})

A2.17. Chlorophyll-a 2000 to 2009.

Primary Component Analysis (PCA) was completed including all variables where data was available between 2000-2009 (Figure A2.17.1).

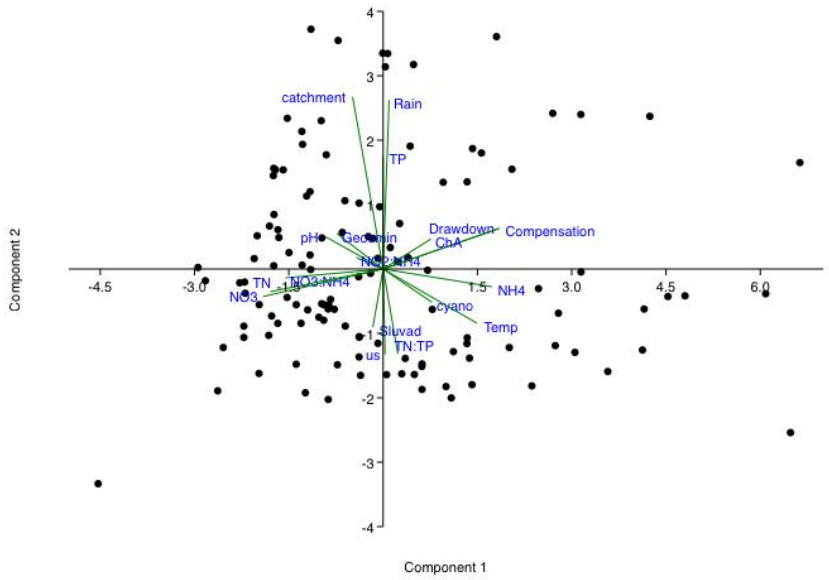

Figure A2.17.1. PCA for all variables 2000-2009. PC1 and PC2 represented 23.12% and 12.31% of the data variation respectively.

The variables that demonstrated correlation with chlorophyll-a over the 1990-1999 sampling period were included in the LM analysis (Table A2.17.1)

Table A2.17.1. variables omitted from LM analysis

Variables
Compensation flow volume (ML/day)
Reservoir level (m)
Rainfall (mm)
TP (mg L^{-1})
Conductivity (µs)
NO_3^-: NH_4^+ (mol/ml)
TN (mg L^{-1})
NO_3^- (mg L^{-1})

Appendix 3a: Primary Component Analysis of data (Chapter 3) by site over the 11-month sampling period

A3a.1. T1

The variables used in the LM/GLM analysis were determined by PC analysis after indicating a correlation with respective P-fractions (Table A3a.1.1; Figures A3a.1.1, A3a.1.2, A3a.1.3 and Table A3a.1.2).

Table A3a.1.1 showing % variance of each PC.

PC	Eigenvalue	% variance
1	8.77458	38.15
2	5.4396	23.65
3	3.36115	14.614
4	2.18429	9.4969
5	1.3715	5.9631
6	1.09936	4.7798
7	0.517685	2.2508
8	0.248292	1.0795
9	0.00353926	0.015388

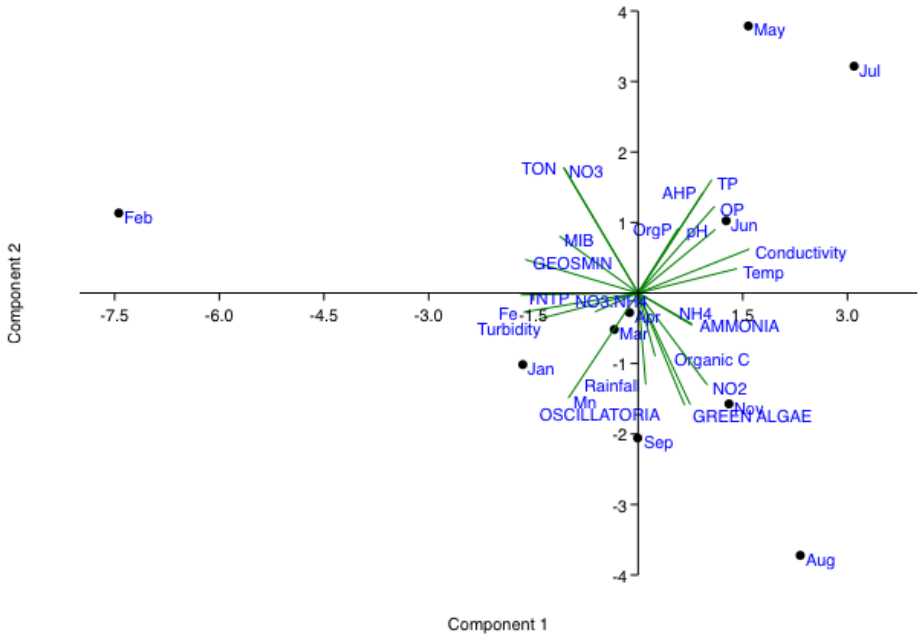

Figure A3a.1.1. PCA of nutrients at site T1

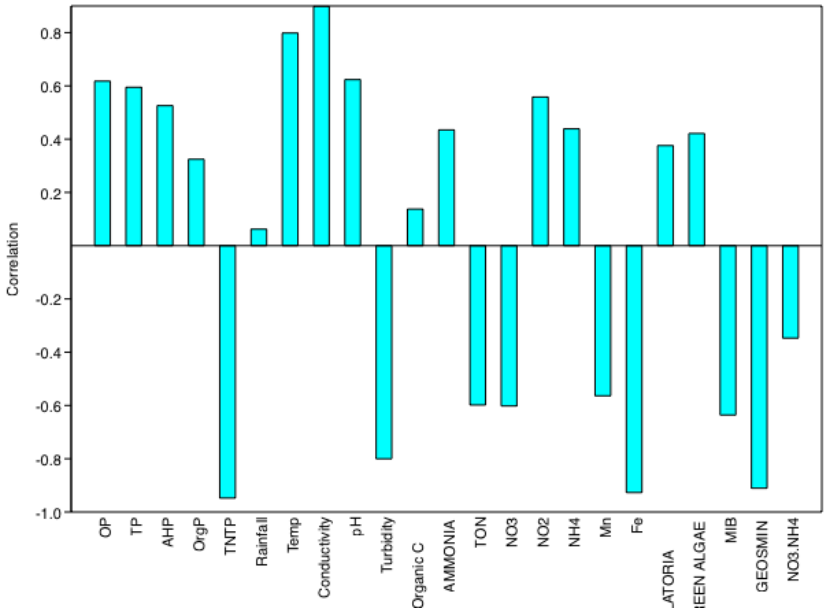

Figure A3a.1.2. PCA loading at site T1 of PC1

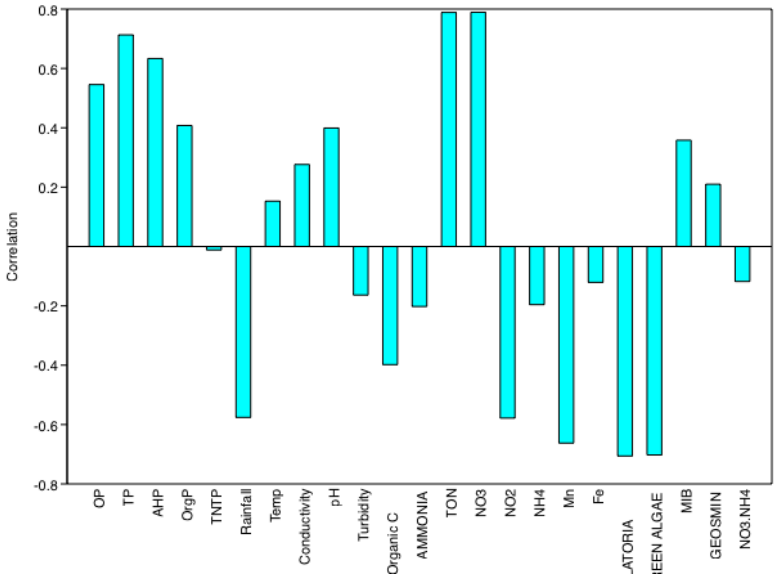

Figure A3a.1.3. PCA loading at site T1 of PC2

Table A3a.1.2. variables for LM analysis

Variables correlating with P-fractions
Conductivity (µs)
Temperature (°C)
Fe^{3+} (mgL^{-1})

Turbidity (ntu)
pH
Rainfall (mm)
Oscillatoria (cfu/ml)
TN:TP (mol/ml)
NO_3^-:NH_4^+ (mol/ml)
Mn (mgL^{-1})

A3a.2. B1

The variables used in the LM/GLM analysis were determined by PC analysis after indicating a correlation with respective P-fractions (Table A3a.2.1; Figures A3a.2.1, A3a.2.2, A3a.2.3 and Table A3a.2.2).

Table A3a.2.1 showing % variance of each PC.

PC	Eigenvalue	% variance
1	7.06792	32.127
2	6.26481	28.476
3	3.15711	14.35
4	1.91741	8.7155
5	1.69894	7.7225
6	0.974669	4.4303
7	0.574956	2.6134
8	0.185634	0.84379
9	0.14602	0.66373
10	0.012529	0.05695

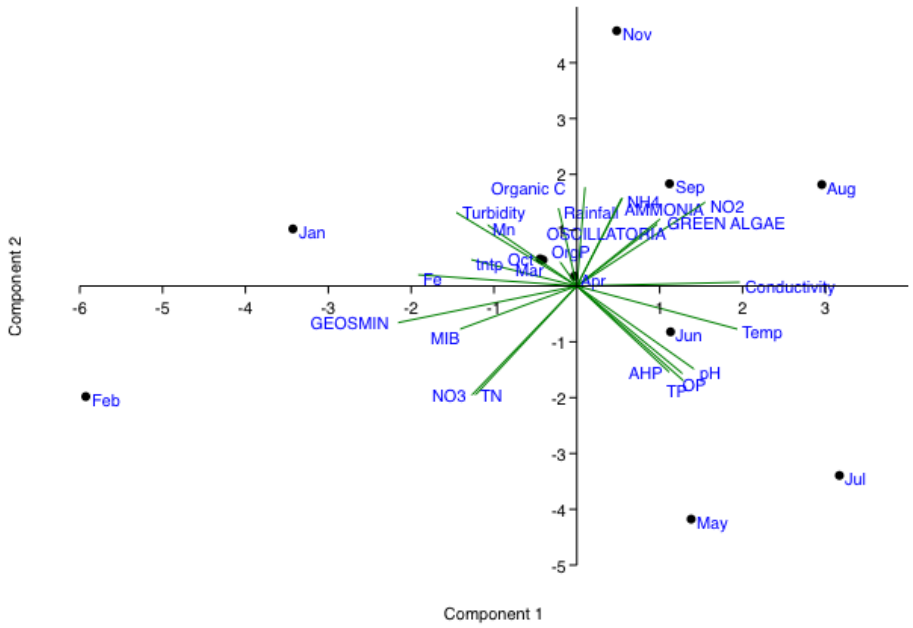

Figure A3a.2.1. PCA of nutrients at site B1

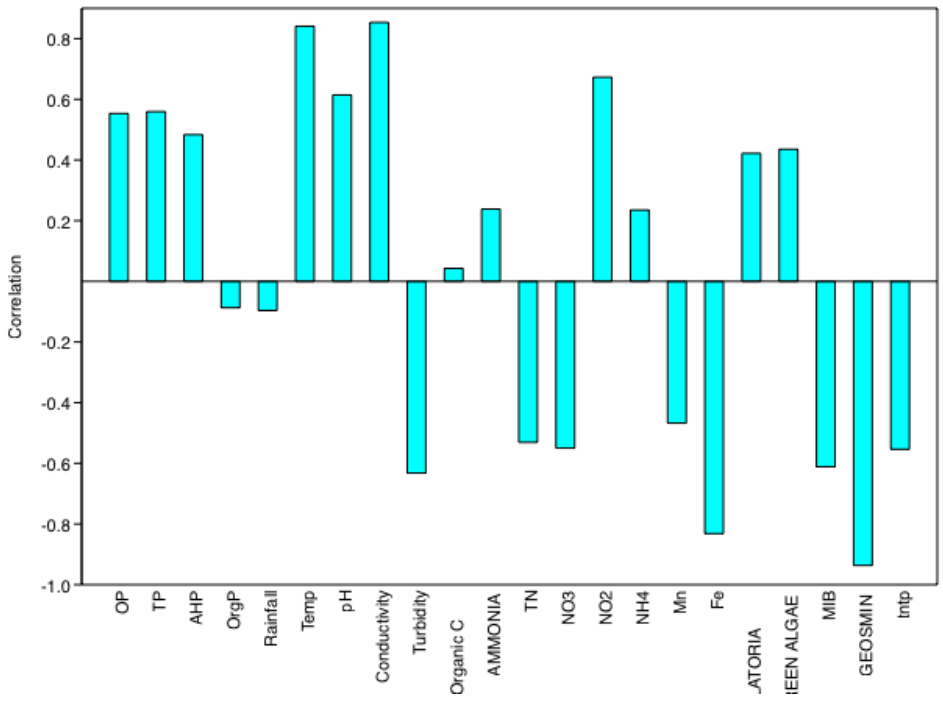

Figure A3a.2.2. PCA loading at site B1 of PC1

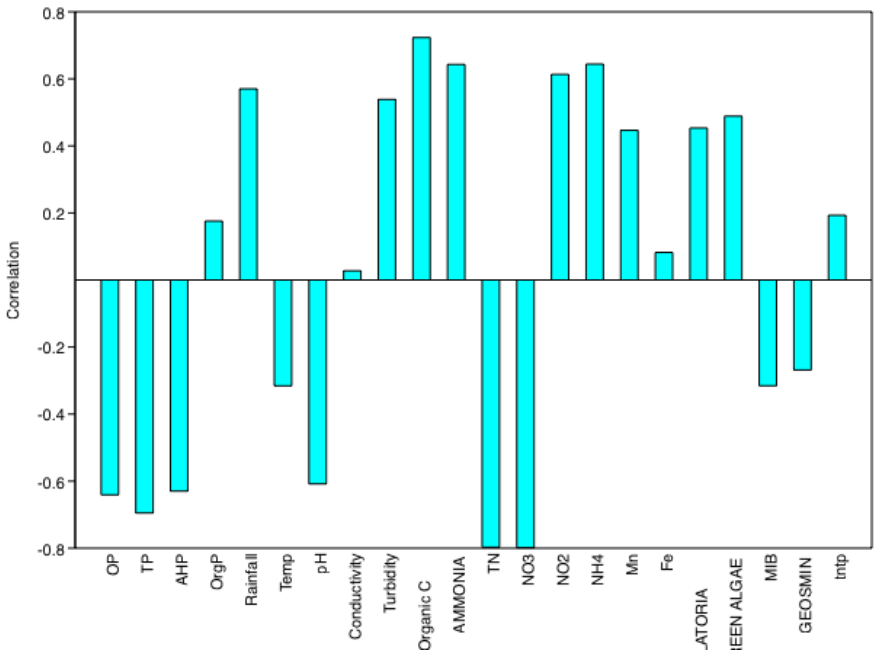

Figure A3a.2.3. PCA loading at site B1 of PC2

Table A3a.2.2. variables for LM analysis

Variables correlating with P-fractions
Temperature (°C)
pH
Turbidity (ntu)
Organic-C (mg L^{-1})
TN:TP (mol/ml)
Oscillatoria (cfu/ml)
Fe_3^+ (mg L^{-1})

A3a.3. T2

The variables used in the LM analysis were determined by PC analysis after indicating a correlation with respective P-fractions (Table A3a.3.1; Figures A3a.3.1, A3a.3.2, A3a.3.3 and Table A3a.3.2).

Table A3a.3.1 showing % variance of each PC.

PC	Eigenvalue	% variance
1	8.14142	40.707
2	4.97653	24.883
3	2.40166	12.008
4	1.5195 7.5975	
5	0.969179	4.8459
6	0.831265	4.1563
7	0.741662	3.7083
8	0.318415	1.5921
9	0.097403	0.48701
10	0.00297526	0.014876

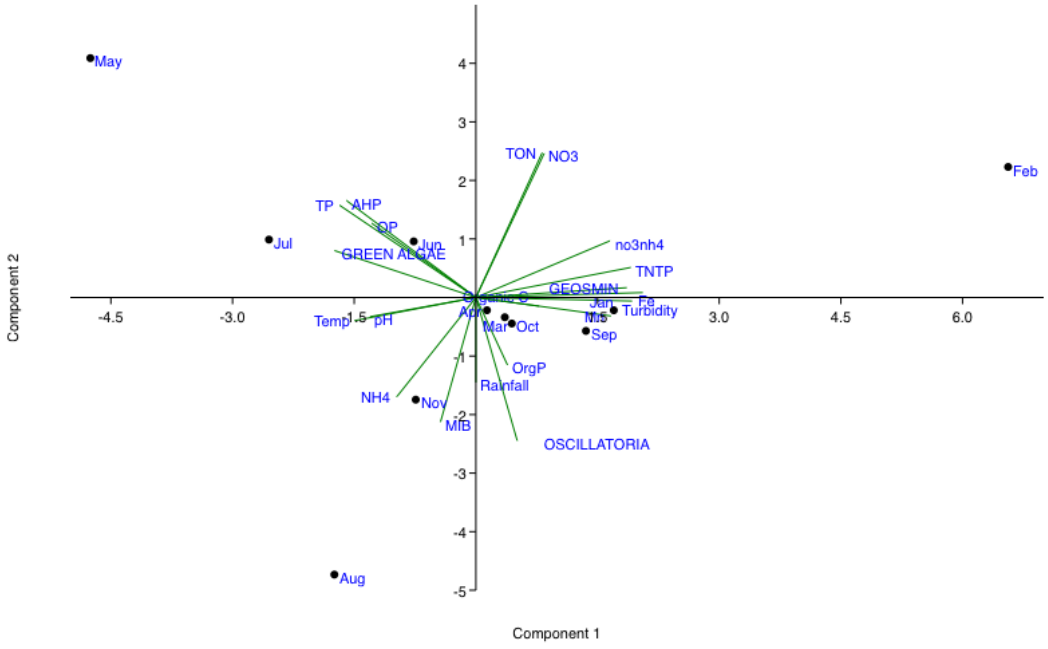

Figure A3a.3.1. PCA of nutrients at site T2

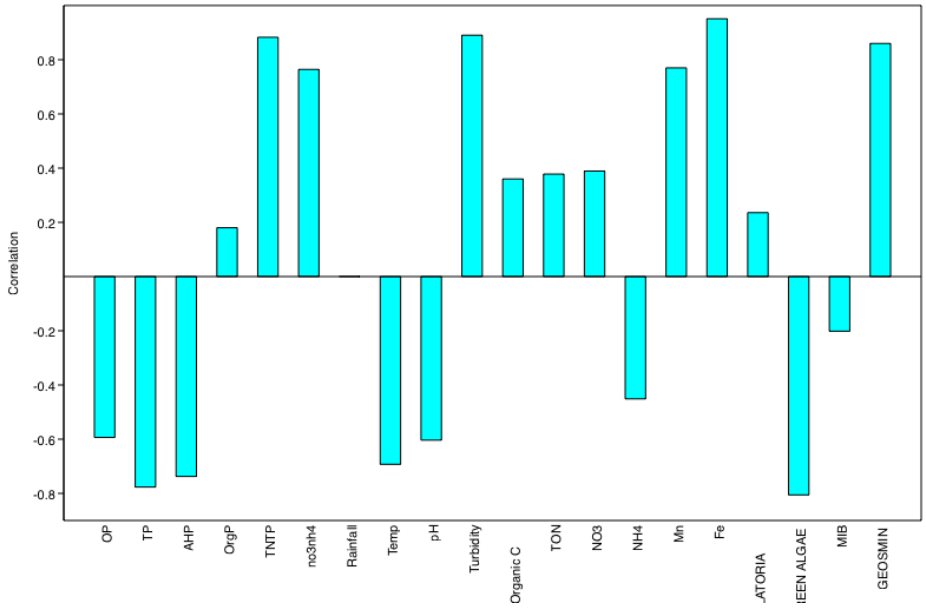

Figure A3a.3.2. PCA loading at site T2 of PC1

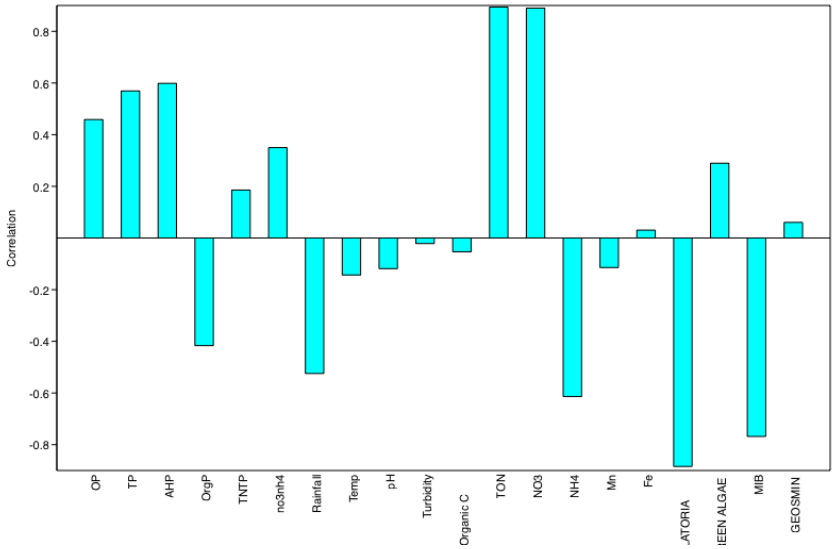

Figure A3a.3.3. PCA loading at site T2 of PC2

Table A3a.3.2. variables for LM analysis

Variables correlating with P-fractions
Green algae (cells/ml)
Rainfall (mm)

Turbidity(ntu)
Oscillatoria (cfu/ml)
Mn (mg L^{-1})
Organic C (mg L^{-1})
Fe_3^+ (mg L^{-1})

A3a.4. B2

PCA determined that OP and TP were positively correlated with one-another, and Org-P was positively correlated with AHP. The variables used in the LM/GLM analysis were determined by PC analysis after indicating a correlation with respective P-fractions (Table A4a.2.1; Figures A4a.2.1, A4a.2.2, A4a.2.3 and Table A4a.2.2).

Table A3a.4.1 showing % variance of each PC.

PC	Eigenvalue	% variance
1	6.90511	38.362
2	4.08498	22.694
3	2.33748	12.986
4	2.04863	11.381
5	1.19732	6.6518
6	0.741952	4.122
7	0.3969 2.205	
8	0.20888	1.1604
9	0.0742207	0.41234
10	0.00453282	0.025182

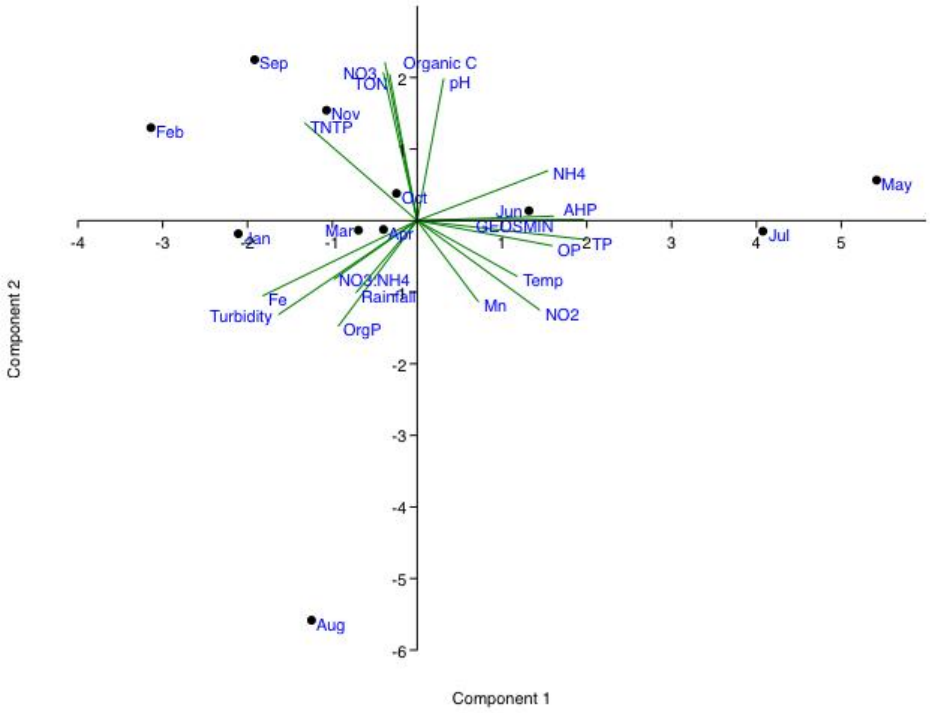

Figure A3a.4.1. PCA of nutrients at site B2

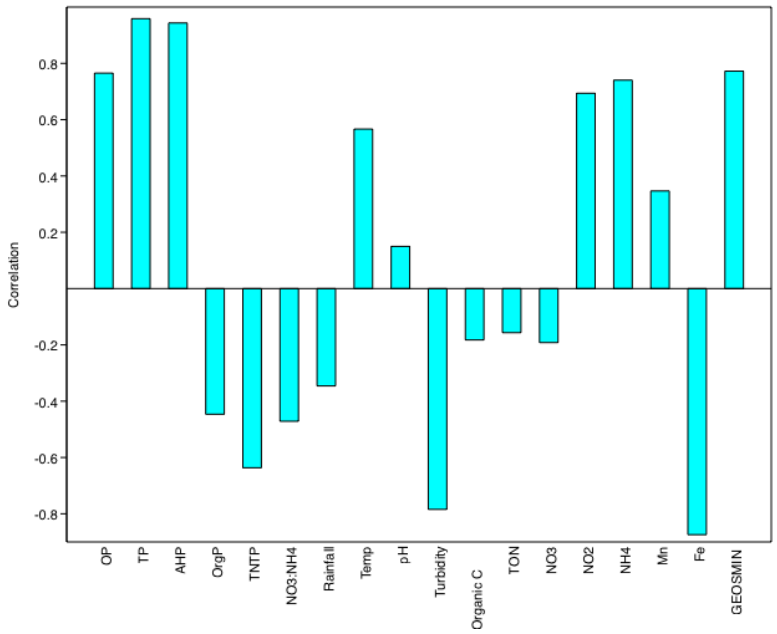

Figure A3a.4.2. PCA loading at site B2 of PC1

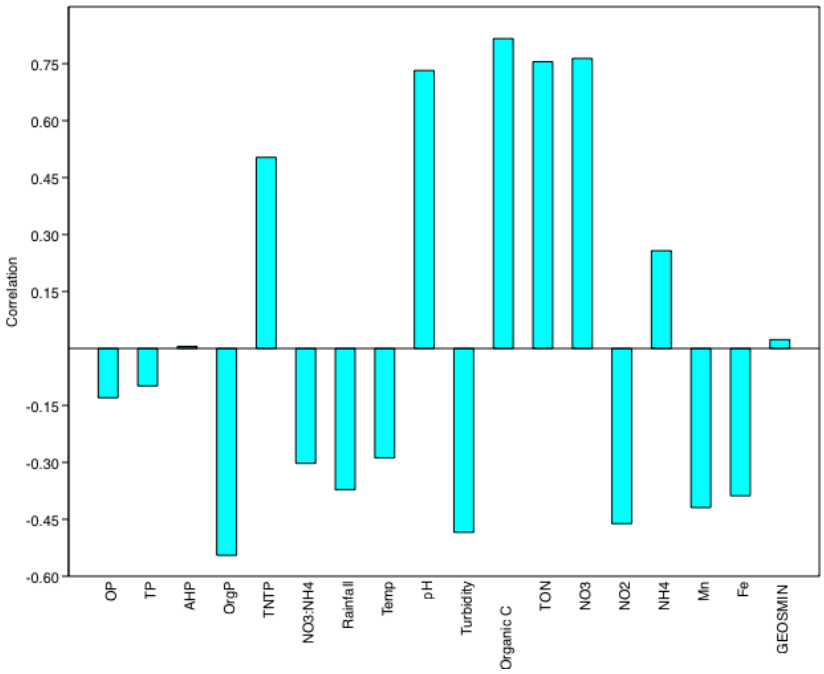

Figure A3a.4.3. PCA loading at site B2 of PC2

Table A3a.4.2. variables for LM analysis

Variables correlating with P-fractions	
OP & TP	Organic P & AHP
Temperature (°C)	pH
Mn (mg L^{-1})	NH_4^+ (mg L^{-1})
NO_2^- (mg L^{-1})	Fe_3^+ (mg L^{-1})
TN:TP (mol/ml)	Turbidity (ntu)
Organic C (mg L^{-1})	NO_3^-: NH_4^+ (mol/ml)
NO_3^- (mg L^{-1})	Rainfall (mm)
TN (mg L^{-1})	
Geosmin (ng L^{-1})	

A3a.5. T3

The variables used in the LM/GLM analysis were determined by PC analysis after indicating a correlation with respective P-fractions (Table A3a.5.1; Figures A3a.5.1, A3a.5.2, A3a.5.3 and Table A3a.5.2).

Table A3a.5.1 showing % variance of each PC.

PC	Eigenvalue	% variance
1	8.1836	37.198
2	4.76918	21.678
3	3.7821	17.191
4	2.09224	9.5102
5	1.17408	5.3367
6	1.02295	4.6498
7	0.627739	2.8534
8	0.331533	1.507
9	0.011534	0.052427
10	0.00504546	0.022934

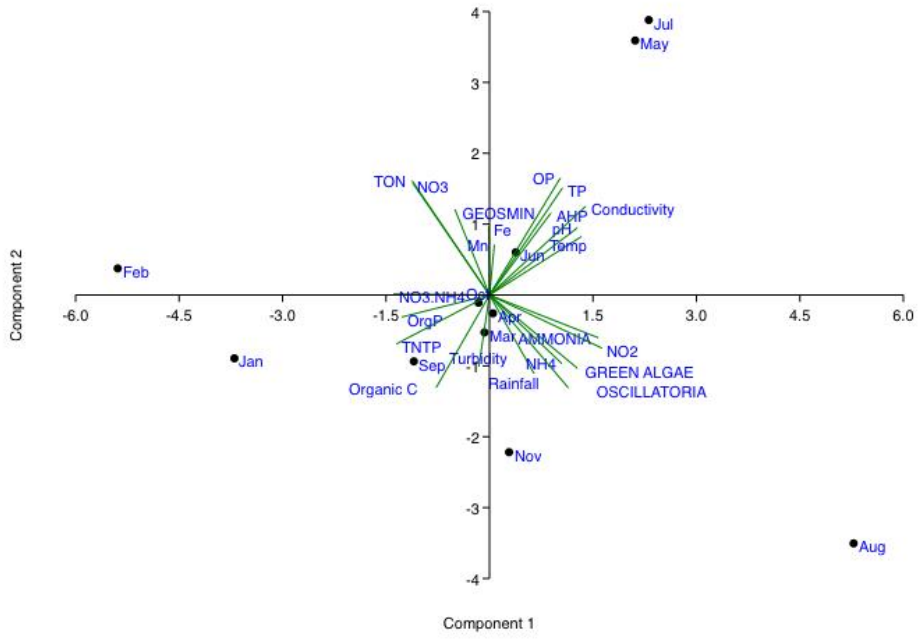

Figure A3a.5.1. PCA of nutrients at site T3

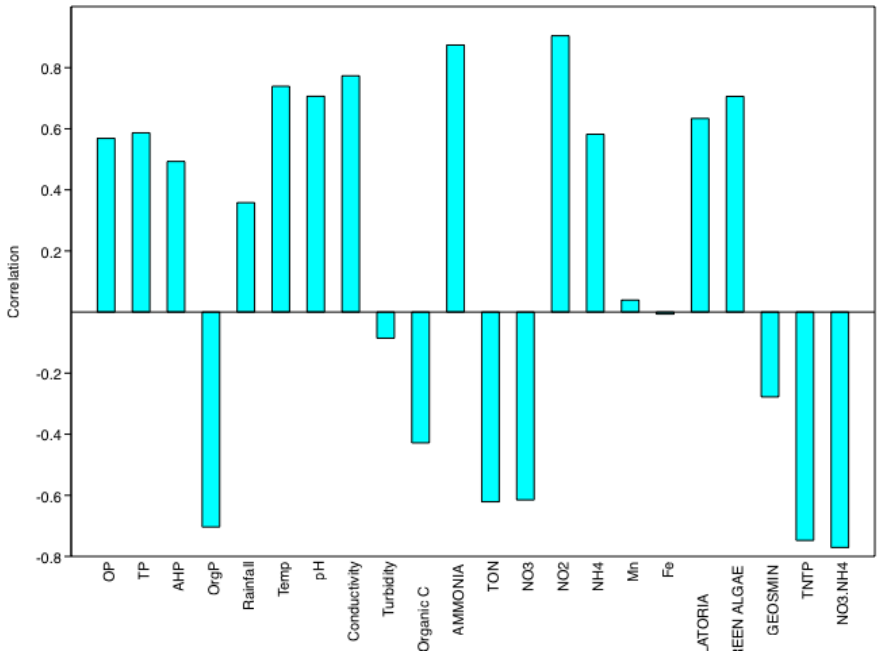

Figure A3a.5.2. PCA loading at site T3 of PC1

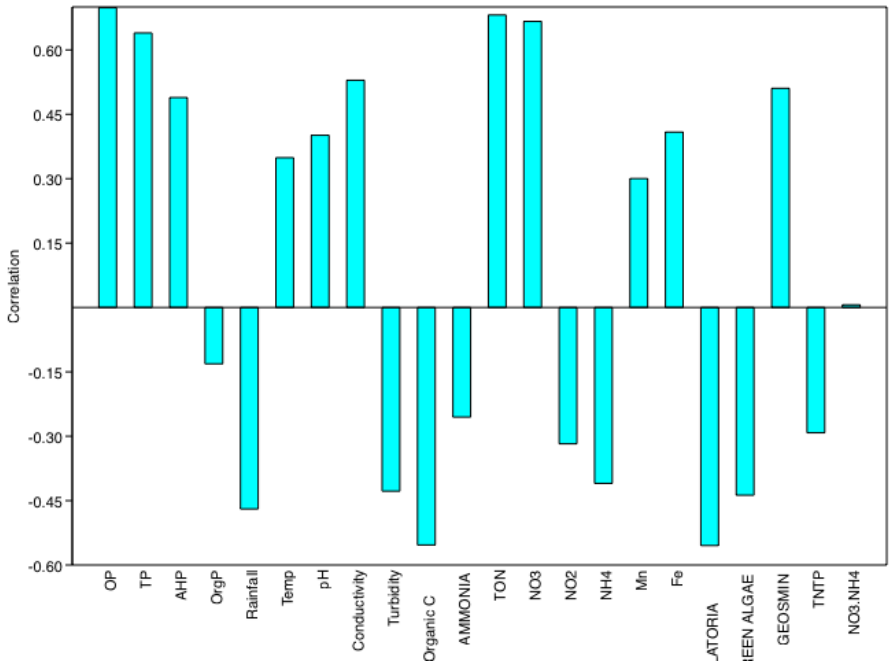

Figure A3a.5.3. PCA loading at site T3 of PC2

Table A3a.5.2. variables for LM analysis

Variables for all P-fractions
Temperature (°C)
pH
Conductivity (µs)
Fe_3^+ (mg L^{-1})
Geosmin (ng L^{-1})
Turbidity (ntu)
TN:TP (mol/ml)
Organic C (mg L^{-1})
NO_3^-: NH_4^+ (mol/ml)

A3a.6. B3

PCA determined that OP, TP and AHP were positively correlated with one-another, however, Organic P was not correlated. The variables used in the LM/GLM analysis were determined by PC analysis after indicating a correlation with respective P-fractions (Table A3a.6.1; Figures A3a.6.1, A3a.6.2, A3a.6.3 and Table A3a.6.2).

Table A3a.6.1 showing % variance of each PC.

PC	Eigenvalue	% variance
1	5.81083	30.583
2	4.83008	25.421
3	3.42535	18.028
4	2.49117	13.111
5	1.00518	5.2904
6	0.61886	3.2572
7	0.46659	2.4557
8	0.281384	1.481
9	0.0673534	0.35449
10	0.00319687	0.016826

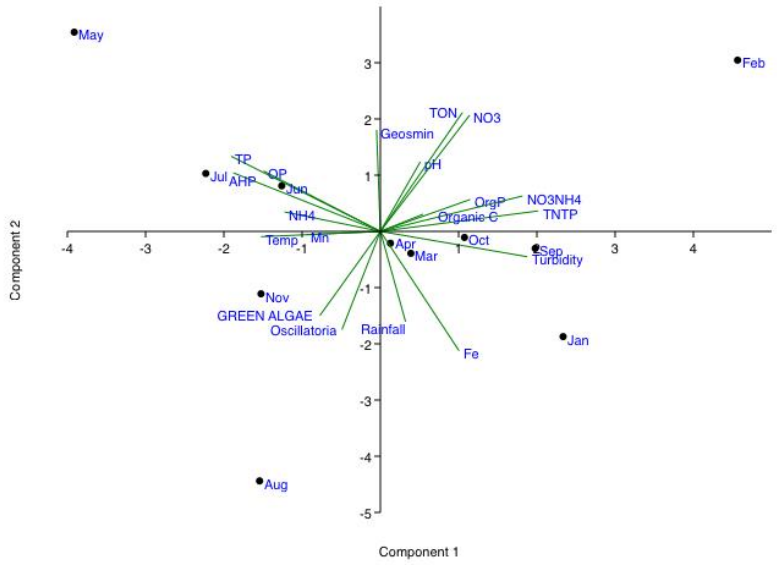

Figure A3a.6.1. PCA of nutrients at site B3

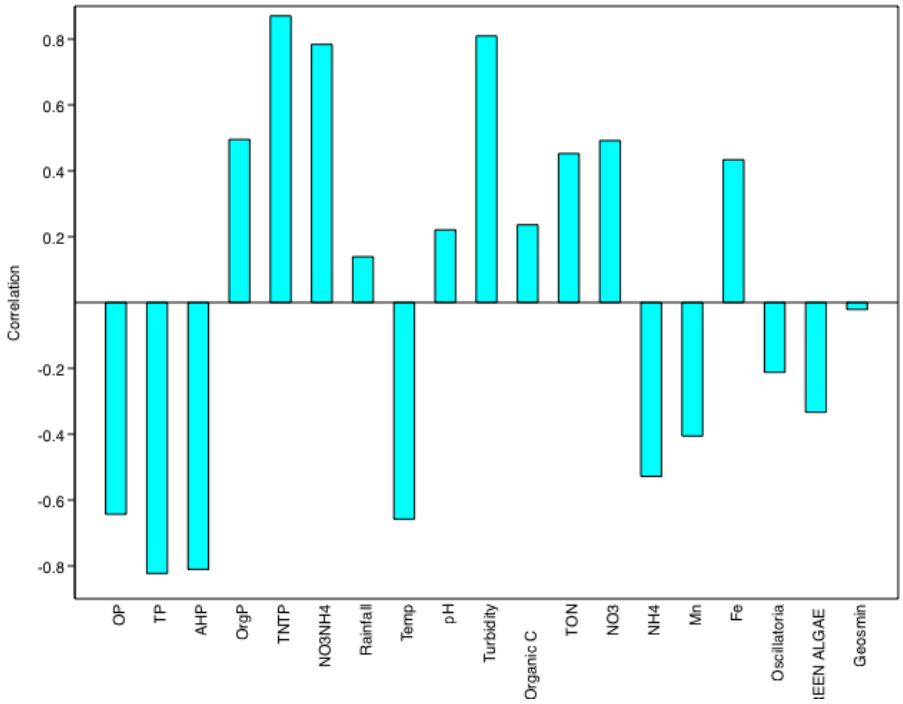

Figure A3a.6.1. PCA of nutrients at site B3

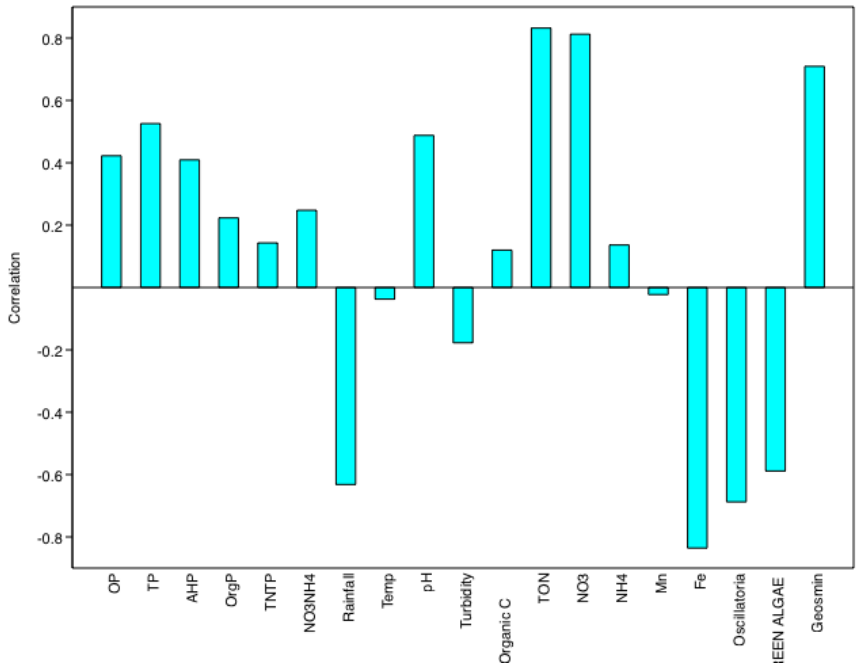

Figure A3a.6.3. PCA loading at site B3 of PC2

Table A3a.6.2. variables for LM analysis

Variables correlating with P-fractions	
PO4, AHP & TP	Organic P
NH_4^+ (mg L^{-1})	Organic C (mg L^{-1})
Rainfall (mm)	TN:TP (mol/ml)
Conductivity (µs)	NO_3^-: NH_4^+ (mol/ml)
Fe_3^+ (mg L^{-1})	pH
Geosmin (ng L^{-1})	Temperature (°C)
Turbidity (ntu)	NO_3^- (mg L^{-1})
	TN (mg L^{-1})
	Oscillatoria (cfu/ml)
	Green algae (cells/ml)
	Mn (mg L^{-1})

A3a.7. T4

PCA determined that OP, TP and AHP were positively correlated with one-another, however, Org-P was not correlated with any other P-fraction. The variables used in the LM/GLM analysis

were determined by PC analysis after indicating a correlation with respective P-fractions (Table A3a.7.1; Figures A3a.7.1, A3a.7.2, A3a.7.3 and Table A3a.7.2).

Table A3a.7.1 showing % variance of each PC.

PC	Eigenvalue	% variance
1	7.40403	35.257
2	5.03089	23.957
3	3.10111	14.767
4	2.19646	10.459
5	1.04983	4.9992
6	0.862086	4.1052
7	0.806596	3.8409
8	0.471138	2.2435
9	0.0744423	0.35449
10	0.00342928	0.01633

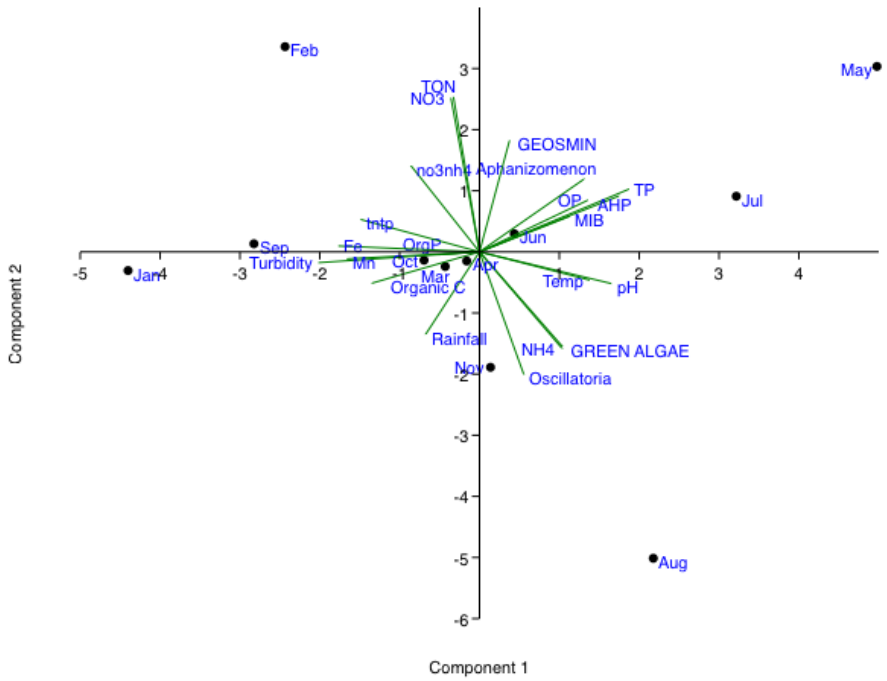

Figure A3a.7.1. PCA of nutrients at site T4

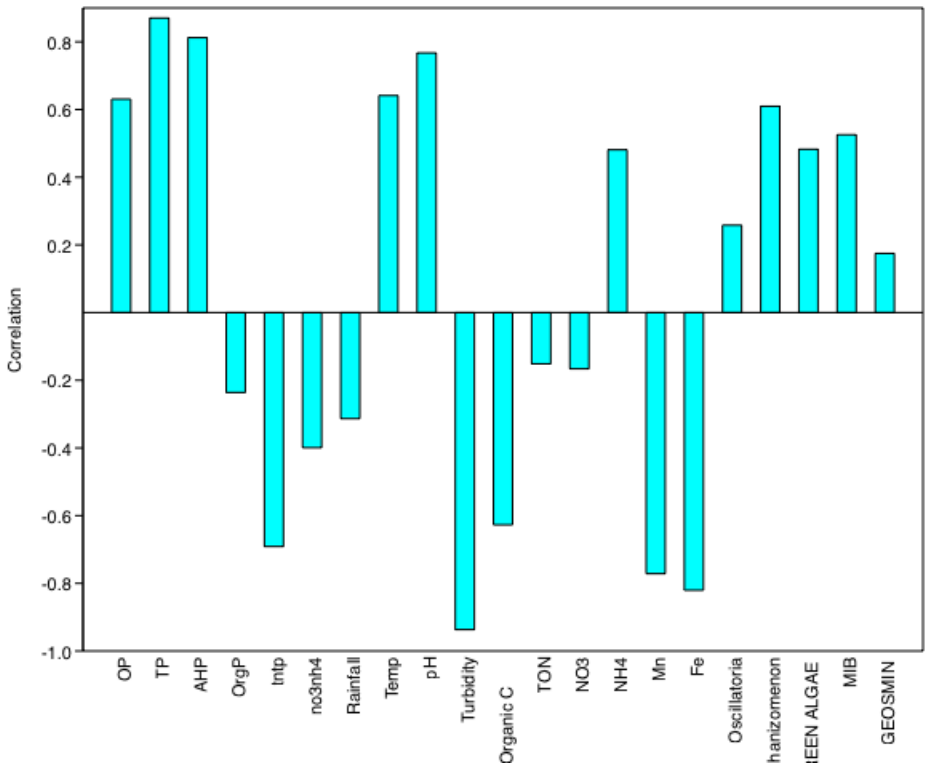

Figure A3a.7.2. PCA loading at site T4 of PC1

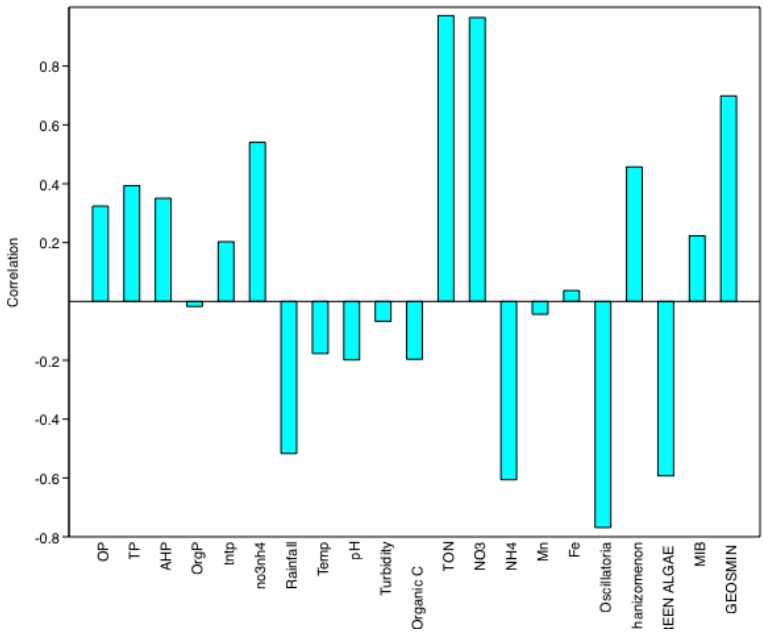

Figure A3a.7.3. PCA loading at site T4 of PC2

Table A3a.7.2. variables for LM analysis

Variables correlating with P-fractions	
OP, AHP & TP	Organic P
Geosmin (ng L^{-1})	TN (mg L^{-1})
Aphanizomenon (cfu/ml)	NO_3^-: NH_4^+ (mol/ml)
Turbidity (ntu)	TN:TP (mol/ml)
Rainfall (mm)	Fe_3^+ (mg L^{-1})
Organic C (mg L^{-1})	Temperature (°C)
Mn (mg L^{-1})	pH
	NH_4^+ (mg L^{-1})
	Oscillatoria (cfu/ml)
	Green algae (cells/ml)

A3a.8. B4

PCA determined that PO4, TP and AHP were positively correlated with one-another, however, Organic P was not correlated with other P-fractions (Table A3a.8.1; Figures A3a.8.1, A3a.8.2, A3a.8.3 and Table A3a.8.2).

Table A3a.8.1 showing % variance of each PC.

PC	Eigenvalue	% variance
1	6.11446	35.967
2	4.2366	24.921
3	2.6861	15.801
4	1.32419	7.7893
5	1.11209	6.5417
6	0.846304	4.9783
7	0.520902	3.0641
8	0.133993	0.7882
9	0.0253632	0.1492
10	7.0609E-32	4.1535E-31

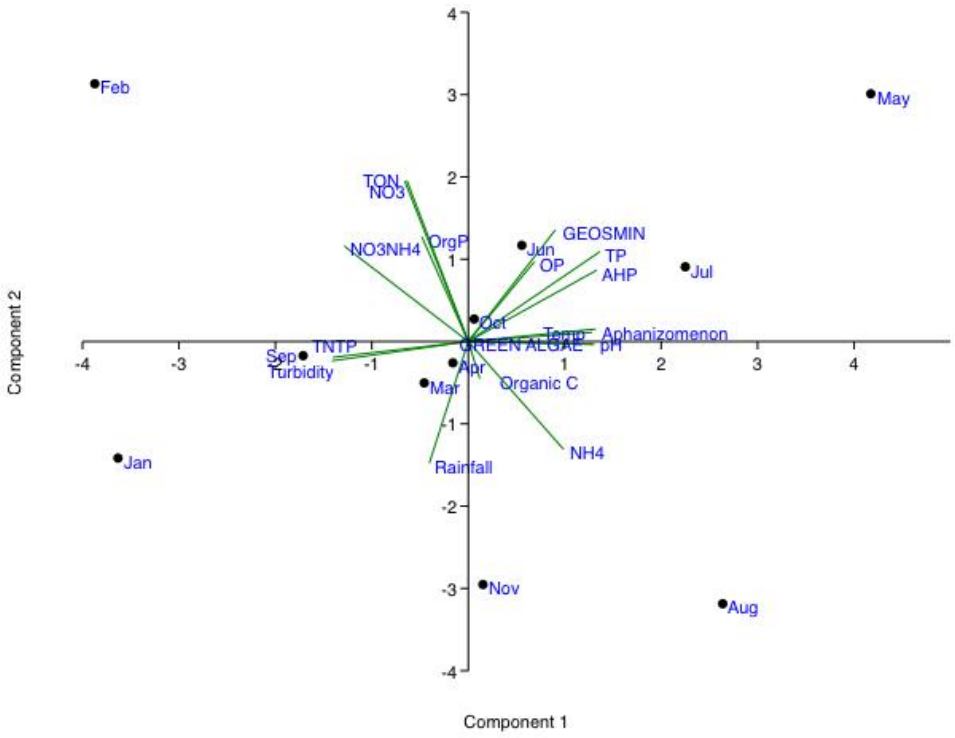

Figure A3a.8.1. PCA of nutrients at site B4

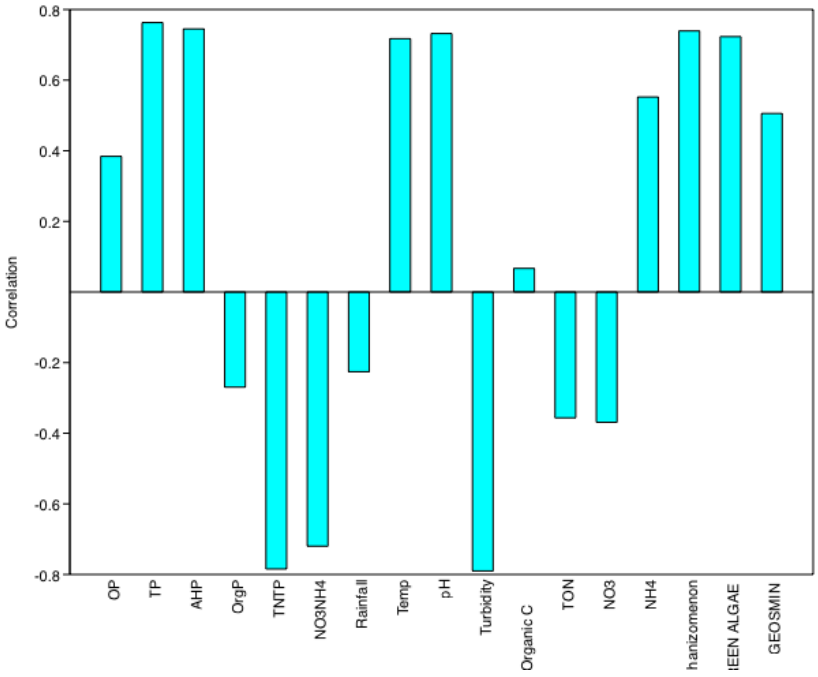

Figure A3a.8.2. PCA loading at site B4 of PC1

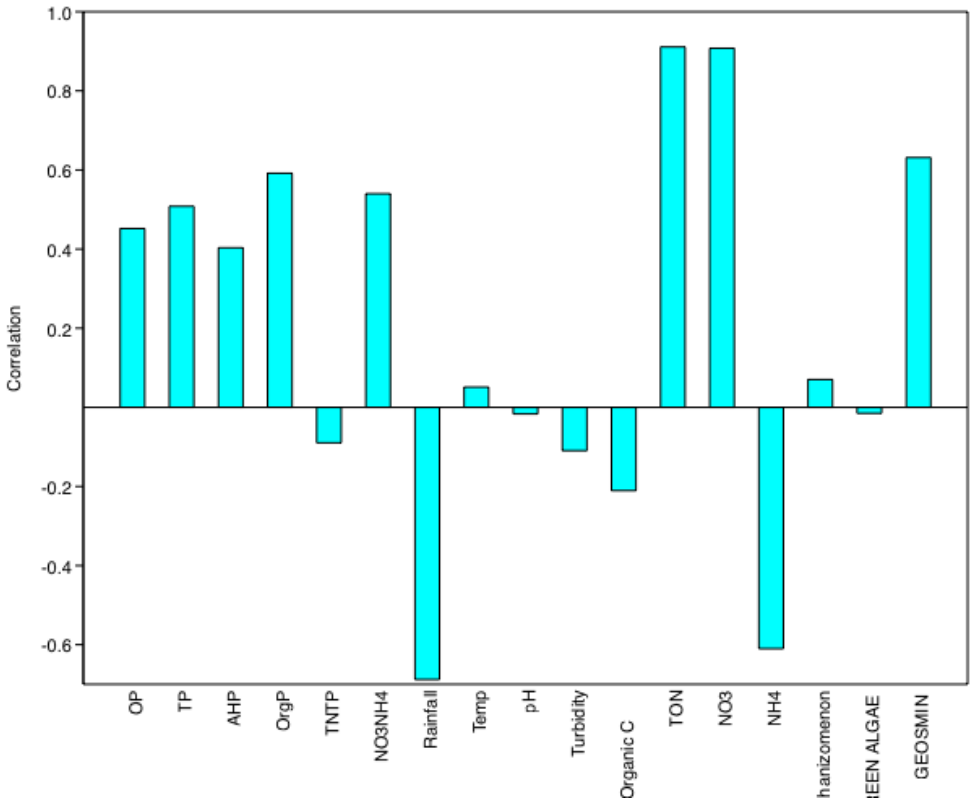

Figure A3a.8.3. PCA loading at site B4 of PC2

Table A3a.8.2. variables for LM analysis

Variables correlating with P-fractions	
OP, AHP & TP	Organic P
Geosmin (ng L^{-1})	NH_4^+ (mg L^{-1})
Aphanizomenon (cfu/ml)	Organic C (mg L^{-1})
Temperature (°C)	Green algae (cells/ml)
Rainfall (mm)	pH
Turbidity (ntu)	NO_3^-: NH_4^+ (mol/ml)
TN:TP (mol/ml)	TN (mg L^{-1})
	NO_3^- (mg L^{-1})
	Oscillatoria (cfu/ml)

Appendix 3b: Model analyses for significant association of P-fractions with water quality and environmental variables at each site from January – November 2018. (Chapter 3)

A3b.1. T1

AHP and TP data were of a parametric distribution and therefore analysed using the Gaussian family (inverse link). The data representing Org-P was not of a normal distribution ($P<0.05$) and was therefore transformed for LM analysis using cubic transformation. OP was omitted from the analysis prior to May due to absence of values/'0' inflated data.

No significant association was determined for any of the P fractions with any variable.

A3b.2. B1 variable associations with P-fractions from January – November 2018.

TP data collected from samples at the benthic site was of a normal distribution whilst that of OP, AHP and Organic P was not. The Gaussian family (inverse link) was used to analyse the relationship between TP and variables. AHP data was transformed using Tukey's ladder of power. OP and Organic P data remained not normally distributed following transformations. Additionally, a GLM using the Gamma link with neither Organic P nor OP data could not be run due to '0' inflated data.

No significant association was determined between TP nor AHP with any of the variables analysed.

A3b.3. T2 variable associations with P-fractions from January – November 2018.

All data were abnormally distributed and therefore had to be transformed.

TP and Organic-P data were transformed using Tukey's ladder of power. A log transformation was used with the AHP data. OP data remained abnormally distributed. LM analysis could not be completed for OP due to '0' inflated data.

No significant association was determined for any P variants with any of the variables analysed.

A3b.4. B2 variable associations with P-fractions from January – November 2018.

TP data were of a normal distribution and was analysed using the Gaussian family (identity link). However, data representing AHP, OP and Organic P were not of a normal distribution and therefore had to be transformed using Tukey's ladder of power (AHP, OP).

No significant association was determined for TP, OP nor AHP with any variables analysed.

A3b.5. T3 variable associations with P-fractions from January – November 2018.

TP data was of a normal distribution whereas that of OP, AHP and Organic P was not normally distributed. Consequently, TP data were analysed using a GLM (Gaussian family; inverse link). AHP was analysed using LM analysis following transformation using Tukey's ladder of power. OP data was analysed using LM once transformed using the square root transformation. Organic P data was '0' inflated, therefore no analyses could be carried out.
No significant associations were determined between TP, OP nor AHP and any of the variables analysed.

A3b.6. B3 variable associations with P-fractions from January – November 2018.

TP data was of a normal distribution and therefore analysis was completed using GLM and the Gaussian family (identity link).
OP data prior to May were omitted from the analyses due to '0' inflated data and absent values. OP data was not normally distributed and transformed for LM analyses through using the square root transformation.
Organic P and AHP were not normally distributed and their data were transformed using cubic transformation method and analysed using an LM.
No significant association was determined for TP, Organic P nor OP with any variable analysed.

A3b.7. T4 variable associations with P-fractions from January – November 2018.

All P data were not normally distributed and was transformed prior to LM analysis.
TP data were transformed using the square root method. AHP data were transformed using Tukey's ladder of power. Organic P data were transformed using the cubic transformation method. OP data remained not normally distributed following cubic, square root, Tukey's and log transformations. Therefore, a GLM was used to analyse the data using a Gamma family (inverse link). Data prior to May was omitted from OP analysis due to '0' inflated data.

No significant association was determined for TP, OP, AHP nor organic P with any of the variables analysed.

A3b.8. B4 variable associations with P-fractions from January – November 2018.

TP data were parametric whereas AHP, OP and Org-P data were not normally distributed. TP data were analysed using GLM and the Gaussian family (inverse link).
AHP data were prepared for analysis using the square root transformation. Both the Org-P and the OP data were transformed through cubing the data.
No significant association was determined for TP, OP, Org-P nor AHP with any of the variables analysed.

Appendix 3c: Nutrient and environmental data

Table. A3c.1. Average monthly values of variables at site T1 from January 2018 through November 2018. Absent data are indicated by grey cells.

Month	Rainfall (mm/month)	Temp (°C)	pH	Turbidity (ntu)	Organic C (mg/L)	Fe_3^+ (mg/L)	Conductivity (µs)	TN (mg/L)	NO_3^- (mg/L)	NH_4^+ (mg/L)	*Oscillatoria* (cfu/ml)	Green algae (cells/ml)	Geosmin (ng/L)
Jan	153.2	9.4	8.20		2.40			0.83	0.83	0.005	0	0	0.75
Feb	49	7.5	8.10	2.30	2.30	0.12	200	1.3	1.3	0	0	0	1.3
Mar	164	9.1											
Apr	129.4	14											
May	56.2	19	8.40	1.20	2.20	0.026	230	1.16	1.1	0.066	0	1426	2.4
Jun	8.4	22.6											
Jul	46	25.4	8.90	1.20	2.40	0.036	230	1.36	1.33	0.03	0	240	1.4
Aug	129.8	21.4	8.50	1.10	2.30	0.044	230	0.58	0.53	0.034	4400	5500	0
Sep	89.8	18.7	8.20	2.00	2.40		220	0.74	0.68	0.07	0	1600	0.31
Oct	48	15.6											
Nov	121	11.9	8.10	1.80	2.50			0.75	0.69	0.11	0	0	0.34

Table. A3c.2. Average monthly values of variables at site B1 from January 2018 through November 2018. Absent data are indicated by grey cells.

Month	Rainfall (mm/month)	Temp (°C)	pH	Turbidity (ntu)	Organic C (mg/L)	TN (mg/L)	NO_3^- (mg/L)	NH_4^+ (mg/L)	*Oscillatoria* (cfu/ml)	Green algae (cells/ml)	Geosmin (ng/L)
Jan	153.2	9.4	8.1	2.8	2.4	0.83	0.83	0.004	0	0	0
Feb	49	7.5	8.1	2.3	2.3	1.3	1.3	0.003	0	0	1.5
Mar	164	9.1									
Apr	129.4	14									
May	56.2	19	8.4	1.2	2.2	1.16	1.1	0.066	0	1426	1.2
Jun	8.4	22.6							0		
Jul	46	25.4	8.9	1.2	2.4	1.39	1.37	0.029	0	240	1.5
Aug	129.8	21.4	8.5	1.1	2.3	0.73	0.7	0.031	4400	5500	0.75
Sep	89.8	18.7	8.2	1.5	2.4	0.82	0.71	0.11	0	0	0.36
Oct	48	15.6									
Nov	121	11.9	7.9	3.1	2.6	0.9	0.61	0.29	0	0	0

Table. A3c.3. Average monthly values of variables at site T2 from January 2018 through November 2018. Absent data are indicated by grey cells.

Month	Rainfall (mm/month)	Temp (C)	pH	Turbidity (ntu)	Organic C (mg/L)	TN (mg/L)	NO_3^- (mg/L)	NH_4^+ (mg/L)	*Oscillatoria* (cfu/ml)	Green algae (cells/ml)	Geosmin (ng/L)
Jan	153.2	9.4			2.4	0.81	0.81	0.004	0	0	0.94
Feb	49	7.5	8.1	2.3	2.5	1.3	1.3	0.003	0	10	1.4
Mar	164	9.1									
Apr	129.4	14									
May	56.2	19	8.4	0.62	2.3	1.168	1.1	0.068	133	532	2.45
Jun	8.4	22.6									
Jul	46	25.4	8.9	1.1	2.6	1.35	1.28	0.071	0	190	1.3

Aug	129.8	21.4	8.6	1	2.4	0.6	0.5	0.1	5000	0	0
Sep	89.8	18.7	8.1	2.2	2.6	0.78	0.67	0.11	0	0	0
Oct	48	15.6									
Nov	121	11.9	8.2	1.5	2.4	0.8	0.69	0.11		190	0.34

Table. A3c.4. Average monthly values of variables at site B2 from January 2018 through November 2018. Absent data are indicated by grey cells.

Month	Rainfall (mm/month)	Temp (°C)	pH	Turbidity (ntu)	Organic C (mg/L)	TN (mg/L)	NO_3^- (mg/L)	NH_4^+ (mg/L)	*Oscillatoria* (cfu/ml)	Green algae (cells/ml)	Geosmin (ng/L)
Jan	153.2	9.4	8.2	2.7	2.4	0.75	0.75	0.007	0	0	0
Feb	49	7.5	8.1	2.3	2.5	1.3	1.3	0.003	0	0	0
Mar	164	9.1									
Apr	129.4	14									
May	56.2	19	8.2	0.71	2.2	1.06	0.97	0.093	0	0	1.5
Jun	8.4	22.6									
Jul	46	25.4	8	0.93	2.6	0.94	0.93	0.014	0	0	2
Aug	129.8	21.4	7.8	4.1	2	0.75	0.73	0.003	0	0	0.94
Sep	89.8	18.7		2.8	2.7	0.78	0.68	0.1	0	0	0
Oct	48	15.6									
Nov	121	11.9		2.8	2.7	0.69	0.68	0.01	0	0	0

Table. A3c.5. Average monthly values of variables at site T3 from January 2018 through November 2018. Absent data are indicated by grey cells.

Month	Rainfall (mm/month)	Temp (°C)	pH	Turbidity (ntu)	Organic C (mg/L)	TN (mg/L)	NO_3^- (mg/L)	NH_4^+ (mg/L)	*Oscillatoria* (cfu/ml)	Green algae (cells/ml)	Geosmin (ng/L)
Jan	153.2	9.4	8.2	3.2	2.4	0.84	0.84	0.005	0	0	0.9
Feb	49	7.5	8.1	2.1	2.5	1.3	1.3	0.003	0	0	1.4
Mar	164	9.1									
Apr	129.4	14									
May	56.2	19	8.4	0.48	2.1	1.12	1.03	0.093	0	1331	2.5
Jun	8.4	22.6									
Jul	46	25.4	8.9	1.1	2.3	1.39	1.37	0.027	0	240	0
Aug	129.8	21.4	8.6	1.2	2.4	0.57	0.5	0.072	6900	7000	0
Sep	89.8	18.7	8	3.1	2.7	0.8	0.69	0.11	0	0	0.34
Oct	48	15.6									
Nov	121	11.9	8.2	17	2.4	0.78	0.67	0.11	0	0	0

Table. A3c.6. Average monthly values of variables at site B3 from January 2018 through November 2018. Absent data are indicated by grey cells.

Month	Rainfall (mm/month)	Temp (°C)	pH	Turbidity (ntu)	Organic C (mg/L)	TN (mg/L)	NO_3^- (mg/L)	NH_4^+ (mg/L)	*Oscillatoria* (cfu/ml)	Green algae (cells/ml)	Geosmin (ng/L)
Jan	153.2	9.4	8.1	3.3	2.4	0.82	0.82	0.005	0	0	0
Feb	49	7.5	8.2	2.3	2.3	1.3	1.3	0.003	0	0	0

Mar	164	9.1									
Apr	129.4	14									
May	56.2	19	8.2	0.75	2.2	1.068	0.97	0.098	0	0	0
Jun	8.4	22.6									
Jul	46	25.4	7.9	1.4	2.6	1.35	1.31	0.04	0		0
Aug	129.8	21.4	8	1.2	2.1	0.72	0.66	0.006	0	0	0.9
Sep	89.8	18.7	8	3	2.7	0.9	0.61	0.29	0	10	0
Oct	48	15.6									
Nov	121	11.9	8.1	1.6	2.4	0.82	0.71	0.11	0	0	0.36

Table. A3c.7. Average monthly values of variables at site T4 from January 2018 through November 2018. Absent data are indicated by grey cells.

Month	Rainfall (mm/month)	Temp (°C)	pH	Turbidity (ntu)	Organic C (mg/L)	TN (mg/L)	NO_3^- (mg/L)	NH_4^+ (mg/L)	*Oscillatoria* (cfu/ml)	Green algae (cells/ml)	Geosmin (ng/L)
Jan	153.2	9.4	8.1	3.8	2.5	0.88	0.88	0.009	0	0	1.2
Feb	49	7.5	8.1	2.2	2.4	1.3	1.3	0.003	0	0	1.6
Mar	164	9.1									
Apr	129.4	14									
May	56.2	19	8.4	0.45	2.2	1.86	1.03	0.83	0	599	3
Jun	8.4	22.6									
Jul	46	25.4	8.9	1.5	2.5	1.374	1.33	0.044	0	0	0
Aug	129.8	21.4	8.6	1.4	2.4	0.58	0.5	0.075	6300	1600	0
Sep	89.8	18.7	8	3.1	2.7	0.8	0.69	0.011	0	0	0.34
Oct	48	15.6									
Nov	121	11.9	8.2	1.7	2.4	0.78	0.68	0.1	0	0	0.31

Table. A3c.8. Average monthly values of variables at site B4 from January 2018 through November 2018. Absent data are indicated by grey cells.

Month	Rainfall (mm/month)	Temp (°C)	pH	Turbidity (ntu)	Organic C (mg/L)	TN (mg/L)	NO_3^- (mg/L)	NH_4^+ (mg/L)	*Aphanizomenon* (cfu/ml)	Green algae (cells/ml)	Geosmin (ng/L)
Jan	153.2	9.4	8.1	2.9	2.3	0.91	0.91	0.006	0	5	0.88
Feb	49	7.5	8.1	2.4	2.4	1.3	1.3	0.003	0	67	1.7
Mar	164	9.1									
Apr	129.4	14									
May	56.2	19	8.4	1.6	2.3	1.1	1.1	0.033	2851	4324	5
Jun	8.4	22.6									
Jul	46	25.4	8.9	1.4	2.6	0.88	0.84	0.042	0	48	1
Aug	129.8	21.4	8.6	1.8	2.6	0.56	0.51	0.056	2400	4600	1.2
Sep	89.8	18.7	8	3.3	2.8	1.1	1	0.012	0	0	0
Oct	48	15.6									
Nov	121	11.9	8.2	2	2.4	0.74	0.68	0.072	0	0	0

Appendix 3d: Primary Component Analysis assignment of data by sampling date

A3d.1. May 14th

PCA determined that OP, TP and AHP were positively correlated with one-another, however, Org-P was not correlated with other P-fractions. Table A3d.1.1. lists the variables analysed using GLM analyses following PC analysis using PC1 and PC2 to determine the most suitable variables for each P-fraction.

Table A3d.1.1. variables for GLM analysis

Variables with correlation with P-fractions	
OP, AHP & TP	Organic P
Geosmin (ng L^{-1})	NH_4^+ (mg L^{-1})
Aphanizomenon (cfu/ml)	Organic C (mg L^{-1})
Temperature (°C)	Green algae(cells/ml)
Rainfall (mm)	pH
Turbidity (ntu)	NO_3^-: NH_4^+ (mol/ml)
TN:TP (mol/ml)	TN (mg L^{-1})
	NO_3^- (mg L^{-1})
	Oscillatoria (cfu/ml)

A3d.2. May 29th

PCA determined that OP, TP and AHP were positively correlated with one-another, however, Org-P was not correlated with other P-fractions. Table A3d.2.1. lists the variables analysed using LM/GLM analysis following PC analysis using PC1 and PC2 to determine the most suitable variables for each P-fraction.

Table A3d.2.1. variables for GLM analysis

Variables included GLM/LM analyses for each P-fraction	
PO4, AHP & TP	Organic P
NO_3^-: NH_4^+ (mol/ml)	Geosmin (ng L^{-1})
Aphanizomenon (cfu/ml)	NO_3^- (mg L^{-1})
Organic C (mg L^{-1})	TN (mg L^{-1})
NH_4^+ (mg L^{-1})	pH
Temperature (°C)	Turbidity (ntu)
Rainfall (mm)	TN:TP (mol/ml)

	Green algae (cell/ml)
	Oscillatoria (cfu/ml)

A3d.3. July 9th

PC analysis using PC1 and PC2 determined correlation for OP fraction with the TP data and Org-P correlated with AHP fractions. Table A3d.3.1. lists the variables analysed using LM/GLM method of determining significant associations between variables. *Aphanizomenon* and *Oscillatoria* were excluded from the PCA due to '0' inflated values.

Table A3d.3.1. variables for GLM analysis

OP & TP	Organic P and AHP
Temperature (°C)	Geosmin (ng L^{-1})
NO_3^-: NH_4^+ (mol/ml)	NO_3^- (mg L^{-1})
Rainfall (mm)	TN (mg L^{-1})
NH_4^+ (mg L^{-1})	pH
Green algae (cells/ml)	Turbidity (ntu)
	TN:TP (mol/ml)

A3d.4. July 23rd

Org-P data were omitted from analysis due to its concentrations remaining undetected at all sites. PC analysis using PC1 and PC2 determined correlation between TP data and AHP fraction data, but neither were correlated with OP data. Table A3d.4.1. lists the variables analysed using LM analysis. *Aphanizomenon* and *Oscillatoria* were excluded from the PCA due to '0' inflated values.

Table A3d.4.1. variables for GLM analysis

TP & AHP	OP
NO_3^-	Rainfall (mm)
NO_3^-: NH_4^+ (mol/ml)	Temperature (°C)
TN:TP (mol/ml)	
NH_4^+ (mg L^{-1})	
Green algae (cells/ml)	
Geosmin (ng L^{-1})	

Oscillatoria (cfu/ml)	
TN (mg L^{-1})	

A3d.5. August 3rd

PCA determined that TP and OP were positively correlated with one-another. Org-P and AHP were also positively correlated with each other but not correlated with other P-fractions. Table A3d.5.1 lists the variables analysed using LM/GLM following PC analysis using PC1 and PC2 to determine the most suitable variables for each P-fraction.

Table A3d.5.1. variables for GLM analysis

OrgP, AHP, OP & TP
Oscillatoria (cfu/ml)
pH
NO_3^-: NH_4^+ (mol/ml)
Aphanizomenon (cfu/ml)
Temperature (°C)

A3d.6. Sept 17th

OP was omitted from the LM analyses as a consequence of '0' inflated values. PCA determined that TP and AHP were positively correlated with one-another. Org-P was not correlated with other P-fractions. Table A3d.6.1. lists the variables analysed with GLM following PC analysis using PC1 and PC2 to determine the most suitable variables for each P-fraction.

Table A3d.6.1. variables for GLM analysis

AHP & TP	OrgP
NH_4^+ (mg L^{-1})	Turbidity (ntu)
Organic C (mg L^{-1})	NO_3^- (mg L^{-1})
TN:TP (mol/ml)	TN (mg L^{-1})
pH	Temperature (°C)
NO_3^-: NH_4^+ (mol/ml)	Green algae (cells/ml)
	Geosmin (ng L^{-1})
	Rainfall (mm)

A3d.7. Nov 12th

PCA determined that Org-P and AHP were negatively correlated with one-another. OP and TP were not correlated with other P-fractions but were positively correlated with each other. Table A3d.7.1. lists the variables analysed using LM/GLM following PC analysis using PC1 and PC2 to determine the most suitable variables for each P-fraction.

Table A3d.7.1. variables for GLM analysis

Organic P & AHP	OP and TP
Organic C (mg L^{-1})	Geosmin (ng L^{-1})
TN:TP (mol/ml)	Temperature (°C)
NO_3^-: NH_4^+ (mol/ml)	Green algae (cells/ml)
pH	NO_3^- (mg L^{-1})
Turbidity (ntu)	TN (mg L^{-1})
Rainfall (mm)	
NH_4^+ (mg L^{-1})	

Appendix 3e: Model analyses for significant association of P-fractions with water quality and environmental variables: January – November 2018. (Chapter 3) (by month).

A3e.1. May 14th cross-site GLM analysis

Both OP and AHP data exhibited a normal distribution (Shapiro-Wilks P>0.05), therefore the Gaussian family (log link) was used in the GLM analysis. However, neither TP nor geosmin data exhibited a normal distribution and remained skewed following transformation attempts. Therefore, the data were analysed using Gamma family (inverse link) as a GLM.
No significant association was determined between TP, OP nor AHP concentrations with any of the variables analysed.

A3e.2. May 29th cross-site LM/GLM analysis

The OP data displayed a normal distribution (P>0.05), whereas data for AHP, TP, OrgP and geosmin did not (P<0.05). TP was transformed using Tukey's ladder of power to create a normal distribution.
No significant association was determined for any P-fractions nor geosmin with any variables analysed.

A3e.3. July 9th cross-site LM/GLM analysis

OP and AHP demonstrated not normally distributed distributions (Shapiro-Wilks P<0.05). OP was transformed using Tukey's ladder of power. AHP was transformed using cubic method. TP and Organic P were normally distributed, therefore GLM analyses were completed using the Gaussian family, log link (TP) and identity link (Organic P).
No significant association for TP, OP, organic P nor AHP with any of the variables analysed.

A3e.4. July 23rd cross-site LM analysis

All data were not normally distributed and were transformed for analyses using Tukey's Ladder of Power.
No significant associations were determined for any P fraction with any of the variables analysed.

A3e.5. August 3rd cross-site LM/GLM analysis

All P-fractions were not normally distributed. TP data were transformed using Tukey's ladder of power.

AHP, organic-P and OP data remained positively skewed following transformation, therefore analysis was completed using GLM with a Gamma family (inverse link; AHP) and Gamma (log link; OP and organic-P).

No significant associations were determined for TP, AHP, OP nor organic P with any of the variables analysed.

A3e.6. September 17th cross-site GLM analysis

All P fraction data were normally distributed, therefore Gaussian family (identity link) was used in the analysis.

No significant association was confirmed between any of the P fractions and any of the variables analysed.

A3e.7. November 12th cross-site LM/GLM analysis

TP and AHP were of a normal distribution therefore the Gaussian family (inverse link) was used for the analysis.

Org-P and OP data were not normally distributed. Despite transformation attempts, OP data remained of a not normally distributed. AHP data transformations were carried out using square root transformation method.

No significant association was determined for P fractions with any variable analysed.

Appendix 3f: P-fraction data

A3f.1. January P-fraction data.

Table A3f.1.1 Orthophosphate (OP), Total Phosphorous (TP), Acid Hydrolysable Phosphorous (AHP), Condensed-P (Con-P) and Organic Phosphorous (Org-P) concentrations (mgL^{-1}, mean ± SD) in surface and benthic water samples at sites along the reservoir during mid-January (19^{th}) 2018.

Site	OP (mgL^{-1})	TP (mgL^{-1})	AHP (mgL^{-1})	Org-P (mgL^{-1})	Con-P (mgL^{-1})	Con-P % of TP
T1	0	0	0	0	0	0
B1	0	0.001	0	0	0	0
T2	0	0.0012	0	0.0012	0	0
B2	0	0.001 ± 0.001	0	0	0.0003	30.00
T3	0	0.001	0	0.001	0	0
B3	0	0	0	0	0	0
T4	0	0	0	0	0	0
B4	0	0.001	0	0	0.0005	50.00

A3f.2. Feb 1^{st}

Table A3f.2.1. Orthophosphate (OP), Total Phosphorous (TP), Acid Hydrolysable Phosphorous (AHP), Condensed-P (Con-P) and Organic Phosphorous (Org-P) concentrations (mgL^{-1}, mean ± SD) in surface and benthic water samples at sites along the reservoir during early February (1st) 2018. Sample Points (SP) indicated as Top (T), Benthic (B) and site reference.

Site	OP (mgL^{-1})	TP (mgL^{-1})	AHP (mgL^{-1})	Org-P (mgL^{-1})	Con - (mgL^{-1})	Con-P % of TP
T1	0	0.001	0	0.001	0	0
B1	0	0.001	0	0.001	0	0
T2	0	0.002	0	0.002	0	0
B2	0	0.003	0	0.003	0	0
T3	0	0.006 ± 0.002	0.001	0.005 ± 0.002	0.001	16.67
B3	0	0.006	0	0.005	0	0
T4	0	0.003 ± 0.001	0	0.003 ± 0.001	0	0
B4	0	0.006 ± 0.002	0	0.006 ± 0.002	0	0

A3f.3. Feb 15^{th}

Table A3f.3.1 Orthophosphate (OP), Total Phosphorous (TP), Acid Hydrolysable Phosphorous (AHP), Condensed-P (Con-P) and Organic Phosphorous (Org-P) concentrations (mgL^{-1}, mean ± SD) in surface and benthic water samples at sites along the reservoir during mid-February (15th) 2018. Sample Points (SP) indicated as Top (T), Benthic (B) and site reference.

Site	OP (mgL^{-1})	TP (mgL^{-1})	AHP (mgL^{-1})	Org-P (mgL^{-1})	Con-P (mgL^{-1})	Con-P % of TP

T1	0	0.002 ± 0.001	0.002 ± 0.002	0	0.002	100.00
B1	0	0.002	0.002	0	0.002	100.00
T2	0	0.001	0.001	0	0.001	100.00
B2	0	0.002 ± 0.001	0.002 ± 0.001	0	0.002	100.00
T3	0	0.001	0	0	0	0
B3	0	0.001	0	0.001	0	0
T4	0	0.005 ± 0.002	0.005 ± 0.002	0	0.005	100.00
B4	0.001	0.002	0.002	0	0.001	50.00

A3f.4. May 2nd

Figure A3f.4.1. Orthophosphate (OP), Total Phosphorous (TP), Acid Hydrolysable Phosphorous (AHP) and Organic-Phosphorous (Org-P) concentrations (mgL^{-1}, mean ± SD) in surface and benthic water samples at sites along the reservoir on 2nd May 2018. Sample Points (SP) indicated as Top (T), Benthic (B) and site reference.

Site	OP (mgL^{-1})	TP (mgL^{-1})	AHP (mgL^{-1})	Org-P (mgL^{-1})	Con-P (mgL^{-1})	Con-P % of TP
T1	0.007 ± 0.002	0.029 ± 0.019	0.023 ± 0.021	0	0.016	55.17
B1	0.008 ± 0.002	0.055 ± 0.01	0.047 ± 0.011	0	0.039	70.91
T2	0.011 ± 0.002	0.056 ± 0.001	0.046	0	0.035	62.50
B2	0.014 ± 0.004	0.057 ± 0.004	0.043	0	0.029	50.88
T3	0.013 ± 0.003	0.043 ± 0.001	0.03 ± 0.001	0	0.017	39.53
B3	0.015 ± 0.001	0.055 ± 0.01	0.04 ± 0.017	0	0.025	45.45
T4	0.009 ± 0.004	0.055 ± 0.003	0.046 ± 0.004	0	0.037	67.27
B4	0.008 ± 0.004	0.031 ± 0.01	0.035 ± 0.009	0	0.027	87.10

A3f.5. May 14th

Table A3f.5.1. Orthophosphate (OP), Total Phosphorous (TP), Acid Hydrolysable Phosphorous (AHP), Condensed-P (Con-P) and Organic Phosphorous (Org-P) concentrations (mgL^{-1}, mean ± SD) in surface and benthic water samples at sites along the reservoir during May (14th) 2018. Sample Points (SP) indicated as Top (T), Benthic (B) and site reference.

Site	OP (mgL^{-1})	TP (mgL^{-1})	AHP (mgL^{-1})	Org-P (mgL^{-1})	Con-P (mgL^{-1})	Con-P % of TP
T1	0.006 ± 0.002	0.04 ± 0.002	0.034 ± 0.004	0	0.028	70.00
B1	0.004 ± 0.003	0.043 ± 0.003	0.039 ± 0.006	0	0.035	81.40
T2	0.001	0.033	0.032 ± 0.008	0	0.031	93.94
B2	0.001 ± 0.001	0.014 ± 0.001	0.013 ± 0.009	0	0.012	85.71
T3	0.003 ± 0.001	0.026 ± 0.001	0.023 ± 0.003	0	0.020	76.92
B3	0.002	0.021	0.018 ± 0.016	0	0.016	76.19
T4	0.007 ± 0.005	0.022 ± 0.005	0.015 ± 0.01	0	0.008	36.36
B4	0.002 ± 0.001	0.034 ± 0.001	0.032 ± 0.008	0	0.030	88.24

A3f.6. May 29th

Table A3f.6.1. Orthophosphate (OP), Total Phosphorous (TP), Acid Hydrolysable Phosphorous (AHP), Condensed-P (Con-P) and Organic Phosphorous (Org-P) concentrations (mgL^{-1}, mean ± SD) in surface and benthic water samples at sites along the reservoir during May (29th) 2018.

Site	OP (mgL^{-1})	TP (mgL^{-1})	AHP (mgL^{-1})	Org-P (mgL^{-1})	Con-P (mgL^{-1})	Con-P % of TP
T1	0.002 ± 0.002	0.02 ± 0.004	0.018 ± 0.003	0.001 ± 0.001	0.016	80.00
B1	0	0.031 ± 0.01	0.03 ± 0.012	0	0.030	96.77
T2	0.002 ± 0.001	0.031 ± 0.001	0.029 ± 0.001	0	0.027	87.10
B2	0.001 ± 0.001	0.034 ± 0.007	0.033 ± 0.008	0	0.032	94.12
T3	0.004 ± 0.005	0.033 ± 0.007	0.029 ± 0.003	0	0.025	75.76
B3	0.003 ± 0.004	0.033 ± 0.007	0.029 ± 0.003	0	0.026	78.79
T4	0	0.03 ± 0.004	0.03 ± 0.005	0	0.030	100.00
B4	0	0.003 ± 0.009	0.003 ± 0.012	0	0.003	100.00

A3f.7. June 11th

Table A3f.7.1. Orthophosphate (OP), Total Phosphorous (TP), Acid Hydrolysable Phosphorous (AHP), Condensed-P (Con-P) and Organic Phosphorous (Org-P) concentrations (mgL^{-1}, mean ± SD) in surface and benthic water samples at sites along the reservoir during June (11th) 2018.

Site	OP (mgL^{-1})	TP (mgL^{-1})	AHP (mgL^{-1})	OrgP (mgL^{-1})	Con-P (mgL^{-1})	Con-P % of TP
T1	0.013 ± 0.003	0.028 ± 0.009	0.014 ± 0.007	0.001 ± 0.001	0.001	3.57
B1	0.01 ± 0.006	0.03 ± 0.006	0.02 ± 0.007	0	0.010	33.33
T2	0.011 ± 0.001	0.027 ± 0.003	0.015 ± 0.004	0	0.004	14.81
B2	0.01 ± 0.005	0.032 ± 0.01	0.022 ± 0.012	0	0.012	37.50
T3	0.007 ± 0.004	0.02 ± 0.005	0.012 ± 0.001	0	0.005	25.00
B3	0.012 ± 0.001	0.022 ± 0.004	0.01 ± 0.006	0	0	0
T4	0.011 ± 0.002	0.016 ± 0.002	0.003 ± 0.002	0.002 ± 0.001	0	0
B4	0.011 ± 0.003	0.025 ± 0.015	0.011 ± 0.015	0.003 ± 0.004	0	0

A3f.8. June 27th

Table A3f.8.1. Orthophosphate (OP), Total Phosphorous (TP), Acid Hydrolysable Phosphorous (AHP), Condensed-P (Con-P) and Organic Phosphorous (Org-P) concentrations (mgL^{-1}, mean ± SD) in surface and benthic water samples at sites along the reservoir during June (27th) 2018.

Site	OP (mgL^{-1})	TP (mgL^{-1})	AHP (mgL^{-1})	OrgP (mgL^{-1})	Con-P (mgL^{-1})	Con-P % of TP
T1	0.004 ± 0.001	0.006 ± 0.001	0.002	0	0	0
B1	0	0.001	0.001	0	0.001	97.94

T2	0.002	0.003	0.001	0	0	0
B2	0.007	0.008 ± 0.005	0	0	0	0
T3	0.001 ± 0.001	0.005 ± 0.003	0.004 ± 0.004	0	0.003	60.00
B3	0.008 ± 0.007	0.011 ± 0.005	0.003 ± 0.002	0	0	0
T4	0.001 ± 0.001	0.002 ± 0.001	0.001	0	0	0
B4	0	0.003 ± 0.003	0.003 ± 0.003	0	0.003	100.00

A3f.9. July 9th

Table A3f.9.1. Orthophosphate (OP), Total Phosphorous (TP), Acid Hydrolysable Phosphorous (AHP), Condensed-P (Con-P) and Organic Phosphorous (Org-P) concentrations (mgL^{-1}, mean ± SD) in surface and benthic water samples at sites along the reservoir on July 9th 2018.

Site	OP (mgL^{-1})	TP (mgL^{-1})	AHP (mgL^{-1})	Org-P (mgL^{-1})	Con-P (mgL^{-1})	Con-P % of TP
T1	0.001 ± 0.001	0.01 ± 0.004	0	0.009 ± 0.005	0	0
B1	0.007 ± 0.005	0.01 ± 0.006	0.002 ± 0.001	0.001 ± 0.001	0	0
T2	0.002 ± 0.001	0.008 ± 0.004	0.003 ± 0.002	0	0.001	12.50
B2	0.002 ± 0.002	0.005 ± 0.003	0.002	0	0	0
T3	0.002 ± 0.001	0.003 ± 0.001	0	0.001	0	0
B3	0	0.008 ± 0.006	0.001	0.007 ± 0.005	0.001	10.65
T4	0.001	0.013 ± 0.01	0.01 ± 0.01	0.002 ± 0.002	0.009	68.38
B4	0.001 ± 0.001	0.002 ± 0.001	0.001	0	0	0.40

A3f.10. July 23rd

Table A3f.10.1. Orthophosphate (OP), Total Phosphorous (TP), Acid Hydrolysable Phosphorous (AHP), Condensed-P (Con-P) and Organic Phosphorous (Org-P) concentrations (mgL^{-1}, mean ± SD) in surface and benthic water samples at sites along the reservoir during July 23rd, 2018.

Site	OP (mgL^{-1})	TP (mgL^{-1})	AHP (mgL^{-1})	Org-P (mgL^{-1})	Con-P (mgL^{-1})	Con-P % of TP
T1	0.004 ± 0.002	0.019 ± 0.005	0.015 ± 0.006	0	0.011	57.89
B1	0.012 ± 0.007	0.033 ± 0.006	0.021 ± 0.001	0	0.009	27.27
T2	0.006 ±.0.004	0.020 ± 0.005	0.014 ± 0.009	0	0.008	40.00
B2	0.008 ± 0.004	0.021 ± 0.004	0.012 ± 0.006	0	0.004	19.05
T3	0.012 ± 0.001	0.019 ± 0.004	0.006 ± 0.004	0	0	0
B3	0.011 ± 0.003	0.018 ± 0.002	0.006 ± 0.001	0	0	0
T4	0.016	0.026 ± 0.002	0.011 ± 0.002	0	0	0
B4	0.012 ± 0.005	0.016 ± 0.006	0.005 ± 0.003	0	0	0

A3f.11. August 3rd

Table A3f.11.1. Orthophosphate (OP), Total Phosphorous (TP), Acid Hydrolysable Phosphorous (AHP), Condensed-P (Con-P) and Organic Phosphorous (Org-P) concentrations (mgL^{-1}, mean ± SD) in surface and benthic water samples at sites along the reservoir during August 3rd, 2018.

Site	OP (mgL^{-1})	TP (mgL^{-1})	AHP (mgL^{-1})	Org-P (mgL^{-1})	Con-P (mgL^{-1})	Con-P % of TP
T1	0.001	0.007 ± 0.006	0.01 ± 0.005	0	0.009	86.05
B1	0	0.01	0.01	0	0.010	100.00
T2	0	0.009 ± 0.001	0.007 ± 0.002	0.002 ± 0.003	0.007	77.78
B2	0	0.01 ± 0.005	0.006 ± 0.004	0.003 ± 0.004	0.006	60.00
T3	0.007 ± 0.008	0.017 ± 0.009	0.01 ± 0.004	0	0.003	17.65
B3	0	0.01 ± 0.003	0.01 ± 0.003	0	0.010	99.96
T4	0	0.009 ± 0.004	0.009 ± 0.004	0	0.009	99.28
B4	0	0.009 ± 0.005	0.009 ± 0.005	0	0.009	99.78

A3f.12. August 20th

Table A3f.12.1 Orthophosphate (OP), Total Phosphorous (TP), Acid Hydrolysable Phosphorous (AHP), Condensed-P (Con-P) and Organic Phosphorous (Org-P) concentrations (mgL^{-1}, mean ± SD) in surface and benthic water samples at sites along the reservoir during August 20th, 2018.

Site	OP (mgL^{-1})	TP (mgL^{-1})	AHP (mgL^{-1})	Org-P (mgL^{-1})	Con-P (mgL^{-1})	Con-P % of TP
T1	0.003 ± 0.001	0.004	0	0.001	0	0
B1	0.003 ± 0.001	0.016 ± 0.016	0.013 ± 0.018	0	0.010	63.19
T2	0.002 ± 0.001	0.004	0	0.001 ± 0.001	0	0
B2	0.004	0.007 ± 0.002	0.002 ± 0.002	0	0	0
T3	0.001 ± 0.001	0.004	0.001	0.001 ± 0.001	0	0
B3	0.001	0.006 ± 0.002	0.003 ± 0.003	0.002 ± 0.001	0.002	29.33
T4	0	0.002	0	0.002	0	1.00
B4	0.001 ± 0.001	0.003	0	0.002	0	0

A3f.13. September 17th

Table A3f.13.1. Orthophosphate (OP), Total Phosphorous (TP), Acid Hydrolysable Phosphorous (AHP), Condensed-P (Con-P) and Organic Phosphorous (Org-P) concentrations (mgL^{-1}, mean ± SD) in surface and benthic water samples at sites along the reservoir during September 17th, 2018.

Site	OP (mgL^{-1})	TP (mgL^{-1})	AHP (mgL^{-1})	Org-P (mgL^{-1})	Con-P (mgL^{-1})	Con-P % of TP
T1	0	0.003 ± 0.002	0.002 ± 0.002	0.001	0.002	64.79
B1	0	0.002	0	0.002	0	0
T2	0	0.001	0.001	0.001	0.001	99.84
B2	0	0.001	0.001	0	0.001	96.57

T3	0	0.004	0.004	0	0.004	99.64
B3	0	0.003 ± 0.001	0.002 ± 0.001	0.001	0.002	66.23
T4	0	0.002	0.001	0.001	0.001	28.14
B4						

A3f.14. October 1st

Table A3f.14.1. Orthophosphate (OP), Total Phosphorous (TP), Acid Hydrolysable Phosphorous (AHP), Condensed-P (Con-P) and Organic Phosphorous (Org-P) concentrations (mgL^{-1}, mean ± SD) in surface and benthic water samples at sites along the reservoir during October 1st, 2018.

Site	OP (mgL^{-1})	TP (mgL^{-1})	AHP (mgL^{-1})	Org-P (mgL^{-1})	Con-P (mgL^{-1})	Con-P % of TP
T1	0	0.007 ± 0.002	0.002 ± 0.003	0.003 ± 0.002	0.002	29.70
B1	0	0.006 ± 0.002	0.001 ± 0.002	0.003 ± 0.002	0.002	24.39
T2	0	0.01 ± 0.004	0.006 ± 0.003	0.003 ± 0.003	0.006	60.54
B2	0	0.009 ± 0.002	0.006 ± 0.001	0	0.006	68.16
T3	0	0.012 ± 0.001	0.006 ± 0.001	0.002 ± 0.003	0.007	52.72
B3	0	0.002 ± 0.001	0	0.002	0	0
T4	0	0.004	0.001 ± 0.001	0.003	0.001	19.96
B4						

A3f.15. November 12th

Table A3f.15.1. Orthophosphate (OP), Total Phosphorous (TP), Acid Hydrolysable Phosphorous (AHP), Condensed-P (Con-P) and Organic Phosphorous (Org-P) concentrations (mgL^{-1}, mean ± SD) in surface and benthic water samples at sites along the reservoir during November 12th, 2018.

Site	OP (mgL^{-1})	TP (mgL^{-1})	AHP (mgL^{-1})	Org-P (mgL^{-1})	Con-P (mgL^{-1})	Con-P % of TP
T1	0.004 ± 0.002	0.015	0.011 ± 0.002	0	0.007	46.67
B1	0	0.006 ± 0.002	0.005 ± 0.002	0	0.005	81.50
T2	0	0.009 ± 0.001	0.006 ± 0.003	0.003 ± 0.003	0.006	65.50
B2	0	0.002	0.002	0	0.002	93.89
T3	0	0.011 ± 0.001	0.01 ± 0.002	0.001	0.010	89.80
B3	0	0.011 ± 0.002	0.011 ± 0.002	0	0.011	98.83
T4	0	0.01 ± 0.003	0.01 ± 0.003	0	0.010	98.85
B4	0	0.009 ± 0.005	0.008 ± 0.005	0	0.008	87.29

Appendix 3g: Molar data

A3g.1. T1

Table A3g.1.1. Mean monthly concentrations at site T1 from January 2018 through November 2018. Absent data are indicated by grey cells. * ratios are undetermined due to a variable having a value of '0'.

Month	TN:TP (mol/ml)	NO_3^-:NH_4^+ (mol/ml)	NO_3^- (mol/ml)	NH_4^+ (mol/ml)	TN (mol/ml)	TP (mol/ml)
Jan	*	48:1	0.0134	0.0003	0.0137	0
Feb	699:1	*	0.0210	0	0.0210	0.00003
Mar						
Apr						
May	22:1	5:1	0.0177	0.0037	0.0214	0.00097
Jun						0.00055
Jul	33:1	13:1	0.0215	0.0017	0.0231	0.00071
Aug	55:1	5:1	0.0085	0.0019	0.0104	0.00019
Sep	149:1	3:1	0.0110	0.0039	0.0149	0.00010
Oct						0.00023
Nov	36:1	2:1	0.0111	0.0061	0.0172	0.00048

A3g.2. B1

Table A3g.2.1. Mean monthly values of variables at site B1 from January 2018 through November 2018. Absent data are indicated by grey cells. * ratios are undetermined due to a variable having a value of '0'.

Month	TN:TP (mol/ml)	NO_3^-:NH_4^+ (mol/ml)	NO_3^- (mol/ml)	NH_4^+ (mol/ml)	NO_2^- (mol/ml)	TN (mol/ml)	TP (mol/ml)
Jan	27:1	60:1	0.0134	0.0002	0	0	0.0005
Feb	*	126:1	0.0210	0.0002	0.0001	0.0212	0
Mar							
Apr							
May	16:1	5:1	0.0177	0.0037	0.0004	0.0218	0.0014
Jun							0.0005
Jul	27:1	14:1	0.0221	0.0016	0.0006	0.0243	0.0009
Aug	35:1	5:1	0.0113	0.0017	0.0011	0.0141	0.0004
Sep	1099:1	2:1	0.0115	0.0061	0.0154	0.0330	0.00003
Oct							0.0002
Nov	35:1	1:1	0.0098	0.0161	0.0011	0.0270	0.0002

A3g.3. T2

Table A3g.3.1. Average monthly values of variables at site T2 from January 2018 through November 2018. Absent data are indicated by grey cells.

Month	TN:TP (mol/ml)	NO_3^-:NH_4^+ (mol/ml)	NO_2^- (mol/ml)	NO_3^- (mol/ml)	NH_4^+ (mol/ml)	TN (mol/ml)	TP (mol/ml)
Jan	443:1	59:1	0	0.0131	0.0002	0.0133	0.00003
Feb	352:1	126:1	0	0.0210	0.0002	0.0211	0.00006
Mar							
Apr							

May	16:1	5:1	0.0001	0.0177	0.0038	0.0216	0.00129
Jun							0.0005
Jul	35:1	5:1	0.0002	0.0206	0.0039	0.0248	0.0007
Aug	70:1	1:1	0.0003	0.0081	0.0056	0.0139	0.0002
Sep	577:1	2:1	0.0004	0.0108	0.0061	0.0173	0.00003
Oct							0.0003
Nov	88:1	2:1	0.0004	0.0111	0.0061	0.0176	0.0002

A3g.4. B2

Table A3g.4.1. Average monthly values of variables at site B1 from January 2018 through November 2018. Absent data are indicated by grey cells.

Month	TN:TP (mol/ml)	NO_3^-:NH_4^+ (mol/ml)	NO_3^- (mol/ml)	NH_4^+ (mol/ml)	NO_2^- (mol/ml)	TN (mol/ml)	TP (mol/ml)
Jan	420:1	31:1	0.0121	0.0004	0.0001	0.0126	0.00003
Feb	236:1	126:1	0.0210	0.0002	0.0001	0.0212	0.00009
Mar							
Apr							
May	19:1	3:1	0.0156	0.0052	0.0006	0.0214	0.0011
Jun							0.0006
Jul	20:1	19:1	0.0150	0.0008	0.0003	0.0161	0.0008
Aug	41:1	71:1	0.0118	0.0002	0.0005	0.0124	0.0003
Sep	544:1	2:1	0.0110	0.0056	0.0001	0.0166	0.00003
Oct							0.0003
Nov	214:1	20:1	0.0110	0.0006	0.0013	0.0128	0.00006

A3g.5. T3

Table A3g.5.1. Average monthly values of variables at site T3 from January 2018 through November 2018. Absent data are indicated by grey cells.

Month	TN:TP (mol/ml)	NO_3^-:NH_4^+ (mol/ml)	NO_3^- (mol/ml)	NH_4^+ (mol/ml)	NO_2^- (mol/ml)	TN (mol/ml)	TP (mol/ml)
Jan	464:1	49:1	0.0135	0.0003	0.0001	0.0139	0.00003
Feb	212:1	126:1	0.0210	0.0002	0.0001	0.0212	0.0001
Mar							
Apr							
May	20:1	3:1	0.0166	0.0052	0.0004	0.0209	0.0011
Jun							0.0004
Jul	40:1	15:1	0.0221	0.0015	0.0006	0.0171	0.0006
Aug	33:1	2:1	0.0081	0.0040	0.0011	0.0132	0.0004
Sep	185:1	2:1	0.0111	0.0061	0.0013	0.0180	0.0001
Oct							0.0004
Nov	46:1	2:1	0.0108	0.0061	0.0013	0.0182	0.0004

A3g.6. B3

Figure A3g.6.1. Average monthly values of variables at site B3 from January 2018 through November 2018. Absent data are indicated by grey cells. * ratios are undetermined due to a variable having a value of '0'.

Month	TN:TP (mol/ml)	NO_3^-:NH_4^+ (mol/ml)	NO_3^- (mol/ml)	NH_4^+ (mol/ml)	NO_2^- (mol/ml)	TN (mol/ml)	TP (mol/ml)
Jan	*	48:1	0.0132	0.0003	0	0.0135	0
Feb	211:1	126:1	0.0210	0.0002	0	0.0211	0.0001
Mar							
Apr							
May	18:1	3:1	0.0156	0.0054	0.0007	0.0218	0.0012
Jun							0.0005
Jul	34:1	10:1	0.0211	0.0022	0.0003	0.0237	0.0007
Aug	401	32:1	0.0106	0.0003	0.0011	0.0121	0.0003
Sep	270:1	1:1	0.0098	0.0161	0.0011	0.0270	0.0001
Oct							0.0001
Nov	47:1	2:1	0.0115	0.0061	0.0013	0.0189	0.0004

A3g.7. T4

Figure A3g.7.1. Average monthly values of variables at site T4 from January 2018 through November 2018. Absent data are indicated by grey cells. * ratios are undetermined due to a variable having a value of '0'.

Month	TN:TP (mol/ml)	NO_3^-:NH_4^+ (mol/ml)	NO_3^- (mol/ml)	NH_4^+ (mol/ml)l	NO_2^- (mol/ml)	TN (mol/ml)	TP (mol/ml)
Jan	*	28:1	0.0142	0.0005	0	0.0147	0
Feb	211:1	126:1	0.0210	0.0002	0	0.0211	0.0001
Mar							
Apr							
May	53:1	1:3	0.0166	0.0461	0.0004	0.0631	0.0012
Jun							0.0003
Jul	31:1	9:1	0.0215	0.0024	0.0006	0.0245	0.0008
Aug	67:1	2:1	0.0081	0.0042	0.0011	0.0133	0.0002
Sep	217:1	18:1	0.0111	0.0006	0.0013	0.0130	0.00006
Oct							0.0002
Nov	59:1	2:1	0.0110	0.0056	0.0013	0.0178	0.0003

A3g.8. B4

Table A3g.8.1. Average monthly values of variables at site B3 from January 2018 through November 2018. Absent data are indicated by grey cells.

Month	TN:TP (mol/ml)	NO_3^-:NH_4^+ (mol/ml)	NO_3^- (mol/ml)	NH_4^+ (mol/ml)	NO_2^- (mol/ml)	TN (mol/ml)	TP (mol/ml)
Jan	500:1	44:1	0.0147	0.0003	0	0.0150	0.00003
Feb	211:1	126:1	0.0210	0.0002	0	0.0211	0.0001
Mar							
Apr							

May	20:1	10:1	0.0177	0.0018	0.0004	0.0200	0.0010
Jun							0.0005
Jul	28:1	6:1	0.0135	0.0023	0.0008	0.0167	0.0006
Aug	62:1	3:1	0.0082	0.0031	0.0011	0.0124	0.0002
Sep		24:1	0.0161	0.0007	0	0.0168	
Oct							
Nov	54:1	3:1	0.0110	0.0040	0.0013	0.0163	0.0003

Appendix h: APA data

A3h. 1. July 9th

Table A3h.1.1. µmoles *p*NPP / µg Chl a / h (mean ± SD) data for all sites 9th July in surface and benthic water samples at sites along the reservoir.

Site	µmoles *p*NPP/ µg Chl a / h
T1	1.13 ± 0.32
B1	1.16 ± 0.26
T2	1.24 + 0.09
B2	1.24 ± 0.22
T3	1.09 ± 0.23
B3	16.13 ± 26.47
T4	0.93 ± 0.35
B4	1.15 ± 0.15

Table A3h.1.2. Orthophosphate (OP), Total Phosphorous (TP), Acid Hydrolysable Phosphorous (AHP) and Organic Phosphorous (OrgP) concentrations (mgL^{-1}, mean ± SD) in surface and benthic water samples at sites along the reservoir during July 9th 2018.

Site	OP (mgL^{-1})	TP (mgL^{-1})	AHP (mgL^{-1})	OrgP (mgL^{-1})
T1	0.001 ± 0.001	0.01 ± 0.004	0	0.009 ± 0.005
B1	0.007 ± 0.005	0.01 ± 0.006	0.002 ± 0.001	0.001 ± 0.001
T2	0.002 ± 0.001	0.008 ± 0.004	0.003 ± 0.002	0
B2	0.002 ± 0.002	0.005 ± 0.003	0.002	0
T3	0.002 ± 0.001	0.003 ± 0.001	0	0.001
B3	0	0.008 ± 0.006	0.001	0.007 ± 0.005
T4	0.001	0.013 ± 0.01	0.01 ± 0.01	0.002 ± 0.002
B4	0.001 ± 0.001	0.002 ± 0.001	0.001	0

A3h.2. July 23rd

Table A3h.2.1. µmoles *p*NPP / µg Chl a / h (mean ± SD) data for all sites 23rd July in surface and benthic water samples at sites along the reservoir.

Site	µmoles *p*NPP / µg Chl a / h
T1	0.96 ± 0.19
B1	1.51 ± 0.82
T2	1.05 ± 0.48
B2	0.74 ± 0.15
T3	0.8 ± 0.17
B3	0.89 ± 0.07

T4	0.84 ± 0.19
B4	2.55 ± 2.98

Figure A3h.2.2. Orthophosphate (OP), Total Phosphorous (TP), Acid Hydrolysable Phosphorous (AHP) and Organic Phosphorous (OrgP) concentrations (mgL^{-1}, mean ± SD) in surface and benthic water samples at sites along the reservoir during July 23rd, 2018.

Site	OP (mgL^{-1})	TP (mgL^{-1})	AHP (mgL^{-1})	OrgP (mgL^{-1})
T1	0.004 ± 0.002	0.019 ± 0.005	0.015 ± 0.006	0
B1	0.012 ± 0.007	0.033 ± 0.006	0.021 ± 0.001	0
T2	0.006 ±.0.004	0.020 ± 0.005	0.014 ± 0.009	0
B2	0.008 ± 0.004	0.021 ± 0.004	0.012 ± 0.006	0
T3	0.012 ± 0.001	0.019 ± 0.004	0.006 ± 0.004	0
B3	0.011 ± 0.003	0.018 ± 0.002	0.006 ± 0.001	0
T4	0.016	0.026 ± 0.002	0.011 ± 0.002	0
B4	0.012 ± 0.005	0.016 ± 0.006	0.005 ± 0.003	0

A3h.3. July 31st

Table A3h.3.1. µmoles *p*NPP / µg Chl a / h (mean ± SD) data for all sites 31st July in surface and benthic water samples at sites along the reservoir.

Site	µmoles *p*NPP / µg Chl a / h
T1	0
B1	1.23 ± 2.13
T2	0
B2	0
T3	24.54 ± 42.5
B3	0
T4	0
B4	0

Figure A3h.3.2. Orthophosphate (OP), Total Phosphorous (TP), Acid Hydrolysable Phosphorous (AHP) and Organic Phosphorous (OrgP) concentrations (mgL^{-1}, mean ± SD) in surface and benthic water samples at sites along the reservoir during July 31st, 2018.

Site	OP (mgL^{-1})	TP (mgL^{-1})	AHP (mgL^{-1})	OrgP (mgL^{-1})
T1	0.016 ± 0	0.038 ± 0.008	0.022 ± 0.009	0.000
B1	0.014 ± 0.002	0.038 ± 0.004	0.025 ± 0.006	0.000
T2	0.01 ± 0.005	0.038 ± 0.01	0.028 ± 0.01	0.000

B2	0.016 ± 0	0.048 ± 0.01	0.032 ± 0.01	0.000
T3	0.016 ± 0	0.032 ± 0.003	0.016 ± 0.003	0.000
B3	0.016 ± 0	0.036 ± 0.004	0.02 ± 0.003	0.000
T4	0.016 ± 0.001	0.038 ± 0.002	0.022 ± 0.002	0.000
B4	0.015 ± 0	0.038 ± 0.003	0.023 ± 0.003	0.000

A3h.4. August 3rd

Table A3h.4.1. µmoles *p*NPP / µg Chl a / h (mean ± SD) data for all sites 3rd August in surface and benthic water samples at sites along the reservoir.

Site	µmoles *p*NPP / µg Chl a / h
T1	2.96 ± 6.23
B1	0.6
T2	8.49 ± 0.09
B2	11.32 ± 17.56
T3	12.93 ± 18.25
B3	0.19 ± 0.16
T4	4.92 ± 6.9
B4	0.23 ± 0.39

Table A3h.4.2. Orthophosphate (OP), Total Phosphorous (TP), Acid Hydrolysable Phosphorous (AHP) and Organic Phosphorous (OrgP) concentrations (mgL^{-1}, mean ± SD) in surface and benthic water samples at sites along the reservoir during August 3rd, 2018.

Site	OP (mgL^{-1})	TP (mgL^{-1})	AHP (mgL^{-1})	OrgP (mgL^{-1})
T1	0.001	0.007 ± 0.006	0.01 ± 0.005	0
B1	0	0.01	0.01	0
T2	0	0.009 ± 0.001	0.007 ± 0.002	0.002 ± 0.003
B2	0	0.01 ± 0.005	0.006 ± 0.004	0.003 ± 0.004
T3	0.007 ± 0.008	0.017 ± 0.009	0.01 ± 0.004	0
B3	0	0.01 ± 0.003	0.01 ± 0.003	0
T4	0	0.009 ± 0.004	0.009 ± 0.004	0
B4	0	0.009 ± 0.005	0.009 ± 0.005	0

A3h.5. August 20th

Table A3h.5.1. µmoles *p*NPP / µg Chl a / h (mean ± SD) data for all sites 20th August in surface and benthic water samples at sites along the reservoir.

Site	µmoles *p*NPP / µg Chl a / h
T1	0
B1	0
T2	0.11 ± 0.09
B2	0
T3	0
B3	0
T4	0
B4	0

Table A3h.5.2. Orthophosphate (OP), Total Phosphorous (TP), Acid Hydrolysable Phosphorous (AHP) and Organic Phosphorous (OrgP) concentrations (mgL^{-1}, mean ± SD) in surface and benthic water samples at sites along the reservoir during August 20th, 2018.

Site	OP (mgL^{-1})	TP (mgL^{-1})	AHP (mgL^{-1})	OrgP (mgL^{-1})
T1	0.003 ± 0.001	0.004	0	0.001
B1	0.003 ± 0.001	0.016 ± 0.016	0.013 ± 0.018	0
T2	0.002 ± 0.001	0.004	0	0.001 ± 0.001
B2	0.004	0.007 ± 0.002	0.002 ± 0.002	0
T3	0.001 ± 0.001	0.004	0.001	0.001 ± 0.001
B3	0.001	0.006 ± 0.002	0.003 ± 0.003	0.002 ± 0.001
T4	0	0.002	0	0.002
B4	0.001 ± 0.001	0.003	0	0.002

Appendix 3i: PC analysis with pNPP

A3i.1. July 9th

Table A3i.1.1. lists the variables analysed using LM following PC analysis using PC1 and PC2 to determine the most suitable variables for LM analysis with *p*NPP.

Table A3i.1.1. Variables included LM analyses with *p*NPP

Geosmin (ng L^{-1})
AHP (mg L^{-1})
TP (mg L^{-1})
Turbidity (ntu)
Organic P (mg L^{-1})
TN (mg L^{-1})
pH
TN:TP (mol/ml)
Temperature

A3i.2. August 3rd

Table A3i.2.1. lists the variables analysed using LM following PC analysis using PC1 and PC2 to determine the most suitable variables for LM analysis with *p*NPP.

Table A3i.2.1. Variables included LM analyses with *p*NPP

Aphanizomenon (cfu/ml)
NH_4^+ (mg L^{-1})
Green algae (cells/ml)
TN (mg L^{-1})
Turbidity (ntu)
Geosmin (ng L^{-1})

Appendix 4: P-fraction, TOC, ion sediment and PCA data (Chapter 4)

A4.1. Mean Fe-P fraction concentrations between April 2016 and July 2018

Table A4.1.1. Mean Fe-P concentrations (mg/g ± SD) throughout the layers of sediment at each sampling point along the trajectory of the reservoir. Greyed cells indicate to an absence of data.

Site	Layer	Apr-16	Jul-17	Apr-18	Jul-18
1	1	0	22.60 ± 15	86.28 ± 54.52	130.69 ± 7.64
	2	0	32.23 ± 2.23	74.45 ± 47.47	
	3	0	17.66 ± 11.36	126.81 ± 6.68	
	4	0	0.86 ± 1.23	111.39 ± 2.77	
	5	0.047 ± 0.06			135.21 ± 7.14
2	1	0.029 ± 0.04	25.38 ± 20.05	100.15 ± 75.05	112.05 ± 0.84
	2	0.30 ± 0.07	5.95 ± 4.84	133.51 ± 16.25	
	3	0.48 ± 0.13	22.21 ± 17.68	123.07 ± 9.32	
	4	0.51 ± 0.09	13.26 ± 12.96	126.30 ± 8.37	
	5	0.45 ± 0.06			133.42 ± 3.95
3	1	0.77	30 ± 23.88	188.54 ± 42.23	109.89 ± 0.96
	2	0.75 ± 0.12	39.13 ± 9.65	66.28 ± 46.9	
	3	0.88 ± 0.14	34.10 ± 7.16	126.29 ± 0.78	
	4	1.38 ± 0.11	15.13 ± 21.39	146.94 ± 58.63	
	5	1.49 ± 0.18			85.70 ± 68.73
4	1	0.44 ± 0.13	12.81 ± 11	35.90 ± 42.89	8.28 ± 11.7
	2	0.48 ± 0.19	19.24 ± 6.4	374.43 ± 524.36	
	3	0.46 ± 0.04	13.91 ± 10.1	0	
	4	0.47 ± 0.06	0	26.32 ± 37.23	
	5	0.46 ± 0.1			114.89 ± 11.9

A4.2. Fe-P April 2016

Table A4.2.1. Fe-P (mg/g) concentrations (mean ± SD) in sediment samples at site 1, 2, 3, 4 & 5 during April 2016. Layer 1 represents the top 0-3cm, layer 2 represents 4-6cm, layer 3 represents 7-9cm, layer 4 represents 10-12cm and layer 5 represents 13-15cm of sediment depth.

Layer	Site 1	Site 2	Site 3	Site 4
1	0	0.029 ± 0.04	0.77	0.44 ± 0.13
2	0	0.30 ± 0.07	0.75 ± 0.12	0.48 ± 0.19
3	0	0.48 ± 0.13	0.88 ± 0.14	0.46 ± 0.04
4	0	0.51 ± 0.09	1.38 ± 0.11	0.47 ± 0.06
5	0.047 ± 0.06	0.45 ± 0.06	1.49 ± 0.18	0.46 ± 0.1

A43. Fe-P July 2017

Table A4.3.1. Fe-P (mg/g) concentrations (mean ± SD) in sediment samples at site 1, 2, 3 & 4 during July 2017. Layer 1 represents the top 0-3cm, layer 2 represents 4-6cm, layer 3 represents 7-9cm and layer 4 represents 10-12cm of sediment depth.

Layer	Site 1	Site 2	Site 3	Site 4
1	22.6 ± 15	25.38 ± 20.05	30 ± 23.88	12.81 ± 11
2	32.23 ± 2.23	5.95 ± 4.84	39.13 ± 9.65	19.24 ± 6.4
3	17.66 ± 11.36	22.21 ± 17.68	34.10 ± 7.16	13.91 ± 10.1
4	0.86 ± 1.23	13.26 ± 12.96	15.13 ± 21.39	0

A4.4. Fe-P April 2018.

Table A4.4.1. Fe-P (mg/g) concentrations (mean ± SD) in sediment samples at site 1, 2, 3 & 4 during April 2018. Layer 1 represents the top 0-3cm, layer 2 represents 4-6cm, layer 3 represents 7-9cm and layer 4 represents 10-12cm of sediment depth.

Layer	Site 1	Site 2	Site 3	Site 4
1	86.28 ± 54.52	100.15 ± 75.05	188.54 ± 42.23	35.90 ± 42.89
2	74.45 ± 47.47	133.51 ± 16.25	66.28 ± 46.9	374.43 ± 524.36
3	126.81 ± 6.68	123.07 ± 9.32	126.29 ± 0.78	0
4	111.39 ± 2.77	126.30 ± 8.37	146.94 ± 58.63	26.32 ± 37.23

A4.5. Fe-P July 2018.

Table A4a.5.1. Fe-P (mg/g) concentrations (mean ± SD) in sediment samples at site 1, 2, 3 & 4 during July 2018. Layer 1 represents the top 0-3cm and layer 5 represents 13-15cm of sediment depth. Layers 2 – 4 were unavailable for analysis on this date.

Layer	Site 1	Site 2	Site 3	Site 4
1	130.69 ± 7.64	112.05 ± 0.84	109.89 ± 0.96	8.28 ± 11.7
2				
3				
4				
5	135.21 ± 7.14	133.42 ± 3.95	85.70 ± 68.73	114.89 ± 11.9

A4.6. Mean Ca-P fraction concentrations between April 2016 and July 2018

Table A4a.6.1. Mean Ca-P concentrations (mg/g ± SD) throughout the layers of sediment at each sampling point along the trajectory of the reservoir. Greyed cells indicate to an absence of data.

Site	Layer	Apr-16	Jul-17	Apr-18	Jul-18
1	1	9.84 ± 0.19	15.21 ± 1.44	1.81 ± 1.46	32.02 ± 0.22
	2	6.55 ± 2	15.25 ± 1.15	2.68 ± 2	
	3	8.67 ± 2.66	20.43 ± 6.26	2.25 ± 1.6	
	4	8.65 ± 1.2	14.63 ± 0.14	12.21 ± 12.5	
	5	11.58 ± 1.42			52.46 ± 1.13
2	1	7.54 ± 1.25	14.73 ± 0.59	1.54 ± 1.19	7.00 ± 4.64
	2	10.32 ± 5.87	15.00 ± 0.52	3.81 ± 2.51	
	3	9.45 ± 3.77	16.93 ± 1.36	1.00 ± 0.91	
	4	10.51 ± 2.02	14.57 ± 0.75	3.52 ± 4.28	
	5	7.35 ± 0.99			96.46 ± 76.32
3	1	0.00	15.88 ± 2.26	1.37 ± 1.93	19.77 ± 1.59
	2	3.61 ± 3.97	14.30 ± 0.62	1.46 ± 2.06	
	3	4.39 ± 6.21	15.27 ± 0.97	1.41 ± 1.99	
	4	2.55 ± 3.61	9.42 ± 6.67	76.53 ± 104.6	
	5	3.16 ± 3.77			18.64 ± 10.32
4	1	8.52 ± 0.77	14.39 ± 0.46	32.53 ± 44.8	71.18 ± 87.81
	2	5.12 ± 2.43	14.76 ± 0.88	3.99 ± 3.86	
	3	3.94 ± 2.47	14.43 ± 0.57	0	
	4	6.23 ± 3.1	8.09 ± 9.06	61.84 ± 87.46	
	5	7.77 ± 2.84			3.23 ± 1.15

A4.7. Ca-P April 2016.

Table A4.7.1. Ca-P (mg/g) concentrations (mean ± SD) in sediment samples at site 1, 2, 3, 4 & 5 during April 2016. Layer 1 represents the top 0-3cm, layer 2 represents 4-6cm, layer 3 represents 7-9cm, layer 4 represents 10-12cm and layer 5 represents 13-15cm of sediment depth.

Layer	Site 1	Site 2	Site 3	Site 4
1	9.84 ± 0.19	7.54 ± 1.25	0	8.52 ± 0.77
2	6.55 ± 2	10.32 ± 5.87	3.61 ± 3.97	5.12 ± 2.43
3	8.67 ± 2.66	9.45 ± 3.77	4.39 ± 6.21	3.94 ± 2.47
4	8.65 ± 1.2	10.51 ± 2.02	2.55 ± 3.61	6.23 ± 3.1
5	11.58 ± 1.42	7.35 ± 0.99	3.16 ± 3.77	7.77 ± 2.84

A4.8. Ca-P July 2017.

Table A4.8.1. Ca-P (mg/g) concentrations (mean ± SD) in sediment samples at site 1, 2, 3 &4 during July 2017. Layer 1 represents the top 0-3cm, layer 2 represents 4-6cm, layer 3 represents 7-9cm and layer 4 represents 10-12cm of sediment depth.

Layer	Site 1	Site 2	Site 3	Site 4
1	15.21 ± 1.44	14.73 ± 0.59	15.88 ± 2.26	14.39 ± 0.46
2	15.25 ± 1.15	15.00 ± 0.52	14.30 ± 0.62	14.76 ± 0.88
3	20.43 ± 6.26	16.93 ± 1.36	15.27 ± 0.97	14.43 ± 0.57
4	14.63 ± 0.14	14.57 ± 0.75	9.42 ± 6.67	8.09 ± 9.06

A4.9. Ca-P April 2018.

Table A4.9.1. Ca-P (mg/g) concentrations (mean ± SD) in sediment samples at site 1, 2, 3 & 4 during April 2018. Layer 1 represents the top 0-3cm, layer 2 represents 4-6cm, layer 3 represents 7-9cm and layer 4 represents 10-12cm of sediment depth.

Layer	Site 1	Site 2	Site 3	Site 4
1	1.81 ± 1.46	1.54 ± 1.19	1.37 ± 1.93	32.53 ± 44.8
2	2.68 ± 2	3.81 ± 2.51	1.46 ± 2.06	3.99 ± 3.86
3	2.25 ± 1.6	1.00 ± 0.91	1.41 ± 1.99	0.00
4	12.21 ± 12.5	3.52 ± 4.28	76.53 ± 104.66	61.84 ± 87.46

A4.10. Ca-P July 2018.

Table A4.10.1. Ca-P (mg/g) concentrations (mean ± SD) in sediment samples at site 1, 2, 3 & 4 during July 2018. Layer 1 represents the top 0-3cm and layer 5 represents 13-15cm of sediment depth. Layers 2 – 4 were unavailable for analysis on this date.

Layer	Site 1	Site 2	Site 3	Site 4
1	32.02 ± 0.22	7.00 ± 4.64	19.77 ± 1.59	71.18 ± 87.81
2				
3				
4				
5	52.46 ± 1.13	96.46 ± 76.32	18.64 ± 10.32	3.23 ± 1.15

A4.11. Labile-P April 2016.

Table A4.11.1. Labile-P (mg/g) concentrations (mean ± SD) in sediment samples at site 1, 2, 3 & 4 during April 2016. Layer 1 represents the top 0-3cm, layer 2 represents 4-6cm, layer 3 represents 7-9cm, layer 4 represents 10-12cm and layer 5 represents 13-15cm of sediment depth.

Layer	Site 1	Site 2	Site 3	Site 4
1	0.017 ± 0.012	0.16 ± 0.23	0	0
2	0.016 ± 0.019	0.02 ± 0.02	0	0
3	0	0.061 ± 0.029	0	0
4	0.086 ± 0.056	0.46 ± 0.47	0	0
5	0.075 ± 0.08	0.141 ± 0.02	0	0

A4.12. Labile-P July 2017.

Table A4.12.1. Labile-P (mg/g) concentrations (mean ± SD) in sediment samples at site 1, 2, 3 & 4 during July 2017. Layer 1 represents the top 0-3cm, layer 2 represents 4-6cm, layer 3 represents 7-9cm and layer 4 represents 10-12cm of sediment depth.

Layer	Site 1	Site 2	Site 3	Site 4
1	18.89 ± 3.59	22.19 ± 1.54	8.70 ± 0.85	6.59 ± 0.25
2	15.41 ± 4.83	20.43 ± 0.65	8.82 ± 1.28	7.76 ± 0.9
3	15.7 ± 5.69	19.19 ± 0.42	8.58 ± 0.9	6.94 ± 0.46
4	10.94 ± 7.96	19.68 ± 1.85	11.15 ± 3.12	5.14 ± 3.63

A4.13. Labile-P April 2018.

Table A4.13.1. Labile-P (mg/g) concentrations (mean ± SD) in sediment samples at site 1, 2, 3 & 4 during July 2017. Layer 1 represents the top 0-3cm, layer 2 represents 4-6cm, layer 3 represents 7-9cm and layer 4 represents 10-12cm of sediment depth.

Layer	Site 1	Site 2	Site 3	Site 4
1	0	65.03 ± 91.97	0	0
2	0	0	30.3 ± 42.85	0
3	0.98 ± 1.39	0	0	0
4	0	1.01 ± 1.43	0	0

A4.14. Labile-P July 2018.

Table A4.14.1. Labile-P (mg/g) concentrations (mean ± SD) in sediment samples at site 1, 2, 3 & 4 during July 2018. Layer 1 represents the top 0-3cm and layer 5 represents 13-15cm of sediment depth. Layers 2 – 4 were unavailable for analysis on this date.

Layer	Site 1	Site 2	Site 3	Site 4
1	3.11 ± 1.69	4.32 ± 1.33	3.37 ± 1.06	188.10 ± 1.61
2				
3				
4				
5	5.13 ± 1.18	9.51 ± 0.65	5.56 ± 1.37	0.34 ± 0.24

A4.15. Mean Total Organic Carbon (TOC) concentrations between April 2016 and July 2018

Table A4.15.1. TOC (mg/g) concentrations (mean ± SD) in sediment samples at site 1, 2, 3 & 4 during April 2016, July 2017, April 2018 and July 2018. Layer 1 represents the top 0-3cm and layer 5 represents 13-15cm of sediment depth. Layers 2 – 4 were unavailable for analysis on this date.

Site Layer	Apr-16	Jul-17	Apr-18	Jul-18

	1	15.00 ± 10.8	26.08 ± 23.27	3.05 ± 0.28	4.21 ± 2.75
	2	6.66 ± 9.42	2.77 ± 3.92	12.41 ± 13.32	
1	3	0	1.23 ± 1.74	3.98 ± 1.59	
	4	8.33 ± 11.78	3.448 ± 3.44	1.96 ± 1.38	
	5	0.00			4.32 ± 0.99
	1	8.33 ± 11.78	4.59 ± 6.5	4.93 ± 1.35	4.26 ± 1.18
	2	8.33 ± 11.78	5.42 ± 5.41	7.18 ± 3.12	
2	3	6.66 ± 9.42	6.27 ± 7	4.20 ± 1.31	
	4	0	2.94 ± 4.15	6.30 ± 3.82	
	5	8.33 ± 11.78			4.36 ± 1.48
	1	14.99 ± 10.8	7.65 ± 2.6	4.10 ± 1.38	4.96 ± 0.11
	2	0	11.32 ± 1.95	2.30 ± 1.64	
3	3	0	8.15 ± 5.38	3.51 ± 2.99	
	4	6.66 ± 9.42	6.74 ± 0.74	1.55 ± 2.19	
	5	23.33 ± 2.35			6.52 ± 3.32
	1	5.55 ± 7.85	76.35 ± 96.65	1.58	1.04 ± 1.43
	2	12.22 ± 8.74	4.11 ± 1.84	0	
4	3	11.11 ± 7.85	5.55 ± 0.73	1.92	
	4	10.83 ± 8.24	7.06 ± 4.84	0	
	5	5.55 ± 7.85			3.79 ± 0.03

A4.16. Total organic carbon April 2016.

Table A4.16.1. Total organic carbon (TOC) (mg/g) concentrations (mean ± SD) in sediment samples at site 1, 2, 3 & 4 during April 2016. Layer 1 represents the top 0-3cm, layer 2 represents 4-6cm, layer 3 represents 7-9cm, layer 4 represents 10-12cm and layer 5 represents 13-15cm of sediment depth.

Layer	Site 1	Site 2	Site 3	Site 4
1	15.00 ± 10.8	8.33 ± 11.78	14.99 ± 10.8	5.55 ± 7.85
2	6.66 ± 9.42	8.33 ± 11.78	0	12.22 ± 8.74
3	0.00	6.66 ± 9.42	0	11.11 ± 7.85
4	8.33 ± 11.78	0	6.66 ± 9.42	10.83 ± 8.24
5	0	8.33 ± 11.78	23.33 ± 2.35	5.55 ± 7.85

A4.17. Total organic carbon July 2017.

Table A4.17.1. Total organic carbon (TOC) (mg/g) concentrations (mean ± SD) in sediment samples at site 1, 2, 3 & 4 during July 2017. Layer 1 represents the top 0-3cm, layer 2 represents 4-6cm, layer 3 represents 7-9cm and layer 4 represents 10-12cm of sediment depth.

Layer	Site 1	Site 2	Site 3	Site 4
1	26.08 ± 23.27	4.59 ± 6.5	7.65 ± 2.6	76.35 ± 96.65
2	2.77 ± 3.92	5.42 ± 5.41	11.32 ± 1.95	4.11 ± 1.84
3	1.23 ± 1.74	6.27 ± 7	8.15 ± 5.38	5.55 ± 0.73
4	3.448 ± 3.44	2.94 ± 4.15	6.74 ± 0.74	7.06 ± 4.84

A4.18. Total organic carbon April 2018.

Table A4.18.1. Total organic carbon (TOC) (mg/g) concentrations (mean ± SD) in sediment samples at site 1, 2, 3 &4 during July 2017. Layer 1 represents the top 0-3cm, layer 2 represents 4-6cm, layer 3 represents 7-9cm and layer 4 represents 10-12cm of sediment depth.

Layer	Site 1	Site 2	Site 3	Site 4
1	3.05 ± 0.28	4.93 ± 1.35	4.10 ± 1.38	1.58
2	12.41 ± 13.32	7.18 ± 3.12	2.30 ± 1.64	0.00
3	3.98 ± 1.59	4.20 ± 1.31	3.51 ± 2.99	1.92
4	1.96 ± 1.38	6.30 ± 3.82	1.55 ± 2.19	0.00

A4.19. Total organic carbon July 2018.

Table A4.19.1. Total organic carbon (TOC) (mg/g) concentrations (mean ± SD) in sediment samples at site 1, 2, 3 & 4 during July 2018. Layer 1 represents the top 0-3cm and layer 5 represents 13-15cm of sediment depth. Layers 2 – 4 were unavailable for analysis on this date.

Layer	Site 1	Site 2	Site 3	Site 4
1	4.21 ± 2.75	4.26 ± 1.18	4.96 ± 0.11	1.04 ± 1.43
2				
3				
4				
5	4.32 ± 0.99	4.36 ± 1.48	6.52 ± 3.32	3.79 ± 0.03

A4.20. Fe^{+} and Mn^{+} ion July 2017

Table A4.20.1. Fe^{+} and Mn^{+} ion data (mean ± SD) through layer 1 (0-3cm), layer 2 (4-6cm and layer 3 (7-9cm) of sediment at sample point 1, 2, 3and 4 during July 2017.

Site	Layer	Fe^{+} ion(mg/g)	Mn^{+} ion (mg/g)
1	1	50.93 ± 0.14	0.996 ± 0.05
	2	44.9 ± 0.31	0.809 ± 0.02
	3	48.66 ± 0.43	0.89 ± 0.04
2	1	53.13 ± 0.34	0.90 ± 0.07
	2	53.93 ± 0.2	0.971 ± 0.06
	3	47.53 ± 0.06	0.98 ± 0.08
3	1	43.56 ± 0.01	0.819 ± 0.13
	2	43.43 ± 0.3	0.63 ± 0.09
	3	42.13 ± 0.16	0.62 ± 0.04
4	1	29.52 ± 0.11	0.42 ± 0.05
	2	28.03 ± 0.13	0.624 ± 0.06
	3	37.23 ± 0.01	0.73 ± 0.05

A4.21. Fe^{+} and Mn^{+} ion April 2018

Table A4.21.1. Fe^{+} and Mn^{+} ion data (mean ± SD) through layer 1 (0-3cm), layer 2 (4-6cm and layer 3 (7-9cm) of sediment at sample point 1, 2, 3and 4 during April 2018.

Site	Layer	Fe^{+} ion (mg/g)	Mn^{+} ion (mg/g)
1	1	51.9 ± 3.31	1.53 ± 0.01
	2	47.73 ± 3.02	0.93 ± 0.1
	3	51.23 ± 1.77	1.05 ± 0.05
2	1	53.03 ± 1.43	0.99 ± 0.01
	2	50 ± 0.58	1.05 ± 0.09
	3	48.26 ± 0.33	1.24 ± 0.1

	1	40.77 ± 5.7	0.89 ± 0.07
3	2	45.33 ± 2	0.60 ± 0.04
	3	44.66 ± 1.18	0.62 ± 0.04
4	1	36.03 ± 0.86	0.50 ± 0.04

A4.22. Fe^{+} and Mn^{+} ions July 2018

Table A4.22.1. Manganese ion (Mn^{+}) and iron ion (Fe^{+} concentrations (pph, mean ± SD) in sediment samples at sites along the reservoir during July 2018. Layer 1 represents the top 0-3cm, layer 2 represents 4-6cm and layer 3 represents 7-9cm of sediment depth.

Site	Layer	Fe+ ion (mg/g)	Mn+ ion (mg/g)
1	1	62.2 ± 1.13	0.99 ± 0.11
2	1	54.23 ± 1.39	0.98 ± 0.05
3	1	48.76 ± 0.44	0.82 ± 0.07
4	1	31.44 ± 0.4	0.35 ± 0.01

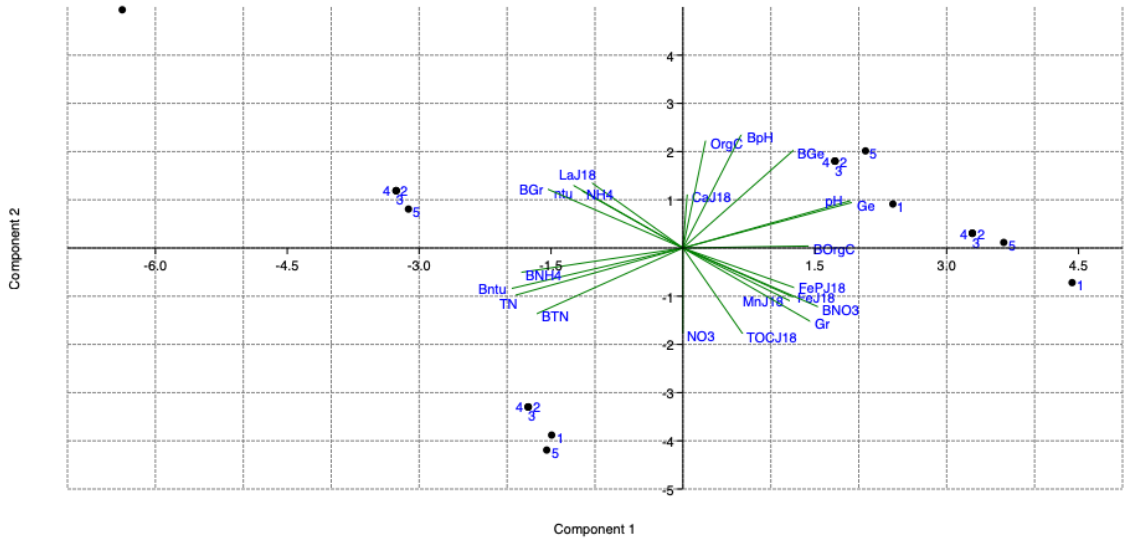

Figure A4.23. PCA for the determination of suitable variables for GLM/LM analyses of July 2018 data

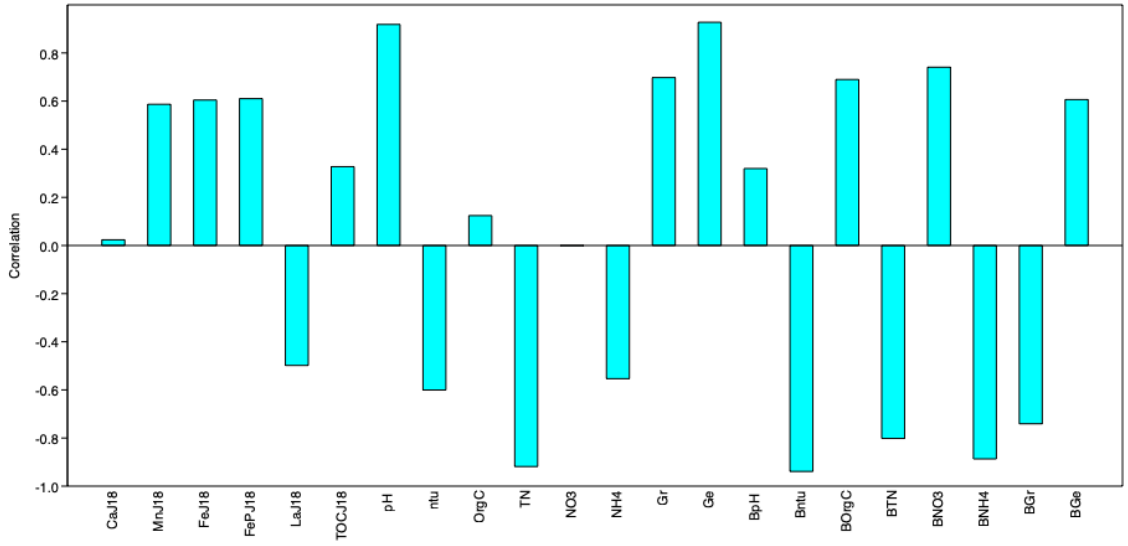

Figure A4. 24. PC1 loading July 2018

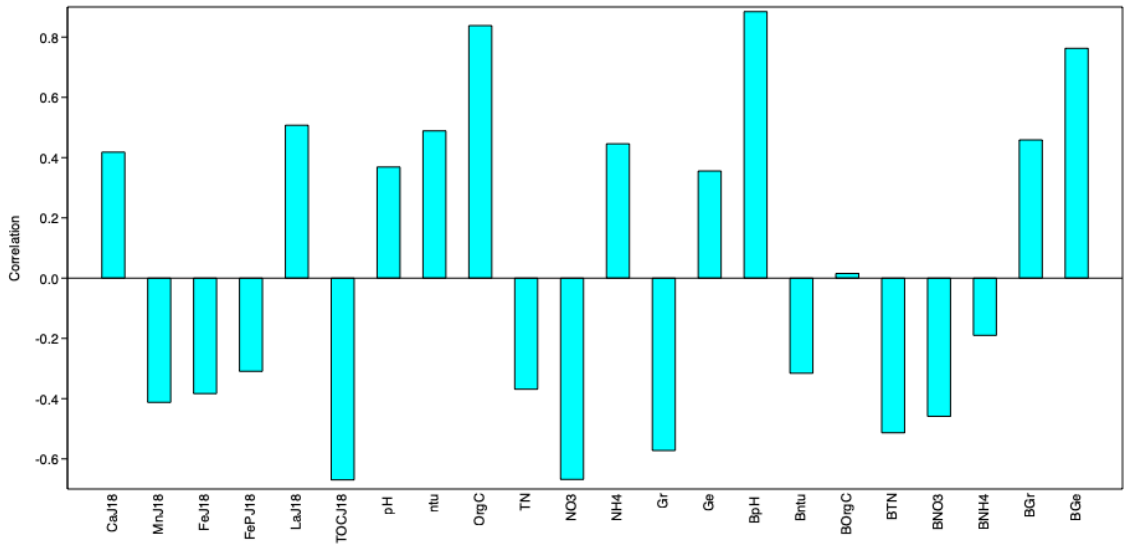

Figure A4.25. PC2 loading for July 2018

Appendix 5: EWE nutrient data

A5.1. Orthophosphate (OP) (mgL^{-1}) site concentrations over the course of the EWE.

Table A5.1.1 Orthophosphate (OP) concentrations (mean mgL^{-1} ± SD) in surface and benthic water samples at sites 1 through 4 along the reservoir on July 9th July 23rd, July 31st and August 3rd of summer 2018.

Site	No pumping, no rain (9th July)	Active pumping, no rain (23rd July)	Active pumping and 1 day post rain (31st July)	Active pumping, 4 days post rain (3rd August)
T1	0.001 ± 0.001	0.004 ± 0.002	0.016	0.009
B1	0.007 ± 0.005	0.012 ± 0.007	0.014 ± 0.002	0
T2	0.002 ± 0.001	0.006 ±.0.004	0.01 ± 0.005	0
B2	0.002 ± 0.002	0.008 ± 0.004	0.016	0
T3	0.002 ± 0.001	0.012 ± 0.001	0.016	0.007 ± 0.008
B3	0	0.011 ± 0.003	0.016	0
T4	0.001	0.016	0.016 ± 0.001	0
B4	0.001 ± 0.001	0.012 ± 0.005	0.015	0

A5.2. Acid hydrolysable phosphate (AHP) (mgL^{-1}) site concentrations over the course of the EWE.

Table A5.2.1. Acid Hydrolysable Phosphate (AHP) concentrations (mean mgL^{-1}± SD) in surface and benthic water samples at sites 1 through 4 along the reservoir on July 9th July 23rd, July 31st and August 3rd of summer 2018.

Site	No pumping, no rain (9th July)	Active pumping, no rain (23rd July)	Active pumping and 1 day post rain (31st July)	Active pumping, 4 days post rain (3rd August)
T1	0	0.015 ± 0.006	0.022 ± 0.009	0.01 ± 0.005
B1	0.002 ± 0.001	0.021 ± 0.001	0.025 ± 0.006	0.01
T2	0.003 ± 0.002	0.014 ± 0.009	0.028 ± 0.01	0.007 ± 0.002
B2	0.002	0.012 ± 0.006	0.032 ± 0.01	0.006 ± 0.004
T3	0	0.006 ± 0.004	0.016 ± 0.003	0.01 ± 0.004
B3	0.001	0.006 ± 0.001	0.02 ± 0.003	0.01 ± 0.003
T4	0.01 ± 0.01	0.011 ± 0.002	0.022 ± 0.002	0.009 ± 0.004
B4	0.001	0.005 ± 0.003	0.023 ± 0.003	0.009 ± 0.005

A5.3. Organic P concentrations (mgL^{-1}) over the course of the EWE.

Table A5.3.1. Organic Phosphate (Org-P) concentrations (mean mgL^{-1} ± SD) in surface and benthic water samples at sites 1 through 4 along the reservoir on July 9th July 23rd, July 31st and August 3rd of summer 2018.

Site	No pumping, no rain (9th July)	Active pumping, no rain (23rd July)	Active pumping and 1-day post rain (31st July)	Active pumping, 4 days post rain (3rd August)
T1	0.009 ± 0.005	0	0	0
B1	0.001 ± 0.001	0	0	0
T2	0	0	0	0.002 ± 0.003
B2	0	0	0	0.003 ± 0.004
T3	0.001	0	0	0
B3	0.007 ± 0.005	0	0	0
T4	0.002 ± 0.002	0	0	0
B4	0	0	0	0

A5.4. Total P (mgL^{-1}) concentrations over the course of the EWE.

Table A5.4.1. Total Phosphorous (TP) concentrations (mean mgL^{-1} ± SD) in surface and benthic water samples at sites 1 through 4 along the reservoir on July 9th July 23rd, July 31st and August 3rd of summer 2018.

Site	No pumping, no rain (9th July)	Active pumping, no rain (23rd July)	Active pumping and 1-day post rain (31st July)	Active pumping, 4 days post rain (3rd August)
T1	0.01 ± 0.004	0.019 ± 0.005	0.038 ± 0.008	0.007 ± 0.006
B1	0.01 ± 0.006	0.033 ± 0.006	0.038 ± 0.004	0.01
T2	0.008 ± 0.004	0.020 ± 0.005	0.038 ± 0.01	0.009 ± 0.001
B2	0.005 ± 0.003	0.021 ± 0.004	0.048 ± 0.01	0.01 ± 0.005
T3	0.003 ± 0.001	0.019 ± 0.004	0.032 ± 0.003	0.017 ± 0.009
B3	0.008 ± 0.006	0.018 ± 0.002	0.036 ± 0.004	0.01 ± 0.003
T4	0.013 ± 0.01	0.026 ± 0.002	0.038 ± 0.002	0.009 ± 0.004
B4	0.002 ± 0.001	0.016 ± 0.006	0.038 ± 0.003	0.009 ± 0.005

A5.5. Oxidised N.

Table A5.5.1. Nitrate (NO_3^-) concentrations (mean mgL^{-1}) in surface and benthic water samples at sites along the reservoir during the dry, active pumping and active pumping 4 days post rainfall event of summer 2018.

Site	No pumping, no rain (9th July)	Active pumping, no rain (23rd July)	Active pumping, 4 days post rain (3rd August)
T1	0.96	0.74	0.53
B1	0.99	0.76	0.7
T2	0.94	0.67	0.5
B2	0.99	0.87	0.73
T3	0.96	0.83	0.5
B3	0.99	0.64	0.66
T4	0.95	0.76	0.5
B4	0.96	0.73	0.51

A5.6. Reduced N over the course of the EWE.

Table A5a.6.1. Ammonium (NH_4^+) concentrations (mean mgL^{-1}) in surface and benthic water samples at sites along the reservoir during the dry, active pumping, and active pumping 4 days post rainfall of summer 2018.

Site	No pumping, no rain (9th July)	Active pumping, no rain (23rd July)	Active pumping, 4 days post rain (3rd August)
T1	0.017	0.027	0.034
B1	0.007	0.044	0.031
T2	0.021	0.1	0.1
B2	0.013	0.003	0.003
T3	0.019	0.016	0.072
B3	0.017	0.051	0.006
T4	0.021	0.046	0.075
B4	0.017	0.05	0.056

A5.7. TN:TP ratio (mol/ml) over the course of the EWE.

Table A5.7.1. TN:TP (mol/ml) concentrations (mean mgL^{-1}) in surface and benthic water samples at sites along the reservoir during the dry, active pumping and active pumping and 4 days post rainfall of summer 2018.

Site	No pumping, no rain (9th July)	Active pumping, no rain (23rd July)	Active pumping, 4 days post rain (3rd August)
T1	5:1	22:1	54:1
B1	55:1	13:1	44:1
T2	55:1	27:1	46:1
B2	84:1	20:1	40:1
T3	167:1	24:1	25:1
B3	57:1	22:1	38:1
T4	42:1	19:1	42:1
B4	166:1	29:1	39:1

A5.8. NO_3^-:NH_4^+ ratio (mol/ml) over the course of the EWE.

Table A5.8.1. NO_3^-:NH_4^+ (mol/ml) ratio during the dry, active pumping and dry and active pumping following a precipitation event.

Site	No pumping, no rain (9th July)	Active pumping, no rain (23rd July)	Active pumping, 4 days post rain (3rd August)
T1	16:1	8:1	5:1
B1	41:1	5:1	7:1
T2	13:1	2:1	1:1
B2	22:1	84:1	71:1
T3	15:1	15:1	2:1
B3	17:1	4:1	32:1
T4	13:1	5:1	2:1
B4	16:1	4:1	3:1

A5.9. Geosmin concentration data analysis

Table A5.9.1. Geosmin concentrations (ngL^{-1}) at the sampling sites throughout the drought sampling period.

Site	No pumping, no rain (9th July)	Active pumping, no rain (23rd July)	Active pumping, 4 days post rain (3rd August)
T1	1.4	0.3	0
B1	1.5	0	0.75
T2	1.3	0	0
B2	2	0.34	0.94
T3	0	0	0
B3	0	0	0.9
T4	0	0.44	0
B4	1	0	1.2

A5.10. Cyanobacteria concentrations (cfu/ml) and distribution.

Table A5.10.1. Incidence of cyanobacteria (cfu/ml) (*Oscillatoria*) throughout the drought and post rainfall sampling period. No other species of cyanobacteria were isolated during the sampling period.

Site	No pumping, no rain (9th July)	Active pumping, no rain (23rd July)	Active pumping, 4 days post rain (3rd August)
T1	0	2200	4400
B1	0	2100	0
T2	0	0	5000
B2	0	2100	0
T3	0	0	6900
B3	0	2500	0
T4	0	0	6300
B4	0	4400	0

A5.11. Green algae (cells/ml) concentrations and distribution.

Table A5a.11.1. Incidence of green algae (cells/ml) throughout the drought and post rainfall sampling period.

Site	No pumping, no rain (9th July)	Active pumping, no rain (23rd July)	Active pumping, 4 days post rain (3rd August)
T1	240	150	5500
B1	0	190	0
T2	190	140	7900
B2	0	86	0
T3	240	1700	7000
B3	0	430	0
T4	0	520	1600
B4	48	5500	4600

Appendix 6: Sequential phosphorous sequestration method

SEDIMENT PHOSPHOROUS EXTRACTION

1. Section cores on day of sampling, eg 0-5, 5-10, 10-15cm sections unless stable core in which case 0-3, 3-6,6-9.9-12,12-15cm if possible.

2. Take sub-core with syringe to 0.5cm depth for algal counts in surface layer, add to 10ml UHPm and add gluteraldehyde.

3. Weigh out about 1g into weighed crucibles and place in oven at 80C overnight, each core section.

4. Freeze dry some sediment of each core section in small plastics for chla analysis.

5. Store remainder at 4C.

6. On day 2 carry out a) dry weights
b) ash-free weights
c) chla
d) start digests

7. Digests
a) To equivalent wet weights equal to 20mg dry weights add the following reagents.
b) 20ml 0.1N NaOH (2g in 500ml) and leave for 17hours.
c) 20ml 0.5N HCl (41.7ml in 500ml of Sp grav 1.18 (12M)) and leave for 24 hours.
d) 20ml 1M NH_4Cl (26.745g in 500ml) neutalised to pH7 with HCl, leave for 2 hours and repeat.

8. Centrifuge at 4500 rpm for 10 mins and proceed for OP analysis. Run standard 10µM as samples in each digest.

9. Removes Fe/Al bound, Ca bound and labile P respectively.

Appendix 7: Alkaline phosphatase Activity (APA) method

Alkaline Phosphatase Activity

Schedule for assay

1. Buffer

HEPES. Dissolve 14.8938 g of HEPES (MWT 238.3) in 100ml and adjust pH to 7.8 with Conc NaOH solution. Pour 100 ml Hepes and add 67ml DO water.

Glycine. Dissolve 4.6919 g glycine (MWT 75.07) in 100ml and adjust pH to 10.3 using conc NaOH solution (Vol = ml).

2. pNPP solution.

Dissolve 1 pNPP (MWT 371.1) tablet (20 mg) in 10 ml buffer solution.

3. Standard pNP solution

Dissolve 0.0348 g pNP (MWT 139.1) in 250ml UHP to give 1 mM. Dilute as required

4. To 20 ml sample add 0.44ml pNPP solution (final conc = 107.78 µM, and 5 µmoles substrate per assay) and 0.89 ml buffer (final conc = 50 mM). Seal and mix transferring to a 25C shaking water bath. Incubate for 1 hour.

5. Add 5N NaOH to terminate reaction (Vol ml). Mix and filter a sub-sample.

6. Transfer 1 ml to a cuvette and read ABS at 405 mM.

7. Run standards, 1 ml in a cuvette and blanks of above procedure but with 45 ml UHP instead of sample.

8. Calculation.

ABS = m. Conc (from standard curve).

ABS of sample = y

Therefore :-

$$\frac{(y/m \,.\, \text{Sample vol } (50))}{\mu g \text{ Chl a /ml} \,.\, 45 \,.\, T \text{ (1 hr)}} \text{ divide by } 2.25$$

= x µmoles pNPP / µg Chl a / h

Appendix 8: Analysis of bi-monthly cross-site P-fraction data over the 11-month sampling period

3.3.7. Analysis of bi-monthly cross-site P-fraction data over the 11-month sampling period

3.3.7.1. P-fraction data analysis

All fractions of P were detected within the reservoir during January, with AHP being the dominant fraction (Figure 3.3.7.1). However, TP predominantly consisted of organic-P during early February with the highest concentrations isolated at bottom and surface of sites 3 (0.005 mgL^{-1} ± SE 0.002) and 4 (up to 0.006 mgL^{-1} ± SE 0.001).

Organic-P decreased in concentration throughout the reservoir through February with AHP becoming the dominant fraction. Organic-P became undetected throughout the reservoir during early and mid-May and AHP remained the dominant fraction (Figure 3.3.7.1). OP concentrations increased throughout the reservoir from February to early May, reaching its highest concentration on May 2nd at site B3 (0.015 mgL^{-1} ± SE 0.001).

OP concentrations decreased through May, however, AHP increased from mid to end of May at each site with the exception of site T1 where a decrease was observed. Organic-P reached its highest concentrations at site 4 (bottom and surface) during early June but was undetected throughout the reservoir at the end of June. Both OP and AHP concentrations decreased through June.

Organic-P increased throughout the reservoir during early July with the exception of bottom sites 2 and 4. Concomitantly, both OP and AHP concentrations decreased early July.

Following a period of heavy rainfall at the end of July, both OP and AHP concentrations increased throughout the reservoir, with the highest OP concentrations isolated at bottom and surface sites 3 and 4. Conversely, surface and bottom sites 1 and 2 recorded the highest AHP concentrations. Organic-P was undetected throughout the reservoir.

All P fractions were lower throughout August relative to that during the summer, with OP undetected throughout the majority of the reservoir over the remaining sampling period. However, both AHP and organic-P concentrations increased during October. Organic-P concentrations decreased by November with AHP the dominant P-fraction (Figure 3.3.7.1).

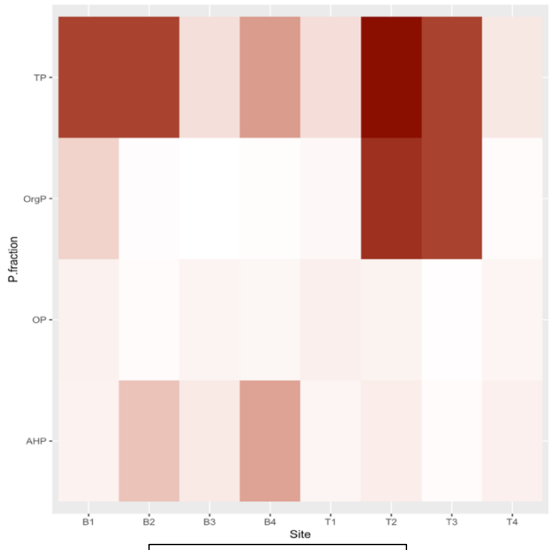

January 19th

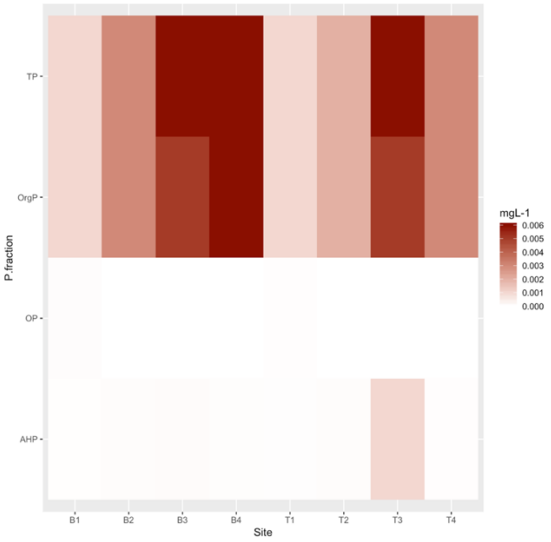

February 1st

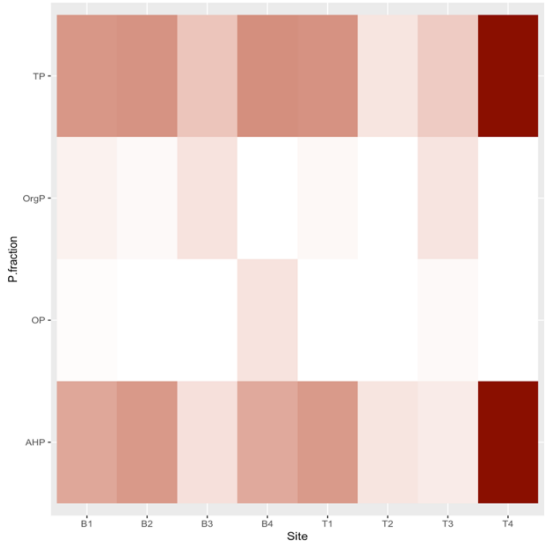

February 15th

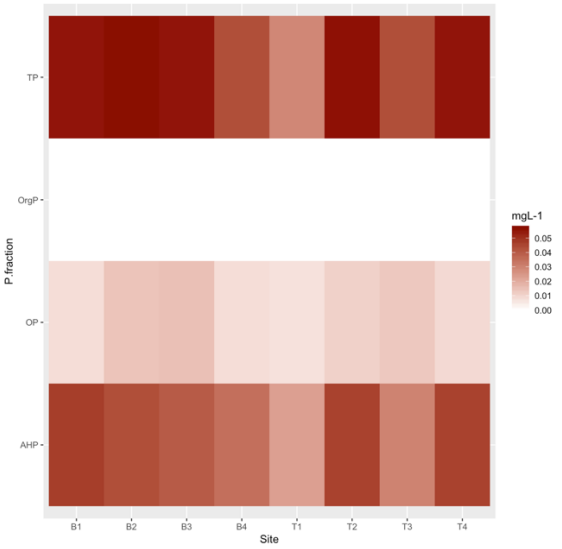

May 2nd

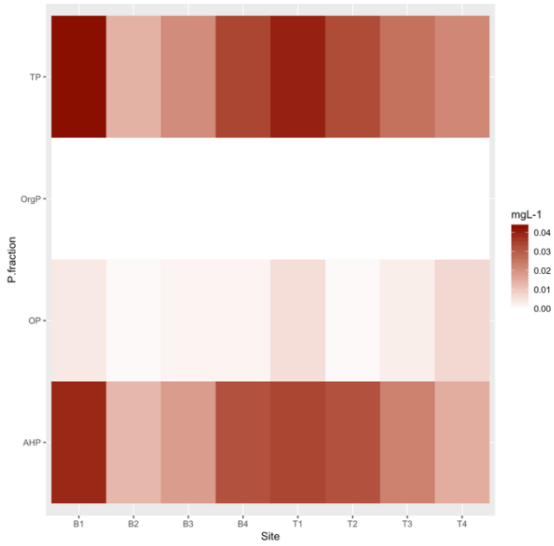

May 14th

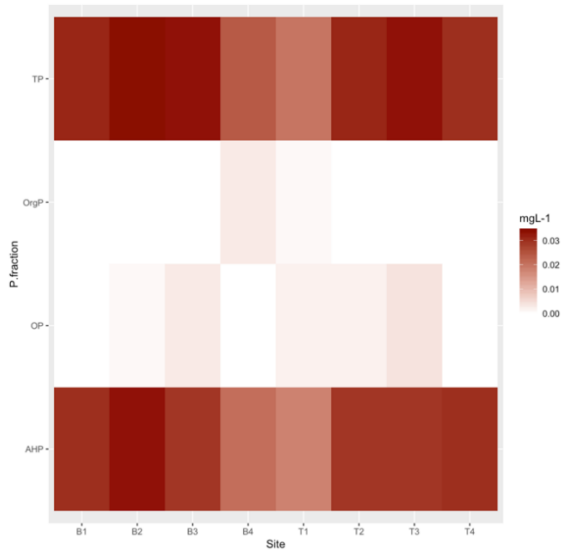

May 29th

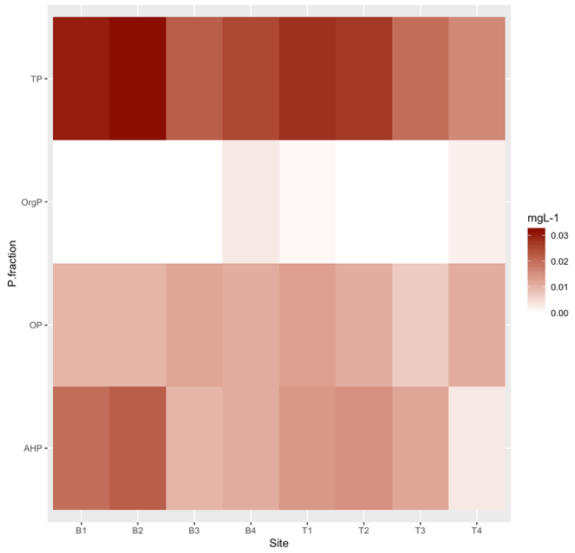

June 11th

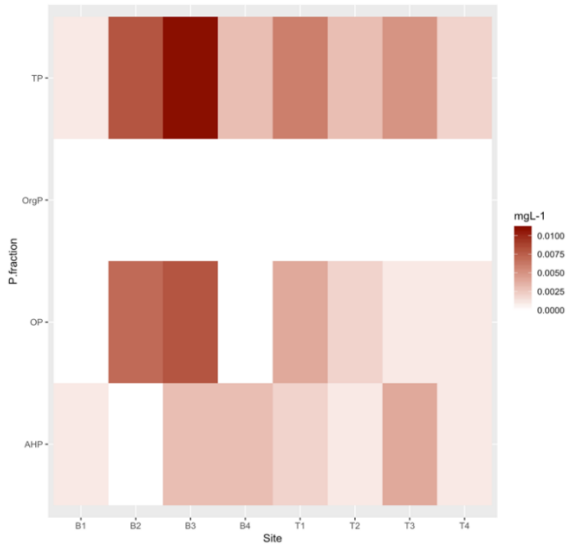

June 27th

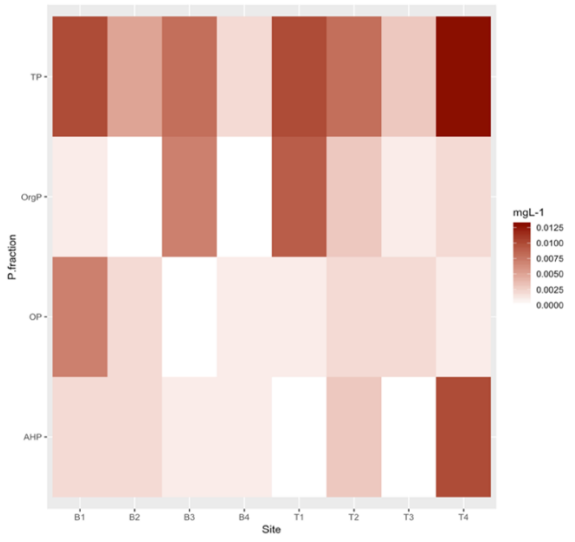

July 9th

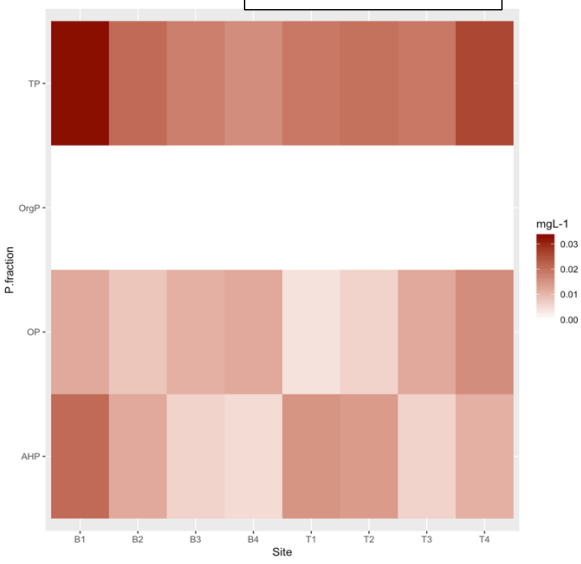

July 23rd

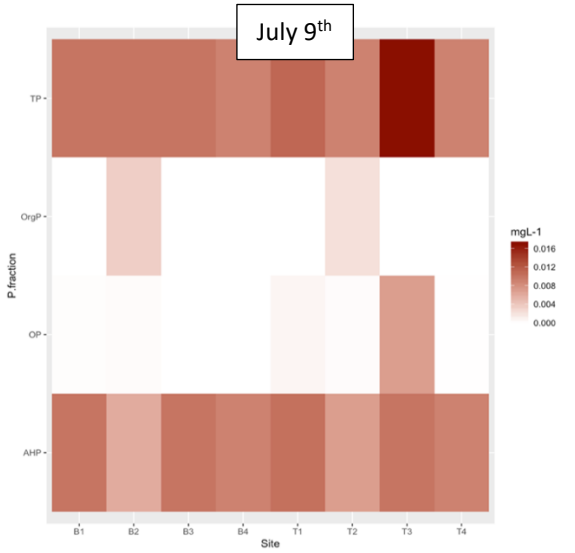

August 3rd

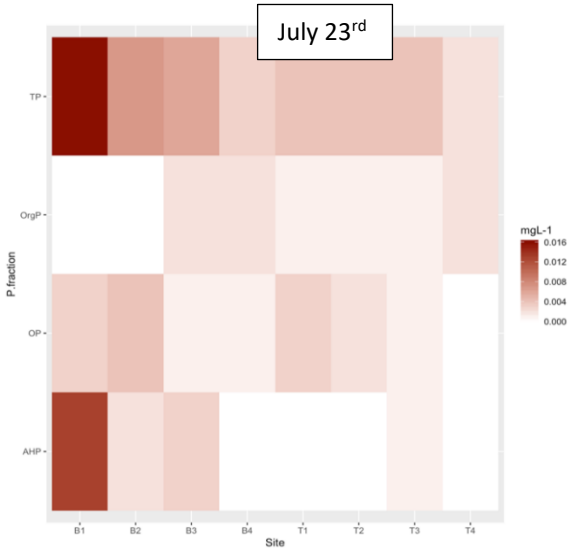

August 20th

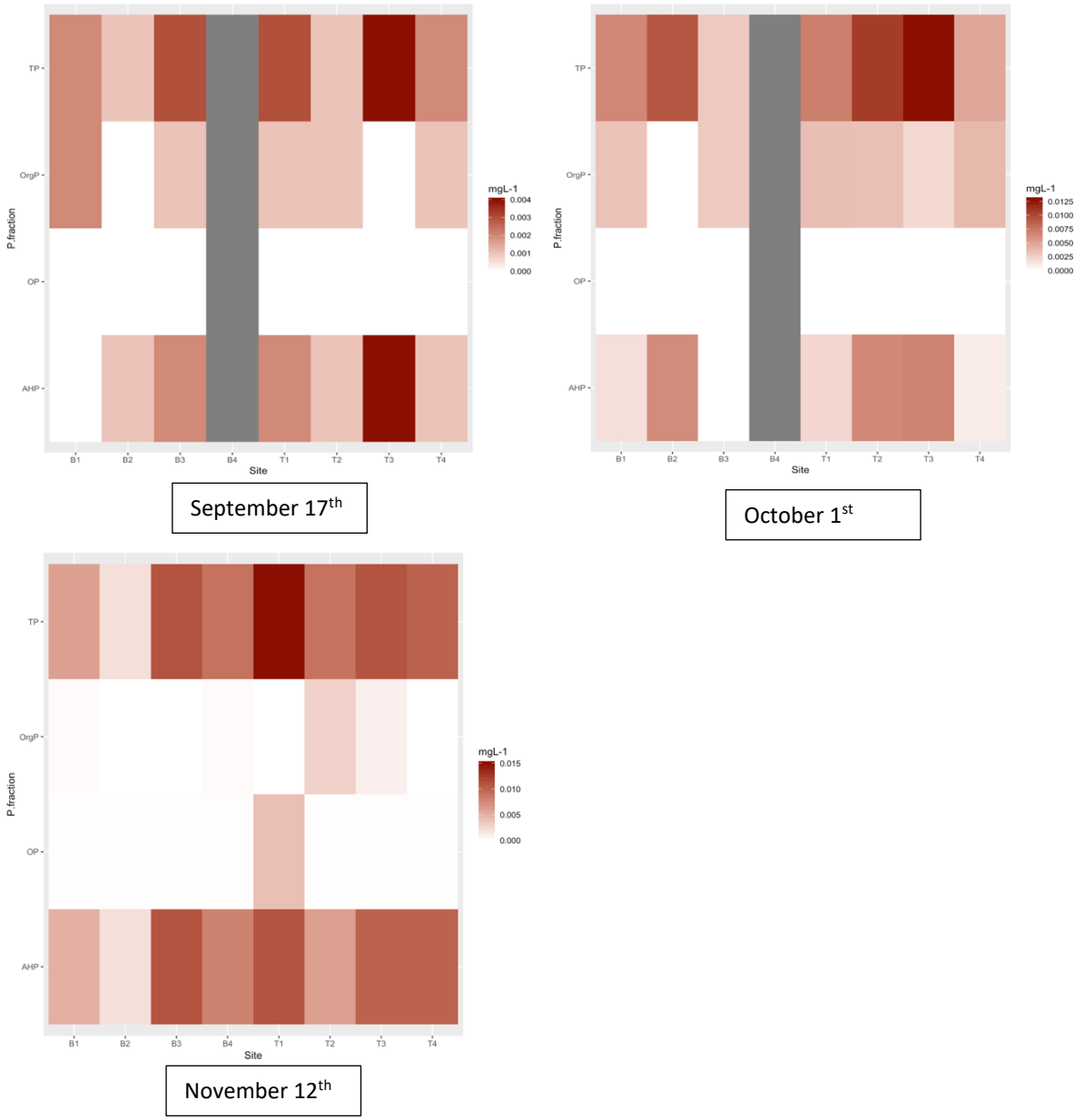

Figure 3.3.7.1. P-fraction (mgL^{-1}) distribution and concentration across each site over the 11-month sampling period. OP availability was increased from May through July at most sites, increasing the risk of water quality degradation.

3.3.8. Models and PCA addressing monthly P-fraction data associations

3.3.8.1. PCA of P-fractions at each sampling site during January and February.

3.3.8.1.1. PC analysis of variable data obtained during sampling on January 16th

The variables, OP, AHP and cyanobacteria were omitted from the PCA as they were not detected at any site.

Higher concentrations of nitrate were positively correlated with high TN:TP (mol/ml) and TN concentrations (Figure 3.3.8.1.1.1) as a consequence of nitrate comprising the greater portion of the TN concentration (99.8%). Likewise, negative correlation between NH_4^+ and the NO_3^- : NH_4^+ ratio is expected.

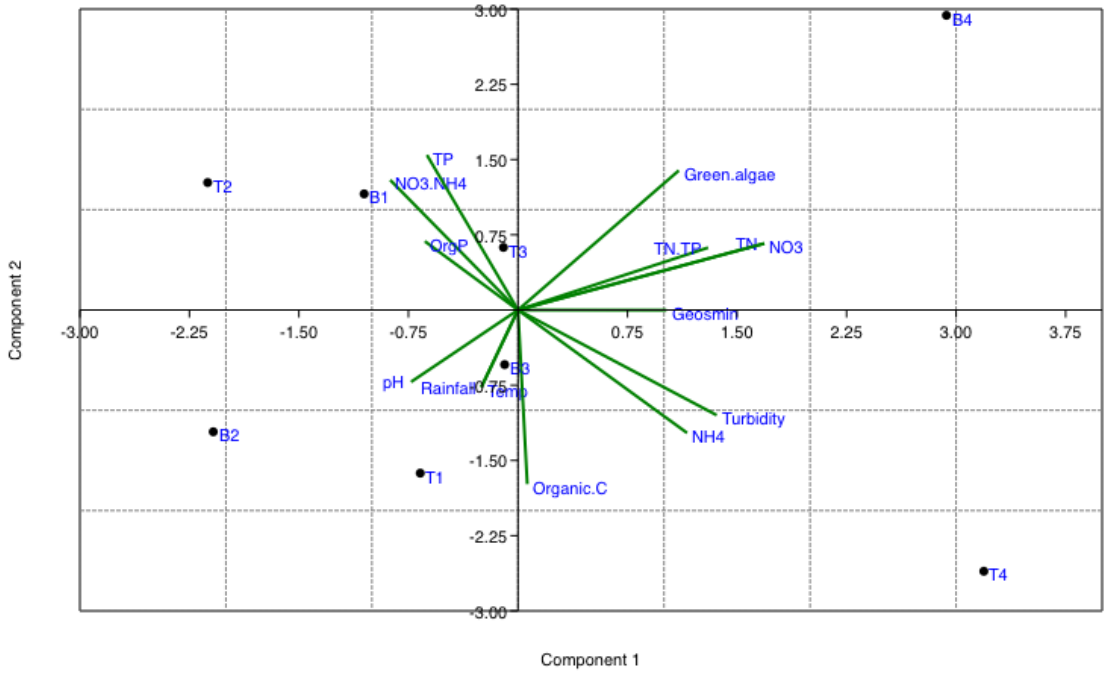

Figure 3.3.8.1.1.1. PCA of surface and bottom sites 1 through to 4 for January 2018. PC 1 and 2 represent 29.8% and 23.6% of the data respectively. High ammonium concentrations were negatively correlated with high NO_3^- : NH_4 ratio, indicating the weight of ammonium concentration upon the ratio.

The negative correlation between nitrate concentrations and rainfall volume suggested that nitrate was not introduced to the reservoir during run-off. An increase in bottom NO_3^- at site 4 was associated with an increase in TN, indicating that the majority of TN was predominantly composed of nitrate. NO_3^- was negatively correlated with pH and sampling sites B2, T1 and T3, indicating increased NO_3^- during periods of low pH, typically recorded at site B4 and indicative of primary production. Raised geosmin concentrations were positively associated with both sampling sites T4 and B4 due to its position directly on the PC2 axis, indicating to site 4 as being the highest risk of geosmin detection during January; however, the negative correlation between geosmin and rainfall suggesting that geosmin was not introduced to the

reservoir entrained in run-off. Lower geosmin concentrations were associated with sites B1, T1 and T2.

3.3.8.1.2. PC analysis of variable data obtained during sampling on February 15th

The green algae, NO_3^- : NH_4^+, *Oscillatoria*, TN and NO_3^- variables were omitted from PCA due to a high number of singularities as a consequence of the variables being undetected throughout the reservoir.

Raised concentrations of Org-P and Org-C were positively correlated with surface and bottom sites 2 and 3 and a negative correlation with increased volumes of rainfall, temperature and the TN.TP molar ratio (Figure 3.3.8.1.2.1).

Raised concentrations of geosmin were positively correlated with increased concentrations of TP (predominantly AHP) and pH, and low concentrations of NH_4^+ and was analogous with site 4.

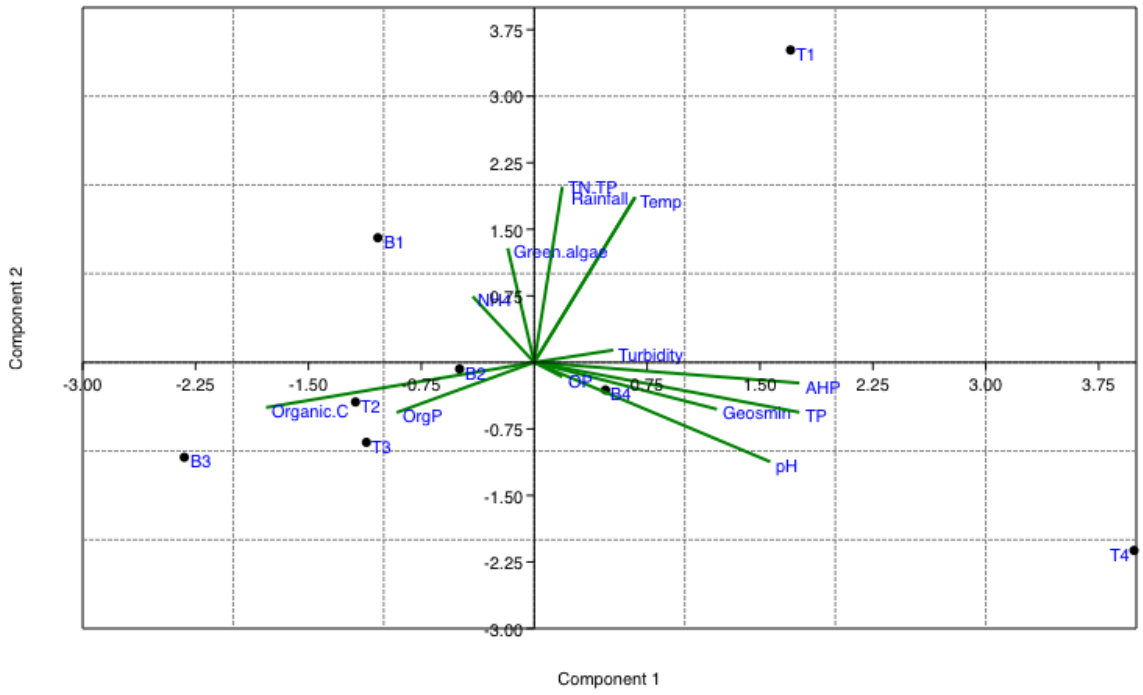

Figure 3.3.8.1.2.1. PCA of surface and bottom sites 1 through to 4 for February 15th, 2018. PC 1 and 2 represents 31.1% and 23.2% of the PCA respectively. Bottom site 4 was positively correlated with increased concentrations of geosmin, pH and AHP.

No correlation was established for geosmin with rainfall volume, therefore, geosmin of a terrestrial origin is unlikely to be the source of the geosmin recorded within the reservoir.